

canadian acoustics

acoustique canadienne

Journal of the Canadian Acoustical Association - Journal de l'Association Canadienne d'Acoustique

SEPTEMBER 2007

Volume 35 -- Number 3

SEPTEMBRE 2007

Volume 35 -- Numéro 3

EDITORIAL / EDITORIAL	3
PROCEEDINGS OF THE ACOUSTICS WEEK IN CANADA 2006/ ACTES DE LA SEMAINE CANADIENNE D'ACOUSTIQUE 2006	
Table of Contents / Table des matières	4
Conference Calendar	11
Plenary Session	16
Aeroacoustics	24
Musical Cognition/ Musical Acoustics	38
Hearing Sciences	66
Noise	88
Speech Sciences	100
Building Acoustics	120
Instrumentation, Signal Processing and Techniques	144
Computational Acoustics	160
Environmental Acoustics	174
Acoustic Materials	196
Micro and Nano Acoustics	206
Abstracts for Presentations without Summary Papers	210
Other Features / Autres Rubriques	
Book Reviews	215
News / Informations	218

PROCEEDINGS

ACOUSTICS WEEK IN CANADA
 SEMAINE CANADIENNE D'ACOUSTIQUE
 ACOUSTICS WEEK IN CANADA
 SEMAINE CANADIENNE D'ACOUSTIQUE
 ACOUSTICS WEEK IN CANADA
 SEMAINE CANADIENNE D'ACOUSTIQUE
 ACOUSTICS WEEK IN CANADA

COMPTES RENDUS

canadian acoustics

THE CANADIAN ACOUSTICAL ASSOCIATION
P.O. BOX 1351, STATION "F"
TORONTO, ONTARIO M4Y 2V9

CANADIAN ACOUSTICS publishes refereed articles and news items on all aspects of acoustics and vibration. Articles reporting new research or applications, as well as review or tutorial papers and shorter technical notes are welcomed, in English or in French. Submissions should be sent directly to the Editor-in-Chief. Complete instructions to authors concerning the required camera-ready copy are presented at the end of this issue.

CANADIAN ACOUSTICS is published four times a year - in March, June, September and December. The deadline for submission of material is the first day of the month preceeding the issue month. Copyright on articles is held by the author(s), who should be contacted regarding reproduction. Annual subscription: \$20 (student); \$60 (individual, institution); \$250 (sustaining - see back cover). Back issues (when available) may be obtained from the CAA Secretary - price \$10 including postage. Advertisement prices: \$600 (centre spread); \$300 (full page); \$175 (half page); \$125 (quarter page). Contact the Associate Editor (advertising) to place advertisements. Canadian Publication Mail Product Sales Agreement No. 0557188.

acoustique canadienne

L'ASSOCIATION CANADIENNE D'ACOUSTIQUE
C.P. 1351, SUCCURSALE "F"
TORONTO, ONTARIO M4Y 2V9

ACOUSTIQUE CANADIENNE publie des articles arbitrés et des informations sur tous les domaines de l'acoustique et des vibrations. On invite les auteurs à soumettre des manuscrits, rédigés en français ou en anglais, concernant des travaux inédits, des états de question ou des notes techniques. Les soumissions doivent être envoyées au rédacteur en chef. Les instructions pour la présentation des textes sont exposées à la fin de cette publication.

ACOUSTIQUE CANADIENNE est publiée quatre fois par année - en mars, juin, septembre et décembre. La date de tombée pour la soumission de matériel est fixée au premier jour du mois précédant la publication d'un numéro donné. Les droits d'auteur d'un article appartiennent à (aux) auteur(s). Toute demande de reproduction doit leur être acheminée. Abonnement annuel: \$20 (étudiant); \$60 (individu, société); \$150 (soutien - voir la couverture arrière). D'anciens numéros (non-épuisés) peuvent être obtenus du Secrétaire de l'ACA - prix: \$10 (affranchissement inclus). Prix d'annonces publicitaires: \$600 (page double); \$300 (page pleine); \$175 (demi page); \$125 (quart de page). Contacter le rédacteur associé (publicité) afin de placer des annonces. Société canadienne des postes - Envois de publications canadiennes - Numéro de convention 0557188.

EDITOR-IN-CHIEF / RÉDACTEUR EN CHEF

Ramani Ramakrishnan
Department of Architectural Science
Ryerson University
350 Victoria Street
Toronto, Ontario M5B 2K3
Tel: (416) 979-5000; Ext: 6508
Fax: (416) 979-5353
E-mail: rramakri@ryerson.ca

EDITOR / RÉDACTEUR

Chantai Laroche
Programme d'audiologie et d'orthophonie
École des sciences de la réadaptation
Université d'Ottawa
451, chemin Smyth, pièce 3062
Ottawa, Ontario K1H 8M5
Tél: (613) 562-5800 # 3066; Fax: (613) 562-5428
E-mail: claroche@uottawa.ca

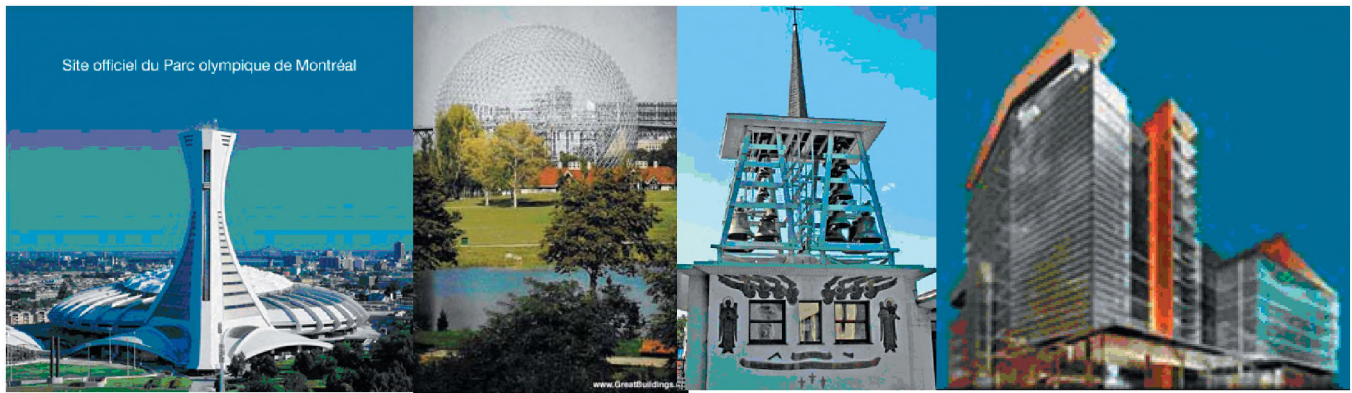
ASSOCIATE EDITORS / REDACTEURS ASSOCIES

Advertising / Publicité

Jason Tsang
7 Parkwood Crescent
Ottawa, ONTARIO
K1B3J5
E-mail: jtsangeng@yahoo.ca

News / Informations

Steven Bilawchuk
aci Acoustical Consultants Inc.
Suite 107, 9920-63rd Avenue
Edmonton, Alberta T6E 0G9
Tel: (780) 414-6373
Fax: (780) 414-6376
E-mail: stevenb@aciacoustical.com



**CAA Montreal 2007
Concordia University
1515 Ste. Catherine West, Montreal, QC, H3G 2W1
9-12 October 2007**

ORGANIZING COMMITTEE

Rama Bhat, Conference Chair
Kamran Siddiqui, Technical Programs Chair
Muthukumar Packirisamy, Exhibits Chair
Zhi Chen, Finance Chair
Sivakumar Narayanaswamy, Publications Chair
Wenfang Xie, Logistics Chair

Sponsors

Engineering and computer Science, Concordia University
CRIAQ - Consortium for Research and Innovation in Aerospace in Quebec
Pratt and Whitney Canada
Bombardier Aerospace

Exhibitors

H. L. Blachford Ltd.
Bruel & Kjaer North America Inc
Dalimar Instruments
Novel Dynamics Inc
Pyrok Inc
Scantek Inc
Soft dB

The organizing committee extends a grateful acknowledgment to Sophie Merineau for French translation assistance



Soundbook™ Designed for You:

- Innovative ✓
- IEC conform ✓
- Inexpensive ✓
- User friendly ✓
- General purpose ✓
- Tough (MIL) ✓
- Reliable ✓

S O U N D B O O K

Multichannel SLM IEC61672-1, IEC60804 & IEC60651 Type 1

SAMURAI Basic Software includes Sound Recorder, Frequency Analyzer, Reverberation time measurement

2/4/8/channels with 40kHz bandwidth, 2x tacho, 5 AUX and 2/4 analog outputs

Various software options for Acoustics and Vibration

Remote Control, Network Integration & wireless synchronization of several devices possible

Alternative packages for ME'scope(direct device), si++workbench, SINUS MATLAB Toolbox

PTB Type Approval



SINUS
G.R.A.S.
SOUND & VIBRATION

LDS
DACTRON

01dB-Stell
IMI technology group

SYRAN
SYSTEMS, INC.

MetroLaser, Inc. *

Vibrant Technology, Inc.

Integrated Solutions from World Leaders

- Precision Measurement Microphones
- Intensity Probes
- Outdoor Microphones
- Hydrophones
- Ear Simulation Devices
- Speech Simulation Devices
- Calibrators
- Array Microphones
- Sound Quality
- Sound Intensity
- Sound Power
- Room Acoustics
- Noise Monitoring
- Dynamic Signal Analyzers
- Multi Channel Dynamic Analyzer/Recorders
- Electro Dynamic Shaker Systems
- Advanced Sound & Vibration Level Meters
- Doppler Laser Optical Transducers (Laser Vibrometers)



New KEMAR Manikin



Ottawa

613-598-0026

info@noveldynamics.com

NOVEL DYNAMICS INC.
Dynamic Test and Analysis Systems



Toronto

519-853-4495

Ametelka@cogeco.ca

EDITORIAL / EDITORIAL

It is with great pleasure that we present the proceedings of the CAA Montreal 2007 conference. The conference will take place on October 9-12, 2007 in the new Engineering and Visual Arts complex of the Concordia University in the downtown Montreal.

The conference has Aeroacoustics as its main theme, while Building Acoustics and Musical Acoustics are two additional subthemes. We will have three keynote lectures, on aeroacoustics by Philip Morris from Pennstate, on building acoustics by Franck Sgard from École Nationale des Travaux Publics de l'État, and musical acoustics by Dmitri Tymozsco from Princeton. There are more than 100 papers organized into 24 sessions.

Thanks are due to the Organizing committee members who were very helpful in every aspect of planning this conference. I also would like to thank the Faculty of Engineering and computer Science, Pratt and Whitney Canada, Bombardier for their generous sponsorship of the conference. The exhibitors with their sponsorship of the conference and their exhibits have added an industrial dimension to the conference and we thank them for their support.

Montreal in October will be a welcoming place with the right weather and atmosphere. The technical papers will provide insights to the various aspects of acoustics that the acoustics community is working on, and there will be the banquet and a special feature presentation for informal get together.

We look forward to the conference and the chance of meeting the Canadian acoustics community.

Prof. Rama Bhat
Concordia University

Il nous fait plaisir de vous présenter le compte rendu de la conférence CAA Montréal 2007 qui aura lieu du 9 au 12 octobre 2007 dans le nouveau pavillon intégré génie, informatique et arts visuels de l'Université Concordia situé au centre-ville de Montréal.

La conférence traitera principalement de l'aéroacoustique ainsi que des deux sous-thèmes suivants: l'acoustique du bâtiment et l'acoustique musicale. Nous aurons trois discours-programme sur: l'aéroacoustique par Philip Morris de Pennstate, l'acoustique du bâtiment par Franck Sgard de École Nationale des Travaux Publics de l'État, et l'acoustique musicale par Dmitri Tymozsco de Princeton. Il y aura plus de 100 exposés répartis en 24 séances.

Nous tenons à remercier les membres du comité organisateur qui ont grandement contribué à tous les aspects de la planification de cette conférence. J'aimerais également remercier la faculté de Génie et d'Informatique, Pratt & Whitney Canada et Bombardier pour leur généreux parrainage. De plus, les exposants apporteront une dimension industrielle à la conférence et nous les remercions pour leur soutien.

Montréal est une ville avec une ambiance accueillante et la température en octobre est plutôt clémente, ce qui constitue un endroit idéal pour cette conférence. Les articles techniques donneront des aperçus des divers aspects du domaine de l'acoustique sur lesquels les chercheurs travaillent. De plus, il y aura un banquet et une présentation spéciale qui permettront aux participants de se réunir de façon informelle.

Nous attendons avec impatience le plaisir de rencontrer les spécialistes du domaine de l'acoustique au Canada lors de cette conférence.

Prof. Rama Bhat
Université Concordia

WHAT'S NEW ??

Promotions
Deaths
New jobs
Moves

Retirements
Degrees awarded
Distinctions
Other news

Do you have any news that you would like to share with Canadian Acoustics readers? If so, send it to:

Steven Bilawchuk, aci Acoustical Consultants Inc., Edmonton, Alberta, Email: stevenb@aciacoustical.com

QUOI DE NEUF ?

Promotions
Décès
Offre d'emploi
Déménagements

Retraites
Obtention de diplômes
Distinctions
Autres nouvelles

Avez-vous des nouvelles que vous aimeriez partager

TABLE OF CONTENTS/TABLES DES MATIÈRES

Organising Committee, Sponsors and Exhibitors	1
Editorial/Éditorial	3
Table of Contents/Tables des matières	4
Conference Calendar	9
Plenary Session	
Jet Noise Prediction: Past, Present and Future Philip Morris	16
Pitch Proximity, Voice Leading, and Acoustic Consonance Dmitri Tymoczko	23
Aeroacoustics I	
Jet Noise Prediction Model for Gas Turbine Engine with Internal Forced Mixers Sid-Ali Meslioui	24
Direct Measurement of a Green's Function for Jet Noise Prediction Werner Richarz	26
Aeroacoustic Noise in the Gas Wiping Process David Arthurs and Samir Ziada	28
Exterior Aeroacoustic Array Measurement on the Bombardier Global Express Antoine Malkoun and Robby Lapointe	30
Application of FEM and SEA in Predicting Vibro-Acoustic Behavior of a Flat Ribbed Panel Structure Reza Madjlesi	32
Aeroacoustics II	
H.S. Ribner and Aero Acoustics at UTIAS (Invited Talk) (no paper) Werner Richarz	
Acoustic Performance Considerations for a 'Once Through Steam Generator'/OTSG Vince Gambino and Payam Ashtiani	34
Experimental and Numerical Investigation of Surface Pressure Fluctuations behind Notched and Uniform Spoilers Palom Mejia, Jong Beom park and Luc Mongeau	36
Musical Cognition/Musical Acoustics I	
Psycho-Acoustic Experiments on the Sensory Consonance of Musical Two-Tones (Invited Talk) Reinhart Frosch	38
Perception of Meter Similarity in Flamenco Music Rafa Absar, Francisco Gomez, Catherine Gustavino, Fabrice Marandola and Godfried Toussaint	46
Psychology-Based Rhythmic Transformations Francisco Gomez, Imad Khoury and Godfried Toussaint	48

Musical Cognition/Musical Acoustics II

Preliminary Results on String Instrument Recognition 50
Jason Smalridge, Luis Rodrigues and Lisa Lorenzino

Wind Instrument Acoustic Research at the Computational Acoustic Modeling Laboratory, McGill University 52
Antoine Lefebvre and Gary Scavone

Playful Tools, Serious Questions 54
Rosemary Mountain

Musical Cognition/Musical Acoustics III

Memory for Musical Intervals: Cognitive Differences for Consonance and Dissonance 56
Susan E. Rogers and Daniel J. Levitin

Effect of Age on Sensitivity to Tonality 58
Daniel Minghella, Frank Russo and M. Kathleen Pichora-Fuller

Eliciting Individual Language Describing Differences in Auditory Imagery Associated with Four Multichannel Microphone Technique 60
William L. Martens, Sungyoung Kim, Kent Walker, David Benson and Wieslaw Woszczyk

Developing Consensus Language for Describing Differences in Auditory Imagery Associated with Four Multichannel Microphone Techniques 62
Sungyoung Kim and William L. Martens

Towards a Spatial Sound Description Interchange Format (SpatDIF) 64
Nils Peters, Sean Ferguson and Stephen McAdams

Hearing Sciences I

Finite Element Analysis of an Earmuff-Earcanal System 66
Mahborbeh Khani, Kechroud Riyad and Soulaïmani Azzedine

Adaptive Environmental Classification System for Hearing Aids 68
Luc Lamarche, Wail Gueaieb, Christian Giguere and Tyseer Aboulnasr

Learning User Volume Control Preferences in Hearing Aids 70
Abimbola Cole, Wail Gueaieb, Christian Giguere and Tyseer Aboulnasr

Spatial Vibration Patterns of the Gerbil Eardrum 72
Nicolas N. Ellaham, Fadi Akache, W. Robert J. Funnell and Sam J. Daniel

Hearing Sciences II

Auditory Spatial Attention in Younger and Older Adults: A Comparison of Laboratory and Self-Report Measures 74
Gurjit Singh and M. Kathleen Pichora-Fuller

Acoustic Cues and Recognition Accuracy in Cross-Cultural Vocal Expression 76
Christopher Trimmer, Robin Meyer-Macleod, Lola L. Cuddy and Laura-Lee Balkwill

Nonlinear Registration of Histological Images for 3-D Middle-Ear Modeling 78
Shruti Nambiar, Mallar M. Charavarty, W. Robert J. Funnell and D. Louis Collins

Variabilité de l'atténuation des protecteurs auditifs mesurée par la méthode Field-MIRE en fonction de la direction du son incident et des bruits du porteur 80
Marc-Andre Gaudreau, Frederic Laville, Jeremie Voix and Hugues Nelisse

Hearing Sciences III

- A Field Study of Preferred Listening Levels for Music Played on Personal Stereo Players in the Urban Environment 82
Frank A. Russo, Mohammad Abdoli-E, Zizhen Lu and Ahlexxi Jelen
- Universal Accessibility and Usability for Hearing: Considerations for Design 84
Danie Fok, Lynn Shaw, Mary Beth Jennings and Margaret Cheesman
- Changing State and the Irrelevant Sound Effect 86
Aimee M. Surprenant, Ian Neath and Tamra J. Bireta

Noise I

- Echo Control in VoIP 88
Samy El-Hennawey
- The Challenge for Telecom Industrial in the Acoustic and Network Echo Cancellation 90
Qu Gary Jin
- Prediction of Noise Generated by a Cabin Outflow Valve using the STAR-CD Code 92
George Waller

Noise II

- Measurement of Perceived Annoyance Due to Low Frequency Content in Broad Spectrum Noises 94
Cheng Qian, Alberto Behar and Willy Wong
- Modeling the Vibroacoustic Response of Multi-Materials Complex Structures under Mechanical Excitation 96
Dilal Rhazi and Nouredine Atalla
- A New Nonlinear Impedance Model for Liners 98
A. Touchais, N. Atalla and R. Panneton

Speech Sciences I

- Speech Enhancement Employing Loudness Subtraction and Over-Subtraction 100
Wei Zhang and Tyseer Aboulnasr
- Articulatory State Estimation from Incomplete Speech Measurements 102
Luis Rodrigues and John Kroeker
- Acoustic Diagnosis of Vocal Tremor 104
Huawei Colin Li, Hilmi R. Dajani, Willy Wong and Pascal van Lieshout
- A Robust Voice Separation Method 106
Yijing Chu, Heping Ding and Xiaojun Qiu
- Effect of Within- and Between-talker Variability on Word Identification in Noise by Younger and Older Adults 108
Huiwen Goy, Kathy Pichora-Fuller, Pascal van Lieshout, Gurjit Singh and Bruce Schneider

Speech Sciences II

- An Algorithm for Formant Frequency Estimation from Noise-corrupted Speech Signals 110
Shaikh Fattah, Wei-Ping Zhu and M. Omair Ahmad
- Débruitage par ondelettes de la parole en milieu industriel 112
Cecile Le Cocq, Frederic Laville and Christian Gargour

A Time-Domain Pitch Extraction Scheme for Noisy Speech Signals Celia Shahnaz, Wei-Ping Zhu and M. Omair Ahmad	114
Simulation of the Three Dimensional Flow in the Human Larynx S. Presault C��r��, A. Lormand, D. Redekop and G. Rouhi	116
Efficient Blind Speech Signal Separation Combining Independent Component Analysis And Beamforming Qiongfeng Pan and Tyseer Aboulnasr	118
Building Acoustics I	
The acoustics of the Hellenistic Theatre of Epidaurus: The Important Role of the Seat Rows Nico F. Declercq and Cindy S. A. Dekeyser	120
Using Speech Intelligibility Scores to Rate Sound Insulation Hyeon Ku Park, John Bradley and Brad Gover	122
Acoustic Ecology and the Cinematic Representation of Architectural Space: Strains of R. Murray Schafer’s Acoustic Design in the Films of Jacques Tati Randolph Jordan	124
Tonal Noise in Buildings: Current Practice in Measurement and Assessment Emanuel Mouratidis and Dean E. Capone	126
Building Acoustics II	
Statistical Basis for Rating Speech Privacy of Closed Rooms Brad Gover and John Bradely	128
Guide for Flanking Sound Transmission in Wood Framed Construction: Issues for Impact Noise J. David Quirt, Trevor R. T. Nightingale and Frances King	130
A Unified Theory for Stresses and Oscillations Himanshu Dehra	132
Acoustic Renovation of Vancouver’s Queen Elizabeth Theatre: 2006 to 2009 John O’Keefe	134
Building Acoustics III	
Measuring and Predicting Speech Privacy in Open-Plan Spaces John Bradley	136
Acoustic Design Of The Esplanade Arts And Heritage Centre, Medicine Hat, Alberta John O’Keefe	138
Comparison of subjective and objective ratings of intelligibility of speech recordings Brad Gover and John Bradley	140
Effects of Structural Flanking on Apparent STC of Steel Stud Wall Clair Wakefield and Andrew Williamson	142
Instrumentation, Signal Processing and Techniques I	
Measurement of the Performance of Sound Level Meters Using IEC 61672-3:2006 Peter Hanes	144

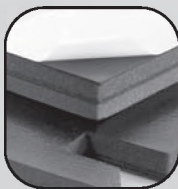
Improved Repeatability for Calibration of Shock Accelerometers Lixue Wu	146
A New Method of Acoustical Remote Evaluation of Defective Structures and Material Characterization E. Mfoumou, C. Hedberg, C. Kao-Walter and S. Narayanaswamy	148
Frequency Analysis of the Acoustic Pressure of Nonlinear Standing Waves Majid Nabavi, M. H. Kamran Siddiqui and Javad Dargahi	150
Instrumentation, Signal Processing and Techniques II	
Ray Trace Modelling of Multipath in Ultrasound Power Measurement System Lixue Wu	152
Monte Carlo Simulation for Calculation of Uncertainty in Reciprocity Calibration of Microphones Peter Hanes	154
A Theoretical Study on Using PVDF in the Acoustic Pump for Biomedical Applications Majid Nabavi, M. H. Kamran Siddiqui and Javad Dargahi	156
Impedance Tube Characterization of Elastic Properties of Expanding Foams Fabian Chevillotte and Raymond Panneton	158
Computational Acoustics I	
Effect of Mean Flow on the Acoustic Trapped Modes of a Cavity-Duct System K. Awny and S. Ziada	160
A Numerical Study on Effect of Vibrator Shape on the Development of Nonlinear Standing Waves in 2-D Acoustical Resonator Majid Nabavi, M. H. Kamran Siddiqui and Javad Dargahi	162
In-Plane Free Vibration of Circular Disks using Characteristic Orthogonal Polynomials in Rayleigh-Ritz Method Salem Bashmal, Rama Bhat and Subash Rakheja	164
Design Optimization of the Thermoacoustic Air Conditioning System of an Automotive Hadi Babaei and Kamran Siddiqui	166
Computational Acoustics II	
Radiation by a Submerged Cylindrical Shell in Response to an External Non-Stationary Acoustic Pulse Sergui Iakovlev	168
Design Optimization for Parallel Plate Heat Exchangers in a Thermoacoustic Device Hadi Babaei and Kamran Siddiqui	170
Effect of Boundary Conditioning on String Inharmonicity Chien-Yu Chen and Rama Bhat	172
Environmental Acoustics I	
A Review of Noise Impacts from Offshore Oil-Gas Production Activities on Marine Biota Sharmin Sultana and Zhi Chen	174
Bayesian Matched-field Geoacoustic Inversion Stan Dosso	178

Assessment of Aircraft Noise Impact on Residential Area Z. Chen, W. B. Amer and J. Yuan	180
Suivi du bruit audible généré par une nouvelle ligne haute-tension à 735 kV Franck Duchassin, Claude Chamberland and Blaise Gossellin	182
Reduction of Noise Levels in Hydraulic System Driven by Swash Plate Pumps by Improving Design of Port Plate M. Chikhalsouk and Rama Bhat	186
Environmental Acoustics II	
Characterization of Sound Emitted by Wind Machines Used for Frost Control Vince Gambino, Tony Gambino and Hugh Fraser	188
Wind Turbine Noise and Meteorological Influences Ramani Ramakrishnan and Nicholas Sylvestre-Williams	190
Impulse Noise Exposure During Personal Weapon Testing on an Outdoor Shooting Range Ann Nakashima and Yushi Hu	192
The Sound that Vortices within Vortices Make Georgios H. Vatistas	194
Acoustical Material	
An Index of Heterogeneity of Sound Absorbing Porous Materials Yacoubou Salissou and Raymond Panneton	196
A new 3D finite element for sandwich structures with viscoelastic materials Kamel Amichi and Noureddine Atalla	198
Inverse Acoustical Characterization of Porous Media Ali Hamoudi and Raymond Panneton	200
Modeling of General Laminate Composite Structures with Viscoelastic Layers Sebastian Ghinet and Noureddine Atalla	202
Symmetry of Viscous Permeability Tensor in Porous Media C. Perrot, F. Chivilotte and R. Panneton	204
Micro and Nano Acoustics	
Dampig and Quality Factor Optimiztion in MEMS Microresonators Gino Rinaldi, Muthukumaran Packirisamy and Ion Stitharu	206
MEMS based acoustic pressure microphones Gino Rinaldi, Muthukumaran Packirisamy and Ion Stitharu	208
Abstracts for Presentations without Summary Papers	210

Better testing... better products.

The Blachford Acoustics Laboratory

Bringing you superior acoustical products from the most advanced testing facilities available.



Our newest resource offers an unprecedented means of better understanding acoustical make-up and the impact of noise sources. The result? Better differentiation and value-added products for our customers.

Blachford Acoustics Laboratory features

- Hemi-anechoic room and dynamometer for testing heavy trucks and large vehicles or machines.
- Reverberation room for the testing of acoustical materials and components in one place.
- Jury room for sound quality development.



Blachford acoustical products

- Design and production of simple and complex laminates in various shapes, thicknesses and weights.
- Provide customers with everything from custom-engineered rolls and diecuts to molded and cast-in-place materials.

Blachford **QS 9000**
REGISTERED

www.blachford.com | Ontario 905.823.3200 | Illinois 630.231.8300



Conference Program - CAA 2007 (Montreal)

October 9, 2007 (Tuesday)

5:00 PM - 9:00 PM	Board Meeting
6:00 PM - 8:00 PM	Registration and Welcome Reception

October 10, 2007 (Wednesday)

8:30 AM - 4:00 PM	Conference Registration
8:30 AM - 9:00 AM	Conference Opening
9:00 AM - 10:00 AM	Planary Session: Jet Noise Prediction: Past, Present and Future (Philip J. Morris)
10:00 AM - 10:40 AM	Coffee Break

	Aeroacoustics I	Music Cognition/Musical Acoustics-I	Hearing Sciences-1
10:40 AM - 11:00 AM	Jet Noise Prediction Model for Gas Turbine Engine with Internal Forced Mixers - Meslioui	Psycho-Acoustic Experiments on the Sensory Consonance of Musical Two-Tones - Frosch	Finite Element Analysis of an Earmuff-Earcanal System - Khani et al.
11:00 AM - 11:20 AM	Direct Measurement of a Green's Function for Jet Noise Prediction - Richarz	(Invited Talk: 40 minutes)	Adaptive Environmental Classification System for Hearing Aids - Lamarche et al.
11:20 AM - 11:40 AM	Aeroacoustic Noise in the Gas Wiping Process - Arthurs and Ziada	Perception of Meter Similarity in Flamenco Music - Absar et al.	Learning User Volume Control Preferences in Hearing Aids - Cole et al.
11:40 AM - 12:00 PM	Exterior Aeroacoustic Array Measurement on the Bombardier Global Express - Malkoun and Lapointe	Psychology-Based Rhythmic Transformations - Gomez et al.	Spatial Vibration Patterns of the Gerbil Eardrum - Ellaham et al.
12:00 PM - 12:20 PM	Application of FEM and SEA in Predicting Vibro-Acoustic Behavior of a Flat Ribbed Panel Structure - Madilesi	Emotion recognition and Autistic Spectrum Disorders (ASD) : Can music help? - Quintin et al.	Is it the Pits? Noise Exposure of Opera Musicians - MacDonald et al.

12:20 PM - 1:40 PM	Lunch Break
--------------------	-------------

	Noise-I	Speech Sciences-I	Building Acoustics-I
1:40 PM - 2:00 PM	Echo Control in VoIP - El-Hennawy	Speech Enhancement Employing Loudness Subtraction and Over-Subtraction - Zhang and Aboulnasr	The acoustics of the Hellenistic Theatre of Epidaurus: The Important Role of the Seat Rows - Declercq and Dekeyser
2:00 PM - 2:20 PM	The Challenge for Telecom Industrial in the Acoustic and Network Echo Cancellation - Jin	Articulatory State Estimation from Incomplete Speech Measurements - Rodrigues and Kroeker	Using Speech Intelligibility Scores to Rate Sound Insulation - Park et al.
2:40 PM - 3:00 PM	Prediction of Noise Generated by a Cabin Outflow Valve using the STAR-CD Code - Waller	Acoustic Diagnosis of Vocal Tremor - Li et al.	Acoustic Ecology and the Cinematic Representation of Architectural Space: Strains of R. Murray Schafer's Acoustic Design in the Films of Jacques Tati - Jordan
3:00 PM - 3:20 PM	Modeling Aircraft Cabin Noise with Statistical Energy Analysis (SEA) - Wareing	A Robust Voice Separation Method - Chu et al.	Tonal Noise in Buildings: Current Practice in Measurement and Assessment - Mouratidis and Capone
3:20 PM - 3:40 PM	Acoustic Echo Cancellation and Noise Removal in the Automobile - Hetherington	Effect of Within- and Between-talker Variability on Word Identification in Noise by Younger and Older Adults - Gov et al.	Noise Control Provisions in Canada's Building Codes - Nightingale and Quirt

3:40 PM - 4:20 PM	Coffee Break
-------------------	--------------

	Instrumentation, Signal Processing and Techniques-I	Computational Acoustics-I	Environmental Acoustics-I
4:20 PM - 4:40 PM	Measurement of the Performance of Sound Level Meters Using IEC 61672-3:2006 - Hanes	Effect of Mean Flow on the Acoustic Trapped Modes of a Cavity-Duct System - Awny and Ziada	A Review of Noise Impacts from Offshore Oil-Gas Production Activities on Marine Biota - Sultana and Chen
4:40 PM - 5:00 PM	Improved Repeatability for Calibration of Shock Accelerometers - Wu	A Numerical Study on Effect of Vibrator Shape on the Development of Nonlinear Standing Waves in 2-D Acoustical Resonator - Nabavi et al.	Bayesian Matched-field Geoacoustic Inversion - Dosso
5:00 PM - 5:20 PM	A New Method of Acoustical Remote Evaluation of Defective Structures and Material Characterization - Mfoumou et al.	In-Plane Free Vibration of Circular Disks using Characteristic Orthogonal Polynomials in Rayleigh-Ritz Method - Bashmal et al.	Assessment of Aircraft Noise Impact on Residential Area - Chen et al.
5:20 PM - 5:40 PM	Frequency Analysis of the Acoustic Pressure of Nonlinear Standing Waves - Nabavi et al.	Design Optimization of the Thermoacoustic Air Conditioning System of an Automotive - Babaei and Siddiqui	Suivi du bruit audible généré par une nouvelle ligne haute-tension à 735 kV - Duchassin et al.
5:40 PM - 6:00 PM	Optical Audio Reconstruction for Stereo Phonograph Records using White Light Interferometry - Li et al.	Modeling transient wave propagation with retarded boundary potentials and waveguide meshes - de Leon and Scavone	Reduction of Noise Levels in Hydraulic System Driven by Swash Plate Pumps by Improving Design of Port Plate - Chikhalsouk and Bhat

8:00 PM - 9:30 PM	Musical Evening
-------------------	-----------------

October 11, 2007 (Thursday)

8:30 AM - 4:00 PM		Conference Registration		
9:00 AM - 10:00 AM		Planary Session: Pitch Proximity, Voice Leading, and Acoustic Consonance (Dmitri Tymoczko)		
10:00 AM - 10:40 AM		Coffee Break		
	Aeroacoustics II	Music Cognition/Musical Acoustics-II	Hearing Sciences-II	
10:40 AM - 11:00 AM	H.S. Ribner and Aero Acoustics at UTIAS - Richarz	Vikrutha Panchama Scales in Carnatic Music Containing both Fourth and Diminished Fifth - Bhat	Auditory Spatial Attention in Younger and Older Adults: A Comparison of Laboratory and Self-Report Measures - Singh and Pichora-Fuller	
11:00 AM - 11:20 AM	(Invited Talk: 40 Minutes)	Preliminary Results on String Instrument Recognition - Smalridge et al.	Acoustic Cues and Recognition Accuracy in Cross-Cultural Vocal Expression - Trimmer et al.	
11:20 AM - 11:40 AM	Acoustic Performance Considerations for a 'Once Through Steam Generator'/OTSG - Gambino and Ashtiani	Wind Instrument Acoustic Research at the Computational Acoustic Modeling Laboratory, McGill University - Lefebvre and Scavone	Nonlinear Registration of Histological Images for 3-D Middle-Ear Modeling - Nambiar et al.	
11:40 AM - 12:00 PM	Valve Noise Control - Meslioui	Playful Tools, Serious Questions - Mountain	Variabilité de l'atténuation des protecteurs auditifs mesurée par la méthode Field-MIRE en fonction de la direction du son incident et des bruits du p - Gaudreau et al.	
12:00 PM - 12:20 PM	Experimental and Numerical Investigation of Surface Pressure Fluctuations behind Notched and Uniform Spoilers - Monneau and Meija	Subharmonic Effects in Some Musical Instruments - Hanssen et al.	Validation of an NVH Simulator Compared to Traditional Laboratory Experiment - Novak and Ule	
12:20 PM - 1:40 PM		Lunch Break		

	Noise-II	Speech Sciences-II	Building Acoustics-II	Micro and Nano Acoustics
1:40 PM - 2:00 PM	Measurement of Perceived Annoyance Due to Low Frequency Content in Broad Spectrum Noises - Qian et al.	An Algorithm for Formant Frequency Estimation from Noise-corrupted Speech Signals - Fattah et al.	Statistical Basis for Rating Speech Privacy of Closed Rooms - Gover and Bradely	Damping and Quality Optimization in MEMS Microresonators - Rinaldi et al.
2:00 PM - 2:20 PM	Modeling the Vibroacoustic Response of Multi-Materials Complex Structures under Mechanical Excitation - Rhazi and Atalla	Débruitage par ondelettes de la parole en milieu industriel - Cocq et al.	Guide for Flanking Sound Transmission in Wood Framed Construction: Issues for Impact Noise - Quirt et al.	MEMS Based Acoustic Pressure Measurements - Rinaldi et al.
2:40 PM - 3:00 PM	A New Nonlinear Impedance Model for Liners - Touchais et al.	A Time-Domain Pitch Extraction Scheme for Noisy Speech Signals - Shahnaz et al.	A Unified Theory for Stresses and Oscillations - Dehra	
3:00 PM - 3:20 PM	SEA Based Model for the Prediction of the Acoustic Performance of Machine Enclosures - Nelisse et al.	Simulation of the Three Dimensional Flow in the Human Larynx - Céré et al.	Acoustic Renovation of Vancouver's Queen Elizabeth Theatre: 2006 to 2009 - O'Keefe	
3:20 PM - 3:40 PM	Integration of Turbulent Boundary Layer (TBL) by using Plate-Backed Cavity to Study the Various TBL Models - Levitte and Atalla	Efficient Blind Speech Signal Separation Combining Independent Component Analysis And Beamforming - Pan and Aboulnasr	Using Annoyance and Loudness Ratings of Transmitted Speech and Music to Evaluate Measures of Sound Insulation - Park et al.	

3:40 PM - 4:20 PM	Coffee Break			
-------------------	--------------	--	--	--

	Acoustic Materials	Music Cognition/Musical Acoustics-III	Instrumentation, Signal Processing and Techniques-II	Environmental Acoustics-II
4:20 PM - 4:40 PM	An Index of Heterogeneity of Sound Absorbing Porous Materials - Salissou and Panneton	Memory for Musical Intervals: Cognitive Differences for Consonance and Dissonance - Rogers and Levitin	Ray Trace Modelling of Multipath in Ultrasound Power Measurement System - Wu	Characterization of Sound Emitted by Wind Machines Used for Frost Control - Gambino et al.
4:40 PM - 5:00 PM	A new 3D finite element for sandwich structures with viscoelastic materials - Amichi and Atalla	Effect of Age on Sensitivity to Tonality - Minghella et al.	Monte Carlo Simulation for Calculation of Uncertainty in Reciprocity Calibration of Microphones - Hanes	Wind Turbine Noise and Meteorological Influences - Ramakrishnan and Sylvestre-Williams
5:00 PM - 5:20 PM	Inverse Acoustical Characterization of Porous Media - Hamoudi and Panneton	Eliciting Individual Language Describing Differences in Auditory Imagery Associated with Four Multichannel Microphone Technique - Martens et al.	A Theoretical Study on Using PVDF in the Acoustic Pump for Biomedical Applications - Nabavi et al.	Performance Parameters for Selecting Equipment to Characterize Sound and Weather Conditions in Remote Natural Environments - Busch
5:20 PM - 5:40 PM	Modeling of General Laminate Composite Structures with Viscoelastic Layers - Ghinet and Atalla	Developing Consensus Language for Describing Differences in Auditory Imagery Associated with Four Multichannel Microphone Techniques - Kim and Martens	Impedance Tube Characterization of Elastic Properties of Expanding Foams - Chevillotte and Panneton	Impulse Noise Exposure During Personal Weapon Testing on an Outdoor Shooting Range - Nakashima and Hu
5:40 PM - 6:00 PM	Symmetry of Viscous Permeability Tensor in Porous Media - Perrot et al.	Towards a Spatial Sound Description Interchange Format (SpatDIF) - Peters et al.	Effect of Demographics on Subjective Jury Testing of an Automotive Application - Ule and Novak	The Sound that Vortices within Vortices Make - Vatisas

6:00 PM - 6:45 PM	CAA Annual General Meeting			
-------------------	----------------------------	--	--	--

7:00 PM - 9:30 PM	Banquet			
-------------------	---------	--	--	--

October 12, 2007 (Friday)

9:00 AM - 10:00 AM	Plenary Session: Innovative Materials for Noise Control in Buildings (Sgard)		
10:00 AM - 10:40 AM	Coffee Break		
	Computational Acoustics-II	Hearing Sciences-III	Building Acoustics-III
10:40 AM - 11:00 AM	Radiation by a Submerged Cylindrical Shell in Response to an External Non-Stationary Acoustic Pulse - Iakovlev	A Field Study of Preferred Listening Levels for Music Played on Personal Stereo Players in the Urban Environment - Russo et al.	Measuring and Predicting Speech Privacy in Open-Plan Spaces - Bradley
11:00 AM - 11:20 AM	Design Optimization for Parallel Plate Heat Exchangers in a Thermoacoustic Device - Babaei and Siddiqui	Universal Accessibility and Usability for Hearing: Considerations for Design - Fok et al.	Acoustic Design Of The Esplanade Arts And Heritage Centre, Medicine Hat, Alberta - O'Keefe
11:20 AM - 11:40 AM	Effect of Boundary Conditioning on String Inharmonicity - Chen and Bhat	Changing State and the Irrelevant Sound Effect - Surprenant et al.	Comparison of subjective and objective ratings of intelligibility of speech recordings - Gover and Bradley
11:40 AM - 12:00 PM	Sound Propagation in Nonstationary, Inhomogeneous and Dispersive Media - Hanssen	Development of Temporary Threshold Shift (TTS) Detector for use in iPods and other Portable Audio Devices - Laroche et al.	Effects of Structural Flanking on Apparent STC of Steel Stud Wall - Wakefield and Williamson
12:00 PM - 12:20 PM		Blink Reflex and Auditory-Speech Perception in Prelingually Cochlear Implanted Children - Emamdiomeh et al.	Acoustics, Noise & Vibration Issues for Technology Research & Manufacturing - Busch

JET NOISE PREDICTION : PAST, PRESENT AND FUTURE

Philip J. Morris

Boeing/A. D. Welliver Professor, Dept. of Aerospace Engineering, Penn State University, 233C Hammond Building,
University Park, PA, USA, 16802. pjm@psu.edu

1. INTRODUCTION

Even with the use of high bypass ratio turbofan engines, jet noise continues to be an important contributor to the total aircraft noise on takeoff. In the case of military fighter aircraft engines, with negligible bypass ratio, jet noise is the dominant noise source at all flight conditions. Thus, jet noise is an important component of community noise in the vicinity of both commercial airports and military bases, and jet noise reduction is an ongoing problem for engine manufacturers. However, after nearly sixty years of research, the prediction of jet noise continues to be a challenging problem. This is especially true if rapid estimates, such as necessary for acoustics to become part of the engine design cycle, are needed. In most instances, such predictions are either based on a company's proprietary experimental database or are based on a Reynolds-averaged Navier-Stokes (RANS) simulation for the jet's mean flow, coupled with an acoustic analogy. Unfortunately, such predictions are often in error, particularly in the peak noise radiation direction. In the present paper the likely reasons for this difficulty are described.

The focus of the present paper is on noise predictions based on relatively simple models. However, there is no question that numerical simulations have made tremendous progress in recent years. Detailed calculations of the full time-dependent, three-dimensional near field, coupled with an extrapolation method to extend the solution semi-analytically to the far field, have shown great promise. For example, Bogey et al. (2003) performed a Large Eddy Simulation of a high subsonic jet. Their calculations also included the acoustic field as part of the simulation. Shur et al. (2005a, 2005b) also performed a Large Eddy Simulation in the near field and then extended the near field solution to the far field using a permeable surface implementation of the Ffowcs Williams- Hawkins (1969) acoustic analogy: see Brentner and Farassat (1998) for an excellent discussion of this technique. Shur et al. considered simple, single axisymmetric jets; jets operating off-design; coaxial jets with chevrons; and heated as well as unheated jets. It is an impressive study. However, these simulations take considerable time and computational resources. In the end, they represent a large numerical experiment and, by themselves, offer no insight into noise generation mechanisms. Without this insight, simpler models and schemes for noise reduction are less likely to be developed.

In the next section a brief review of previous theory and predictions is given. This is followed by a discussion of jet noise measurements, how well they support previous theory, and what help they can give in suggesting new directions. Finally, a simple model is proposed for the generation and radiation of noise by the large scale turbulent structures in the jet shear layer. It is argued that this mechanism, lacking in traditional acoustic analogy approaches, is dominant in the peak noise radiation direction at both subsonic and supersonic jet operating conditions.

2. BACKGROUND

The theory of aerodynamic noise was developed by Sir James Lighthill (1952, 1954). This was the first use of an acoustic analogy. In an acoustic analogy the equations of motion are rearranged into the form of an expression for propagation on the left hand side of the equation and the remaining terms are treated as equivalent sources. In Lighthill's acoustic analogy the propagator is the wave equation in an undisturbed medium at rest. Lighthill identified the sources as having a quadrupole form – by analogy with classical acoustics. Using simple scaling arguments Lighthill deduced that jet noise power should scale with the eighth power of the jet exit velocity and the square of the jet exit area. Lighthill's acoustic analogy was extended to turbulence convecting at high speed by Ffowcs Williams (1963). He argued that due to non-compactness effects, the power radiated by a jet should scale with three powers of jet exit velocity at sufficiently high Mach numbers. All these results were confirmed by the available experimental evidence. Features of the theory at this time included “convective amplification” and Doppler frequency shifts. These effects were argued to increase the noise radiation in the jet downstream direction with five inverse powers of the (modified) Doppler factor and shift the spectrum to higher frequencies. Again there was general agreement with experiments. However, measurements by Lush (1971) and others, showed that in the downstream direction the peak frequency actually decreased and that convective amplification over-predicted the sound pressure levels. It was argued by Lilley (1973) and Goldstein (1976) that these discrepancies could be explained if the propagation of the sound, once generated, through the non-uniform mean flow was included. This led to the development of Lilley's equation which includes refraction effects. This is an acoustic analogy in which the propagator describes the propagation of sound through a non-uniform (in velocity and speed of sound) mean flow. In the special

case of a parallel mean flow, which is a reasonable approximation to the actual slowly varying mean flow, the equivalent source terms are second-order in the fluctuations. General solutions to Lilley's equation must be obtained numerically, but high and low frequency approximations are available: see, for example, Goldstein (1976), Mani (1978), and Balsa (1980). These solutions were coupled to a simple model of the jet flow by Balsa et al. (1978) and Morfey et al. (1978). This provided the first attempt to make noise predictions based on a flow solution, though the latter model used experimental data to define a master spectrum in the absence of mean flow/acoustic interaction effects.

In the theory and predictions outlined above, there are several common features. First, refraction effects are included in the propagation predictions. Second, a model is required for the statistical properties of the turbulence. In particular the two-point space-time correlation of the velocity fluctuations must be modeled. Ffowcs Williams (1963) assumed that the correlation took a Gaussian form in both space and time and this assumption was used for many years. It should be noted that Ffowcs Williams emphasized that this was a model, chosen for ease of analysis. It was not necessarily based on experimental observations. However, it is only with this model that five inverse powers of convective amplification are predicted. In fact, there are very few measurements of the two-point properties of the turbulence. The measurements by Davies et al. (1963) have often been used as guidance for the models – and they do not have a Gaussian form. Another feature of the analysis was the use of a moving reference frame to describe these turbulence properties. It was argued, correctly, that in a reference frame convecting with the turbulence, the sources could be treated as compact up to higher jet velocities. It also removes the apparently high frequency content of the fluctuations due to convection effects, which are unrelated to the frequency of the noise radiation. To a great extent, this represents the theoretical framework that is still used today for jet noise prediction. The primary advance has been the use of RANS solutions to describe the mean flow and the turbulence length and time scales: see Khavaran et al. (1994) for example.

In the present paper it is not possible to provide all the background analysis and only the appropriate references are provided. First, it is important to repeat that the five inverse powers of convective amplification are tied to the Gaussian model for the space-time correlation of the velocity fluctuations. Models based more closely on experimental measurements, such as those given by Harper-Bourne (2003), result in negligible convective amplification: see Morris and Boluriaan (2004) and Raizada and Morris (2006). In addition, Morris et al. (2002) showed that whether the turbulence statistics are described in a moving or stationary reference frame the same prediction for the radiated noise is obtained. Also, it should be noted that

noise predictions at or near 90 degrees to the jet axis provide excellent agreement with experiment. An example is shown in Fig. 1. This prediction uses the method described by Raizada and Morris (2006). However, using the same acoustic analogy model, and including the mean flow/acoustic interaction effects as described by Lilley's

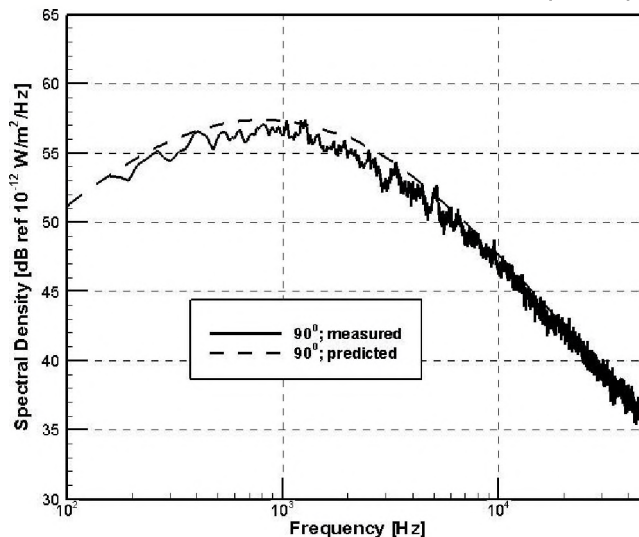


Fig. 1. Comparison of measured and predicted spectral density at 90° to the jet axis. $M_j = 0.9$, $D_j = 6.223$ cm.

equation, predictions in the peak noise direction, close to the jet downstream axis, fail to match noise measurements.

3. EXPERIMENTAL OBSERVATIONS

In recent years there have been a series of experiments conducted in a high quality facility and new interpretations of experimental data that shed light on the prediction problems described at the end of the previous section. Viswanathan (2004) made measurements in single axisymmetric jets at a wide range of jet operating conditions. Prior to undertaking this study a careful examination of the quality of the experimental facility was conducted. Comparisons were also made with previous measurements in other anechoic jet facilities and problems with these prior measurements were identified. Details of the experimental facility and comparisons with other data are given by Viswanathan (2003). For example, previous measurements of jet noise from heated jets had suggested a change in the shape of the spectrum for heated, low speed jets. This data had been used, by Morfey et al. (1978) for example, to propose that a dipole-like noise source, generated by temperature fluctuations in the jet, was responsible for change in spectral shape. However, measurements in different diameter jets showed that the spectrum returned to the shape of the unheated jet spectrum as the diameter, and the Reynolds number, of the jet increased. This is a case where modelers were misled by measurements.

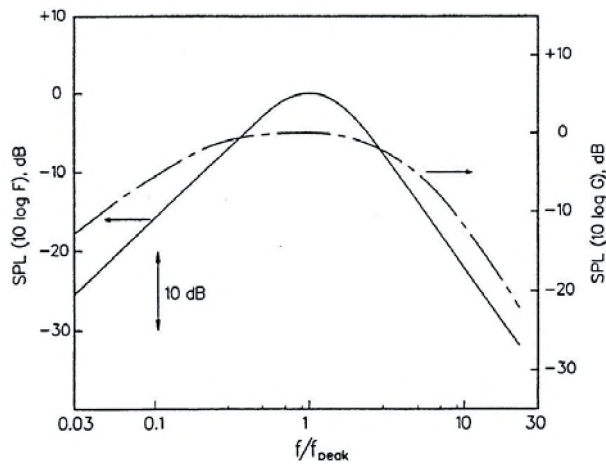


Fig. 2. LSS spectrum (denoted as F) and FSS spectrum (denoted as G). From Tam et al. (1996)

Before examining some of Viswanathan's measurements another experimental observation is useful. Tam et al. (1996) examined and correlated a large database of noise measurements from NASA Langley Research Center and other facilities. They observed that the spectra at all angles to the jet and for a wide range of operating conditions could be collapsed using two spectral shapes. These were named the Fine Scale Similarity (FSS) and the Large Scale Similarity (LSS) spectra. The FFS spectrum is a broad, fairly flat spectrum and the LSS spectrum is much more peaked. The spectrum shapes are shown in Fig. 2. At large angles to the jet downstream axis the FSS spectrum alone fitted the data and at small angles to the jet downstream axis the LSS spectrum alone fitted the data. At intermediate

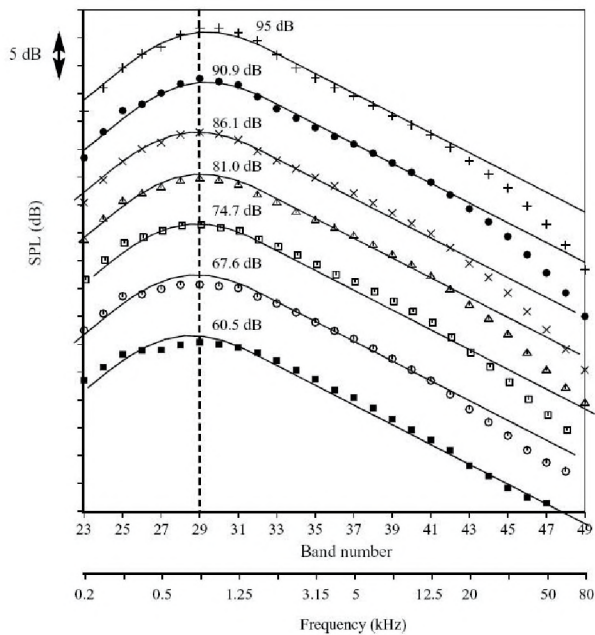


Fig. 3. Comparison of measured spectra with large-scale similarity spectrum. Unheated jets. $D = 2.45$ in., angle = 160° . ■, $M = 0.4$; ○, 0.5; □, 0.6; △, 0.7; ×, 0.8; ●, 0.9; +, 1.0. From Viswanathan (2004).

angles the spectra could be fitted with a linear combination

of the two spectral shapes. Tam et al. (1996) argued that their observations could be explained by the existence of two separate noise generation mechanisms. They argued that the LSS spectrum is generated by the large scale structures in the jet shear layer. Morris and Tam (1977) and Tam and Burton (1984) had shown how the large scale structures could generate noise when the structures travel supersonically with respect to the ambient speed of sound. They modeled the large scale structures as instability waves and explained the noise generation mechanism with a wavy wall analogy. This is discussed further below. The agreement between prediction and experiment in both the jet's near and far fields gave no room for doubt that the large scale structures are the dominant noise source in convectively supersonic jets. What is surprising is that exactly the same spectrum shape is observed in the peak noise directions in convectively subsonic jets! Figure 3, from Viswanathan (2004) shows unheated jet spectra at jet exit Mach numbers ranging from 0.4 to 1.0. If the convection velocity of the large structures is assumed to be 70% of the jet exit velocity, then all these cases are convectively subsonic with respect to the ambient speed of sound. However, the LSS spectrum shape fits all the data very well. There is another striking feature in this figure. The spectral peak is independent of jet Mach number. If there were a Doppler frequency shift effect then the spectral peak should move to a higher frequency as the Mach number increases. This strongly suggests that there is no Doppler shift associated with the LSS spectrum shape. The traditional explanation for this observation is that there is a

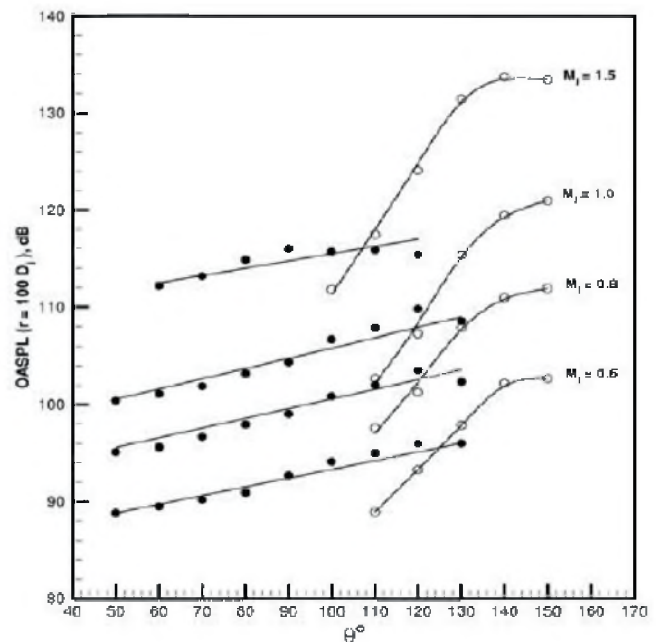


Fig. 4. Variation of OASPL with angle to the jet upstream axis as a function of jet Mach number divide into contributions from the LSS and FSS spectrum sources. Heated jet, $T_t/T_a = 2.2$. From Tam et al. (2007).

Doppler shift, but mean flow acoustic interaction effects

would cause the higher frequency components of the spectrum to be reduced due to refraction. At the relatively low Mach numbers of the jets considered, these effects might be expected to be relatively small. Also, it is far from clear that the offsetting effects of several phenomena – Doppler frequency shift, convective amplification, and mean flow/acoustic interaction effects – would balance so beautifully that the spectral shape would remain unchanged with Mach number. A more rational explanation is that the noise radiation in the peak noise radiation direction is controlled by a different mechanism.

Additional experimental evidence for there being a different mechanism for noise radiation in the peak noise radiation direction has been given by Tam et al. (2007). For example, Fig. 4 shows the variation of overall sound pressure level (OASPL) with angle for a heated jet at different Mach numbers. The OASPL has been separated into two contributions by fitting the LSS and FSS spectra to the measured spectra. For angles close to the downstream jet axis (note that the angles are measured from the upstream axis in this figure) the measured spectrum can be fitted with the LSS spectrum alone. At larger angles from the jet downstream axis the measured spectra can be fitted by the FSS spectrum alone. At intermediate angles, both spectra are required to fit the experimental data. It is clear that the OASPL contributions from sources associated with the LSS and FSS spectra have a quite different behavior. The FSS source contributions increase only slightly as the angle to the downstream jet axis decreases whereas that from sources associated with the LSS have a much stronger variation. For example, there are changes of the order of 20 dB over 40 degrees. The other feature to note is that the peak OASPL occurs at approximately 150 degrees to the jet upstream axis for all but the highest Mach number case. In this highest speed case, the peak moves to a polar angle of 140 degrees.

The contribution to the OASPL from the sources associated with the FSS spectrum can be predicted with the traditional, acoustic analogy-based, methods. Clearly, there is little variation with angle, which is consistent with an absence of convective amplification. This is also reinforced by the observation that the variation with angle from the fine-scale sources is independent of jet Mach number. If convective amplification were present, even if the number of inverse powers of Doppler factor were less than five, the OASPL would vary more rapidly with angle as the jet exit velocity increased. For example, if three inverse powers of Doppler factor are assumed for convective amplification, as suggested by Harper-Bourne (2003), and the convection velocity is assumed to be 70% of the jet exit velocity, then there would be a 4 dB increase from 90 to 130 degrees, relative to the jet upstream axis, for the $M_j = 0.6$ case and an increase of 8 dB in the $M_j = 1.5$. If anything, the measurements show a smaller increase in the higher Mach number case.

It is clear that a different approach is required to make predictions of the noise from the LSS spectrum sources. A simple model for the source mechanism is given in the next section.

4. A MODEL FOR NOISE GENERATION BY LSS SPECTRUM SOURCES

It has long been realized that if the amplitude of a travelling wave generated in the vicinity of the jet is constant, and if its convection velocity is subsonic, relative to the ambient speed of sound, then the pressure fluctuations it generates decay exponentially with distance for the jet. This is well-explained using the wavy wall analogy. However, if the amplitude varies with axial distance then some sound radiation will be possible. Crow (1972), based on his observations of large scale structures in excited jets [Crow and Champagne (1971)], proposed a “line-antenna” model. This consists of a traveling wave with a Gaussian amplitude variation in the axial direction. This was also considered by Crighton (1975) and Ffowcs Williams and Kempton (1978). Experiments in a low speed jet, motivated by the line antenna model, were conducted by Laufer and Yen (1983) who measured some of the growth and decay properties of the large scale turbulent structures. A formal matching of the instability waves in a two-dimensional shear layer with their acoustic radiation was described by Tam and Morris (1980) and this procedure was applied to axisymmetric jets by Morris and Tam (1977) and Tam and Burton (1984) – the latter paper providing a complete analysis of the asymptotic matching. In these papers, the large scale structures were modeled as instability waves supported by the mean flow. Their growth and decay were calculated from the linearized, inviscid equations of motion. These could be reduced to the so-called “Rayleigh equation” of hydrodynamic stability. Special care had to be taken when calculating the decaying stage of the wave, but comparisons with viscous calculations showed that the inviscid results were a good approximation to the viscous solutions, except at very low Reynolds numbers. Tam and Morris (1980), in their calculations for the two-dimensional mixing layer, showed that the rate of growth and decay given by the linear instability analysis was not sufficiently rapid to lead to significant noise radiation. It should be noted that comparisons of linear instability wave models provide a good description of the growth phase of the large scale structures, based on comparisons with measurements using excitation: see Gaster et al. (1985) for example. However, it is unlikely that the rate of decay of the large scale structures is controlled by a linear analysis. This breakdown involves the nonlinear transfer of energy to smaller scale motions. The modeling and prediction of this breakdown process remains an unanswered problem.

However, it is still useful to reexamine the line antenna model. Assume that the pressure fluctuation generated on a

cylindrical surface of radius a in the near field of the jet can be written as¹,

$$p(a, z, t) = \text{Re} \{ \hat{p}(z, t) \} = \text{Re} \{ A(z) \exp [i(\alpha(z) - \omega t)] \} \quad (1)$$

Then it is straightforward to show, using the method of stationary phase, that the far field pressure is given by,

$$\hat{p}(R, \theta) = -\frac{i}{\pi R} \frac{P(a, \omega \cos \theta / c_\infty)}{H_0^{(1)}(\omega a \sin \theta / c_\infty)} \exp(i\omega R / c_\infty) \quad (2)$$

where $P(a, s)$ is the Fourier transform of the pressure on the cylindrical surface with respect to the axial wavenumber s and c_∞ is the ambient speed of sound. Note that the axial wavenumber spectrum is to be evaluated at the wavenumber that gives a sonic velocity at a polar angle θ relative to the jet downstream axis. $H_0^{(1)}(\cdot)$ is the Hankel function of the first kind and order zero. In this simple model only an axisymmetric disturbance on the cylindrical surface has been considered. In addition, only a single frequency is examined. A more complete model would involve a random superposition of all frequencies and azimuthal mode numbers. For example, the surface pressure fluctuation could be written as,

$$\hat{p}(a, \phi, z, t) = \int_{-\infty}^{\infty} \sum_{n=-\infty}^{\infty} a_n(\omega) \exp \{ i[\chi_n(z, \omega) + n\phi - \omega t] \} d\omega \quad (3)$$

where $\chi_n(z, \omega)$ is the axial phase variation of the component with frequency ω and azimuthal mode number n . $a_n(\omega)$ is a random amplitude of the n -th azimuthal mode with frequency ω . In addition, the surface surrounding the jet could be conical to allow for the spreading of the jet.

Returning to the simple, axisymmetric, single frequency case, assume that the wave has a constant phase velocity and a Gaussian amplitude envelope. That is,

$$\hat{p}(a, z) = A \exp \left[-b(z - z_s)^2 \right] \exp(i\alpha_o z) \quad (4)$$

The corresponding solution for $P(a, s)$ is,

$$P(a, s) = A \sqrt{\frac{\pi}{b}} \exp \left[-iz_s (\alpha_o - s) \right] \exp \left[-\frac{(\alpha_o - s)^2}{4b} \right] \quad (5)$$

¹ It should be noted that this wave packet representation has been used by several researchers. Most recently by Tam et al. (2007).

There are several things to notice. First, the peak in the amplitude of $P(a, s)$ occurs at $s = \alpha_o$. Thus, if $\alpha_o > \omega / c_\infty$, the peak wavenumber components of the pressure signal will not radiate. Secondly, the width of the Gaussian envelope for the transform is controlled by the rate of amplitude change of the pressure with axial distance: the factor b . Thus if the amplitude of the instability wave is changing very slowly, that is if $b \ll 1$, the transform's amplitude will have a very narrow bandwidth. This corresponds to highly directional radiation and would give negligible radiation for subsonic convection velocities. This is the classical wavy wall problem – with constant amplitude. However, if there is a relatively rapid change in the amplitude of the wave packet, the bandwidth of the transform will be much greater and more radiating components will be generated.

Some example calculations have been performed to estimate the far field directivity associated with this model. The predictions, shown in Fig. 5, correspond to a Strouhal number of 0.2 and different convective Mach numbers. The polar angle is chosen to be relative to the jet upstream axis, to correspond to Fig. 4. It should be noted that the peak radiation direction is located at 150° for subsonic convection Mach numbers. This is due to the weighting by the Hankel function in the denominator in Eqn. (2) for the far field pressure. Also, as the convective Mach number becomes supersonic, the peak in the directivity moves to smaller polar angles. It should be noted that the Mach angle for $M_c = 1.1$ is equal to 165° , so the influence of the Hankel function weighting is still felt. However, at higher convective Mach numbers, the peak direction is controlled primarily by the phase velocity – it is 132° for $M_c = 1.5$. All of these features are consistent with the observations shown in Fig. 4.

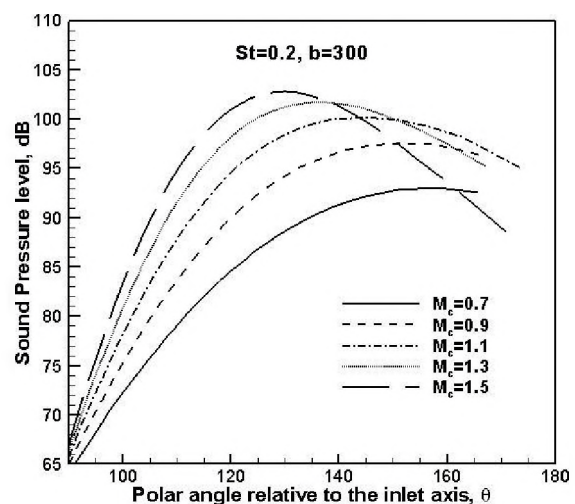


Fig. 5. Calculated variation of far field pressure for Strouhal number 0.2 instability waves at different convective Mach numbers.

Calculations have also been performed for more general variations in the axial amplitude and phase, including more rapid amplitude decay than growth and a variable phase velocity. In these cases it is necessary to perform the Fourier transform numerically. However, the trends are as expected. Increasing the phase velocity moves more wavenumber components into the radiating region and increasing the amplitude variation broadens the directivity.

5. DISCUSSION

In the previous section a simple explanation of the observed jet noise radiation in the peak noise directions was proposed. It clearly provides a reasonable explanation of the measurements shown in Fig. 4. However, as noted in the previous section, a more general model is needed to include more frequencies and azimuthal mode numbers. In addition, there is really no *prediction* involved, as the amplitude and phase variations have been chosen arbitrarily. One could try to use noise measurements to work backwards to find the pressure variation that would give rise to those measurements. However, this is not as simple as it might appear. The problem is that only a limited range of wavenumbers will actually radiate to the far field: those for which $|s| \leq \omega / a_\infty$. So the reconstructed pressure pattern in the near field would be based on a low-pass filtered version of the actual pressure signal. This is a common feature of far field phased array measurements when trying to reconstruct the source distribution. Another possibility would be to use a microphone array in the near field.

Even though such inverse methods would supply useful information, they would not provide a true *predictive* capability. There is a clear need for a model that can describe the axial phase and amplitude characteristics of the instability waves. A possibility would be to extend the linear stability wave model to a nonlinear one. A possible approach would be to use the Parabolized Stability Equations (PSE) [see Malik and Chang (2000) for an application to jet stability]. In the PSE multiple modes and their interactions can be included, though still within the framework of locally linear analysis. Some progress along these lines has been made by Cheung et al. (2007). However, they did not pursue the complete nonlinear capability of the PSE. The development of a predictive model is clearly a need for the *future* of jet noise prediction.

REFERENCES

- Balsa, T. F., Gliebe, P. R., Kantola, R. A., Mani, R. and Stringas, E. J. (1978) High Velocity Jet Noise Source Location and Reduction, Task 2 Final Report: Theoretical Development and Basic Experiments. CR-FAA-RD-76-79.
- Balsa, T. F. (1976) The Far Field of High Frequency Convected Singularities in Sheared Flows, with an Application to Jet-Noise Prediction. *J. Fluid Mech.* 74, 193-208.
- Bogey, C., Bailly, C. and Juve, D. (2003) Noise Investigation of a High Subsonic, Moderate Reynolds Number Jet Using a Compressible LES. *Theo. Comp. Fluid Dyn.* 16(4), 273-297.
- Brentner, K. S. and Farassat, F. (1998) Analytical Comparison of Acoustic Analogy and Kirchhoff Formulation for Moving Surfaces. *AIAA Journal.* 36(8), 1379-1386.
- Cheung, L. C., Bodony, D. J. and Lele, S. K. (2007) Noise Radiation Predictions From Jet Instability Waves Using A Hybrid Nonlinear PSE-Acoustic Analogy Approach. *AIAA Paper 2007-3638.*
- Crighton, D. G. (1975) Basic Principles of Aerodynamic Noise Generation. *Prog. Aero. Sci.* 16, 31-95.
- Crow, S. C. (1972) Acoustic Gain of a Turbulent Jet. *Bull. Am. Phys. Soc.*, paper IE.6.
- Crow, S. C. and Champagne, F. H. (1971) Orderly Structure in Jet Turbulence. *J. Fluid Mech.* 48, 547-591.
- Davies, P. O. A. L., Fisher, M. J. and Barratt, M. J. (1963) The Characteristics of the Turbulence in the Mixing Region of a Round Jet. *J. Fluid Mech.* 15, 337-367.
- Ffowcs Williams, J. E. (1963) The Noise From Turbulence Convected at High Speed. *Phil. Trans. Roy. Soc. Lond.* A255, 469-503.
- Ffowcs Williams, J. E. and Hawkings, D. L. (1969) Sound Generation by Turbulence and Surfaces in Arbitrary Motion. *Phil. Trans. Roy. Soc. Lond.* A264, 341-362.
- Ffowcs Williams, J. E. and Kempton, A. J. (1978) The Noise from the Large Scale Structure of a Jet. *J. Fluid Mech.* 84, 673-694.
- Gaster, M., Kit, E. and Wagnanski, I. (1985) Large-Scale Structures in a Forced Turbulent Mixing Layer. *J. Fluid Mech.* 150, 23-59.
- Goldstein, M. E. (1976) *Aeroacoustics*, McGraw-Hill, New York.
- Harper-Bourne, M. (2003) Jet Noise Turbulence Measurements. *AIAA Paper 2003-3214.*
- Khavaran, A., Krejsa, E. A. and Kim, C. M. (1994) Computation of Supersonic Jet Mixing Noise for an Axisymmetric Convergent Divergent Nozzle. *J. Aircraft.* 31(3) 603-609.
- Laufer, J. and Yen, T.-C. (1983) Noise Generation by a Low-Mach-Number Jet. *J. Fluid Mech.* 134, 1-31.
- Lighthill, M. J. (1952) On Sound Generated Aerodynamically: I. General Theory. *Proc. Roy. Soc. Lond.* A211, 564-587.
- Lighthill, M. J. (1954) On Sound Generated Aerodynamically: II. Turbulence as a Source of Sound. *Proc. Roy. Soc. Lond.* A222, 1-32.
- Lilley, G. M. (1973) On the Noise from Jets, in *Noise Mechanisms*, AGARD-CP-131, 13.1-13.11.
- Lush, P. A. (1971) Measurements of Jet Noise and Comparison with Theory. *J. Fluid Mech.* 46(3), 477-500.
- Malik, M. R. and Chang, C. L. (2000) Nonparallel and Nonlinear Stability of Supersonic Jet Flow. *Computers and Fluids.* 29(3), 327-365.
- Mani, R. (1976) The Influence of Jet Flow on Jet Noise. *J. Fluid Mech.* 80, 753-793.
- Morfey, C. L., Szweczyk, V. M. and Tester, B. J. (1978) New Scaling Laws for Hot and Cold Jet Mixing Noise Based on a Geometrics Acoustics Model. *J. Sound Vib.* 61(2), 255-292.

Morris, P. J. and Boluriaan, S. (2004) The Prediction of Noise from CFD Data. AIAA Paper 2004-2977.

Morris, P. J., Boluriaan, S., Lilley, G. M. and Long, L. N. (2002) Two-Point Cross Correlations of Turbulence and Noise Predictions – Analysis and Simulation. AIAA Paper 2002-0071.

Morris, P. J. and Tam, C. K. W. (1977) Near and Far Field Noise from Large-Scale Instabilities of Axisymmetric Jets. AIAA Paper 77-1351.

Raizada, N. and Morris, P. J. (2006) The Prediction of Noise From High Speed Subsonic Jets Using an Acoustic Analogy. AIAA Paper 2006-2596.

Shur, M. L., Spalart, P. R. and Strelets, M. Kh. (2005) Noise Prediction for Increasingly Complex Jets. Part I: Methods and Tests. Int. J. Aeroacoustics. 4(3&4), 213-245.

Shur, M. L., Spalart, P. R. and Strelets, M. Kh. (2005) Noise Prediction for Increasingly Complex Jets. Part II: Applications. Int. J. Aeroacoustics. 4(3&4), 247-266.

Tam, C. K. W. and Burton, D. E. (1984) Sound Generation by the Instability Waves of Supersonic Flows. Part 2. Axisymmetric Jets. J. Fluid Mech. 138, 273-295.

Tam, C. K. W., Golebiowski, M. and Seiner, J. M. (1996) On the Two Components of Turbulent Mixing Noise from Supersonic Jets. AIAA Paper 96-1716.

Tam, C. K. W. and Morris, P. J. (1980) The Radiation of Sound by the Instability Waves of a Compressible Plane Turbulent Shear Layer. J. Fluid Mech. 98(2), 349-381.

Tam, C. K. W., Viswanathan, K., (2007) The Sources of Jet Noise: Experimental Evidence. AIAA Paper 2007-3641.

Viswanathan, K. (2003) Jet Aeroacoustic Testing: Issues and Implications. AIAA Journal 41(9), 1674-1689.

Viswanathan, K. (2004) Aeroacoustics of Hot Jets. J. Fluid Mech. 516, 39-84.

ACKNOWLEDGEMENTS

The author would like to thank the conference organizers for the opportunity to present this paper. My first postgraduate job was in Canada at the University of Toronto Institute for Aerospace Studies. I had sent out more than a hundred job applications following my Ph.D. and had received no offers. Fortunately my application letter was forwarded to Professor H. S. (Herb) Ribner (1913-2005) and he offered me a research position. It is hard to believe that Herb was 92 at his death. We had been communicating on jet noise issues until shortly before his death. He was extraordinary scholar and he is missed by everyone who knew him – even if we didn't agree on every technical point. Herb was generally correct and always insightful. I would also like to acknowledge many conversations with Dr. Viswanathan of the Boeing Company and Prof. Chris Tam of the Florida State University (who was also a product of Canadian higher education: McGill).

FIVE COMPONENTS OF TONALITY

Dmitri Tymoczko

Princeton University, Princeton, New Jersey, USA

In my talk, I will argue that there are five forms of pitch structure that are present in a wide range of musical genres, Western and non-Western, past and present, and which jointly contribute to a sense of tonality:

1. *Conjunct melodic motion*: melodies tend to move by short distances from note to note.
2. *Acoustic consonance*: consonant harmonies are preferred to dissonant harmonies, and tend to be used at points of musical stability.
3. *Harmonic consistency*: the harmonies in a passage of music, whatever they are, tend to be structurally similar to one another.
4. *Macroharmony*: the music tends to use a relatively small number of notes (often between 5 and 7) over moderate spans of musical time.
5. *Centricity*: over moderate time spans, one or more notes is heard as being more stable and important than others, appearing more frequently and serving as the goal of melodic motion.

tonality: which is the most significant, and are there any interesting interactions between them? (For instance, is harmonic consistency more important in the context of some scales than others?) Theoretically, we might ask how the various features can *in principle* be combined. Is it the case, for example, that diatonic music necessarily involves a “tonic” note? Conversely, is chromatic music necessarily non-centric? What sorts of chords can be used to construct contrapuntal music, in which a series of independent melodies articulate structurally similar chords? Finally, we can ask a historical question about how different Western styles have in fact combined and recombined these five ingredients of tonality—treating the five properties as articulating a space of possible tonal musics, and exploring the way previous composers have investigated this space. I will conclude the talk by sketching an alternative history of Western music emphasizing the changing interactions of these five musical features.

My goal is to try to think very broadly about composers can combine these five features to produce interesting tonal effects. This project has empirical, theoretical, and historical components. Empirically, we might ask how each of the five features contributes to listeners’ perceptions of

JET NOISE PREDICTION MODEL FOR TURBOFAN ENGINES WITH INTERNAL FORCED MIXERS

Sid-Ali Meslioui

Pratt & Whitney Canada Corp., 1000 Marie-Victorin, Longueuil, QC, Canada, J4G 1A1, Sid-Ali.Meslioui@pwc.ca

1 INTRODUCTION

Many turbofan engine exhaust designs feature internal forced mixers to rapidly mix the hot core flow with the cold bypass flow before the nozzle exit, primarily to enhance mixing and thus improve Specific Fuel Consumption (SFC). The low frequency jet noise is reduced as a result of the lower relative mixed jet velocity compared to a confluent nozzle, at the expense of an increase of the high frequency noise attributed to the mixer. Due to the complexity of the flow field downstream of forced mixer, the effect of mixer geometry on noise is difficult to capture analytically or from noise databases. There is no industry standard on predicting noise from such complex jets. The existing empirical models, such as SAE ARP876D [1] or ESDU98019 [2], for far field noise spectra prediction of single stream jets are not adequate, but remain essential for the engineering community. More accurate methods are deemed essential to increase the confidence level of noise control measures.

Various approaches are being used to assess the noise from jet engines. Numerical methods based on CFD / CAA solvers, such as Direct Numerical Simulation (DNS) and Large Eddy Simulation (LES), remain complex and computationally expensive, thus limited to academic researchers. Other simplified methods use CFD results for the near field flow sources region, solving the acoustic far field with the acoustic analogy, e.g RANS solution coupled with Ffowcs-Williams and Hawkins formulation may present a good compromise if properly pursued.

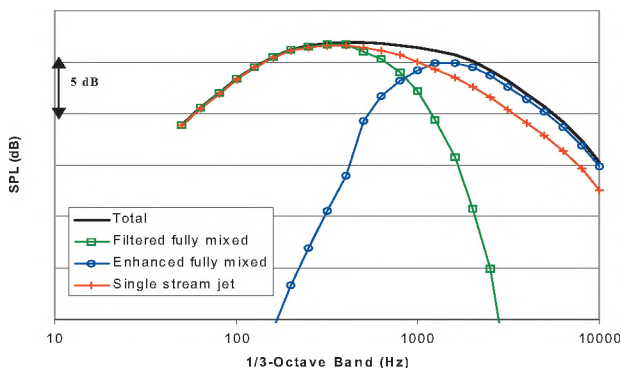


Figure 1: Jet noise prediction using the filtered single stream jets method.

One recent approach developed by Tester et al. [3], and Garrison et al. [4] relies on SAE ARP876D or ESDU98019 far field noise spectra predicted for single stream jets, with appropriate filtering to decompose the spectrum on an enhanced jet spectrum and a fully mixed

jet spectrum. In the present study, far field jet noise predictions were performed for seven lobed mixer configurations and compared to full scale engine noise data obtained in an outdoor test facility. The required turbulence scales are deduced from a data fitting exercise of test data and compared with similar quantities obtained from RANS-CFD for two mixer configurations [5].

2 JET NOISE MODEL

The jet noise modeling approach consists of dividing the jet plume into two regions. The upstream region or “Enhanced fully mixed jet”, close to the nozzle exit, is modeled using the far field single stream jet spectra in which the low frequency part is filtered out. A hypothetical turbulence factor is added to the equation to account for the enhanced turbulence due to mixing inside the nozzle. The downstream region or “filtered fully mixed jet” is also predicted using the far field single stream jet method with the high frequency filtered and removed. More details of the method can be found in Ref. [3, 4, 5].

The total jet noise of an engine with an internal forced mixer is the sum of two jet sources: the enhanced fully mixed jet given by

$$SPL_{enhj} = SPL_s + 10 \text{Log}_{10}(1 - FilterF) + 40 \text{Log}_{10}(Fm)$$

and the fully mixed filtered jet given by

$$SPL_{mixj} = SPL_s + 10 \text{Log}_{10}(FilterF), \quad SPL_s \text{ is the single stream}$$

jet noise spectrum at the fully mixed condition. The characteristic of the filter function is defined as

$$FilterF = \exp(-u) \left[1 + u + \frac{1}{2}u^2 + \frac{1}{6}u^3 \right], \text{ where } u = 4f/f_c, \quad f \text{ is}$$

the frequency and f_c is the cut off frequency of the filter defined by its Strouhal number $S_t = f_c D_m / V_m$ and

$$f_c = \frac{(X/D)_{PC} V_m}{LenJ D_m}, \quad V_m \text{ is the fully mixed jet velocity. } LenJ \text{ is}$$

defined as the length of the enhanced region, $(X/D)_{PC}$ is the axial location of the end of the potential core, and Fm is the turbulence factor. A sample result that shows the effect of both jet components and the total jet noise is shown in Figure 1.

3 DISCUSSION

The accuracy of the predictions depends on the accuracy of the empirical model used to calculate the far field of single stream jets, i.e. SAE ARP876D or ESDU 98019. It was reported that this prediction method can be accurate within +/- 3-5 dB in amplitude, but may also result in a substantial discrepancy in the spectral shape compared to the measured

noise data. Although the accuracy may be found acceptable for engineering use, it yields significant errors in the interpretation of the engine sources noise when performing engine sources noise breakdown, for instance.

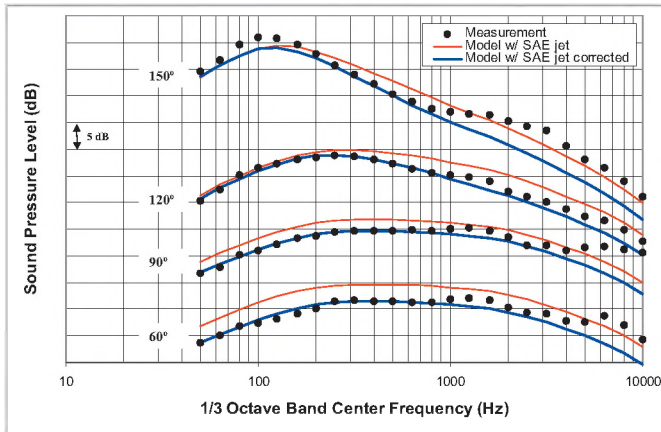


Figure 2: Jet noise prediction vs. measurement for Engine A for high power- Data was offset for clarity.

A study was conducted for seven turbofan engines all featuring an internal exhaust forced mixer, where the predicted noise spectra were compared to the measured far field noise spectra of the corresponding engines. It was found that the two-source method reasonably predicts the noise from jets with internal forced mixers, despite the existence of amplitude and spectral shape discrepancies at given angles and engine power settings. The SAE method was found to over-predict the jet noise at most forward angles relative to the inlet axis, and a large discrepancy exists in the spectral shape for aft angles. Extensive data analyses established a first amplitude correction to the jet noise spectra predicted with the SAE single stream jet noise method. The amplitude correction was then applied to all predicted jet spectra of all engines studied independent of engine power setting and type.

A second correction was then developed to correct for the spectral shape discrepancy. The latter correlation was established using a surface fitting function since the irregularity varies with the frequency and the observation angle. Figure 2 and Figure 3 show sample results for Engine A and B at various directivity angles. The figures show a comparison of the measured noise spectra with jet noise spectra predicted using ISVR / Purdue university method using the SAE single stream jet noise model. Also shown is the prediction using the same method but with the improved or corrected SAE jet noise model. It is shown that more accurate results are obtained when including the amplitude and spectral shape corrections. It should be noted that the very high frequencies (above 3 kHz) are not dominated by jet noise sources.

The improved jet noise model was validated with full-scale engine data with mixed exhaust flow temperature

ratios between 1.3 and 1.6, Bypass ratios (BPR) between 3 and 5, and Mach numbers between 0.5 and 1.1. This covers a wide range of small to medium size commercial turbofan engine designs and operating conditions.

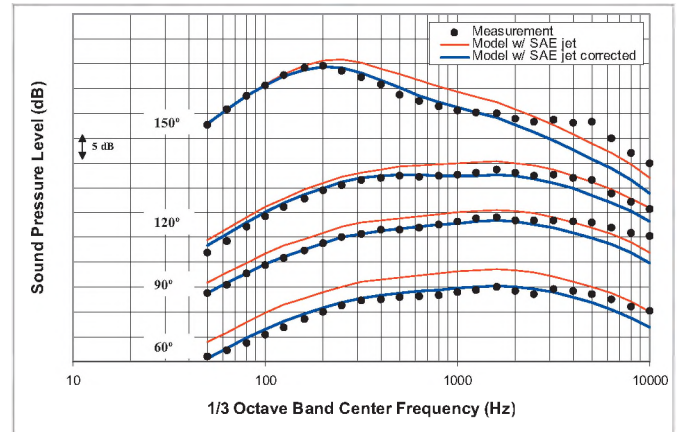


Figure 3: Jet noise prediction vs. measurement for Engine B for high power- Data was offset for clarity.

ACKNOWLEDGMENTS

I would like to thank Mark Cunningham for the CFD work.

REFERENCES

- [1] Society of Automotive Engineers Inc., "Gas Turbine Jet Exhaust Noise Prediction", SAE ARP876D, 1993.
- [2] ESDU 98019, "Computer-based procedure for single-stream jet noise: including far field, static jet mixing noise database for circular nozzles".
- [3] B.J. Tester, M.J. Fisher and W.N. Dalton, "A contribution to the understanding and prediction of jet noise generation in forced mixers", 10th AIAA/CEAS Aeroacoustics Conference, paper 2004-2897.
- [4] L.A. Garrison, W.N. Dalton, A.S. Lyrintzis, G.A. Blasidell, "On the development of semi-empirical models for the prediction of the noise from jets with forced mixers", 10th AIAA/CEAS Aeroacoustics Conference, paper 2004-2898.
- [5] S-A. Meslioui, M. Cunningham, P. Germain, "Determination of CFD Turbulence Scales for Lobed Mixer Jet Noise Prediction", ASME Turbo Expo, GT2007-28334.

DIRECT MEASUREMENT OF A GREEN'S FUNCTION SUITABLE FOR PREDICTION OF SUBSONIC JET NOISE

Werner G. Richarz

Aercoustics Engineering Ltd. Toronto, ON

werner@aercoustics.com

INTRODUCTORY REMARKS

An analytical formulation of a suitable Green's function has eluded jet noise researchers to date. This paper explores the possibility of direct measurement of a Green's function. To this end a point source is placed in the jet flow and the amplitude and phase of radiated signal are extracted. In principle, this information leads to a semi-empirical model Green's function.

JET NOISE REFRACTION (SHIELDING)

Lighthill's acoustic analogy^{1,2} yields less than satisfactory predictions when source and fluid motion are not accounted for. Whereas source motion can be dealt without great difficulty^{3,4,5}, the interaction of the acoustic field and the hydrodynamic field poses far greater challenges. The influence of flow and temperature gradients on sound was demonstrated by a rather elegant set of experiments, wherein a small point source, emitting a single tone, was placed in a jet flow^{6,7}. Schubert⁸, Mani⁹, Lilley¹⁰, Balsa¹¹, and others have added their perspectives on refraction (or fluid shielding) effects.

GREEN'S FUNCTION FOR JET FLOWS

Ribner¹² described a 'road-map' for dealing with all the key features of jet noise including source convection and refraction by flow and temperature gradients, but no explicit solution was provided. It is assumed that the Green's function $G(x-y, t-t', M) = G_N G_0(x-y, t-t')$ is the product of G_N , the normalized Green's function and G_0 the free field Green's function ($M=0$). G_N is measured for discrete frequencies, at it is possible to determine both amplitude and phase quite accurately using a lock-in amplifier technique.

For discrete frequencies $G_N = |G_N| e^{i\delta\phi}$ applies. $|G_N|$ is expected to be less than one whenever the field point x subtends a small angle with respect to the jet axis. At right angles to the jet axis the numerical value should tend to unity and the phase angle $\delta\phi$ to zero. There is no reason to expect that the normalized Green's function is invariant with the source location y . Both source location in the jet as well as the source-observer vector are parameters. (viz. $G_N(y, x-y, \omega)$).

PRELIMINARY RESULTS

Measurements were performed in the anechoic room at the University of Toronto Institute for Aerospace Studies. A 'point source' was placed in the flow of a 1.9 cm diameter model air-jet. The radiated sound was measured by a

condenser microphone mounted on a boom which is centered on the jet exit¹³.

Measured values of $|G_N|$ are shown in figure 1. Figure 2 illustrates the phase shift induced by the flow. The effects is quite small at low Mach numbers, but become more significant at moderate Mach numbers ($M = 0.28$).

CONCLUDING REMARKS

A means of obtaining a Green's function appropriate for sound radiated from subsonic jet flows has been described. The data available to date is not sufficient to permit one to deduce an appropriate empirical model.

REFERENCES

1. Lighthill, M.J., "On Sound Generated Aerodynamically- I General Theory", Proc. Roy. Soc. London, Vol 211, Ser. A., 1952.
2. Lighthill, M.J., "On Sound Generated Aerodynamically- II Turbulence as a Source of Sound", Proc. Roy. Soc. London, Vol 222, Ser. A., 1954.
3. Ffowcs-Williams, J.E., "The Noise from Turbulence Convected at High Speed", Proc. Roy. Soc. London, Vol 255, Ser. A., 1963.
4. Ribner, H.S., "Aerodynamic Sound from Fluid Dilatations: A Theory of Sound from Jets and Other Flows", UTIA Rep. 86, AFOSR TN 3420, 1962.
5. Pao, S.P., Lowson, M.V., "Some Applications of Jet Noise Theory", AIAA Paper 70-233, 1970.
6. Atvars, J., Schubert, L.K., Grande, E., Ribner, H.S., "Refraction of Sound by Jet Flow or Temperature", UTIAS TN-109, 1965, NASA CR-494, 1966.
7. Grande, E., "Refraction of Sound by jet Flow and Jet Temperature II", UTIAS TN-110, 1966, NASA CR-840, 1967.
8. Schubert, L.K., "Numerical Study of Sound Refraction by a Jet Flow II, Wave Acoustics", JASA, Vol 51, 1972
9. Mani, R., "The Influence of Jet Flow on Jet Noise. Part 1. The Noise of Unheated Jets." JFM, Vol. 73, 1976.
10. Lilley, G.M., "The Generation and Radiation of Supersonic Jet Noise". Vol IV. AFAPL-TR-53, 1972.
11. Balsa, T.F., "The Acoustic Field of Sources in Shear Flow with Application to Jet Noise: Convective Amplification", JFM, Vol 79, No. 1, 1977.
12. Ribner, H.S., "Effects of Jet Flow on Jet Noise via an Extension of the Lighthill Model", JFM, Vol. 321, 1996.
13. Richarz, W.G., "Direct Correlation of Noise and Flow of a Jet using Laser Doppler", UTIAS Report 230, 1978.

Figure 1. Measured Normalized Green's Function $|GN|$,
 $y/D=6, r/D=0.5$

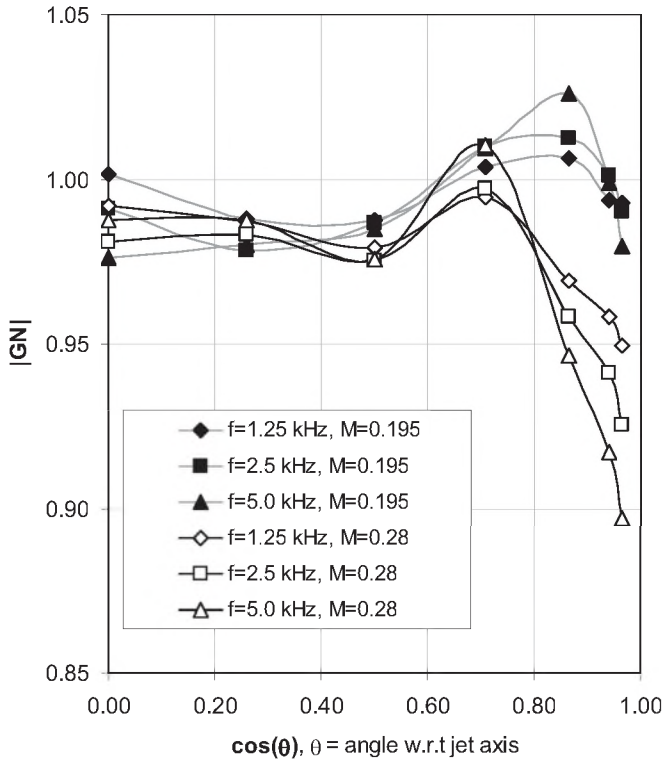
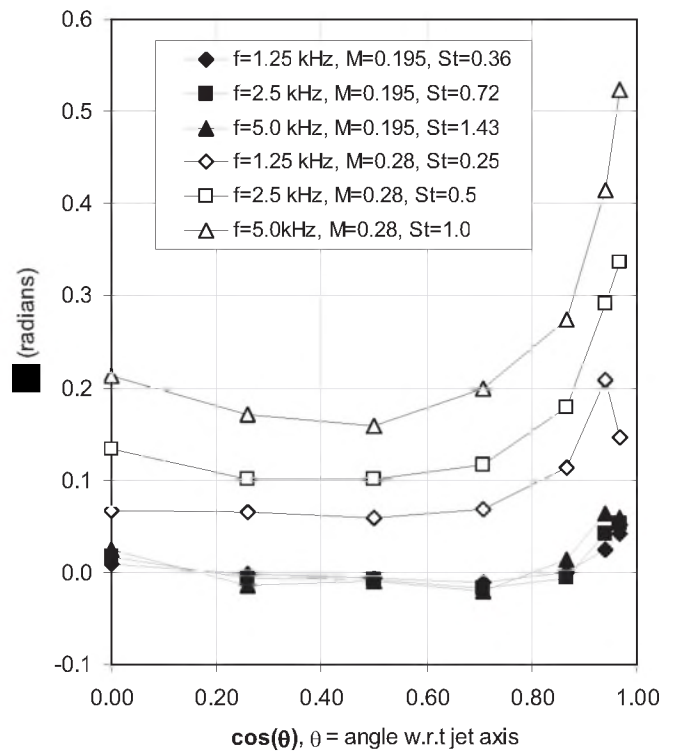


Figure 2. Measured Phase Shift ($\delta\phi$)
 $y_1/D=6, y_2/D=0.5, R/D=60$



Why Purchase from a Single Manufacturer... ...When You Can Have the Best in the Industry From a Single Supplier?

Scantek is the company to call when you want the most comprehensive assortment of acoustical and vibration equipment. As a major distributor of the industry's finest instrumentation, we have the right equipment at the right price, saving you time and money. We are also your source for instrument rental, loaner equipment, product service, technical support, consulting, and precision calibration services.

Scantek delivers more than just equipment. Since 1985, we have been providing solutions to today's complex noise and vibration problems with unlimited technical support by acoustical engineers that understand the complex measurement industry.

Suppliers of Instruments and Software:

- Norsonic
- RION
- CESVA
- DataKustik (Cadna & Bastian)
- KCF Technologies
- BSWA
- Castle Group
- Metra
- RTA Technologies
- G.R.A.S.

Scantek
 Sound and Vibration
 Instrumentation and Engineering

Applications:

- Building Acoustics & Vibration
- Occupational Noise and Vibration
- Environmental and Community Noise Measurement
- Sound Power Testing
- Calibration
- Acoustical Laboratory Testing
- Loudspeaker Characterization
- Transportation Noise
- Mechanical Systems (HVAC) Acoustics

Scantek, Inc. • 7060 Oakland Mills Road • Suite L • Columbia, MD 21046 • 800•224•3813 • www.scantekinc.com

NOISE GENERATED BY IMPINGEMENT OF A PLANAR JET ON A FLAT PLATE

David Arthurs¹ and Samir Ziada²

^{1,2}Dept. of Mechanical Engineering, McMaster University, 1280 Main Street W., ON, Canada, L8S 4L7

1. INTRODUCTION

High speed impinging planar jet flows are used in a number of industrial applications such as hot dip galvanization, coating control and high performance cooling applications. These flows can be liable to flow-excitation mechanisms, leading to the generation of excessive acoustic tones, noise and vibration. Although the problem of flow excitation of axisymmetric impinging jets has been thoroughly investigated by many authors such as Petrie [1] and Ho & Nossier [2, 3], relatively little research has been performed on noise generated by impinging planar jets. The present study examines acoustic excitation of planar jets impinging on an infinite flat plate, as well as the effects of plate inclination on the generated acoustic tones.

2. EXPERIMENTAL APPARATUS

All experimental work was conducted using a planar air jet constructed out of Plexiglas® and Aluminum. A series of internal baffles located immediately upstream of the nozzle outlet were utilized to ensure uniform flow exiting across the jet span. The jet allows the adjustment of the slot thickness h , to be varied within a range of $0 \leq h \leq 7.5$ mm, with a jet slot width of $h = 1.45$ mm used for all present testing. Additionally, the span of the jet was $L = 406$ mm resulting in an aspect ratio of $L/h = 280$. Reynolds numbers based upon the jet slot width vary between $Re_h \approx 7,000$ and 14,000.

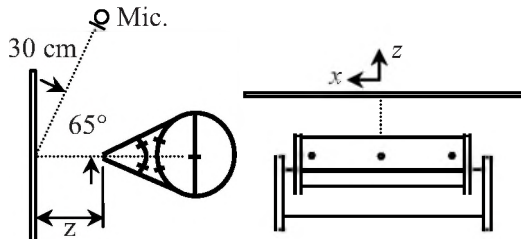


Fig. 1: Simplified schematic of experimental planar jet-plate impingement setup.

The jet was pressurized by a 10 HP Sonic Air Systems 70 Series centrifugal blower connected to a piping system and plumbed to an air plenum feeding both ends of the jet, to ensure uniform flow distribution. Measurements have been performed to ensure even flow across the entire span of the jet. Furthermore, the piping system employs several flow conditioning devices including screens and honeycomb sections to reduce the noise or turbulence levels exiting the blower. Plenum pressure was modulated from $P = 0$ to 0.315 Bar with a ball valve located well upstream of the jet

and flow conditioners. The isentropic flow velocity (V_i) of the jet was calculated using Eq. (1) derived from compressible flow equations for a standard isentropic nozzle, where c is the speed of sound and P_∞ is standard atmospheric pressure.

$$V_i = c \sqrt{\frac{2 \left[\left(\frac{P_\infty}{P + P_\infty} \right)^{\frac{\gamma-1}{\gamma}} - 1 \right]}{\gamma - 1}} \quad (1)$$

The flat plate used for jet impingement was constructed of aluminum and measured 205 mm×490 mm. The plate was mounted on a 3-axis traverse which could be manipulated in the x - y - z directions to within ± 0.025 mm. In order to study the effects of plate inclination on noise generation, the plate could also be inclined up to $\kappa = 5^\circ$ in the span-wise direction, and the jet could be inclined up to $\zeta = 45^\circ$ for testing of stream-wise inclination. Schematics of both stream-wise and span-wise inclination are shown in Figure 2.

Noise measurements were performed using a single $\frac{1}{2}$ " G.R.A.S. pressure microphone with a flat frequency response to 10 kHz, and a PC based data acquisition system utilizing LabView®.

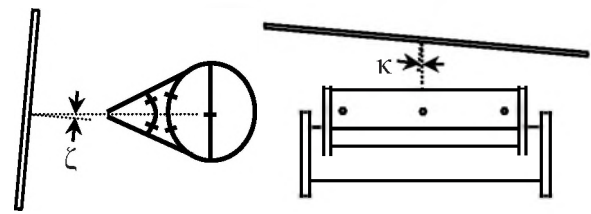


Fig. 2: Simplified schematic of stream-wise (ζ) and span-wise (κ) jet-plate inclination angles.

3. RESULTS

3.1. NORMAL JET-PLATE IMPINGEMENT

Experiments were performed for a series of jet-to-plate impingement cases with plenum pressure varying from 0.07 Bar to 0.315 Bar in 0.035 Bar increments for normal jet inclination ($\zeta = \kappa = 0^\circ$). Microphone measurements were taken at a point 65° from the jet plane, 30 cm from the point of impingement at the center of the jet span. Acoustic spectra up to 10 kHz were constructed using a 50s measurement broken down into 50 spectral averages to refine the acoustic spectra.

Figure 3 shows a series of waterfall plots of the jet-plate frequency response as a function of impingement ratio

(z/h) for varying plenum pressures. A strong acoustic tone was excited for all jet-plate impingement cases with plenum pressures exceeding $P = 0.14$ Bar ($V_i \approx 153$ m/s). The acoustic tone strength increases with increasing plenum pressure and the tone is excited over increasingly larger ranges of impingement ratio as the plenum pressure increases. Furthermore, the frequency is proportional to the isentropic flow velocity of the jet and approximately the inverse of the impingement ratio, (z/h).

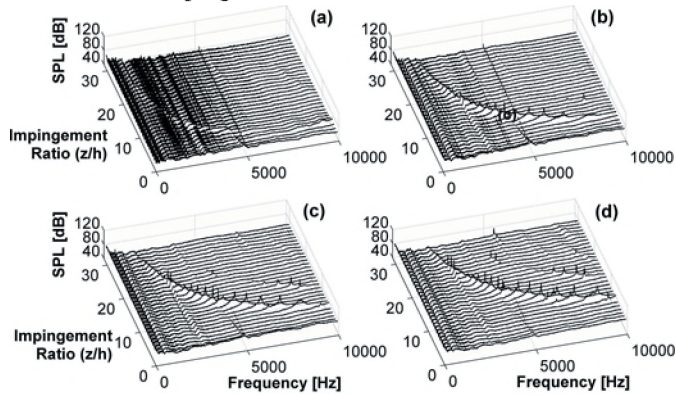


Fig. 3: Aeroacoustic response of planar jet-plate impingement as a function of impingement ratio (z/h) for isentropic jet velocities of $V_i = 108$ m/s (a), 153 m/s (b), 187 m/s (c) & 216 m/s (d).

The frequency of the jet-plate acoustic tone divided by the isentropic flow velocity as a function of impingement ratio for varying plenum pressures is shown in Figure 4. The data points of all three flow velocities with jet-plate mode excitation collapse on a single curve, showing that the frequency of the tone scales with the flow velocity of the impinging jet. The frequency of the jet-plate tone can be accurately predicted by the expression given in Eq. (2).

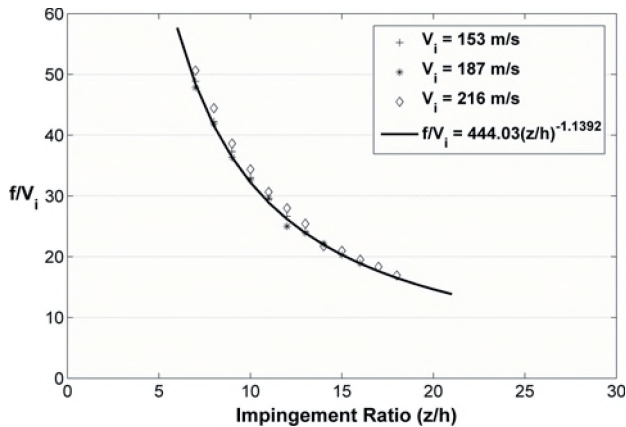


Fig. 4: Frequency of jet-plate acoustic tone divided by the isentropic jet velocity, V_i as a function of impingement ratio (z/h).

$$f = 444.01 \left(\frac{z}{h} \right)^{-1.1392} V_i \quad (2)$$

4. EFFECT OF PLATE INCLINATION

The effect of jet-plate inclination, both in the stream-wise and span-wise directions, was investigated as a method to reduce the intensity of the tone generation of the jet-plate tones. Stream-wise inclination angles of $\zeta = 0^\circ, 5^\circ, 10^\circ$ and 15° have been tested, in addition to span-wise inclination angles of $\kappa = 0^\circ, 1.25^\circ$. The results of changing the plate inclination angles for both cases is shown in Figure 5, with the peak SPL of the jet-plate tone shown as a function of varying impingement ratio. The amplitude of the acoustic jet-plate tones is much more sensitive to span-wise inclination (κ) than to stream-wise inclination angle, with a complete suppression of the jet-plate mode occurring for inclination of only $\kappa = 1.25^\circ$. Stream-wise inclination angle was also effective at suppressing these modes, however, much larger inclination angle were required in order to adequately suppress these modes.

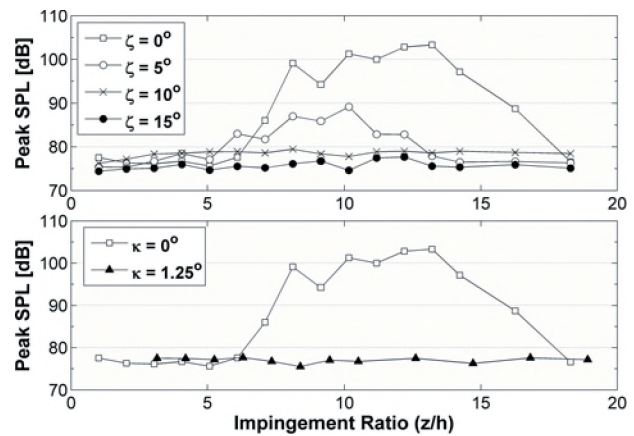


Fig. 5: Effect of jet-plate inclination in the stream-wise (ζ) and span-wise (κ) directions.

5. CONCLUSIONS

The acoustic excitation of a planar jet impinging on an infinite plate was investigated. The frequency of the dominant tone was shown to be proportional to the flow velocity of the jet and the inverse of the dimensionless impingement length as given by Eq. (2). Jet-plate inclination was shown to be an effective method to suppress acoustic excitation, with the pulsations being roughly 10 times as sensitive to changes in span-wise inclination compared to stream-wise inclination.

6. REFERENCES

- [1] A. M. Petrie, "An experimental investigation of the noise produced by air jet impingement on flat plates," *Applied Acoustics*, 7, 117-126 (1974).
- [2] N. S. Nossier & C. Ho, "Dynamics of an impinging jet. Part 1. The feedback mechanism" *J. Fluid Mech.* 105, 119-142 (1980).
- [3] N. S. Nossier & C. Ho, "Dynamics of an impinging jet. Part 2, The noise generation" *J. Fluid Mech.* 116, 379-391 (1982).

EXTERIOR ACOUSTIC ARRAY MEASUREMENTS ON THE BOMBARDIER GLOBAL EXPRESS

Antoine Malkoun, Robby Lapointe

Acoustics and Vibration Department, Bombardier, Aerospace division, Dorval, QC, H4S 1Y9, Canada
E-mail: antoine.malkoun@aero.bombardier.com, robbly.lapointe@aero.bombardier.com

1. INTRODUCTION

Because of the increase of aircraft traffic and population around airports, governments are putting pressure on international ruling agencies to become more stringent on community noise certification limits. Some airports have also taken the liberty of imposing on the airliners landing fees that vary according to the noise emitted by their aircraft. As a result, and in line with its constant efforts to offer its customers aircraft with minimized operating costs, Bombardier has funded research and development projects over the last few years to study and reduce the noise from its aircraft.

The microphone array project exposed in this article served to identify and measure noise coming from individual aircraft components such as landing gears, flaps, slats, engine, etc (see Fig. 1). In collaboration with the Transportation division of Bombardier in Sweden, which had already performed sound source localization on high-speed trains and possessed the necessary hardware, a methodology and in-house software were developed. The first measurements with microphone array at the Aerospace division of Bombardier were done in November 2005 on a Global Express, an ultra-long range business jet.

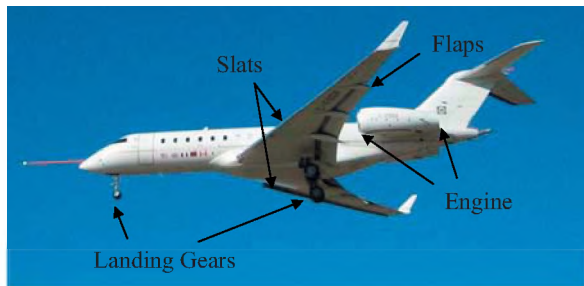


Fig. 1. Major noisy components of a Bombardier Global Express on approach

2. METHOD

The method consists in using a large number of microphones (microphone array) to focus on sound coming from a specific direction. Based on similar work done in the past to localize sound sources on moving vehicles [1], a temporal delay-and-sum beamforming technique was developed at Bombardier to process the phased array data. In this method, the sensor outputs are delayed by

appropriate amounts and added together reinforce the signal emanating from a specific region in space. It can be described as an acoustic camera, where the focus can be electronically shifted in space by manipulating the phases of the signals, similarly to how a parabolic antenna is mechanically aimed (see Fig. 2).

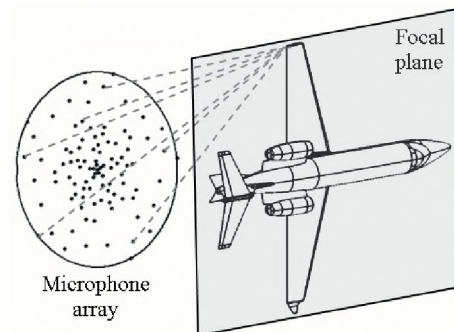


Fig. 2 - Principle of the acoustic camera, ability to focus on a specified region

3. FLIGHT TESTS

A site was selected with very low aircraft traffic and the array was placed on the extended runway centerline (see Fig. 3). The phased microphone array composed of 95 transducers was used to record aircraft noise during a series of flyovers at an altitude of 30 meters. A compromise was found to distribute the microphones semi-randomly in an 8.5-meter diameter circle (see array represented in Fig. 2) to sample the acoustic field with an optimized resolution. The electret microphones were installed on plastic plates nailed to the ground. The space between the edges of the plates and the ground was filled with sand to reduce acoustic scattering. Their membranes were assumed to be located in the reflection plane resulting in a doubling of the sound pressure [2].

Information collected by a Differential-GPS (DGPS) and an Inertial Reference System allowed aircraft tracking with high precision, 5 times per second. Flush-mounted piezoelectric noise generators producing tonal sources were attached below the aircraft wing tips to help for the method calibration. A time-synchronization was done between the flight data recorded onboard and the acoustic data recorded on the ground via an event-tone transmitted over VHF.

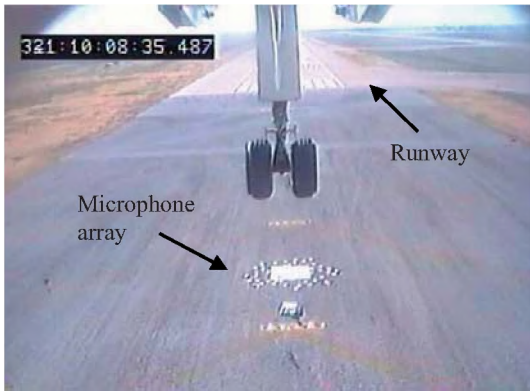


Fig. 3 - Picture from aircraft camera during flight test

4. RESULTS

Fig. 4 shows a typical source localization map of the Global Express in an approach flight condition, with landing gears down and high-lift devices (slats/flaps) deployed. The colors correspond to the sound pressure levels of mid-frequency sources in dB(A), relative to the maximum level in the map. The A-weighting was chosen because the low frequencies are dominating the noise emission seen by the array. The 10 dB scale on the graph means that no source could be detected 10 dB below the maximum level found in that 1/3 octave band. The observation angle is 90° relative to the flight direction, which means that the aircraft was overhead when this acoustic map was computed. All sources are studied under this angle, which means that the nose landing gear is studied at an earlier time in the flyover than the main landing gear.

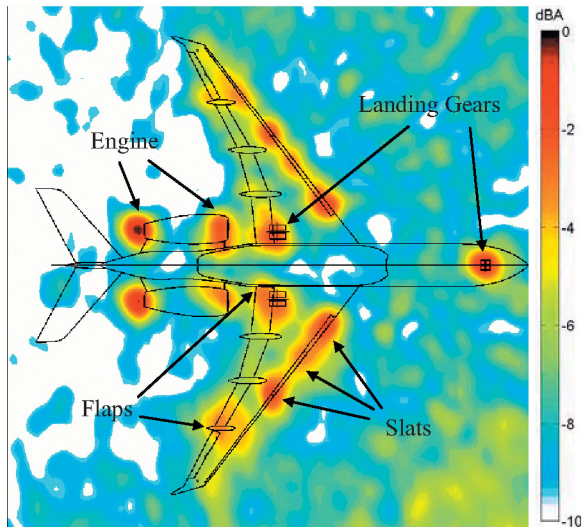


Fig. 4 - Localization of mid-frequency sources on the Global Express during a normal landing configuration; observation angle 90° (overhead); aircraft seen from below

In Fig. 4, the noise of the nose landing gear is clearly visible. Other sources are localized all along the slats and at the engine entrances. The loudest noise sources shown in

black are located near the exhaust, near the slat edges and near the landing gears. Noise sources can also be localized at the outboard flap side edges of the wings. The slat edge noise generated at the slat junction with the fuselage can also be seen as a dominant source. This source was already detected as being an important noise contributor in previous wind tunnel measurements with a 7 %-scaled CRJ700 model [3].

5. CONCLUSION

At Bombardier, the phased microphone array has been shown to be a powerful tool for localizing the sound sources on a flying aircraft. The main sources of noise that could be found were due to turbulence and vortices created by the airflow around high-lift devices, landing gears, and flow excited acoustic resonators. The acoustic data collected on the Global Express aircraft in landing configuration revealed important information for future designs of Bombardier aircraft. Thanks to the reference sources, to the low flyover altitude chosen during the tests and to the accurate tracking system, a good definition of noise sources was found. Both detection of the loudest sound sources on the aircraft and evaluation of precision and performance of the method were achieved. An extension of this work would be a quantification of absolute source levels in order to relate microphone array results to the overall aircraft noise.

REFERENCES

- [1] A. Nordborg, J. Wedemann and L. Willenbrink, "Optimum Array Configuration", 29th International Congress Inter-Noise, Nice, France, 27-30 August 2000
- [2] J. F. Piet, U. Michel and P. Böhning, "Localization of the Acoustic Sources of the A340 with a Large Phased Microphone Array during Flight Tests", AIAA 2002-2506, Onera and DLR, 2002
- [3] P. Soderman, F. Kafyke, N. Burnside, R. Chandrasekharan, S. Jaeger, J. Boudreau, "Airframe Noise Study of a CRJ-700 Aircraft Model in the NASA Ames 7- by 10- Foot Wind Tunnel No. 1", AIAA-2002-2406, 8th AIAA/CEAS Aeroacoustics Conference and Exhibit, Breckenridge, Colorado, June 17-19, 2002

ACKNOWLEDGEMENTS

The authors would like to thank all the supporting staff of the Bombardier Flight Test Center and the Bombardier Aerospace Experimental group who got involved in the test preparation and achievements. Also, this work would not have been possible without the collaboration of the Acoustic team of the Transportation division of Bombardier in Sweden (Västerås), who lent the acoustic equipment.

APPLICATION OF FEM AND SEA IN PREDICTING VIBRO-ACOUSTIC BEHAVIOR OF A FLAT RIBBED PANEL STRUCTURE

Reza Madjlesi

Acoustics and Vibration, Bombardier Aerospace, 123 Garratt Blvd, Toronto, ON, Canada, M3K 1Y5

1. INTRODUCTION

In today's market the passenger comfort is driving the interior design of the aircraft. The basic requirement of the comfort is low noise and vibration environment. Considering the effect of extra mass on the performance of the aircraft and cost to improve the comfort later in the program, the fuselage structure must be designed for low noise at the early stages of design. This highlights the need for better design tools that can be used with a high confidence to design the cabin for acoustics and vibration comfort.

In this paper two major design tools in predicting acoustical response of the coupled structure-cavity are presented. The response of a structure (flat ribbed panel) excited by a point force is predicted using Finite Element Method (FEM) and Statistical Energy Analysis (SEA).

For FE modeling, structural testing was required to confirm integrity of the FE model of the structure. Modal testing was performed on the ribbed panel. First 5 non-rigid body modes and mode shapes were calculated and used for correlation. For SEA modeling all required parameters such as damping loss factor and absorption inside the box was measured and imported to the model.

2. Experimental Set-up

The experimental setup to measure vibro-acoustic response of a coupled structure-cavity is shown in Figure 1. The ribbed panel installed in the window of a reverberation box. The volume of the box is 0.6999 m^3 . The size of the box restricted the low frequency limit of reliable measurement to 250 Hz. Above this frequency enough number of acoustical modes are available. It is assumed that the boundary of the panel installed in the window of the box is simply supported.

The ribbed panel shown in Figure 1 has three frame- stringer bays. Measurement was performed with the panel installed in the window. Response of the structure and cavity to a point force excitation was studied. A shaker was attached to the center of the middle frame-stringer bay. Random signal was used as the excitation signal at this location. The force at the excitation point was measured using a force sensor. Response of the interior cavity was measured with four microphones located randomly inside the box.



Figure 1: Experimental setup

Reverberation time of the box was measured using interrupted method. A speaker was located inside the box and generated burst random signal. Response of the cavity to this excitation was recorded at 4 microphone locations. The sound pressure data at these locations were used to calculate reverberation time and interior absorption.

Frequency Response Functions (FRFs) of the structure mounted in the box window were measured at three random points using impact hammer method. Modal damping of structure at each mode was extracted using half-power bandwidth method.

For FE model, the modal response of the structure is used for structural correlation. Fine FRF measurement was performed on the suspended ribbed panel. Modes and mode shapes of the ribbed panel structure were extracted from FRF data using LMS modal software.

Sound pressure data was used to correlate FEM and SEA prediction with measured interior noise.

3. FEM Modeling

The ribbed panel structure was modeled with 9600 Quad8 shell elements. The cavity inside the box was modeled with 31000 Hexa8 solid elements. Based on Structural FRF measurement viscous damping of 1-3% was considered for the FE model of the bare ribbed panel. Reverberation time measurement was shown that the acoustical damping of the cavity is around 0.5%.

FE model of coupled structure-cavity is shown in Figure 2. Measured excitation force at the center of the panel was imported to the FE model. Response of the structure-cavity to this excitation was predicted using LMS FE Acoustic Module.

Structural modes of the panel and cavity modes of the box were calculated up to 1500 Hz. Averaged sound pressure response of the cavity was predicted in 1/3-Octave bands. Predicted noise at four microphone locations were averaged and compared to the measured data. Figure 3 is the acoustical modes of the box as well as structural modes of the ribbed panel structure.

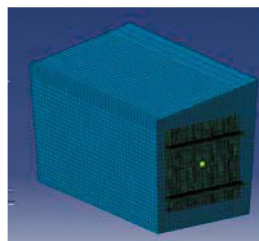


Figure 2: FEM Model of ribbed panel and box

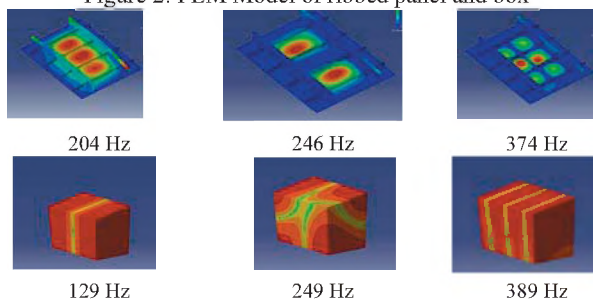


Figure 3: Structural and Acoustical Modes

4. SEA Modeling

The structure was modeled as a ribbed panel subsystem in SEA. Properties of the cross sections of the frames and stringers were calculated in MSC Patran and imported to the SEA model. Loss factor of the box cavity was measured using reverberation time method. 1% damping loss was considered for the ribbed panel structure. 1/3-Octave measured force data at the center of the panel was imported to the SEA model as the excitation. Averaged predicted sound pressure level was compared to the measurement at the four microphone locations. Figure 4 shows the SEA model of the panel-box.

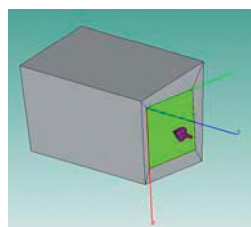


Figure 4: SEA Model of ribbed panel and box

5. RESULTS

Predicted response of coupled structure-cavity system using SEA is presented in Figure 5. The SEA prediction correlates well with the measured data above

400Hz. For mid-high frequencies range, SEA is the only tool to predict response of a vibro-acoustic system.

FE modeling is used to predict the response of the system for low-mid frequency range. Structural and acoustical modes of the system are shown in Figure 3. Predicted average interior noise of the box-ribbed panel system when excited by a point force is shown in Figure 5. FE predictions correlate well with the measured sound pressure level for frequency range of 200-1000 Hz.

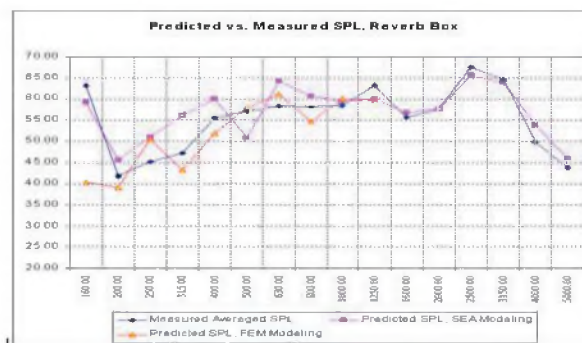


Figure 5: Measurement vs. Predicted Interior Noise, FEM and SEA Modeling

6. DISCUSSION

Predicting acoustical response of a coupled structure-cavity was presented in this paper. The FE modeling technique can be used to predict the response of the structure when excited by different sources. For low-mid frequency range the FE modeling technique gives detailed information on the sound pressure level distribution across the acoustic field. The SEA modeling should be used to predict average response of the system for mid-high frequency range.

REFERENCES

- 1 S.De Rosa, F. Franco (1999). Full Validation of The Structural-Acoustic Response of A Simple Enclosure. Journal of Aircraft, Vol.36, No.5.
- 2 J. M. Montgomery (2004). Modeling of Aircraft Structural-Acoustic Response to Complex Source Using Coupled FEM-BEM Analysis. AIAA 2004-2822
- 3 Numerical Acoustics, LMS International Manual.
- 4 Frank Fahy, Sound and Structural Vibration. ISBN: 0-12-247671-9
- 5- E. B. Davis (2004). By Air, By SEA. Noise Con 2004

ACOUSTIC PERFORMANCE CONSIDERATIONS FOR A 'ONCE THROUGH STEAM GENERATOR' (OTSG)

Vince Gambino and Payam Ashtiani

Aercoustics Engineering Limited 50 Ronson Drive,
Toronto, Ontario, Canada, M9W 1B3

1. Introduction

Once Through Steam Generators (OTSG) are used by electricity power plants and a host of other industrial and/or commercial centers to recover the heat from a gas turbine exhaust stream. The OTSG works by passing the hot exhaust over tube bundles. The steam can then be either fed into a steam turbine generator to obtain electricity, or used for heating and humidification in a variety of applications. Figure 1 shows the standard arrangement of an OTSG in a typical cogeneration plant. An OTSG can attenuate gas turbine exhaust noise ($L_w \sim 150$ dB re 1pW). Parameters governing the acoustic performance of an OTSG under both steam generating and dry running conditions are discussed herein.

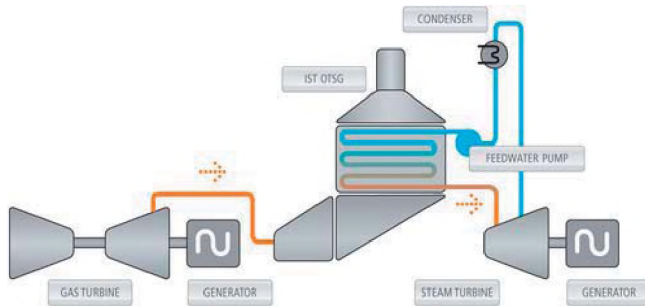


Figure 1 : OTSG in Cogeneration Plant

2. Sources of Noise in an OTSG

The OTSG is generally comprised of the following sections: The inlet from the turbine, inlet plenum (sometimes fitted with a silencer), environmental controls, tube bundles, exhaust hood and exhaust stack. The main source of noise in the OTSG originates from the aerodynamic and combustion noise. It is critical to have reliable input sound power from the gas turbine to the OTSG. The noise from the turbines exits the circuit in two ways: casing/wall radiated noise, and noise exiting from the exhaust stack. There is also some flow induced noise from the exhaust gas stream going through the various OTSG components. The interaction of this sound field with the various components inside the OTSG results in a significantly modified sound spectrum at the OTSG outlet. The acoustic performance of an OTSG cannot be determined from a simple speaker test alone that is conducted under ambient temperature and static conditions. The higher speed of sound and the regenerated noise from interactions of the gas flow with the OTSG components

result in unique noise reduction characteristics that vary case by case.

3. Acoustic Environment inside an OTSG

Studies on the acoustic environment and related existing phenomena have been conducted on for HRSGs [4], and the prediction of sound attenuation using scale modelling techniques [2]. The following are areas of study that require systematic consideration when analyzing the noise control mechanisms, which dictate the acoustic performance of an OTSG.

3.1 Elevated Gas Temperature

Power systems involving Once-Through-Steam-Generators can be run in two modes: Simple or Combined cycle. Simple cycle mode involves the gas turbines running without producing any additional steam, i.e. no water is fed through the OTSG tubes and no steam is produced. In this mode, the temperature of the exhaust gas stream can reach near 650°C . In combined cycle operation the OTSG unit produces steam. In this mode OTSG inlet gas temperatures are near 815°C and approximately 95°C at the stack. This strong thermal gradient has a significant effect on affect the sound propagation through the OTSG.

3.2 Gas Flow Conditions & Flow Induced Noise

Gas flow from the exhaust stream of the gas turbine generators can reach or at times exceed flow velocities of 75 m/s at the OTSG inlet (i.e. exhaust of the GT). At these velocities, flow induced noise mechanisms such as vortex generation and other effects have the potential to become problematic in the OTSG. The insertion of environmental control stages and tube bundles inherently causes turbulence in the flow and can further augment flow induced noise and vibration, which can also give rise to fatigue damage.

4. Summary of Sensitive Parameters

4.1 Geometry

Geometry plays a major role in the acoustic performance of the OTSG. Area changes in the flow can cause acoustic reflections back upstream of the flow. The reduction due to partial sound reflection is a function of the ratios of the area change [1]. The design, however, should

weigh in the benefits of the number of area change reflections with respect to the pressure drop caused by the area changes. Similarly, a change in the flow direction (for e.g. through L-Junctions) also provides attenuation at the cost of flow disturbance and increased pressure drop.

4.2 Casing construction

Casing construction is an important consideration to ensure that there are no acoustic compromises in the overall performance of an OTSG. The construction of an OTSG casing involves heavy and temperature resistant materials to ensure long term viability and to minimize heat loss. A typical construction will have an isolated internal shell, typically made of a moderate gauge steel plate, and an outer shell typically with a heavier/thicker steel construction. The two layers are usually separated by ceramic fibre or similar insulation. Low frequency noise reduction is crucial in this application, so it is important to keep the mass and stiffness of the casing wall high in order to attenuate sound in this frequency range.

4.3 Tube bundle arrangement and flow considerations

Tube banks have the ability to reduce noise due to reactive effects of cross sectional area changes as seen by the flow, as well as propagation losses due to the flow resistivity of the tube bundles (viscous loss). The location and orientation of the tube bundles must be very carefully considered in the design. There is potential for flow induced acoustical vortex shedding which can potentially give rise to significant flow related acoustic and structural integrity concerns. Several studies

[3] [5] show the potential effects of flow through different tube bundle arrangements. The analysis involves obtaining a Strouhal number, S , based on tube separation ratios. The vortex shedding frequency is then $f_{VS} = S \times V_{max} / D$ (Hz). The frequency f is dependant on the flow velocity V_{max} and the diameter D of the tubes in the array. Care has to be taken to ensure that the vortex shedding frequencies do not coincide with the resonant frequencies of the tubes or other structures, or with the acoustic modes in the OTSG duct and plenum. It is also important to consider the effects of any environmental controls, plates, cavities or any other obstructions that may impede the flow.

5. Conclusion Remarks

OTSG's can be quite effective in mitigating the noise emissions from a gas turbine exhaust. Successful designs minimize vortex generation, detune acoustic and/or structural resonances. The degree of noise reduction that can be realized is illustrated in **Figure 2**. The OTSG affords significant attenuation over the entire audible range.

6. References

- [1] **Leo L. Beranek**, *Noise and Vibration Control (Revised Edition)*, Ch11 (I. L. Ver, C. I. Holmer), Institute of Noise Control Engineering, 1988.
- [2] **M. Bracken, M. Barman and V. Gambino**, *Prediction of Heat Recovery Steam Generator (HRSG) noise attenuation using scale model testing*, Aercoustics Engineering Limited, Proceedings of the Spring Environmental Noise Conference, Alberta EUB, 1996.
- [3] **S. Joiner**, *Acoustical Analysis of Nepco-Brownsville Peaking Plant*, Innovative Steam Technologies (IST), November 1998.
- [4] **G. F. Hessler**, *Issues in HRSG System Noise*, Proceedings at the 1997 NOISE-CON at Pennsylvania State University, June 1997.
- [5] **F. L. Eisinger and R. E. Sullivan**, *Unusual Acoustic Vibration in Heat Exchanger and Steam Generator Tube Banks Possibly Caused by Fluid-Acoustic Instability*, Journal of Engineering for Gas Turbines and Power Vol. 115,pg 411, April 1993.

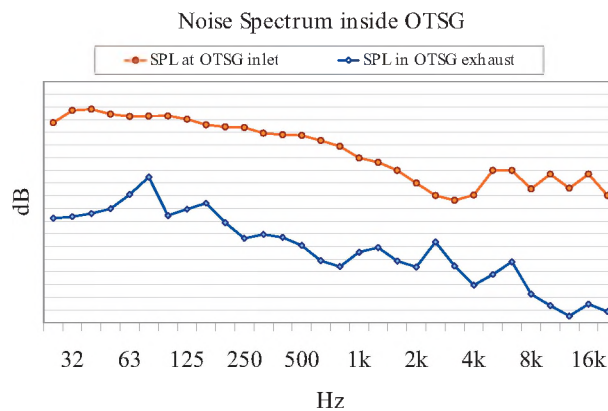


Figure 2: Sound at the inlet and discharge of an OTSG. 1/3rd octave sound level spectra were obtained using a calibrated high temperature microphone assembly with an anechoic termination.

EXPERIMENTAL AND NUMERICAL INVESTIGATION OF SEPARATED-REATTACHED FLOWS BEHIND UNIFORM AND NOTCHED SPOILERS

Paloma Mejia, Jong Beom Park¹, and Luc Mongeau¹

The Ray W. Herrick Laboratories, Purdue University, 140 S. Intramural Dr., West Lafayette, IN, USA, 47906

¹Now: Dept. of Mechanical Engineering, McGill University, 817 Sherbrooke St., Montreal, Qc, Canada, H3A 2K6

1. INTRODUCTION

Interior noise in road vehicles is an important source of discomfort, leading to reduced speech intelligibility, and passenger fatigue. Aerodynamically excited noise from the open sunroof of a vehicle is of particular interest due to the high pressure oscillations that may be generated inside the cabin for certain vehicle speeds. Spoilers are often used to reduce interior noise by deflecting the flow stream over the opening.

Notched spoilers have frequently been observed to be more effective than uniform spoiler for buffeting suppression. It is generally understood that the notches break down the coherence of the flow downstream of the spoiler, leading to a reduction in the equivalent excitation pressure due to local interferences between the fluctuating pressures at different locations. The study of the turbulent wall pressure fluctuations^{1, 2} downstream of a wall mounted notched spoiler may thus be useful in order to develop a better understanding of vortex shedding and convection over the region where a sunroof would normally be located, and quantify the single point and two-points statistics of the hydrodynamic and acoustic pressure fields.

2. METHODS

2.1 Experimental Instrumentation

The experimental cases under investigation consisted of uniform and notched automobile sunroof spoilers mounted into the test section of a low-speed, quiet wind tunnel. The notched spoiler used was from a Fiat Lancia Y. The spoiler was trimmed on each side to fit in the wind tunnel test section, maintaining the symmetry with respect to the center of the spoiler. The spoiler height, h , was varied for both notched and uniform spoiler cases with heights of 20 mm and 24 mm from the floor of the wind tunnel test section. The angle of the frontal spoiler surface was approximately 62 degrees with respect to section floor.

A circular plate of a rectangular array of 15 x 22 pinholes was installed 5 cm downstream from the spoiler to measure static and dynamic surface pressures (Fig. 1). To allow flush mounted microphone installation, the 10.26 mm diameter array holes were counter-sunk to a depth of 11.7 mm. A 0.5 mm pinhole was then drilled through the center of each array hole and the superior surface of the plate. The

separation distance between each measurement point in the rectangular grid was constant at 12.7 mm.

A dual sensor hot-wire probe was employed to measure streamwise and vertical velocity components of the mean flow. The hot-wire measurements included x-y and y-z field scanning in the flow where streamwise, cross-streamwise (or transverse) and vertical directions were coordinated as x, y and z, respectively. Flow visualization was also performed using an oil based smoke generator.

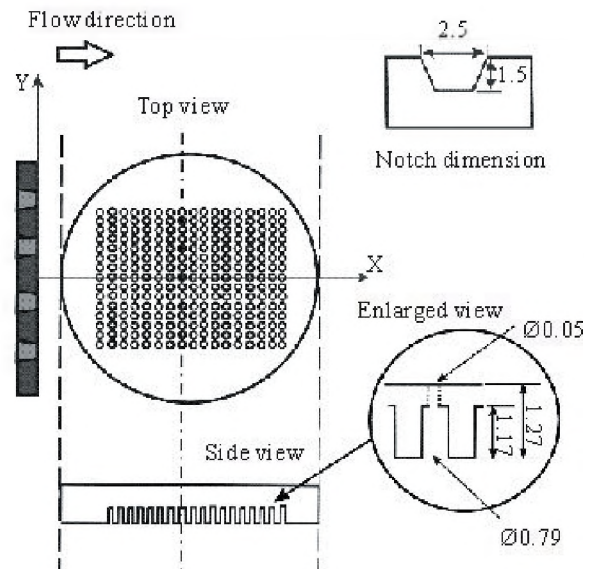


Fig. 1. Schematic of the experimental apparatus. The circular plate with 330 microphone pinholes is located 5 cm behind (downstream of) the spoiler. Dimensions in cm.

2.2 Numerical Simulations

The commercial software PowerFLOWTM was used. A number of pre- and post-processing operations were followed in order to prepare and verify the spoiler geometry, to set flow parameters, define variable resolution regions, impose boundary conditions, and analyze results. PowerFLOWTM consists of a range of specialized modules that were used at various stages to retrieve, visualize, check, and set-up the case. The simulation results were verified based on comparisons between the simulation results and measured flow field statistics from hot-wire anemometry.

3. RESULTS

The reattachment point of the mean flow over the spoiler was observed to occur approximately at $x/h \sim 15$ for the uniform spoiler and $x/h \sim 13$ for the notched spoiler. The reattachment point was estimated using several methods: zero static pressure gradient ($\Delta p \sim 0$), root mean square value of pressure fluctuations, and flow visualization. The numerical simulations predicted a reattachment location further downstream (at $x/h \sim 15$ for the notched spoiler).

It was observed from the static surface pressure distribution and the mean flow field obtained from the hot-wire as well as the numerical simulations that the notches created a smaller flow-recirculation zone behind the spoiler.³ The notches moved the reattachment point closer to the spoiler, and reduced the pressure drop across the spoiler and thus the pressure drag.

Cross-stream variations of the unsteady surface pressure distribution were induced by notches. The coherence of the dynamic surface pressures along cross-stream locations was lower at low frequencies for the notched spoiler (Fig. 2). The numerical simulations yielded similar general trends of coherence spectrum variation. In addition, the cross-stream decay rate⁴ of the coherence was larger for the notched spoiler. It was observed that a consistent phase difference existed in the unsteady surface pressures along the cross-stream direction near the notches.

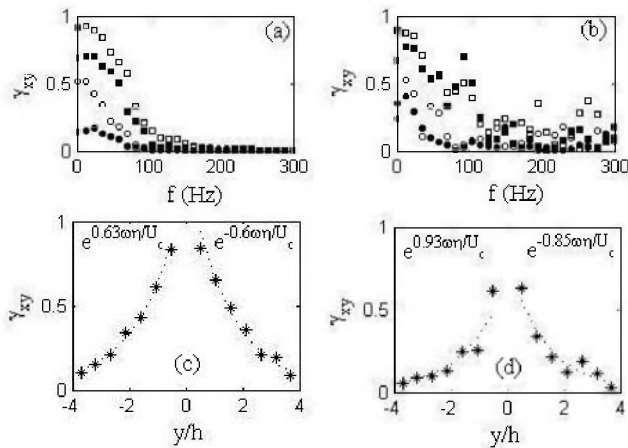


Fig. 2. Coherence spectrum of surface pressures obtained (a) experimentally and (b) numerically between the center reference point ($y/h=0$) and two other transverse locations: $y/h \sim 0.5$ (\square : uniform; \blacksquare : notched), $y/h \sim 2.08$ (\circ : uniform; \bullet : notched). The streamwise distance of the points is $x/h \sim 4.4$. The transverse decay of the maximum coherence at $f=25$ Hz is shown for (c) uniform and (d) notched spoilers, respectively, at the streamwise distance of $x/h \sim 5.4$.

4. DISCUSSION

The cross-stream reduction in surface pressure coherence confirms that the notches create turbulent and de-correlated fluctuations, leading to destructive interferences and randomness in vortex development along the span. As a result, the aerodynamically generated surface force obtained by integrating the surface pressure over a surface area roughly equivalent to that of a sunroof is decreased over a wide range of frequency, as shown in Fig. 3, where the excitation force was obtained from the surface integration of the measured unsteady surface pressure values. The numerical simulations allowed the spectrum of the surface pressure to be predicted for frequencies up to 2 kHz. But significant discrepancies were observed around 1 KHz between measured and predicted surface spectra. The simulations did however faithfully reproduce the main trends of the flow- and surface pressure fields.

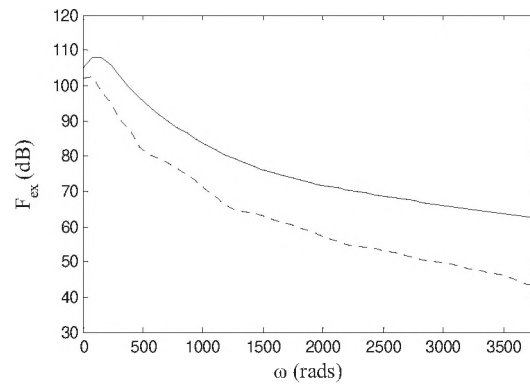


Fig. 3. Estimated excitation force spectra for the uniform (—) and the notched (---) spoilers.

REFERENCES

- Blake, W.K. (1970). Turbulent boundary-layer wall pressure fluctuations on smooth and rough walls. *Journal of Fluid Mechanics*, 44(4), 637-660.
- Farabee, T. M. and Casarella, M. J. (1986). Measurements of fluctuating wall pressure for separated/reattached boundary layer flows. *Journal of Vibration, Acoustics, Stress, and Reliability in Design*, 108, 301-307.
- Mejia, P., Park, J. B., and Mongeau, L. (2007). Surface pressure fluctuations in separated-reattached flows behind notched spoilers. *Journal of the Society of Automotive Engineers*, SAE Paper No. 2007-01-2399.
- Corcos, G.M. (1964). The structure of the turbulent pressure field in boundary layer flows. *Journal of Fluid Mechanics*, 18(3), 353-378.

ACKNOWLEDGEMENTS

Thanks are expressed to Drs. David Freed, Siva Senthoooran, Bernd Crouse, and Gana Balasubramanian from Exa Corporation for their assistance and their financial support.

PSYCHO-ACOUSTIC EXPERIMENTS ON THE SENSORY CONSONANCE OF MUSICAL TWO-TONES

Reinhard Frosch

Sommerhaldenstrasse 5B, CH-5200 Brugg, Switzerland

PSI (Paul Scherrer Institute), Villigen and ETH (Eidgenoessische Technische Hochschule), Zurich (retired)

1. INTRODUCTION

The topic of the present study is the sensory consonance of two-tones (i.e., pairs of simultaneous tones) composed of two harmonic complex tones similar to vibrato-less bowed-string tones. Per definition, a complex tone contains two or more simultaneous “simple” (i.e., sinusoidal) partial tones; in a *harmonic* complex tone, all partial-tone frequencies are integral multiples of the fundamental frequency f , i.e., of the frequency of the first partial.

According, e.g., to Plomp and Levelt (1965), *sensory consonance* is approximately equivalent to pleasantness, euphony, and beauty.

In previous sensory-consonance experiments with bowed-string-like tones, it was found that the *consonance curve* (i.e., the sensory consonance of the studied two-tone plotted versus its fundamental-frequency ratio $R = f_2 / f_1$) forms narrow peaks at small-integer ratios R such as $3/2$, $5/3$, etc.

The abscissa of the experimental consonance curve shown in Fig. 1 [taken from Section 3.2 of Frosch (2002)] is the *interval size* x of the two-tone:

$$x = (1200 \text{ cents}) \cdot \frac{\log(R)}{\log(2)} ; \quad (1)$$

e.g., an *octave* ($R = 2$) has an interval size $x = 1200$ cents, and a *perfect fifth* ($R = 3/2$) has $x \approx 702$ cents.

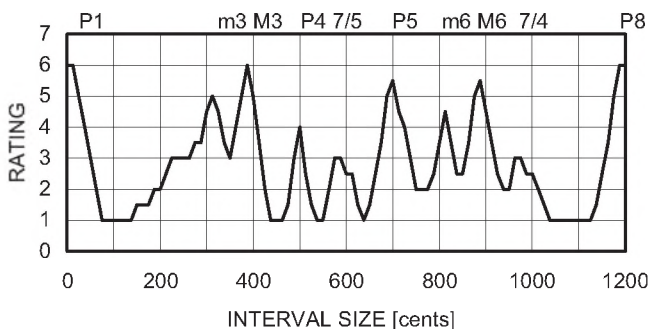


Fig. 1. Results of my “one-man” experiment on the sensory consonance of bowed-string-like two-tones; $f_1 = 264$ Hz; rating 6 means “very consonant”, and rating 1 means “very dissonant”.

The symbols P1, m3, ... above Fig. 1 are the standard names of the diatonic intervals corresponding to the consonance peaks. Seven of these symbols are explained in Table 1. The names “perfect prime”, “minor third”, etc. can be under-

stood by counting notes on a diatonic scale; e.g., the minor third $E4-G4$ involves three notes (namely $E4$, $F4$, $G4$); one of the two corresponding steps, $E4-F4$, is a diatonic semi-tone, and the other step $F4-G4$, is a diatonic whole tone; see Section 3.6 of Frosch (2002).

Interval	Symbol	R	x [cents]
Perfect prime	P1	1 / 1	0
Minor third	m3	6 / 5	316
Major third	M3	5 / 4	386
Perfect fourth	P4	4 / 3	498
Perfect fifth	P5	3 / 2	702
Major sixth	M6	5 / 3	884
Perfect octave	P8	2 / 1	1200

Table 1. Interval name, symbol, frequency ratio R , and interval size x of seven two-tones yielding consonance peaks in Fig. 1.

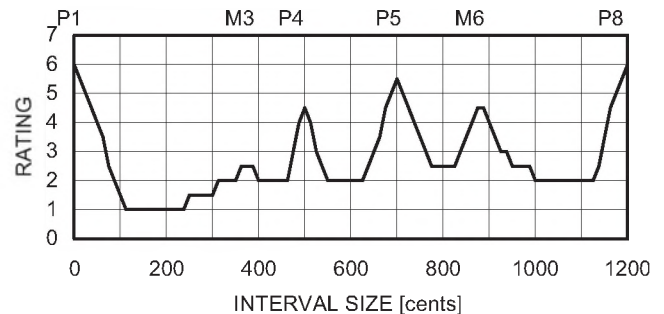


Fig. 2. Same as Fig.1; $f_1 = 99$ Hz.

In the case of Fig. 1, the deeper of the two simultaneous bowed-string-like tones had a fundamental frequency f_1 of 264 Hz; i.e., its note was $C4$. The fundamental frequency f_2 of the higher of the two simultaneous tones was chosen to be higher than f_1 by 0, 12.5, 25, 37.5, ... , 1200 cents; i.e., as many as 97 different two-tones were judged. The two-tones were generated at a sound-pressure level of about 70 dB on a Yamaha DX11 music synthesizer. The “voice” (i.e., the timbre) of the synthesizer was chosen to be “harmonica”. The corresponding partial-tone spectrum differs little from that of vibrato-less bowed-string tones.

The experimental details of Fig. 2 were equal to those of Fig.1, with the exception of the fundamental frequencies. For Fig. 2, the frequency f_1 was 99 Hz; i.e., the note of the deeper tone was $G2$. Thus the two-tones of Fig. 1 were in the female-singing pitch region, whereas those of Fig. 2 were in the bass region. In comparison with Fig. 1, Fig. 2 contains fewer consonance peaks, its peaks are wider, and

he peak heights differ; e.g., the major-third peak (M3) of Fig. 2 is lower than that of Fig. 1.

Tests similar to that just described have been done by other authors; e.g., the experiments of Hall and Hess (1984) and of Vos (1986) both yielded solid evidence for narrow sensory-consonance peaks at small-integer fundamental-frequency ratios. These experiments, however, did not yield complete sets of consonance-peak heights in the interval range 0–1200 cents.

The just mentioned interval range was covered fairly completely in the old experiment of Kaestner (1909); see Figs. 3 and 4. The method of complete paired comparisons used by Kaestner will be briefly described in Section 2 below.

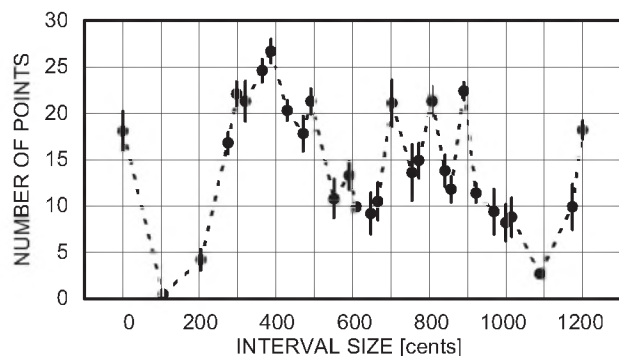


Fig. 3. Numbers of points obtained by 30 different two-tones in the range 0–1200 cents in the experiment of Kaestner (1909); deeper-tone frequency $f_1 = 256$ Hz.

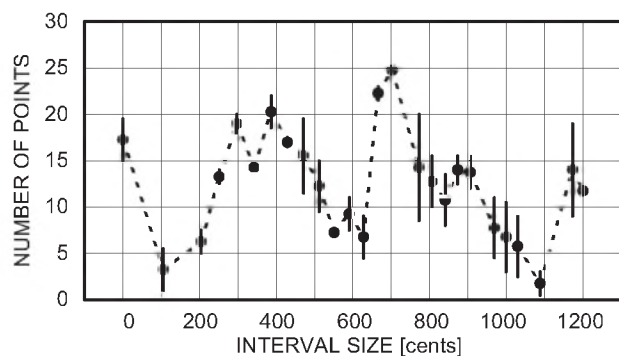


Fig. 4. Same as Fig. 3; $f_1 = 128$ Hz.

The points with error bars in Fig. 3 represent the means of the point numbers obtained by 5 observers and the standard errors of those means. In the case of Fig. 4 there were 26 different two-tones and 2 observers.

My one-man experiment (Figs. 1 and 2) and the experiment of Kaestner (Figs. 3 and 4) both yielded consonance peaks at small-integer frequency ratios. The ranking order of the peak-heights, however, disagrees in several cases; the octave (1200 cents), e.g., in Figs. 1 and 2 obtains the first place (jointly with other two-tones); in Figs. 3 and 4, however, the octave is relegated to 7th place. In the deep-tone case (Figs. 2 and 4), disagreeing peak heights may be due to pitch differences (deeper-tone notes G_2 and C_3 , respec-

tively); in the higher-tone case (Figs. 1 and 3), however, the deeper-tone frequencies differ little (note C_4 in both cases). In order to determine more reliably the relative consonance-peak heights, I conducted two “peak-height experiments” featuring complete paired comparisons similar to those of Kaestner (1909). These newer experiments, first reported in Frosch (2003) and Frosch (2005), will be briefly described in the following two sections.

2. PEAK-HEIGHT EXPERIMENT AT FEMALE-SINGING PITCH

In this experiment, the seven two-tones specified in Table 1 were judged by 18 subjects (no professional musicians). Table 1 contains all fundamental-frequency ratios R that have values ranging from 1.0 to 2.0 and are equal to ratios of integers m and n ranging from 1 to 6. The consonance curve in Fig. 1 has peaks at the interval sizes x corresponding to these seven R -values. Thus the purpose of the experiment was to determine the relative heights of the seven consonance peaks. The frequency of the deeper of the two simultaneous bowed-string-like tones was equal to that for Fig. 1 (i.e., 264 Hz, note C_4). The properties of the tones were as described in the text below Fig. 2.

The 18 subjects were asked to listen to an audio-tape recording lasting about 15 minutes. The seven stimuli S_i ($S_1 =$ prime, $S_2 =$ minor third, etc.) were made to take part in a championship consisting of $7 \cdot 6 = 42$ matches. In contrast to Kaestner (1909), return matches were included, because they allowed the reliability of the subjects to be verified (see below). The order of the 42 matches was chosen at random; e.g., game 1 came out to be S_1 versus S_6 , game 2 was S_3 versus S_1 , etc.; the return match of game 1, i.e., S_6 versus S_1 , turned out to be game 22.

Sequence of events on audio tape:

- 1) spoken words “game one” (duration: 2 seconds);
- 2) break (2 seconds);
- 3) stimulus S_1 is played (1 second);
- 4) break (0.5 second);
- 5) stimulus S_6 is played (1 second);
- 6)–9) repeat 2)–4) (4.5 seconds);
- 10)–13) repeat 2)–4) (4.5 seconds);
- 14) break (4 seconds; subjects write down their judgment);
- 15) spoken words “game two” (2 seconds); etc.

Possible judgments:

- same as those in experiment of Kaestner (1909);
- “A”: the first of the two stimuli is more consonant;
- “B”: the second of the two stimuli is more consonant;
- “X”: the two stimuli are equally consonant.

Data taking:

Before judging the above-mentioned audio-tape recording, each of the 18 subjects was given a one-page form on which they were to write down their judgments on the 42 games, and they were instructed to attempt to decide which of the

two stimuli taking part in a game was more pleasant, euphonious, and beautiful.

Total number of judgments:

Among the $18 \cdot 42 = 756$ judgments, there were 274 judgments *A*, 302 judgments *B*, and 180 judgments *X*. In a Monte-Carlo calculation based on the assumption that the probabilities of *A* and *B* were both equal to the arithmetic mean of $274/756$ and $302/756$, i.e., equal to 0.381, it was found that the judgment-number ratio *A/B* was smaller than its experimental value of $274/302$ in about 12200 of 100000 Monte-Carlo experiments; i.e., the (unexpected) difference between the just mentioned experimental judgment numbers 274 and 302 was found to be statistically not very significant.

Reproducibility of judgments:

The 42 judgments per subject form 21 pairs; each pair consists of a home match (e.g., stimulus S_6 versus stimulus S_2) and its return match (S_2 versus S_6). The judgment pairs *AB*, *BA*, and *XX* are consistent, whereas the remaining six combinations (*AA*, *AX*, *BB*, *BX*, *XA*, *XB*) signify that the subject has not judged consistently. A second Monte-Carlo program based on the judgment probabilities $274/756$, $302/756$, and $180/756$ (see above) and on the assumption of random judgments yielded the bad-pair number distribution given by black discs in Fig. 5. The experimental histogram

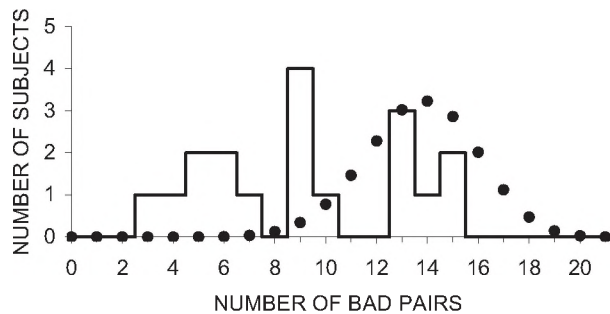


Fig. 5. Solid line: histogram of the numbers of subjects who totalled the number of bad judgment pairs specified on the abscissa. Black filled circles: numbers of subjects expected if the judgments are assumed to have been made at random (see text).

In Fig. 5 indicates that indeed 6 of the 18 subjects must be suspected to have judged randomly. The remainder of the analysis was restricted to the 12 subjects which had ≤ 10 bad pairs.

The twelve “reliable” subjects made a total of $12 \cdot 42 = 504$ judgments. If a judgment was either *A* or *B*, the winning stimulus received one point. In case of a draw (judgment *X*) each of the two participating stimuli was given 0.5 point. Each of the 7 stimuli took part in 12 games. The summed numbers of points are listed in Table 2. It is seen that subject 1 attributed a total of 5.0 points to the perfect prime (P1, the single complex tone C4), whereas subject 8 gave the maximum of 12.0 points to that stimulus, and subject 10

attributed the minimum of 0.0 point. In the last column of Table 2, the sum of the 7 numbers of points from the considered subject is listed, and is seen to be equal to the number of judgments, i.e., to 42.0, as expected.

Results:

Subject	P1	m3	M3	P4	P5	M6	P8	Sum
1	5.0	9.0	11.0	2.0	5.0	6.5	3.5	42.0
2	6.0	9.5	12.0	0.0	2.5	7.0	5.0	42.0
3	10.5	7.0	6.5	7.0	6.0	5.0	0.0	42.0
4	4.0	9.0	12.0	6.0	6.0	5.0	0.0	42.0
5	5.5	10.0	9.0	6.5	2.5	7.5	1.0	42.0
6	7.5	8.0	8.5	5.5	5.5	5.5	1.5	42.0
7	1.0	11.0	7.0	6.0	6.0	8.0	3.0	42.0
8	12.0	3.5	7.0	6.5	6.5	3.5	3.0	42.0
9	6.5	9.5	10.0	4.0	2.5	6.0	3.5	42.0
10	0.0	5.0	8.5	6.0	7.5	8.0	7.0	42.0
11	6.0	10.5	10.5	7.5	4.0	3.5	0.0	42.0
12	5.5	3.0	10.0	8.0	7.5	7.0	1.0	42.0
Mean	5.79	7.92	9.33	5.42	5.13	6.04	2.38	42.0
Standard error	0.97	0.78	0.55	0.67	0.53	0.45	0.63	
x [cents]	0	316	386	498	702	884	1200	

Table 2. Results of the peak-height experiment at female-singing pitch.

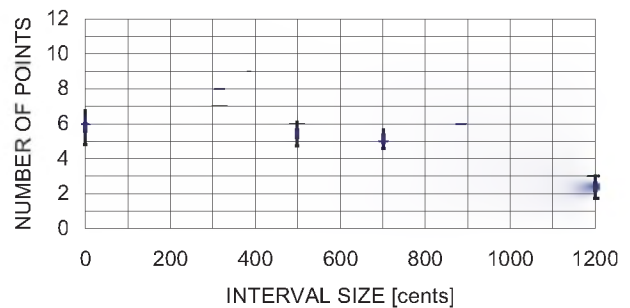


Fig. 6. Mean numbers of points obtained by the seven two-tones in Table 2; deeper-tone frequency $f_1 = 264$ Hz.

In the 14th line of Table 2, and also in Fig. 6, the arithmetic mean of the 12 numbers of points for the considered stimulus is presented. The 15th line of Table 2 and the error bars in Fig. 6 give the standard errors of those means.

The ranking order of the seven two-tones obtained by an attitude scale construction according to Edwards (1957) was equal to that of the seven mean point numbers in Table 2 and Fig. 6. That ranking order is similar to that obtained by Kaestner (1909); see Fig. 3 and Table 6 below.

3. PEAK-HEIGHT EXPERIMENT AT BASS PITCH

The details of this second experiment were similar to those of the female-singing pitch experiment described in the previous section; the fundamental frequency of the deeper

of the two simultaneous bowed-string-like tones, however, was 99 Hz; i.e., the note of that tone was G2. Twenty-nine subjects (no professional musicians) took part. The histogram of the number of bad judgment pairs was similar to that shown in Fig. 5. Eighteen subjects had ≤ 10 bad pairs and were thus considered as reliable. In this second experiment, too, the total number of judgments *B* was greater than that of judgments *A*. Among the $18 \cdot 42 = 756$ judgments of the 18 reliable subjects, there were 291 judgments *A*, 316 judgments *B*, and 149 judgments *X*. The deviation of that ratio $316/291$ from 1.0 was again found not to be statistically significant; the corresponding number (~ 15700) of Monte-Carlo experiments was even greater than that for the first experiment (~ 12200 ; see previous section).

Results:

Subject	P1	m3	M3	P4	P5	M6	P8	Sum
1	10.0	0.0	3.0	3.0	6.5	8.5	11.0	42.0
2	7.5	0.0	3.0	9.0	11.0	5.5	6.0	42.0
3	12.0	2.5	7.0	5.0	6.5	7.0	2.0	42.0
4	11.0	0.0	7.0	5.0	4.0	5.0	10.0	42.0
5	7.0	3.0	2.5	3.5	4.0	12.0	10.0	42.0
6	4.0	7.5	11.0	6.5	9.5	2.5	1.0	42.0
7	12.0	0.0	6.5	7.5	5.5	8.0	2.5	42.0
8	7.5	9.0	3.5	5.5	5.5	4.0	7.0	42.0
9	12.0	2.5	3.5	3.5	4.5	6.0	10.0	42.0
10	2.5	6.5	11.5	3.5	9.0	5.5	3.5	42.0
11	3.0	6.0	5.0	10.0	11.0	5.5	1.5	42.0
12	2.0	10.5	10.5	5.0	2.5	8.5	3.0	42.0
13	10.5	4.0	10.5	4.5	2.0	3.0	7.5	42.0
14	6.0	6.0	6.5	6.5	6.5	4.0	6.5	42.0
15	4.0	2.5	4.0	6.0	6.5	7.0	12.0	42.0
16	11.0	2.0	6.0	3.5	6.5	6.5	6.5	42.0
17	11.0	6.0	8.0	5.5	7.0	3.0	1.5	42.0
18	10.0	4.0	9.5	3.0	3.0	4.0	8.5	42.0
Mean	7.94	4.00	6.58	5.33	6.17	5.86	6.11	42.0
Standard error	0.84	0.75	0.71	0.47	0.63	0.57	0.86	
x [cents]	0	316	386	498	702	884	1200	

Table 3. Results of the peak-height experiment at bass pitch.

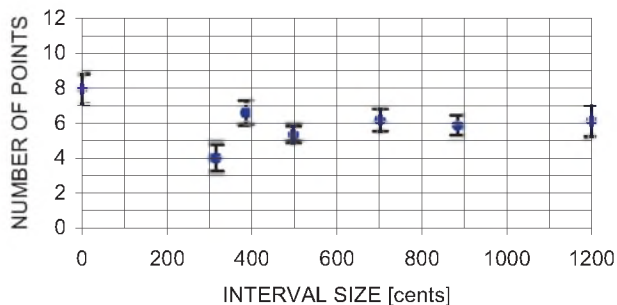


Fig. 7. Mean numbers of points obtained by the seven two-tones in Table 3; deeper-tone frequency $f_1 = 99$ Hz.

The resulting mean numbers of points obtained by the seven bass-pitch two-tones are presented in Table 3 and Fig. 7, and are seen to differ strongly from those obtained by the corresponding female-singing-pitch two-tones (Table 2 and Fig. 6).

4. HELMHOLTZ CONSONANCE THEORY

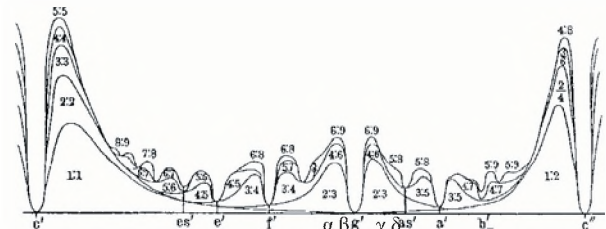


Fig. 8. Reproduction of Fig. 60a of von Helmholtz (1913); deeper-tone frequency $f_1 = 264$ Hz; abscissa: interval size (c': 0 cent; c'': 1200 cents; g': 702 cents, etc.); ordinate: roughness (\approx dissonance). The added symbols $\alpha, \beta, \gamma, \delta$ are defined in Table 4 below.

In Fig. 8, the fundamental frequency of the deeper of the two simultaneous bowed-string-like tones is assumed to be $f_1 = 264$ Hz, i.e., to have the note C4. The ordinate of Fig. 8 is the roughness caused by beats generated by pairs of partial tones having nearly equal frequencies.

point	higher tone [Hz]	2 nd harmonic [Hz]	beats per second	relative roughness
α	376	752	40	0.5
β	386	772	20	1
g'	396	792	0	0
γ	406	812	20	1
δ	416	832	40	0.5

Table 4. Five points of the curve “2:3” in Fig. 8.

In Table 4, five points of the curve “2:3” in Fig. 8 are listed. The number “3” signifies that one of the two beating partials is the third harmonic of the deeper of the two complex tones and thus has a frequency of $3 \cdot 264 = 792$ Hz. The number “2” means that the other beating partial is the second harmonic of the higher of the two complex tones. At point α , e.g., that second harmonic has a frequency of $2 \cdot 376 = 752$ Hz, so that $792 - 752 = 40$ beats per second are generated. Von Helmholtz judged that these 40 beats per second cause a relative roughness of about 0.5; see Table 4 above and Appendix XV of von Helmholtz (1957). [There is a misprint in the last equation of that appendix: the second of the two brackets in the denominator has to be squared.]

At point β in Fig. 8, the two just defined partials generate $792 - 772 = 20$ beats per second and are judged to cause a relative roughness of 1.0; thus point β is one of the two peaks of the partial-roughness curve “2:3”.

My own synthesizer experiments on the roughness caused by two sine-tones of frequencies f_A and f_B (done at deeper-sine-tone frequencies $f_A = 132, 264, 528, \text{ and } 1056$ Hz) have yielded roughness maxima at beat rates $b = |f_B - f_A|$ such that

$$b(\text{maximal roughness}) \approx k \cdot \sqrt{(f_A + f_B)/2} . \quad (2)$$

My experimental results for the constant k in Eq. (2) were

$$k = (1.068 \pm 0.052) \text{ s}^{-1/2} \text{ and } k = (1.075 \pm 0.099) \text{ s}^{-1/2} \quad (3)$$

at sound pressure levels of 50 and 70 dB, respectively. The maximal-roughness beat-rates given by Eqs. (2) and (3) tend to be lower than those found in the published studies on this topic; see, e.g., Fig. 1 of Terhardt (1974) and Fig. 7 of Kameoka and Kuriyagawa (1969a). [The maximal-dissonance beat rates experimentally determined by these latter authors themselves are particularly high. A different feature of that study, namely the method of adding partial dissonances described in Kameoka and Kuriyagawa (1969b), has been criticized by Vos (1986).]

According to Eqs. (2) and (3), the peak of the curve “2:3” in Fig. 8 (point β ; higher-complex-tone frequency 386 Hz) should be shifted to a beat rate of about 30 s^{-1} , i.e., to the left, to a higher-complex-tone frequency of about 381 Hz.

In Fig. 8, the dissonances defined by the various curves such as “2:3”, “4:6”, etc. are added linearly. Aures (1985) has found that linear roughness addition is valid in a case which shares some features with the present one (namely in the case of two sine tones which are both amplitude-modulated at modulation frequencies of 40 Hz), if the two carrier frequencies differ from each other by several critical band widths or more.

The relative heights of the various curves in Fig. 8 are based on the partial-tone amplitudes of bowed-string tones. According, e.g., to Section 10.2.4 of Terhardt (1998), however, the partial dissonances in Fig. 8 decrease too strongly with rising partial-tone number; e.g., the curve “4:6” is too shallow. The correction of this inaccuracy shifts the total-roughness peak to the right, i.e., back towards its original position in Fig. 8.

It is seen in Fig. 8 that the Helmholtz theory predicts dissonance minima at small-integer fundamental-frequency ratios (e.g., $e' = 5/4$, $g' = 3/2$, etc.)

Theoretical consonance curves based on roughness due to beating partial-tone pairs have been presented also in recent years, e.g. in Fig. 12.15 of Terhardt (1998) and in Fig. 11 of Rasch and Plomp (1999). As specified in Table 5, the consonance rankings of the seven dyads treated in Section 2 above defined by these two more recent curves differ little from those defined by the Helmholtz curve (i.e., by our Fig. 8).

frequency ratio of dyad	ranking according to ...		
	Helmholtz	Terhardt	Rasch and Plomp
1/1 (P1)	1(a)	1	1(a)
6/5 (m3)	7	7	6
5/4 (M3)	6	6	7
4/3 (P4)	5	5	5
3/2 (P5)	3	4	3
5/3 (M6)	4	3	4
2/1 (P8)	1(b)	2	1(b)

Table 5. Consonance ranking of the seven dyads treated in Section 2 above, according to the Helmholtz consonance theory and to two of its modern versions (see text).

In Table 6 below, the theoretical consonance ranking order given in the Helmholtz column of Table 5 is compared with the experiment described in Section 2 and with the experiment of Kaestner (1909) [see our Fig. 3].

frequency ratio of dyad	ranking according to ...		
	Helmholtz theory	Experiment Kaestner	Experiment R. F.
1/1 (P1)	1(a)(!)	6(a)	4
6/5 (m3)	7(!)	3(a)	2
5/4 (M3)	6(!)	1	1
4/3 (P4)	5	3(b)	5
3/2 (P5)	3	5	6
5/3 (M6)	4	2	3
2/1 (P8)	1(b)(!)	6(b)	7

Table 6. Consonance ranking of the seven dyads treated in Section 2 above (deeper-complex-tone frequency 264 Hz), according to the Helmholtz consonance theory (Table 5 and Fig. 8), to the experiment of Kaestner (1909; our Fig. 3), and to the experiment described in Section 2 (Table 2 and Fig. 6).

The symbol (!) in Table 6 indicates that this theoretical ranking differs from at least one of the two experimental rankings by 5 or more.

Perfect prime (P1) and perfect octave (P8): Kaestner (1909) noted that his observers found these two dyads “dull”, and thus not pleasant. The twelve “reliable” subjects of the experiment described in Section 2 were not asked to comment on their judgments; they, however, attributed few points to these two dyads, too.

Major third (M3) and minor third (m3): The experimental rankings of these two dyads are better than the theoretical ones. Most composers of the last few centuries appear to have shared this preference of thirds at female-singing pitch. For the last 200 years, children have heard equal-temperament thirds (300 cents, 400 cents) more often than just thirds (316 cents, 386 cents). Nevertheless, the consonance peaks in our Fig. 1, and also those in Fig. 3 of Hall and Hess (1984) and in Fig. 2a of Vos (1986) occur at the just-third interval sizes, indicating that such preferences are not due to

education, but rather to the physiological properties of our hearing system.

5. A MODIFIED CONSONANCE THEORY

It is hereby postulated that the sensory consonance of a dyad (i.e., of a two-tone) formed of two simultaneous harmonic complex tones is high if the dyad fulfils both of the following conditions.

Condition a:

The dyad contains few or no pairs of partial tones which generate disagreeable beats.

Condition b:

In the excitation pattern generated by the dyad on the basilar membrane of the inner ear there are few or no wide gaps.

The just specified condition a is the “Helmholtz condition”; see, e.g., Chapter X and Appendix XV of von Helmholtz (1954). Condition b (which constitutes our proposed modification of the Helmholtz theory) has been presented first in Section 3.3 of Frosch (2001), and then (in English) in Section 3.4 of Frosch (2002).

The structure of the mammalian cochlea is described in many textbooks, e.g., in Slepecki(1996) and in Zwicker and Fastl (1999). The basilar membrane (BM) in the human cochlea is about 35 mm long. The BM end near the base of the cochlea, i.e., near the oval window, is usually given the coordinate $x_{BM} = 0$, and the other end, near the apex of the cochlea and near the helicotrema, is said to be at $x_{BM} \approx 35$ mm. The BM supports the organ of Corti, which contains inner and outer hair cells (OHC’s).

Because of strong amplification in the OHC’s of a healthy inner ear, a soft or medium-level sine-tone causes a strong vibration of an about 1 mm long piece of the BM. At high frequency (typically 10 kHz), the vibration peak is near $x_{BM} = 0$, at low frequency (~ 0.1 kHz) the peak is near $x_{BM} = 35$ mm, and at medium frequency (~ 2 kHz) it is near $x_{BM} = 17.5$ mm.

In Fig. 6.11 of Zwicker and Fastl (1999), e.g., a linear relationship between the vibration-peak coordinate x_{BM} and the *critical-band rate* z is presented. In Chapter 10 of Hartmann (1998) it is pointed out that the quantity z is not a rate, and the better designation *critical-band number* is introduced. Chapter 10 of Hartmann (1998) also contains the definitions of the Bark (or “Munich”) scale and the ERB (or “Cambridge”) scale; “ERB” stands for “equivalent rectangular bandwidth”. In the mentioned first presentation of condition b, Frosch (2001), Munich critical bands were used; in the later publication, Frosch (2002), I switched to Cambridge critical bands. Both these treatments yielded that condition b leads to an improvement of the bad agreement between theory and experiment specified in Table 6 above.

Equation (10.29) of Hartmann (1998) gives the following relation between the sine-tone frequency f and the Cambridge critical-band number z :

$$z = 9.26 \cdot \ln \left(\frac{f}{229 \text{ Hz}} + 1 \right); \quad (4)$$

Hartmann (1998) commented that this equation “possibly ... correlates with the mapping of frequency in the cochlea”. As mentioned above, such a correlation appears to be more positively inferred in Zwicker and Fastl (1999); in the remainder of the present study, the following relation between the vibration-peak coordinate x_{BM} and the (Cambridge) critical-band number z is assumed to hold approximately:

$$z \approx 35 - x_{BM} [\text{mm}]. \quad (5)$$

In Fig. 9 below, the partial-tone patterns of the seven two-tones treated in Section 2 above are presented.

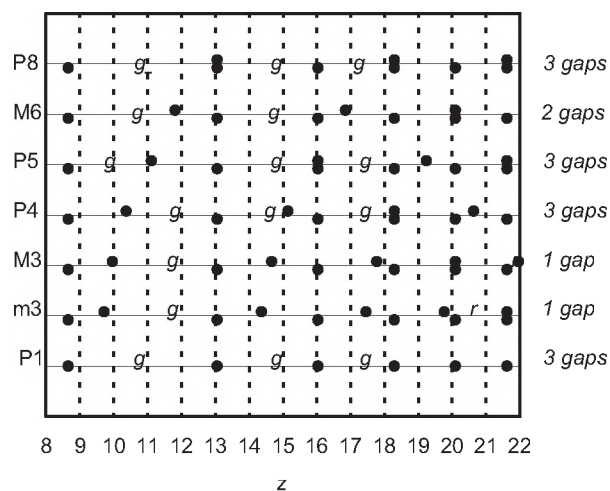


Fig. 9. Partial-tone patterns of the seven two-tones defined in Table 1, at female-singing pitch ($f_1 = 352$ Hz; note F4); details see text.

In Figs. 9 and 10, the critical-band numbers z corresponding, according to Eq. (4) above, to the partial-tone frequencies f occurring in each of the seven dyads are indicated by filled circles. Pairs of adjacent partials separated by a critical-band-number difference $\Delta z > 2$ (and thus yielding, on the BM, excitation peaks separated approximately by a distance $\Delta x_{BM} > 2$ mm) are conjectured to cause a disagreeable gap, and are indicated, in Figs. 9 and 10, by the symbol g . If Figs. 9 and 10 are extended to higher critical-band numbers z , no additional gaps with $\Delta z > 2$ are found in any of the seven dyads. Pairs of partials yielding, via Eq. (2), a constant k ranging from 0.5 to 2.0 are thought to cause strongly disagreeable roughness, and are indicated in Figs. 9 and 10 by the symbol r .

In Fig. 9, the major third (M3) and the minor third (m3) are seen to fulfil condition b especially well (only one gap), so that their good ranking in the two experimental columns of Table 6 is understandable.

The minor sixth (m6, $R = 8/5$, not shown) yields two gaps in Fig. 9, as does the major sixth (M6, $5/3$).

In Fig. 9, the deeper-tone complex-tone frequency f_1 has been chosen to be 352 Hz (note F4), near the centre of the range of the corresponding frequencies chosen in our Section 2 above (264 Hz), in our Fig. 3 (Experiment of Kaestner, 256 Hz), in our Fig. 8 (Theory of von Helmholtz, 264 Hz), in Fig. 12.15 of Terhardt (1998, theoretical curve, 440 Hz), and in Fig. 11 of Rasch and Plomp (1999, theoretical curve, 250 Hz). If in our Fig. 9 the deeper complex tone F4 is replaced by C4 (264 Hz), then the only different number of gaps is that of the perfect fourth (P4; $4/3$; 2 gaps). If, on the other hand, F4 is replaced by C5 (528 Hz), then the only different number of gaps is that of the perfect fifth (P5; $3/2$; 4 gaps).

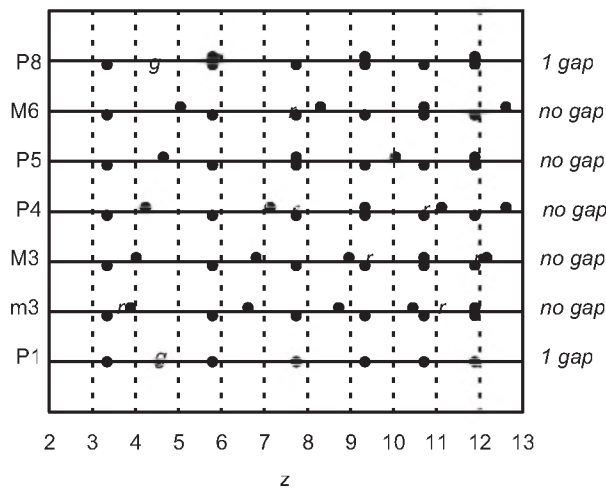


Fig. 10. Same as Fig. 9; bass pitch ($f_1 = 99$ Hz, note G2).

According to this modified theory, sensory consonance is *subtle*: An increase of dissonance is avoided if the frequency difference of two neighbouring partial tones is *large enough* (no disagreeable beats) but also *small enough* (no disagreeable gap in the excitation pattern on the BM).

Condition b (i.e., consonance is high if there are no or few wide gaps in excitation pattern on BM) becomes fairly plausible if one considers *dyads of deep tones* (i.e., of tones at bass pitch; deeper of the two simultaneous complex tones at ~ 100 Hz; see Fig. 10).

In the case of Fig. 10, perfect primes (P1), perfect fifths (P5), and octaves (P8) have no or one gap and no strongly disagreeable beats. In this case, condition b is about equally well fulfilled for all seven stimuli. The thirds (M3 and m3) are predicted to be dissonant because they violate condition a (the Helmholtz condition): each of them includes two pairs of partial tones (marked by the symbol r in Fig. 10) which generate strongly disagreeable beats [constant k in Eq. (2) between 0.5 and 2.0]. Thus the modified consonance theory explains, e.g., that the numbers of points for the

thirds (M3 and m3) are high in Fig. 6 (female-singing pitch), but are distinctly lower in Fig. 7 (bass pitch).

6. CONCLUSIONS

The consonance curves for two simultaneous bowed-string-like harmonic complex tones (sensory consonance versus fundamental-frequency ratio $R = f_2 / f_1$) form narrow peaks.

The R -values of the peaks ($R = m / n$; m and n are small integers) agree with the Helmholtz consonance theory (rates of beats of partial tones in a certain range cause dissonance).

The relative *heights* of the consonance peaks become more understandable if one considers, in addition to the Helmholtz theory, also “condition b” (sensory consonance is high if there are no or few wide gaps in the excitation pattern caused by the partial tones on the basilar membrane in the inner ear).

REFERENCES

- Aures, W. (1985). Ein Berechnungsverfahren der Rauigkeit. *Acustica*, 58, 268-281.
- Edwards, A. L. (1957). *Techniques of Attitude Scale Construction*. Irvington Publishers, New York. Chapters 1-3.
- Frosch, R. (2001). *Mitteltönig ist schöner! Studien über Stimmungen von Musikinstrumenten*. Peter Lang, Bern. Sections 3.2 and 3.3.
- Frosch, R. (2002). *Meantone Is Beautiful! Studies on Tunings of Musical Instruments*. Peter Lang, Berne. Sections 3.2-3.6.
- Frosch, R. (2003). *Psycho-Acoustic Experiment on the Sensory Consonance of Musical Two-Tones*. Contribution to Swiss Physical Society meeting in Basel, March 21.
- Frosch, R. (2005). *Psycho-Acoustic Experiment on the Sensory Consonance of Deep Musical Two-Tones*. Contribution to Swiss Physical Society meeting in Berne, July 14.
- Hall, D. E. and Hess, J. T. (1984). Perception of Musical Interval Tuning. *Music Perception*, 2, 166-195.
- Hartmann, W. M. (1998). *Signals, Sound, and Sensation*. Springer, New York. Chapter 10.
- von Helmholtz, H. (1913). *Die Lehre von den Tonempfindungen*. Vieweg, Braunschweig. 6th ed. Chapter 10.
- Helmholtz, H. (1954). *On the Sensations of Tone*. Dover, New York. Chapter X and Appendix XV.
- Kaestner, G. (1909). Untersuchungen über den Gefühlseindruck unanalysierter Zweiklänge. *Psychologische Studien*, 4, 473-504.

Kameoka, A. and Kuriyagawa, M. (1969a). Consonance Theory Part I: Consonance of Dyads. *J. Acoust. Soc. Am.*, 45, 1451-1459.

Kameoka, A. and Kuriyagawa, M. (1969b). Consonance Theory Part II: Consonance of Complex Tones and Its Calculation Method. *J. Acoust. Soc. Am.*, 45, 1460-1469.

Plomp, R. and Levelt, W. J. M. (1965). Tonal Consonance and Critical Bandwidth. *J. Acoust. Soc. Am.*, 38, 548-560.

Rasch, R. and Plomp, R. (1999). The Perception of Musical Tones, in: *The Psychology of Music*, D. Deutsch, ed., 2nd ed., Academic Press, San Diego, 89-112. Section III C.

Slepecki, N. B. (1996). Structure of the Mammalian Cochlea, in: *The Cochlea*, P. Dallos, A. N. Popper, and R. R. Fay, eds., Springer, New York, 44-129.

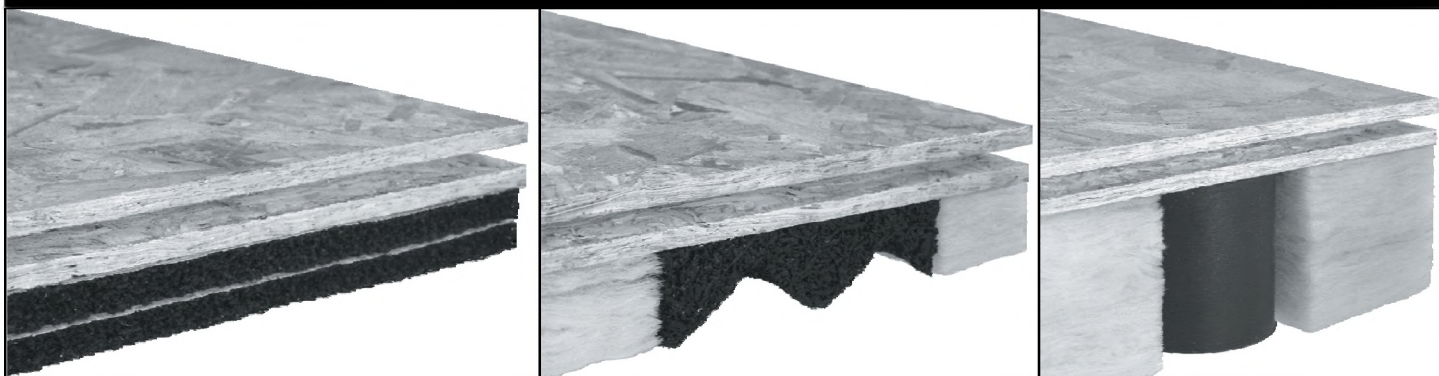
Terhardt, E. (1974). Pitch, consonance, and harmony. *J. Acoust. Soc. Am.*, 55, 1061-1069.

Terhardt, E. (1998). *Akustische Kommunikation*. Springer, Berlin. Section 12.1.4.

Vos, J. (1986). Purity Ratings of Tempered Fifths and Major Thirds. *Music Perception*, 3, 221-258.

Zwicker, E. and Fastl, H. (1999). *Psycho-Acoustics, Facts and Models*. Springer, Berlin. Chapters 3 and 6.

SOUND CONTROL SUBFLOOR PANELS



AcoustiGuard Subfloor Panels are available for a wide variety of applications including:

- BUILDING CONVERSIONS
- EQUIPMENT & MECHANICAL ROOMS
- HOME THEATRE & MEDIA ROOMS
- AEROBIC & DANCE FLOORS
- GYPSUM OR CONCRETE POUR OVER

AcoustiGuard™
Sound Control for Buildings

WILREP LTD.

Noise & Vibration Control Since 1977

1-888-625-8944

1515 Matheson Blvd. East Unit C-10
Mississauga, Ontario L4W 2P5
905-625-8944

www.wilrep.com

info@wilrep.com

PERCEPTION OF METER SIMILARITY IN FLAMENCO MUSIC

Rafa Absar^{1,2}, Francisco Gómez³, Catherine Guastavino^{1,2}, Fabrice Marandola^{1,4}, Godfried Toussaint^{1,5}

¹Centre for Interdisciplinary Research on Music Media and Technology (CIRMMT) and McGill University,

²School of Information Studies, McGill University 3459 McTavish, H3A 1Y1 Montreal, QC, Canada,

rafa.absar@mail.mcgill.ca, catherine.guastavino@mcgill.ca

³Applied Mathematics Dpt., School of Computer Science, Polytechnic Univ. of Madrid, fmartin@eui.upm.es

⁴Schulich School of Music, fabrice.marandola@mcgill.ca

⁵School of Computer Science, godfried@cs.mcgill.ca

1. INTRODUCTION

Flamenco music is characterized by hand clapping patterns whose underlying meter is composed of a pattern of soft and accented claps. A mathematical analysis of the five 12/8 metric patterns used in flamenco music was recently conducted to establish several musicological hypotheses [1]. This analysis relied on the similarity between the metric patterns. Such similarity was measured with two different rhythmic similarity measures, namely, the *chronotonic* measure and the *directed swap* distance. Presented in this paper are the results of a listening test conducted to evaluate the perceived similarity of the five metric patterns used in flamenco music. The goal of this experiment includes testing out the validity of those measures from a perceptual point of view. Twelve subjects participated in three experimental sessions, corresponding to three tempi (slow, medium, fast). In each session, participants were asked to rate the dissimilarity of all non-identical pairs of the five MIDI-generated patterns, presented twice in counterbalanced order. Dissimilarity ratings were analyzed using multi-dimensional scaling and phylogenetic analysis. The perceptual measures of similarity were then compared with mathematical measures of rhythmic similarity used in [1] to determine which measure best matches human judgments.

2. METHOD

2.1 Participants

12 listeners (mean age: 25, S. D. 4) with an average of 3 years of musical training were recruited from the student population at McGill University. They received 10\$ for their participation.

2.2 Stimuli

The listeners listened to the following rhythms (in box notation): (1) Fandango: [x . . x . . x . . x . .]; (2) Soleá: [. . x . . x . . x . . x]; (3) Bulería: [. . x . . . x . . x . . x]; (4) Seguiriya: [x . x . x . x . . x . .]; (5) Guajira: [x . . x . . x . . x . .]

The sound files were generated using the music notation software Finale. The output was MIDI-generated sounds of hand clapping (channel 10, key 39) produced through the native instruments audio unit of Finale. The rhythms were generated at three different tempi, namely, 50, 70 and 90 dotted quarter notes per minute, respectively (or 400 ms, 285 ms and 222 ms between consecutive claps).

2.3 Procedure

The graphical interface was programmed in Java on a MacPro computer. The experiment took place in an acoustically treated room. Sounds were presented over headphones (AKG 240) after digital-to-analog conversion and amplification (Motu 828 MKII). The experiment consisted of 3 sessions corresponding to the aforementioned tempi. In each session, participants were first asked to listen to the 5 rhythmic patterns presented in the experiment to become familiar with the range of variation. After 3 randomly chosen practice trials, they were asked to rate the dissimilarity for all possible non-identical pairs of the 5 patterns (10 pairs). Pairs were presented twice in counterbalanced order, resulting in 20 trials in total. The order of presentation was randomized across trials within each session. The order of presentation of the 3 sessions was counterbalanced across participants using a Latin square design. Dissimilarity ratings were made with the mouse on a scale presented on the computer screen with end points labeled "very similar" and "very different". Scale values were digitized on a 0 to 100 scale. Listeners were allowed to listen to the patterns as many times as desired before entering their ratings. They were requested to keep their rating strategy as constant as possible. After the experiment, they were asked to freely describe the differences between the sounds presented and explain how they made their ratings.

3. RESULTS

3.1 Phylogenetic analysis

A dissimilarity matrix was created for each participant based on their ratings. These values were averaged for every participant to symmetrize the matrix. A global dissimilarity

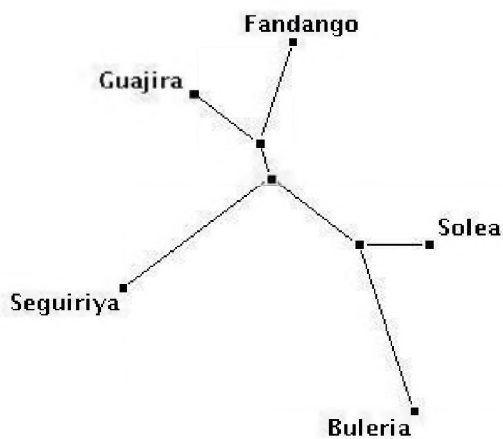
matrix was obtained by summing individual matrices across the 12 participants. Afterwards the BioNJ phylogenetic program [3] was used to construct the phylogenetic tree for each tempo (see Figure 1 and 2).

It can be seen that there is very little difference between the trees for each tempo. Guajira and fandango always form one cluster, soleá and bulería form another cluster, and seguiriya is isolated from the others. Bulería comes out as the most different from all the rhythms, according to the chronotonic distance, and guajira and fandango come out as the two most similar.

3.2 Comparison with mathematical measures

The results confirm the mathematical results from [1]. Specifically human judgment matches the similarity measures using the chronotonic distance more than that using the directed swap distance [2].

Slow-tempo LS fitness 99.98



Medium-tempo LS fitness 99.71

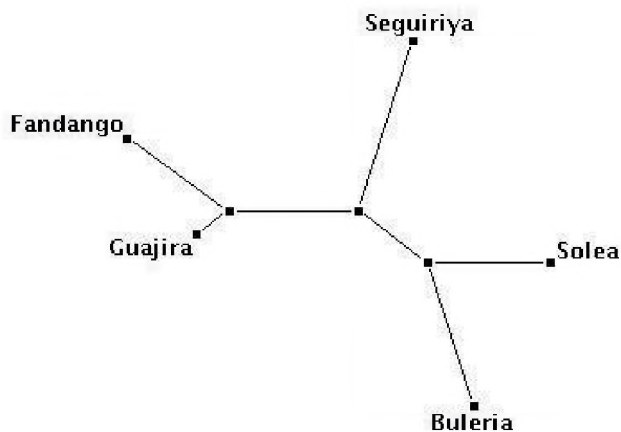


Fig 1: Phylogenetic trees for the slow and medium tempi

Fast-tempo LS fitness 99.57

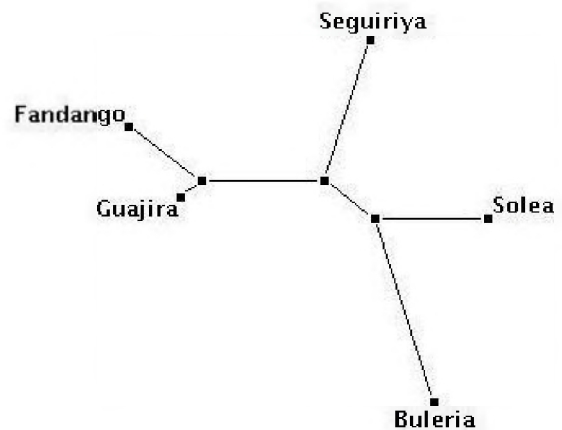


Fig 2: Phylogenetic tree for the fast tempo.

4. FUTURE DIRECTIONS

For future research, we will analyze the effect of the order of the three tempi during the counterbalanced presentations to investigate potential learning effects. We will also replicate the study with the same rhythmic patterns repeated a number of times to evaluate the effect of repeated presentation. Furthermore, we will carry out the study with classically trained musicians and flamenco players to investigate the effect of expertise on perceived rhythmic similarity.

ACKNOWLEDGEMENTS

This research is supported by Strategic Innovation Funding from the Centre for Interdisciplinary Research on Music Media and Technology (CIRMMT). The authors would like to thank Eric Thul for help with obtaining the figures.

5. REFERENCES

- [1] J.-M. Díaz-Báñez, G. Farigu, F. Gómez, D. Rappaport, and G. T. Toussaint, "Similaridad y evolucion en la rítmica del flamenco: una uncursion de la matematica computacional," *La Gaceta de la Real Sociedad de Matematica Española*, 8:(2), pp. 489-509, 2005.
- [2] M. Díaz-Báñez, G. Farigu, F. Gómez, D. Rappaport and G. T. Toussaint, "El compás flamenco: A phylogenetic analysis," *Proceedings of BRIDGES: Mathematical Connections in Art, Music, and Science*, Southwestern College, Winfield, Kansas, July 30 to August 1, pp. 61-70, 2004.
- [3] O. Gascuel, "BIONJ: an improved version of the NJ algorithm based on a simple model of sequence data," *Molecular Biology and Evolution*, 14, pp. 685-695, 1997.

PSYCHOLOGY-BASED RHYTHMIC TRANSFORMATIONS

Francisco Gómez¹ Imad Khoury² Godfried Toussaint²

¹Dept. of Applied Mathematics, Polytechnic University of Madrid, Madrid, Spain. E-mail: fmartin@eui.upm.es

²School of Computer Science and Centre for Interdisciplinary Research in Music Media and Technology, Schulich School of Music, McGill University, Montréal, Québec, Canada. E-mail: [fjelkhol](mailto:fjelkhol@cs.mcgill.ca), [godfried](mailto:godfried@cs.mcgill.ca) @cs.mcgill.ca

1. INTRODUCTION

In most musical traditions rhythmic transformations including rephrasing, displacement, changes of division, metric modulation and segmentation are applied to rhythmic cells (Anku, 1997). Many examples may be drawn from music with developed percussion such as that in the Afro-Cuban tradition, the Indian *tabla* and Indonesian *gamelan* traditions, or jazz music. Rhythmic transformations have also been used to study the evolution of music. For example, Pérez-Fernández proposed a theory of how rhythms in some regions of Latin America may have originated from West-African rhythms, and consequently how one musical tradition may have evolved from another as a result of cultural interaction (Pérez-Fernández, 1986).

Musical cyclic rhythms with a cycle length (timespan) of 8 or 16 pulses are called *binary*; those with 6 or 12 pulses are called *ternary*. The process of mapping a ternary rhythm of, say 12 pulses, to a rhythm of 16 pulses, such that musicologically salient properties are preserved is termed *binarization*. By analogy the converse process of mapping a binary rhythm to a ternary rhythm, proposed here, is referred to as *ternarization*. Pérez-Fernández's theory relies heavily on this binarization transformation. However, this theory has its opponents. Indeed several critiques of this theory have already been published. Gómez et al., (2007) introduced a class of purely mathematical rhythmic transformations, called snapping rules, to binarize and ternarize rhythms, which snap onsets of one representation to onsets of another representation on the basis of proximity rules. However, since the listener has the last word in judging music, the perceptual standpoint should not be overlooked.

Neil McLachlan in *A Spatial Theory of Rhythmic Resolution* (McLachlan, 2000) analyzed music from the African and Javanese musical traditions using Gestalt theory and mathematical group theory. Some of his constructions actually lead to our snapping rules for binarization. In this paper we generalize McLachlan's constructions to include ternarizations and other timespans such as 6 and 8. A second goal of this paper is to test the snapping rules

derived from McLachlan's rhythmic constructions. Following the approach of Gómez et al. (2007), we compare our results to those of Pérez-Fernández. More specifically, we tested the validity of McLachlan's constructions as music-perception-based binarization and ternarization transformations.

2. RHYTHMIC TRANSFORMATIONS AND GESTALT PSYCHOLOGY

Prompted by the idea that onset proximity should be a criterion to maintain perceptual resemblance among rhythms, Gómez et al. defined the *nearest neighbour* rule (NN) and the *furthest neighbour* rule (FN). The nearest neighbour rule snaps an onset to the nearest neighbour, whereas the furthest neighbour rule snaps it to the furthest neighbour. They also introduced snapping rules based on direction such as the *clockwise neighbour* rule (CN), which moves an onset to the next neighbour in a clockwise direction; and *counter-clockwise neighbour* rule (CCN), which moves the onsets in a counter-clockwise direction. Onsets belonging to both pulses are snapped to themselves (i.e., they do not move). It may seem counter-intuitive to use the FN rule. However, in our study this rule was used to fully understand the snapping process, and because it actually gave good results in some cases. We note that snapping rules have been used previously in the study of rhythmic patterns in the context of automatic pattern generation and the formal definition of families of rhythms (Toussaint, 2002), (Demaine et al., 2005).

McLachlan used several Gestalt psychology principles to define rhythmic transformations (McLachlan, 2000). Of particular interest is his transformation from a 12-pulse rhythm to a 16-pulse rhythm. In the presence of a rhythm with timespan length divisible by 4, the superposition of two groups of 3 pulses each over two groups of 4 pulses each is, from the perceptual point of view, sufficient to generate a 12-pulse rhythm (refer to Figure 1). Following the Gestalt principle of simplest organization, this is the minimum information (or minimum resolution in the

PRELIMINARY RESULTS ON STRING INSTRUMENT RECOGNITION

Jason Smalridge¹, Luis Rodrigues¹, and Lisa Lorenzino²

¹Dept. of Mechanical and Industrial Engineering, Concordia University, Montreal, Canada, luisrod@encs.concordia.ca

²Schulich School of Music, McGill University, Montreal, Canada, lisa.lorenzino@mcgill.ca

ABSTRACT

This paper analyzes and compares the spectrum of three string instruments obtained from the Fast Fourier Transform of the sound waves. It is shown that comparing the spectrums of different instruments holds a strong potential to be used as a first stage of an automatic instrument recognizer.

1. Introduction

The most important elements required to identify musical instruments are: envelope, timbre and spectrum.

1.1 Envelope

The envelope of a sound is the shape of its amplitude over time and is divided into 4 parts: attack, decay, sustain and release (ADSR). The attack and decay are often referred to as the transient portion of the sound, with attack being the onset of the sound. They are both important in identifying a source because they hold information about the way the sound is produced. A sound produced from a bowed instrument (violin) will have a longer transient than a struck instrument (guitar). If the sustained portion and release of the sound is played by itself without the transient, then it is very difficult to identify the source.

1.2 Timbre

The most important aspect of a sound is unfortunately the most difficult to analyze. The word timbre (pronounced Tam-ber) describes the aspect of a sound which allows the ear to distinguish two different sound sources which are playing the same pitch at the same level. Even though there are no direct answers as to how to analyze the timbre of a sound, it has to do with the slight variations of both the pitch (and partials) which is called vibrato or jitter and amplitude which is called tremolo. Other factors may include the way that the instrument is constructed and how it resonates certain frequencies. Some instruments tend to have a low common partial throughout all their frequencies that is the product of the materials used for constructing them having their own natural resonant frequency.

1.3 Spectrum

By analysing the spectrum of a note, one can obtain an instrument's signature harmonic series. The Fast Fourier

Transform [1] is the mathematical tool used to produce the spectrum and therefore the signature. Often the fundamental frequency is the first and most dominant partial, but sometimes the instrument produces noise and sub-harmonics that create partials below the true fundamental [2]. Sometimes the fundamental can even be removed without affecting the tonal quality.

In the 1960s Claude Risset at Bell Laboratories performed experiments analyzing and synthesizing a trumpet. He discovered that removing certain frequencies did not change how the human ear perceives the instrument. By removing the partials above the 4000 Hz threshold a trumpet could still be identified. He discovered that the important characteristics for identifying an instrument were the slight variations in frequency (vibrato) and of amplitude (tremolo) of the partials over the duration of the sound [3]. Based on these results, in this paper we will analyze and compare the spectrum of three string instruments.

2. Methodology and Results

In this paper we analyze the spectrum of a Fender acoustic guitar, a Fender Telecaster electric guitar and a Fender short scale Squire electric bass. Six notes were sampled for each instrument and then the Fast Fourier Transform function was used to obtain the spectrum. The six notes were:

-LowE(0):	82Hz
-A(1):	110Hz
-D(1):	146Hz
-G(1):	195Hz
-B(2):	246Hz
-HighE(2):	329Hz

2.1 Acoustic Guitar

We noticed that depending on where the string was plucked, the partials would change amplitudes. When the string was plucked above the sound hole, there was normally only an average of 4 partials with significant peaks. The rest of the partials had such low amplitudes that they were almost equal to the background noise. When the string was plucked close to the bridge (Figure 1) there was a much more even distribution of the partials' amplitudes. When the string was plucked above the soundboard (middle of the string), the partials were completely inconsistent in amplitude.

Problems that arose when recording the data were due to a natural resonant frequency from the guitar. This partial constantly appeared throughout all the notes before the fundamental. In some cases it merged with the harmonic series and created a second harmonic partial that was an octave above the first. In other cases it merged with the fundamental to create two peaks side by side, therefore confusing the location of the fundamental.

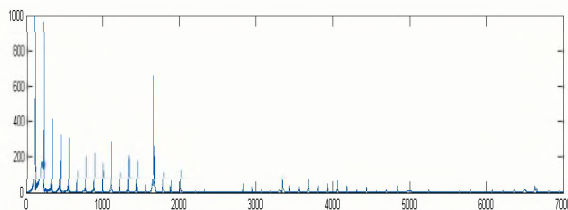


Figure 1 – A string when plucked at the bridge (acoustic guitar)

2.2 Electric Guitar

We noticed a difference in the bass strings and the treble strings in the electric guitar. The electric guitar is fabricated with a slanted single coil pickup. This allows the pickup to be closer to the bridge under the high pitched strings and farther away for the low pitch strings. This would allow the higher strings to pick up more energy in the higher partials much like when the acoustic guitar strings were struck near the bridge (Figure 2). The only difference being that the acoustic guitar could not project enough amplitude to allow the microphone to record it.

Problems arose when analyzing the fundamental frequency for the high pitch strings because the fundamental was much lower in amplitude than the rest of the partials. The position of the pick up explains why the fundamental, and the lower partials, have less amplitude in the higher strings than in the lower strings.

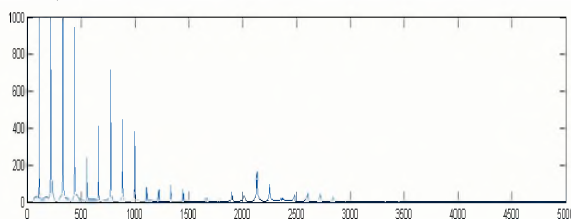


Figure 2 – A string (electric guitar)

2.3 Electric Bass

We had a difficult time with the data from the bass. The first partial in the series acted differently than in previous recordings. The low strings had partials that were almost nonexistent, but the higher strings had the same partials with higher amplitudes (Figure 3). The highest string produced the highest amplitude for this partial. We believe that the microphone used to record the sample did not have a high frequency response at that level. As this partial moved higher, the microphone was able to pick up the frequency better.

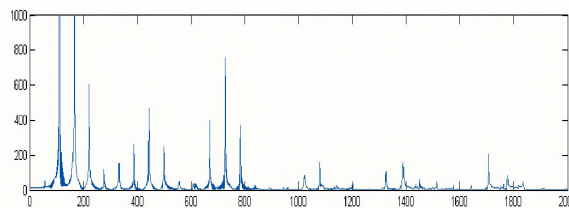


Figure 3 – A string (electric bass)

As can be seen in Figure 4, the frequency response only really begins at 55 Hz. The first two tones the bass produces have fundamentals below this point. The samples that were taken were seen to be one octave lower than the samples taken from the guitar.

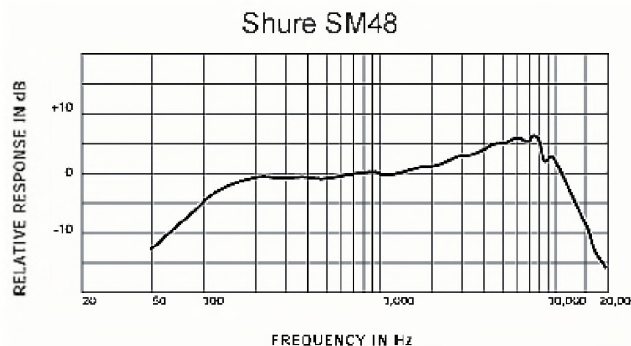


Figure 4 – Frequency response of the microphone

3. CONCLUSIONS

In this paper we analyzed and compared the spectrum of three string instruments obtained from the Fast Fourier Transform of the sound waves. It was seen that comparing the spectrums of different instruments holds a strong potential to be used as a first stage in an automatic instrument recognizer. The potential applications of automatic musical instrument recognition range from assisting hearing impaired subjects to aiding an individual to identify musical selections from a database containing a given instrument.

REFERENCES

- [1] A. V. Oppenheim, *Digital Signal Processing*, Prentice Hall, 1974.
- [2] H. F. Olson, *Music, Physics and Engineering*, 2nd. Edition, Dover, 1967.
- [3] J. R. Pierce, *The Science of Musical Sound*, W.H. Freeman Company, 1983.

ACKNOWLEDGEMENTS

The authors would like to acknowledge Mr. Paulo Tavares for stimulating discussions about the potential applications of an automatic musical instrument recognizer. The second author would also like to acknowledge NSERC, NATEQ and Concordia's Co-op Institute for partially funding this research.

WIND INSTRUMENT ACOUSTIC RESEARCH IN THE COMPUTATIONAL ACOUSTIC MODELING LABORATORY, MCGILL UNIVERSITY

Antoine Lefebvre and Gary Scavone

Computational Acoustic Modeling Laboratory (CAML)

Centre for Interdisciplinary Research in Music Media and Technology (CIRMMT)

Music Technology, McGill University, 555 Sherbrooke St. West, Montreal, Quebec, Canada, H3A 1E3

1. INTRODUCTION

The Computational Acoustical Modeling Laboratory (CAML)¹ of the Music Technology area, Schulich School of Music, McGill University, was established in 2004 by Gary Scavone. Research conducted in CAML includes 1) Studies and measurements to gain a theoretical understanding of the fundamental acoustic behavior of music instruments and other sounding objects, 2) Development of computer-based mathematical models that implement these acoustic principles as accurately as possible, 3) Development of efficient, real-time synthesis algorithms capable of producing convincing sounds (perhaps informed by psychoacoustic data), and 4) Development of appropriate human-computer interfaces for use in controlling and interacting with real-time synthesis models. The laboratory has been funded in large part through a Canadian Foundation for Innovation (CFI) New Opportunities grant awarded in October 2004, as well as an NSERC Research Tools and Instruments grant.

2. SUMMARY OF INVESTIGATIONS

An overview of our recent results, as well as work in progress, is reported in this section with references to submitted and/or published articles.

2.1 Development of input impedance measurement techniques for wind instruments

We recently investigated two methods for measuring the acoustic input impedance of wind instruments. In the first approach, commonly referred to as the two-microphone transfer function method, a tube is connected to the instrument and excited with a broad-band stimulus. Signals recorded at microphone pairs placed along the tube are then analyzed to estimate the instrument input impedance. The second technique, a novel variant of pulse reflectometry, makes use of a long tube with a single microphone located at its midpoint. Using a long-duration broad-band source signal, the impulse response is measured for the tube, first with a rigid termination, and then with the

system to be characterized attached. The system reflectance, and therefore its impedance, is found by comparing the first reflection from the tube end for both measurements. (Lefebvre et al., 2007).

The measurement techniques have been compared for various acoustic systems, including an alto saxophone neck and fabricated conical objects. Both methods show good agreement though there are some discrepancies with theoretical results that might arise from object curvature, under-estimation of boundary losses and temperature fluctuations. Further analysis of these results is planned.

2.2 Comparisons of theoretical and measured impedances of saxophones

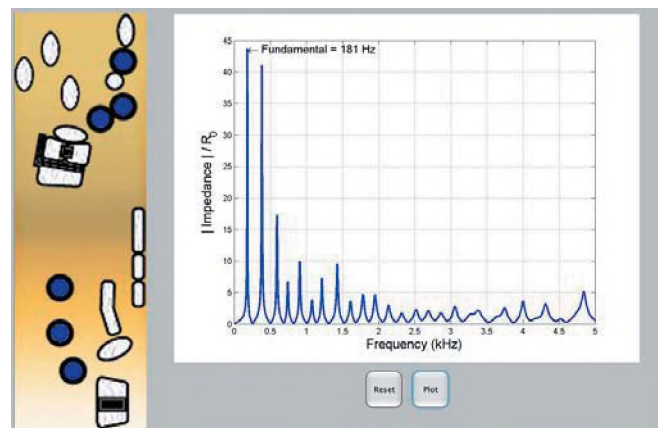


Fig. 1. Saxophone impedance web interface.

A general computational structure has been implemented that allows for the evaluation of the input impedance of an arbitrary acoustic object in terms of cylindrical and conical segments and toneholes (Matthews and Scavone, 2007). A Web-based interface, as shown in Fig. 1, has been created to allow general user access to the computed results for saxophones and comparisons with measurements. By approximating the saxophone's response computationally for different combinations of open toneholes, one can make predictions of the instrument's timbre and tuning. Future work will focus on validating or improving the current

¹ <http://www.music.mcgill.ca/musictech/caml/>

theoretical model of toneholes in conjunction with conical air columns.

2.3 Identification of key features leading to instrument quality

In order to improve woodwind designs, we hope to find correlations between geometric, acoustic, and subjective features of instruments. From that, we hope to determine a set of ideal frequency responses and use an iterative computational approach to find optimized designs. Specifically, we will look at intonation, timbre uniformity, ease of response, dynamic range, playing action, etc.

2.4 Study of vocal-track influence in the performance of saxophones

An approach for analyzing vocal-tract influence in single-reed instruments during performance has been developed. The system provides a relative comparison of the upstream windway and downstream air column impedances under playing conditions and a visual display that allows players to investigate the effect of vocal-tract manipulations in real time. The measurement approach assumes continuity of volume flow on either side of the reed, which leads to a direct proportionality between the upstream and downstream pressures and impedances. Playing experiments were designed to explore vocal-tract influence over the full range of the saxophone, as well as when performing special effects such as pitch bending, multiphonics, and “bugling”. The results indicate that vocal-tract influence is required when playing in the extended register of the saxophone, as well as when pitch bending notes high in the traditional range of the instrument. Subtle timbre variations via tongue position changes can affect spectral content in the range 500 – 2000 Hz and are possible for most notes in the saxophone’s traditional range. Instances of timbre variation are assumed to make use of a wide bandwidth vocal-tract resonance, whereas significant upstream influence involves a narrow bandwidth resonance. An article has been submitted to the *Journal of the Acoustic Society of America* on this subject.

2.5 Investigation of tonehole design improvements

Traditional woodwind toneholes, when closed, leave a non-negligible volume on the inside of the air column that has a negative effect on the acoustics of the instrument. Current instrument designs include various geometrical corrections to account for this effect. We are investigating a tonehole design in a conical air column that eliminates closed-hole chimney volumes, as illustrated in Fig. 2. The keys are curved to fit the hole shape and are closer to the body to allow the hole space to be filled when the key is closed. Experiments are planned for the theoretical characterization of these toneholes so that calculations can be performed to determine correct

positioning and diameter parameters. Possible changes to timbre will also be evaluated.



Fig. 2. Experimental tonehole design without chimney.

2.6 The use of innovative materials and fabrication techniques

The use of composite material for the molding of musical instruments is under investigations. Possible benefits include reduced weight, improved resistance to shock and temperature variations, elimination of discontinuities between sections, increased flexibility on the fabrication of complex shapes (like curved toneholes), etc. Conical objects have been built and their qualities are under investigation.

REFERENCES

- Lefebvre, A., Scavone, G., Abel, J. and Buckiewicz-Smith, A. “A Comparison of Impedance Measurements Using One and Two Microphones.” *Proceedings of the 2007 International Symposium on Musical Acoustics*, Barcelona, Spain, September 2007.
- Matthews, T. and Scavone, G. “An Online System for Viewing the Input Impedance of Saxophones.” *Proceedings of the 2007 International Symposium on Musical Acoustics*, Barcelona, Spain, September 2007.
- Scavone, G., Lefebvre, A., and da Silva, A. “Measurement of Vocal-Tract Influence during Saxophone Performance.” Submitted to *Journal of the Acoustical Society of America*, 2007.

ACKNOWLEDGEMENTS

This work is funded in part by grants from the Natural Sciences and Engineering Research Council (NSERC) of Canada, the Quebec Fonds de Recherche sur la Société et la Culture (FQRSC), the Fonds Québécois de la Recherche sur la Nature et les Technologies (FQRNT), the Centre for Interdisciplinary Research in Music Media and Technology (CIRMMT), Hexagram, and in-kind donations from AuSIM Engineering, Apple Computer, Dell Computer, Universal Audio, National Instruments, Media Musique, and Cycling '74.

PLAYFUL TOOLS, SERIOUS QUESTIONS

Rosemary Mountain

Dept. of Music, Concordia University, 7141 Sherbrooke St. W., RF 322, Qc, Canada, H4B 1R6
mountain@alcor.concordia.ca

1. INTRODUCTION

The *Interactive Multimedia Playroom*¹ is a research project that explores the diverse ways in which people identify & describe sounds and sound - image combinations. The Playroom is characterized by a mixture of technology and traditional aspects in a playful and easily-navigated environment, and is set up to link closely with other research projects both locally and internationally.

The paper gives an overview of the project and suggests how it can function as a tool for investigating our perception of various acoustic properties of sounds. Short sound and image files, triggered by the user through barcode technology, are associated with descriptors in a 3-D space or in sorting bins. An installation of the project is presented in the Hexagram - Concordia Black Box during the conference, and for the first time in the project's development, there will be 3 different 3-D grids to encourage users to 'sort' the clips by mood, properties, or sound-image interaction, as well as means for indicating colour associations. The tool can function at various levels: to encourage users to discriminate between subtle differences in acoustic properties of sound, to test the relevance & accuracy of descriptors used by acoustic researchers, or simply to explore the diversity of associations with sounds of different kinds.

The current report is an update on the project, subsequent to its first major public installation. The report has two major aspects: explanation of the physical setup (through verbal and visual documentation) including several new components and refinements of previous aspects; and summaries of feedback from collaborators, research assistants, and visitors to the installation. The feedback is being received in several formats, ranging from formal data collection to observations by the research assistants (who often act as guides) on the delights and difficulties encountered by users. The report concludes with projections of future developments.

¹ Funded by Hexagram Institute for Research & Creation in Media Arts & Technologies (www.hexagram.org) - a dynamic 80-member media arts institute founded in Montreal in 2001 by Concordia and UQAM; now with several academic & industry partners.

2. BACKGROUND

The *Interactive Multimedia Playroom* is formulated to explore the various ways in which people may listen to, think about, and classify music and music-image-movement interactions. The *Playroom* was developed out of the *Multimedia Thesaurus* project, which presents users with a framework and specific banks of sounds and images to be "sorted" according to their salient characteristics. The *Thesaurus* aspect can also serve to investigate human perception of the acoustic properties of sounds, and the potential impact of visual aspects on that perception.

The project emerged from various concerns of the author in her various guises as composer, musicologist, and professor with long-standing interest in cross-disciplinary research and art-forms. In particular, her work in the composition and, more recently, analysis of electroacoustic music has led to her to appreciate the blurring of boundaries between that field and acoustics.

The *Playroom* is structured to function as a stimulant to discourse and collaboration, and is also designed to facilitate a scientific study of the area. By incorporating physical representation of 3-D grids, it familiarizes its participants with the psychologists' study of perceptual discrimination, similarity ratings, and terminology. The project employs a set of research strategies that lie halfway between those commonly used by the humanities and the sciences, designed to address the shortcomings of each.²

The IMP project has been presented to a variety of academic communities, including electroacoustic and computer music, music perception & cognition, and music information retrieval conferences. Further background information can be found in the proceedings from these previous presentations.³

3. RELEVANCE TO ACOUSTICS

The Playroom can be used in a variety of ways. For those involved with acoustics, three of these seem most relevant: pedagogy, research into perception, and vocabulary.

² The approach is outlined in the Armchair Researcher project – see author's website www.armchair-researcher.com

³ Details on website under "Writings".

Pedagogically, it is an engaging tool for children & adults alike, and the tangibility of the clips helps compensate for the ephemeral nature of sound. Sounds of instruments or acoustic phenomena can be demonstrated easily, and matched with appropriate visuals and terminology.

Its suitability for research into perception ranges from the specific—such as a comparison study of speakers or room acoustics—to more fundamental issues which can benefit from conversations among experts in relevant fields, including sound engineers, sound designers, musicians, cognitive scientists, etc. The project design enables interested colleagues to import clips of their own into the Playrooms giving access to wider response as well as contributing the flexibility and easy interface that is part of its fundamental design.

Vocabulary is one of the main interests of the project participants, as many who work with sound come from different fields whose usage of terminology is often at variance, and sometimes in direct conflict. Without presuming to establish a common vocabulary, the project aims at least to sensitize participants to the diversity of interpretation in descriptors such as bright, grainy, or low; it also enables participants to grasp quickly what another person or discipline means by a specific word.

4. DETAILS OF DESIGN

The installation has various types of components: the media itself, the computers and software for triggering the playing of the media, databases, sorting labels, explanatory texts, reference material, illustrative props, furniture, the SmartBoard and video camera, and the chain grid. Although many of the components can be viewed as 'interim' in their current state, all of them are considered fundamental to the project design.

Physical handheld objects are linked via barcode to short sound, still image, or video clips in a computer bank. Each clip is also linked to a specific database entry, giving source and copyright details, characteristics, and other useful data. A user (or "player") can scan a still image or video clip, and while looking at it, scan a sound clip to study the interaction of the two. The players can also sort the clips into trays, onto racks, or onto a position on one of several chains that together represent a 3-dimensional grid representing those used by psychologists in similarity ratings.⁴

The sound clips chosen for the conference installation emphasize acoustic characteristics of timbre, amplitude envelope, pitch variation, and spatial properties; and include the representation of a variety of styles, instrumentation and cultures, as well as sounds from natural and urban environments and examples of auditory streaming and other psychoacoustical phenomena.

In order to help clarify the participants' focus, we have just introduced a new grid in the Playroom setup. Now, the user needs to choose whether s/he wishes to focus on "statistical" qualities or prefers to indicate the mood or character of the sound. The 'statistical' qualities include acoustical properties and those relating to musical structure, such as texture, gesture, harmony, and rhythm.

New developments in the project include: more automated data collection; easier re-assignments of clips, newer database forms for clip information, explicit directions for various "games", clarification of terminology, more suggestions for axis labels, and an updated website. We are also refining the physical design of the Playroom in various ways, which contribute both to the attractiveness of the space and to the clarity of response from participants.

Plans for future developments include: multiple installations in various places internationally, connected by a virtual hub on the Internet; live video streaming of sessions; database subsets for in-depth studies; and a tighter integration with cognate projects. As we are still developing several aspects of the project, we are eager to receive feedback from acoustics specialists on the designs that could maximize its usefulness for them.

ACKNOWLEDGEMENTS

Thanks to Hexagram, CIAM (Centre Interdisciplinaire des Arts Médiatiques), SSHRC, Smart Technologies, Oboro Gallery, Concordia University, the research assistants, team members, and all the colleagues and visitors to the installation who have offered feedback. A list of the current team members (including student assistants) and related projects can be found on the website.

⁴ See website for images and more detail.

MEMORY FOR MUSICAL INTERVALS: COGNITIVE DIFFERENCES FOR CONSONANCE AND DISSONANCE

Susan E. Rogers and Daniel J. Levitin

Dept. of Psychology, McGill University, 1205 Dr. Penfield Avenue, Montréal, Québec, Canada, H3A 1B1

1. INTRODUCTION

When two tones are produced simultaneously, the resulting sound – a *dyad* – may be judged along several continua such as from smooth to rough, pleasant to unpleasant, and *consonant* to its opposite – *dissonant* [1]. Infants and adults display heightened sensitivity to and a preference for consonant over dissonant musical intervals, leading to speculation that consonant intervals are inherently easier to process than dissonant [2]. Regardless of whether consonance and dissonance are learned or innate distinctions, the contrast is reflected in two independent measures – one based on the frequency separation between two tones (sensory consonance/dissonance); the other based on the frequency ratio between two tones (musical consonance/dissonance). The present study used a short-term memory (STM) paradigm to examine the influence of frequency separation versus frequency ratio on the processing of pure-tone dyads presented outside of a musical (tonal) context.

When the frequency separation between a dyad's two tones is less than a single critical bandwidth (auditory filter) the physical interaction produces a sensation termed *beating* when the separation is less than 15 Hz, and *roughness* when the two tones are separated by roughly 25% to 40% of the bandwidth [3]. Models of *sensory* consonance/dissonance (C/D) predict that all pure-tone dyads with frequency differences greater than a critical bandwidth should be judged consonant [4]. *Musical* C/D, on the other hand, is a term used by music theorists and relates C/D to the size of the integers defining the frequency ratio relationship between two tones. Most adults describe small-integer ratio dyads such as octaves (1:2) as consonant compared with large-integer ratio dyads such as tritones (32:45), described as dissonant [5, 6].

The representation of musical C/D typically reflects an integration of the sensory properties of a *complex-tone* signal, the musical context, and the listener's exposure to intervals. The perception of musical C/D is thus a "knowledge-driven" process [7]. Subjective evaluations, however, of the "beauty" and "pleasantness" of pure-tone dyads show that frequency ratio size influences C/D judgments in the absence of tonal context [8, 9]. An outstanding question is the extent to which distinctions

between sensory and musical C/D are reflected in higher-level cognitive processes. We recruited musicians and nonmusicians to explore these distinctions in a novel/familiar recognition memory task.

2. METHOD

Seventy-two dyads of 500 ms duration each were created by summing two sine tones. Root notes ranged from C3 (130 Hz) to B4 (494 Hz). The 12 musical intervals of the chromatic scale (m2, M2, m3, M3, p4, tritone, p5, m6, M6, m7, M7, octave) were assigned to each of the root notes by random number table. Each musical interval was represented at 6 different root notes; each pitch chroma was represented by 6 different musical intervals. The stimulus set was partitioned into four levels of musical C/D by integer-ratio size, labeled from most to least consonant as follows: MC, mc, md, and MD. The same stimulus set was also partitioned into four levels of sensory C/D by frequency separation and critical bandwidth, labeled from most to least consonant as follows: SC, sc, sd, and SD.

Eight musicians (≥ 5 years training) and eight nonmusicians (≤ 2 years training) heard each dyad twice, first as a novel and later as a familiar stimulus. Novel/familiar pairs were separated by as few as 0 or as many as 6 intervening dyads, corresponding to memory retention periods ranging from 7.75 to 48.00 s. At each trial participants judged whether a dyad was novel or familiar by responding with a keystroke ("yes" or "no" – the "1" and "3" keys, respectively) to the question "Have you heard this before?," displayed on a computer screen. Dyads were presented at 55 dB(A) through stereo headphones in a soundproof booth.

3. RESULTS

At long retention periods (40.75 s and 48.00 s) nonmusicians recognized MD and md, but not MC or mc, dyads significantly better than chance [MC: $\chi^2(1, N = 48) = 0.75, p = 0.39$; mc: $\chi^2(1, N = 40) = 2.50, p = 0.11$; md: $\chi^2(1, N = 40) = 10.00, p < 0.01$; MD: $\chi^2(1, N = 56) = 23.14, p < 0.001$] (see Fig. 1a). Nonmusicians recognized only two levels of sensory C/D dyads (SD and SC) significantly better than chance at the longest retention periods [SC: $\chi^2(1, N = 40) = 10.00, p < 0.01$; sc: $\chi^2(1, N = 48) = 2.08, p = 0.15$; sd: $\chi^2(1, N = 56) = 1.14, p = 0.29$; SD: $\chi^2(1, N = 40) = 8.10, p < 0.01$] (see Fig. 2a).

Musicians recognized all levels of musical and sensory C/D dyads significantly better than chance at 40.75 and 48.00 s [MC: $\chi^2(1, N = 48) = 6.75, p < 0.01$; mc: $\chi^2(1, N = 40) = 12.10, p = 0.001$; md: $\chi^2(1, N = 40) = 16.90, p < 0.001$; MD: $\chi^2(1, N = 56) = 16.07, p < 0.001$; SC: $\chi^2(1, N = 40) = 10.00, p < 0.01$; sc: $\chi^2(1, N = 48) = 5.33, p < 0.03$; sd: $\chi^2(1, N = 56) = 25.79, p < 0.001$; SD: $\chi^2(1, N = 40) = 12.10, p = 0.001$] (see Figs. 1b and 2b).

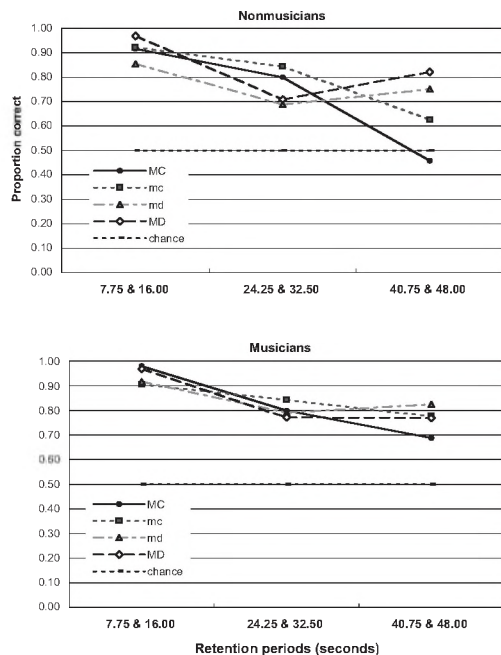


Figure 1. Mean proportion of correct recognitions by nonmusicians (a) and musicians (b) with increasing retention period for dyads categorized by musical consonance/dissonance.

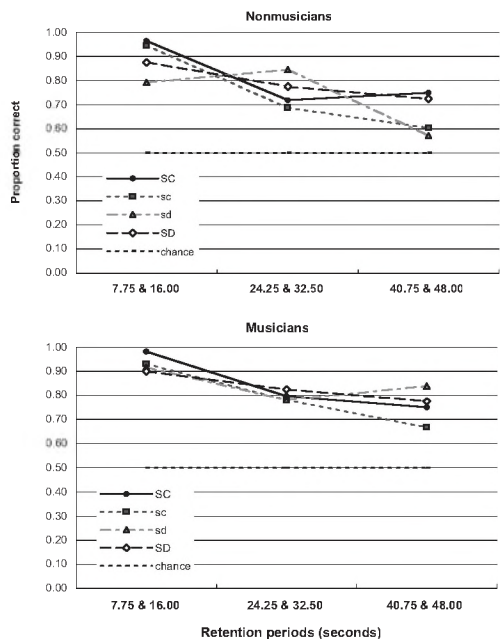


Figure 2. Mean proportion of correct recognitions by nonmusicians (a) and musicians (b) with increasing retention period for dyads categorized by sensory consonance/dissonance.

4. DISCUSSION

The present finding shows auditory STM to be robust and accurate for some dyads beyond the generally understood limit of 30 s retention [10], despite interference from other sounds. Groups of dyads with similar frequency ratio relationships (musical C/D), as opposed to frequency separation (sensory C/D), were processed similarly, particularly by nonmusicians. Nonmusicians displayed more accurate memory for large-integer compared with small-integer ratio dyads. Musicians showed slightly better memory performance overall than did nonmusicians, and less variation between categories of dyads.

Musicians' scores may have reflected a higher degree of explicit music knowledge and familiarity with musical intervals, while nonmusicians' scores may have been driven more by interval distinctiveness [7]. Exposure to musical intervals and their frequency of occurrence allows nonmusicians to internalize the rules of harmonic relationships between notes and chords [1, 7]. Early passive exposure to complex-tone intervals present in speech and music may account for the privileged position of consonance over dissonance and the influence of integer-ratio size on the processing of pure-tone dyads [2,9]. Differential memory for consonance and dissonance implies processing differences in the computation of musical intervals and suggests that certain auditory features are particularly salient.

REFERENCES

- [1] Krumhansl, C. L. (1991). "Music psychology: Tonal structures in perception and memory," *Ann. Rev. Psychol.*, 42, 277-303.
- [2] Schellenberg, E.G., & Trainor, L. (1996). "Sensory consonance and the perceptual similarity of complex-tone harmonic intervals: Tests of infant and adult listeners," *J. Acoust. Soc. Am.*, 100, 3321-3328.
- [3] Zwicker, E. & Fastl, H. (1990). *Psychoacoustics: Facts and Models*. (Springer-Verlag: Berlin).
- [4] Plomp, R., & Levelt, W.J.M. (1965). "Tonal consonance and critical bandwidth," *J. Acoust. Soc. Am.*, 38, 548-560.
- [5] Cazden, N. (1980). "The definition of consonance and dissonance," *Int. Rev. Aesthet. Sociol. Music*, 11, 123-168.
- [6] Helmholtz, H.L.F. von (1954). *On the Sensations of Tone as a Physiological Basis for the Theory of Music*, A.J. Ellis, ed., trans. (Dover: New York), 2nd ed. (Originally published 1885).
- [7] Bigand, E. & Tillman, B. (2005). "Effect of context on the perception of pitch structures," in *Pitch: Neural Coding and Perception*, C. Plack, A. Oxenham, R. Fay, and A. Popper, eds. (Springer: NY).
- [8] Van de Geer, J., Levelt, W. & Plomp, R. (1962). "The connotation of musical consonance," *Acta Psychol.* 20, 308-319.
- [9] Tramo, M., Cariani, P., Delgutte, B., & Braidia, L. (2003). "Neurobiology of harmony perception," in *The Cognitive Neuroscience of Music*, I. Peretz and R. Zatorre, eds. (Oxford: NY)
- [10] Winker, I. *et al.* (2002). "Temporary and longer-term retention of acoustic information," *Psychophys.* 39, 530-534.

EFFECT OF AGE ON SENSITIVITY TO TONALITY

Danielle Minghella¹, Frank Russo², M. Kathleen Pichora-Fuller¹

¹University of Toronto at Mississauga, Department of Psychology, 3359 Mississauga Rd N, Mississauga, Ontario L5L 1C6

²Ryerson University, Department of Psychology, 350 Victoria St., Toronto, Ontario M5B 2K3

1. INTRODUCTION

The purpose of our study was to determine if there are differences in how younger and older adults process pitch relations in music, and more specifically tonality.

Pitch may be referred to as the attribute of auditory sensation by which sounds are ordered on a musical scale (Plack, Oxenham, Fay, & Popper, 2005). Tonality refers to the hierarchical organization of pitches around the tonic or key-note of a piece of music. In Western music, this organization has been described as a four-level hierarchy of stability. The hierarchy is theoretically ordered as follows: 1. *Do* (highest level); 2. *Mi, So*; 3. *Re, Fa, La, Ti*; and 4. non-scale notes (lowest level). Krumhansl, & Kessler (1982) have validated this tonal hierarchy using the probe-tone technique with a variety of musical contexts, arriving at a standardized profile of ratings. Sensitivity to the tonal hierarchy is affected by pitch range as well as the periodicity of tones (Cuddy, Russo & Galembo, 2007; Russo, Cuddy, Galembo & Thompson, 2007).

Many older adults, even those with relatively good audiometric thresholds, are believed to have age-related declines in various aspects of auditory temporal processing that may account for the problems that they experience understanding speech in noise (Pichora-Fuller, & Souza, 2003). One such aspect of auditory aging is believed to be a loss of periodicity or synchrony coding. Age-related differences in psychoacoustic measures such as low-frequency frequency difference limens (Abel, Krever, & Alberti, 1990) and in speech measures such as voice fundamental frequency difference limens (Vongpaisal, & Pichora-Fuller, in press) are consistent with the notion that older adults may be less able than younger adults to use periodicity coding. A jitter simulation of loss of synchrony that temporally distorts the fine structure of speech has been used to mimic the effects of aging on intelligibility when younger adults listen to speech in noise (Pichora-Fuller, Schneider, MacDonald, Pass, & Brown, 2007). Reduced ability to code periodicity could have a negative effect on the perception of musical pitch relations, especially for lower frequency notes that are more dependent on temporal coding. Such reductions might be observed in older adults listening to intact music or in younger adults listening to music distorted by the jitter simulation.

In the present experiment, we test sensitivity to tonality using the probe-tone technique. We investigate whether or not there are differences due to age (younger or older),

periodicity of the stimulus (normal or jittered), and frequency range (mid- or low-frequency).

2. METHOD

Participants

A total of 30 participants completed the study, including 15 younger adults (18-28 years of age; mean = 20.7; *SE* = 0.67), and 15 older adults (66-79 years of age; mean = 71.2; *SE* = 0.92). All participants had clinically normal audiometric pure-tone air-conducted thresholds (0 to 25 dB HL) across the speech range from .25 to 3 kHz (Mencher, Gerber, & McCombe, 1997).

Musical training was not a criteria for inclusion in the study, although the number of years of formal musical training was recorded for each participant. For the younger adults, musical experience ranged from 0 to 12 years of formal training (mean = 3.27; *SE* = 1.05), with 10 of the 15 younger adults having had some musical training. For the older adults, musical experience ranged from 0 to 10 years of formal training (mean = 2.36; *SE* = 0.88), with 8 of the 15 older adults having had some musical training. To adjust for differences between private and group instruction, if the participant had received training in a group setting (e.g., choir, band) then the number of years of that type of training was halved in calculating the total years of training.

Equipment and Stimulus Presentation

All testing was conducted in a 10 x 12 ft IAC double-walled sound-attenuating booth. A Tucker Davis Technology (TDT) System III was used to present the musical tones which were heard by the participants through Sennheiser HD 265 earphones in both ears.

All tones were produced using the General MIDI Protocol. Both mid- and low-frequency tones were utilized. The mid-frequency piano tones spanned the pitch range from C3 (~ 131 Hz) to E4 (~ 330 Hz). The low-frequency piano tones spanned the pitch range from C1 (~ 33 Hz) to E2 (~ 82 Hz). A trial consisted of a key-defining context (implying either C Major or F# Major) followed by a probe tone. The key-defining context consisted of 4 contiguously presented tones (*Do, Mi, Do, So*). The duration of all tones was 333 milliseconds and an interval of one second separated the probe tone from the context. Each trial was separated by 4 seconds.

Two sets of 4 blocks each were prepared and the order of sets was counterbalanced across participants. The first set of blocks always consisted of normal tones, and the final set always consisted of tones distorted by temporal jittering (i.e., difficulty increased). Each block consisted of 12 probe tones, drawn from the chromatic scale starting on the keynote of the implied key (C for C Major and F# for F# Major). The first two blocks were in the mid-frequency range and the second two were in the low-frequency range (i.e., difficulty increased). Each block consisted of 12 probe tones, representing all 12 chromatic notes starting on the keynote of the key implied by the context.

Task

In each trial, participants were asked to rate the degree to which each probe tone fit with the preceding context. Ratings were made on a 7-point scale that ranged from “Fits very poorly” (1) to “Fits very well” (7). Participants were encouraged to use the entire 7-point scale when assessing each tone. The experiment lasted approximately 20-30 minutes per participant.

3. RESULTS

For each participant and in each block, the set of probe tone ratings was correlated with the standardized profile. The correlation value is referred to as the recovery score and can be interpreted as a measure of tonal sensitivity (Russo et al., 2007). As may be seen in Figure 1, the recovery scores for the younger adults were higher than those for the older adults. Furthermore, the recovery scores for the normal tones were higher than those for the jittered tones. This description was confirmed by an Analysis of Variance with age (young or older) as a between-subjects factor and periodicity (normal or jittered) and frequency range (mid or low) as within-subjects factors. There were significant main effects of age, $F(1, 28) = 5.60, p < .03$, and periodicity, $F(1, 28) = 5.16, p < .04$. No other effects reached significance. Although the effect of frequency range did not reach significance, the trend is as expected with low-frequency tones yielding weaker recovery scores than mid-frequency tones (mean = 0.69; $SE = 0.02$ for the low-frequency range; mean = 0.72; $SE = 0.02$ for mid-frequency range). A Student Newman-Keuls post-hoc test indicated that the recovery scores for the younger adults with jittered tones (mean = 0.72; $SE = 0.03$) did not differ significantly from those of the older adults with normal tones (mean = 0.67; $SE = 0.03$), $p > .1$. The scores for the older adults for normal (mean = 0.67; $SE = 0.03$) and jittered tones (mean = 0.63; $SE = 0.03$) did not differ significantly, $p > .1$, but the scores for the younger adults were significantly better for normal (mean = 0.78; $SE = 0.02$) than for jittered tones (mean = 0.72; $SE = 0.03$), $p < .05$; and for normal tones the recovery scores of the younger adults (mean = 0.78; $SE = 0.02$) were significantly greater than those of the older adults (mean = 0.67; $SE = 0.03$), $p < .05$.

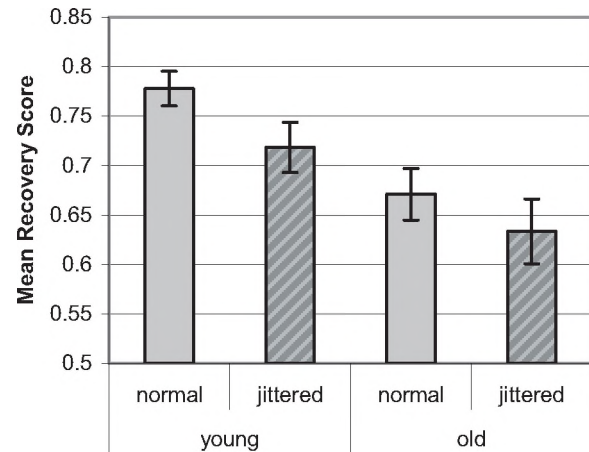


Figure 1. The mean recovery scores for younger and older adults in the normal and jittered conditions.

4. DISCUSSION

We found significant effects of age and stimulus periodicity on tonal sensitivity. The finding that the younger adults were better than the older adults overall in terms of tonal sensitivity provides new evidence of an age-related deficit in periodicity coding. Furthermore, jittering the stimulus to disrupt periodicity negatively influenced tonal sensitivity in both groups.

REFERENCE

- Abel, S.M., Krever, E.M., & Alberti, P.W. (1990). Auditory detection, discrimination and speech processing in aging, noise-sensitive and hearing impaired listeners. *Scandinavian Audiology*, 19, 43-54.
- Cuddy, L. L., Russo, F. A., & Galembo, A. (2007). Tonality of low-frequency synthesized piano tones. *Archives of Acoustics*, 32, 3-12.
- Krumhansl, C.L., & Kessler, E.J. (1982). Tracing the dynamic changes in perceived tonal organization in a spatial representation of musical keys. *Psychological Review*, 89, 334-368.
- Mencher, G., Gerber, S., & McCombe, A. (1997). *Audiology and Auditory Dysfunction*. Needham Heights, MA: Allyn & Bacon.
- Pichora-Fuller, M.K., Schneider, B., MacDonald, E., Brown, S., & Pass, H. (2007). Temporal jitter disrupts speech intelligibility: A simulation of auditory aging. *Hearing Research*, 223, 114-121.
- Pichora-Fuller, M.K., & Souza, P. (2003). Effects of aging on auditory processing of speech. *International Journal of Audiology*, 42 (Supp 2), S11-S16.
- Plack, J. Oxenham, A.J., Fay, R.R., & Popper, A.N. (2005). *Pitch: Neural coding and perception*. New York: Springer.
- Russo, F.A., Cuddy, L.L., Galembo, A., & Thompson, W.F. (2007). Sensitivity to tonality across the pitch range. *Perception*, 36, 781-790.
- Vongpaisal, T., & Pichora-Fuller, M.K. (in press). Effect of age on use of F_0 to segregate concurrent vowels. *Journal of Speech, Hearing, and Language Research*.

ELICITING INDIVIDUAL LANGUAGE DESCRIBING DIFFERENCES IN AUDITORY IMAGERY ASSOCIATED WITH FOUR MULTICHANNEL MICROPHONE TECHNIQUES

William L. Martens, Sungyoung Kim, Kent Walker, David Benson, and Wieslaw Woszczyk
Schulich School of Music, McGill University, 555 Sherbrooke Street W., Montreal, QC, Canada H3A 1E3
wlm@music.mcgill.ca

1. INTRODUCTION

When different listeners hear several versions of a single piano performance, each of which is different from the others in a number of ways, those individual listeners might use any number of words to describe the differences that they hear. It is worth questioning whether they are hearing the same distinctions on identifiable auditory attributes, even though they name those distinctions differently. This question generally needs to be addressed in a systematic perceptual evaluation of modern techniques used for multichannel sound recording. The work described in this paper attempted to address this question through a controlled verbal elicitation that was followed by an examination of ratings on individualized attribute scales constructed from the results of the verbal elicitation for each of five listeners.

In contrast to a recent related investigation that focused upon the development of a consensus language for a group of listeners with similar training (Martens & Kim, 2007), the current study relied upon the modern descriptive analysis technique termed the Repertory Grid (RepGrid) Technique. This approach, perhaps first introduced to the sound quality evaluation community by Kjeldsen (1998), was employed with good results for the sensory evaluation of multichannel sound reproduction by Berg & Rumsey (2000; 2006). In their verbal elicitations they collected both descriptive and attitudinal features of multichannel reproduced sound, and used cluster analysis to organize the obtained terms. In the current study, five trained listeners were asked to focus their attention primarily upon spatial attributes that could be used to discriminate between stimuli presented in groups of three. Always, a given triadic comparison was made between three different versions of a single solo piano performance. By focusing only upon multiple versions of a solo piano performance, the current investigation was not too ambitious in its exploration of reproductions that were very similar to one another in many respects, and were indeed all acceptable reproductions of piano performances that were captured simultaneously using four different multichannel microphone techniques. A full explanation of the RepGrid approach is beyond the scope of this paper, and so the reader is referred to the manual for commercial software enabling the analysis of such data (Fransella et al, 2003).

2. METHOD

Two short excerpts of each of four solo piano pieces composed in the European concert musical tradition were chosen for this study: works by Bach, Schubert, Brahms, and a contemporary improvisation by Plaunt. It was hypothesized that some microphone techniques might be preferred for certain musical selections within the performance space, which was the 600-seat Pollack Concert Hall located at McGill University, and expert advisors agreed that the following four surround microphone arrays were appropriate selections for comparison: Fukada Tree, Polyhymnia Pentagon, Optimized Cardioid Triangle combined with a Hamasaki Square, and a SoundField microphone. All musical excerpts were performed in the same concert hall by a single musician, and played on a single piano. The details of the recording procedure are well documented in Kim, et al. (2006).

The 32 five-channel stimuli were presented via five active full bandwidth loudspeakers (Dynaudio model BM15A) positioned at a height of 1.2 m from the floor and at a radius of 1.5 m from the central listening position (no LFE signal was prepared, and no subwoofer was employed). This surround sound reproduction system was located in MARLAB (Multichannel Audio Research LABORatory) at McGill University. The five listeners had all participated in previous listening tests conducted in MARLab, and were all either professors in the Sound Recording Area within the Schulich School of Music of McGill University, or were students enrolled in the School's doctoral program in Sound Recording.

The details of the experimental method are similar to those that were well described in the recent report by Martens & Kim (2007), although that study was focused upon the development of a consensus language for a group of listeners with similar training. None of the five listeners had participated in that previous study, though they were all well aware of that study's results. For the current study, no examples were presented prior to listening sessions, such as stimuli exhibiting extreme positions on any of the attributes identified in the previous study. Also, no group discussions were held, in order to avoid any bias other than that which comes from training in sound recording.

3. RESULTS

The following table gives a summary of some of the bipolar adjectives that were elicited from the five listeners, along with the relative frequency with which they were generated.

<p>Listener 1: wide vs. narrow 10/32 focused vs. diffuse 9/32 tight-bass vs. muddy-bass 8/32 distant vs. close 3/32 bright vs. dark 2/32 not reverberant vs. reverberant 2/32</p> <p>Listener 2: sparkling, bright vs. dull, muddy 10/32 wide vs. narrow 16/32 close, near vs. far, distant 4/32 more spacious vs. less spacious 2/32</p> <p>Listener 3: narrow vs. wide 14/32 defined vs. diffused 6/32 open vs. closed 4/32 far vs. close 4/32 bright vs. dark 4/32</p> <p>Listener 4: strong-centre vs. well-spread 15/32 clear vs. blurry 5/32 distant vs. close 4/32 dull vs. bright 3/32 surrounding vs. less surrounding 3/32</p> <p>Listener 5: narrow vs. wide 12/32 covered, muffled vs. clear 8/32 thin, narrow bass vs. fat, wide bass 5/32 spiky, pointy vs. smooth, warm, even 4/32</p>

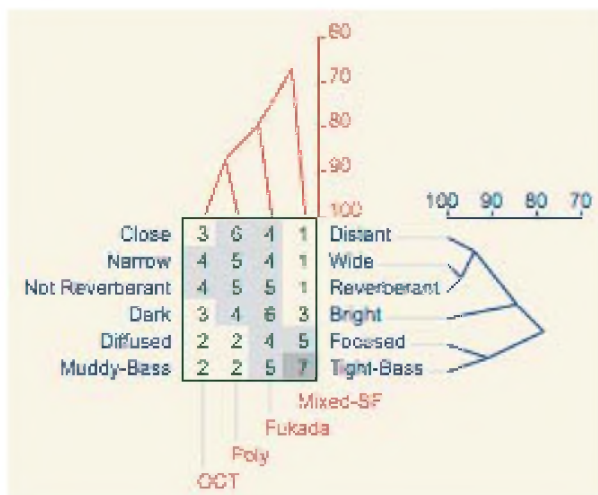


Fig. 1. Results of RepGrid cluster analysis relating Mic. Techniques to ratings on the 6 attribute scales constructed for Listener 1 from his elicited bipolar constructs.

Figure 1 shows the results of Repertory Grid (RepGrid) cluster analysis performed on ratings obtained from just one of the five listeners. Note that instead of running the RepGrid analysis on ratings for all 32 stimuli, the centroid response dataset was calculated from the combined ratings for all 8 of the musical programs for each of the four microphone techniques (and rounded to integer values as required). Thus, the average responses given for each of the four microphone techniques, regardless of which musical selection was being rated, were submitted to RepGrid analysis, thereby giving a general overview for each. This analysis for Listener 1 gave a tight cluster between obtained ratings on three attribute scales: on the <wide-narrow> scale, the <distant-close>, and the <not reverberant-reverberant> scale. A second tight cluster was observed between ratings on the <focused-diffuse> and the <tight(bass)-muddy(bass)> scale. Ratings on the <bright-dark> scale separated out from the other attributes in that this attribute described timbral rather than spatial character of the reproduced musical performances.

REFERENCES

Martens, W. L., and Kim, S. (2007) Verbal Elicitation and Scale Construction for Evaluating Perceptual Differences between Four Multichannel Microphone Techniques. In Proc. Audio Engineering Society 122nd Int. Conv., Vienna, Austria.

Kjeldsen, A. D. (1998) The measurement of personal preferences by repertory grid technique. In Proceedings of 104th Conv., Amsterdam, The Netherlands.

Berg, J., and Rumsey, F. (2000) In search of the spatial dimensions of reproduced sound: Verbal protocol analysis and cluster analysis of scaled verbal descriptors. In Proc. Audio Engineering Society 108th Conv., Paris, France.

Berg, J., and Rumsey, F. (2006) Identification of Quality Attributes of Spatial Audio by Repertory Grid Technique. J. Audio Eng. Soc., 54(5):365-379, 2006.

Fransella, F., Bell, R. and Bannister, D (2003) A Manual for Repertory Grid Technique, 2nd Edition. John Wiley & Sons, Inc., New York, NY.

Kim, S., Martens, W. L., Marui, A. and Walker, K. (2006) Predicting Listener Preferences for Surround Microphone Technique through Binaural Signal Analysis of Loudspeaker-Reproduced Piano Performances. In Proc. Audio Engineering Society 121st Int. Conv., San Francisco, CA.

ACKNOWLEDGEMENTS

This work was supported in part by the Social Sciences and Humanities Research Council of Canada (SSHRC), within the project entitled "Recording and auralization of the acoustics of concert halls and sonic spaces." Additional support was provided by the Canada Foundation for Innovation (CFI) New Opportunities Program, and also by McGill University's Centre for Interdisciplinary Research in Music Media and Technology (CIRMMT).

DEVELOPING CONSENSUS LANGUAGE FOR DESCRIBING DIFFERENCES IN AUDITORY IMAGERY ASSOCIATED WITH FOUR MULTICHANNEL MICROPHONE TECHNIQUES

Sungyoung Kim and William L. Martens

Schulich School of Music, McGill University, 555 Sherbrooke Street W., Montreal, QC, Canada H3A 1E3

sungyoung.kim@mail.mcgill.ca

1. INTRODUCTION

Eight listeners who had already completed a series of descriptive analysis (DA) sessions on the stimuli employed in this study (Martens & Kim, 2007) made ratings on the stimuli during two experimental test sessions separated in time by 6 months using the bipolar adjective scales that resulted from those DA sessions. This retest was initiated to examine the consistency with which the eight listeners could make ratings on three of the bipolar adjective scales that had been used to describe perceptual differences within a set of 32 stimuli comprising solo piano performances captured using four different multichannel microphone techniques. It was hypothesized that the auditory attributes associated with these bipolar adjective scales may represent relatively permanent perceptual characteristics of reproduced musical sound that might be assessed subjectively in a similar manner over time for a given stimulus domain. If this were so, then the ratings that a given listener produces on one occasion for a restricted set of stimuli should be highly correlated with the ratings that same listener produces on another occasion, removed in time from the first so as to represent an independent assessment of the characteristics of those stimuli. The reliability of the listeners' ratings was examined in a number of ways. First, inter-subject consistency was examined using Procrustes Analysis (Dijksterhuis, 1996). Then, for a selected subset of listeners showing highest agreement with each other, intra-subject consistency was examined through comparison of ratings made by each of these eight listeners before and after the 6-month break between rating sessions. Finally, Principal Component Analysis was employed in order to find relatively stable perceptual components underlying the listener's ratings.

In the study to be described in this paper, the experimental variable that was under direct control was the multichannel microphone technique that was used to record a selection of solo piano performances. Another important factor here was the selection of musical program material to be used in evaluating the results of using the microphone techniques to be evaluated. Previous reports on this project have already given more in-depth introduction to these issues (Martens & Kim, 2007), and only details relevant to this particular longitudinal study will be provided here.

2. METHOD

2.1 Listeners

A total of eight masters students in the Sound Recording program of McGill University participated in the listening experiments. While these students could not be regarded as experts either in sensory evaluation nor in sound recording practice, they were all engaged in the training that follows the *Tonmeister* tradition, in which they develop skills in microphone placement and in aural evaluation of the results.

2.2 Attribute Ratings

The same eight individuals who participated in this longitudinal attribute rating study completed a verbal elicitation task using a triadic comparison method to explore the adjectives that could be used to describe differences between solo piano performances captured using four different multichannel microphone techniques. The attribute rating scales employed in this study were anchored by the following pairs of bipolar adjectives upon which the eight listeners had reached some consensus: Wide–Narrow, Focused–Diffused, and Tight-Bass–Muddy-Bass.

3. RESULTS

The mean ratings over the two sessions for each individual listener were submitted to Procrustes Analysis (Dijksterhuis, 1996) in order to gauge how similarly the attributes scales were being used by the eight listeners. First the centroid response dataset was calculated from the combined ratings of all eight listeners. This centroid was used as a basis for comparison, and Procrustes Analysis (PA) was used to determine a linear transformation (translation, reflection, orthogonal rotation, and scaling) of the points in each individual dataset to best conform them to the points in this centroid dataset. The “goodness-of-fit” criterion is a dissimilarity measure D , which is the sum of squared deviations of the individual dataset from the centroid response dataset. For each of the listeners the analysis produced a minimized value of D , standardized by a measure of the scale of the centroid (i.e., the sum of squared elements of a centered version of the centroid response dataset). The average obtained dissimilarity for the five listeners who were in best agreement was $D = 0.390$,

while the average dissimilarity for the three listeners who were judged to be outliers was $D = 0.534$.

Pearson correlation coefficients between the first and second ratings on each of the three attributes were calculated for each of the five selected listeners (who were in best agreement according to PA results). The observed correlations are plotted in Figure 1, with the correlation coefficient value of $r = .345$ marked by the horizontal dashed line. Correlation coefficients smaller than criterion might indicate either that listeners in these cases were inconsistent in how they understood the attributes on which they were required to make their ratings, or that they simply were not able to make consistent magnitude estimates for these attributes, though they might have understood well the meaning of the anchors defining the extremes for each attribute scale. Regardless of the reason, three subjects, were separated out from the other five as relatively poor in producing ratings that matched their previous ratings. Since combining such inconsistent perceptual responses would provide a poor definition of the auditory attributes under investigation here, the ratings from these three relatively inconsistent subjects were excluded from the subsequent Principal Components Analysis (PCA) designed to examine the underlying perceptual structure for the obtained attribute ratings.

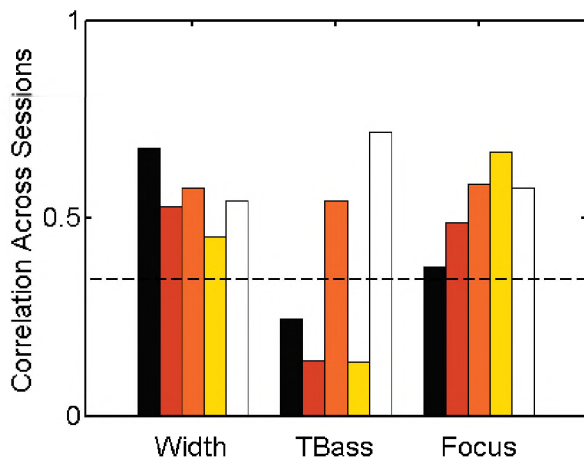


Fig. 1. Pearson correlation coefficients between the first and second ratings on each of the three attributes were calculated for each of the five selected listeners. The horizontal dashed line indicates the criterion for statistical significance (at probability $\alpha < .05$ of incorrectly retaining the null hypothesis).

The PCA results shown in Figure 2 reveal the relationship between these three sets of collected attribute ratings, with ratings from the two separate sessions treated as distinct variates (i.e., a matrix of 6 columns was submitted to PCA, with a total of 160 rows containing ratings on 32 stimuli from each of 5 listeners). Loadings on each PC are plotted separately for each rating session, so there are two corresponding symbols for each of the three attributes.

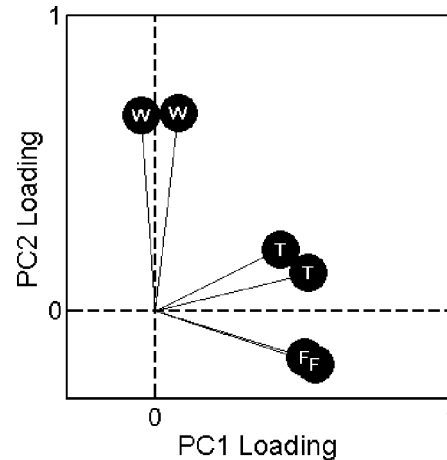


Fig. 2. Attribute loadings on the first two principal components (PCs) plotted separately for each of two rating sessions, with symbols corresponding to each of the three attributes labeled as follows: W for Width, T for Tight-Bass, and F for Focus.

4. DISCUSSION

It was shown that the attributes found most salient in a previous study could be reliably rated in well separated sessions by 5 out of the 8 listener tested here. These 5 listeners were also in good agreement on how to use the attribute scales in describing the restricted set of 32 stimuli presented here. Only for one of the attribute scales (Tight-Bass) were ratings not significantly correlated between first and second sessions. For the other two attributes, (Width and Focus), ratings produced by each of the five selected listeners always were found to be correlated significantly with the ratings that the same listener produced on another occasion 6 months later. The PCA results indicate that a relatively stable perceptual structure may be said to underlie the attribute ratings obtained on such temporally separated occasions.

REFERENCES

Martens, W. L., and Kim, S. (2007) Verbal Elicitation and Scale Construction for Evaluating Perceptual Differences between Four Multichannel Microphone Techniques. In Proc. Audio Engineering Society 122nd Int. Conv., (Vienna, Austria), Preprint 7043.

Dijksterhuis, G. (1996) Multivariate analysis of data in sensory science, volume 16 of Data handling in science and technology, chapter 7: Procrustes analysis in sensory research, pages 185–217. Elsevier, Amsterdam, The Netherlands.

ACKNOWLEDGEMENTS

This investigation was supported by grant No. 110403 awarded to the first author by the FQRSC. Additional support was provided by the CFI New Opportunities Program, and also by McGill University's Centre for Interdisciplinary Research in Music Media and Technology (CIRMMT).

Towards a Spatial Sound Description Interchange Format (SpatDIF)

Nils Peters¹, Sean Ferguson², Stephen McAdams¹

¹Music Technology Area - Music Perception and Cognition Lab

²Music Composition Area - Digital Composition Studios

Centre for Interdisciplinary Research in Music Media and Technology (CIRMMT)

Schulich School of Music, McGill University, Montréal*

1 Introduction

This paper presents the need for a Spatial Sound Description Interchange Format (SpatDIF) with the aim of creating, storing and sharing information for 3D audio applications.

2 Initial Problem

Our research includes a review of several spatialization algorithms and their implementations:

- Vector Based Amplitude Panning (VBAP), [7]
- (Higher Order) Ambisonics, e.g. [8]
- Spatialisateur (SPAT), [5]
- Space Unit Generator (SUG), e.g. [11]
- Virtual Microphone Control (ViMiC), [2]
- Wavefield Synthesis (WFS), e.g. [1]

We found that each spatialization algorithm uses a self-contained syntax and data format, wherein sequences of control messages (e.g. trajectories to move a sound in space) programmed for one application are incompatible with another implementation. Furthermore, like the recently opened *Allosphere*¹ in Santa Barbara, CA more and more concert halls and research facilities are equipped with a large number of loudspeakers. Although these venues might provide a good environment for 3D audio applications, they often differ in terms of room size, their technical specifications and the applied audio rendering concept. This lack of a standardized format for controlling spatialization across different rendering platforms and venues complicates the portability of compositions and requires manual synchronization and conversion of control data - a time consuming affair. Incompatible data formats also prevent collaboration between researchers and institutions. Therefore we call for developing of SpatDIF - a format to describe spatial audio information in a structured way to support real-time and non-real-time applications.

*Correspondence should be addressed to nils.peters@mcgill.ca
¹<http://www.mat.ucsb.edu/allosphere/>

3 Implementation

According to the Sound Description Interchange Format (SDIF) [9], SpatDIF should have the following properties:

Platform independence Any 3D audio rendering algorithm on any computer platform should technically be able to understand SpatDIF;

Easily understandable syntax to prevent misunderstandings when stored data are shared;

Extendability Easy adding of descriptors to extend the specification especially as long as SpatDIF is in development;

Free and open source to increase the acceptance and widespread usage of this new format;

Easy to connect with interfaces, controllers and sensors for real-time control of spatialization, e.g. through GDIF [4];

Use of existing standards to focus on conceptual rather than technical development.

SpatDIF builds on the well-known Open Sound Control (OSC) address space standard [10] for real-time purposes. A SpatDIF OSC stream could also be stored as streams in audio sequencer programs, or in SDIF files (see Figure 1). For now, a SpatDIF interpreter receives and converts a SpatDIF OSC stream into the low-level data format according to the applied spatialization algorithm, but we hope that developers will integrate SpatDIF directly into their software.

3.1 Example for SpatDIF

Changing the position of virtual sound sources is the most common controllable parameter in spatialization applications. We briefly demonstrate SpatDIF by using this parameter as an example. There are several ways a position in space is defined:

1. Perspective: a position can be defined either in allocentric (relative to an external framework) or in egocentric (relative to the listener) perspectives;

2. Coordinate system: two or three dimensional, cartesian or spherical coordinate systems;
3. Absolute or relative (normalized) parameter values.

We propose an egocentric and normalized coordinate system as used in VBAP and several Ambisonic implementations. A control message for describing the position of sound source Nr.3 could be defined in cartesian (1) and spherical (2) coordinates. It should also be possible to change just a single coordinate dimension, e.g. the azimuth component in absolute values (3), or in incremental/decremental steps (4):

```
(1) /SpatDIF/source/3/xyz -0.5 0.5 0.0
(2) /SpatDIF/source/3/aed -45.0 0.0 0.0
(3) /SpatDIF/source/3/a -46.0
(4) /SpatDIF/source/3/a:+
```

If absolute positions are defined (as in [11]), a conversion factor needs to be initialized to rescale normalized coordinates. Initial parameters that are necessary for setting up the spatialization algorithm as well as other descriptive meta-information, should also be storable.

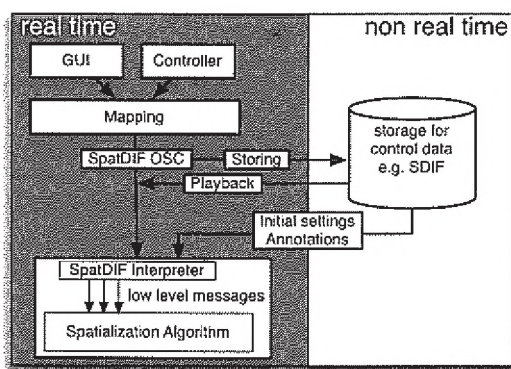


Figure 1: SpatDIF in real-time and non-real-time applications.

4 Conclusion and Acknowledgment

An interchangeable namespace for describing, storing and sharing data for 3D audio applications was presented. For now SpatDIF handles elementary parameters, but we also want to describe higher level data, such as reverberation or complex sound scenes. SpatDIF is being tested in three projects related to live electronics: Integra [3], Jamoma [6], and an NSERC/CCA New Media Initiative project at CIRMMT. Researchers from McGill University, the University of Oslo and the Bergen Center for Electronic Arts are involved in the development - others are welcome to join.

This work is funded by the Canadian Natural Sciences and

Engineering Research Council (NSERC) and the Canada Council for the Arts. Special thanks to Alexander Jensenius, Trond Lossius and Joseph Malloch.

References

- [1] M. A. Baalman, T. Hohn, S. Schampijer, and T. Koch. Renewed architecture of the WONDER software for Wave Field Synthesis on large scale systems. In *proceedings of the Linux Audio Conference*, Berlin, Germany, 2007.
- [2] J. Braasch. A loudspeaker-based 3D sound projection using virtual microphone control (ViMiC). In *Convention of the AudioEng. Soc. 118, Barcelona, Spain, Preprint 6430*, 2005.
- [3] J. Bullock and H. Frisk. libIntegra: a system for software-independent multimedia module description and storage. In *Proceedings of the International Computer Music Conference*, Copenhagen, Denmark, 2007.
- [4] A. Jensenius, T. Kvifte, and R. Godøy. Towards a gesture description interchange format. In *Proceedings of the 2006 conference on New interfaces for musical expression*, pages 176–179. Paris, France, 2006.
- [5] J.-M. Jot. The Spat Processor and its Library of Max Objects - Introduction. Technical report, IRCAM, Manual, Ver. Oct. 2006.
- [6] T. Place and T. Lossius. Jamoma: A modular standard for structuring patches in Max. In *Proceedings of the International Computer Music Conference 2006*, New Orleans, US, 2006.
- [7] V. Pulkki. Virtual sound source positioning using vector base amplitude panning. *AES Journal*, 45(6):456 – 466, 1997.
- [8] J. C. Schacher and P. Kocher. Ambisonics spatialization tools for max/msp. In *Proceedings of the 2006 International Computer Music Conference*, pages 274 – 277, New Orleans, US, 2006.
- [9] M. Wright, A. Chaudhary, A. Freed, D. Wessel, and X. Rodet. New Applications of the Sound Description Interchange Format. In *Proceedings of the International Computer Music Conference*, pages 276–279, Ann Arbor, US, 1998.
- [10] M. Wright, A. Freed, and A. Momeni. OpenSound Control: state of the art 2003. In *Proceedings of the 2003 conference on New Interfaces for Musical Expression*, pages 153–160, Singapore, 2003.
- [11] S. Yadegari, F. R. Moore, H. Castle, A. Burr, and T. Apel. Real-time implementation of a general model for spatial processing of sounds. In *Proceedings of the 2002 International Computer Music Conference*, pages 244 – 247, San Francisco, CA, USA, 2002.

FINITE ELEMENT ANALYSIS OF AN EARMUFF-EARCANAL SYSTEM

Mahborbeh Khani¹, Kechroud Riyad¹, and Soulaïmani Azzeddine¹

¹Dept. of Mechanical Engineering, Ecole de Technologie Supérieure, 1100, Notre Dame Ouest, Québec, Canada, H3L2G9
azzeddine.soulaimani@etsmtl.ca

1. INTRODUCTION

The use of earmuffs is one of the useful ways to protect against hearing loss in environments where noise levels are not controllable within safe limits. Whenever the use of earplugs is impossible or impractical, the use of earmuffs provides a means of reducing sound intensity, and in many instances to a degree even greater than that provided by earplugs. Also, earmuffs tend to deliver higher in-field noise protection in many high frequency noise environments than most earplugs.

This research presents the direct coupling of FEM models of an earmuff-like structure and acoustic cavity (air cavity plus ear canal). Vibro-acoustic steady-state and transient responses are predicted for a hearing protection device (HPD, such as an earmuff that attenuates the pressure wave prior to its reception by the eardrum). The modeling of the coupled structure-acoustic-cavity system is important to predict the level of protection achievable for the wearer. Therefore, the FEM technology is essential for the analysis of this kind of problem.

1. METHODOLOGY

1.1 FEM formulation for the structure

For a general elastic structure, the differential equations governing the motion can be written in the following matrix form as:

$$[M_s]\{\ddot{u}\} + [C_s]\{\dot{u}\} + [K_s]\{u\} = \{F(t)\} \quad (1)$$

Where $[M_s]$, $[C_s]$ and $[K_s]$ are respectively the mass, damping and stiffness matrix. $\{\ddot{u}\}$, $\{\dot{u}\}$, $\{u\}$ and $\{F\}$ are respectively the nodal acceleration, velocity and load vector.

1.2 FEM formulation for the acoustic cavity

The discretization of the pressure-wave equation by the finite element method leads to the following differential system of equations:

$$[M_a]\{\ddot{p}\} + [K_a]\{p\} = \{0\} \quad (2)$$

Where $[M_a]$ and $[K_a]$ are respectively the fluid mass and stiffness matrix. $\{p\}$ is the nodal pressure vector.

1.3 Acoustic fluid-structure coupling

At the interface between the structure and acoustic cavity, the boundary conditions must satisfy the compatibility and equilibrium coupling conditions. First, the displacement of the structure must coincide with the displacement of the acoustic particle. Secondly, the dynamic equilibrium condition requires that the normal force produced by the vibrating structure at the interface must be to the total acoustic pressure force:

$$n \cdot \nabla p = -\rho n \cdot \{\ddot{u}\} \quad (3)$$

The governing finite element matrix equations for the coupled structure-cavity system are then written as (time-dependent solutions):

$$\begin{bmatrix} M_s & 0 \\ \rho R^T & M_a \end{bmatrix} \begin{Bmatrix} \ddot{u} \\ \ddot{p} \end{Bmatrix} + \begin{bmatrix} C_s & 0 \\ 0 & 0 \end{bmatrix} \begin{Bmatrix} \dot{u} \\ \dot{p} \end{Bmatrix} + \begin{bmatrix} K_s & R \\ 0 & K_a \end{bmatrix} \begin{Bmatrix} u \\ p \end{Bmatrix} = \begin{Bmatrix} F(t) \\ 0 \end{Bmatrix} \quad (4)$$

With the assumption of time-harmonic evolution of the system (steady case), the governing equation (4) takes the following form in the frequency domain:

$$\begin{bmatrix} -\omega^2 M_s + j\omega C_s + K_s & R \\ -\omega^2 \rho R^T & -\omega^2 M_a + K_a \end{bmatrix} \begin{Bmatrix} \ddot{u} \\ \ddot{p} \end{Bmatrix} = \begin{Bmatrix} \ddot{F} \\ 0 \end{Bmatrix} \quad (5)$$

Where ω is the pulsation of the load.

2. ANALYSIS OF AN EARMUFF-EARCANAL SYSTEM

The earmuff normally consists of a plastic-shell earcup with a cushion sealing it to the flesh around the ear. When the earmuff is worn, an air cavity is created within the ear-cup. This cavity extend into the ear-canal up to the eardrum which represented by a specific impedance ($Z=5026.55\text{Pa.s/m}$). An acoustic pressure wave impinges on the outside surface of the ear-cup, causing it to vibrate. For the earmuff-earcanal system modelled [Vergara(2002)], the

dimensions and the physical parameters are reported in Fig. 1 and Table 1..

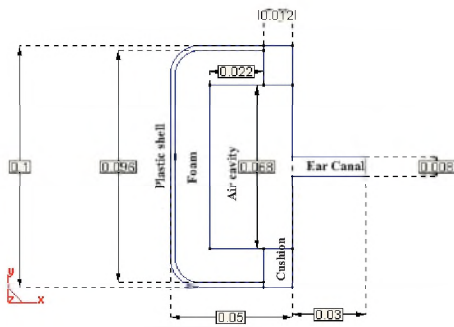


Fig. 1. Dimensions in meters of the earmuff-earcanal system studied.

2.1 Transient response

A triangular pressure impulse simulating gun shot is applied uniformly over the earmuff shell to get the transient response at the eardrum. The assumed pulse shape, presented in Fig. 2, has a rising time of 1 ms and a duration of 3.0 ms. The maximum and the minimum pressure are respectively set to 1130 Pa and -100 Pa. The resulting FEM transient pressure history from the FEM at the eardrum is shown in Fig. 2.

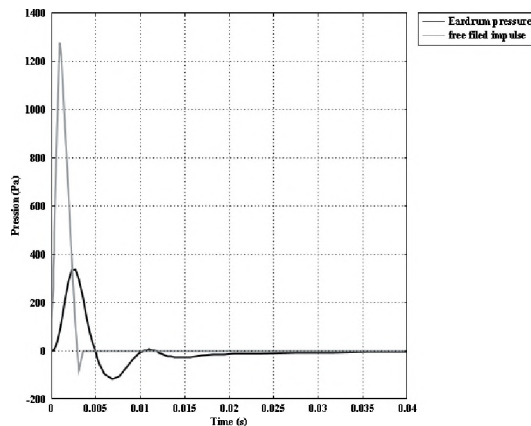


Fig. 2 Pressure vs time histories for the free field excitation and FEM predicted tympanic pressure.

The predicted FEM attenuation provided by the studied earmuff is equal to 12.00 dB which is close to 12.6 dB as measured by Vergara & al [Vergara (2002)]

2.2 Steady state response

The internal pressure level response is predicted at the eardrum over the frequency range of 25Hz to 5kHz (Fig.3). The attenuation of the earmuff is weak around the first resonant 140 Hz of the coupled system. This frequency is very close to the resonant frequency of the structure 141 Hz.

Table 1. Physical properties.

material	Young modulus (Pa)	Poisson coefficient	Density (kg/m ³)	Sound celerity (m/s)
Plastic	$1.94 \cdot 10^{+9}$	0.38	1200	
Foam	$3.34 \cdot 10^{+7}$	0.33	320	
Rubber	$2.5 \cdot 10^{+5}$	0.49	1522	
Air			1.21	343

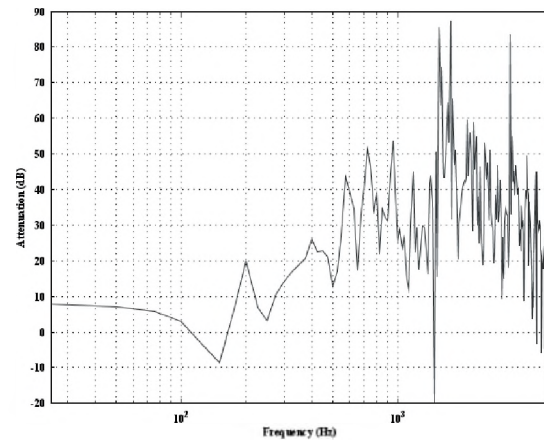


Fig. 3. Steady state response of earmuff-earcanal system for a uniform external pressure.

3. CONCLUSION

A FEM model has been developed to predict the steady-state and transient responses for an earmuff-earcanal system. Good agreement between the model and available experimental data for the configuration studied has been obtained.

REFERENCES

Lee, C.-M.; Royster, L.H.; Ciskowski, R. D. (1995). Formulation for an FE and BE coupled problem and its application to the earmuff-earcanal system. *Engineering Analysis with Boundary Elements*, v 16, no. 4, Dec, 1995, p 305-315.
 Vergara, F.; Gerges, S.N.; Birch, R.S. (2002). Numerical and experimental study of impulsive sound attenuation of an earmuff. *Shock and Vibration*, v 9, n 4-5 SPEC., Cobem 2001, 2002, p 245-251

ADAPTIVE ENVIRONMENTAL CLASSIFICATION SYSTEM FOR HEARING AIDS

Luc Lamarche, Wail Gueaieb, Christian Giguère, and Tyseer Aboulnasr

School of Information Technology and Engineering, University of Ottawa, 800 King Edward Ave., Ottawa ON, K1N 6N5
llama101@site.uottawa.ca

1. INTRODUCTION

Hearing aids are customized for the user's specific type of hearing loss and are typically programmed to optimize each user's audible range and speech intelligibility. There are many different types of prescription models that may be used for this purpose [1], the most common ones being based on hearing thresholds and discomfort levels. Each prescription method is based on a different set of assumptions and operates differently to find the optimum gain-frequency response of the device for a given user's hearing profile. In practice, the optimum gain response depends on many other factors such as the type of environment, the listening situation and the personal preferences of the user. The optimum adjustment of other components of the hearing aid, such as noise reduction algorithms and directional microphones, also depend on the environment, specific listening situation and user preferences. It is therefore not possible to optimize the listening experience for all environments using a fixed set of parameters for the hearing aid. It is widely agreed that a hearing aid that changes its algorithm or features for different environments would significantly increase the user's satisfaction [2]. Currently this adaptability typically requires the user's interaction through the switching of listening modes.

New hearing aids are now being developed with automatic environmental classification systems which are designed to automatically detect the current environment and adjust their parameters accordingly. This type of classification typically uses supervised learning with predefined classes that are used to guide the learning process. This is because environments can often be classified according to their nature (speech, noise, music, etc.). A drawback is that the classes must be specified a priori and may or may not be relevant to the particular user. Also there is little scope for adapting the system or class set after training or for different individuals.

In this paper, an adaptive environmental classification system is introduced in which classes can be split and merged based on changes in the environment that the hearing aid may encounter. This results in the creation of classes specifically relevant to the user. This process would continue to develop during the use of the hearing aid and therefore adapt to evolving needs of the user.

2. METHOD

2.1 Overall System

Figure 1 shows the block diagram for the adaptive classification system. First, the sound signal received by the hearing aid is sampled and converted into a feature vector via feature extraction. This step is a very crucial stage of classification since the features contain the information that will distinguish the different types of environments [3]. The resulting classification accuracy highly depends on the selection of features. The feature vector is then passed on to the adaptive classifier to be assigned into a class, which in turn will determine the hearing aid settings. However, the system also stores the features in a buffer which is periodically processed to provide a single representative feature vector for the adaptive learning process. Finally, the post processing step acts as a filter, to remove spurious jumps in classifications to yield a smooth class transition. The buffer and adaptive classifier are described in more detail below.

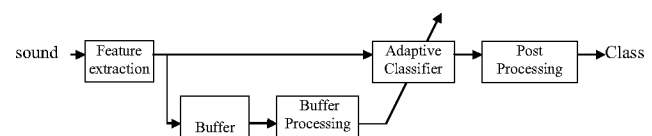


Fig. 1: Adaptive Classification System

2.2 Buffer

The buffer stage consists of an array that store past feature vectors. Typically, the buffer stage can be 15-60 seconds long depending on the rate at which the adaptive classifier needs to be updated. This allows the adaptation of the classifier to run at a much slower rate than the ongoing classification of input feature vectors. The buffer processing stage calculates a single feature vector to represent all of the buffered data, allowing a more accurate assessment of the acoustical characteristics of the current environment for the purpose of adapting the classifier.

2.3 Adaptive Classifier

The adaptive classification system is divided into two phases. The first phase, the initial classification system, is the starting point for the adaptive classification system when the hearing aid is first used. The initial classification system organizes the environments into four classes: speech,

speech in noise, noise, and music. This will allow the user to take home a working automatic classification hearing aid. Since we are training the system to recognize specific initial classes, a supervised learning algorithm is appropriate.

The second phase is the adaptive learning phase which begins as soon as the user turns the hearing aid on following the fitting process, and modifies the initial classification system to adapt to the user-specific environments. The algorithm continuously monitors changes in the feature vectors. As the user enters new and different environments the algorithm continuously checks to determine if a class should split and/or if two classes should merge together. In the case where a new cluster of feature vectors is detected and the algorithm decides to split, an unsupervised learning algorithm is used since we do not have any a priori knowledge about the new class.

3. TEST RESULTS

The following example illustrates the general behavior of the adaptive classifier and the process of splitting and merging environment classes. The initial classifier was trained with two ideal classes, meaning the classes have very defined clusters in the feature space as seen in Figure 2a). The squares in the center of each cluster represent the class centers. These two classes represent the initial classification system. Figure 2b) shows the test data that will be used for testing the adaptive learning phase. As the figure shows, there are four clusters present, two of which are very different than the initial two in the feature space. The task for the algorithm is to detect these two new clusters as being new classes. To demonstrate the merging process, the maximum number of classes is set to three. Therefore two of the classes must merge once the fourth class is detected.

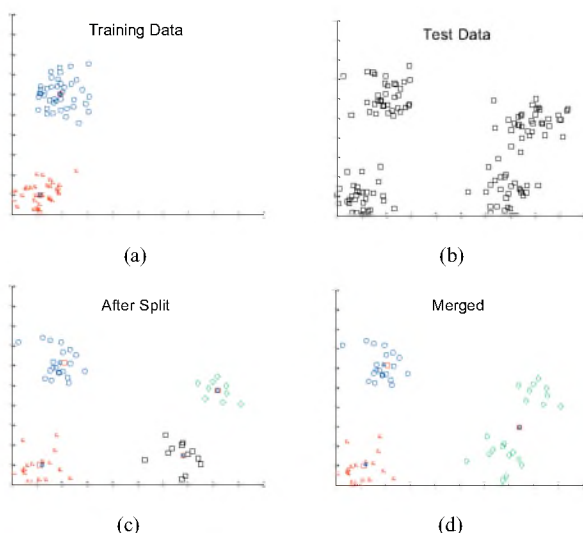


Fig. 2: a) Training data for initial classification; b) Test data for adaptive learning algorithm; c) After splitting two times; d) After merging of two classes

3.1 Splitting

While introducing the test data, a split criterion is continuously monitored and checked until enough data lies outside of the cluster area. This sets a flag that then triggers the algorithm to split the class into two. Figure 2c) shows the data after the algorithm has split and detected the two new classes.

3.2 Merging

Once the fourth cluster is detected and the splitting process occurs, as shown in Figure 2c), the merging process begins where two classes must merge into one. Figure 2d) shows the two closest clusters merging into one, thus resulting with three classes, the maximum set in this example.

4. DISCUSSION

This paper introduced a new adaptive classification system for hearing aids which would allow the device to track and define environmental classes relevant to each user. Once this is accomplished the hearing aid may then aim to learn the user preferences (volume control, directional microphone, noise reduction, etc.) for each individual class. Further work is ongoing to determine the best algorithm for the split and merge process.

REFERENCES

- [1] H. Dillon, *Hearing Aids*, Sydney: Boomerang Press, 2001
- [2] D. Fabry, and P. Stypulkowski. Evaluation of fitting procedures for multiple-memory programmable hearing aids. In: Paper presented at the annual meeting of the American Academy of Audiology, 1992.
- [3] M. Büchler, "Algorithms for Sound Classification in Hearing Instruments," PhD Thesis at Swiss Federal Institute of Technology, Zurich, 2002, no 14498.

ACKNOWLEDGEMENTS

This project is funded under a NSERC CRD research grant.

LEARNING USER VOLUME CONTROL PREFERENCES IN HEARING AIDS

Abimbola Cole, Christian Giguère, Wail Gueaieb, Tyseer Aboulnasr

School of Information Technology and Engineering, University of Ottawa, 800 King Edward Ave., Ottawa ON, K1N 6N5
acole027@site.uottawa.ca

1. INTRODUCTION

It has been reported that many users are not satisfied with their hearing aids and would rather not wear them. Some reasons given are the presence of background noise, no perceived added benefit, discomfort, and the difficulty and frequency in which the volume control of the hearing aid has to be adjusted [1]. This paper focuses on advancements in the learning of user control preferences in order to minimize the amount of adjustments being made to the hearing aids over time. Reducing the need for frequent adjustments would create a better listening experience and draw less attention to the fact that an assistive hearing device is being worn. The gains prescribed during the hearing aid fitting process are a good starting point to compensate an individual's hearing loss. However, these gains still need to be adjusted during follow up visits to the audiologist after being worn in real life situations. This process can be tedious and long for both the patient and clinician. Moreover, optimal gain and other control setting requirements may differ according to the specific environments and listening situations encountered by the user, and it is difficult to resolve these needs in the clinic.

The concept of self-learning hearing aids addresses the issues of fine tuning and optimal adjustment by learning what settings the user prefers in environments that are presented on a daily basis. The device has memory and remembers previous settings. At specified points in time, it adjusts the present settings to some combination of the previous settings. Some research has already gone into this and a few devices with self-learning features are currently on the market. The SAVIA[®] hearing aid from Phonak has a datalogging component that analyzes and stores the volume changes made by the user as they go about their day-to-day activities in each environment. Based on the analysis a volume setting is suggested [2]. The clinician makes a decision on whether or not to include this suggestion at next follow up visits as the device does not automatically update the volume. The CENTRA hearing aid by Siemens is able to learn user preferences for volume in different listening environments. Each time the hearing is turned on it calculates the weighted average of past volume preferences and sets the volume accordingly. The device is typically able to learn the volume preferences for a specific environment on average by the end of the first week [3]. Another hearing aid manufacturer, GN Resound, approaches

this issue in a slightly different way. The gain function of the device is adjusted after each volume control change. Features are extracted from the input signal and used in the Automatic Volume Control (AVC) module to calculate a gain. The gain is applied to the input to produce the output that will be heard by the user. The system absorbs changes in the volume control register every time into the AVC module [4]. The parameters of the AVC are adjusted so that the gains applied will put the input at a level preferred by the user.

Currently, a fixed time constant or weighted average is typically used to learn or memorize past user control settings. This should suffice if all users had the same behavior and if this behavior would be identical in all situations or environments. This, however, is not generally the case, and it would be expected that the optimum time constant for learning should be dependent on the user's behavior and environment. In this research, the use of a fixed time constant was tested in different behavioral scenarios for learning volume control preferences; then three adaptive exponential smoothing algorithms were analyzed. The task was to learn what volume control settings the user prefers in different environments with the goal of being able to predict what the user would like when they re-enter the same environments again. Over the course of the day the user switches between different environments. The device should be able to recommend the best initial setting when the user goes into a specific environment.

2. METHOD

The learning algorithm should be robust enough to learn different user behaviors. In order to test the fixed and adaptive methods, it is necessary to have data and performance measures with which to make comparisons. Real volume control preferences selected by users over time are difficult to obtain; therefore, different user behaviors were simulated in this research to supplement any real data to be collected in the future. A user is assumed to have a desired mean volume control setting and a standard deviation around the mean to generate more or less variability in the user's decisions. The basic behaviors generated are fairly constant, fairly fluctuating and fluctuating user. More complex behaviors were generated as combination of these basic behaviors. The volume control setting profile for each user behavior was made up of

several phases, where the start and end of a phase signify entering and leaving an environment. These behaviors varied in the amount of time the user spends in an environment, the frequency of changing the volume control, the amount of change and variations in the desired mean within a user profile.

The goal of the learning algorithms is to minimize user intervention when entering a new phase in a given environment. A good learning algorithm should reduce the number of times that the user changes the settings. Even if this calculated value is not exactly what the user wants, it should be as close as possible. In the process of learning, the algorithm should adjust according to the data being used in the analysis and should not give one-sided estimates that are consistently lower or higher than the first initial setting by the user. It is with these considerations in mind that four performance error measures were identified. The first error is the average over all phases in a user profile of the difference between the learned value for a phase and what the user actually sets the device to. The second error measures the average bias of the learned value over all phases of the user profile. The third error is the average root mean squared error between the learned volume setting and the actual user settings for a phase. The last error measure is the percentage of phases in a profile for which the learned value and the initial setting by the user differ by more than 3dB.

In analyzing the fixed method, the optimum time constant for each profile was found. This was to investigate if the best time constant would be the same for each user behavior. This also allowed establishing a baseline reference from which to compare the adaptive algorithms. These were modified from their original implementation to update the time constants at the end of each phase and not on each sample point. Also, the update is based on the value of one of the four errors discussed above.

Firstly, it important to confirm that the adaptive algorithms could indeed perform as well the optimum time constant for a given profile. In doing the comparison for a given profile, the parameters for each of the three adaptive algorithms were tuned to the best values for the profile and the four error measures were calculated. This was then compared to the optimum fixed time constant for the profile.

The performance of the adaptive algorithms was also analyzed over a wide range of profiles. The best adaptive parameters on average were used for these tests since, in practice, the clinician might not able to tune the adaptive algorithms for each user. This was compared to the optimum fixed time constant on average over all user profiles.

3. RESULTS AND DISCUSSION

In finding the best fixed constant for the different profiles generated, it was found that the value of this optimum varied, as expected. The range of time constant that performed best was different for the different profiles. No single time constant would be able to minimize the errors for all the profiles. When the optimum parameters for the Taylor and Chow adaptive methods are used, they are able to perform as good as the best fixed time constant on a profile-by-profile basis. Figure 1 below shows the values obtained for error 1 for a given user profile using some fixed time constants (including the optimum one for the profile) and three adaptive methods. The best average parameter values are used in the adaptive methods.

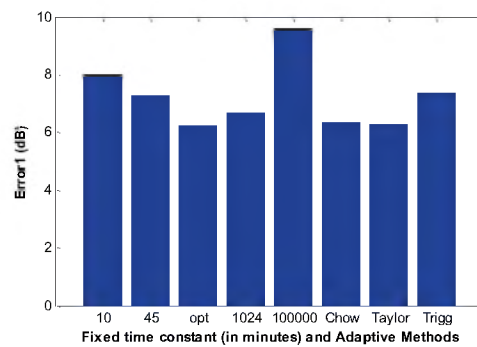


Fig.1. Comparisons of fixed methods and adaptive algorithms using best average parameter values.

It can be seen that very short time constants give a higher error value than the optimum one (about 2 dB). The methods by Chow and Taylor perform as good as the optimum. The simulations carried out show that without having prior knowledge of a person’s behavior, using an adaptive algorithm with a good initialization, hearing aid volume control preferences can be learned as well as if the optimum time constant was used for a particular user.

REFERENCES

- [1] S. Kochkin, “MarkeTrak V – Why my hearing aids are in the drawer: The consumers’ perspective,” *The Hearing Journal*, vol. 53, No. 2 (February 2000).
- [2] D.A. Fabry, “DataLogging: A clinical tool for meeting individual patient needs,” *The Hearing Review* (January 2005).
- [3] Siemens, “DataLearning & Learning VC: Learning Preferred Gain Settings in Everyday Life,” <http://mvsiemens.siemens-hearing.com/admin/documents/08139.pdf> (2006).
- [4] A. Ypma, B. de Vries & J. Geurts, “Robust Volume Control Personalisation from on-Line Preference Feedback,” *IEEE Proc. Signal Processing Society Workshop on Machine Learning for Signal Processing*, Sept. 2006, p. 441-446 (2006).

ACKNOWLEDGEMENTS

This project is funded under a NSERC CRD research grant.

SPATIAL VIBRATION PATTERNS OF THE GERBIL EARDRUM

Nicolas N. Ellaham¹, Fadi Akache², W. Robert J. Funnell^{1, 2}, and Sam J. Daniel²

¹Dept. of BioMedical Engineering, McGill University, Montréal, QC, Canada, robert.funnell@mcgill.ca

²Dept. of Otolaryngology, McGill University, Montréal, QC, Canada

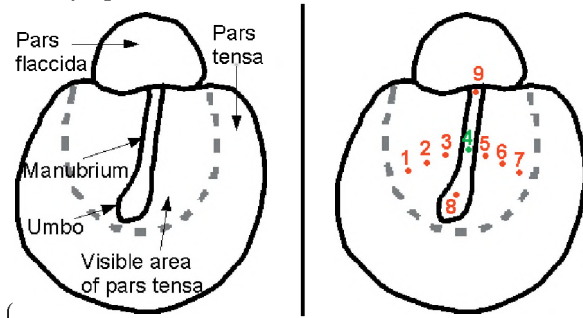
1. INTRODUCTION

Located between the external ear and the inner ear, the middle ear extends from the eardrum to the oval window and includes a chain of three ossicles (malleus, incus and stapes) suspended in an air-filled cavity. The middle ear plays a key role in hearing and is the site of many infections, congenital defects, injuries and other diseases that contribute to hearing loss. To date, non-invasive diagnostic procedures and the quality of middle-ear prostheses are often inadequate. A better understanding of middle-ear mechanics would contribute to advancements in diagnosis and treatment of hearing loss. To this end, many groups have conducted research on mammalian middle ears. Gerbils in particular have become widely used in this field.

Studies investigating eardrum vibrations in mammalian ears have shown simple vibration patterns at low frequencies and more complex ones at high frequencies (Tondorf & Khanna, 1972; Decraemer & Khanna, 1996; Rosowski et al., 2007). The motion of the malleus-incus complex has traditionally been described as a simple rigid rotation around a fixed axis (Békésy, 1960), but studies in cats have shown evidence of shifting of the axis of rotation, and of manubrial bending at high frequencies (Decraemer et al., 1991 & 1994; Funnell et al., 1992). There is, however, a lack of such data for the gerbil.

The use of laser Doppler vibrometry (LDV) has become very common in the study of middle-ear vibrations. LDV is an optical technique used to measure the velocity of a vibrating surface at the nanometer level without mass

After the gerbil is sacrificed and decapitated, the lower jaw is removed to expose the bulla which encloses the middle-ear cavity. The external ear is removed and parts of the bony ear canal are drilled away to maximize exposure of the tympanic membrane and to reveal the umbo



loading. In this work we present LDV measurements at multiple points along the manubrium of the malleus and along a line on the eardrum perpendicular to the manubrium, in order to study the spatial vibration patterns.

2. MATERIALS AND METHODS

Measurements were carried out on 5 Mongolian gerbils (*Meriones unguiculatus*) from Charles-River (St-Constant, QC). The experimental protocol is described briefly here; a more detailed description was given by Ellaham et al. (2007).

Fig. 1). A large hole is drilled in the bulla to equalize the pressures on the two sides of the eardrum, and to permit experimental steps to correct for temporal effects (Ellaham et al., 2007).

Fig. 1). The coupler is an acoustically sealed aluminum cavity. An ER-2 Tube-phone (Etymotic Research) is used for sound delivery and an ER-7C probe-microphone system

The gerbil head is attached to a coupler with dental cement at the opening of the ear canal with an orientation that allows an optimal view of the eardrum

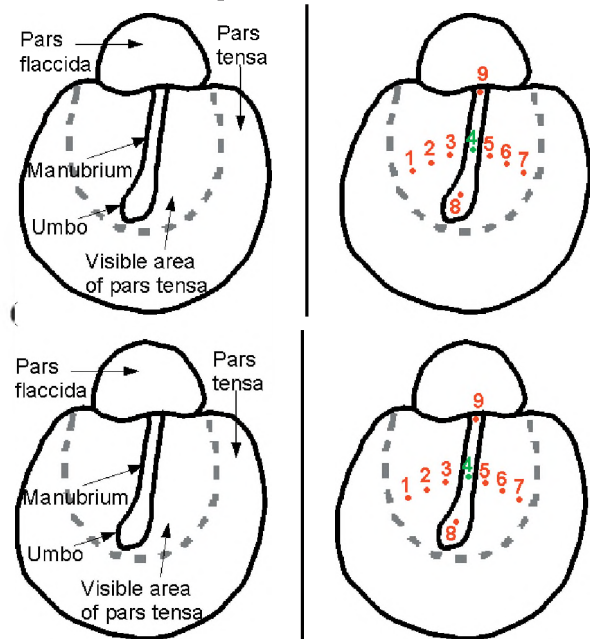


Fig. 1: LEFT: Schematic illustration of the tympanic membrane. Outlined in grey is the area of the pars tensa visible under the microscope. RIGHT: Locations of measurements.

(Etymotic Research) is used to monitor the sound pressure level (SPL) at 2 to 3 mm from the eardrum. A 15-cm PE-50 tube (I.D. = 0.58mm, O.D. = 0.96mm) is used as a vent to prevent static pressure from building up inside the coupler. An antireflection-coated glass window (T47-518, Edmund Optics) covers the top of the cavity. Measurements are performed inside a double-walled sound-proof room (Génie Audio, St-Laurent, QC) to attenuate interference from outside noise.

Fig. 1) to increase reflectivity and thus improve the signal-to-noise ratio (SNR) of the measured signal. Measurements are acquired starting about 2 hours after the animal is sacrificed. The stimulus is a 128-ms sinusoidal sweep over the frequency range of 0.1 to 10 kHz. The displacements acquired are normalized to the SPL and averaged over 100 samples. The frequency responses below 0.15 kHz are not presented because of low SNR's at the lowest frequencies.

3. RESULTS

3.1. Eardrum vibrations

Fig. 2). The frequency response is flat at low frequencies, and features a peak at about 6.5 kHz and a larger peak at about 9.5 kHz. The frequency responses all have a similar shape over the whole frequency range. Displacements measured on the pars tensa are larger than those on the manubrium, with the magnitude increasing with the distance from the manubrium on both the anterior and posterior sides of the eardrum.

A comparison between symmetrically located points on each side of the manubrium reveals that displacements seem to be larger on the anterior side in all specimens studied. In some specimens, measurements were taken in both the

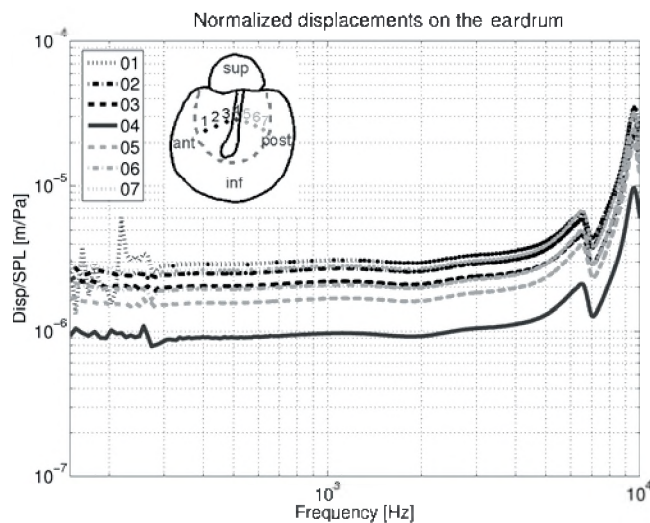


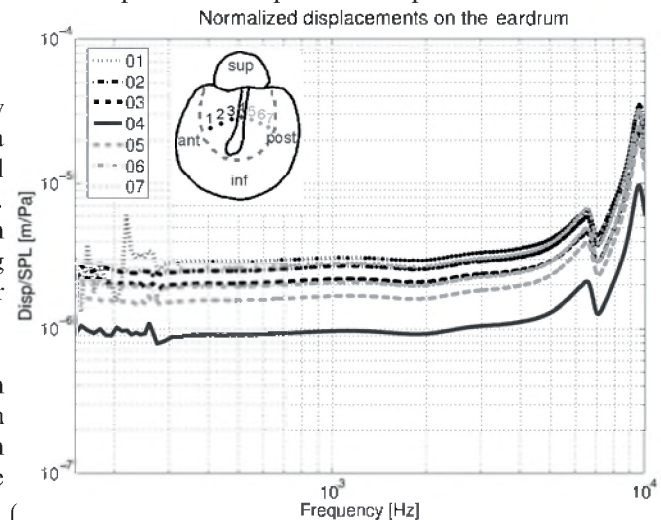
Fig. 2: Normalized displacements on the eardrum. Point 4 is on the manubrium (solid line, dark grey). Measurements on the anterior side of the pars tensa are shown in black, those on the posterior side are shown in light grey, using dashed, dot-dashed, and dotted lines as we move away from the manubrium.

inferior and superior portions of the pars tensa; displacements were found to be larger in the inferior portion.

3.2. Manubrial vibrations

Normalized displacements recorded along the manubrium showed the same frequency-response shape as on the pars tensa. Manubrial displacements are generally largest at the umbo and decrease as the distance from the umbo to the point of measurement increases. In one gerbil, the shapes of the responses change beyond 6 kHz, and over a small range of frequencies (from 8 to 9 kHz) the manubrial displacements at a point superior to the umbo are actually larger than those at the umbo. These discrepancies may be

A large number of measurements was performed on all five gerbils. We present here only the normalized displacements from one specimen, measured across the width of the visible portion of the pars tensa at points 1 to 7

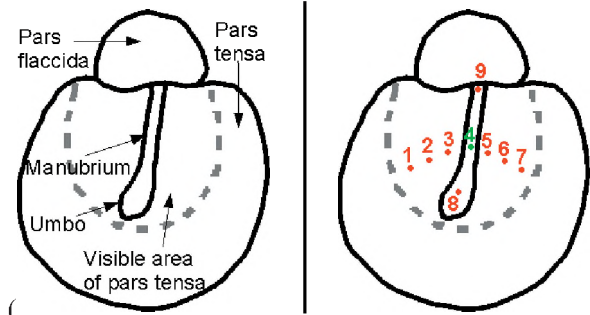


attributable to significant temporal effects in that specimen.

4. CONCLUSION

This paper presents displacement measurements at

This experimental setup is positioned under an operating microscope (OPMI 1-H, Zeiss) mechanically coupled to the sensor head of a laser Doppler vibrometer (Polytec HLV-1000). Glass micro beads (diameter 90-150 μm , Sigma) are placed at the points of measurement



AUDITORY SPATIAL ATTENTION IN YOUNGER AND OLDER ADULTS: A COMPARISON OF LABORATORY AND SELF-REPORT MEASURES

Gurjit Singh and M. Kathleen Pichora-Fuller

Department of Psychology, University of Toronto, 3359 Mississauga Rd N, Mississauga, Ontario, Canada L5L 1C6
Toronto Rehabilitation Institute, 550 University Ave, Toronto, Ontario, Canada M5G 2A2

1. INTRODUCTION

A common situation for most people is to hear sounds coming simultaneously from different sources. Typically, each sound signal originates from a unique point in space. In order to make sense of the wall of sound arriving at our ears, mechanisms of attention serve to select relevant information for further information processing [e.g., 1]. Auditory spatial attention, or the process by which a listener focuses listening resources along a spatial vector to a target, represents one such mechanism [2-3].

Recent investigations of auditory spatial attention have examined the contribution of auditory and cognitive factors to age-related differences in auditory spatial attention [4]. We studied younger adult and older adult listeners with normal audiometric thresholds in the speech range (see Fig. 1) who were simultaneously presented with a target sentence and two competing sentences. All sentences had the structure: “Ready [CALLSIGN] go to [COLOUR] [NUMBER] now” with a closed set of options for callsign (e.g., Baron, Charlie), colour, and number [5]. Each sentence was presented from one of three different loudspeaker locations. Target callsign identity was cued on a visual display either before or after sentences were presented. One of four different probability specifications was visually displayed to indicate the likelihood of the target being presented at the left, centre, and right locations (0-100-0, 10-80-10, 20-60-20, 33-33-33), where 10-80-10 indicated that the target would be presented from the centre location on 80% of the trials and from each of the left and right locations on 10% of the trials.

Figure 2 shows the results from this study. Overall, younger adults outperformed older adults. Collapsing across

all conditions, mean word identification was approximately 6.5% better for younger than for older adults. Furthermore, for both age groups, performance improved with target location certainty and with *a priori* target cueing.

Interestingly, we did not observe a significant interaction of age with location certainty. This is noteworthy because the location certainty manipulation permits the examination of different attentional mechanisms. On trials where location certainty = 0.8 or 0.6, the target sentence would usually be presented from the more likely centre location, but occasionally it would be presented from the less likely, left or right loudspeaker location. Presumably, by inducing spatial expectation, if the target is presented at a ‘likely’ location, listeners are engaged in a focused attention task, unlike when the target is presented from an ‘unlikely’ location, and listeners must ‘shift’ attentional focus between locations, thus engaging attention switching processes.

Comparing performance on likely and unlikely trials, it was found that although younger adults performed better than older adults by an average of 9%, the cost of switching attention was equivalent for older and younger adults, suggesting a lack of age-related differences in the ability to switch attention when listening in a multi-talker environment. This finding agrees with evidence suggesting that for simple tasks, younger and older adults can switch attention equally well [6], but it does not agree with findings of greater age differences in more complex attention switching tasks [7]. In studies of vision, the general finding is that there is a disproportionate age-related difference for

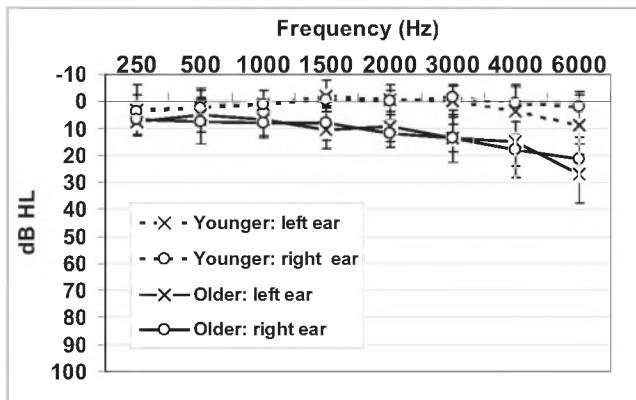


Fig. 1. Mean audiometric thresholds for younger (dashed lines) and older (solid lines) participants. Circles indicate right ears and crosses indicate left ears. Standard error bars are shown.

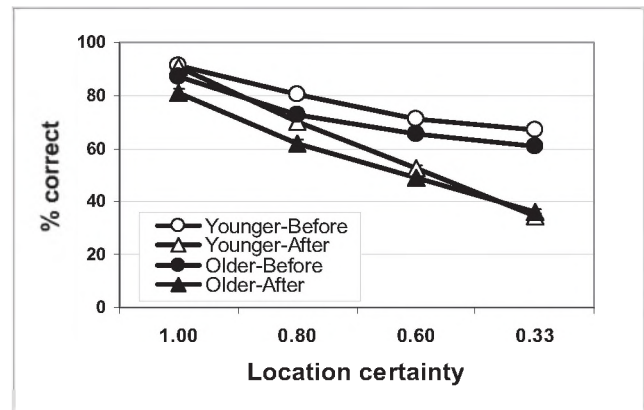


Fig.2. Mean percent correct identification scores and standard errors of the mean for younger (unfilled symbols) and older (filled symbols) adults across the four location certainties. Identification correct is calculated as the percentage of trials where participants identified the colour and number associated with the target callsign. Circles indicate the callsign was cued before stimulus presentation and triangles indicate the callsign was cued after stimulus presentation.

slower, more controlled behaviours, but not for faster, reflexive behaviours. It may be that speech perception in auditory spatial displays is at times relatively simple and/or reflexive and at other times more complex and/or automatic.

The main purpose of this report is to compare this laboratory data with performance on a self-report measure of auditory experience measuring a broad range of hearing functions, the *Speech, Spatial, and Qualities of Hearing* (SSQ) scale [8]. Whereas traditional self-report measures focus on listening situations where sound is predictable in both space and time, the SSQ is designed to address listening in more dynamic listening situations. The SSQ comprises three scales. The first (*speech*) assesses ability to hear speech in a variety of contexts. The second (*spatial*) assesses directional, distance, and movement components of spatial hearing. The third (*qualities*) assesses a range of hearing qualities including segregation (sounds are heard as separate and distinct), clarity, and naturalness. The subscales of the SSQ evaluate more peripheral (e.g., audibility) as well as more cognitively mediated (e.g., divided and switching attention) components of hearing [7].

2. METHOD

2.1 Participants

Participants from the laboratory study [4] also completed this study except for one younger adult and one older adult. Participants were 7 younger (mean age = 24.0 years, $SD = 3.1$) and 7 older adults (mean age = 71.0, $SD = 3.7$). All participants spoke English as a first language, and had pure-tone audiometric thresholds of ≤ 25 dB HL at frequencies from .25 to 3 kHz binaurally (see Fig. 1).

2.2 Questionnaire

After completing the laboratory measures obtained in [4], participants completed the SSQ, usually requiring about 20 minutes. An example question (question 8 of the *qualities* scale) is “When you listen to music, does it sound clear and natural?”. Responses are made on an 11-point ruler scale, where 0 represents a complete inability or absence of a quality, and 10 represents complete ability or presence of a quality. A research assistant was available to respond to questions.

3. RESULTS

3.1 SSQ

Table 1 shows the performance of younger and older adults. Older adults indicated significantly greater impairment on scales measuring *speech* [$F(1, 12) = 7.96, p \leq 0.05$], *audibility* [$F(1, 12) = 7.00, p \leq 0.05$], *divided and switching attention* [$F(1, 12) = 8.09, p \leq 0.05$], *qualities* [$F(1, 12) = 9.36, p \leq 0.01$], and *segregation* [$F(1, 12) = 5.73, p \leq 0.05$].

3.2 Covariate analysis

A final analysis was performed that compared the performance of the age groups on the SSQ, after statistically controlling for binaural pure-tone average (PTA). Older adults reported significantly greater impairment on scales measuring *divided and switching attention* [$F(2, 11) = 3.97, p \leq 0.05$] and *qualities* [$F(2, 11) = 4.41, p \leq 0.05$].

Table 1. Mean (SD) SSQ results. Asterisks indicate significant between-group differences * = ($p \leq 0.05$); ** = ($p \leq 0.01$). Bolded scales indicate significant between group-differences, after statistically controlling for binaural pure-tone average threshold ($p \leq 0.05$)

SSQ Scales& subscales	Younger	Older
<i>Speech</i> *	8.97 (0.57)	7.36 (1.40)
<i>Audibility</i> *	9.41 (0.53)	8.22 (1.07)
<i>Divided/switching attention</i>*	8.52 (0.82)	6.50 (1.69)
<i>Spatial</i>	8.53 (1.10)	7.59 (1.82)
<i>Qualities</i>**	9.35 (0.32)	8.55 (0.61)
<i>Segregation</i> *	9.73 (0.28)	9.29 (0.57)
<i>Clarity and naturalness</i>	9.46 (0.44)	8.06 (1.48)

4. DISCUSSION

The goal of the present study was to compare laboratory measures examining auditory spatial attention with self-report measures of auditory function. In general, the results are in agreement. On the SSQ, older adults reported significantly more trouble on the *speech*, *audibility*, *divided and switching attention*, *qualities*, *segregation*, and *clarity and naturalness* scales (see Table 1). This is comparable to the main effect of age observed in the laboratory [4], whereby younger adults outperformed older adults in all conditions (see Fig. 2). Interestingly, we observed significant age-group differences on the SSQ, despite both groups having ‘normal’ audiometric thresholds in the speech range (see Fig. 1). However, because there were minor between-group audiometric differences, we performed an analysis to statistically control for binaural PTA. Our assumption was that, after accounting for PTA, significant differences tapping more peripheral hearing phenomena (e.g., audibility) should be minimized, but not differences on scales that are less dependent on the cochlea (e.g., the divided and attention switching subscale). This pattern is precisely what we observed. These findings suggest that aspects of divided and attention switching are important contributors to age-related differences in the experience of listening in everyday contexts and environments.

REFERENCES

- [1] Cherry, E.C. (1953). Some experiments on the recognition of speech, with one and two ears. *JASA*, 25, 975-979.
- [2] Spence, C.J., & Driver, J. (1994). Covert spatial orienting in audition: Exogenous and endogenous mechanisms *JEP: HPP*, 20, 555-574.
- [3] Mondor, T.A., & Zatorre, R.J. (1995). Shifting and focusing auditory spatial attention. *JEP: HPP*, 21, 387-409.
- [4] Singh, G., Pichora-Fuller, M.K., & Schneider, B.A. (submitted). Auditory spatial attention in conditions of real and simulated spatial separation by younger and older adults.
- [5] Bolia, R.S., Nelson, W.T., Ericson, M.A., & Simpson, B.D. (2000). A speech corpus for multitalker communications research. *JASA*, 107, 1065-1066.
- [6] Somberg B.L., & Salthouse, T.A. (1982). Divided attention abilities in young and old adults. *JEP: HPP*, 8, 651-663.
- [7] McDowd, J.M., & Craik, F.I.M. (1988). Effects of age and task difficulty on divided attention performance. *JEP: HPP*, 14, 267-280
- [8] Gatehouse, S., & Noble, W. (2004). The speech, spatial, and qualities of hearing scale (SSQ). *IJA*, 43, 85-99.

ACKNOWLEDGEMENTS

This research was funded by CIHR and NSERC.

ACOUSTIC CUES AND RECOGNITION ACCURACY IN CROSS-CULTURAL VOCAL EXPRESSION OF EMOTION

Christopher G. Trimmer, Robin Meyer-MacLeod, Lola L. Cuddy and Laura-Lee Balkwill
Dept. of Psychology, Queen's University, Kingston, Ontario, Canada, 4cgt1@qmlink.queensu.ca

1. INTRODUCTION

Telecommunications play a vital role in today's global culture, and as a result, accurate communication of vocal emotion between distinct cultures has become increasingly important. Based on discrepant findings, two alternative theories of cross-cultural vocal emotion transmission have been put forth (Thompson & Balkwill, 2006). The universal cue theory proposes that basic emotions (anger, joy, fear and sadness) are recognized at above chance accuracy regardless of the encoder's culture and language background, whereas an opposing view states that emotion cues are not universal, and emotion recognition is largely dependent on the culture of the decoder (for a review, see Elfenbein & Ambady, 2002). We investigate this theoretical disagreement by testing participants' recognition accuracy for emotional speech in familiar and unfamiliar languages and paralleling the results with acoustic analyses of the same test stimuli.

A feature of the current study is that English-speaking listeners were asked to rate emotional speech presented in two non-European languages—Mandarin and Dari—as well as in English. Since Mandarin and Dari are geographically and linguistically distinct from English, cultural differences in emotional expression (if they exist) should be most evident for these languages. Also, the present study reversed the design of previous research. Most cross-cultural research designs have presented emotions spoken in one language to many groups and compared recognition across groups (Elfenbein & Ambady, 2002). In the present study, each listener decoded emotion from a variety of cultural groups, and as such, acted as her own control.

It was predicted that English-speaking listeners would recognize basic emotions in each language with above chance accuracy due to the existence of universal cues of emotion expression. A variety of acoustic cues were analyzed to directly compare the cues involved in vocal emotion expressions across cultures. It was anticipated that the pattern of acoustic cues for each emotion would generally adhere to the patterns described in Juslin and Laukka's (2003) review of vocal emotion communication, irrespective of culture. However, it was also predicted that the degree of adherence would vary by culture, which would be a mediating influence in recognition accuracy.

2. METHODS

2.1 Participants

Participants were 30 female Queen's University students (*mean age* = 22, *range* = 18 – 53). All reported normal hearing. All were native English speakers and did not speak or read either Mandarin or Dari.

2.2 Materials

Stimuli consisted of the semantically neutral sentence "The bottle is on the table", uttered in English and, in translation, in Mandarin and Dari. There were 120 utterances formed by the cross-classification of four native speakers of each language x two speaker genders x three languages x five emotions (anger, fear, joy, sadness, and neutral). Each speaker recorded the sentence with intent to express each of the five emotions. Each utterance was confirmed to be a typical display of emotion as judged by an independent female rater native to the relevant culture.

A Power Mac G4 computer running PsyScope X b46 software (Cohen, MacWhinney, Flatt, & Provost, 1993) was used for all stimuli presentation and data collection.

2.3 Procedure

Following demographic data collection, the listening portion of the study was conducted in a sound-attenuated booth with the rating scales presented in PsyScope. Participants were instructed to rate each utterance on four 11-point scales (0 = not present and 10 = extremely present) based on the degree of anger, fear, joy and sadness in the utterances. Participants were not informed about the presence of neutral utterances.

The values on the emotional scales were converted into difference scores using a procedure outlined by Resnicow, Salovey and Repp (2004). The difference scores represent the degree to which an intended emotion was successfully transmitted by an emotional utterance (anger, fear, joy or sadness) relative to a participant's ratings of the neutral utterance. Chance accuracy is zero.

Each utterance was analyzed as a wav file using Praat v 4.5.16 software (Boersma and Weenink, 2005). The acoustic cues analyzed in this study were: speech rate (mean syllable per second), fundamental frequency (mean, median and standard deviation), proportion of pauses, proportion of jitter, first formant (mean and bandwidth) and intensity (mean, median, and standard deviation). These are

commonly analyzed acoustic cues in vocal emotion research (for a review, see Juslin and Laukka, 2003).

3. RESULTS

Recognition accuracy

The descriptive statistics for recognition accuracy for each language and emotion are reported in Table 1. Participants recognized all four emotions in each of three languages with above chance accuracy.

Table 1
Descriptive Statistics of Recognition Accuracy (Difference Score) Across Language and Emotion (n= 30)

Factor	Group	M	SD	Confidence Interval (95 %)*
Language	English	.51	.13	.45 - .55
	Mandarin	.22	.08	.19 - .25
	Dari	.10	.05	.07 - .12
Emotion	Anger	.42	.12	.37 - .47
	Fear	.24	.09	.21 - .27
	Joy	.22	.09	.18 - .25
	Sadness	.22	.09	.19 - .25

Note.* Lower bound of all the confidence intervals is greater than zero indicating that emotional recognition was above chance across emotions and languages.

A repeated-measures analysis of variance was conducted on the difference scores with language (English, Mandarin, and Dari), emotion (anger, fear, sadness, and joy), gender (male, female) and speaker (four speakers) as the experimental factors. There was a significant main effect for language, $F(2, 58) = 248.68, p < .01$, and emotion, $F(3, 87) = 45.69, p < .01$. A paired sample t-test revealed that participants recognized emotion in their own language with significantly higher accuracy than Dari, $t(29) = 17.43, p < .01$, or Mandarin, $t(29) = 16.78, p < .01$, though recognition of Mandarin vocal emotion was significantly greater than Dari, $t(29) = 7.60, p < .01$.

Acoustic cues

Eleven separate mixed-model analyses of variance (emotion as the within-speaker factor, language as the between-speaker) were conducted for each measured acoustic cue to determine whether acoustic cues for an emotion differed across languages. Table 2 shows that significant differences across emotions were found for seven of the eleven acoustic cues. In addition, the analyses of variance yielded several significant interactions between emotion and language.

Further analysis of the variation among languages revealed that acoustic cues underlying perception of pitch and rhythm showed similar patterns across emotions for English and Mandarin, but not for Dari utterances. For example, Figure 1 shows that Dari utterances have little variation in fundamental frequency and percent of pauses across emotions relative to English and Mandarin. Given the low accuracy for which participants recognized emotion in Dari speech, the large deviation of acoustic cue patterns in Dari from English appears to be a likely cause for the decreased recognition of emotion.

Table 2
Analyses of Variance for the Main Effects of Emotion on Acoustic Cues

Cue	Value	F(3, 63)	Partial η^2	p
Speech Rate (syllables/s)	Mean	13.20*	0.68	.01
	Median	14.20*	0.69	.01
Pitch	Mean	13.72*	0.68	.01
	Std. Dev.	5.33*	0.46	.01
Pauses	Mean	16.9*	0.73	.01
Jitter	Mean	2.33	0.27	.11
First formant	Mean	1.72	2.13	.20
	Bandwidth	Mean	3.00	0.32
Intensity	Mean	12.36*	0.66	.01
	Median	6.93*	0.52	.01
	Std. Dev.	0.48	0.07	.70

Note. * $p < .01$

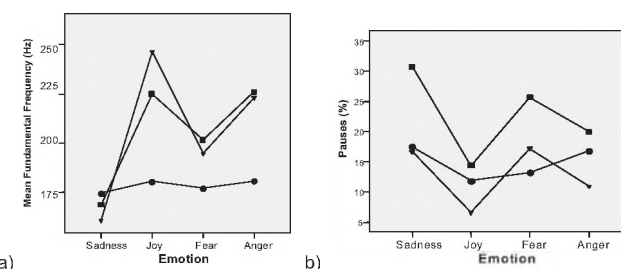


Figure 1 - Measures of (a) mean fundamental frequency (Hz) and (b) percentage of pauses for English, Mandarin, and Dari utterances across the basic emotions [■ English ▼ Mandarin ● Dari]

4. DISCUSSION

All emotions were recognized with above chance accuracy across the three languages. As expected, the English-speaking listeners displayed an in-group advantage in their emotional recognition for English speech compared to Mandarin and Dari. However, the degree to which an individual recognizes emotion conveyed by speech in an unfamiliar culture may be directly related to the acoustic similarities of the expression of emotion in both languages.

REFERENCES

- Boersma, P., & Weenink, D. (2005). Praat: Doing phonetics by computer (version 4.3.21) [Computer software]. Amsterdam, Netherlands: University of Amsterdam.
- Cohen, J. D., MacWhinney, B., Flatt, M., & Provost, J. (1993). PsyScope: A new graphic interactive environment for designing psychology experiments. *Behavioral Research Methods, Instruments, and Computers*, 25, 257-271.
- Elfenbein, H. A., & Ambady, N. (2002). On the universality and cultural specificity of emotion recognition: a meta-analysis. *Psychological Bulletin*, 128, 203-235.
- Juslin, P. N., & Laukka, P. (2003). Communication of emotions in vocal expression and music performance: Different channels, same code? *Psychological Bulletin*, 129, 770-814.
- Resnicow, J. E., Salovey, P., & Repp, B. H. (2004). Is recognition of emotion in music performance an aspect of emotional intelligence? *Music Perception*, 22, 145-158.
- Thompson, W. F., & Balkwill, L.-L. (2006). Decoding speech prosody in five languages. *Semiotica*, 158, 407-424.

ACKNOWLEDGEMENTS

Research supported by NSERC Discovery Grant to LLC.

NON-LINEAR REGISTRATION OF HISTOLOGICAL IMAGES FOR 3-D MIDDLE-EAR MODELLING

Shruti Nambiar¹, Mallar M. Chakravarty^{1,3}, W. Robert J. Funnell^{1,2}, and D. Louis Collins^{1,3}

¹Department of BioMedical engineering, McGill University, Montréal, QC, Canada, robert.funnell@mcgill.ca

²Department of Otolaryngology, McGill University, Montréal, QC, Canada

³McConnell Brain Imaging Centre, Montréal Neurological Institute, Montréal, QC, Canada

1. INTRODUCTION

Hearing loss is the most common sensory impairment. It has been estimated that more than 560 million people worldwide suffer from mild or worse hearing loss (Davis, 1995). Conductive hearing losses involve middle-ear disorders. Advances in otology and biomechanical engineering have led to new surgical techniques and to developments in the design of implantable hearing aids. Further advances will demand detailed analyses of the acoustical and mechanical properties of the middle ear.

A comprehensive and reliable finite-element model of the human middle ear can provide a better understanding of the biomechanics of its many interrelated structures. The middle ear, situated within a physiologically complex milieu, consists of an air-filled cavity extending from the eardrum (tympanic membrane) to the oval window (the interface with the inner ear). The cavity contains three bones, two muscles and several ligaments and other structures. Geometries of models are often based on microscopic X-ray computed tomography (microCT) or magnetic resonance microscopy (MRM). Due to the limited contrast and resolution of these imaging modalities, however, it is not possible to distinguish details like the different tissue types in the ear canal, the fine details of the middle-ear ligaments and joints, and the distinct ossified and cartilage components of the bones. Histological images offer much better image contrast and resolution, and permit one to identify the sub-structural intricacies of the middle ear. Such details are important for realistic finite-element modelling of middle-ear mechanics and acoustics. However, serious spatial misalignments and distortions are introduced at the time of histological tissue processing. The usual approach is to employ a suitable registration technique to account for the misalignments. Various warping strategies are available. Linear transformations are most commonly used to align the images with one another, but this cannot correct for all of the distortions. Non-linear registration techniques also exist and one such algorithm, developed at the Brain Imaging Centre (BIC) at McGill University, has been used for the creation of a brain atlas from serial histological data (Chakravarty et al., 2003). In this paper, we investigate the adaptation of the above non-linear warping algorithm for registration of a human middle-ear histological data set. Preliminary results are presented, with an emphasis on the

long-term goal of obtaining a reliable and refined finite-element model of the human middle ear.

2. METHODS

2.1 Histological data acquisition

The histological data set of the adult human middle ear was acquired from C. Northrop (Temporal Bone Foundation, Boston). The histological block was cut into 20- μ m-thick sections and every tenth slice was stained with hæmatoxylin and eosin to yield a total of 56 slices. Each slice was digitized using a slide scanner to form images of size 3644 \times 2152 pixels. The histological images were then downsampled by a factor of 4 for speed of processing.

2.2 Non-linear registration algorithm

The non-linear warping algorithm used is a variant of the Automatic Nonlinear Image Matching and Anatomical Labelling (ANIMAL) algorithm (Collins and Evans, 1997). The aim is to maximize the slice-to-slice (source-to-target) anatomical consistency between adjacent slices in order to achieve global 3-D consistency. The ANIMAL algorithm defines a 2-D regular lattice of control nodes and computes a vector for each node that maximizes the correlation ratio for the local intensity neighbourhood centred at each of these lattice points. The non-linear spatial registration transformation is computed in a hierarchical fashion: deformations are first estimated on slices blurred with a Gaussian kernel having a large full width at half maximum (FWHM) and then the transformations are further refined by estimating deformations on slices with Gaussian kernels having smaller FWHM's. This blurring is done three times, and for each step the ANIMAL algorithm is applied iteratively. The transformations are represented by deformation fields which are defined to be locally translational, so the deformation vector at each node can be considered independently from its neighbours. This is followed by a smoothing step to ensure continuity of the deformation fields. Both the local and smoothing processes are carried out iteratively to achieve global optimization. The overall optimization is thus achieved by amalgamation of all the local optimizations computed at each lattice point. The quality of the non-linear transformation can be altered by three parameters: the *similarity cost ratio*, the *stiffness* and the *weight*. The transformation thus obtained can be applied to the coördinates of the segmented contours, the surface triangulation of which yields a 3-D model.

3. RESULTS

Here we present preliminary results of the application of the algorithm described above. Sample histological images are shown in the figures to illustrate the registration principle. Fig. 1 shows the source slice, which is registered onto the target slice (Fig. 2). Fig. 3 shows the source slice after registration.

Some of the anatomical parts of the temporal bone are marked in the figures: semicircular canal (a), stapes footplate (b), cochlea (c) and external ear canal (d). The geometry of the stapes footplate in the source slice seems to have been registered well onto the target, as seen in Fig. 3. The smooth rounded outlines of the semicircular canal and cochlea, however, have been seriously distorted, and the region of the ear canal has become smeared.



Fig. 1: Source slice of human temporal bone.

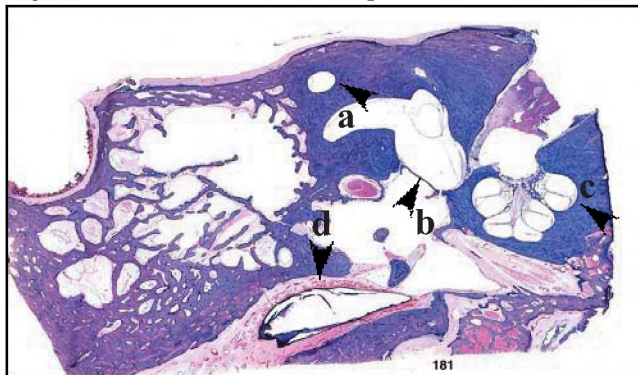


Fig. 2: Target slice.

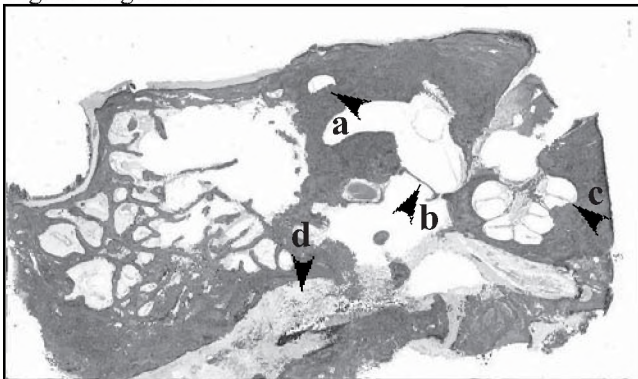


Fig. 3: Registered slice.

4. CONCLUSION

The preliminary application of the registration algorithm led to good results for some structures but poor results for other structures. Various approaches can be taken to improve the outcome. For example, the 2-D slice-to-slice algorithm relies on a set of parameters that was initially optimized by Chakravarty et al. (2006) for certain areas of the human brain (basal ganglia and thalamus). The optimization was done by using an exhaustive search strategy to minimize the mean chamfer distance between the source and target contour data. Redoing this parameter optimization for the middle-ear histological data may allow more successful registrations, leading to more accurate mechanical and acoustical models and thus to new insights into the function of the middle ear.

REFERENCES

Chakravarty, M.M., Bertrand, G., Descoteaux, M., Sadikot, A.F., Collins, D.L. (2003). *The creation of a brain atlas for image guided neurosurgery using serial histological data*. In: Ellis, R.E., Peters, T.M. (Eds.), Fifth International Conference on Medical Image Computing and Computer Assisted Intervention MICCAI 2003, Lecture Notes in Computer Science, Montréal, Canada. Springer, pp. 343–350.

Chakravarty, M.M., Bertrand, G., Hodge, C.P., Sadikot, A.F., Collins, D.L. (2006). *The creation of a brain atlas for image guided neurosurgery using serial histological data*. *NeuroImage*, 30, 359–376.

Collins, D.L., Evans, A.C. (1997). *ANIMAL: validation and application of non-linear registration based segmentation*. *Int. J. Pattern Recogn. Artif.Intell.*, 1271–1294.

Davis, A. (1995): As cited by http://www.hearingreview.com/issues/articles/2006-02_10.asp

ACKNOWLEDGEMENTS

This work was supported by the Canadian Institutes of Health Research and by the Natural Sciences and Engineering Research Council of Canada.

VARIABILITÉ DE L'ATTÉNUATION DES PROTECTEURS AUDITIFS MESURÉE PAR LA MÉTHODE FIELD-MIRE EN FONCTION DE LA DIRECTION DU SON INCIDENT ET DES BRUITS DU PORTEUR.

Marc-André Gaudreau¹, Frédéric Laville¹, Jérémie Voix¹ et Hugues Nélisse²

¹École de technologie supérieure, 1100, rue Notre-Dame Ouest, Montréal, Canada, H3C 1K3, frederic.laville@etsmtl.ca

²IRSST, 505, Boul. De Maisonneuve Ouest, Montréal, Canada, H3A 3C2, nelisse.hugues@irsst.qc.ca

1. INTRODUCTION

Dans le cadre d'un projet de recherche visant à étudier la protection réelle obtenue par les travailleurs en milieu bruyant, certains résultats obtenus lors de tests préliminaires laissent penser que la position de la source de bruit par rapport au sujet pourrait influencer l'atténuation mesurée [1]. La présente étude vise à apporter un éclairage sur l'influence de la position de la source sonore (directivité) sur la mesure de protection obtenue grâce à la méthode F-MIRE (Field Microphone-in-Real-Ear), [2]. L'étude a aussi permis de mettre en évidence l'influence d'autres facteurs tels la variation dans le temps du système porteur-protecteur et l'effet du repositionnement des protecteurs.

2. PROCÉDURES EXPÉRIMENTALES

Deux types de protecteur ont été étudiés, des coquilles de protection E-A-R modèle 1000 et des bouchons moulables SonoCustom (Sonomax santé auditive inc.). Pour chaque oreille, le protecteur est instrumenté d'un doublet microphonique miniature (microphones miniatures de Knowles Acoustics - FG series) permettant la mesure des signaux protégés et non-protégés. Les coquilles ont été modifiées afin d'insérer le microphone à l'intérieur tout en assurant l'étanchéité tandis que les bouchons moulés sont déjà équipés d'un canal de mesure destiné à l'usage du doublet microphonique. Chaque doublet est raccordé à un petit enregistreur numérique deux voies. Le système permet l'enregistrement de fichier en format WAV avec une fréquence d'échantillonnage de 44.1 kHz. Un générateur de bruit et un amplificateur connectés à un haut-parleur ont été utilisés pour générer un bruit rose de 102 dB(A). Les mesures ont été réalisées dans une salle semi-anéchoïque. Le sujet est assis sur une chaise pivotante placée à 1 mètre d'une source fixe. Le principe de la mesure consistait à prendre des enregistrements (environ 8 scc) des signaux protégés et non-protégés pour chaque oreille à différentes positions en faisant une rotation du sujet de 30° entre chaque enregistrement (12 positions pour un tour complet).

Il est fait l'hypothèse que le fait de faire tourner le sujet par rapport à la source est équivalent à faire tourner la source par rapport au sujet. On choisit comme position de référence

le cas où la source est face au sujet (0°). Selon la convention choisie, pour les figures qui suivent, un angle de 90° signifie que la source est pointée vers l'oreille droite du sujet, l'oreille gauche étant cachée derrière la tête du sujet (voir figure 1).

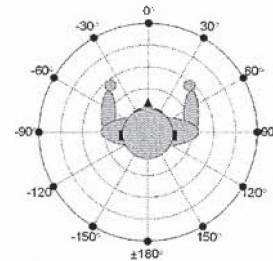


Fig. 1. Positions de la source (•) par rapport au sujet

Les signaux enregistrés sont ensuite analysés à l'aide de routines développées dans MATLAB. L'analyse permet notamment d'obtenir les niveaux de pressions protégés et non-protégés en bande de tiers d'octaves (100 à 10000 Hz) et de les représenter dans les domaines temporel et fréquentiel.

3. RÉSULTATS ET ANALYSE :

Avant d'étudier la directivité de l'atténuation, différents facteurs pouvant influencer les résultats ont été analysés : directivité des microphones, variations dans le temps du système porteur-protecteur et repositionnement des protecteurs.

3.1 Variation causée par la directivité des microphones

Les résultats de mesures de directivité en champ libre des microphones ont confirmé une directivité uniforme, la variation du niveau étant négligeable en basses fréquences et inférieure à 0.4 dB en hautes fréquences (4 kHz).

3.2 Variation dans le temps du système porteur-protecteur

La variation de la protection, pour un sujet et une source immobile, en fonction du temps et en fonction du repositionnement des protecteurs a été analysée en effectuant une série d'enregistrements. Trois

enregistrements espacés d'une minute pendant lesquels le sujet ne devait ni bouger, ni toucher à ses protecteurs ont été réalisés. Deux autres enregistrements ont ensuite été réalisés où le sujet devait enlever ses protecteurs et les repositionner lui-même entre chaque enregistrement. Les résultats sont similaires tant pour les bouchons moulés que pour les coquilles et bien que l'échantillonnage soit faible, les données obtenues dans la présente étude permettent d'observer des variations inférieures à 0.5 dB dans le cas de la répétition des essais dans le temps et des variations de inférieures à 8 dB dans le cas où les protecteurs sont repositionnés. Ces résultats sont en accord avec ceux obtenus par Voix [2].

3.3 Variation de la protection mesurée en fonction de la position de la source (directivité)

La figure 2 montre l'affaiblissement acoustique (noise reduction NR) mesuré avec les coquilles en fonction de l'angle d'incidence pour chaque oreille sur deux bandes de tiers d'octave (500 et 2000 Hz). La source tournant de façon horaire autour de la tête, les données de l'oreille droite ont été inversées (antihoraire) afin que les 2 courbes puissent être directement comparables en fonction d'un même angle d'incidence pour les 2 oreilles.

A 500 Hz, non seulement il a peu de variation du NR en fonction de la position de la source, mais en plus, on retrouve la même valeur de NR autant pour l'oreille gauche que pour l'oreille droite. A 2000 Hz, le NR varie en fonction de la position et de plus, la valeur du NR est différente entre les deux oreilles; cependant, malgré les différences, les deux courbes semblent avoir le même patron de directivité.

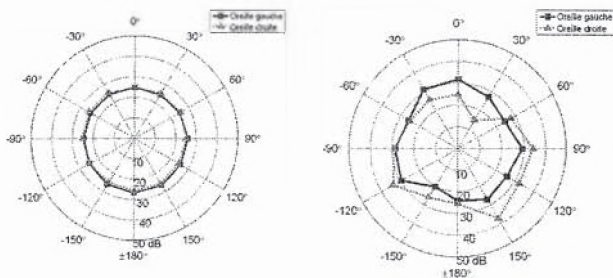


Fig. 2. Affaiblissement acoustique brut ($NR(\theta)$), pour les oreilles droite et gauche, en fonction de la position de la source pour les bandes de tiers d'octave centrées sur : a) 500 Hz; b) 2000 Hz.

Pour mieux observer la directivité, on peut tracer le patron de directivité de l'atténuation sous la forme d'un écart entre le NR à un angle donné et le NR à 0° ($NR(\theta) - NR(0^\circ)$). La figure 3 montre cet écart (qui peut être négatif ou positif) en dB en fonction de l'angle obtenu pour l'oreille gauche avec les coquilles pour différentes bandes de tiers d'octave. On observe que pour les fréquences inférieures à 1000 Hz, le patron de directivité est à toute fin pratique un cercle (peu de variations en fonction de la position), les écarts obtenus

étant manifestement sous les écarts qui peuvent être générés par d'autres facteurs. Lorsque la fréquence augmente, le patron de directivité devient plus complexe et des écarts importants sont observés laissant suggérer que l'atténuation peut dépendre de la position de la source.

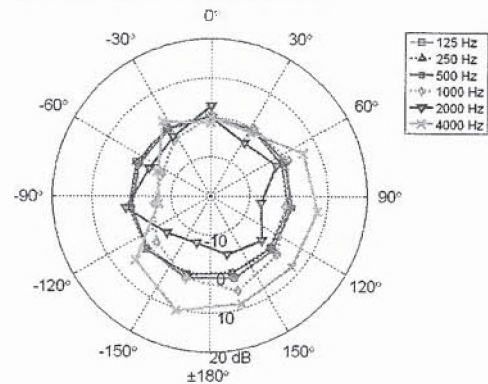


Fig. 3. Écart de l'affaiblissement ($NR(\theta) - NR(0^\circ)$) pour l'oreille gauche avec les coquilles pour certaines bandes de tiers d'octave.

Le même type d'analyse a été effectué sur les bouchons moulés et des résultats semblables ont été obtenus, le patron de directivité montre, par contre, des variations plus faibles que pour les coquilles.

4. CONCLUSION

Des mesures en laboratoire ont permis de mettre en évidence que l'atténuation obtenue par des protecteurs auditifs dépend de la position de la source par rapport à la tête du porteur. Ces variations sont supérieures aux variations dues à d'autres facteurs (directivité des microphones, variation dans le temps du système porteur-protecteur). Les résultats obtenus pour les deux types de protecteurs testés suggèrent : a) une variation significative de l'atténuation en fonction de la position de la source pour des fréquences supérieures à 1000 Hz; b) une variation plus importante dans le cas des coquilles que dans le cas des bouchons. Ces premiers résultats, qui restent à être confirmés par des études approfondies, montrent d'ores et déjà que la directivité de la protection auditive est un facteur à prendre en compte dans les études sur la protection réelle obtenue en milieu de travail.

RÉFÉRENCES

- Nélisse, H., et al. *A Preliminary Study on the Measurement of Effective Hearing Protection Device Attenuation During a Workshift*. in *Noise at Work 2007*. 2007. Lille, France.
- Voix, J., *Mise au point d'un bouchon d'oreille "intelligent"*. Thèse de doctorat, 2006, École de technologie supérieure Montréal, 223 p.

REMERCIEMENTS

Les auteurs remercient l'IRSST pour son soutien financier et Sonomax santé auditive pour son soutien logistique.

A FIELD STUDY OF PREFERRED LISTENING LEVELS FOR MUSIC PLAYED ON PERSONAL STEREO PLAYERS

Frank A. Russo¹, Mohammad Abdoli-E², Zizhen Lu², & Ahlexxi Jelen¹

¹Dept. of Psychology, Ryerson University, Toronto, Ontario, Canada, M5B 2K3; russo@ryerson.ca

²School of Occupational and Public Health, Ryerson University, Toronto, Ontario, M5B 2K3

1. INTRODUCTION

Over the last decade, audio devices and music consumption habits have changed dramatically. Larger amounts of music are being consumed via Personal Stereo Players (PSPs). These portable devices allow continuous playback of large collections of music. Public concern over the extent to which PSP use represents a hearing health risk has increased rapidly, and some manufacturers have responded by making volume limiters available. Although the level of risk is difficult to assess and will likely remain controversial, it may be particularly acute for at least a subgroup of listeners who have a preference for high music levels (Ahmed et al., 2007). Laboratory studies indicate that the risk level may be further exaggerated in noisy environments (Ahmed et al., 2007; Hodgetts, Rieger, & Szarko, 2007). Preferred music listening levels tend to be higher in high background noise environments than in low background noise environments. This study provides ecological validation of these laboratory findings by demonstrating a relationship between music level and background noise level in the field. Simultaneous recordings were made of PSP sound output levels and ambient noise levels in three environments in the city of Toronto: the subway (TTC), a busy street corner (Dundas Square), and a university library (Ryerson).

2. METHOD

2.1 Participants

Previous research has shown that earphone type influences PSP sound output levels (Filgor & Cox, 2004). Samples were thus limited to listeners using insert earphones (i.e., earbuds). Our sample of 75 participants included 46 men and 29 women with an average age of 24.6 years (SD = 7.04).

2.2 Procedure and Apparatus

Potential participants were approached in the same environment in which recordings were made. The initial contact was made nonverbally by gesturing for the user to remove the earphones. The majority of users followed the nonverbal request by removing one or both of the earbuds. Those users who manipulated sound levels in addition to or instead of removing the earbuds were not considered in the final sample. Thus, the reported sound level measurements reflect actual listening levels.

All music and background noise level measurements were based on 10-second samples obtained from consenting PSP users. Music levels were obtained by porting headphone-out of the PSP directly to mic-in of laptop and applying a correction factor to approximate the sound level that would be obtained with earbuds (some variability exists across manufacturers). Background noise levels were obtained with a Bruel and Kjaer preamplified microphone (model 2671) that was connected to the same laptop via a National Instruments analog input module USB-9233 4-Channel, +5V, 24-Bit IEPE. Music and background noise levels were obtained simultaneously.

3. RESULTS

Mean and standard deviation of music level and background noise level (dBA) in each environment is displayed in Figure 1. Music levels were highest in the street (M = 96.61; SD = 15.14), and were comparable in the subway (M = 77.10; SD = 16.83) and the library (M = 76.29; SD = 15.36). Background noise levels were highest in the subway (M = 77.68; SD = 4.54), lowest in the library (M = 58.71; SD = 2.58), and intermediate in the street (M = 69.30; SD = 5.09).

Music levels were significantly higher than background noise levels in the street, $t(25) = 6.88, p < .0001$, and in the library, $t(18) = 4.85, p < .0001$, but there was no significant difference in the subway, $t(29) < 1$.

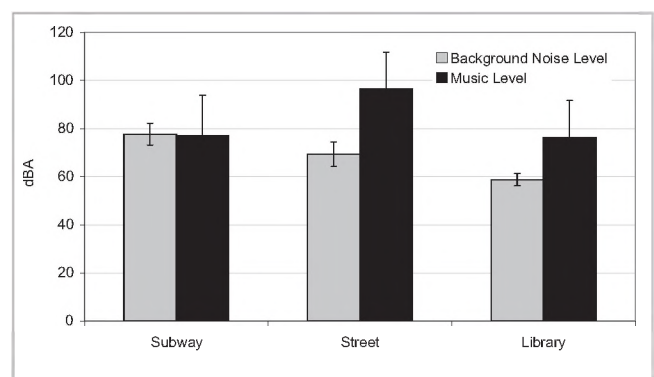


Fig. 1. Background noise and music levels (dBA) in three environments. Error bars represent standard deviation.

It is interesting to note that music levels in the subway and library did not differ significantly, $t(47) < 1$. This pattern of results might be interpreted to suggest that background noise level has no influence on preferred music listening

levels; however, there are numerous social factors that likely moderate the effect of background noise level, making comparisons across environments misleading.

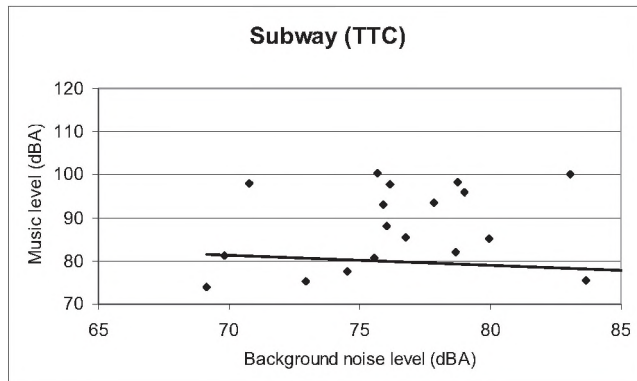


Fig. 2. Background noise and music levels (dBA) in the subway environment, $r(28) = -.07$, n.s.

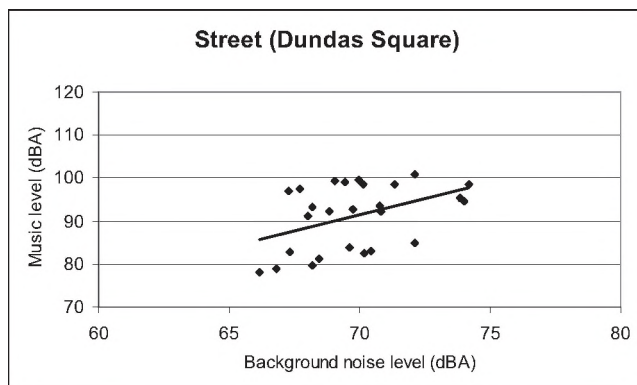


Fig. 3. Background noise and music levels (dBA) in the street environment, $r(24) = .43$, $p < .05$.

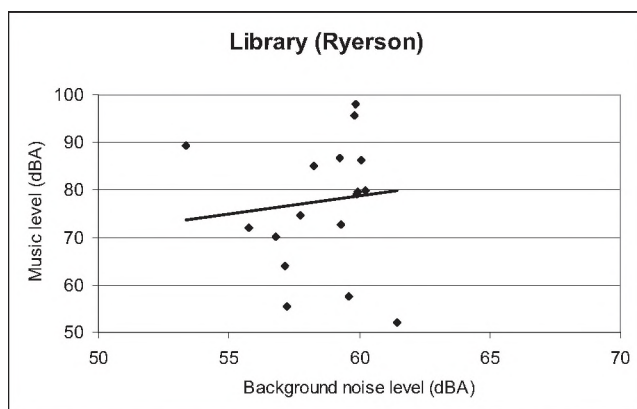


Fig. 4. Background noise and music levels (dBA) in the library environment, $r(17) = .11$, n.s.

Scatter plots comparing music level and background noise level for each environment are provided in Figure 2 (subway), Figure 3 (street) and Figure 4 (library). A significant correlation between music level and background

noise level may only be observed in the scatter plot for the street environment.

4. DISCUSSION

The highest music levels were observed in the street environment. A substantial percentage of the measurements obtained in the street (42.3%) revealed dangerous listening levels (>94 dBA) that would present a hearing health risk for exposures in excess of 1-hour per day (NIOSH). These music levels are considerably higher than preferred listening levels obtained in laboratory studies utilizing background traffic noise. The lower preferred listening levels observed in laboratory studies may reflect a bias towards pleasing the experimenter and/or the absence of visual clutter.

Preferred music listening levels were higher than background noise levels in the street and library but not in the subway. The subway environment is unique in that people tend to be stationary and in very close proximity to one another. These factors may lead some PSP users to be self conscious about their music listening levels. Although social expectations may also constrain the preferred listening levels in the library environment, PSP users have more flexibility to isolate themselves.

Social expectations in the urban streetscape are minimal and the movement of pedestrians provides an acoustic blanket of anonymity. Indeed, a significant correlation between background noise levels and music levels was only observed in the street environment.

REFERENCES

- Ahmed, S. A., Fallah, S., Garrido, B., Gross, A., King, M., Morrish, T., Pereira, D., Sharma, S., Zaszewska, E., & Pichora-Fuller, M. K. (2007). Use of portable audio devices by university students. *Canadian Acoustics*, 35, 35-52.
- Filgor, B. J., & Cox, L. C. (2004). Output levels of commercially available portable compact disc players and the potential risk to hearing. *Ear and Hearing*, 25, 513-527.
- Hodgetts, W. E., Rieger, & Szarko, R. A. (2007). The effects of listening environment and earphone style on preferred listening levels of normal hearing adults using an MP3 player. *Ear and Hearing*, 28, 290-297.

ACKNOWLEDGEMENTS

We thank Gabe Nespoli for his assistance with data collection and preparation.

UNIVERSAL ACCESSIBILITY AND USABILITY FOR HEARING: CONSIDERATIONS FOR DESIGN

Daniel Fok¹, Lynn Shaw², Mary Beth Jennings³ and Margaret Cheesman³

¹Faculty of Health Sciences, Health & Rehabilitation Sciences Program, The University of Western Ontario.

²Faculty of Health Sciences, School of Occupational Therapy, The University of Western Ontario.

³Faculty of Health Sciences, National Centre for Audiology, The University of Western Ontario.

1. INTRODUCTION

Hearing loss is the most prevalent and fastest growing sensory-related chronic disability in North America. Despite this trend, the accessibility and usability for hearing in community and public spaces is severely underemphasized in research and practice. Traditionally, designs for persons with disabilities in the built environment have focused on removing physical barriers through barrier-free design ideology. For the past decade, the universal design (UD) movement has played an instrumental role through informing building and product standards and policies. However, like its predecessor, UD concepts and their application have largely remained restricted to physical, and to a lesser extent, visual domains. Considerations for universal accessibility and usability for hearing in the built environment, by a person with or without a hearing loss, continues to be deficient. In this article, an interdisciplinary team of researchers draw attention to the need for a companion guideline to the original UD principles as it relates to hearing.

1.1 Universal Design

The term “universal design” was coined by the late Ron Mace whose work inspired architects and many other professionals to think beyond the boundaries of barrier-free design. According to Mace, Hardie and Place (1991), universal design means designing all products, buildings and exterior spaces to be usable by all people to the greatest extent possible without special adaptations. UD principles include: (1) equitable use; (2), flexibility in use; (3) simple and intuitive use; (4) perceptible information; (5) tolerance for error; (6) low physical effort; and (7) size and space for approach and use (The Center for Universal Design, 1997). Although all seven principles should be considered for designs, from the authors’ perspective, four of these are particularly relevant for activities that involve hearing. First, principle (1) elaborates that designs should avoid segregating or stigmatizing any users. This is consistent with assistive technology literature which has shown that designs that segregate or stigmatize the user are likely to be abandoned. Although this may be less of a problem for contemporary hearing aids that have small and highly marketed mainstream form factors, other hearing technologies such as FM systems are sometimes left unused or are abandoned as they stigmatize along with requiring training and or a cumbersome set of steps to operate and use (Lederman & Hendricks, 2003; Myers, 2003). Principles (3)

and (6) also speak to this latter point. In many cases, these *end-of-pipe* solutions are implemented to compensate for a failure to consider factors such as building acoustics and other assistive listening systems during the initial design phase. Second, from principle (2), the idea of choice in the methods of use is an important notion for hearing accessibility and usability. Third, principle (4) draws attention to the idea of using different modes for redundant presentation of information. Good examples to demonstrate this principle are the various applications of captioning technology to present visual along with auditory information, on the television, during a presentation and most recently, on the telephone. Finally, under principle (5), the idea of discouraging unconscious action that require vigilance is also important and needs to be put in the context of the sensory task of hearing.

2. AN OCCUPATIONAL APPROACH

The development of this initial set of universal design for hearing (UDH) guidelines used an occupational approach focused on what people do, need to do, and want to do, in community and public environments where hearing activities take place. An occupational approach helps to understand how people *do* or participate in everyday life but also what constrains participation in occupations. As such, an occupational approach considers the complexity of interactions between person, environment, occupation (Law et al., 1996) and objects (Hocking, 1994). Hamilton (2004) also underscores that humans need to be occupied in a diversity of spaces, and that places shape what we do, or can do, over the course of a lifetime. In essence, participation in occupations is vital to health and quality of life (Wilcock, 1998). It follows that the lack of accessible and usable spaces can limit participation in daily, work and enjoyment occupations. Thus, occupational relationships and concepts can provide a backdrop for critically examining how environments support or hinder hearing accessibility and usability for persons who engage in community occupations (e.g. banking and grocery shopping) and use public spaces (e.g. train stations and airports).

This project enacted a participatory action method to bring together experts and consumers to critically analyze the literature, develop an evidence-based guideline for creating hearing accessible spaces in the community and validate it with consumers and stakeholders. To date, an interdisciplinary team of researchers from the fields of

human factors, audiology, hearing science, occupational therapy and occupational science drew upon their unique disciplinary knowledge as well as an occupational approach, to come up with an initial set of UDH guidelines that warrants further discussion, refinement and validation.

3. PRELIMINARY THEMES

Preliminary themes written in the form of initial UDH guidelines include:

- (i) Design hearing environments that maximize the capabilities of a person to hear without a hearing device or with their current hearing device
- (ii) Optimize object-person interactions for hearing
- (iii) Consider designs that require low cognitive and physical effort
- (iv) Allow for choice of interaction
- (v) Design environments that support single-function or multi-functions, to allow for a range of planned or unplanned occupations that involve hearing

4. DISCUSSION

In this section, the authors will briefly discuss how the occupational approach was used, and will further emphasize it as a potential conceptual framework that may be adopted by related practicing professionals for the analysis of occupations that involve hearing. Based on the wording of (i) the authors emphasized the importance of considering environmental factors and their interactions with the person and objects. The interaction between the environment and the occupation(s) is more explicitly stated in (v). One of the key points in guideline (i) is that individuals should not be expected to obtain a new hearing device in order to participate and engage in occupations in a given environment. The design of the built environment should benefit most if not all individuals to hear better regardless of their hearing abilities. Examples of factors that should be considered include: reverberation, background noise and intelligibility.

In guideline (ii), the interaction between persons and objects are highlighted. Designers, engineers and architects need to be mindful of the positioning and maintenance of objects that generate unwanted noise like lights, fans and HVAC systems and that the impact of these for persons with hearing loss are far greater than can be predicted from persons with good hearing abilities. The relative distance between the person and the desired noise source (e.g. objects like loudspeakers) must also be considered.

The idea of choice was further developed from UD principles and examined through an occupational approach. All forms of interpersonal interaction needs to be considered as the preclusion of any particular method may affect individual experience and participation. Depending on the situation, a built environment may need to afford one-to-one, one-to-many and many-to-one hearing and

communication activities. Other related central notions include the choice of interaction across and in different contexts.

Finally, being able to hear in a built environment should not be a chore. A person should be able to walk into an environment and be able to hear the necessary information right away without having to expand considerable, or ideally any, cognitive or physical efforts, before, during or after the occupation involving hearing. The design of spaces for participation in community based occupations needs to become more seamless. The potential for integration of extant (e.g. inductive loop) and emerging technologies (e.g. Bluetooth, ultrawide band) in the appropriate context presents exciting, disciplinary, interdisciplinary and inter-professional possibilities and challenges to all stakeholders including, but not limited to, end-users, designers, engineers, architects, legislators and health professionals.

REFERENCES

- Hamilton, T. (2004). Occupations and places. In C.H. Christiansen & E.A. Townsend (Eds.), *Introduction to occupation: The art and science of living* (pp. 173-196). Upper Saddle River, NJ: Prentice Hall.
- Hocking, C. (1994). A model of interaction between objects, occupation, society and culture. *Journal of Occupational Science*, 1(3), 28-45.
- Law, M., Cooper, B., Strong, S., Stewart, D., Rigby, P., & Letts, L. (1996). The Person-Environment-Occupation model: A transactive approach to occupational performance. *Canadian Journal of Occupational Therapy*, 63, 9-23.
- Lederman, N. & Hendricks, P. (2003). Induction loop assistive listening systems: A venerable technology meets the new millennium. *Seminars in Hearing*, 24(1), 81-92.
- Mace, R., Hardie, G. & Plaice, J. (1991). Accessible environments: Toward universal design. In W.E. Preiser, J.C. Vischer, E.T. White (Eds.), *Toward a more humane architecture* (pp. 1-49). Reinhold, NY: Van Nostrand Reinhold.
- Myers, D. (2003). The coming world of hearing-aid-compatible assistive listening. *Hearing Loss*. November/December, 22-26.
- The Center for Universal Design. (1997). The principles of universal design (version 2.0). Raleigh, NC: NC State University.
- Wilcock, A. (1998). *An occupational perspective of health*. Thorofare, NJ: Slack.

ACKNOWLEDGEMENTS

The first author would like to acknowledge funding support from the Mary Horney Fellowship in Rehabilitation administered through the Aging, Rehabilitation and Geriatric Care Program at Lawson Health Research Institute, St. Joseph's Health Care - Parkwood Hospital.

CHANGING STATE AND THE IRRELEVANT SOUND EFFECT

Aimée M. Surprenant¹, Ian Neath¹, and Tamra J. Bireta²

¹Dept. of Psychology, Memorial University of Newfoundland, St. John's, NL, Canada, A1B 3X9 asurpren@mun.ca

²Dept. of Psychology, The College of New Jersey, Ewing, NJ, USA, 08628

1. INTRODUCTION

When a stream of irrelevant sound is present during an immediate memory task, serial recall is typically impaired even when the to-be-remembered items are visual. This “irrelevant sound effect” (ISE) is very robust and the magnitude of the typical effect can be large (Beaman & Jones 1997; LeCompte & Shaibe, 1997; Surprenant, LeCompte, & Neath, 2000). The semantic content of the irrelevant speech (Salamé & Baddeley, 1982) and the phonological similarity between the irrelevant speech and memory items (LeCompte & Shaibe, 1997) seem to have little effect on the amount of disruption.

Not all irrelevant auditory stimuli will cause an ISE, however. There is much less disruption when the irrelevant sound consists of a single, repeated item compared to the case in which the irrelevant sound is changing. A steady-state stimulus of any kind, such as a repeating vowel or a continuous pitch glide, does not cause a decrease in performance (Beaman & Jones, 1997; Jones, Macken, & Murray, 1993). This “changing state effect” has been identified as a critical feature in producing an ISE.

Unfortunately, despite numerous attempts, there is still no clear definition of what ‘changing’ is, other than in intuitive terms; for example, white noise ‘changes’ less than tones which ‘change’ less than speech. The current experiments were designed to explore the definition of ‘changing’ relating to the dynamic spectral and temporal properties of the irrelevant stimuli.

Fluent speech varies over time on a number of different dimensions, the most salient of which are frequency and amplitude. The approach we have taken in this research is to begin by taking a stimulus that we know results in an ISE and constructing a new stimulus that varies by the same amount on one of those dimensions while keeping the other dimension constant.

We started by looking at amplitude variation and created an irrelevant stimulus that was equated for amplitude modulation with the base sound but that had no changes in frequency. This “envelope stimulus” was constructed by outlining the amplitude envelope of the base passage and then replacing the time-varying frequency information with a pure tone or white noise. Essentially we kept the amplitude-modulated segment of the signal but replaced the frequency-modulated elements with a static stimulus. Thus,

the only difference between the base passage and the envelope stimulus are the changes in frequency. If ‘changing’ means changes in amplitude over time, an equally amplitude-modulated irrelevant sound should result in an equal decrement in recall.

In subsequent experiments we tested the effect of backward speech and sinewave speech modeled after the base stimulus. Backward speech has segmental and suprasegmental properties that are very different from those of forward speech; however, it retains similar phonetic and temporal information. A sinewave speech stimulus is constructed by replacing the noise in speech formants with sinewaves at the center frequency of the formant. The stimulus changes in frequency at the same rate as the base stimulus and has similar suprasegmental (prosodic) features but contains little or no phonetic information and is seldom even identified as a speech sound (Remez & Rubin, 1990).

2. METHOD

Subjects. Thirty different Purdue University undergraduates participated in each experiment.

Materials. The to-be-remembered stimuli were random permutations of the letters F K L M R X Q (the dissimilar letters from Colle & Welsh, 1976).

The irrelevant sounds were all modifications of the base sound consisting of a passage (in German) from *Die Wilden* by Franz Kafka recorded by a female talker. This passage was modified by: Experiment 1) outlining the amplitude envelope of the German passage and replacing the time-varying frequency information with a 400 Hz pure tone; Experiment 2) using the same technique except filling the envelope with white noise; Experiment 3) playing the base stimulus backward; Experiment 4) replacing the base stimulus with forward and backward sinewave speech constructed from the base stimulus. The sinewave speech was constructed by performing an LPC re-synthesis on the base stimulus in order to extract the formant values for the first three formants. These were then converted to sinewave speech using sinewave speech source code obtained from Ellis (2005).

Design. The design was within-subjects with each participant receiving twenty-five trials of each of three conditions; no noise and two types of irrelevant sound (depending on the experiment). The order of presentation of

the three conditions was random.

Procedure. Each letter was shown in the middle of a computer monitor for 1 s. On irrelevant sound trials the sound was played through headphones at a comfortable level and subjects were instructed to ignore the sounds. After the final letter was shown, seven response buttons became active and were labeled with the seven letters in alphabetical order. The subjects were asked to indicate the presentation order by clicking on appropriately labeled buttons on the screen using the mouse.

3. RESULTS

Figure 1 shows the results from Experiments 1-2. There was a small ISE in the tone condition but, upon examination of the spectrogram, it appeared that there was some spurious frequency modulation in the stimulus. This was not the case for the white noise envelope stimuli and did not give rise to an ISE. It is clear, therefore, that amplitude changes, by themselves, do not play a large part in the 'changing state' effect.

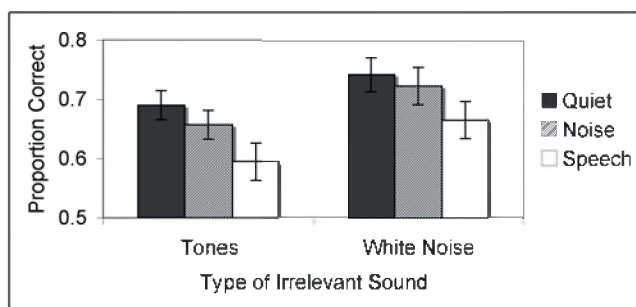


Fig. 1. Mean proportion correct as a function of type of irrelevant speech for Experiments 1-2.

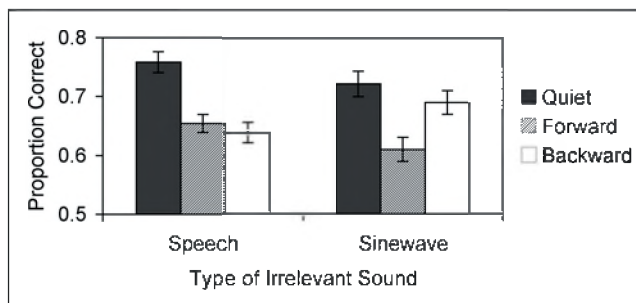


Fig. 2. Mean proportion correct as a function of type of irrelevant speech for Experiments 3-4.

Figure 2 shows the results of Experiments 3-4 in which the irrelevant stimuli included backward speech and forward and backward sinewave speech. The natural speech (both forward and backward) significantly disrupted performance on the memory task but the sinewave speech had an effect only when it was played forward.

4. DISCUSSION

The data from Experiments 1 and 2 are consistent with a great deal of speech perception research that shows

that in perceiving speech, the perceiver uses the coherent pattern of frequency variation and gross signal energy, but probably gets rather little information from tracking the precise details of the energy envelope (Remez and Rubin, 1990). Change in amplitude by itself gives little or no information about the content of the stimulus and, therefore, does not attract much in the way of attentional resources.

The backward speech used in Experiment 3 has segmental and suprasegmental properties that are very different from those of forward speech; however, it contains similar phonetic and temporal information. In contrast, the sinewave speech from Experiment 4 has similar segmental properties and similar temporal information as natural speech but very different phonetic information. Backward sinewave speech has little in common with speech with very little recognizable phonetic information, a very different prosodic form, and no apparent segmental properties. It is perhaps perceived rather like a continuous pitch glide which does not result in an ISE (Jones, et al., 1993).

Thus, it seems that in order to produce an ISE the stimulus must hold some informational value for the listener.

REFERENCES

- Beaman, C. P., & Jones, D. M. (1997). Role of serial order in the irrelevant speech effect: Tests of the changing-state hypothesis. *Journal of Experimental Psychology: Learning, Memory, and Cognition*, 23, 459-471.
- Colle, H. A., & Welsh, A. (1976). Acoustic masking in primary memory. *Journal of Verbal Learning and Verbal Behavior*, 15, 17-32.
- Ellis, D. (2005, March 28). Sinewave speech analysis/synthesis in Matlab. Retrieved July 24, 2007 from <http://labrosa.ee.columbia.edu/matlab/sws/>
- Jones, D. M., Macken, W. J., & Murray, A. C. (1993). Disruption of visual short-term memory by changing-state auditory stimuli: The role of segmentation. *Memory & Cognition*, 21, 318-328.
- LeCompte, D. C., & Shaibe, D. M. (1997). On the irrelevance of phonological similarity to the irrelevant speech effect. *Quarterly Journal of Experimental Psychology*, 50A, 100-118.
- Remez, R. E. & Rubin, P. E. (1990). On the perception of speech from time-varying attributes: Contributions of amplitude variation. *Perception & Psychophysics*, 48, 313-325.
- Salamé, P., & Baddeley, A. D. (1982). Disruption of short-term memory by unattended speech: Implications for the structure of working memory. *Journal of Verbal Learning and Verbal Behavior*, 21, 150-164.
- Surprenant, A. M., LeCompte, D. C., & Neath, I. (2000). Manipulations of irrelevant information: Suffix effects with articulatory suppression and irrelevant speech. *Quarterly Journal of Experimental Psychology* 53A, 325-348.

ACKNOWLEDGEMENTS

We gratefully acknowledge the assistance of Don Gallant in constructing the envelope stimuli.

ECHO CONTROL IN VoIP

Samy El-Hennawey, Ph.D., P.Eng., SM-IEEE
Nortel - Enterprise Solutions
Belleville, Ontario, Canada, K8N 5M1
Email: hennawey@nortel.com

1. INTRODUCTION

Echo control in public-switched telephone networks (PSTN) using echo cancellers have been exercised for nearly the past 40 years. While a great deal of success has been achieved, the recent deployment of voice over the Internet protocol (VoIP) equipment has faced additional challenges. As it is well known, perception of echo and its annoyance is a function of the level of echo as well as its associated round-trip delay. While the percentage of all-PSTN calls that requires echo control is relatively very small, all VoIP calls need echo control due to the inherent latency of all VoIP calls accessing any 2-wire connection including PSTN. As such, echo cancellation is an inevitable functionality of any voice media gateway.

2. SOURCES OF ECHO

In telephone conversation, there are primarily two classes of echo. The first class is due to the use of a 2-to-4 wire conversion using hybrid circuits. Echo control of this class is achieved by a line echo canceller (LEC). The other class is due to the use of handsfree mechanisms where there is significant acoustical feedback coupling between the receiver speaker and the receiver microphone. Echo control of this class is achieved using an acoustic echo canceller (AEC). This paper is primarily concerned with the first class. Additional sources of echo need to be dealt with the LEC as shown in Figure 1 below.

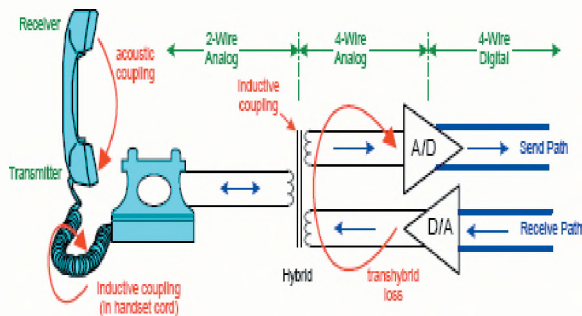


Figure 1 Echo Sources

3. ROUND-TRIP DELAYS IN VoIP

In any VoIP call, voice is packetized either at the IP-phone itself or in the voice gateway. While voice packets

can vary in duration, a typical value is 20 milliseconds. At each side of the IP network of the call, a jitter buffer is part of the receiver to account for the asynchronous reception of the packets due to passing through the IP network. A typical inserted delay in the jitter buffer is twice the packet size, i.e. about 40 milliseconds. The path of the speech packets through the IP network involve many switches and routers and as such will encounter additional delays. Noting that echo encounters both ways, it is the round-trip delay and its typical value is in the neighborhood of 200 milliseconds. In reality, one should expect longer round-trip delays. It is well known that the maximum round-trip delay NOT needing any echo control is approximately 50 milliseconds. Therefore, the use of echo cancellation is inevitable when there is echo.

4. PERCEPTION OF ECHO

As mentioned earlier, the perceived annoyance of echo is a function of the echo level in dB as well as the round-trip delay. Figure 2 below depicts the level of annoyance with these two parameters.

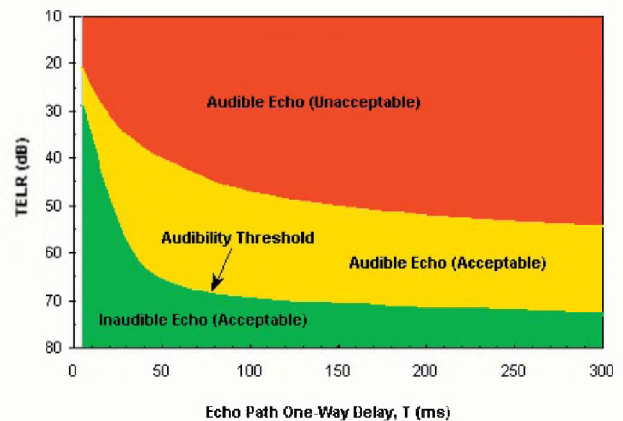


Figure 2 Echo Perception

With the minimum round-trip delay of 200 milliseconds, and with the help of Figure 2, the “total echo loss rating (TELR) has to exceed 55 to 70 dB, with the upper range meant for high-profile users. This definitely represents a major challenge facing LEC designers. Achieving this level of cancellation using fixed-point DSP techniques in an adaptive filter is rather impossible. Therefore, echo suppression mechanisms are used in

addition to the adaptive filter operation for better cancellation. This is done by using a non-linear processor (NLP) that is activated only when the signal coming is only echo, i.e. the person at the other end is not talking. This mandates the existence of a double-talk detector and a sophisticated NLP mechanism. NLP has become a standard module of an LEC as shown in Figure 3 drawn from the G.168 Recommendation of the ITU-T.

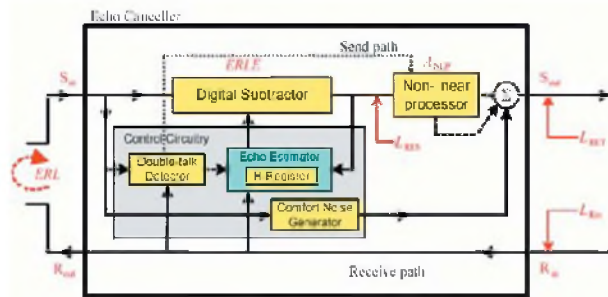


Figure 3 The Line Echo Canceller Modules

The design of double-talk detectors is another challenge for VoIP gateway design. On one hand an aggressive operation of the NLP will lead to cut or clip portions of real speech from the other end. This leads to double-talk choppiness distortion that is very annoying. On the other hand, a very lenient NLP operation leads to echo leakage in single-talk, which is also very annoying. Most double-talk detectors are energy-based. With the non-homogeneous loss plan with a wide variety of call scenarios in addition to the interruptability caused by the long delay add to the challenge.

5. ADDITIONAL CHALLENGES

Conferencing also represents a major challenge to the LEC designers. Some conference participants are IP phone users and others are connected to the bridge from the PSTN through a voice gateway. The number of PSTN participants could be large and each of them usually joins the conference bridge at a different time. Each PSTN participant then may have a different echo path with different loss and round-trip delay. This means the LEC initially adapts to the first PSTN participant echo path. Each time a new PSTN participant joins the conference bridge the overall echo path changes with possible dispersion different from the previous ones. This mandates the use of either a very long tail delay full filter LEC or sparse LEC. In both cases, a re-training procedure has to take place that may cause echo to occur for some duration of time. In the case of full filter LEC, the number of filter coefficient becomes too large which will slow the speed of convergence, hence possibility of echo leakage for longer duration of time. In the case of sparse LEC, a new allocation of window is needed for one or more participants depending on the new dispersion location(s). This adds to the complexity of the canceller hence limiting the channel capacity.

Another challenge seen in deploying VoIP with voice gateways to interface with PSTN is that some PSTN local loops have peculiar characteristics. Some local loops are nonlinear in nature and if this nonlinearity is significant the LEC will be unable to cancel echo efficiently unless using an aggressive NLP with its associated choppiness possibility. Some other local loops are seen to use pair gain technique where some very primitive cancellers are used. This results in canceller tandeming. The voice gateway will track the other primitive canceller and thus seeing a time-varying echo path. This will eventually lead to longer convergence time and as such more leakage of echo or choppiness if an aggressive NLP operation is used.

6. ECHO MEASUREMENT

With multi-vendor networks, it is expected to have the DSP module of the voice gateway manufactured by a different vendor than the network management and QoS monitoring module. Therefore, it is highly desirable to measure echo at the end user of an IP phone. One way to achieve this is through the use of the RTCP-XR protocol of the IETF. However, this relies on the LEC itself for estimating the echo leakage. Another more efficient process is developed at Nortel to provide a complete suite of impairments measurement located at the end user of an IP phone. An important impairment, that is to be measured, is echo with its echo path loss and its associated round-trip delay. The effect of each impairment on the voice quality is reported along with the overall quality measure based on the mean opinion score (MOS). More details can be found in the references provided. The work is also being discussed for the new P.CQO Recommendation of the ITU-T that is in progress.

7. DEMONSTRATION

During the presentation of the paper, it is intended to provide demonstrations of some calls recorded in real life at customer sites showing some of the challenges faced the deploying team. As well, a simple demonstration will be given to illustrate the effect of echo amplitude and delay in the perception of echo.

REFERENCES

- M.S. El-Hennawy, R.A. Goubran, L. Ding, A. Radwan, "Non-intrusive single-ended voice quality assessment in VoIP based on voice payload", United States patent application filed by Nortel Networks on June 15, 2005.
- M.S. El-Hennawy, R.A. Goubran, L. Ding, A. Radwan, "Method and Apparatus for Non-Intrusive Single-Ended Voice Quality Assessment in VoIP", European Patent Application: WO2006136900, Publication Date: December 28, 2006.
- L. Ding, M.S. El-Hennawy and R.A. Goubran, "Nonintrusive Measurement of Echo-Path Parameters in VoIP Environment", IEEE Trans. on Instrumentation and Measurement, Vol. 55, No. 6, December 2006.

THE CHALLENGE FOR TELECOM INDUSTRY IN THE ACOUSTIC AND NETWORK ECHO CANCELLER

Qu Gary Jin

Zarlink Semiconductor, Ottawa, Ont., Canada K2K 3H4, gary.jin@zarlink.com

1. INTRODUCTION

The echo cancellation has been a major challenge for the voice quality in telephone conversation since the phone was invented 100 years ago by Alexander Graham Bell. The real progress was made about 50 years ago when the LMS adaptive algorithm was introduced. At first, the algorithm is thought too expensive and complicate to be implemented. In the last few decades, the semiconductor industrial experienced a dramatic technology revolution. The processor speed doubles and memory size halves every 18 months. Now, the adaptive algorithm can be easily implemented in silicon and telephone voice quality improved dramatically. In the mean time, the telecom industrial raises the standard bar again. About 20 years ago, we were starting to talk about full-duplex conversation.

In general, the adaptive algorithm is a linear echo cancellation algorithm; it can model a linear echo path and cancel the echo if both echo and far-end signals are independent Gaussian white signals. However, the echo path is not a linear time-invariant system and speech is strongly correlated signal. The residual echo can still be heard after adaptive echo canceller. How to get rid of the remaining echo while maintain the far end speech and background noise (or music) untouched is still a challenge problem. Today, IP phone is widely used and the conversation delay increases with IP network. This means that a much smaller residual is required for the same speech quality because the human tolerant to the speech distortion is inversely related to the delay between speakers.

On another front, wireless mobile phone is also widely used. In many countries, it becomes mandatory requirement that the phone in the car has to be handsfree. We all know that the loud background noise in the car makes conversation and echo canceller very difficult. These are all challenges we are going to face in today's echo canceller.

With Zarlink Semiconductor TruePlex technology, we are designing echo cancellation chip to give the best speech quality under server environment and with minimum cost.

2. Zarlink Truplex Technology

Zarlink Trueplex Echo canceller technology is shown in Fig.1. Trueplex is patented technology provide a

real (True) Full-duplex conversation with both network and acoustic echo cancellation.

The major function blocks are as follows:

Linear adaptive filter is the main filter which emulates the linear echo path to cancel the majority of echo in the received path. This filter can be either LMS based or RLS based linear adaptive filter.

Non-linear echo canceller is to cancel some non-linear components in the echo so that the residual can be further reduced by 10dB+. This will emulate the non-linear behavior of the echo with a non-linear gain being added for different signal level. This can also being done in frequency domain with sub-band decomposition.

Noise Reduction (NR) is to reduce background noise to make speech more understandable. This is especially important in the mobile phone where noise power is much stronger than speech. The common used noise reduction method is spectral subtraction. In the spectral subtraction method, the signal is first being decomposed into different sub-band, the noise power is measured in each sub-band and then subtracted from the signal spectrum.

Equalizer (EQ) is to adjust low end and high end frequency response and also to compensate resonance. In general, the speaker driver is highly non-linear with signal level at some frequency. The Equalizer will identify these frequency and put appropriate gain for different frequency band.

Nonlinear Processor (NLP) is to further reduce echo residual and also maintain far end speech undistorted and background noise uninterrupted. NLP is the last stage of echo canceller and any small amount of echo has to be eliminated and in the mean time, make an intelligent decision which part of speech is echo and which part is incoming speech. The remaining echo residual is very small but also very difficult to cut out without interrupt the incoming speech signal.

Automatic Level Control (ALC) is to automatic adjust speech to a comfortable level no matter the speaker speaks load or soft, or is far away or close to microphone. At low SNR cases (SNR=-20dB), the ALC has to make sure the microphone is not saturated with sudden burst noise such as when window is opened while car runs on high way.

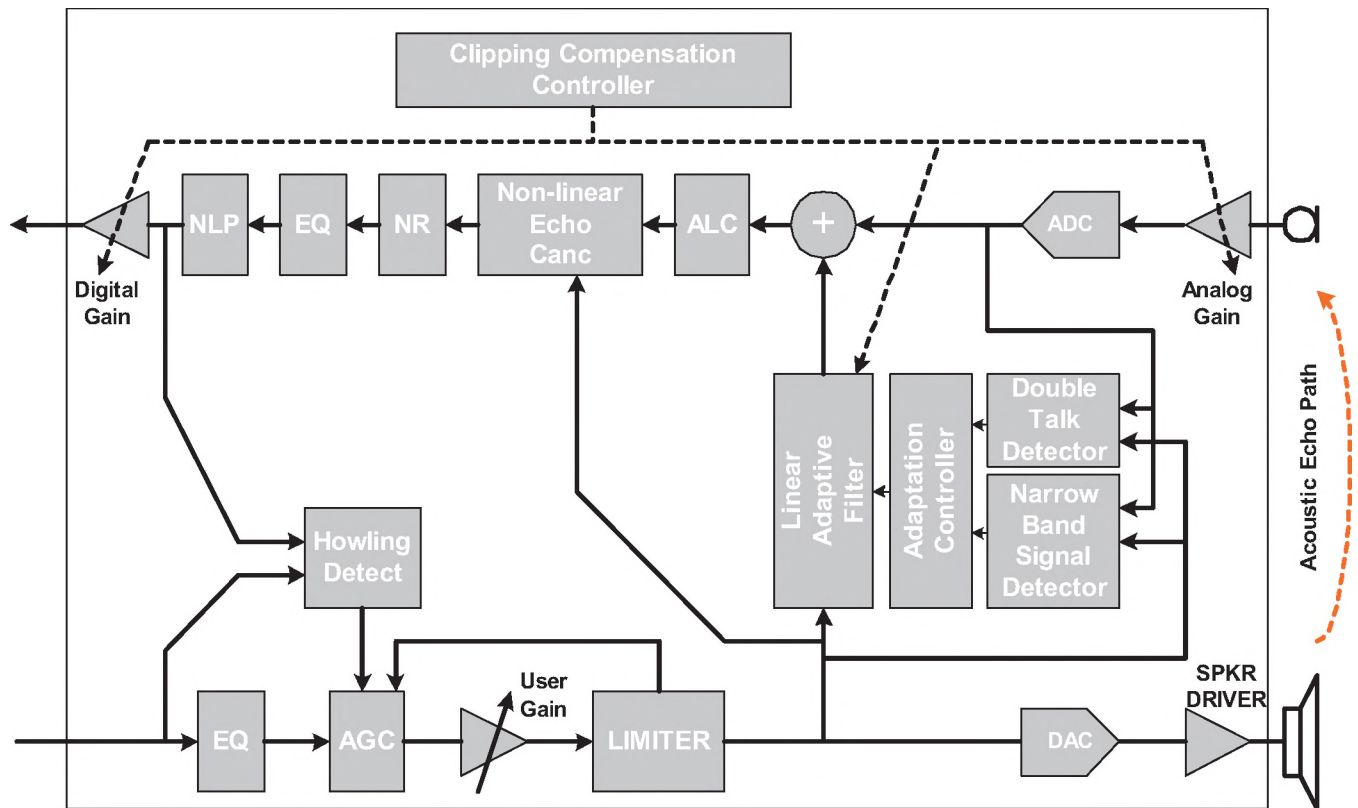


Fig.1 Zarlink Trueplex Technology

Narrow Band Signal Detection is another function block controlling filter adaptation to avoid filter divergence when narrow band tones are sent on either end of communication channels.

Clipping Compensation exchange codec gain with a digital gain so that the microphone will not clip under server condition such as when the car window is opened on the high way during the conversation. It also maintains the original speech level when the background noise is cancelled and environment changes.

Automatic Gain Control (AGC) automatically adjusts the speaker volume for the best conversation and echo cancellation.

Output Limiter emulates DAC clipping so that the adaptive filter still see a linear echo path even the speaker clips.

Anti-Howling controls the loop stability during initial convergence or when echo path changes. It includes two parts: howling detector and howling gain control. When the loop stabilized, the howling gain should be release to 0dB.

Double Talk Detector is to detect whether far end speaker is talking or not. The purpose is to stop adaptation (or control its step size) during double talk to avoid filter divergence. It also controls NLP so that the non-linear processor wouldn't cut a lot of far end speech.

All these function blocks make our chip to fully cancel the echo without affecting the incoming speech quality under server condition such as lower than -20SNR and enhanced echo return of 10dB.

REFERENCES

- ITU-T G.168. (2004). Digital network echo cancellers.
- ITU-T G.VED (2004) Draft Recommendation G.VED (Voice Enhancement Devices).
- Q.Jin, G.Reesor and T.Qian (2003), "Double-Talk Insensitive Normalized Least-Mean Square (DNLMS) Algorithm for Acoustical Echo Cancellation", US patent #US6608897B1.
- Q.Jin, G.Reesor and T.Qian (1999), "Advanced Non-Linear Processor for Acoustic Echo Canceller", France Patent,#FR2770361.
- Q.Jin and G.Reesor (2000), "Tone and Periodical Signal Detection", US Patent, #US6122652.

PREDICTION OF NOISE GENERATED BY A CABIN OUTFLOW VALVE USING THE STAR-CD CODE

George Waller,

Bombardier Aerospace, 123 Garratt Blvd., ON, CANADA, M3K 1Y5 e-mail:George.Waller@aero.bombardier.com

1. INTRODUCTION

Cabin comfort is a paramount concern for business aircraft design. To maintain cabin pressures at equivalent to 8000 feet above sea-level whilst flying at 45000 feet requires careful maintenance of the airflow exhausting from the cabin. This is normally achieved using a servo-controlled flap outflow valve, such as that shown in Figure 1. Unfortunately the air pressure ratio across the outflow valve can be as high as 7, so a lot of shock and screech noise can be generated as well as the jet noise from the highly separated flow behind the valve.

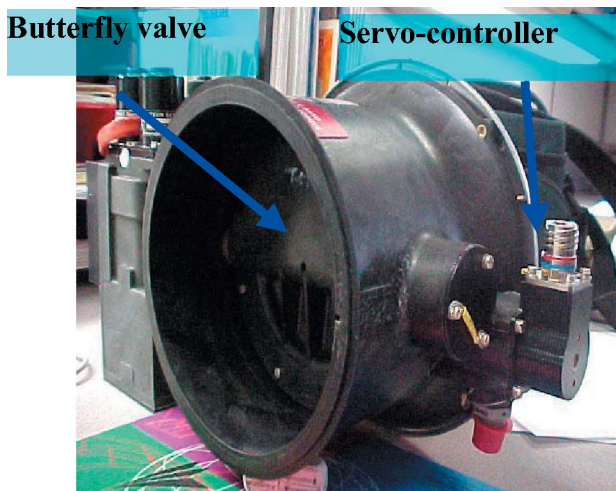


Fig. 1. Cabin outflow valve

As part of a noise reduction exercise on a business jet, noise measurements were made on a rig consisting of a full-scale outflow valve exhausting horizontally through a circular steel plate, with 4 microphones centered on the exhaust plane, as shown in Figure 2.

Commercial Navier-Stokes codes have been used for computational aero-acoustic (CAA) predictions for flows around bluff bodies, internal flows and fans. It was decided to use the STAR-CD code to predict the noise of the outflow valve at sub-critical pressure ratios. The flow is of the jet-type i.e. dominated by quadrupole noise sources due to the turbulent shear stresses. This would be a good validation case similar jet flows found in aircraft systems such as APU exhausts.

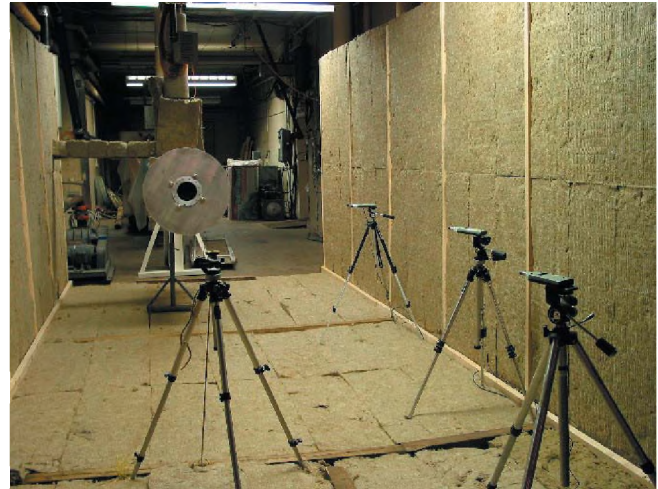


Figure 2. Cabin outflow valve noise measurement

2. STAR-CD Computation

STAR-CD is a commercially available thermofluids analysis system developed by the CD-adapco Group. The solver is an implicit finite-volume method, with pressure calculated from a pressure correction equation using the SIMPLE algorithm. The user can select either a high or low order spatial discretisation scheme and either a fully implicit or a second-order Crank-Nicholson temporal discretisation scheme. For the outflow valve case spatial discretisation used MARS (monotone advection and reconstruction scheme) and the Crank-Nicholson second-order time marching scheme. The solver used an AMG (algebraic multi-grid) method to solve the linear equations.

The unstructured grid used prism and tetrahedral cells, with a total of 4.98×10^6 cells, with the majority of the cells clustered around the butterfly valve and downstream over the region of the jet as shown in Figure 3. An initial, steady state solution was run at a pressure ratio of 1.43. The turbulence was modeled using a detached eddy simulation (DES) based on a modified Spalarat-Allmaras turbulence model. The unsteady solution used a time-step of 1.0e-05 seconds, run for 6000 iterations.

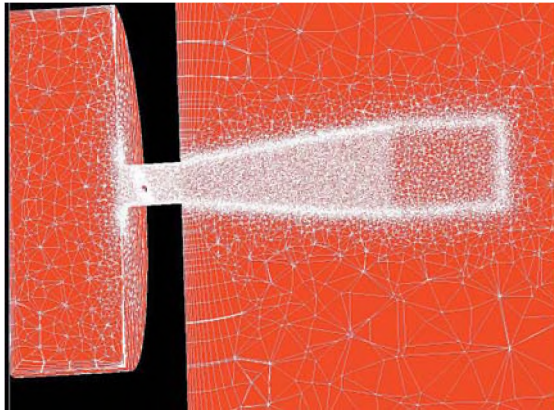


Figure 3 Outflow valve mesh

The unsteady velocities on a survey plane surrounding the exhausting jet were recorded at every time step. An integral acoustic code, based on the porous Ffowcs Williams-Hawkings method¹, was written to predict the far-field acoustic pressures at the microphone positions. The results at the closest microphone position are shown in Figure 4. The results for the first 0.02 seconds were assumed to be affected by the start up transients of the calculation and were discarded. The pressures were converted to the frequency domain using a Hanning window with a 64 Hz bandwidth, to match the experimental results.

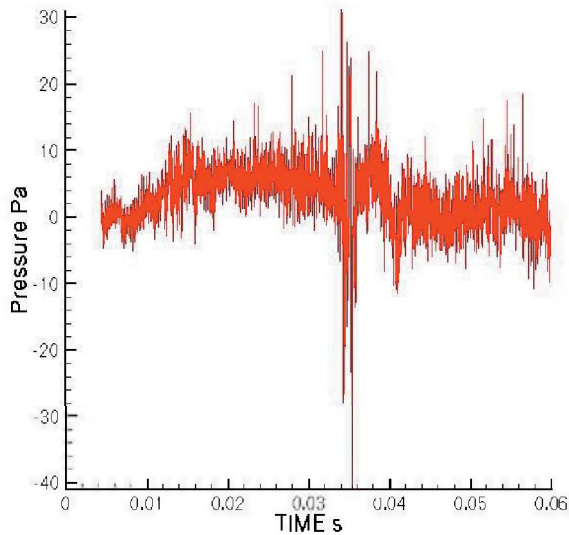


Figure 4 STAR-CD unsteady pressure prediction

3.RESULTS

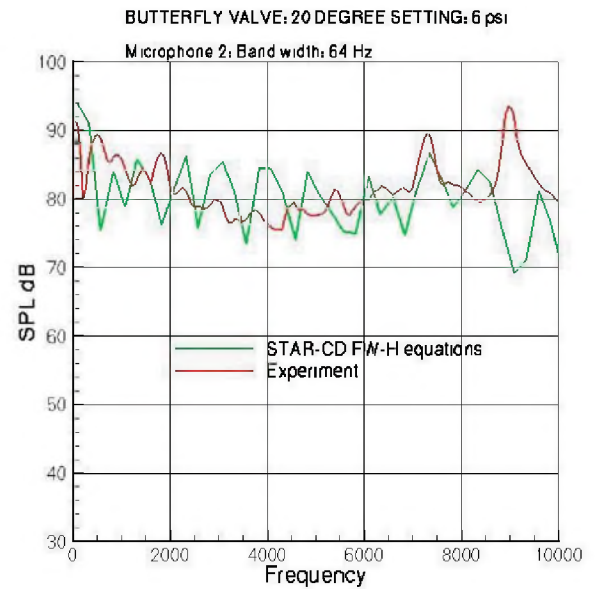


Figure 5 STAR-CD noise prediction at microphone 2

The predicted noise compared to the measured noise at the second microphone position, starting from the closest microphone to the valve as shown in Figure 2, is shown in Figure 5. The agreement is good up to all but the highest frequency, 9kHz, where STAR-CD does not capture a local peak. The results at higher pressure ratios showed this peak developing into a screech tone, so it is likely created by locally supersonic flow around the valve which is probably not resolved by STAR-CD.

4.DISCUSSION

The prediction of the noise generated by a cabin outflow valve operating at sub-critical pressure ratio by STAR-CD was very good. Unlike a conventional jet, which has the shear layer and mixing developing slowly with distance downstream, the flow here is dominated by highly separated flow with large-scale vertical structures. This flow is well adapted to the DES turbulence model in that the flow structures are large relative to the mesh size so that it will operate in its Large Eddy Simulation mode.

REFERENCES

1. Lyrintzis, A.S., Uzun, A., (2001), 'Integral Techniques for Jet Aeroacoustics Calculations' AIAA Paper 2001-2253

MEASUREMENT OF PERCEIVED ANNOYANCE DUE TO LOW FREQUENCY CONTENT IN BROAD SPECTRUM NOISES

Cheng Qian¹, Alberto Behar², and Willy Wong^{1,2}

¹Edward Rogers Sr. Dept of ECE, University of Toronto, 10 Kings College Rd., Toronto, ON, Canada, M5S3G4

²IBBME, University of Toronto, 4 Taddle Creek Rd., Toronto, ON, Canada, Country, M5S3G9 qianch@ecf.utoronto.ca

1. INTRODUCTION

Environmental noise is a growing problem in the workplace and in homes, inducing annoyance and hearing loss, and affecting productivity and well-being. Current by-laws and regulations use SL measured in the dBA to assess both annoyance and potential hearing loss. While dBA-based measurements are fairly effective in assessing risk of hearing loss, noise annoyance arises from many factors other than loudness (Guski 1999) which cannot be measured using only this weighting. Annoyance is especially difficult to assess when the noise in question contains significant energy with Low Frequency (LF) content.

In the past, a number of experiments have tried to correlate annoyance with LF content with rather specific methods, using pure tones (Moller, 1987; Nakamura and Inukai, 1998), verbal scales for judgment (Inukai et al, 2000), or field data with real noises and assessments (Broner and Leventhall, 1983). While individually, useful results are often obtained, it is difficult to generalize such specific results into a versatile method of assessing LF annoyance in the field. In the present work, we generate and use a set of broadband noises of continuous spectra similar in shape to common pink noise. Subjects listen to each noise followed by a reference white noise of a known level and adjust the volume of the test noise until both noises reach equal annoyance. The idea is to quantitatively determine how LF spectral content contributes to noise annoyance.

Our goal is to develop a means to assess the annoyance of a noise by measuring it in both dBC and dBA. The difference dBC-dBA is an index of low frequency energy in a noise. Since dBA understates low frequencies while dBC does not, a greater proportion of noise energy in the LF region will show a larger difference between dBC and dBA. Furthermore, dBC and dBA are both easily measured in the field using any sound level meter. Thus, an attractive way to assess noise annoyance while account for low frequency content may be to use the standard dBA measurement result and add a “penalty” based on the measured C-A value.

This C-A idea has been explored in the past by Kjellberg (1997) where it was suggested that any C-A value of greater than 15 should incur a +6 dBA penalty. Our approach differs by seeking an appropriate penalty for each C-A value

through the testing of subjects in the laboratory. We present an experimental method that is straightforward and scalable, and which may eventually offer a simple means to adjust for LF content in assessing noise annoyance.

2. METHOD

Test noises used were generated artificially for simple control of desired spectra and levels. Noise generation was done via MATLAB by the Inverse Fast Fourier Transform of a random-phase, $1 / (f \wedge n)$ shaped spectrum. For the spectra, n is referred to as the ‘slope’ of the spectrum and corresponds to the amount of low frequency content. The spectra were band-limited between 31.25Hz and 8kHz, representing a total 8 octave bands: 6 octaves focused on the pertinent region of hearing around 1kHz, while extending 2 extra octaves in the LF direction. The noises were balanced in software to the level in dB linear. The .wav files were then stored at $F_s=22050$ Hz for later playback. Table 1 contains the four spectra used and their values under different indices of LF content.

Table 1. Various noise spectra used in preliminary tests

Slope(n)	dB/octave	dBC-dBA
0.5	-3	2.00
1.0	-6	9.94
1.5	-9	18.33
2.0	-12	24.35

The calibration and experiment were both performed inside an IAC Audiometric Cabin. The noise signals were sent from the computer through a Digital Audio Labs CardDeluxe sound card into a Rotel RA-810A power amplifier, after which the signal was binaurally reproduced via AKG K301xtra circumaural headphones, worn by the subject inside the sound cabin. Calibration of the noise levels were performed by measurement through an artificial ear setup consisting of a human head mannequin containing a Bruel & Kjaer Type 4134 microphone connected through a B&K 2804 amplifier to a B&K 2231 sound level meter. Adjustments were made directly in software.

For the preliminary tests, 6 young adult subjects, 3 male and 3 female were asked to adjust pairs of noises to obtain the same annoyance. The noise pairs were presented as one reference white noise and one “coloured” noise for which the LF content varied. After each listening, the subject adjusted the volume of the “coloured” noise and listened to

the noise pair again, repeating until both noises appeared equally annoying. Each of six subjects performed three runs of the experiment. Each run consisted of 20 pairs of noises, with 5 slopes (Table 1) at 40, 50, 60, and 70 dB linear.

To assist our subjects, “annoyance” was elaborated as “disturbance”, “unpleasantness”, or “nuisance” as these terms best represent annoyance according to noise research experts from seven nations (Guski, 1998).

3. PRELIMINARY TESTS

The tests conducted were intended to establish the performance of a straight dBA measurement of noise annoyance. The results show dBA tending to underestimate annoyance in noises with high LF content. Total variability in the limited data was large, making quantitative claims difficult. However, these differences arose mostly between subjects. Figure 1 shows each subject’s results with the $n=2.0$ “coloured” noise. The dotted line through each figure represents when A-weighting correctly measures annoyance. 4 of 6 subjects had found LF content more annoying, 1 was neutral, 1 found it less annoying. The relative consistency within each individual suggests that the method is reasonably reliable and may hold potential.

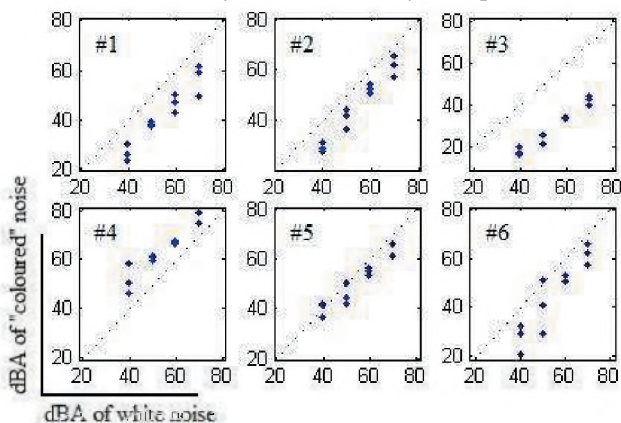


Fig. 1. Plots of equal annoyance between “coloured” and white noises. Each point represents one observation.

A second observation was that overall level of the noises did not have any discernable effect on the annoyance of LF content. This result suggests that following tests should reduce the number of levels used, hence reducing testing time per subject, freeing up time to test more subjects.

Variability is the main concern. To reach our goal of a dBC-dBA assessment method, more coherent results are required. The source of variations likely includes the set of personal moderators proposed by Guski (1999) which include sensitivity, anxiety and personal evaluation of noise source, and coping capacity. Of these, sensitivity and evaluation of the noise source are the primary contributors to variability. In a controlled laboratory, anxiety about noise source and coping capacity are unlikely to be real concerns as the subject has full control over delivery of the noise dose.

Feedback from subjects indicated that association with memories and environments directly influence their response to noise. From figure 1, subject 4 described the LF noises as sounding like a soothing waterfall, while subject 1 was reminded of the noise inside an airplane cabin. This has clearly introduced a large discrepancy between the subjects’ responses. Thus, any further experiment should include a simple survey component to allow subjects to describe their associations with the noise, separating subjects into positive and negative responder groups. Because only one in six of the subjects had found “coloured” noise less annoying than white noise, and since the noises are typically encountered in workplaces or homes where they tend to distract or disturb, positive responses to LF noise will be uncommon. It is logical to use only data from individuals with negative associations, thus providing more coherent data in determining our dBC-dBA penalty values. Finally, figure 2 is an idealized example of the dBC-dBA penalty plot using only the mean values of the limited data collected thus far.

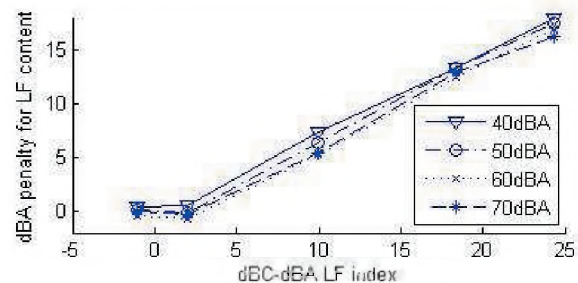


Fig. 2. Plausible end application of LF annoyance data. An operator can use dBC and dBA measurement of real noise to determine the dBA penalty due to LF energy.

4. CONCLUSION

The method developed here confirmed the inadequacy of the dBA system in measuring LF noise annoyance. Suggestions were made to further improve the method toward tighter results. Further testing is required to gather enough data to realize a dBC-dBA approach to noise annoyance assessment for LF-intensive noises.

REFERENCES

Broner, N., and Leventhall, H. G. (1983): Low frequency noise annoyance assessment by Low Frequency Noise Rating (LFNR) Curves. *Jnl Low Freq Noise Vib* **2**, 20-28.
 Guski, R., Felscher-Suhr, U. (1998): The concept of noise annoyance: how international experts see it. *Journal of Sound and Vibration* **223**(4), 513-527.
 Guski, R. (1999): Personal and social variables as codeterminants of noise annoyance. *Noise and Health* **1**, 45-56.
 Inukai, Y., Nakamura, N., and Taya, H. (2000): Unpleasantness and acceptable limits of low frequency sound. *Jnl Low Freq Noise Vib* **19**.
 Kjellberg, A., Tesarz, M., Holberg, K., and Landstrom, U. (1997): Evaluation of frequency-weighted sound level measurements for prediction of low-frequency noise annoyance. *Environmental International* **23**, 519-527.
 Moller, H. (1987): Annoyance of audible infrasound. *Jnl Low Freq Noise Vib* **6**, 1-17.

MODELING THE VIBROACOUSTIC RESPONSE OF MULTI-MATERIALS COMPLEX STRUCTURES UNDER MECHANICAL EXCITATION

Dilal RHAZI¹, Nouredine ATALLA²

^{1,2}GAUS, Dept. of mechanical engineering, University of Sherbrooke, Qc, Canada

1. INTRODUCTION

The prediction of the acoustic and vibration behavior of a multi-layer structure, made up of parallel and homogeneous layers is of interest to several industries. A typical configuration consists of a master structure with an attached Noise Control Treatment (NCT) in both single wall and double wall configurations. The Transfer matrix methods (TMM) is extensively used and well validated for solving the above problem (Allard [1], ATALLA [2] and MUNJAL [3, 4]). However, it is mainly limited to acoustic excitation (plane wave or diffuse field). Few works have been published on the use and validity of the method for a structure-borne excitation. For instance, Villot and all [5] rapidly hinted to the use of the TMM to solve the response of a multilayer with a mechanical excitation, including correction for the size effect using spatial windowing; but didn't present example or validation results.

Therefore, a rigorous work is still lacking for the mechanical excitations (structure-borne). The presented work concentrates on the latter. It presents the study and validation of three different approaches to model the vibration and acoustic response of a mechanically excited structure with added NCT. The first approach is based on the propagation of plane waves in the main structure and the layers of the NCT. The second uses SEA (Statistical Energy Analysis) for the main structure and calculates an equivalent damping to account for the NCT. The last approach uses the modal technique by calculating the equivalent impedance for the added treatment. In the three approaches, the transfer matrix method is used to model various multilayered acoustic control treatments. Applying these approaches to some aircraft structures confirm their relevance in relation to more exact and costly methods, such as the finite elements method.

2. THEORY

The Multilayer separates two semi-infinite fluids. Moreover the mechanical excitation and the response of the structure are assumed harmonic. In the first approach (referred to by the wave approach), the studied structures are assumed of infinite extent and excited by a point load $f(x, y)$. In wavenumber space (k_x, k_y) , the field

$f(x, y)$ can be considered to be constructed from an infinite number of plane waves. For each wavenumber, Transfer Matrix Method is used to compute the input and output (transfer) indicators (velocities, impedance, pressure, etc.). For example, the quadratic velocity of the main structure takes the form:

$$\langle \bar{V}^2 \rangle = \frac{1}{8\pi^2 S} \int_0^{2\pi+\infty} \int_0^{\infty} \left| [V(k_x, k_y)]_{z=0} \right|^2 k_r dk_r d\varphi$$

$$\text{Where: } [V(k_x, k_y)]_{z=0} = \frac{1}{Z_{S,TMM} + Z_{B,\infty}}$$

$Z_{S,TMM}$ is the impedance of the multilayer, seen from the excitation side. It is calculated using the TMM.

$$Z_{B,\infty} = \frac{k_0 Z_0}{\sqrt{k_0^2 - (k_x^2 + k_y^2)}} \text{ is the radiation impedance, seen}$$

from the emission side, k_0 the acoustic wavenumber, Z_0 the characteristic impedance in the emission domain, and S is the surface of the multilayer.

Note that the panel's size is accounted for in the calculation of the acoustic indicators using the Finite Transfer Matrix Method (FTMM). The application of this method for calculation of the radiated power is shown by the following equation:

$$\pi_{rad} = \frac{1}{8\pi^2} \left[\int_0^{2\pi} \int_0^k \frac{Z_0 \sigma_{finie}(k_r, \varphi)}{|Z_{B,\infty} + Z_{S,TMM}|^2} k_r dk_r d\varphi \right]$$

$$\text{Where: } \sigma_{finie} = \frac{\Re(Z_R)}{Z_0 S}$$

And:

$$Z_R = i\omega\rho_0 \iint_{s \ s} e^{-i(k_x x_0 + k_y y_0)} G(M, M_0) e^{i(k_x x + k_y y)} dS(M_0) dS(M)$$

This term represents a geometrical correction to account for the finite size effect. And it depends only on the geometry

of the panel. $G(M, M_0) = \frac{\rho^{-ik_0 R}}{2\pi R}$ is the half space

Green's function. The principle of the approach is to replace the radiation efficiency in the receiving medium by the radiation efficiency of an equivalent baffled window. Let us note that the approach is valid strictly for planar structures. Figure 2 shows the relevance of the technique for an aluminum plate of thickness 0.003 (m).

In the second approach, based on SEA for the main structure, a light coupling is assumed between the structure and the sound package. The effect of the sound package is accounted for through an equivalent damping η_{eq} , the latter is calculated for each structural wavenumber, from the TMM applied to the NCT in a piston motion.

The same methodology is used for the modal approach (third approach). The first layer is modeled by a modal technique. Next, the transfer matrix methods is used to evaluate for each mode (m, n) the expression of the equivalent impedance of the treatment $Z_{eq, mn}$. The total impedance: $Z_{eqT} = Z_{mn}(Bar\ plate) + Z_{eq, mn}$.

3. RESULTS

In this section the comparison between the three presented approaches is illustrate by the example of a double panel made up from a Plate-Fiber-Plate. The aluminums plates have the same thickness: $h=0.003$ (m) and the fiber of thickness $H=0.01$ (m) is modeled as a limp porous layer. The force has unit magnitude, and the results are plotted in third of octaves. In order to compare the three methods, a comparison to the finite element method (FEM) is presented. The FE prediction is carried out with the Novafem software, developed at GAUS. The plates were modeled using xyz cquad4 elements while the fiber was modeled using xyx bricks equivalent fluid elements (limp porous) elements. The plates were assumed baffled for acoustic radiation. Due to the cost of the FE calculation, the calculations were done for a fixed force position while the presented approaches assume a rain on the roof type of excitation. A comparison of the quadratic velocity computed using the three presented approaches and the FEM is illustrated in figure 1. Good agreement is observed between the FTMM, modal and FE calculations. The latter depicts modal fluctuations at lower frequencies (recall that data are presented in 1/3 octave bands). The SEA approach overestimates the quadratic velocity. This is related to the assumption of slight coupling that only accounts for equivalent damping while neglecting the effects of stiffness and mass of the treatment.

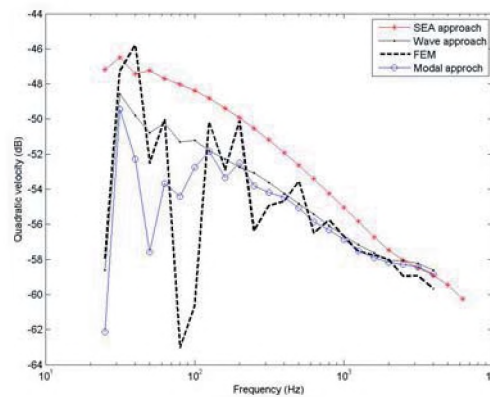


Fig.1. Quadratic velocity of a Plate-Fiber-Plate system excited by a random force.

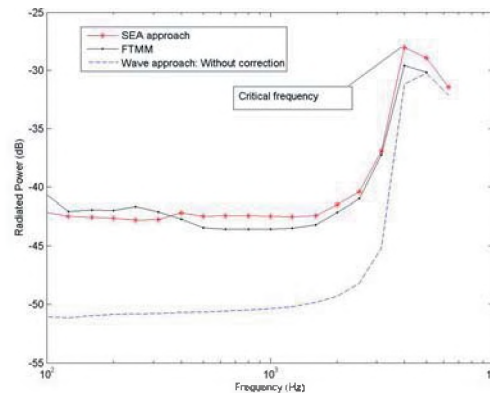


Fig.2. Radiated power of a single plate excited by a random force.

4. CONCLUSION

Three methods are presented and compared for the quick estimation of the structure-borne response of complex flat structures with added sound packages. They represent an attractive alternative to finite element method for quick assessment of Sound package effects. The three methods are shown to work correctly within their assumptions. A combination of the methods can be used to eliminate the assumption of low coupling classically assumed in SEA calculations.

REFERENCES

- [1] Allard, J.F. (1993) Propagation of sound in porous media: modeling sound absorbing materials, Elsevier, New York.
- [2] Atalla, N. (2004). An overview of the numerical modeling of poroelastic materials. Congrès SAPEM, France.
- [3] Munjal, M, L. (1993) Response of a multi-layer infinite plate to an oblique plane wave by means of transfer matrices, Journal sound and vibration 162 (2), 333 p.
- [4] Munjal, M, L., Sastry, J, S. (1995) A transfer matrix approach for evaluation of the response of a multi-layer infinite plate to a two-dimensional pressure excitation, Journal sound and vibration 182 (1), 109 p.
- [5] Villot, M., Guigou, C., Gagliardini L. (2001) Predicting the acoustical radiation of finite size multi-layered structures by applying spatial windowing on infinite structures. Journal of Sound and Vibration 245(3), 433-455.

A NEW NON-LINEAR IMPEDANCE MODEL FOR LINERS

Touchais A, Atalla N, and Panneton R

Dept. of mechanical engineering, University of Sherbrooke, Québec, Canada, J1K2R1.

1. INTRODUCTION

Acoustic treatments are extensively used in commercial gas turbine engine nacelle system to reduce aircraft noise in flight. The liners usually consist of a single degree of freedom resonator made up of a cavity filled by honeycomb construction on which a perforated sheet is bonded. These kinds of liners exhibit nonlinear impedance characteristics that depend on sound pressure level (SPL) [1]. At high sound pressure levels (starting at 120 dB), the resistance and reactance are modified to account for nonlinear effects. Classical nonlinear models such as Hersh's model [2] and Crandall's model [3] are respectively too empirical and not applicable for a thickness- diameter ratio over 0.80. A more accurate model is still needed for single degree of freedom non linear liners. In this paper, an attempt to develop such a model is presented. It uses Maa's [4] model for the linear component of the impedance and Melling's [5] model for the nonlinear effects on the resistance. It takes also into account a frequency shift toward high frequencies when sound pressure level increases. This phenomenon is especially visible on absorptions curves and the imaginary part of the impedance. The model considers only the effects of resonator geometry and incident sound pressure amplitude according to frequency. Normal incidence impedance measurements, in a high intensity impedance tube, are presented to corroborate the validity of the developed model.

2. IMPEDANCE MODEL

2.1 Model without frequency shift

Maa's impedance model [4] is given by

$$\zeta = R + j\omega m,$$

with ζ , R and ω are respectively impedance, resistance and reactance and

$$R = \frac{32\eta t}{\phi \rho_0 c_0 d^2} * \left[\sqrt{1 + \frac{x^2}{32}} + \sqrt{\frac{2xd}{8t}} \right],$$

With d , t , ϕ , ρ_0 , c_0 , and η are respectively the diameter, thickness, porosity, density, speed of sound and cinematic viscosity; and

$$\omega m = \left[\frac{\omega y}{\phi c_0} \right] * \left[1 + \frac{1}{\sqrt{9 + \frac{x^2}{2}}} + 0.85 \frac{2\varepsilon}{t} \right],$$

where $x = d \sqrt{\frac{\omega \rho_0}{4\eta}}$, and the length correction ε is

$$\varepsilon = 0.48 * \sqrt{\pi * \left(\frac{d}{2}\right)^2}.$$

To account for non linear effects, a nonlinear resistance component is added. Melling's nonlinear resistance model is used [5]. It is given by the expression

$$R_{NL} = 1.2 \frac{(1 - \phi^2)}{2c_0(\phi C_D)} V_a,$$

with C_D is the discharge coefficient given by:

$$C_D = 0.80695 * \sqrt{\frac{\phi^{0.1}}{e^{-0.5072 * \frac{t}{d}}}},$$

and V_a is the acoustic particle velocity.

2.2 Frequency shift

When sound pressure levels increase, a frequency shift of the zero of the imaginary part of impedance (or maximum of the absorption) is observed experimentally. This phenomenon is visible in both the imaginary part of impedance and the absorption coefficient. An example is shown in Fig.1 for a single degree of freedom resonator made up of cavity construction on which a perforate sheet is bonded. The perforated plate has perforation diameter of 1mm, a porosity of 4.5%, a thickness of 2mm and a cavity depth of 25mm. It is clearly seen that the absorption's maxima increases with SPL and shifts towards high frequency.

To account for this frequency shift, the radius and thickness of the perforations are modified as a function of the acoustical Mach number. The latter is used for homogeneity reasons. The proposed modifications are based on an experimental parameters study. It resulted in the following expressions:

$$\Delta r = -6,15 \cdot 10^{-3} * M_a + 20 * M_a^2 - 2660 * M_a^3,$$

$$\Delta t = 0.301 * M_a - 97.50 * M_a^2 + 11400 * M_a^3.$$

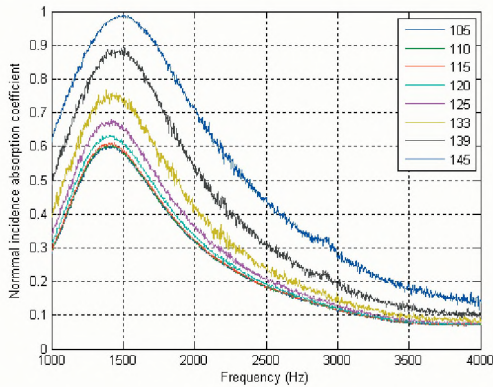


Fig.1 Absorption coefficients at different SPL with normal incidence impedance tube for a single degree of freedom resonator

According to these expressions, the effective radius and thickness of the perforations decrease at high SPL [6]. These corrections are added to Maa's model for the linear component of the impedance and Melling's model for the nonlinear effects on the resistance.

3. RESULTS

The complete model gives good approximation versus measurements, as shown in Fig. 2 for the absorption, in Fig. 3 for the resistance and in Fig. 4 for the reactance. On the other hand, the classical models of Hersh and Crandall fail to predict the results of the presented example.

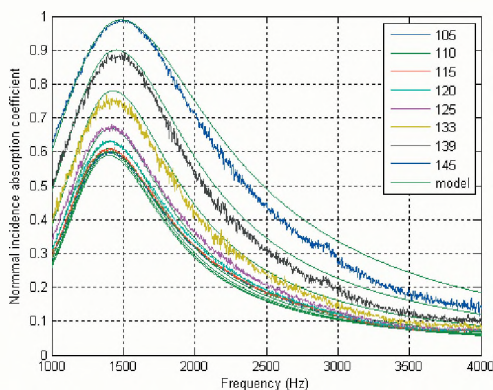


Fig. 2 Comparison experiments versus model for the absorption coefficient.

4. CONCLUSION

Thanks to Maa's model for the linear part and the proposed nonlinear resistance, including the frequency shift effects, the proposed model allows for simulations of various perforated plates configurations, such as microperforated plates at high SPL. This is an enhancement over classical models. However, its full validity is still to be confirmed using an experimental study on various SDOF liners

configurations.

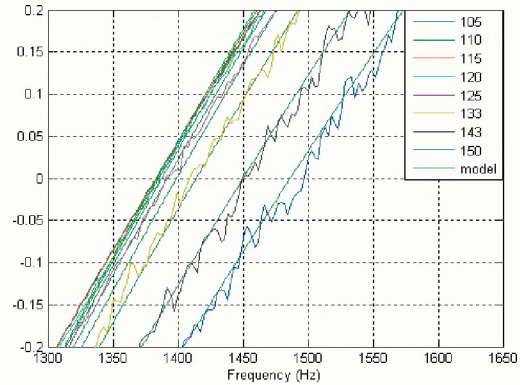


Fig. 3 Imaginary part of normal impedance at different SPL. When SPL increase, imaginary part of impedance decrease.

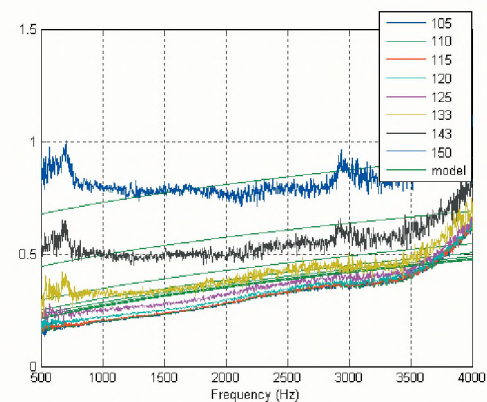


Fig. 4. Real part of normal impedance at different SPL. When SPL increase, real part of impedance increases too.

REFERENCES

- [1] Motsinger R.E. and Kraft (1991), Design and Performance of Duct Acoustic Treatment, Chap 14, Volume 2, Aeroacoustics of flight Vehicles : Theory and Practice.
- [2] Hersh, A.S., Walker B.E. and Celano J.W. (2003), Helmholtz Resonator Impedance Model, Part1: Nonlinear Behavior, AIAA, vol. 41, No. 5, 795-808.
- [3] Crandall I. B. (1926), Theory of Vibrating Systems and Sound, pp.229.
- [4] Maa D.Y. (1988). Design of microperforated panel construction. Acta Acust., vol 13, 174–180.
- [5] Melling T. H. (1973), The Acoustic Impedance Of Perforates at Medium And High Sound Pressure Levels, J. Sound and Vibration, 29, No. 1, 1-65.
- [6] Ingard U. (1967), Acoustic nonlinearity of an orifice, JASA, Vol.42, No.1, 6-17.

SPEECH ENHANCEMENT EMPLOYING LOUDNESS SUBTRACTION AND OVER-SUBTRACTION

Wei Zhang and Tyseer Aboulnasr

School of Information Technology and Engineering, University of Ottawa, K1N 6N5, Ottawa, ON, Canada

Email:zhangw,aboulnas@site.uottawa.ca

1. INTRODUCTION

In classical speech enhancement algorithms, the focus is on the removal of additive noise. The simplest type of speech enhancement is based on spectral subtraction. The estimate of the average noise spectrum is subtracted from the noisy speech spectrum to give the enhanced speech spectrum. This model often leads to large residual noise and musical artifacts. It has been discussed extensively and summarized with a generalized form in [1].

While reducing the power of the noise in the signal results in SNR improvement, it is known that the correlation between the subjective quality of the speech and SNR is very weak [2]. Better measures to evaluate the subjective quality of speech are designed considering the human hearing system. For example, loudness can better simulate the subjective quality of the speech and was used in the ITU-T P.862 recommendation [3]. A loudness subtraction method has been presented in [4] and we will derive a more statistically precise model based on the Laplacian speech model [5].

For the spectral subtraction approach, the remaining noise after the enhancement is still high when the SNR is low. The spectral over-subtraction method has been proposed to provide further improvement [6]. It implements a SNR dependent subtraction factor which applies a higher subtraction factor in the lower SNR frames and vice versa. We will extend the over-subtraction approach to the proposed approach in loudness domain.

This paper is organized as follows. The speech enhancement approaches based on the loudness subtraction and the proposed over-subtraction model are discussed in Section 2 and 3, respectively. In Section 4, simulation results are given. Conclusions are given in Section 5.

2. LOUDNESS SUBTRACTION MODEL

In the PESQ measure, the relative quality of a speech signal depends on the difference in the loudness domain between the signal and the reference (clean) speech signal. This suggests implementing a speech enhancement in the loudness domain. For simplicity, we will use the power law of loudness: $N' = C \cdot I^\alpha$, where N' is the specific loudness in a frequency band, I is the physical intensity. C and α are constants. In this paper, we assume $\alpha = 0.27$.

A generalized loudness subtraction algorithm is proposed as follows:

$$\hat{X}^2 = \left((Y^2)^\alpha - a(Y^2)^\alpha \right)^{\frac{1}{\alpha}}, \quad (1)$$

where a is defined as the subtraction factor. To maintain the loudness of the reconstructed speech at the same levels as the original clean speech, we can show that

$$a = E\{Y^{2\alpha} - X^{2\alpha}\} / E\{N^{2\alpha}\} \quad (2)$$

Define the Noisy-Signal-to-Noise Ratio (NSNR) as: $NSNR = E\{Y^2\} / E\{N^2\}$. The parameter a is determined in terms of the measurable signals as follows. Two independent sources are used to simulate the speech and noise in the frequency domain. The clean speech X is assumed to have Laplacian distribution, while the noise N is Gaussian [5]. Both sources are zero mean and with variances determined by the specified NSNR. The resulting selection of a is shown in Figure 1 (the solid line) as a function of the NSNR.

3. PROPOSED LOUDNESS OVER-SUBTRACTION MODEL

The approach in the previous section subtracts a portion of the average loudness of the noise from the noisy speech signal. Given that the noise is random, the actual loudness of the noise will not be the same for all the samples. There will always be fluctuations around average which will lead to large noise residues in the enhanced signal.

In this paper, we focus on removing an over-estimate of the noise from the noisy signal in the loudness domain. This can be done through increasing the value of a . As a increases, more noise will be deducted but the enhanced speech will likely be more distorted. If a is chosen carefully, the improvement of the SNR will compensate for the larger distortion of the speech.

Using the general nature of the spectral over-subtraction factor in [6], we adjusted a to optimize the performance in the algorithm in loudness domain. This over-subtraction scaling factor is chosen to be 5 below 0dB NSNR, 1 beyond 20dB NSNR and changing linearly between 0 and 20 dB. This scaling factor will be multiplied by a selected in the last section using (2) before being used in (1). The resulting subtraction factor is depicted in Figure 1 with the dotted line.

4. SIMULATIONS

In this section, the subtraction and over-subtraction approaches are compared in both loudness and spectral domains. White stationary noise is added to the clean speech signal with different SNRs from 0 dB to 20dB. The FFT of the noisy speech is obtained on a frame-by-frame basis. The phase of the FFT is maintained separately for reconstruction. The loudness of the noise is estimated with the use of a noise memory [5]. The spectrum of enhanced speech components is estimated using (1). The subtraction factor of subtraction and over-subtraction in loudness domain is shown in Figure 1. The approach in [4] is a different loudness subtraction algorithm with $a = 1$. The noisy speech signal is enhanced with the spectral subtraction and over-subtraction, loudness subtraction (both the algorithm in [4] and the proposed algorithm) and over-subtraction.

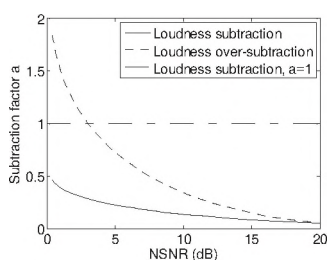


Figure 1: The subtraction factors for loudness domain approaches. The enhanced speech is then reconstructed with the original phase and inverse FFT. The PESQ, a popular objective measure of speech subjective quality, is shown in Table 1 for enhanced signals. The results confirm that using the over-subtraction of noise in an adaptive way in the loudness domain leads to the highest PESQ scores. Similar tests have been done with the segmental SNR and Log-Likelihood Ratio (LLR) measures showing that the loudness over-subtraction continues to provide an improvement. For the LLR measures, the loudness over-subtraction has slightly higher distortion than the loudness subtraction. Both methods in the loudness domain have lower distortion than the corresponding methods in spectral domain.

5. CONCLUSIONS

In this paper, we presented speech enhancement approaches based on loudness subtraction and over-subtraction. The subtraction factor is selected adaptively for each frame based on the NSNR of the speech signal. These approaches in the loudness domain result in improved Segmental SNR, improved PESQ scores and less distortion compared to the corresponding algorithms in the spectral domain.

REFERENCES

- [1] B. L. Sim, Y. C. Tong, J. S. Chan and T. T. Chin, "A parametric formulation of the generalized spectral subtraction method," *IEEE Transactions on Speech and Audio Processing*, Vol. 6, No. 4, pp. 328-337, July, 1998.
- [2] S. Quackenbush, T. Barnwell, and M. Clements, *Objective Measures of Speech Quality*, Englewood Cliffs, NJ, Prentice Hall, 1988.
- [3] A.W. Rix, J. G. Beerends, M. P. Hollier and A. P. Hekstra, "Perceptual evaluation of speech quality (PESQ)- a new method for speech quality assessment of telephone networks and codecs," *Proceedings of ICASSP*, Vol. 2, pp. 749-752, 7-11 May, 2001.
- [4] T. Petersen and S. Boll, "Acoustic noise suppression in the context of a perceptual model," *Proceedings of ICASSP*, Vol. 6, pp. 1086-1088, April, 1981.
- [5] S. Gazor and W. Zhang, "Speech probability distribution," *IEEE Signal Processing Letters*, Vol. 10, No. 7, pp. 204-207, July 2003.
- [6] M. Berouti, R. Schwartz and J. Makhoul, "Enhancement of speech corrupted by acoustic noise," *Proceedings of ICASSP*, Vol. 4, pp. 208-211 April, 1979.

Table 1: Comparison of PESQ scores for spectral subtraction, spectral over-subtraction, loudness subtraction, loudness over-subtraction and the approach in [4].

Speech Type	Input		PESQ score				
	SNR (dB)	Input Signal	Spectral Subtraction	Approach In [4]	Loudness Subtraction	Spectral over-Subtraction[6]	Loudness Over-Subtraction
Female	0	1.122	1.299	1.573	1.420	1.581	1.812
	10	1.819	2.334	2.076	2.209	2.345	2.418
	20	2.637	2.764	2.823	2.924	2.920	2.976
Male	0	1.390	1.461	1.575	1.478	1.573	1.696
	10	1.839	2.205	2.005	2.050	2.222	2.298
	20	2.488	2.581	2.657	2.701	2.742	2.762

ARTICULATORY STATE ESTIMATION FROM INCOMPLETE SPEECH MEASUREMENTS

Luis Rodrigues¹ and John Kroeker²

¹Dept. of Mechanical and Industrial Engineering, Concordia University, Montreal, Canada, luisrod@encs.concordia.ca

²Eliza Corporation, Beverly, MA, USA, jkroeker@elizacorp.com

ABSTRACT

This paper presents a method to find the unknown components of the state of articulators that produce a given speech signal. The proposed method reconstructs the unknown states such that the energy needed to produce the recorded speech is minimized.

1. Introduction

Although increasingly sophisticated models for human speech production have been developed in the past thirty years [1], they have made little impact on the progress of computer synthesized human speech. From a practical point of view, these models are either too complicated to implement, or lack the comprehensiveness in covering all classes of sounds, or both. On the other hand, the current approach used in commercial speech synthesizers cannot provide the natural transitions between phonemes as the human articulatory system does. However, two important computational models in speech synthesis have led to promising results: the Haskins Laboratory computational model [2] and the University of Waterloo nonlinear observation articulatory dynamical model [3], with close connections to the linear observation hidden dynamic model (HDM) from the University of Edinburgh [4].

Traditionally, human speech has been seen as having two structures: one considered physical, the other cognitive. The relation between the two structures is generally not an intrinsic part of either description. Articulatory Phonology was first suggested by [5] at the Haskins Laboratory, and it offers the different assumption that these apparently different domains are, in fact, the low and high level description of a single complex feedback system. Crucial to this approach is the identification of phonological units with dynamically specified units of articulatory action, called *gestures*. Thus, an utterance is described as an act that can be decomposed into a small number of primitive units, with a particular spatio-temporal configuration. Examples of gestures for different words can be found in [1]. This paper uses the dynamical model from [3] (based on the articulatory theory of speech production described in [1]), and proposes a method that reconstructs the unknown articulatory states such that the energy needed to produce a given speech signal is minimized.

2. Problem Formulation

We assume a mathematical model for speech production consisting of a discrete-time linear and time-invariant dynamical system [3]. The state then evolves according to

$$x_{k+1} = \Phi x_k + w_k \quad (1)$$

with $x \in R^n$ being the state vector of positions of the different articulators and $w \in R^m$ being the forcing input vector. We furthermore assume that the state vector is not completely known. In other words, at each instant k of discrete-time, some components of x_k are not known and some components of x_{k+1} are also not known. We will use the following notation: an upper index in a variable corresponds to the row index when the variable is a component of a vector or matrix; a lower index corresponds to the time index when the variable is a component of a vector and to the column index when the variable is an entry of a matrix. Using this notation, suppose that, without loss of generality, for a given instant of discrete-time k , the component l of x_k (x_k^l) and the component m of x_{k+1} (x_{k+1}^m) are unknown. The problem then, for each instant k , is to compute the unknown components of both x_k and x_{k+1} such that the input energy

$$J = w_k^T w_k \quad (2)$$

is minimized. In other words, the problem to be solved is

$$\begin{aligned} \min_{x_k^l, x_{k+1}^m, l \in I_l, m \in I_m} w_k^T w_k \\ \text{s.t.} \quad (1) \end{aligned} \quad (1)$$

3. Problem Solution

To solve this problem we start by noting that from (1) the forcing input vector w_k is

$$w_k = x_{k+1} - \Phi x_k \quad (3)$$

and the functional (2) can then be rewritten as

$$J = (x_{k+1} - \Phi x_k)^T (x_{k+1} - \Phi x_k) \quad (4)$$

Then, the solution that minimizes (4) must verify

$$\frac{\partial J}{\partial x_k^l} = 0, \quad \frac{\partial J}{\partial x_{k+1}^m} = 0. \quad (5)$$

From (4), the first condition leads to

$$\frac{\partial J}{\partial x_k^l} = 0 \Leftrightarrow 2(x_{k+1} - \Phi x_k)^T \frac{\partial}{\partial x_k^l} (x_{k+1} - \Phi x_k) = 0, \quad (6)$$

$$\Leftrightarrow (x_{k+1} - \Phi x_k)^T (-\Phi_l) = 0$$

where Φ_l is the column l of matrix, i.e.,

$$\Phi_l = [\Phi_l^1 \quad \dots \quad \Phi_l^n]^T.$$

Using (4), the second condition from (5) leads to

$$\frac{\partial J}{\partial x_{k+1}^m} = 0 \Leftrightarrow 2(x_{k+1} - \Phi x_k)^T \frac{\partial}{\partial x_{k+1}^m} (x_{k+1} - \Phi x_k) = 0 \quad (7)$$

$$\Leftrightarrow (x_{k+1} - \Phi x_k)^T e_m = 0$$

where e_m is the m th unitary coordinate vector, i.e.,

$$e_m = \underbrace{[0 \quad \dots \quad 1 \quad \dots \quad 0]^T}_m.$$

Note that equations (6) and (7) express the fact that the approximation error between x_{k+1} and the linear model Φx_k must be orthogonal to all vectors Φ_l (for l in the set of indices of unknown components of x_k) and to all coordinate vectors e_m (for m in the set of unknown components of x_{k+1}). Rearranging equations (6)-(7) we finally get the following set of linear equations to be solved

$$\begin{cases} \Phi_l^T x_{k+1} - \Phi_l^T \Phi x_k = 0, & l \in I_l \\ e_m^T x_{k+1} - e_m^T \Phi x_k = 0, & m \in I_m \end{cases} \quad (8)$$

Note that (8) is a system of linear equations, which has the advantage that it can be solved numerically very efficiently. If we use the subscript *knownk* for all column indices corresponding to known values of x_k , *knownk1* for all column indices corresponding to known values of x_{k+1} , *unknownk* for all column indices corresponding to unknown values of x_k and *unknownk1* for all column indices corresponding to unknown values of x_{k+1} , then the system of equations (8) can be rewritten as

$$Ax = b \quad (9)$$

where

$$A = \begin{bmatrix} \Phi_{unknownk}^T \\ e_{unknownk1}^T \end{bmatrix} \begin{bmatrix} I_{unknownk1} & -\Phi_{unknownk} \end{bmatrix}$$

$$b = - \begin{bmatrix} \Phi_{unknownk}^T \\ e_{unknownk1}^T \end{bmatrix} \begin{bmatrix} I_{knownk1} & -\Phi_{knownk} \end{bmatrix} \begin{bmatrix} x_{k+1} \\ x_k \end{bmatrix}_{known}$$

$$x = \begin{bmatrix} x_{k+1} \\ x_k \end{bmatrix}_{unknown}$$

4. Numerical Example

Consider

$$\Phi = \begin{bmatrix} 1.75 & 0.8 \\ -0.95 & 0 \end{bmatrix}, \quad k=1, \quad l=1, \quad m=2,$$

$$x_1 = \begin{bmatrix} a \\ 1 \end{bmatrix}, \quad x_2 = \begin{bmatrix} 1 \\ b \end{bmatrix}$$

The system of linear equations (8) to be solved is

$$\begin{cases} 3.965a + 0.95b = 0.35 \\ 0.95a + b = 0 \end{cases}$$

and the solution is $a = 0.1143$, $b = -0.1086$.

REFERENCES

- [1] R. D. Kent, S. G. Adams, and G. S. Turner, "Principles of Experimental Phonetics", chapter in *Models of Speech Production*, pp. 2–45, Mosby, 1996, Edited by N.J. Lass.
- [2] Haskins Laboratory, "Introduction to Articulatory Phonology and the Gestural Computational Model", <http://www.haskins.yale.edu/research/gestural.html>
- [3] L. J. Lee, P. Fieguth, L. Deng, "A Functional Articulatory Dynamic Model for Speech Production", *Proc. IEEE International Conference on Acoustics Speech and Signal Processing*, Salt Lake City, Utah, May 2001.
- [4] S. King and A. Wrench, "Dynamical system modelling of articulator movement", *Proc. International Congress of Phonetic Sciences*, San Francisco, California, pp.2259–2262, 1999.
- [5] C. P. Browman and L. Goldstein, "Towards an articulatory phonology", *Phonology Yearbook*, 3:219–252, 1986.

ACKNOWLEDGEMENTS

The first author would like to acknowledge NSERC and NATEQ for partially funding this research.

ACOUSTIC DIAGNOSIS OF VOCAL TREMOR

^{1,2}Huawei Colin Li, ³Hilmi R. Dajani, ^{1,2}Willy Wong and ¹Pascal van Lieshout

¹Institute of Biomaterials and Biomedical Engineering, University of Toronto, Toronto, ON

²Department of Electrical and Computer Engineering, University of Toronto, Toronto, ON

³School of Information Technology and Engineering, University of Ottawa, Ottawa, Canada

1. INTRODUCTION

Tremor is an unintentional muscle movement involving oscillations of one or more parts of the body. Vocal tremor is known to be associated with neurological disorders such as Parkinson's disease, essential tremor, and cerebellar ataxia. These vocal tremors are associated with a low-frequency modulation of the vocal folds. Characterizing the frequency, level and intensity of these modulations may help in diagnosing and treating a disorder. The primary non-invasive quantification of vocal tremor has been through acoustic analysis, which involves measuring the variation in the pitch contour or the fundamental frequency in a sustained voice signal.

While much work towards measuring the variation of the pitch contour using time domain techniques has been done [1-3], these methods are not able to classify abnormal phonations accurately. There are two important limitations associated with the current methods: (a) they cannot extract the fundamental frequency in an accurate and precise manner; (b) they have not provided a fine structural display of the variation in the acoustic energy across frequency domain with respect to time. To overcome these limitations, a method involving time-frequency analysis using the Fine Structure Spectrogram (FSS) [4] is proposed as a potential analysis tool for abnormal phonations, in particular, Parkinson's disease. Results between normal and abnormal phonations are compared.

2. METHOD

Vocal tremor characteristics are best analyzed in terms of the modulations in the fundamental frequency (F0), i.e. the pitch contour. As shown in Figure 1, F0 of the acoustic signal of the sustained /a/ from pathological and normal voices can be first extracted using our custom-built speech processing algorithm: FSS. The design of FSS was inspired by the human auditory system and can provide a detailed picture of the fine-structure found in the time-frequency display of acoustic energy in a speech signal. The fundamental frequency is the component with lowest frequency in the display. More details about this approach can be found in [4]. In our implementation here, we first preprocessed the raw acoustic signal by performing half-wave rectification, then down-sampling to 1kHz to reduce computational time. The average F0 was then extracted and

a band-pass filter with cut-off frequencies 15Hz above and below the average F0 is applied to eliminate undesired noise. In the next stage, we apply FSS to extract F0. We used a range of 25Hz below the average F0 to 25Hz above for FSS to extract the pitch contour. The fundamental frequency was then further processed with the following steps: (a) subtraction of the mean (b) removal of linear trend (c) smoothing through low-pass filtering (cut-off at 20Hz).

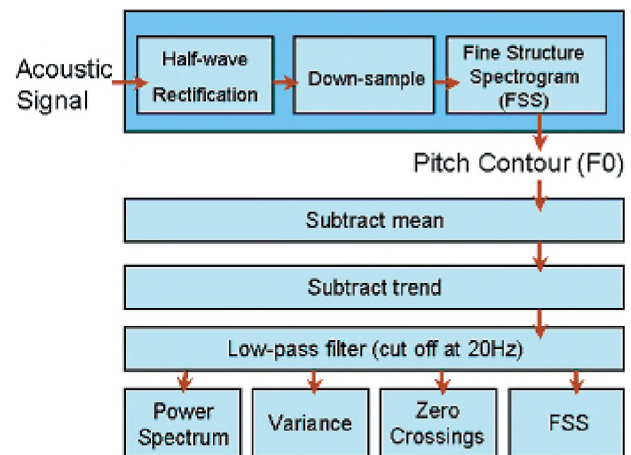


Fig. 1. Overview of the stages in vocal tremor analysis

Four analytical approaches were then applied to this output: (a) Power Spectrum (b) Variance of F0 across frequency (c) Zero-crossing technique (d) Spectrographic display of F0 using FSS. Power spectrum provides a display of the spectral density of F0. F0 variance is a single number quantitatively measuring the overall variability of the fundamental frequency. Zero-crossings measure is also a single number, which acts as an estimation of the most dominating modulating frequency of F0. Lastly, FSS provides a high-resolution time-frequency display of the acoustic energy in F0.

3. RESULTS AND DISCUSSION

The results show that modulations in F0 is the primary difference between normal and pathological speech. From the FSS output, consistent low frequency modulations in F0 over time were observed in the pathological phonations. Variance of the modulations was much higher in the pathological phonations than in the normal. Shown in Figure 2 is an example of the comparison between the two.

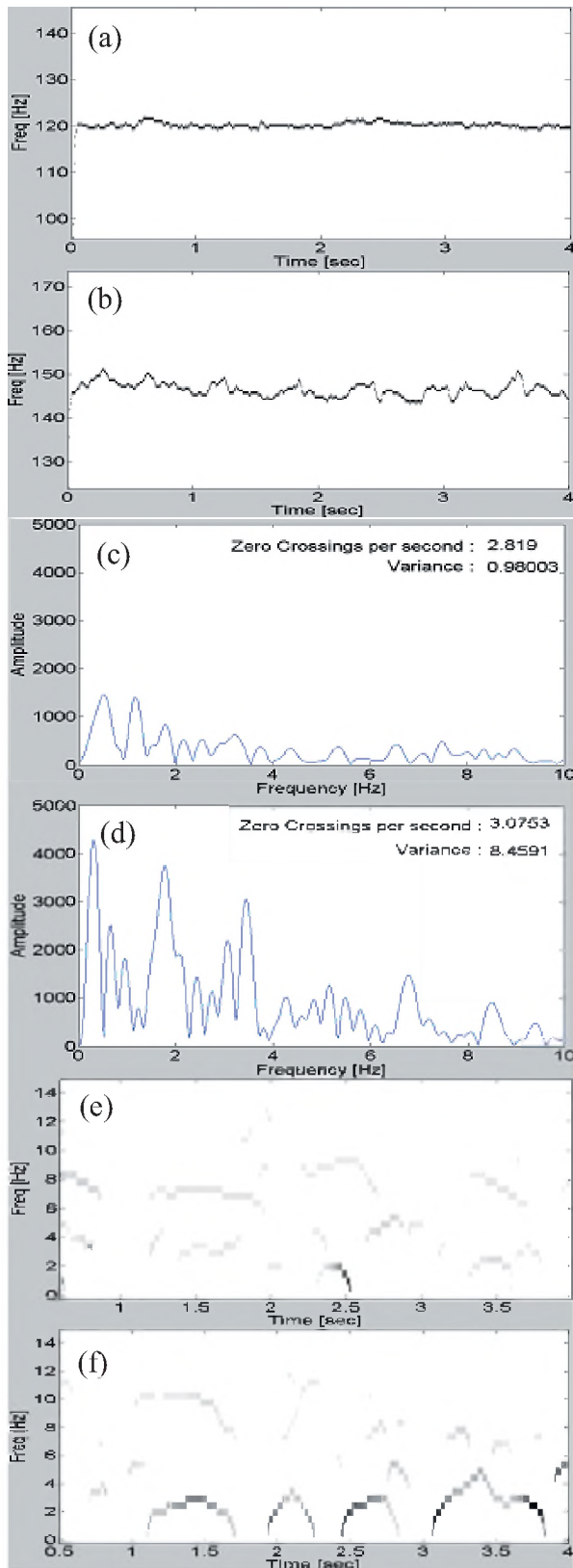


Fig. 2. (a) F0 of a normal phonation of /a/. (b) F0 of a pathological phonation of /a/. (c) Analysis of F0 of the normal phonation. (d) Analysis of F0 of the pathological. (e) FSS display of F0 of the normal. (f) FSS display of F0 of the pathological

Figure 2(a) and (b) show the F0 of a normal phonation and a pathological phonation respectively. It is easy to observe the low frequency modulation in F0. Figure 2(c) and (d) provide a more in-depth analysis showing spectral density, the dominant frequency and the variance in F0. The visible difference in the spectral density and variance offers a qualitative and quantitative cue in separating between the two types of speech. The zero crossings display also shows information, which may potentially be used to distinguish between various types of vocal tremors. Shown in Figure 2(e) and (f) are FSS display of the F0 from the normal and pathological phonations respectively. Through FSS, a relatively consistent modulating frequency is observed in the pathological phonation, in contrast to the normal case.

4. Conclusion

The method proposed here involving the Fine Structure Spectrogram is capable of extracting the fundamental frequency or pitch track contour in an accurate and precise manner. The technique shows the capacity of discriminating between two populations of speech (normal versus pathological) based on modulations found in F0. It is promising in future work to develop a classifier in distinguishing between normal and pathological phonations for a clinical environment.

REFERENCES

1. William S. Winholtz and Lorraine Olson Ramig (1992). "Vocal Tremor Analysis With the Vocal Demodulator" *American Speech-Language-Hearing Association* Vol. 35 562-573
2. Eugene H. Buder and Edythe A. Strand (2003). "Quantitative and Graphic Acoustic Analysis of Phonatory Modulations: The Modulogram" *Journal of Speech, Language, and Hearing Research* Vol. 46, 475-490
3. Laurence Cnockaert, Francis Grenez, Jean Schoentgen (2005). "Fundamental Frequency Estimation and Vocal Tremor Analysis by Means of Morlet Wavelet Transforms" *ICASSP'05*
4. Dajani, H., Willy Wong and Hans Kunov (2005). "Fine structure spectrogram and its application in speech" *J. Acoust. Soc. Am.* Vol. 117, No. 6, 3902-3918

ACKNOWLEDGEMENTS

This work was carried out under the support of OGS and NSERC.

A ROBUST VOICE SEPARATION METHOD

Yijing Chu¹, Heping Ding², and Xiaojun Qiu³

^{1,3}Key Laboratory of Modern Acoustics and Institute of Acoustics, Nanjing University, 210093, China

²Acoustics and Signal Processing, IMS, National Research Council, 1200 Montreal Rd., Ont., Canada K1A 0R6

¹zhuyijing@nju.org.cn ²heping.ding@nrc-cnrc.gc.ca ³xjqiu@nju.edu.cn

1. Introduction

It is often needed to separate mixed voice signals, e.g., in a cocktail party environment. Blind source separation (BSS) techniques based on the independent component analysis [1] and so on work well in simulations where the source signals are independent and identically distributed (i.i.d.), but perform poorly in real life because actual sources are hardly i.i.d.. In addition, other practical issues such as complexity, convergence and tracking rate, and noise immunity also need to be resolved in the existing techniques.

In [3], a robust quasi-BSS method that addresses the above-mentioned practical issues was proposed. Assuming there are two voice sources and two microphones (the numbers can be generalized but are both two here for simplicity) in the room, Fig. 1 shows the signal flow diagram of the method, where the sources $s_1(n)$ and $s_2(n)$ acoustically go through linear mixing filters $\{H_{ij}, \forall i, j=1,2\}$ of the room before reaching the microphones. In the processing realm, the microphone signals $x_1(n)$ and $x_2(n)$ are fed to separation filters $\{W_{ij}, \forall i, j=1,2\}$, which are so chosen that $s_1(n)$ and $s_2(n)$ appear maximally separated in the outputs $u_1(n)$ and $u_2(n)$.

The key therefore is to find a solution to $\{W_{ij}, \forall i, j=1,2\}$. According to [3], such a solution exists if H_{1j} and H_{2j} ($j=1,2$) share no common zeros and the noises in $x_1(n)$ and $x_2(n)$ are i.i.d. and independent of the sources. Next, [3] shows that a solution to $\{W_{j1}, W_{j2}\}$ ($j=1,2$) can be estimated by minimizing

$$J_j(n) = \overline{u_j^2(n)}, \quad (1)$$

a certain kind of time-average of the squares of $u_j(n)$ samples (or energy level of $u_j(n)$), during one source active (1SA) time periods where source $s_{3-j}(n)$ is active and $s_j(n)$ is silent. Furthermore, the solution can be found adaptively by using the affine projection algorithm (APA) [4] with a constraint that the first element of the impulse response in $\{W_{1j}, j=1,2\}$ be unity.

Simulations based on real audio recordings made in a typical listening room (RT30 at 1 kHz around 0.3 s), 8 kHz

sampling rate, and each of $\{W_{ij}, \forall i, j=1,2\}$ having 800 coefficients [3] reveal that the proposed quasi-BSS method outperforms conventional methods, such as that in [2], in terms of convergence and tracking rate, achievable signal to interference ratio, and immunity to ambient noise.

Nevertheless, [3] did not give a complete solution to the BSS problem. In order to function properly, the proposed quasi-BSS method relies on

1. the condition that there are 1SA periods available, and
2. reliable detection of the 1SA periods.

In fact, “1” is not regarded as a problem since 1SA periods are almost always present in real human conversations, and “2” is a practical issue that [3] did not address.

In the following, we present a simple and effective scheme that detects the 1SA periods and controls the adaptation for $\{W_{ij}, \forall i, j=1,2\}$, so as to complete the work in [3] and form a complete BSS solution.

2. Detection and Control Scheme

Our proposed scheme is based on the proposition that, in general, a solution to $\{W_{j1}, W_{j2}\}$ ($j=1,2$), which makes (1) satisfactorily low, only exists during a 1SA period. Given that, we introduce a pair of detection filters $\{D_1, D_2\}$, which are of the same structure as any $\{W_{j1}, W_{j2}\}$ ($j=1$ or 2) and are connected the same way as the latter, as shown in Fig. 2.

For fast convergence and tracking, $\{D_1, D_2\}$ always adapt using the APA at a large step size. The output energy level

$$J_D(n) = \overline{u_D^2(n)} \quad (2)$$

is constantly monitored. As discussed above, (2) stays high as long as both sources $s_1(n)$ and $s_2(n)$ are active. The fact that (2) starts to drop is an indication of a 1SA period having been entered and $\{D_1, D_2\}$ converging on it. When $\{D_1, D_2\}$ have converged during the 1SA period, indicated by (2) having dropped below a certain threshold T , the coefficients of $\{D_1, D_2\}$ are copied to a pair of separation filters $\{W_{j1}, W_{j2}\}$ ($j=1$ or 2), which then start to produce the output $u_j(n)$ and adapt at a low rate (small step size) to track small variations (if any) in the mixing filters. When another

1SA (the other source active) period is entered, indicated by both (2) and $J_j(n)$ jumping, we stop adapting $\{W_{j1}, W_{j2}\}$ to prevent them from diverging. When (2) falls again – result of $\{D_1, D_2\}$ converging on this new 1SA period – we copy the $\{D_1, D_2\}$ to $\{W_{3-j,1}, W_{3-j,2}\}$, which then start to produce the output $u_{3-j}(n)$ and slowly adapt – as $\{W_{j1}, W_{j2}\}$ did earlier. From now on, $\{W_{j1}, W_{j2}\}$ ($j=1$ or 2) adapt if $J_j(n)$ is small, and is frozen otherwise. Also at this point, $\{D_1, D_2\}$ can be decommissioned if large variations in mixing filters $\{H_{ij}, \forall i, j=1,2\}$ are not expected in the future.

In a nutshell, 1SA periods are detected and adaptation for $\{W_{ij}, \forall i, j=1,2\}$ is controlled based on (1) ($j=1,2$) and (2).

3. Experimental Results

This proposed detection and control scheme has been applied to the method in [3] to process real audio recordings described in Section 1 (details in [3]).

The results are illustrated in Fig. 3. The microphone signals $x_1(n)$ and $x_2(n)$ consist of three consecutive periods: $s_1(n)$ active only, $s_2(n)$ active only, and both $s_1(n)$ and $s_2(n)$ active. At each of the two moments marked by the vertical lines, (2) becomes less than a threshold T . This triggers a copying action from $\{D_1, D_2\}$ to certain $\{W_{j1}, W_{j2}\}$, which then start to perform the mission task, as discussed in Section 2.

It can be seen that the proposed 1SA period detection and adaptation control scheme is quite effective and fast-acting. Audio demos showing the separation results under a couple of ambient noise levels will be played during the presentation of this paper.

4. Conclusion

This paper presents a scheme for controlling the adaptive filters associated with a previously proposed method for BSS. The scheme is proven to be effective and with a very small algorithmic overhead in implementation. The complete BSS solution can be further simplified by replacing the APA used with a fast affine projection (FAP), such as a one proposed in [5].

References

- [1] S. Choi, A. Cichocki, H.M. Park and S.Y. Lee, "Blind source separation and independent component analysis: A review," *Neural Information Processing - Letters and Reviews*, Vol. 6, No. 1, pp. 1–57, Jan. 2005
- [2] L. Parra and C. Spence, "Convolutional Blind Separation of Non-Stationary Sources," *IEEE Trans. Speech and Audio Processing*, Vol. 8, No. 3, pp. 320–327, May 2000
- [3] Y. Chu, H. Ding, and X. Qiu, "Quasi-Blind Source Separation Algorithm for Convolutional Mixture of Speech," *Proceedings of the 12th IEEE Digital Signal Processing Workshop*, pp. 233–

238, Jackson Hole, WY, U.S.A., Sept. 2006

- [4] H.C. Shin and A.H. Sayed, "Mean-square performance of a family of affine projection algorithms," *IEEE Trans. Signal Proc.*, Vol. 52, No. 1, pp. 90–102, Jan. 2004
- [5] Heping Ding, "Fast Affine Projection Adaptation Algorithms with Stable and Robust Symmetric Linear System Solvers," *IEEE Transactions on Signal Processing*, Vol. 55, No. 5, pp. 1730–1740, May 2007

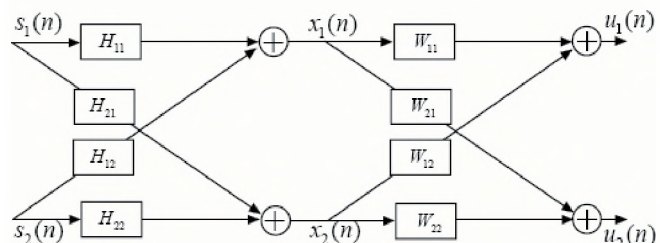


Fig. 1. Signal flow of proposed voice separation method [3]

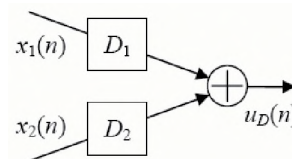


Fig. 2. Detection filters

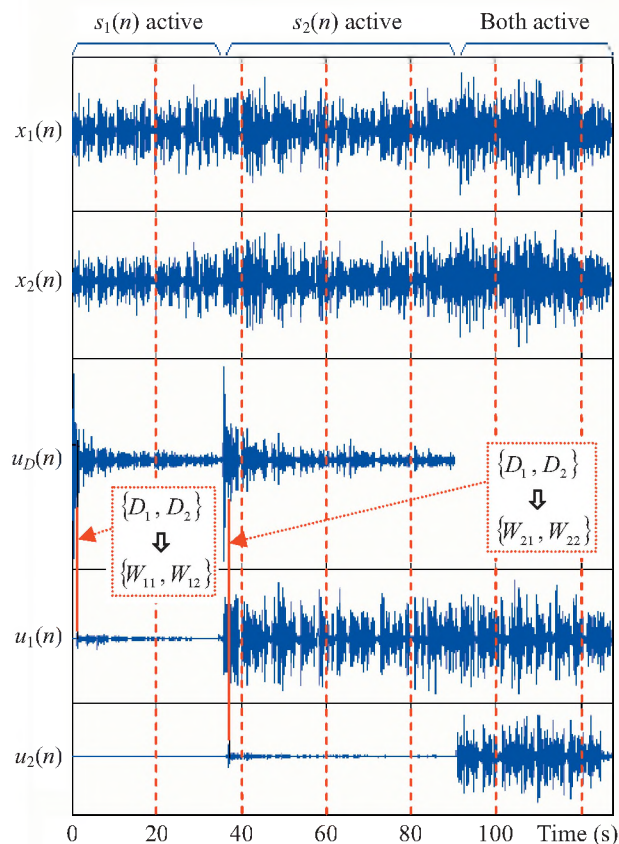


Fig. 3. The proposed detection and control scheme in action

EFFECT OF WITHIN- AND BETWEEN-TALKER VARIABILITY ON WORD IDENTIFICATION IN NOISE BY YOUNGER AND OLDER ADULTS

Huiwen Goy¹, Kathy Pichora-Fuller^{1,3}, Pascal van Lieshout^{1,2,3,4}, Gurjit Singh^{1,3} and Bruce Schneider¹

¹Dept. of Psychology, University of Toronto, Mississauga, 3359 Mississauga Rd North, Ontario, Canada L5L 1C6

²Dept. of Speech-Language Pathology, University of Toronto, 160-500 University Ave, Ontario, Canada M5G 1V7

³Toronto Rehabilitation Institute, 550 University Ave, Ontario, Canada M5G 2A2

⁴Institute of Biomaterials and Biomedical Engineering, University of Toronto, 164 College St, Ontario, Canada M5S 3G9

1. INTRODUCTION

Speech produced in noise differs from speech produced in quiet. The Lombard Effect is the reflex by which talkers increase their vocal effort as environmental noise increases [1]. Other speech differences include increased fundamental frequency (F_0) [2], word duration [3], and high-frequency energy [4]. Although the Lombard Effect is well-documented, standardized tests of speech intelligibility in noise usually use speech materials recorded in quiet, with background noise added later. However, word recognition in noise is significantly better for speech materials produced in noise than for materials produced in quiet, even when vocal level differences are removed [4].

Older adults, even if they have audiometric thresholds within clinically normal limits, often have more trouble than younger adults understanding speech in noise [5]. The intelligibility advantage seen when listeners are tested with speech produced in conditions matched to the listening condition may be even greater for older than for younger adults. The main purpose of the present study was to investigate age-related differences in the extent to which results of speech intelligibility testing might be improved if more ecologically appropriate spoken versions of materials were used. Another purpose was to examine the possible acoustical explanations for any differences in intelligibility.

2. METHOD

2.1 Participants

Participants were 16 younger adults (mean age = 19.9 years, $SD = 1.7$) and 16 older adults (mean age = 69.0 years, $SD = 4.1$). All participants spoke English as a first language, and had pure-tone audiometric thresholds of ≤ 25 dB HL at frequencies from .25 to 3 kHz in the test ear. The vocabulary scores on the Mill Hill test were 13/20 ($SD = 2$) for the younger and 16/20 ($SD = 3$) for the older group.

2.2 Stimuli

The stimuli used were the eight sentence lists of the SPIN-R test. Each list contains 25 low-context and 25 high-context sentences. List 1 of the original SPIN-R recordings was used [6]. A new male talker (DF) with similar F_0 and speaking rate as the original SPIN-R talker recorded the eight lists in different speaking environments. Based on measures for sentences in List 1, the average F_0 was 121.7 Hz for DF and 120.5 Hz for the original talker. The average speaking rate was 4.3 syllables/sec for both talkers. List 1

was spoken by DF in quiet without headphones, and Lists 2, 7 and 8 were spoken in quiet while DF wore headphones (Sennheiser HD265 Linear). DF was instructed to “speak normally” for Lists 1 and 2, to “speak clearly” for List 7, and to “speak loudly” for List 8. Lists 3 to 6 were spoken while DF heard noise presented over headphones: Lists 3 and 5 were spoken in speech spectrum noise at 62 and 66 dB SPL, respectively; Lists 4 and 6 were spoken in multi-talker babble at 62 and 66 dB SPL, respectively. All sentences were digitized at 24 kHz, low-pass filtered at 6 kHz, and matched on RMS level.

2.3 Experiment procedure

Each participant was tested on the eight lists (eight talking conditions), with list order counterbalanced. Sentences were presented monaurally under TDH-50P earphones at 50 dB SL (relative to participant’s average pure-tone threshold for 0.5, 1, and 2 kHz). Each sentence was presented with corresponding files of multi-talker babble at 0 dB S:N. Participants were instructed to report the last word of every sentence. There were no time constraints on responding, and guessing was encouraged.

2.4 Acoustical analysis procedure

Several acoustical measures were taken of the stimuli, using the PRAAT speech analysis program [7]. For every sentence, the time boundaries of target words and their phonemes were marked. A script was then used to generate measures of duration, F_0 , and intensity for each target word, as well as F_1 to F_3 for the vowel in the word.

3. RESULTS

3.1 Word identification

Figure 1 shows the performance of younger and older adults. In general, words were identified better in the high-context than low-context conditions. Younger adults correctly identified more words in noise than older adults, especially in the low-context condition. Both age groups found the new talker to be more intelligible than the original one. Word identification was best for talking conditions with louder noise environments (conditions 4 and 6), when the type of noise in the talking environment matched that of the listening environment (conditions 3 and 4), and when the talker was instructed to “speak loudly” (condition 8).

This description was confirmed by an Analysis of Variance (ANOVA) with age as a between-subjects factor, and talking condition and context as within-subjects factors.

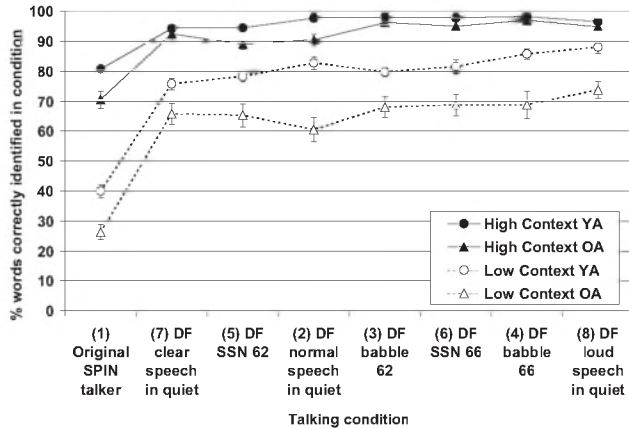


Fig. 1. Mean percent of correctly identified target words in 8 talking conditions, for 16 younger adults (YA) and 16 older adults (OA). Results are categorized into high- and low-context conditions. Standard error bars are shown.

There were main effects of age, $F(1,30) = 17.03, p < 0.001$, context, $F(1,30) = 531.02, p < 0.001$, and talking condition, $F(7,210) = 173.99, p < 0.001$. Performance in all conditions with the new talker was better than with the original talker, and performance in the set of conditions 3, 6, 4 and 8 was equivalent, but better than in all other conditions ($p = 0.05$). There were significant interactions of age and talking condition, $F(7, 210) = 3.260, p < 0.01$, and age and context, $F(1,30) = 24.83, p < 0.001$, with age-related differences being greater in the low-context condition ($p = 0.01$).

3.2 Talker differences

Compared to the original talker, DF's speech had more energy in the higher frequency range (Fig. 2). For DF, his speech in noise had more energy in the 2-5 kHz range than his speech in quiet. Clear speech had less energy in the 3-4 kHz, but more energy in the 4-5 kHz range, whereas loud speech was the opposite, with more energy in the 2-4 kHz and less in the 4-6 kHz range.

There were significant differences between lists for target word properties (Table 1), as confirmed by one-way ANOVAs for duration, $F(4, 120) = 3.76, p < 0.01$, intensity, $F(4, 120) = 11.58, p < 0.001$, and F_0 , $F(4, 120) = 14.23, p < 0.001$, but not for F_1, F_2 or F_3 . Tukey's *HSD* test showed that duration, F_0 , and intensity were not significantly different between the original talker and DF. Within-talker, there were no significant differences between Lists 2, 4, and 7, but word duration in Lists 4 and 7 was slightly longer than in List 2 ($p = 0.05$). List 8 words had significantly higher F_0 and intensity compared to other lists ($p = 0.01$).

Table 1. Acoustical measures of target words in five selected lists

Background	Quiet				Babble at 66 dB
	No	Yes	Clear	Loud	Yes
Headphones	Normal				Normal
Instructions	SPIN 1	DF 2	DF 7	DF 8	DF 4
Talker & list	SPIN 1	DF 2	DF 7	DF 8	DF 4
Duration (ms)	488	521	559	522	547
Intensity (dB)	66.1	66.8	66.1	68.1	66.8
F_0 (Hz)	112	121	102	145	117
F_1 (Hz)	578	637	576	648	610
F_2 (Hz)	1437	1429	1529	1528	1516
F_3 (Hz)	2434	2493	2447	2524	2462

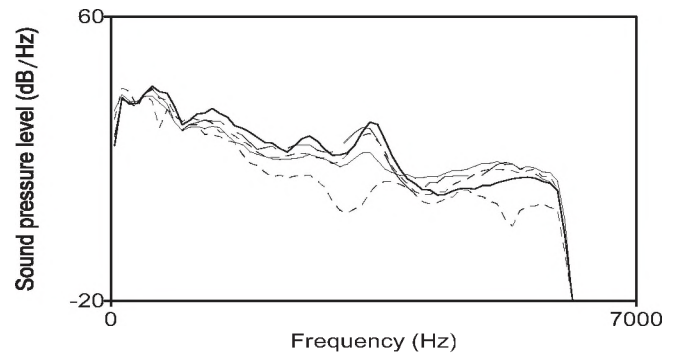


Fig. 2. Long-term average spectrum of target words spoken by the original talker (lower dotted line); DF in quiet (upper dotted line); DF in 66 dB SPL babble (dashed line); DF "speaking clearly" (non-bolded line) and DF "speaking loudly" (bolded line).

4. DISCUSSION

Our results support previous findings that speech produced in noise is more intelligible than speech produced in quiet, when tested in noise. For both age groups, accuracy was influenced by within- and between-talker differences, but older adults seemed to benefit more from speech produced in relevant conditions. Since all sentences were equated for overall intensity, the differences in intelligibility between lists may be due to properties of the target word itself. Specifically, there were changes in the intensity, duration, and F_0 of the target words. Although target words spoken by DF in quiet were more intelligible than those of the original talker, they did not differ significantly in duration, F_0 or intensity. However, as shown in Fig. 2, DF produced more high-frequency energy, which may account in part for the between-talker differences. For DF, words spoken in noise were more intelligible than words spoken in quiet, but they do not differ significantly in duration, F_0 or intensity. However, words spoken "loudly" had greater F_0 and intensity compared to words spoken "normally" in quiet, which may explain their greater intelligibility in noise. A combination of acoustic cues may be needed to explain the pattern of results.

REFERENCES

- [1] L. E. Lombard. (1911). Le signe de l'elevation de la voix. *Ann. Mal. Oreil. Larynx*, 37, 101-119.
- [2] T. Letowski, T. Frank, & J. Caravella. (1993). Acoustical properties of speech produced in noise presented through supra-aural earphones. *Ear & Hearing*, 14, 332-338.
- [3] J. Junqua. (1993). The Lombard reflex and its role on human listeners and automatic speech recognizers. *JASA*, 93, 510-524.
- [4] W. V. Summers, D. B. Pisoni, R. H. Bernacki, R. I. Pedlow & M. A. Stokes. (1988). Effects of noise on speech production: Acoustic and perceptual analyses. *JASA*, 84, 917-928.
- [5] M. K. Pichora-Fuller & P. Souza. (2003). Effects of aging on auditory processing of speech. *Int. J. Audiol*, 42, S11-S16.
- [6] R. Bilger, J. Nuetzel, W. Rabinowitz & C. Rzeczkowski. (1984). Standardization of a test of speech perception in noise. *JSHR*, 27, 32-48.
- [7] P. Boersma and D. Weenik, "Praat: Doing phonetics by computer (version 4.5.08)" [Computer program], 2006 Apr 4 [cited 2007 Jul 22], Available HTTP: <http://www.praat.org/>

ACKNOWLEDGMENTS

This project was funded by CIHR and NSERC.

AN ALGORITHM FOR FORMANT FREQUENCY ESTIMATION FROM NOISE-CORRUPTED SPEECH SIGNALS

Shaikh Anowarul Fattah, Wei-Ping Zhu, and M. Omair Ahmad

Centre for Signal Processing and Communications, Dept. of Electrical and Computer Engineering
Concordia University, Montreal, Quebec, Canada H3G 1M8
{shaik_fa, weiping, omair}@ece.concordia.ca

1. INTRODUCTION

Formant frequency estimation of speech signals plays an important role in speech synthesis, compression, and recognition. For example, formant information serves as a significant acoustic feature and offers a phonetic reduction in speech recognition. It plays a vital role in the design of some hearing aids [1]. Free resonances of the vocal-tract (VT) system are called formants. Formants are associated with peaks in the smoothed power spectrum of speech. Among different formant estimation techniques, linear predictive coding (LPC) based methods have received considerable attention [2]. In this case, formant frequencies are computed from the autoregressive (AR) parameters of the VT system. Most of the formant frequency estimation methods, so far reported, deal only with noise-free environments. However, formant estimation from noisy speech signals is difficult but an essential task as far as practical applications are concerned. In order to handle noisy environments, recently in [1], a method based on an adaptive band-pass filter-bank, later referred as AFB method, has been proposed where the estimation accuracy depends on initial estimates.

In this paper, we propose a scheme for accurately estimate the formant frequencies of speech signals in a noisy environment. First, a frequency domain noise reduction scheme is proposed. The ACF of the resulting noise-compensated speech signal is then employed in a modified form of least-squares Yule-Walker equations (LSYWE) to estimate poles of the VT system. Finally, a pole selection criterion has been introduced for extracting the desired formants which enables the proposed scheme to avoid errors associated with weak formants. Experimental results on natural and synthetic vowels in the presence of additive white noise are presented.

2. PROPOSED METHOD

The overall vocal-tract (VT) filter can be represented by a P -th order AR system with a transfer function given by

$$H(z) = \frac{G}{A(z)} = \frac{G}{1 - \sum_{i=1}^P a_i z^{-i}} = \frac{G}{\prod_{i=1}^P (1 - p_i z^{-1})} \quad (1)$$

where G is the gain factor, $\{a_i\}$ the AR parameters of the filter $A(z)$, and the system pole $p_k = r_k e^{j\omega_k}$ with a pole magnitude r_k and angle ω_k . During a short duration of time, a speech signal, the output of the VT filter, is generally assumed to be stationary. A pair of complex conjugate poles is required to model the formant frequency (F_k) and bandwidth (B_k), respectively, defined as

$$F_k = \frac{F_s}{2\pi} \omega_k; \quad B_k = -\frac{F_s}{\pi} \ln(r_k) \quad (2)$$

where F_s is the sampling frequency. In the autocorrelation method, formants are estimated from the AR parameters using a least-squares (LS) solution of the following relation [2]

$$r_x(\tau) = \sum_{k=1}^P a_k r_x(\tau - k), \quad \tau = 1, 2, \dots, P \quad (3)$$

where $r_x(\tau)$ is the autocorrelation function (ACF) of an N length sequence $x(n)$ and its estimate can be computed as

$$r_x(\tau) = \frac{1}{N} \sum_{n=0}^{N-1-|\tau|} x(n)x(n+|\tau|), \quad \tau = 0, 1, \dots, L'-1; L' \leq N \quad (4)$$

In order to reduce the estimation variance, a combination of more than P equations can be used in the LS estimation.

In the presence of noise $v(n)$, the observed signal is given by

$$y(n) = x(n) + v(n) \quad (5)$$

The ACF of $y(n)$ can be expressed as

$$r_y(\tau) = r_x(\tau) + r_w(\tau), \quad r_w(\tau) = r_v(\tau) + r_{vv}(\tau) + r_{xv}(\tau) \quad (6)$$

It can be observed that in the presence of $r_w(\tau)$, the ACF introduced by the noise, it is difficult to obtain an accurate estimate of $r_x(\tau)$. Even in the case of white Gaussian noise, at a heavy noisy condition, the effect of $r_w(\tau)$ on $r_x(\tau)$ cannot be completely neglected just after the zero lag. In order to reduce the noise effect, instead of directly using the noisy signal, first, we proposed to obtain a noise-compensated signal as

$$\tilde{y}(n) = F^{-1} \left[|Y_C(\omega)| e^{j\angle Y(\omega)} \right], \quad Y_C(\omega) = |Y(\omega)| - \lambda |Y_{HF}(\omega)| \quad (7)$$

If $Y_C(\omega) \leq 0$, set $Y_C(\omega) = 0$

where $Y(\omega)$ is the Fourier transform (FT) of $y(n)$, $\hat{Y}_{HF}(\omega)$ is the average value computed from the high frequency region of $Y(\omega)$, and λ is a scaling factor with $\lambda \leq 1$ to avoid overcompensation. Since, in practical applications it is sufficient to estimate first few formants and speech spectrum shows a decaying nature, only the high frequency region is considered to obtain $\hat{Y}_{HF}(\omega)$. Note that, in the inverse FT operation, we have utilized the phase information of the noisy signal and negative values of $Y_C(\omega)$ are forced to zero to obtain a better result in a noisy environment. In addition, very low frequency region (<100 Hz) is excluded which is not in our interest. Thus, the effect of additive white Gaussian noise $v(n)$ on $x(n)$ is significantly reduced and from $\tilde{r}_y(\tau)$, the ACF of $\tilde{y}(n)$, one may obtain an estimate of $r_x(\tau)$ as

$$\hat{r}_x(\tau) = \begin{cases} \tilde{r}_y(\tau) - r_v(\tau), & \text{for } \tau = 0 \\ \tilde{r}_y(\tau), & \text{for } \tau \neq 0 \end{cases} \quad (8)$$

Since, the zero lag value causes a significant error, considering $\tau = P + 1, \dots, P + S$ in (4), a modified form of LSYW equations excluding zero lag can be obtained as

$$\begin{bmatrix} \tilde{r}_y(P) & \tilde{r}_y(P-1) & \dots & \tilde{r}_y(1) \\ \tilde{r}_y(P+1) & \tilde{r}_y(P) & \dots & \tilde{r}_y(2) \\ \vdots & \vdots & & \vdots \\ \tilde{r}_y(P+S-1) & \dots & \dots & \tilde{r}_y(S) \end{bmatrix} \begin{bmatrix} a_1 \\ a_2 \\ \vdots \\ a_P \end{bmatrix} = - \begin{bmatrix} \tilde{r}_y(P+1) \\ \tilde{r}_y(P+2) \\ \vdots \\ \tilde{r}_y(P+S) \end{bmatrix} \quad (9)$$

Here S governs the number of equations. An estimate of AR parameters can be obtained from the LS solution of (9) as

$$\hat{\mathbf{a}} = (\hat{\mathbf{R}}^T \hat{\mathbf{R}})^{-1} \hat{\mathbf{R}}^T \hat{\mathbf{f}} \quad (10)$$

Thus, system poles are estimated and an estimate of formant frequencies can be obtained using (2). In our implementation, we perform the formant estimation every 10 ms with a 20 ms window applied to overlapping voiced speech segments. In literature, the region of formant frequencies has been well studied [2]. There exists a high degree of overlaps between the formant frequency regions. First, we estimate F1 from a pole with the highest magnitude inside the F1-region. The pole, outside F1 but within F2-region, having the highest magnitude is chosen for F2. In this way the three formants are estimated. A spectral peak-picking operation is performed to estimate a formant if no pole is obtained in a particular region.

3. SIMULATION RESULTS

The proposed formant frequency estimation algorithm has been tested using different synthetic vowels synthesized using the Klatt synthesizer [2] and natural vowels from the North Texas speech database [3], and some natural sentences from the TIMIT speech database with their reported formant references [4]. For the performance comparison, the 12th order LPC [2] and the AFB methods [1] are considered and the percentage root-mean-square error (RMSE) at different noise levels are computed with $S = 4P$ where each noise level consists of 20 independent trials of noisy environments.

Table 1. %RMSE (Hz) for Synthetic Vowels

Vowels			0 dB			5 dB		
			Prop.	LPC	AFB	Prop.	LPC	AFB
Male	/a/	F1	12.63	23.63	31.29	8.93	15.87	11.74
		F2	13.57	27.78	34.82	4.62	15.53	9.51
		F3	11.65	19.28	19.34	7.28	13.19	8.23
	/i/	F1	23.54	28.53	28.16	15.93	19.28	16.25
		F2	4.02	9.68	4.27	2.94	7.54	3.33
		F3	5.78	13.29	7.75	3.81	7.82	3.97
Female	/a/	F1	11.51	17.76	16.76	5.71	9.76	15.67
		F2	9.52	19.43	14.39	5.35	8.68	7.49
		F3	3.84	9.26	4.57	2.11	3.18	2.34
	/i/	F1	30.29	39.81	32.27	17.75	28.27	19.14
		F2	11.92	26.21	13.78	5.89	12.43	6.19
		F3	3.04	15.83	3.78	2.31	7.63	2.78

Table 2. %RMSE (Hz) for Natural Vowels

Vowels			0 dB			5 dB		
			Prop.	LPC	AFB	Prop.	LPC	AFB
Male	/a/	F1	12.14	14.33	13.93	7.34	9.57	8.54
		F2	19.29	44.93	28.76	14.62	28.27	16.29
		F3	14.93	38.01	23.34	12.28	23.67	18.31
Female	/i/	F1	10.72	21.19	16.84	5.72	8.61	5.95
		F2	13.17	23.78	19.49	6.81	11.28	10.21
		F3	15.48	31.29	24.82	5.28	21.92	14.58

In Table 1, the estimated %RMSE (Hz) is shown for two synthesized vowels at SNR = 0 dB and 5 dB. It is clearly observed that the proposed method is able to provide lower %RMSE at low SNRs for both male and female speakers. In Table 2, estimation accuracy in terms of %RMSE (Hz) for natural vowels /a/ and /i/ (contained in the words ‘‘hod’’ and ‘‘heed’’) are shown. It is found that the proposed method provides better estimation accuracy at both conditions.

4. CONCLUSION

The proposed formant frequency estimation algorithm is capable of handling noisy environments, since, a noise-compensated speech signal is used in a modified form of LSYW equations along with an effective formant selection criterion. Experimental results on natural and synthetic speech signals show the efficacy of the proposed method in estimating formant frequencies at a moderate to low levels of SNR.

REFERENCES

- [1] Mustafa, K. and Bruce, I.C. (2006). Robust formant tracking for continuous speech with speaker variability. *IEEE Trans. Audio Speech Lang. Processing*, 14, 435–444.
- [2] O’Shaughnessy, D. (2000). *Speech Communications: Human and Machine* (2nd ed.). IEEE Press, NY.
- [3] Hillenbrand, J.M., Getty, L.A., Clark, M.J., and Wheeler, K. (1995). Acoustic characteristics of American English vowels. *J. Acoust. Soc. Am.*, 97, 3099–3111.
- [4] Deng, L., Cui, X., Pruvencok, R., Huang, J., Momen, S., Chen, Y., and Alwan, A. (2006). A database of vocal tract resonance trajectories for research in speech processing. *In Proc. ICASSP’06*, 1, 369–372.

DÉBRUITAGE PAR ONDELETTES DE LA PAROLE EN MILIEU INDUSTRIEL

Cécile Le Cocq¹, Frédéric Laville¹ et Christian Gargour²

¹Département de génie mécanique, ²Département de génie électrique,
École de Technologie Supérieure, 1100 rue Notre-Dame Ouest, Montréal (Qc) H3C1K3
cecile.lecocq@etsmtl.ca

1. INTRODUCTION

Dans l'industrie, bon nombre de travailleurs sont exposés à des niveaux sonores élevés qui peuvent causer des pertes auditives. Afin de préserver l'audition des travailleurs, le port de protecteur auditifs est une solution efficace et peu coûteuse mais qui entraîne une diminution des capacités à percevoir les signaux d'alarme et à comprendre la parole. De nombreuses techniques de débruitage de la parole existent ; elles sont couramment utilisées dans le domaine de la téléphonie. Ces méthodes peuvent-elles pour autant être appliquées dans un milieu industriel où les bruits sont différents et surtout où leur niveau sonore est beaucoup plus élevé ?

L'étude réalisée ici porte sur le débruitage par ondelettes de la parole en milieu industriel. Le but de cette étude est de poser les premières bases d'une recherche portant sur l'amélioration de la compréhension de la parole par les travailleurs du milieu industriel qui portent des protecteurs auditifs. Avant de présenter les méthodes considérées ainsi que les résultats obtenus, une brève mise en contexte est réalisée afin de présenter le milieu sonore dans lequel oeuvrent les travailleurs de l'industrie.

2. LE CONTEXTE SONORE EN MILIEU INDUSTRIEL

Trois types de signaux sonores sont présents en milieu industriel : le bruit des machines, que nous qualifierons «industriels», les signaux d'alarme et la parole.

- Les bruits industriels peuvent être classés en deux catégories : les bruits non-stationnaires et les bruits stationnaires. Les bruits non-stationnaires sont par exemple des coups de marteaux donnés sur des plaques de métal. Les bruits stationnaires sont par exemples générés par les transformateurs électriques. Le niveau sonore dans les entreprises est la plupart du temps compris entre 70 et 110 dBA. À faible niveau les bruits industriels vont causer une gêne, à fort niveau ils vont entraîner des pertes auditives en l'absence de protecteurs.
- Les signaux d'alarme transmettent des informations importantes aux travailleurs. Il peut s'agir par exemple de l'alarme incendie, de l'avertisseur de recul de véhicule ou d'un signal sonore délivré par une machine pour indiquer un mauvais fonctionnement de celle-ci. Il est donc primordial que les travailleurs puissent entendre, distinguer et comprendre la signification de ces signaux.
- Le niveau normal de la parole est d'environ 60 dBA. Les travailleurs de l'industrie qui oeuvrent en milieu bruyant auront tendance à crier pour se faire comprendre.

3. MÉTHODES

De nombreuses variantes de la technique du débruitage par ondelettes de la parole existent. Ne sont présentées ici que les méthodes testées. Le débruitage de la parole par ondelettes consiste à appliquer un algorithme de seuillage THR sur les coefficients de la transformée en ondelettes du signal bruité, en fonction d'un seuil T . Soient s un signal de parole «propre» et w un bruit industriel. Le signal bruité x est défini par $x = s + w$. Dans le domaine de la transformée en ondelettes, cette expression devient : $X = S + W$. Le signal débruité \tilde{S} s'obtient alors par : $\tilde{S} = \text{THR}(X, T)$. L'algorithme de seuillage THR dépend de trois paramètres que sont la règle de seuillage, l'estimation de l'écart type du bruit $\tilde{\sigma}$ et le calcul du seuil T .

- Les premières règles de seuillage ont été définies par Donoho et Johnstone [1]. Il s'agit des seuillages mou THR_m et dur THR_d qui sont définis de la manière suivante :

$$\text{THR}_m(X, T) = \begin{cases} \text{sgn}(X)(|X| - T) & |X| \geq T \\ 0 & |X| < T \end{cases} \quad (1)$$

$$\text{THR}_d(X, T) = \begin{cases} X & |X| \geq T \\ 0 & |X| < T \end{cases} \quad (2)$$

Ces deux règles de seuillages ont l'inconvénient d'altérer le signal de parole, en raison des coefficients qu'elles forcent à zéro. Dans le but d'éviter ce problème, d'autres règles de seuillage ont été proposées. Nous considérerons ici deux règles «hybrides» des seuillages mou et dur qui ont été proposées par Nordström et all. [2] ; il s'agit des seuillages super mou THR_{sm} et dur mou THR_{dm} qui dépendent du paramètre $\alpha \in [0, 1]$ qui correspond au gain appliqué au signal bruité quand l'amplitude du dit signal est inférieure au seuil T :

$$\text{THR}_{sm}(X, T) = \begin{cases} \text{sgn}(X)(|X| - (1 - \alpha) T) & |X| \geq T \\ \alpha X & |X| < T \end{cases} \quad (3)$$

$$\text{THR}_{dm}(X, T) = \begin{cases} X & |X| \geq T \\ \alpha X & |X| < T \end{cases} \quad (4)$$

- L'estimation de l'écart type du bruit sera calculé pour chaque niveau d'analyse selon la formule $\tilde{\sigma}_j = \text{MAD}(X_j)/0.6745$ proposée par Johnstone et Silverman [3] où $\text{MAD}(X_j)$ représente l'écart absolu médian au niveau j d'analyse.
- Le seuil universel, qui a été introduit au départ par Donoho et Johnstone [1], sera utilisé avec la formulation pro-

posée par Johnstone et Silverman [3] pour les bruits colorés : $T_u(j) = \tilde{\sigma}_j \sqrt{2 \log N}$.

4. ÉVALUATION DES PERFORMANCES

Afin d'évaluer les performances des différentes méthodes présentées dans un milieu industriel, les algorithmes ont été testés sur dix phrases, prononcées par un homme, extraites de la base de données TIMIT. Ces signaux de parole ont été altérés par deux bruits industriels stationnaires issus de la base de données NOISEX selon les rapports signal à bruit (SNR) de -10 dB, -5 dB, 0 dB et 5 dB. La transformée en ondelette discrète avec l'ondelette Daubechies d'ordre 4 sur 10 niveaux d'analyse a été appliquée aux signaux débruités. Le paramètre α des règles hybrides de seuillage a été choisi égal à 0.1. Pour quantifier les performances du débruitage, deux critères quantitatifs ont été utilisés : le gain en terme de SNR et la mesure de distorsion d'Itakura-Saito (IS) [4]. Les tableaux 1 et 2 présentent les performances obtenues en terme de gain du SNR et de la mesure IS pour les quatre règles de seuillage considérées et pour les différents SNR du signal bruité.

Tableau 1. Performances moyennes obtenues en terme de gain du rapport signal à bruit

SNR	dur	mou	super mou	dur mou
-10	9.7	9.8	10.1	10.0
-5	6.3	5.7	6.3	6.9
0	3.1	1.7	2.5	3.9
5	0.3	-1.9	-1.1	1.1

Tableau 2. Performances moyennes obtenues en terme de mesure de distorsion d'Itakura-Saito

SNR	dur	mou	super mou	dur mou
-10	2400	2500	7.7	6.1
-5	2300	2400	9.4	7.0
0	4000	4200	10.6	7.3
5	5900	6200	11.0	7.1

Il est à remarquer sur le tableau 2 que les performances moyennes obtenues en terme de mesure IS pour les règles de seuillages dur et mou sont très élevées, beaucoup plus élevées que celles couramment rencontrées dans la littérature. L'écoute des signaux correspondant a permis de confirmer qu'ils étaient inintelligibles. La mesure IS (voir tableau 2) permet de vérifier que les règles de seuillages dur et mou, qui forcent des coefficients à zéro, dégradent beaucoup l'intelligibilité de la parole. Les règles de seuillages hybrides, qui ont été définis afin de résoudre ce problème, n'altèrent que très légèrement l'intelligibilité de la parole. Il est également à remarquer que la règle de seuillage dur mou donne une plus faible distorsion de la parole que la règle de seuillage super mou. En effet le seuillage dur mou ne modifie pas les coefficients d'ondelette significatifs, alors que le seuillage super mou les diminue. Les performances en terme de gains du SNR (voir tableau 1) sont légèrement supérieures pour les règles de seuillages hybrides que pour les règles de seuillages dur et mou. De plus, pour les SNR élevés, la règle de seuillage dur mou donne un gain en terme de SNR plus important

que la règle de seuillage super mou. Selon les deux critères considérés, la règle de seuillage dur mou permet donc d'obtenir les meilleures performances.

5. CONCLUSION

La présentation du contexte sonore en milieu industriel a permis d'explicitier les différentes problématiques en terme de santé et sécurité des travailleurs. Parmi les méthodes considérées et dans les conditions testées, la règle de seuillage dur mou permet d'obtenir les meilleures performances en terme de gain du SNR et de mesure IS pour le débruitage de la parole en milieu industriel. Cette première étude réalisée sur le débruitage par ondelettes en milieu industriel a permis de mettre en évidence l'importance du choix de la méthode de débruitage afin de conserver l'intelligibilité de la parole : la règle de seuillage choisie ne doit forcer aucun coefficients à zéro et doit éviter de diminuer les coefficients d'ondelette significatifs. L'algorithme de débruitage utilisant la règle de seuillage dur mou n'est pas pour autant le choix «optimal». En effet cette règle de seuillage est discontinue et doit donc diminuer l'intelligibilité du signal de parole. Par ailleurs nous n'avons testé que le seuil universel pour lequel il a été montré que dans certaines conditions expérimentales il n'est pas le plus approprié [5]. En résumé, les performances du débruitage de la parole en milieu industriel devraient pouvoir être améliorées en utilisant une règle de seuillage continue, qui ne force aucun coefficient à zéro et qui n'atténue pas les coefficients d'ondelettes significatifs, avec un seuil approprié.

REMERCIEMENTS

Les auteurs expriment leur reconnaissance à la compagnie SONOMAX HEARING HEALTHCARE INC. et au CRSNG (Conseil de recherches en sciences naturelles et en génie du Canada) pour leur soutien à ce projet.

BIBLIOGRAPHIE

- [1] David L. Donoho and Iain M. Johnstone. Ideal spatial adaptation by wavelet shrinkage. *Biometrika*, 81(3):425–455, 1994.
- [2] F. Nordström, B. Holst, and B. Lindoff. Time and frequency dependent noise reduction in speech signals. In *The International Conference on Signal Processing Applications and Technology*, Orlando, Florida, USA, 1999.
- [3] I. M. Johnstone and B. W. Silverman. Wavelet threshold estimators for data with correlated noise. *Journal of the Royal Statistical Society Series B-Methodological*, 59(2):319–351, 1997.
- [4] John H.L. Hansen and Bryan Pellom. An effective quality evaluation protocol for speech enhancement algorithms. In *ICSLP-98: Inter. Conf on Spoken Language Processing*, volume 7, pages 2819–2822, Sydney, Australia, 1998.
- [5] David L. Donoho and Iain M. Johnstone. Adapting to unknown smoothness via wavelet shrinkage. *Journal of the American Statistical Association*, 90(432):1200–1225, 1995.

A TIME-DOMAIN PITCH EXTRACTION SCHEME FOR NOISY SPEECH SIGNALS

Celia Shahnaz, Wei-Ping Zhu, and M. Omair Ahmad

Centre for Signal Processing and Communications, Dept. of Electrical and Computer Engineering
Concordia University, Montreal, Quebec, Canada H3G 1M8

{c_shahna, weiping, omair}@ece.concordia.ca

1. INTRODUCTION

Pitch is the primary acoustic cue in several applications like voiced/unvoiced classification, speaker recognition, speech enhancement, synthesis, coding, and articulation training for the deaf learning to speak. During the production of speech, the vibration of vocal folds appears to be periodic and the estimation of pitch involves determination of the fundamental frequency (F_0) or fundamental period (T_0) of this vibration. The extraction of pitch is the object of research over the past several decades [1]-[3]. All the algorithms proposed in the literature for clean speech may be broadly classified into three categories, namely, algorithms using time domain properties, algorithm using frequency domain properties and algorithms using both time and frequency domain properties of the speech signals. However, performance of these methods degrades under noisy conditions as noise obscures the periodic structure of speech.

In this paper, a new time-domain pitch extraction scheme for speech signals subject to noise degradation is presented. In order to remove the deleterious vocal-tract information, we propose to pass the pre-processed noisy speech through an inverse filter whose parameters are derived from the Linear Prediction (LP) analysis, yielding an output referred to as the LP residual. The novelty of the proposed scheme lies in the introduction of a new average magnitude sum function (AMSF) of the LP residual which is expected to reveal more prominent peaks at integral multiples of the pitch period compared to that revealed by the LP residual. With a view to quell the pitch-errors considerably in a severe noisy scenario, the peaks of AMSF at different pitch-harmonic locations are added and weighted by a periodicity dependent weighting factor for every possible pitch period. The resulting weighted and harmonically summed AMSF of the LP residual is globally maximized to extract the desired pitch period. The proposed method is able to reflect its efficacy to a significant extent for extracting pitch of both low and high-pitched speakers in the white or car environmental noise.

2. PROPOSED METHOD

Let $x(n)$ and $v(n)$ denote clean speech and uncorrelated additive noise, respectively. The observed noisy signal $y(n)$, given by, $y(n) = x(n) + v(n)$, is divided into

overlapping frames with frame size N by applying a window function $w(n)$. The windowed noisy frame denoted as $y_w(n)$ is filtered using a low-pass filter (LPF) to retain only the first formant (e.g., the 0-900 Hz range). The time domain pre-processed noisy speech is denoted as $y_{PPS}(n)$.

The instant at which the closure of vocal folds occurs within a pitch period is defined as the GC event. One approach to derive information about the GC events for the extraction of pitch of speech signal is the Linear Prediction (LP) analysis. In the LP analysis, assuming $y_{PPS}(n)$ as the output of an autoregressive (AR) spectral shaping filter [1], the predicted sample of $y_{PPS}(n)$ can be modeled by a linear combination of the p previous output samples, $\tilde{y}_{PPS}(n) = -\sum_{k=1}^p a_k y_{PPS}(n-k)$,

here, p is the order of prediction and $\{a_k\}$ are the LP Coefficients (LPCs) computed using the following equations,

$$R_y(l) = -\sum_{k=1}^p a_k R_y(l-k), \quad l=1,2,3,\dots,p \quad (1)$$

here, $R_y(l)$, the ACF of $y_{PPS}(n)$, can be estimated as,

$$R_y(l) = \frac{1}{N} \sum_{n=0}^{N-1-l} y_{PPS}(n) y_{PPS}(n+l), \quad l \geq 0 \quad (2)$$

In order to handle the noisy environment, $l = p+1, p+2, \dots, p+S$ are considered in (1) and thus yielding the following modified least-squares Yule-Walker (MLSYW) equations,

$$\begin{bmatrix} R_y(p) & R_y(p-1) & \dots & R_y(1) \\ R_y(p+1) & R_y(p) & \dots & R_y(2) \\ \vdots & \vdots & & \vdots \\ R_y(p+S-1) & \dots & \dots & R_y(S) \end{bmatrix} \begin{bmatrix} a_1 \\ a_2 \\ \vdots \\ a_p \end{bmatrix} = - \begin{bmatrix} R_y(p+1) \\ R_y(p+2) \\ \vdots \\ R_y(p+S) \end{bmatrix} \quad (3)$$

where, S governs the number of equations in (3). In order to reduce the estimation variance of Yule-Walker method, a combination of more than p equations are used. Least squares solution of (3) provides AR parameters $\{a_k\}$. To remove the information of vocal-tract (formants) from the extraction procedure of pitch, $y_{PPS}(n)$ is passed through an inverse or prediction filter which is given by,

$$A(z) = 1 + \sum_{k=1}^p a_k z^{-k} \quad (4)$$

where, $\{a_k\}$ are already derived from the LP analysis.

The output of the inverse filter is the error between the actual sample $y_{PPS}(n)$ and the predicted sample $\tilde{y}_{PPS}(n)$, which is referred to as the LP residual signal given by,

$$e(n) = y_{PPS}(n) + \sum_{k=1}^p a_k y_{PPS}(n-k) \quad (5)$$

As GC event is the place of significant excitation, large error is associated with GC event in the LP residual. One approach for the extraction of pitch is to detect the peaks at the GC events in the LP residual. It is possible to obtain the information about the pitch period (T_0) from the time difference of successive peaks of the LP residual. However, as a more convenient approach for the extraction of pitch from a noisy speech, an average magnitude sum function (AMSF) of the LP residual is proposed as,

$$\mathfrak{R}(l) = \frac{1}{N} \sum_{n=0}^{N-1} |e(n) + e(n+l)| \quad (6)$$

where, the property of high correlation among the samples of the LP residual around the GC events is exploited. For a quasi-periodic frame of voiced speech, $\mathfrak{R}(l)$ exhibits local maxima at $l = \rho T_0$, where ρ is an integer, $\rho=0,1,2,\dots$ and T_0 is the pitch period. Exploiting this feature, a weighted and harmonically summed AMSF of the LP residual is formulated as,

$$\chi(\tau) = \tau \sum_{\gamma=1}^{\partial} \mathfrak{R}(\gamma\tau), \quad \tau = \tau_{\min}, \dots, \tau_{\max} \quad (7)$$

where, τ represents the possible pitch-period that ranges from τ_{\min} to τ_{\max} . In general, for most male and female speakers, τ_{\min} and τ_{\max} are found, respectively, as $[F_s/(500\text{Hz})]$ and $[F_s/(50\text{Hz})]$ where, F_s is the sampling frequency. In (7), ∂ is the number of pitch-harmonics and it should be chosen such that $\partial\tau \leq M$. It is important to note that instead of considering only the global maximum of $\mathfrak{R}(l)$, since we sum up the peaks of $\mathfrak{R}(l)$ at different harmonics of every possible pitch-period with a periodicity dependent weighting factor, $\chi(\tau)$ exhibits clear and quite sharper peaks for voiced frames. Therefore, by searching for the global maximum of $\chi(\tau)$, the desired pitch frequency \hat{F}_0 is obtained as, $\hat{F}_0 = F_s/\hat{T}_0$ and $\hat{T}_0 = \underset{\tau}{\text{argmax}}[\chi(\tau)]$ is the estimated pitch period.

3. SIMULATION RESULTS

We have defined percentage gross pitch-error which is the ratio of the number of frames giving ‘‘incorrect’’ pitch values to the total number of frames. As reported in [3], estimated \hat{F}_0 is considered as ‘‘incorrect’’ if it falls outside 20% of the true pitch value F_0 . The performance of the proposed method is evaluated using the *Keele* reference database [4]. This database provides a reference pitch at a frame rate of 100 Hz with 25.6 ms window. The *Keele* database has studio quality, sampled at 20 kHz with 16-bit resolution. In order to use this database, we have chosen the same analysis parameters (frame rate and basic window size).

Table 1. Percentage gross pitch-error for the white noise corrupted speech at SNR = 5 dB

Speaker	Proposed Method	ACF Method	AMDF Method
Male	11.22	19.75	28.75
Female	6.12	16.54	19.4

Table 2. Percentage gross pitch-error for the car noise corrupted speech at SNR = 5dB

Speaker	Proposed Method	ACF Method	AMDF Method
Male	20.24	27.75	32.29
Female	10.26	17.31	21.25

For simulation, white and car noises from the *NOISEX'92* database are used as the additive background noises. The noisy speech with SNR varying from 5 dB to ∞ dB is considered for Simulations. For windowing operation, we have used a normalized hamming window. In the estimation of $\{a_k\}$ parameters by (3), S is chosen as $5p$ with $p=10$. We have evaluated and compared the performance of the proposed pitch detection scheme with the conventional average magnitude difference function (AMDF) and autocorrelation function (ACF) methods [2]. For a speaker group, the percentage gross pitch-error (GPE(%)) is calculated considering two male (or female) speakers. In Table 1. and Table 2., GPE(%) for male and female speaker group are summarized considering the white noise and car noise-corrupted speech signals, respectively, at an SNR=5 dB. It is evident that in comparison to the ACF and AMDF methods, GPEs(%) of the proposed algorithm are significantly reduced for both female and male speakers in the presence of a stationary white or a car noise.

4. CONCLUSION

In this paper, a new pitch detection algorithm for speech corrupted by a white or a car noise is presented considering the LP residual of the pre-processed speech as a representation for the GC events. A weighted and harmonically summed AMSF of the LP residual is proposed that is able to effectively quell the pitch-errors in the presence of a noise. Simulation results have shown that the proposed method significantly outperforms some of the reported pitch detection algorithms implemented in the same noisy environment.

REFERENCES

- [1] O'Shaughnessy, D. (2000). *Speech Communications: Human and Machine* (2nd ed.). IEEE Press, NY.
- [2] Rabiner, L., Cheng, M., Rosenberg, A., and McGonegal, C. (1976). A comparative performance study of several pitch detection algorithms. *IEEE Trans. Acoust., Speech, Signal Process.*, 24, 399–418.
- [3] Chevengne, Alain de, and Kawahara, Hideki (2002). YIN, a fundamental frequency estimator for speech and music. *J. Acoust. Soc. Amer.*, 111, 1917-1930.
- [4] Meyer, G., Plante, F., and Ainsworth, W.A. (1995). A pitch extraction reference database. *In Proc. EUROSPEECH'95*, 827-840.

SIMULATION OF THE THREE-DIMENSIONAL FLOW IN THE HUMAN LARYNX

S. Préseault Céré¹, A. Lormand², D. Redekop³ and G. Rouhi⁴

Dep. of Mechanical Engineering, University of Ottawa, 161 Louis-Pasteur, Ontario, CANADA, K1N 6N5
¹spres091@uottawa.ca, ²alorm055@uottawa.ca, ³dredkop@uottawa.ca, ⁴grouhi@uottawa.ca

1. INTRODUCTION

Human phonation has been studied using various methods since Flanagan's two mass model [1]. Titze [2], Alipour [3], and Scherer [4] have produced studies ranging from ex-vitro experiments using excised canine larynxes, duct type Plexiglas steady flow, and dynamic models and many using computational simulation and finite element methods. The role of the vocal fold is well explained and the fundamental frequency relatively well documented. Work has mostly been centered on the glottis, and other parts of the human larynx have only been the topic of a few studies. Three-dimensional analysis of airflow has only been a topic recently included in a few relatively recent works [5-6]. Open questions lie in explaining the hysteresis between the onset and offset threshold pressures in phonation [7], and the nature of the effect of the ventricular fold and supraglottis on the airflow—particularly on the separation point. This project is intended to build on these experiments in order to provide more details about these open questions.

2. METHOD

The three dimensional model was constructed as to represent realistic structures from the trachea up to the epiglottis. The model was designed using approximations based on a collection of average male values taken from morphometric studies. The subglottic and supraglottic zones were constructed based on morphometric measurements taken from [8] and [9]. The ventricular folds data is coming from laminographic tracings extracted from [4 and 10]. The lungs are treated as a constant pressure source. The flow assumed to be at steady state. Although some experiments do caution about using the quasi-steady assumption, as discussed in [11], it was considered appropriate for the current simulation. It is justified by the fact that the simulation is mostly intended as a qualitative investigation of the flow characteristics around the ventricular folds and that the model complexity is already inflicting a high computational cost.

The model geometry was also inspired from a collection of histological cuts of the human larynx in an attempt to mimic the variation in cross section of the ventricular folds. This tissue fold encloses the ventricular ligament that is attached on the thyroid cartilage and at the other end to the arytenoid cartilage. The lower border of this ligament, enclosed in mucous membrane, forms a

free crescentic margin, which constitutes the upper boundary of the ventricle of the larynx [12]. This feature seems to have been included in only two other models so far—a 2D model symmetrical about the larynx coronal plane [12] and in a coarse mesh 3D fluid structure model by [5]. Therefore, the current model has focused on the flow dynamics aspect of the problem using a more complex structure.

The CFD software that was used for the numerical work is coming from a package that is included with the CAD software SolidWorks with which the model was shaped. The solver numerically solves the Navier-Stokes equation, and the fluid elements are brick elements. No slip boundary condition on the wall was imposed, and the surface roughness was set to zero. The first of these assumptions might not be the most accurate simplification to apply considering the nature of the mucosa covering the inner walls of the larynx, but certainly should not greatly affect the results obtained in this study. Adiabatic walls were deemed to bring a sufficiently accurate simplification for the simulation as well.

Variable parameters were the lung pressures, vocal fold frontal angles (VFFAs), and vocal fold opening angles (VFOAs). The various geometrical parameter values used to modify the model shape are shown in Table 1.

Table 1: Model parameters

VFFA	-5°, 0°, 5°, 10°, 15°
VFOA	0°, 0.5°, 1°, 2°, 3°, 4°, 5°

3. RESULTS

The simulation highlighted the interaction between the VFFAs and flow rate. This was an expected result, as the shape of the opening facilitates flow the glottal impedance should decrease. Also, the flow rate and maximum velocity increased with increasing the lung pressure, which again is an expected result.

Study of the velocity profiles showed that when the VFFA were of divergent shape (5°, 10°, 15°) the highest velocity—and lowest pressure—occurred at the

inferior part of the vocal fold. The converging shape and flat (VFFA -5° , 0°) proved to bring the higher velocities closer to the superior edge of the vocal fold. The position of the peak flow velocities did correspond with the location of the lowest pressure; the lower pressure zone taking more span of the vocal fold length when the shape was diverging. Flow separation showed to occur at the superior tip of the vocal fold when the shape was flat and converging.

When flow adhered to one of the sides of the glottis—through the Coanda effect—noticeable recirculation occurred in the ventricle found on the same side. This is shown in Figure 1 and 2. Z-axis is the axis that is perpendicular to the plane of the cut and the Y-axis is positive pointing upward. Varying the VFOA did not show any significant effect on the flow behavior other than affecting the flow rate coming through the larynx.

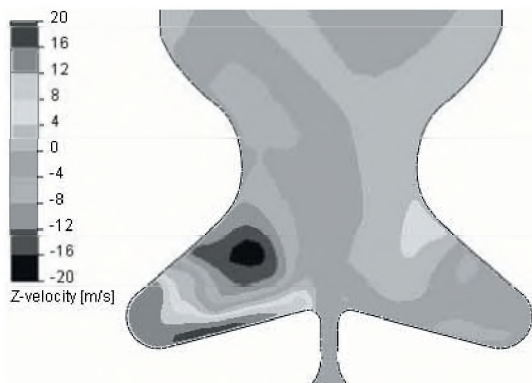


Figure 1: Recirculation in ventricle—VFFA= 0°

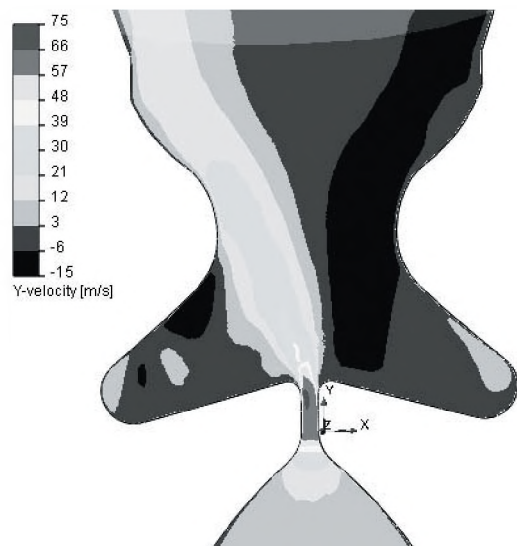


Figure 2: Y-Velocity—VFFA= 0°

4. DISCUSSION

The recirculation occurring in the ventricle when combined with the Coanda effect is enhancing the hypothesis that this effect could be a significant element on the behavior of the ventricular folds. For example, it could explain the action these folds have within a certain range of phonation, especially for certain singing techniques involving the vibration of these folds and screaming.

The relationship between the lowest pressure and the VFFA links the angle with the forced vibration induced by the flow circulating through the glottis. It leads to speculate on the importance of this on the hysteresis between onset and offset phonation pressure. In this context, a more complex simulation can confirm this hypothesis.

REFERENCES

- [1] Flanagan J, Ishizaka K, Synthesis of voiced sounds from a two-mass model of the vocal cords, *Bell System Tech Journal*, 1972, 51, 1233-1268
- [2] Titze IR, Phonation threshold pressure: A missing link in glottal aerodynamics, *J. Acoust. Soc. Am.* May 1992, 2926-2935
- [3] Alipour F, Scherer RC. Pulsatile airflow during phonation: an excised larynx model. *J. Acoust. Soc. Am.* 1995, 1242-1248
- [4] Scherer RC, De Witt KJ, Zhang C. Intraglottal pressure profiles for a symmetric and oblique glottis with a divergence angle of 10 degrees. *J. Acoust. Soc. Am.* 2001, 1616-1630
- [5] De Oliveira Rosa M, Pereira JC, Towards full-scale three-dimensional larynx simulation. *ICPVB 2004*
- [6] Li S, Scherer RC, The effects of three-dimensional geometry on intraglottal quasi-steady flow distributions and their relationship with phonation. *Science in China, Series C Life Sciences* 2006, 82-88
- [7] Plant RL, Freed GL, Plant RE. Direct measurement of onset and offset phonation threshold pressure in normal subjects. *J. Acoust. Soc. Am.* 2004, 3640-3646
- [8] Eckel HE, Sittel C, Morphometry of the larynx in horizontal sections. *American J. of Otolaryngology* 1995, 40-48.
- [9] Sprinzl GM, Eckel HE, Sittel C, Pototschnig C, Koebeke J. Morphometric measurements of the cartilaginous larynx: an anatomic correlate of laryngeal surgery. *Head and Neck* 1999, 743-750
- [10] Agarwal M, Scherer RC, Hollien H, The false vocal folds: shape and size in frontal view during phonation based on laminagraphic tracings. *Journal of Voice* 2002, 97-113
- [11] Li S, Scherer RC, The effect of glottal angle on intraglottal pressure, *J. Acoust. Soc. Am* 2006, 539-548
- [12] Gray, H, *Anatomy of the human body*, 20th Ed, 2000
- [13] Iijima H, Miki N and Nagai N, *Fundamental consideration of finite element method for the simulation of the vibration of vocal cords*, Hokkaido University, 1989.

EFFICIENT BLIND SPEECH SIGNAL SEPARATION COMBINING INDEPENDENT COMPONENT ANALYSIS AND BEAMFORMING

Qiongfeng Pan and Tyseer Aboulnasr

School of Information Technology and Engineering, University of Ottawa, 800 King Edward Ave., Ottawa ON, K16 6N5
aboulnasr@eng.uottawa.ca

1. Introduction

Teleconferencing is a common application where we need to separate different speakers whose speech is picked up by any given microphone. Such a problem has been tackled using Blind Source Separation (BSS) algorithms utilizing time and frequency domain information [1] and beamforming (BF) algorithms utilizing spatial information [2] from different point of views.

We investigate ways to combine these two approaches for improved overall system performance. While the popular BF approach utilizes the spatial information about the mixing system and/or source signals, BSS exploits a strong statistical condition: independence between source signals. These approaches have much in common since source signals coming from different locations in a BF scenario are likely to be independent as well. As such, it is worthwhile to explore the possibilities of combining their advantages. Recently, the relationship between convolutive BSS and BF has been investigated in [3] and some interesting results have been obtained. Based on these results, some combinations of convolutive BSS and BF have been proposed [7] to solve problems in BSS and obtained improved separation results.

In this paper, we propose a new approach combining BSS and BF for blind speech signal separation in real acoustic environment building on the work in [7]. In the beamforming stage, the Directions of Arrival (DOA)s of sources of interest are estimated blindly; then beamformers are constructed to extract signals from these directions. In the BSS stage, frequency domain convolutive algorithm is utilized to further reduce the interference in the given direction and improve the separation performance. Compared with existing systems, the proposed approach significantly reduces the computational complexity while maintaining comparable separation performance.

2. Convolutive Blind Source Separation and Beamforming

The convolutive BSS model is illustrated in Fig. 1. N source signals $\{s_i(k)\}$, $1 \leq i \leq N$, pass through an unknown N -input, M -output linear time-invariant mixing system to yield the M mixed signals $\{x_j(k)\}$. All source signals $s_i(k)$ are assumed to be statistically independent.

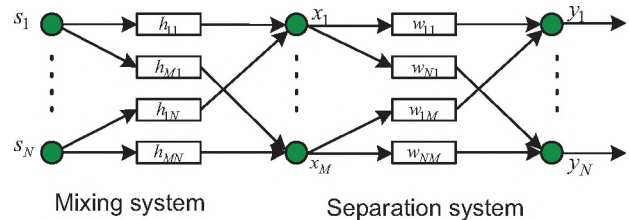


Fig. 1: Structure of convolutive blind source separation system

The j th sensor signal can be obtained by

$$x_j(k) = \sum_{i=1}^N \sum_{l=0}^{L-1} h_{ji}(l) s_i(k-l) \quad (1)$$

where $h_{ji}(l)$ is the impulse response from source i to sensor j , L defines the order of the FIR filters used to model this impulse response.

The i -th output of the unmixing system is given as:

$$y_i(k) = \sum_{j=1}^M \sum_{l=0}^{Q-1} w_{ij}(l) x_j(k-l) \quad (2)$$

By extending the instantaneous BSS algorithm to the convolutive case, we get the time domain update for the convolutive BSS algorithm using the natural gradient optimization approach [6]:

$$\Delta \underline{\mathbf{W}} = -\mu \frac{\partial D}{\partial \underline{\mathbf{W}}} \underline{\mathbf{W}}^T \underline{\mathbf{W}} = \mu \left[\mathbf{I} - E(\varphi(\mathbf{y}) \mathbf{y}^T) \right] \underline{\mathbf{W}} \quad (3)$$

where $\underline{\mathbf{W}}$ the unmixing matrix with FIR filters as its components. Convolutive BSS can also be performed in the frequency domain by using short-time Fourier Transform. This method is based on transforming the convolutive blind source separation problem into an instantaneous BSS problem at every frequency bin.

In [7], independent component analysis (ICA) is used to perform blind source separation at every frequency bin and the unmixing matrix obtained. Accordingly, the directivity pattern at each frequency bin can be obtained from its unmixing matrix. Directions of arrival (DOA) of source signals are estimated from the directions of nulls at all frequency bins. In the adaptation process, at each frequency bin, the null direction in the directivity pattern is compared with the estimated DOA of source signals. If it is steering to the proper direction, the unmixing matrix from ICA algorithm is used. If not, the null-steering beamformer constructed from the estimated DOA information is used to

substitute for the unmixing matrix. By doing so, the unmixing matrix can recover from a local minimum in the optimization procedure to improve its convergence speed.

At every iteration and at each frequency, the ICA algorithm is used to update the weight coefficients; then the DOA information at this frequency is obtained by searching for the null from the directivity pattern of unmixing matrix; the beamformer is formed for every frequency and a comparison is conducted between ICA and beamformer directions. All these operations are very time consuming and require significant computation. The separation performance is also very sensitive to the frame length of the frequency domain BSS algorithm and requires large frame lengths further increasing the computational complexity.

Studying the approach in [7], we can show that: i) low and high frequency bands do not provide good estimations of the DOA, ii) the accuracy of estimated DOAs is effectively independent of frame length, iii) A subset of frequency bands is sufficient to determine the unmixing matrix at every frequency bin to obtain DOA estimation.

3. Proposed Combined BF- BSS System and Simulation Results

The proposed system has two stages: i) blind BF used to obtain signal from estimated source directions and reduce reverberation effects ii) frequency domain BSS to further separate residual interferences in the selected direction and improve the separation performance.

In the BF stage, we implement a new DOA estimation algorithm [5] where the DOA can be independently estimated for mid frequency bins only effectively reducing the computational complexity. In the convolutive BSS stage, an unmixing system \mathbf{W} is adaptively adjusted to make the outputs as independent as possible to recover the independent source signals.

The mixed signals are generated by convolving speech signals with measured real room impulse responses. One signal is located at a DOA of 20 degrees and the other one is at a DOA of 60 degrees. The PESQ (Perceptual Evaluation of Speech Quality) score [4] is used to measure the subjective quality of the recovered speech signal compared to the original speech signal at each stage. The PESQ scores for the mixed signals, output signals from BF stage and output signals from BSS stage compared with the original signals are shown in Table 1. For the original mixture, each mixed speech signal is almost equally similar to both sources. BF and BSS stage ensure each output signals is more biased to one source and away from the other. This was confirmed by our informal listening test. Since the reverberant effects have been already reduced by the beamforming stage, the frame size of the FFT is much

smaller than that used in [7]. Thus, the computational complexity is further reduced.

Table 2 shows the PESQ improvement (defined as the sum of the PESQ score away from one source and PESQ score bias to the other source). Table 2 shows that the proposed system performs very well for speech separation in a real acoustic environment with reduced complexity and flexible system structure.

PESQ	Mixtures		Outputs from BF stage		Outputs from BSS stage	
	x1	x2	y1	y2	z1	z2
s1	1.62	1.60	1.73	0.63	2.11	0.25
s2	1.47	1.50	1.07	2.16	0.59	2.32

Table 1: PESQ scores from different stages

PESQ Improvement	BF Stage		BSS Stage	
s1	0.26	0.87	0.38	0.38
s2	0.55	0.56	0.48	0.16
Total	0.81	1.43	0.86	0.54

Table 2: PESQ improvement from different stages

4. Conclusions

By utilizing the properties of the unmixing matrix in the freq. domain, we propose a reduced complexity combined BF-BSS algorithm for speech separation in real acoustic environment. Performance is confirmed using PESQ scores.

REFERENCES

- [1] S. Haykin, ed., Unsupervised adaptive filtering (Volume I: Blind Source Separation), John Wiley & Sons, 2000.
- [2] B. D. Van Veen and K. M. Buckley, "Beamforming: A versatile approach to spatial filtering," IEEE ASSP Mag., Apr. 1988, pp.4-24.
- [3] S. Araki, S. Makino, Y. Hinamoto, R. Mukai, T. Nishikawa, and H. Saruwatari, "Equivalence between frequency domain blind source separation and frequency domain adaptive beamforming for convolutive mixtures," EURASIP Journal on Applied Signal Processing, vol. 2003, no. 11, pp. 1157-1166, Nov. 2003.
- [4] ITU-T Recommend P.862, "Perceptual evaluation of speech quality (PESQ), an objective method for end-to end speech quality assessment of narrowband telephone network and speech codecs," May 2000.
- [5] H. Sawada, R. Mukai, S. Araki, and S. Makino, "A robust and precise method for solving the permutation problem of frequency-domain blind source separation," IEEE Trans. Speech Audio Processing, vol. 12, no. 5, pp. 530-538, Sept. 2004.
- [6] S. Amari and A. Cichocki, "A new learning algorithm for blind signal separation," In advances in neural information processing systems 8, pp.757-763, MIT press, 1996.
- [7] H. Saruwatari, T. Kawamura, T. Nishikawa, A. Lee and K. Shikano, "Blind source separation based on a fast-convergence algorithm combining ICA and beamforming," IEEE Trans. Speech Audio Processing, Mar. 2006.

THE ACOUSTICS OF THE HELLENISTIC THEATRE OF EPIDAUROS : THE IMPORTANT ROLE OF THE SEAT ROWS

Nico F. Declercq and Cindy S. A. Dekeyser

Georgia Institute of Technology, George W. Woodruff School of Mechanical Engineering, 801 Ferst Drive, Atlanta, GA 30332-0405, USA; nico.declercq@me.gatech.edu

& Georgia Tech Lorraine, UMI Georgia Tech – CNRS 2958, Laboratory for Ultrasonic Nondestructive Evaluation, 2 rue Marconi, 57070 Metz-Technopole, France

1. INTRODUCTION

The Hellenistic theater of Epidaurus, on the Peloponnese in Greece, attracts thousands of visitors every year who are all amazed by the fact that sound coming from the middle of the theater reaches the outer seats, apparently without too much loss of intensity. The theater, renowned for its extraordinary acoustics, is one of the best conserved of its kind in the world. It was used for musical and poetical contests and theatrical performances. The presented numerical study reveals that the seat rows of the theater, unexpectedly play an essential role in the acoustics – at least when the theater is not fully filled with spectators. The seats, which constitute a corrugated surface, serve as an acoustic filter that passes sound coming from the stage at the expense of surrounding acoustic noise. Whether a coincidence or not, the theater of Epidaurus was built with optimized shape and dimensions. Understanding and application of corrugated surfaces as filters rather than merely as diffuse scatterers of sound, may become imperative in the future design of modern theaters. *The contents of this paper have been published as Nico F. Declercq, Cindy S. A. Dekeyser, J. Acoust. Soc. Am. 121(4), 2011-2022, 2007. We kindly refer to this paper for more details and for references*

2. BACKGROUND

In the classical world, the ‘asclepieion’ at Epidaurus was the most celebrated and prosperous healing center; in its vicinity there was the amphitheater, designed by Polycleitus the Younger in the 4th century BC and famous for its beauty and symmetry. The original 34 seat rows were extended in Roman times by another 21 rows. The theater is well preserved because it has been covered for centuries by thick layers of earth. A recent picture of the theater is presented in Fig. 1. Marcus Vitruvius Pollio (first century BC) describes in his famous books ‘De Architectura’ the state of the art in architecture and shows evidence that man was aware of the physical existence of sound waves. He writes, “Therefore the ancient architects following nature’s footsteps, traced the voice as it rose, and carried out the ascent of the theater seats. By the rules of mathematics and the method of music, they sought to make the voices from the stage rise more clearly and sweetly to the spectators’ ears. For just as organs which have bronze plates or horn sounding boards are brought to the clear sound of string instruments, so by the

arrangement of theaters in accordance with the science of harmony, the ancients increased the power of the voice.”

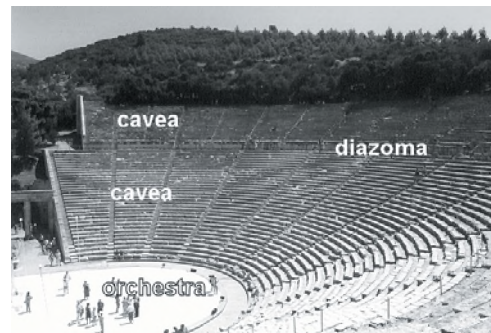


Fig. 1. -picture of the theater of Epidaurus (picture taken by the authors)

This indicates that the construction of theaters was performed according to experimental knowledge and experience and that it was done such as to improve the transmission of sound from the center of the theater (the orchestra) towards the outer seats of the ‘cavea’. It has however always been believed, even in the same chapter written by Vitruvius, or the work by Izenour, that it was mainly the aspect of the slope of the theater, as a result of the constructed seats, rather than the seats themselves, that have been a key factor in the resulting acoustic properties. The current study was triggered by the marvels of Epidaurus and by recent advances in the explanation of a variety of diffraction effects on corrugated surfaces. The theory of diffraction of sound is based on the concepts of the Rayleigh decomposition of the reflected and transmitted sound fields. The theory, earlier applied to describe a number of diffraction effects for normal incident ultrasound on corrugated surfaces, has been used successfully to understand the generation of ultrasonic surface waves in the framework of nondestructive testing. The theory was later expanded to include inhomogeneous waves and enabled a description and understanding of the backward displacement of bounded ultrasonic beams obliquely incident on corrugated surfaces, a phenomenon which had been obscure for 3 decades. Even more, it was later exposed that predictions resulting from that theory were in perfect agreement with new experiments. An expansion of the theory to pulsed spherical acoustic waves revealed special acoustic effects at Chichen Itza in Mexico. The advantage of the theory is its ability to make quantitative simulations as

they appear in reality. From those simulations, it is then possible to detect and characterize patterns and characteristics of the diffracted sound field such as in the case of a short sound pulse incident on the staircase of the El Castillo pyramid in Chichen Itza. The study indicated that the effects were slightly more complicated than the earlier considered principle of Bragg scattering. In the meantime, the fact that the Quetzal echo at Chichen Itza is influenced by the properties of the sound source as well as the existence of the ‘raindrop effect’, have been experimentally verified by J. Cruz et al. Bilsen later showed that if one is only interested in the position of time delay lines on a sonogram and not in the entire amplitude pattern, that it is possible to apply a simpler model based on the gliding pitch theory. For a study of acoustic effects at Epidaurus however, we are not interested in the response to a pulse. We are merely interested in how, for each frequency, sound behaves after interaction with the seats of the theater. Therefore the extensive diffraction theory, as used earlier, is the pre-eminent tool. Until now, there have appeared a number of ‘explanations’ for the excellent acoustics of Epidaurus, such as that sound is driven by the wind because the wind is mostly directed from the orchestra towards the cavea. The wind direction has indeed some influence, but it is also known that the acoustics of Epidaurus is very good when there is no wind or when wind comes from other directions; wind even has a general negative effect because it produces undesirable noise. Another theory is the importance of the rhythm of speech but there are also modern performances taking place at Epidaurus where the typical rhythm of Hellenistic poems and performances composed by Homer, Aeschylus, Sophocles or Euripides is not there; still the acoustics seems perfect. The last theory is that special masks, worn by performers, may have had a focusing effect on the generated sound, but that does not explain why speakers with weak voices are also heard throughout the theater. Izenour points out that the acoustics is so good because of the clear path between the speaker and the audience. The current proves numerically that the effect of diffraction on the seat rows is probably an even more important effect than the ‘clear path effect’. In what follows, we describe the geometry of the theater. Consequently we explain briefly how the numerical simulations are performed. Then we present and explain the numerical results. We end our paper with the most important conclusions. The material parameters at Epidaurus have been taken as: 2000 kg/m^3 for the density of the theater’s limestone, and a shear wave velocity of 2300 m/s and longitudinal wave velocity of 4100 m/s . For the air at Epidaurus, we have taken two cases: ‘summer’, corresponding to an air density of 1.172 kg/m^3 and a (longitudinal) wave velocity of 348.04 m/s ; and ‘winter’, corresponding to an air density of 1.247 kg/m^3 and a (longitudinal) wave velocity of 337.50 m/s .

3. CONCLUSIONS

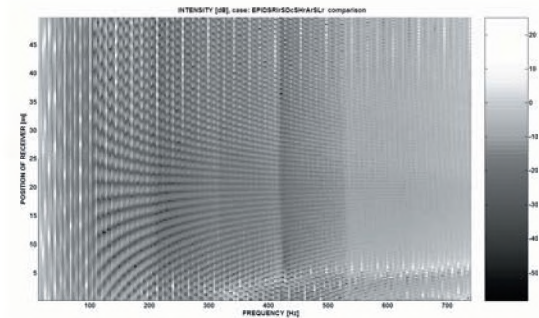


Fig. 2-This figure highlights the effect of diffraction due to the installation of seat rows. At most positions and for most frequencies, the intensity is diminished. However for frequencies beyond 530 Hz, one can see a relatively increased intensity. This is due to the filter effect caused by the seat rows.

It is shown that reflections on the foreground of the theater result in a better distribution of sound throughout the cavea so that all positions become acoustically similar to one another. The installation of seat rows on a smooth cavea generates diffraction effects that change the acoustic properties of the theater. The intensity observed by the audience will be lower than in the case of a smooth cavea. This is not dramatic because the human ear is capable of adapting its sensitivity. More important is that the damping effect is frequency dependent: the seat rows acts like a filter. For frequencies beyond a certain threshold, second order diffracted sound plays an important role and causes sound to be backscattered from the cavea to the audience making the audience to receive sound from the front, but also backscattered sound from behind. This has a positive outcome on the reception of sound. For frequencies below the threshold (mostly noise), the effect of backscattering is less important and is to a great extent filtered out of the observed sound. The threshold frequency of the filtering effect is mainly determined by the periodicity of the seat rows in the cavea of the theater. For Epidaurus this threshold is around 500 Hz, which is usually the upper limit for wind noise. The slope of the cavea does not really influence the frequency values where the amplified frequency band appears and there is no significant difference between the acoustics in summer and the acoustics in winter.

REFERENCES

Nico F. Declercq, Cindy S. A. Dekeyser, “Acoustic diffraction effects at the Hellenistic amphitheater of Epidaurus: seat rows responsible for the marvelous acoustics”, *J. Acoust. Soc. Am.* 121(4), 2011-2022, 2007

Using Speech Intelligibility Scores to Rate Sound Insulation

Hyeon Ku Park, John S. Bradley and Bradford N. Gover

Institute for Research in Construction, National Research Council, Montreal Rd., Ottawa, K1A 0R6

Introduction

Airborne sound insulation ratings can be evaluated in terms of their correlation with various subjective ratings of sound insulation. This paper considers sound insulation ratings in terms of the intelligibility of transmitted speech because speech is a common type of disturbing sound and because speech intelligibility tests can provide accurate subjective ratings.

Airborne sound insulation is usually rated in terms of the ISO *Weighted Sound Reduction Index* (R_w) or the ASTM *Sound Transmission Class* (STC). Previously, Vian et al. [1] related subjective ratings of sound insulation to frequency limited (125 Hz – 4k Hz) A-weighted level differences. Tachibana et al. [2] found judgements of the loudness of transmitted sounds to be predicted by a simple arithmetic average transmission loss over frequency. Recent research has shown the intelligibility of speech from meeting rooms to be well related to frequency-weighted signal-to-noise ratios [3], suggesting possible new wall transmission loss ratings.

Experimental Procedures

Listening tests were carried out in a sound isolated and acoustically dead test space. Subjects heard speech sounds, modified to include the transmission characteristics of 20 different walls, presented from loudspeakers in front of them. At the same time, noise with a -5 dB/octave spectrum shape and an overall level of 35 dBA was played from loudspeakers above the subject.

The characteristics of the 20 simulated walls were chosen to represent a range of STC values evenly distributed from STC 34 to 58 (R_w 33 to 56). They included a variety of construction types and transmission characteristics including wood stud, steel stud and concrete block walls.

The speech tests used the Harvard sentences [4]. These are phonetically balanced English sentences with content that is of low predictability, which is important to minimize the effects of guessing. The sentences were all recorded by the same clear-speaking male talker. The speech source level and the ambient noise levels were held constant throughout the tests. Only the sound transmission characteristics of the simulated walls were varied.

Fifteen subjects heard 5 different sentences for each of the 20 different simulated walls. The speech intelligibility scores of the 75 combinations of 5 sentences and 15 subjects per wall were averaged and plotted versus various sound insulation ratings.

Results were analyzed by fitting Boltzmann equations to plots of mean speech intelligibility scores versus various airborne sound insulation measures [5]. Various insulation ratings were compared in terms of the R^2 value of each relationship since there were always 20 average intelligibility scores.

Standard Sound Insulation Measures

Figure 1 compares the variation of STC values and mean speech intelligibility scores and their standard errors versus wall number with the walls ordered in terms of increasing STC value. Although the even distribution of STC values is evident, the mean intelligibility scores do not closely follow the same trend.

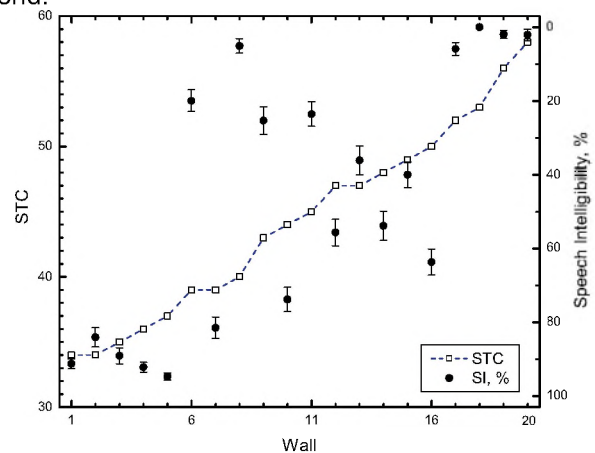


Figure 1. Mean speech intelligibility scores (right hand axis) with error bars indicating the related standard errors and Sound Transmission Class (STC) values on left hand axis versus wall number.

Boltzmann equation fits to intelligibility scores for STC values and R_w values led to significant ($p < 0.05$) but low R^2 values (0.510 and 0.542 respectively).

Varying the 8 dB rule in the STC measure led to modest increases in R^2 values and with the 8 dB rule completely removed an R^2 of 0.661 was obtained.

Speech Intelligibility Type Measures

A number of measures were evaluated that are derived from or related to measures of speech intelligibility. The *Articulation Class* (AC) is a single number attenuation rating derived from the *Articulation Index* (AI) and includes the same frequency weightings. Table 1 lists the R^2 values for relationships with the various speech intelligibility related measures and shows a value of 0.856 for AC values. The *Articulation Index* (AI) and the *Speech Intelligibility Index* (SII) are similarly better predictors of the intelligibility of the transmitted speech.

Recent work [3] on the speech security of meeting rooms showed that frequency-weighted signal-to-noise ratios of the transmitted speech and ambient noise were good predictors of speech security. Several of these measures, SNR_{ai}, SNR_{sii22}, and SNR_{uni32} again led to higher R^2 values. However the simple A-weighted speech – noise level difference (SNR(A)) was not a good predictor of intelligibility scores

Measure	R^2
AC	0.856
AI	0.864
SII	0.899
SNR _{ai}	0.896
SNR _{sii22}	0.913
SNR _{uni32}	0.853
SNR(A)	0.259

Table 1. R^2 values for predictions of intelligibility scores by speech intelligibility type measures.

Some Better Predictors of Intelligibility

Previous work on the speech security of meeting rooms indicated that a simple arithmetic average of *transmission loss* (TL) values over frequencies important for speech was a successful predictor of the intelligibility of transmitted speech. AA(200-2.5k), an arithmetic average of TL values from 200 to 2.5k Hz, was strongly related to intelligibility scores ($R^2 = 0.959$).

Alternatively a new spectrum weighting term ($C_{400-2.5k}$) added to R_w values led to an R^2 value of 0.951. The $C_{400-2.5k}$ term equally weighted frequencies from 400 to 2.5k Hz with zero attenuation and strongly attenuated other frequencies. Further details of this and other results can be found in reference [5].

Conclusions

The standard sound insulation ratings STC and R_w were not strongly related to intelligibility scores. However, removing the 8 dB rule from the STC rating or limiting the included frequency range led to improved R^2 values.

Measures in which decibel values are arithmetically averaged over a range of frequencies, were all generally quite successful. These included: AA(160-5k), AA(200-2.5k), AI, SII, SNR_{ai}, SNR_{sii22}, SNR_{uni32}, and AC values. However, when measures included energy averaging of values at various frequencies, results tended to be less successful.

The arithmetic average transmission loss measure AA(200-2.5k) and the R_w measure with the new spectrum weighting term $C_{400-2.5k}$ provided very good relationships with mean speech intelligibility scores and are considerable improvements over existing standard measures. The new spectrum weighting is also appealing because it adds to an existing standardized approach. However, these new ratings must now be tested in terms of responses to other types of sounds with different acoustical characteristics than speech.

Acknowledgements

This work was supported by the Korea Research Foundation Grant funded by the Korean Government (MOEHRD) (KRF-2006-352-D00200) to Dr. Hyeon Ku Park..

References

- [1] J-P Vian, W.F. Danner and J. W. Bauer, "Assessment of significant acoustical parameters for rating sound insulation of party walls", J. Acoust. Soc. Am., 73 (4) 1236-1243 (1983).
- [2] H. Tachibana, Y. Hamado, and F. Sato, "Loudness evaluation of sounds transmitted through walls – Basic experiments with artificial sounds", J. Sound Vibr. 127 (3) 499-506 (1988).
- [3] B. N. Gover and J.S. Bradley, "Measures for assessing architectural speech security (privacy) of closed offices and meeting rooms," J. Acoust. Soc. Am. 116 (6) 3480-3490 (2004).
- [4] "IEEE recommended practice for speech quality measurements," IEEE Trans. Audio and Electroacoustics, 17, 227–246 (1969).
- [5] H.K. Park, J.S. Bradley and B.N Gover, "Evaluation of Airborne Sound Insulation in Terms of Speech Intelligibility", IRC Research Report, IRC RR-228, February 2007. (available at <http://irc.nrc-cnrc.gc.ca/pubs/html>)

ACOUSTIC ECOLOGY AND THE CINEMATIC REPRESENTATION OF ARCHITECTURAL SPACE: STRAINS OF R. MURRAY SCHAFER'S ACOUSTIC DESIGN IN THE FILMS OF JACQUES TATI.

Randolph Jordan

Dept. of Humanities, Concordia University, 1455 de Maisonneuve Ouest, Canada, H3G 1M8

1. INTRODUCTION

R. Murray Schafer's 1977 book *The Tuning of the World* examines the study of our sonic environments, how they have changed since the industrial revolution, and the effects of these changes on human experience. His goal is to implement the project of Acoustic Design: to develop awareness about the way modern spaces create and shape sound, and move towards the design of such spaces with an appreciation for how their sound affects their inhabitants. French filmmaker Jacques Tati made a career out of fashioning cinematic explorations of the sonic differences between old-world community spaces, urban environments, and the increasing sprawl to suburbia in the 50s and 60s. The culmination of the director's work can be found in his 1967 film *Playtime*, and it is here that we find a virtual template for Schafer's project of Acoustic Design and the ideologies inherent within. This paper examines *Playtime* through *The Tuning of the World*, demonstrating the theoretical and practical connections between both texts so that we might better understand each in light of the other. Without suggesting any direct influence of either of these men on the other, I believe that Schafer's work offers the best means through which Tati's use of sound can be understood as the foundation for the ideologies expressed in his films. In return, I suggest that Tati's aesthetic explorations of the cinematic representation of architectural space yield fascinating inroads into the real-world application of Acoustic Ecology.

2. METHOD

My methodology here is based on a standard Film Studies approach to formal/stylistic analysis. I will compare and contrast different sections of *Playtime* in terms of their presentation of architectural space in both visual and auditory terms. It will be shown that the film sets up a rigorous approach to the relationship between sound and setting for the first half, only to gradually break this relationship down resulting in a climactic scene in which sound is no longer governed by space as it once was. The difference between the film's beginning and ending will then be addressed in terms of the narrative progression between these two points, followed by an assessment of how this change in the film's relationship between sound and setting can be understood in terms of R. Murray Schafer's concept of Acoustic Design.

3. RESULTS

My intended results for this analysis are twofold. First, I simply hope to demonstrate Tati's formal and aesthetic approach to the cinematic representation of architectural space, and relate this approach to the larger thematics of the film as a whole. Second, I hope to illustrate how thinking of film sound in terms of Acoustic Ecology in general, and the work of R. Murray Schafer in particular, can offer a new paradigm in which formal and aesthetic analysis can be carried out within the discipline of Film Studies. In turn I will suggest how studying the cinematic representation of space can offer new paths for exploration within the field of Acoustic Ecology, ultimately forging connections between fields that have as yet remained quite separate.

REFERENCES

- Schafer, R. Murray (1977). *The Tuning of the World: The Soundscape*. Toronto: Mclelland and Stewart.
- Tati, Jacques (1967). *Playtime*. France: Jolly Film + Specta Films.

AUTHOR NOTES

This paper is part of my dissertation on the intersections between Film Studies, Acoustic Ecology, and Electroacoustic Music. This work is being done as part of the Interdisciplinary PhD Humanities program at Concordia University in Montreal.

For
Digital Recorders

Introducing

For
USB A/D Systems

PHANTOM POWER

7052PH

Measurement Mic System

7052H Type 1.5™

Titanium Diaphragm

3Hz to >20 kHz

<20 dBA > 140 dB SPL

MK224 (<14 dBA to >134 dB SPL) Optional

4048 Preamp

Superior

IEC 1094 Type 1

Long-term Stability

Temperature and Humidity

Performance

Now in Stock



**Phantom
to IEPE/ICP
Adaptor
Supplies 3-4 mA
Power
Accelerometers
Microphones**

ICP1248

A **B**
C **e**
O **g**
u **i**
S **n**
t **s**
i **w**
**c *it*
S **h**
O **A**
S **C**
O **O****



**MATT™
Family**

Mic Attenuator

Handle Higher Sound Pressure Levels

ACO Pacific, Inc., 2604 Read Ave., Belmont, CA 94002

Tel: (650) 595-8588 FAX: (650) 591-2891 E-Mail: sales@acopacific.com

Web Site: www.acopacific.com

TM

TONAL NOISE IN BUILDINGS: CURRENT PRACTICE IN MEASUREMENT AND ASSESSMENT

Emanuel Mouratidis¹, and Dean E. Capone²

¹Jacques Whitford Limited, 7271 Warden Avenue, Markham, ON, L3R 5X5, emourati@jacqueswhitford.com. ²Applied

²Research Laboratory at The Pennsylvania State University, Post Office Box 30, State College, PA 16804, dec5@psu.edu

1. INTRODUCTION

Within today's buildings, noise sources and humans are often in close proximity, leaving little space for acoustic precautions and noise controls. Avoiding problems during the design stage and mitigating them should they be identified afterward remains an ongoing concern due to increasing occupant demands for space comfort. Audible tones may be generated by a variety of mechanical and electrical equipment. Public sensitivity towards noise has resulted in research dealing with impulsive, cyclic, and tonal characteristics. This paper is a review of the research and guidelines for tones that may be applied towards buildings.

2. BACKGROUND AND GUIDELINES

A tone is defined as a sound where most of the energy is concentrated at a single frequency, and is more likely to be detected at low levels. One of the earliest evaluations of tones is Fletcher's equal loudness contours [Fletcher¹]. This work demonstrates that the human perception of loudness varies for tones at different frequencies. The concept was used to form the equal loudness contours. Zwicker's tone to noise ratio [Zwicker²] is considered one of the initial tone correction procedures. The work included critical band theory used by researchers and international standards that followed. Tones are rarely found in areas without considerable background noise or masking. Masking was found to be dependant on both the level of the tone over the background noise, and the level of the background noise itself [Stevens³]. This work was a starting point in the evaluation of tones that followed, including correction methods [Wells and Blazier⁴]. Pearsons [Pearsons et al⁵] completed a study on tones with variable background noise. The work applied two different background spectra that resulted in a negligible change in reported noisiness, with maximum noisiness reported when the tone to noise ratio reached 25 dB.

Kryter and Pearsons [Kryter and Pearsons⁶] developed a methodology based on the judgment of random train noise containing a pure tone, resulting in the Tone Corrected Perceived Noise Level. The Federal Aviation Regulation (FAR) Part 36 [FAR⁷, 1969] describes a tonal correction based on subjective responses to aircraft. FAR 36, Section A36.4 outlines the process known as the Effective Perceived Noise Level (EPNL) which is a single number evaluator of the subjective effects of noise. The EPNL correction increases with increasing tone to noise ratio. Patsouras [Patsouras⁸] investigated the behavior of 14 subjects when exposed to synthesized simulations of high speed train

interiors. With a focus on rail and motor noise, the results indicated that receptor annoyance scores increased with higher tone prominence. Early environmental work [Kryter⁹, Scharf and Hellman¹⁰] found that common metrics such as dBA and L_{dn} underestimated the perceived impact of tones. Experiments confirmed that a single tone contributes more to annoyance than an equivalent amount of energy spread over a wide range of frequencies, resulting in a 2 to 15 dB Tonal Penalty (TP). Scharf and Hellman found that tone correction was most suitable for constant noise, as found within most buildings, instead of the variable tones emitted from transportation sources. Landstrom [Landstrom et al¹¹] studied the impact of three ventilation noise spectra. Subject concentration levels were found to be lower for the tone exposure as compared with the masked tone. The National Physical Laboratory [Porter¹²] studied the subjective response to traffic, compressor, and fan noise, including development of a TP for added annoyance. The study reaffirmed that the lower the background level, the more severe a TP. At 35 dBA, the study revealed a TP of more than 10 dB. As background levels increase to 60 dBA, the TP approaches zero. Of the common types of industrial sources, 35% were fans, with 80% of all sources having distinct characteristics (50% described as tonal).

Standards development has moved forward with the research on environmental noise and psychoacoustics. The British Standard for rating industrial emissions onto sensitive receptors [BS 4142¹³] provides one of the earliest prediction methodologies, including a TP. The standard addresses mechanical noise and the additional measurements for tone identification. A popular standard for the assessment of noise is ISO 1996 [ISO 1996-1¹⁴], that includes correction factors for increased annoyance. Although the methodology used to evaluate a TP differs from country to country, the principles are based on the provisions outlined in ISO 1996. Most countries have adopted a TP in the assessment of transportation and industrial noise between 2 to 6 dB. The ANSI S12.9 Part 3 [ANSI S12.9¹⁵] standard outlines the 1/3-octave band procedure for the description and measurement of environmental sounds. The ANSI S12.10 standard [ANSI S12.10¹⁶] provides a detailed assessment of tones through the Prominence Ratio (PR), based on the tonal sound level compared with the average level of the two adjacent bands. The ISO 9296 [ISO 9296¹⁷] explains there is no current international consensus on objective methods for rating the character of tones. The Air-Conditioning and Refrigeration Institute (ARI) standards have adopted tone adjusted ratings, such as ARI 350 [ARI 350¹⁸] for indoor equipment. This is

supported in ARI 1140 [ARI 1140¹⁹] with a Sound Quality Indicator (SQI), where “levels are weighted to adjust for psychoacoustic sensitivity to frequency distribution and any discrete tones...converted to a single number SQI” (ARI 1140, page 2). The adjustment is required for any band that exceeds its two adjacent bands by more than 1.5 dB. The corrected levels are converted into indices weighed by frequency and level, “...by which complex sounds of various levels and spectra may be ordered and compared on a scale of subjective magnitude...provide a means to evaluate the quality of the product sound.” (ARI 1140-2006, page 3).

An indoor setting is dependant on many non-acoustical factors, including room aesthetics and occupant occupation. A recent study by Health Canada [Health Canada²⁰] found that while less than 10% of the people surveyed were either very bothered or extremely bothered by noise exposure, there appeared to be significant variance amongst populations (5% very bothered in urban areas versus 1% very bothered in rural areas) and amongst geographical regions (e.g. 5% very bothered in Ontario versus 2.4% very bothered in Alberta). One may conclude that if a tone study were conducted in an industrial, rural town, they may receive significantly different results if the same study was conducted in a non-industrial, urban area.

3. TONALITY IN BUILDINGS

Present room criteria may be used as the basis of an acoustical design, evaluating the background noise against the preference of the occupants. The criteria do not sufficiently characterize the effects of tones. Using the current guidelines as a starting point, a refined approach may be available for the initial building design stage and an in-field evaluation, such as commissioning and troubleshooting. Adverse effects are present if the occupant has the ability to distinguish the tone over the background. Low noise work spaces often entail high concentration levels. Critical design criteria call for more stringent evaluations of audibility, often applied through the critical band masking concept [Zwicker and Fastl²¹] where only noise within a critical band can determine tone audibility.

4. DISCUSSION

Acoustic comfort has emerged as a key building design issue. Tonality may be a significant occupant issue as a result of annoyance. Although the literature lacks clear tone criteria for a building, there appears to be agreement on the identification of tones, primarily mechanical systems. It is evident that there are practical solutions available that may protect building occupants from tones. In lieu of reliable indoor tone criteria, designers should consider:

1. TP for all applicable building equipment and services under existing noise criteria (dBA, NC, RC)

Or;

2. TP on the noise criteria, analogous to those applied in environmental ordinances (margin of safety).

Obtaining tone-penalized ratings is a feasible option and a first step towards protecting building occupants from annoyance, reduced productivity, and costly repairs.

REFERENCES

- [1] Fletcher, H., Munson, W.A., Loudness: Definition, Measurement and Calculation, *J. Acoust. Soc. Am.*, 5, 82, 1933.
- [2] Zwicker, E., *Über Psychologische und Methodische Grundlagen der Lautheit*, *Acustica* 8, 237-258, 1958.
- [3] Stevens, Procedure for Calculating Loudness, Mark VI, *J. Acoust. Soc. Am.*, 33 P157-1585, 1961.
- [4] Blazier, W.E. and Wells, R.J., *ASHRAE Transactions, Procedure for Computing the Subjective Reaction to Complex Noise*, ASHRAE, 1963.
- [5] Pearsons, K.S., Horonjeff, R.D., Bishop, D.E., *Noisiness of Tones Plus Noise*, NASA CR-1117, 1968.
- [6] Kryter, K.D. and Pearsons, K., *Judged Annoyance of a Band of Noise Containing a Tone*, *J. Acoust. Soc. Am.*, 38, 106-112, 1965.
- [7] FAR Part 36, Appendix 36.4, *Calculation of the Perceived Noise Level*, FAA, 1969.
- [8] Patsouras, C., Fastl, H., Widmann, U., Holzl, G., *Psychoacoustic Evaluation of Tonal Components in View of Sound Quality Design for High-Speed Train Interior Noise*, *Acoustical Science and Tech.*, Vol.23-2, 2002.
- [9] Kryter, K.D., *Review of Research and Methods for Measuring the Loudness and Noisiness of Sounds*, NASA CR 422, 1966.
- [10] Scharf and Hellman, R., *Comparison of Various Methods for Predicting the Loudness and Acceptability of Noise*, US EPA Rep. 550/977-101, 1977.
- [11] Landstrom, U., Kjellberg, L., *The Effects of Broadband, Tonal and Masked Ventilation Noise*, *Jnl Low Frequency Noise Vibration*, 10:112-122, 1991.
- [12] Porter, N.D., *The Assessment of Industrial Noise – Subjective Tests and Objective Assessment*, NPL Report RSA 57C, 1995.
- [13] BS 4142:1997, *Method for Rating Industrial Noise Affecting Residential and Industrial Areas*, BSI British Standards, London, 1997.
- [14] International Standard ISO 1996-1: 1982, *Acoustics - Description and Measurement of Environmental Noise Part 1: Basic Quantities and Procedures*, International Organization for Standardization, Switzerland, 1990.
- [15] ANSI S12.9-1993/Part 3 (R1998), *American National Standard Quantities and Procedures for Description of Sound*, Part 3, ANSI, New York, 2003.
- [16] ANSI S12.10-1985 (R1997), *American National Standard Methods for the Measurement and Designation of Noise Emitted by Business Equipment (Rev. of ANSI S1.29-1979)*, ANSI, 2002.
- [17] International Standard ISO 9296:1988 (E), *Acoustics - Declared noise emission of computer and business equipment*, International Organization for Standardization, 1988.
- [18] ARI Standard 350-2000, *Sound Rating of Non-Ducted Indoor Air-Conditioning Equipment*, *Air Cond. and Refrig. Inst.*, 2000.
- [19] ARI Standard 1140-2006, *Sound Quality Evaluation for Air-Conditioning and Refrigeration Equipment*, *Air Cond. and Ref. Inst.*, Arlington, 2006.
- [20] Health Insider Report No.7 – *Noise Questions for Health Canada*, National Survey Centre, Ottawa, 2002.
- [21] Zwicker, E., and Fastl, H., *Psychoacoustics – Facts and Models*, 2nd Ed., Springer-Verlag, 1999.

STATISTICAL BASIS FOR RATING SPEECH PRIVACY OF CLOSED ROOMS

Bradford N. Gover and John S. Bradley

Institute for Research in Construction, National Research Council, Ottawa, ON K1A 0R6, Canada
brad.gover@nrc-cnrc.gc.ca

1. INTRODUCTION

The degree of privacy offered by a closed room is an indication of how audible or intelligible conversations occurring within are in the adjoining spaces. This depends not only on the passive sound insulation provided by the building, but also on the levels of speech and background noise. The sound insulation is a fixed physical quantity that can be measured, but the speech and noise levels fluctuate from moment to moment: they are statistical quantities. The degree of privacy can therefore be described in a “risk” sense, where a particular level of sound insulation will be associated with a certain probability of a privacy lapse, when speech levels are high and/or noise levels are low. This paper describes results from using measured statistical distributions of speech and noise levels to rate and predict the privacy of closed rooms [1].

2. SPEECH PRIVACY METHOD

Previous investigations have identified a signal-to-noise index that is well correlated with the intelligibility of speech transmitted through walls [2]. This index (SNR_{UNI32}) is the arithmetic average (i.e., uniformly-weighted sum) of the 1/3-octave band level differences of speech ($L_{S,Rec}$) and noise (L_N) at the listening position, over the 16 bands from 160 to 5k Hz:

$$SNR_{UNI32} = \frac{1}{16} \sum_{160Hz}^{5kHz} [L_{S,Rec}(f) - L_N(f)]_{-32dB}. \quad (1)$$

The subscript $-32dB$ indicates that the quantity in brackets is to be clipped to a minimum of -32 dB.

The speech level at the listening position $L_{S,Rec}$ can be determined from the speech level inside the closed room L_S and a measure of the sound insulation to the listening position, LD . In each 1/3-octave band, $LD(f)$ is the difference in levels between a diffuse-field average test noise field in the closed room and the corresponding received level at the listening position. This is measured using broadband noise, several loudspeaker and microphone positions within the room, and microphones at receiving positions in the adjoining spaces, usually 0.25 m from the boundaries of the room [3].

Substituting $L_{S,Rec} = L_S - LD$ into Eq. (1), the expression for the index becomes

$$SNR_{UNI32} = \frac{1}{16} \sum_{160Hz}^{5kHz} [L_S(f) - LD(f) - L_N(f)]_{-32dB} \quad (2)$$

which, by ignoring the -32 dB limit and summing the terms individually, can be written

$$L_S(avg) - L_N(avg) = LD(avg) + SNR_{UNI32}, \quad (3)$$

where “(avg)” indicates the arithmetic average of 1/3-octave band values from 160 to 5k Hz. $LD(avg)$, then, is a single-number indicator of the sound insulation. Through the index SNR_{UNI32} , Eq. (3) relates the difference between average speech level *inside* the closed room and the background noise level at the listening position *outside* the room, to the sound insulation.

By setting $SNR_{UNI32} = -16$ dB (which is the threshold of intelligibility, where 50% of listeners could correctly identify at least one word) Eq. (3) becomes

$$L_S(avg) - L_N(avg) = LD(avg) - 16dB. \quad (4)$$

For given speech and noise levels, Eq. (4) indicates the required $LD(avg)$ to obtain threshold conditions. That is, the minimum required sound insulation to ensure speech privacy. Conversely, for a known $LD(avg)$, Eq. (4) indicates speech and noise level combinations that result in threshold conditions.

3. SPEECH AND NOISE LEVELS

The cumulative distribution functions of speech and noise levels can be used to determine the probability that the speech will be loud enough and the noise will simultaneously be quiet enough so that speech will be intelligible. This probability then can be used in rating the speech privacy.

Fig. 1 shows the cumulative probability of occurrence of speech and noise levels ($10 \text{ s } L_{eq}$) measured for a large range of meetings in different buildings [4]. It indicates that 10% of the time the speech level was higher than 64 dBA, and 10% of the time the noise level was lower than 33 dBA. Assuming independence, the joint probability of speech exceeding 64 dBA and the noise simultaneously being lower than 33 dBA was 1%. By assuming reasonable spectral shapes for the speech and noise (to convert dBA to dB(avg))

the data in Fig. 1 are converted to yield Fig. 2. The horizontal axis is the difference between the average speech level in the closed room and the average noise level at the listening position outside the room: precisely the quantity on the left-hand side of Eq. (4).

4. STATISTICAL RATING

Using Eq. (4), the axes of Fig. 2 can simply be re-labelled as shown in Fig. 3. This graph indicates the probability of speech being intelligible for a given value of $LD(avg)-16$ dB, which is the single-number measure of sound insulation (from measurements) offset by 16 dB.

The individual data points (♦) in Fig. 3 correspond to measurements of $LD(avg)$ made through a real wall. There is one data point for each of 63 receiving positions tested (all were 0.25 m from the wall). The shaded areas and “Risk Category” labels were added to aid users in interpreting the results: for the measured data, most locations were “Risk Category 3” (1–5 likely privacy lapses per day) but several were “Risk Category 4” (5–26 lapses per day), corresponding to a higher likelihood of speech being intelligible, owing to lower sound insulation to those points. It is up to the user to decide on requirements.

5. CONCLUSIONS

To rate the speech privacy of a closed room, measurements of the sound insulation are required. Using distributions of speech and noise levels measured in meetings allows interpretation of the sound insulation measurements in a statistical manner. In this way, the physical measurements of sound insulation can be translated directly to a “risk” of privacy lapse.

REFERENCES

- [1] J.S. Bradley and B.N. Gover, “Designing and Assessing the Architectural Speech Security of Meeting Rooms and Offices”, IRC Research Report RR-187, Aug. 2006. Available at <http://irc.nrc-cnrc.gc.ca>
- [2] B.N. Gover and J.S. Bradley, “Measures for assessing architectural speech security (privacy) of closed offices and meeting rooms”, J. Acoust. Soc. Am., **116**, 3480–3490 (2004).
- [3] J.S. Bradley and B.N. Gover, “Measurement of Sound Transmission from Meeting Rooms”, IRC Research Report, RR-220, Mar. 2006. Available at <http://irc.nrc-cnrc.gc.ca>
- [4] J.S. Bradley and B.N. Gover, “Speech and Noise Levels Associated with Meeting Rooms”, IRC Research Report RR-170, Mar. 2004, revised Dec. 2004. Available at <http://irc.nrc-cnrc.gc.ca>

ACKNOWLEDGEMENTS

This work jointly funded by NRC Institute for Research in Construction, the Royal Canadian Mounted Police, and Public Works and Government Services Canada.

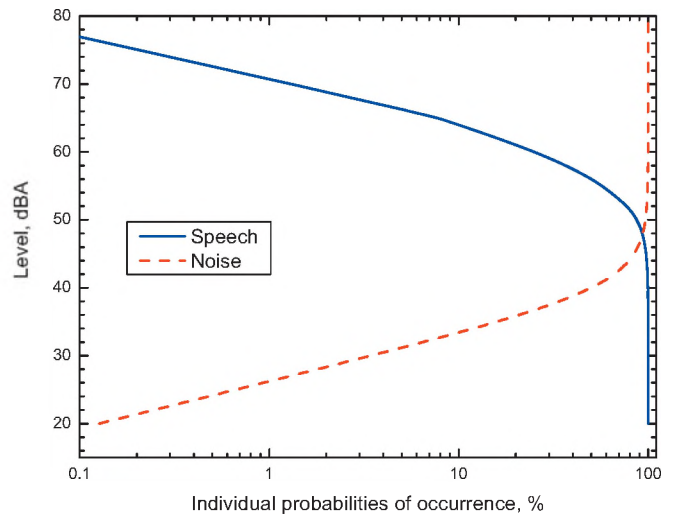


Fig 1: Probability of occurrence of speech and noise levels.

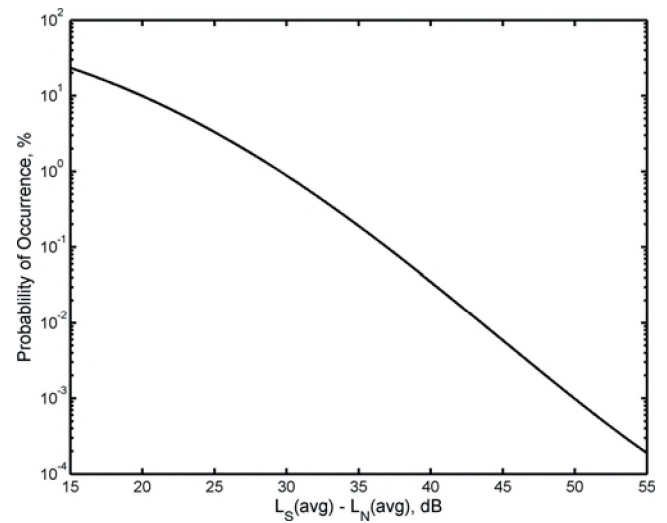


Fig 2: Joint probability of occurrence of speech–noise differences.

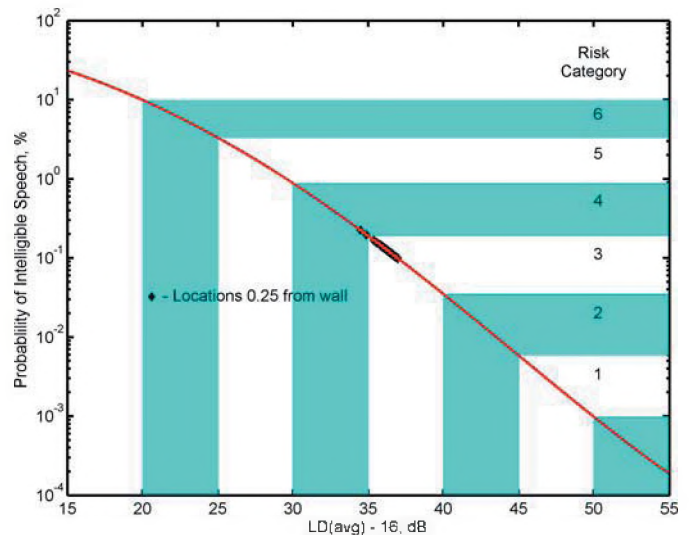


Fig 3: Speech privacy risk chart.

GUIDE FOR FLANKING SOUND TRANSMISSION IN WOOD FRAMED CONSTRUCTION: ISSUES FOR IMPACT NOISE

J. David Quirt, Trevor R.T. Nightingale, Frances King

Inst. for Research in Construction, National Research Council, Ottawa, K1A 0R6, Canada

1. INTRODUCTION

This paper reports results from continuing studies of sound transmission between adjacent units in wood-framed multi-dwelling buildings. Previous papers¹ discussed the basis for a design guide² to predict sound insulation in typical wood-framed row housing or apartment buildings, for airborne noise sources. This paper addresses the rather different issues that apply for impact (footstep) noise. In both cases, the flanking transmission is governed by the same basic propagation of structure-borne vibration. However, differences between airborne and impact sources shift the importance of specific elements of the construction, and increase the significance of source location for impact sound. The paper presents a brief overview of key concerns, and how they are handled in the design guide.

Results in this paper apply to wood-framed constructions, with the wall and floor assemblies shown in Figure 1, or variants on them. Specifications and architectural drawings are given in detail elsewhere.³

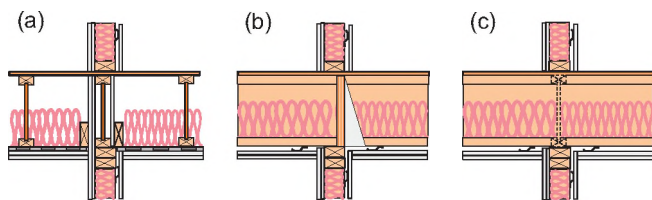


Figure 1: Construction details of the 3 wall/floor systems. Joists were oriented (a) parallel to the wall, (b) perpendicular to the wall, or (c) with joists continuous across the wall, perpendicular to it.

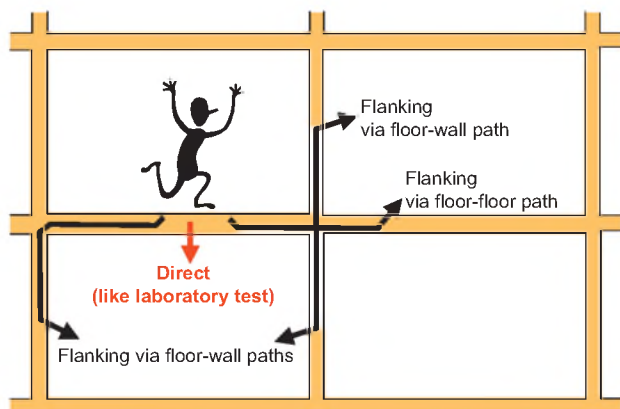


Figure 2: Typical paths for transmission of impact sound (both direct and flanking) to adjacent units below and beside.

Impact transmission to adjacent units in a wood-framed building typically involves transmission via several paths, as illustrated in Figure 2. Impact noise to the unit below combines direct transmission through the floor/ceiling assembly with flanking via 4 floor-wall paths, as discussed previously. Impact transmission to the unit beside (the focus of this paper) includes only flanking – mainly via the floor-floor path, although the floor-wall path also contributes in some cases. The term “Apparent-NISPL” (and single-number rating “Apparent-IIC”) are used here to mark it as a special case ignored in ASTM standards.

2. RESULTS AND DISCUSSION

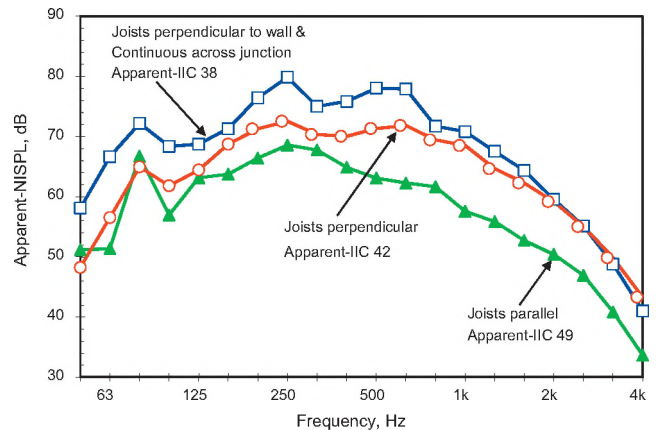


Figure 3: Impact level (Apparent-NISPL in unit beside due to flanking transmission) for the three constructions in Figure 1, with source positions ~2 m from separating wall.

As shown in Figure 3, there is strong transmission of impact sound to the adjacent unit when the floor surface is just the basic OSB panels. Most apartment dwellers experiencing such sound insulation would be seriously annoyed. As noted in previous papers, the three cases differ markedly, because the framing changes strongly affect attenuation across the floor assemblies and the floor/wall junction.

Figure 4 illustrates the change in transmitted impact sound when a topping is added over a basic OSB subfloor. In this case the topping is 25 mm thick gypsum concrete. At low frequencies the impact level is lower (better), due to the weight and stiffness of the concrete. At high frequencies the impact levels increase because the standard impact hammers inject more power into the hard concrete surface, but fortunately this effect is offset by adding compliant flooring such as vinyl or carpet over the topping (See Figure 5).

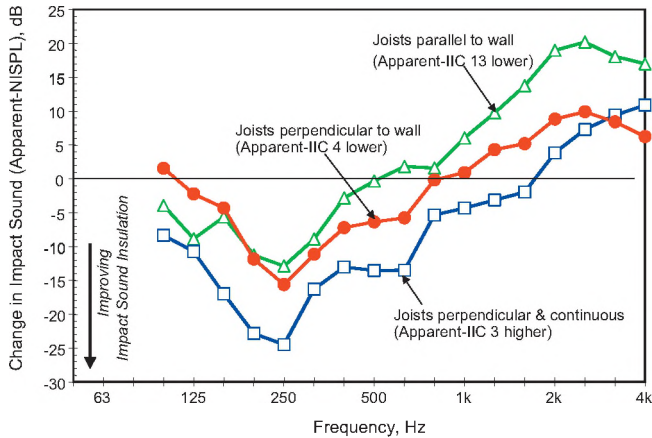


Figure 4: Change in impact level (Apparent-NISPL in unit beside due to flanking transmission) for the 3 constructions shown in Figure 1, due to 25 mm gypsum concrete applied over subfloor.

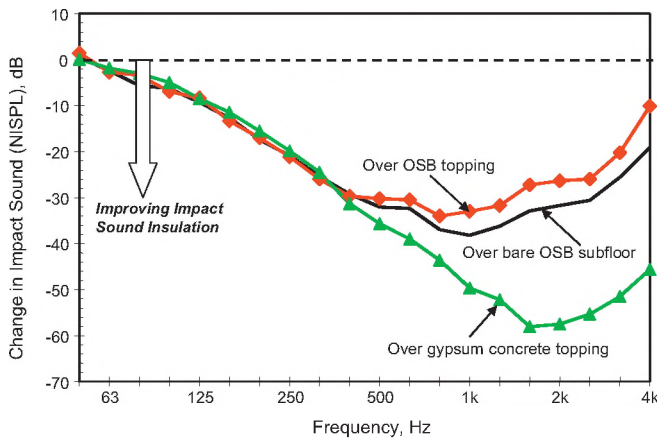


Figure 5: Change in impact level (for either flanking or direct transmission) due to carpet added on the subfloor or over topping.

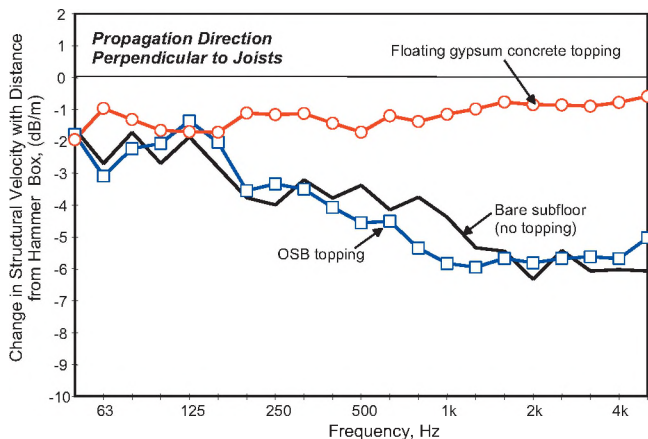


Figure 6: Attenuation of transmitted vibration (dB/metre separation of impact source from floor/wall junction..

Location of the impact source is important, because attenuation of the structure-borne vibration across the floor assembly also has a strong effect; this depends on joist orientation and on the floor topping over the basic floor. Figure 6 shows the attenuation for three treatments with one orientation of the joists; comparable curves have been determined for other toppings and propagation parallel to

the joists. For transmission to the room below, this effect averages out as discussed elsewhere^{1,2} but Apparent-NISPL in the room beside depends appreciably on location of the impact. To include these effects, scenarios with a range of typical source positions were evaluated. For each source position, the combined attenuation due to all the construction variables were evaluated for potentially-significant flanking paths, and the resulting Apparent-NISPL values were calculated. Fortunately just a few cases suffice to provide a basis for practical design.

Table 1: Apparent-IIC to unit beside the source of impacts when floor and wall constructions match detail (b) in Figure 1.

Flooring finish:	Bare Vinyl Carpet			Bare Vinyl Carpet		
Floor Surface:	Apparent IIC (Impacts at 1-3 m)			Apparent IIC (Corridor- impact at 1 m)		
No topping (basic)	42	43	63	39	40	63
19 mm OSB stapled to subfloor	47	47	61	44	44	61
25 mm gypsum concrete bonded to subfloor	38	43	62	35	40	61
38 mm gypsum concrete + resilient mat on subfloor	46	50	68	46	49	66

In the guide, tables like Table 1 present the combined effect of all paths for typical variants of the construction elements. The table gives two sets of values – one set for impact sources 1 to 3 m from the separating wall (typical range of source positions in an adjacent room), the other for impact sources 1 m from the separating wall (typical for an adjacent corridor). Apparent-IIC in a given building will not exactly match these values, but the trends should apply.

3. SUMMARY AND REFERENCES

This paper provides a terse overview of how experimental characterization of the direct and flanking sound transmission paths in wood-framed construction leads to a manageable set of path transmission terms to represent the effect of specific design tradeoffs. By combining the energy transmitted via all paths, estimates of the Apparent-IIC for typical constructions can be derived. Results are presented in a design guide for many common constructions.

We wish to acknowledge the support of our industry partners: CMHC, Forintek Canada, Marriott International, Owens Corning, Trus Joist, and USG.

- Quirt, J.D. Nightingale, T.R.T., King, F. (2005, 2006) Canadian Acoustics, vol. 33, 68-69 and vol. 34, 88-89
- Quirt, J.D. Nightingale, T.R.T. King, F. Guide for Sound Insulation in Wood Frame Construction, **RR219**, NRC-IRC Canada, (2006)
- Nightingale, T.R.T. Quirt, J.D., King F., Halliwell, R.E. Flanking Transmission in Multifamily Dwellings: Phase IV, **RR218**, NRC-IRC Canada, (2006).
(Note that the reports are available on the IRC website at <http://irc.nrc-cnrc.gc.ca/ircpubs/>.)

A UNIFIED THEORY FOR STRESSES AND OSCILLATIONS

Himanshu Dehra¹

¹American Institute-Industry Forum on Energy, 1-140 Av. Windsor, Lachine, QC, Canada, H8R 1P7

1. INTRODUCTION

The aim of the paper is to introduce a unified theory for stresses and oscillations. The stresses developed on a particle due to various forces are classified as: i) fundamental stresses; ii) internal stresses; and iii) external stresses. The fundamental stresses are developed due to presence of gravitational and electromagnetic forces of a solar system. The internal stresses are developed under the influence of fundamental stresses and are defined by properties of composition of a particle. The external stresses are developed under an external source of energy. The oscillations of a particle are assumed to be generated because of stress development with cyclic load of day/night, heating/cooling and compression/expansion.

1.1. Free body analysis

In order to support this hypothesis, a full scale experimental setup for an external photovoltaic cavity wall was installed in an outdoor room facility located at Concordia University, Montréal, Canada (Dehra, 2004). The free body diagram showing energy balance of major composite loads acting on system of a photovoltaic cavity wall is illustrated in Fig. 1. The photovoltaic cavity wall was an amplifier, constituting of a parallel plate photovoltaic device connected to a potentiometer. The cavity wall was constructed with a pair of glass coated photovoltaic (PV) modules forming a parallel plate duct with a plywood board and connected to a potentiometer. A potentiometer, a wire-wound variable resistor of up to 50 Ω was a wire-wound circular coil with a sliding knob contact (Dehra, 2004). It was used to vary electrical resistance across connected PV modules without interrupting the current.

The various forces acting on a photovoltaic cavity wall system were identified. The gravitational force (Mg) act on mass of photovoltaic cavity wall system. The short wave electromagnetic force was applied on a photovoltaic cavity wall due to rotation and movement of the Earth around the Sun. The day/night on the Earth's surface causes periodic force of solar intensity (S) incident on surface of photovoltaic module. Electricity (E) was generated from a photovoltaic module under the influence of gravitational force of the Earth and electromagnetic force of the solar system, which results in generation of electricity due to incident sunlight on electrical system of photovoltaic module. The unutilized absorbed solar radiation was dissipated as electrical noise from a solid state device of photovoltaic module, which results in generation of heat

(H). The generated heat was exchanged with the surrounding environmental system by modes of heat conduction, convection and radiation. The long wave radiation heat exchange occurs between photovoltaic module and plywood board. The heat storage was due to heat storage elements in photovoltaic cavity wall. The major heat storage was due to polystyrene filled plywood wall. Thermal force (T) was developed because of energy dissipation in the vertical and horizontal members from thermal system of photovoltaic cavity wall. Thermal storage was due to thermal storage elements in photovoltaic cavity wall. The major thermal storage was due to glass coated semi conductor material of photovoltaic module. The combination of thermal force and heat exchange has resulted in heating/cooling load on thermal-fluid system of photovoltaic cavity wall. The combination of thermal force and heating/cooling load results in compression/expansion load on structural system of photovoltaic cavity wall. The ambient air entering into ventilation system of photovoltaic cavity wall was set in motion due to differences in temperature between walls of cavity wall and that of air entering into cavity wall.

The enhancement in air flow rate through a cavity wall was achieved by means of an external source of energy of an exhaust fan-induced velocity (EF). The enhancement in air flow rate of ventilation system of photovoltaic cavity wall was also achieved in presence of wind force (WF) applied on photovoltaic cavity wall. The internal sound force (ISF) was generated in photovoltaic cavity wall due to air velocities of wind and fan. The external sound force (ESF) was also applied on sound insulation system of photovoltaic cavity wall due to sound propagation from the surrounding environmental system of photovoltaic cavity wall.

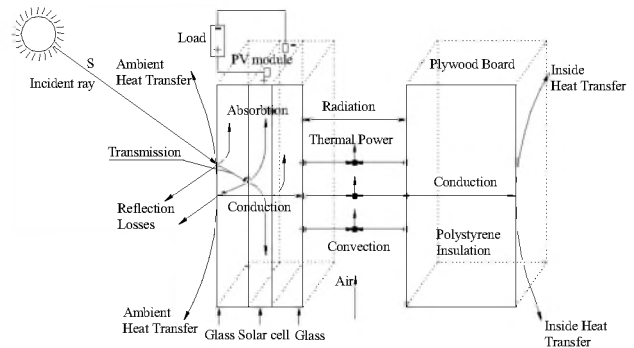


Fig. 1. Free body diagram of major composite loads acting on a photovoltaic cavity wall

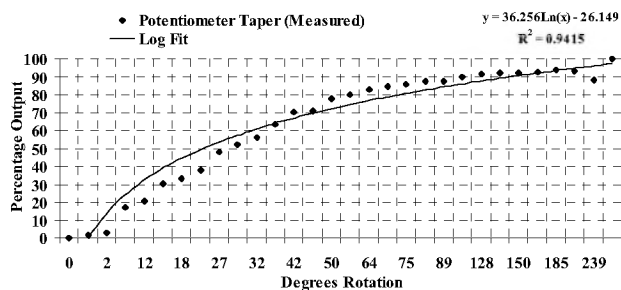


Fig. 2. Potentiometer Taper (Measured) with percentage voltage output

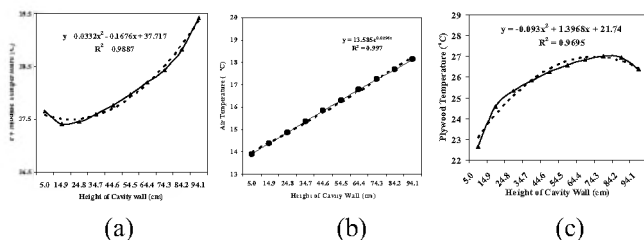


Fig. 3. Temperature plots with height of PV cavity wall: (a) PV module; (b) air; and (c) plywood board

2. AMPLIFICATION RESULTS

The characteristics of a parallel plate photovoltaic device connected to a potentiometer were established by varying electrical resistance with rotation of knob of a potentiometer (Dehra, 2004). The current-voltage measurements were obtained for determining electric power output with a series electrical circuit connection of a pair of vertically inclined PV modules installed on a wooden frame. The results of the power output from a potentiometer with rotation of circular knob are illustrated in Fig. 2.

A mathematical model for prediction of temperature distributions varying with volume of a parallel plate photovoltaic device was developed (Dehra, 2004). The model is used to predict temperature distributions at pre-defined locations in PV module, plywood board and air flowing through a cavity wall based on input measurement data of solar intensity, air velocity and ambient and room air temperatures. The results of the temperature plots are illustrated from Fig. 3 (a) to Fig. 3 (c).

3. DISCUSSIONS

The amplification results of the graphs of Figs. (2) and (3) show that the gain in steady state electrical and thermal functions for a photovoltaic cavity wall is a factor of its volume or resistance. The electrical analog is used herewith to illustrate the resonance phenomenon at amplification for equivalent mechanical, hydraulic and thermal systems for a parallel plate photovoltaic cavity wall, which was connected to a potentiometer. The two cases of series and parallel L-C-R circuit resonance are illustrated in Fig. 4.

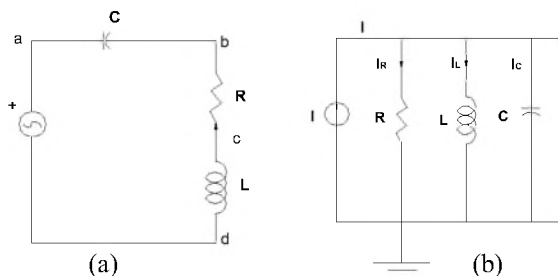


Fig. 4. (a) L-C-R series arrangement of resonance; (b) L-C-R parallel arrangement of resonance

The cases of resonance are visualised at occurrence of phenomenon of photovoltaic amplification. Inductance is mass for the mechanical system for propagation of elastic waves. Capacitance is heat storage capacities of photovoltaic modules, air and polystyrene filled plywood board. Polystyrene filled plywood board is vulnerable to fire as soon as heat waves propagated with frequency matching with its latent heat of vapourisation is reached. Resistance is developed due to electrical, thermal and fluid resistance in energy storage elements of photovoltaic modules, air and polystyrene filled plywood board. The series case of L-C-R resonance occurs with power transfer due to elastic waves and electricity transmission from a photovoltaic cavity wall. The parallel case of L-C-R resonance occurs with power transfer due to electricity, heat waves (C-R) and fluid surface waves (C-R) in conjunction with inductance (L) due to mass of photovoltaic cavity wall and resistance (R) due to temperatures of ground surface and ambient air.

4. CONCLUSION

A unified theory for stresses and oscillations is introduced with an example of an external cavity wall made up of a parallel plate photovoltaic device. The theory has discussed the propagation of acoustic waves caused due to various stresses and oscillations of a cavity wall. The theory is eligible for defining new criteria for generation of acoustic resonance to include waves propagated with transmission of light, sound, noise, heat, electricity, fluid and fire from a cavity wall. A mathematical model has been formulated for the theory based on field experiments conducted on a cavity wall with one degree of freedom.

REFERENCES

- Dehra, H. (2004). A numerical and experimental study for generation of electric and thermal power with photovoltaic modules embedded in building façade, *submitted/unpublished Ph.D. thesis*, Department of Building, Civil and Environmental Engineering, Concordia University, August 2004.

ACOUSTIC RENOVATION OF VANCOUVER'S QUEEN ELIZABETH THEATRE: 2006 – 2009

John O'Keefe

Aercoustics Engineering Limited, 50 Ronson Drive, Suite 165, Toronto, Canada, M9W 1B3, jokeefe@aercoustics.com

1. INTRODUCTION

The Queen Elizabeth Theatre (QET) is a seminal building in the history of North American theatre design. The 1956 competition was won by a design team that would go on to build most of Canada's large post war auditoria. The cities of Regina, Winnipeg, Ottawa, Montreal and Charlottetown – to name a just few – all have venues designed by this team. The acousticians included a young Russell Johnson, making one of his first major contributions to auditorium design. In the Johnson oeuvre the QET is second only to the Tanglewood Music Shed and, even then, only by a few weeks¹.

The building opened in 1959 with the 2929 seat main auditorium. Erected in an age before the importance of lateral sound was known², it was wide and flat. With the advantage of hindsight, we now know that that was a lethal combination³. In 1962, the 668 seat Playhouse Theatre was added to the north end of the building. In 1962, rock and roll acts rarely performed in a venue like the QET and, if they did, their sound equipment could easily have been transported in the back of a station wagon. Structure borne noise control was not a concern at the time. That is hardly the situation today, in this age of tractor-trailer touring shows. This led inevitably to the first phase of the renovation.

2. STRUCTURE-BORNE NOISE

With "soft seat" rock and roll now a major income source for any performing arts centre, the need to extend beyond normal air-borne noise control designs is obvious. The solution at the QET was at once simple and radical: the building was cut in two. In the summer of 2006, while the Playhouse Theatre was dark, the two rooms were separated by a 75 mm acoustic joint extending from the east side of the building to the west along the north side of the QET flytower. This was a formidable task, given that the concrete footings for the flytower were several feet deep.

3. SPATIAL SOUND

The remainder of the renovation will be completed in the summers of 2007, 2008 and 2009. In 2007, the ceiling was removed to increase the height of the room. This has increased the enclosed volume and, consequently, the Reverberation Time. More importantly, it has improved the

Height to Width ratio of the room which, as discussed elsewhere³, will increase the Early Decay Time (EDT).

Typical of its age, the room is very wide: 32 m. Mindful of the seat count but recognising the need for lateral reflections, the renovation design borrows from two obvious ante-decedents: Christchurch Town Hall⁴ and Berliner Philharmonie⁵. With the ceiling removed, an elliptical array of lateral reflectors has been installed in the truss space, similar to the Christchurch model. Lateral reflections are also provided by a terraced floor plan similar to the recently renovated Jubilee Auditoria⁶; a design influenced by Berlin⁵.

The overhead lateral reflectors went through several generations of design prior the final version. They started out as four large, flat and rather awkward looking reflectors located towards the back of the room, providing lateral energy mostly to the balconies. Later on they developed into the final elliptical plan but the individual panels still remained flat. Concerns about image shift generated by the flat panels suggested a need for diffusion. Diffusion would also spread the sound out, increasing the zone of coverage. The question was how much diffusion was enough and how much was too much. An early scheme provided diffusion in the form of a three layer fractal, 2-dimensional Quadratic Residue Diffuser (QRD). This was questioned by the architects on aesthetic grounds. Acoustically, there was also concern that the 2-D QRD provided too much diffusion and that lateral energy levels received by listeners would be too low. These concerns were corroborated by Jerry Hyde, who kindly shared some of his experience with the design of the lateral reflectors at the Michael Fowler Centre.⁷

Reflection coverage zones were easily determined using CATT Acoustic 8.0. Aiming the reflectors was easy; determining where to aim them was not. Should a reflector aim for seats on its side of the room or the opposite side? Aiming for the opposite side of the room meant a larger zone of coverage but, because the room is so large, the reflections were arriving rather late; between 60 and 70 ms in the orchestra level. If a reflector was aimed towards the same side of the room the reflections arrived earlier but the angle of incidence became more vertical than lateral. The decision, once again, was informed by the Christchurch Town Hall design – in this case its descendent, the 1982 Michael Fowler Centre. A quick method of images study of an AutoCAD version of the drawings⁸ confirmed that the

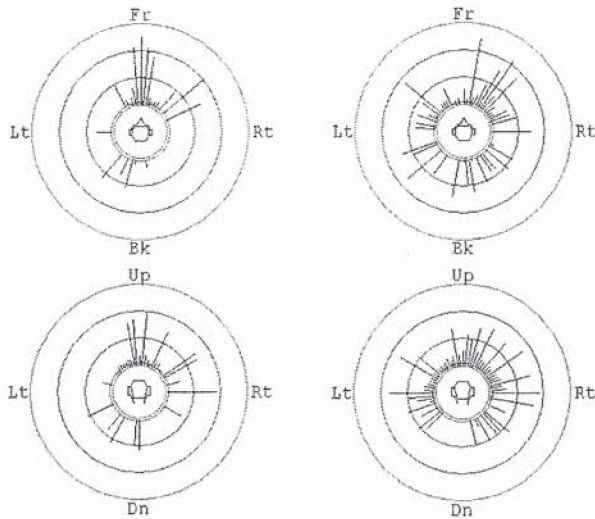


Figure 1 Computer model calculation for a seat in the orchestra level of the existing room demonstrating the paucity of laterally reflected sound.

Figure 2 Computer model calculation for the same seat as Figure 1. Laterally reflected sound has been increased by the overhead reflectors and the terraced floor plan.

Before and after computer model calculations, shown in Figures 1 and 2, indicate a significant increase in laterally reflected sound.

4. MULTI-PURPOSE ACOUSTICS

The Queen Elizabeth Theatre is, above all, a multi-purpose venue. Although much of the acoustic design was centred around the needs of Vancouver Opera, most of the bookings for the room rely on amplified sound. The traditional solution, of course, is to provide the appropriate room volume for opera and when amplified productions are on stage, absorb the excess reverberation with adjustable acoustic banners. Recognising that these banners don't absorb low frequency sound very well, the client stated that they wanted something better. Discussions between the author and the architect led to a novel solution.

Coupled volumes have long been used to extend the Reverberation Time of a room. While there are many successful examples, some acousticians remain sceptical. What most agree on, however, is that coupled volumes can be used as very efficient low frequency absorbers. We informed the architect of this and a few days later he came up with a proposal to put a series of doors in the side walls, opening them up to the Sound and Light Lock (SLL) corridors that run down the sides of the auditorium. The SLLs will be lined with as much glass fibre as possible, typically 100 mm thick and more. The doors will be 55 mm thick wood. For opera, ballet, etc. these doors will be closed and will provide strong early lateral reflections. For amplified sound, the doors will be open, exposing the absorption material to the room. Other absorption will be

reflectors could indeed be safely aimed to the opposite side of the room.

found on the back walls, in the form of moveable fabric covered panels, and in the ceiling, in the form of vertical roll-up curtains at the catwalks.

5. ENHANCEMENT SYSTEM

If there was a "prime directive" from the client, it would be to maintain the seat count. The result is a wide room with 2 very long balcony overhangs. The wide room will be compensated for with the lateral reflectors, described above. An electro-acoustic enhancement underneath the balconies will compensate for their problematic geometry. The enhancement system is limited to the balcony areas. Enhancement is not used in the main body of the auditorium or on the side wall boxes. A late design change deleted two rows from the 1st balcony thus eliminating the need for enhancement at the back of the orchestra level.

6. OTHER ISSUES

A number of other modifications are being made to improve acoustics. The side walls are currently lined with thin wood panels that absorb low frequency sound and will consequently be removed. To improve acoustic warmth, all surfaces exposed to the auditorium will be massive, either 50 mm plaster or the equivalent weight.

The existing Heating Ventilation and Air Conditioning (HVAC) system is very noisy. Substantial re-design of the system, necessitated in part by the removal of the ceiling, will see HVAC noise levels reduced to Preferred Noise Criterion (PNC) 15 or lower.

REFERENCES

1. Johnson, R. (2007) Private communication.
2. Barron, M. (1974) The subjective effects of first reflections in concert halls - the need for lateral reflections, *J. Sound & Vibration* 15, pp 481-502
3. O'Keefe, J. (2002) Acoustical Problems in Large Post-war Auditoria. *Proceedings of the Institute of Acoustics*, Vol. 24.
4. Marshall, A.H. (1978) Aspects of the Acoustical Design and Properties of Christchurch Town Hall, New Zealand, *J. Sound & Vibration*, Vol.62, Pt. 2, pp 181-194.
5. Cremer, L., Muller, H.A. & Schultz, T.J. (1978) Principles and Applications of Room Acoustics, Vol. 1, Applied Science.
6. Jordan, N.V., Rindel, J.H. (2006) The Alberta Jubilee Halls reborn with up-to-date acoustics. *Proceedings of the Institute of Acoustics*, Vol. 28. Pt. 2 pp 297-304.
7. Hyde, J. (2007) Private communication.
8. The Venue Web, http://www.venueweb.co.nz/wcc_mfc/aud/mfc_aud.htm.

ACKNOWLEDGEMENTS

I should like to dedicate this paper to the memory of Russell Johnson, who passed away as it was being written.

Measuring and Predicting Speech Privacy in Open-Plan Spaces

John S. Bradley

Institute for Research in Construction, National Research Council, Montreal Rd., Ottawa, K1A 0R6

Introduction

The acoustical design of an open-plan office should attempt to minimize the intelligibility and disturbance of unwanted speech from nearby workstations. The success of the design can be assessed in terms of signal-to-noise ratio type measures such as the *Articulation Index (AI)* or its newer replacement the *Speech Intelligibility Index (SII)*. In Europe the use of *Speech Transmission Index (STI)* has been proposed for evaluating open-plan offices.

Successful designs can be most reliably achieved by a combination of quantitative design procedures and subsequent validation measurements. This paper reviews the elements for good design and describes new software tools that make quantitative design and assessment more easily achievable.

Rating Open-Plan Office Acoustics

Subjective studies [1] have confirmed conventional recommendations that the combination of speech from an adjacent workstation and ambient noise levels should correspond to $SII \leq 0.20$ (or $AI \leq 0.15$, or $STI \leq 0.17$) (See Fig. 1). In calculating these values an *Intermediate Office Speech Level (IOSL)* was used which is representative of the lower speech levels found in open-plan offices [2,3].

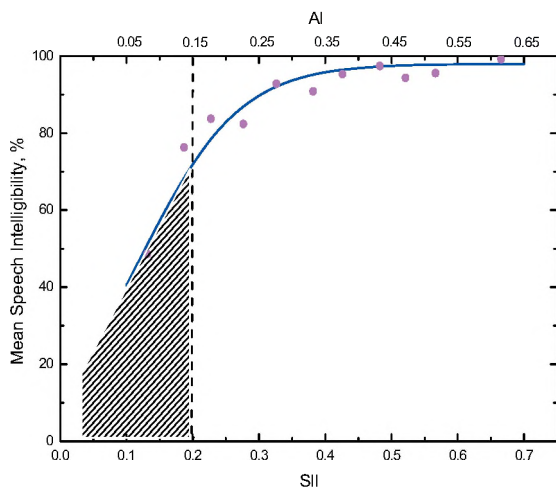


Fig. 1. Mean speech intelligibility scores versus AI and SII values aggregated in 0.05 intervals.

While increased ambient noise levels can better mask unwanted speech sounds and lead to reduced AI ratings, too much noise is disturbing and causes people to talk louder. An ambient/masking noise level

of 45 dBA is recommended as an optimum compromise for open-plan offices [1,3].

Key Requirements for Open-Plan Offices

Open-plan offices must be designed to have appropriate ambient/masking noise levels (≈ 45 dBA) and should attenuate the propagation of speech as much as possible to ensure adequate speech privacy (i.e. $SII \leq 0.20$). The most important 2 elements of the design are a highly sound absorbing ceiling, to minimize reflected sound, and adequate height workstation panels (≥ 1.7 m) to block speech propagation to adjacent workstations. Fig. 2 shows combinations of these two parameters that will meet the design criterion of $SII \leq 0.20$.

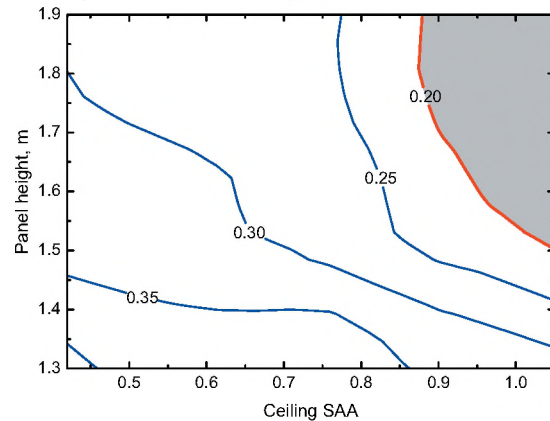


Fig. 2. Shaded area indicates combinations of ceiling absorption (SAA) and panel height providing $SII \leq 0.20$.

It is also important that workstations not be too small (at least 2m by 2m), and that the workstation panels are sound absorptive ($SAA \geq 0.70$). The type and location of lighting fixtures can also affect the success of the acoustical design. Ceiling lights with flat reflective lens should be avoided.

COPE-Calc, Software Design Tool

The COPE-Calc software [4] provides accurate estimates of the expected speech privacy between two adjacent rectangular workstations. It uses an image sources approach [5-8] and includes all significant reflections. The user specifies the dimensions and selects material properties from the programs database. The user can add new materials to the database. Finally, the user specifies speech levels and ambient/masking noise levels and the program calculates AI and SII values.

The program makes it easy to compare various designs and also allows the user to hear audio simulations of speech from an adjacent workstation with the specified ambient/masking noise for each design. The program also gives advice on how to improve privacy based on a range of calculated increases in each parameter.

Figure 3 shows a view of the edit screen illustrating the selection of a ceiling tile material from the database.

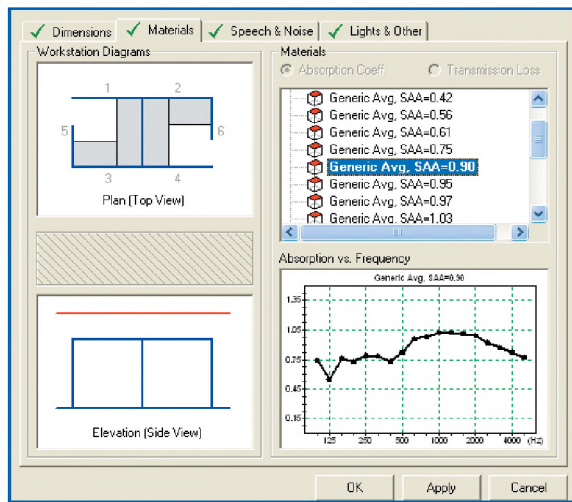


Fig. 3. COPE-Calc edit screen.

SPMsoft, Speech Privacy Measurement Tool

It is also important to be able to measure the degree of speech privacy in offices to either quantify problems or to validate the success of new designs. The new speech privacy measurement software (SPMsoft) is being developed to permit more convenient speech privacy measurements using impulse response techniques. The sound source is first calibrated to have a known output at 1 m in a free field and then the program can measure attenuations from a source workstation to nearby workstations.

The user selects an appropriate speech source level such as the IOSL [1-3] and when combined with the measured attenuation gives the expected speech level at the receiver location. The ambient noise level is either measured or a reference value is read from the program's database. The program then calculates values of AI, SII and STI from the impulse response, as well as the speech and noise levels.

If the user enters the dimensions of the workstations and the positions of the source and receiver, the program will identify the expected time of arrival of the main ceiling reflection and the initial diffracted path over the separating screen. The relative energy

in these two main features of the impulse response indicates whether one should first increase the screen height or the ceiling absorption to most effectively improve speech privacy. (See Fig. 4).

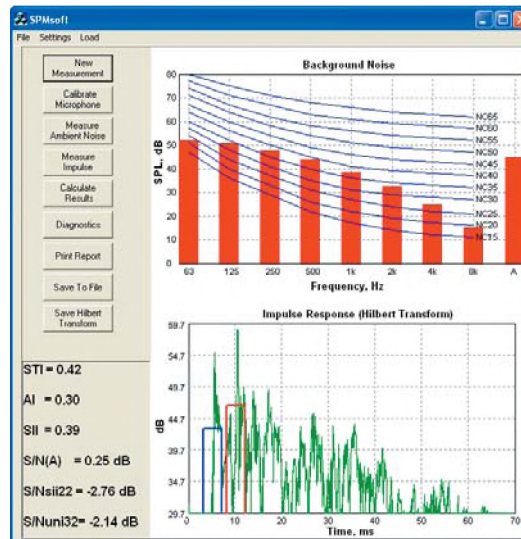


Fig. 4 Main screen of SPMsoft showing measured noise levels (upper) and measured impulse response (lower).

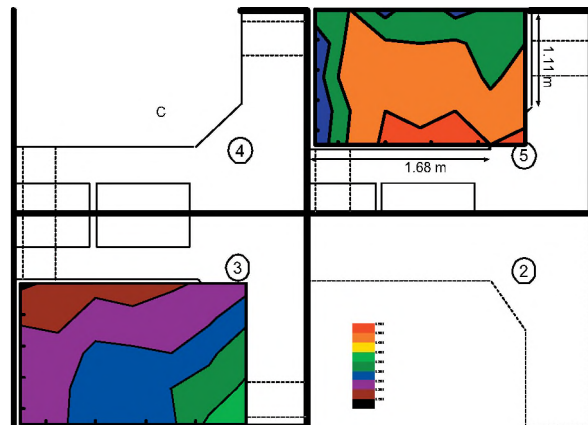


Fig. 8. Contours of AI values for speech propagation from workstation #4 to workstations #3 and #5 from measurements at 0.30 m intervals.

References

- [1] Construction Technology Update #63 IRC-NRC (2004).
- [2] Can. Acoust. 31(2) 23-30 (2003).
- [3] Paper N1034, Inter Noise (2003).
- [4] COPE-Calc, is available at <http://irc.nrc-cnrc.gc.ca/ie/cope/index.html>
- [5] App. Acoust., 63(8) 849-866 (2002).
- [6] App. Acoust., 63(8) 867-883 (2002).
- [7] App. Acoust., 63 (12) 1335-1352 (2002).
- [8] App. Acoust., 63 (12) 1353-1374 (2002).

ACOUSTIC DESIGN OF THE ESPLANADE ARTS AND HERITAGE CENTRE, MEDICINE HAT

John O'Keefe

Aercoustics Engineering Limited, 50 Ronson Drive, Suite 165, Toronto, Canada, M9W 1B3, jokeefe@aercoustics.com

1. INTRODUCTION

The \$32M Esplanade Arts and Heritage Centre consists of a museum, a 150 seat studio theatre and the 700 seat main auditorium. This paper will focus on the latter. The 700 seat, single balcony theatre is located in the north-east corner of the building and is surrounded on three sides by a 50 mm acoustic joint. To simplify construction, a corridor between the north façade of the building and the audience chamber was left unisolated. Carpet on the corridor floor controls noise from footfall. The room is designed for music and theatre, both community based and professional.

2. NOISE CONTROL

The Esplanade, like many new performing arts centres, uses a displacement system to ventilate the room. The floors of the orchestra and balcony levels are perforated with a series of 150 mm diameter holes. A room below the orchestra level and the ceiling space underneath the balcony act as their respective plena. Air is inserted into these plena, where it mixes and slowly moves upward to ventilate the audience chamber. These systems have become quite popular of late but there is little, if any, information in the literature to guide design. Industry standard calculations such as ASHRAE¹ do have calculation procedures for plena but not of the kind considered here. So, how does one calculate the noise attenuation of a typical displacement system plenum?

Analysis of plenum noise control presents a dilemma. Each hole in the floor is an aperture into the plenum and can thus be considered a noise source. Good sight lines, of course, make for good sound paths. With that in mind, should we concern ourselves with all these noise sources or just the few that can be "seen" by a listener sitting in his or her seat? And, if one takes this "line of sight" approach, how many noise sources are there? A listener seated in the orchestra level, for example, can see only four or five noise sources. On the other hand, in a room like the Esplanade, a listener located on the catwalk can see hundreds of noise sources. An appropriate analysis, of course, must consider both listener scenarios.

Recognising that the listener on the orchestra level is always close to the noise sources while the listener on the catwalk is always far away, a concept of Near and Reverberant Fields was developed, similar to but not quite the same as the Direct and Reverberant field solution of traditional room

acoustics theory. For the near field, the calculation model is of a partially blocked pipe. For the reverberant field the procedure is similar to a noise intrusion calculation from one room to another, where the Transmission Loss (TL) of the common partition is calculated as an area ratio combining the concrete floor and the partially blocked pipe.

Measurements have now been performed on three displacement systems: Mississauga Living Arts Centre, The Esplanade, Medicine Hat and the Four Seasons Centre for Performing Art in Toronto. The measurements to date consistently suggest the Reverberant Field is louder than the Near Field. Typical results are shown in Figure 1. At most frequencies, the Noise Reduction for the Reverberant Field is lower than the Near Field. This means that the Reverberant Field will be louder inside the auditorium. The only exceptions occur at what one might suspect to be the pipe resonance frequencies. This exception however, is limited in effect and it is a safe 1st order approximation to assume that the prediction algorithm can be limited to the Reverberant Field. This is fortunate because of the two, the Reverberant Field is easier to calculate.

Results from a recent project, the Four Seasons Centre for the Performing Arts, are shown in Figure 2. There is good agreement at most frequencies, the only exceptions being at low frequencies. It is suspected that the discrepancies may be related to pipe resonances.

3. SCALE AND COMPUTER MODELLING

Like most new auditorium designs, the original intention for The Esplanade was to predict the room's acoustical behaviour using 3-D computer models. However, the architect's desire for a low, "acoustically transparent" ceiling above the audience presented a challenge beyond the capabilities of modern computer modelling algorithms. A 1:20 scale model was built and tested. All of the 20 scale model measurements were augmented with the post-processing algorithm developed by Grillon². This routine, executed in MatLab, extends both the frequency and dynamic ranges of acquired signals. Unlike previous scale model conditioning routines³, the Grillon algorithm maintains the reactive component of the signal and, in so doing, permits auralization. The ability to "listen" to how the ceiling affected sound incident at small grazing angles proved critical.

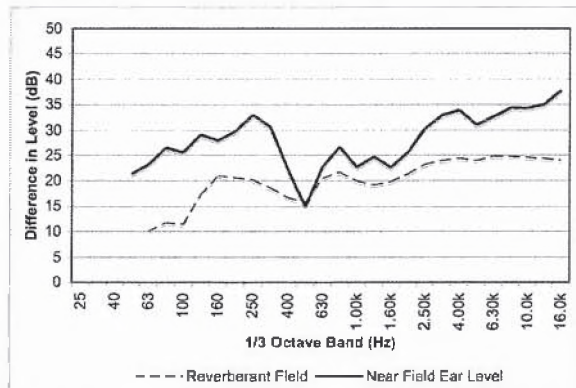


Figure 1. A comparison of Near and Reverberant Field Noise Reduction at The Esplanade.

Building and testing the scale model proved fortuitous because it turns out that the computer model had trouble dealing with the fly-tower. Through a number of trials and experiments, it consistently overestimated the effect of soft goods stored in the fly-tower above the (partially open) orchestra shell ceiling. Modern computer algorithms are known to have problems with coupled spaces like a fly-tower, an issue that was addressed by Summers et al.⁴ Even when the late energy correction developed in [4] was applied, the computer model predicted Early Decay Time (EDT) in the range of 1.5 s, far short of the goal for the symphonic programme anticipated at The Esplanade. The scale model predicted EDTs in the range of 2.2 s.

It is suspected that the problem is not with the software (an otherwise reliable commercial product) but with a fundamental anomaly in computer modelling algorithms. Computer model algorithms assume that sound behaves like light and that the path of the reflections can be quantified with rays and lines. The boundaries of the room and objects

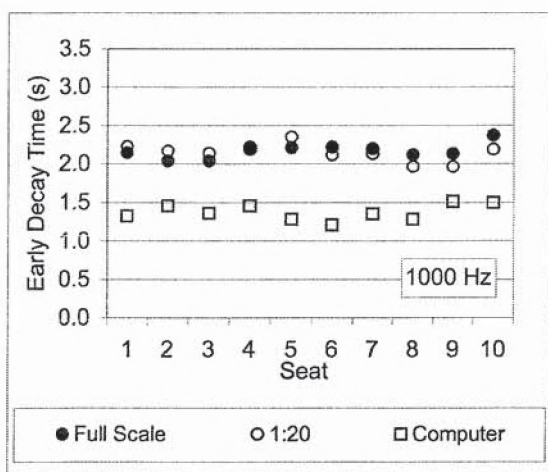


Figure 3. Predicted and measured Early Decay Times. Seats 1 to 6 are on the orchestra level, 7 to 10 in the balcony.

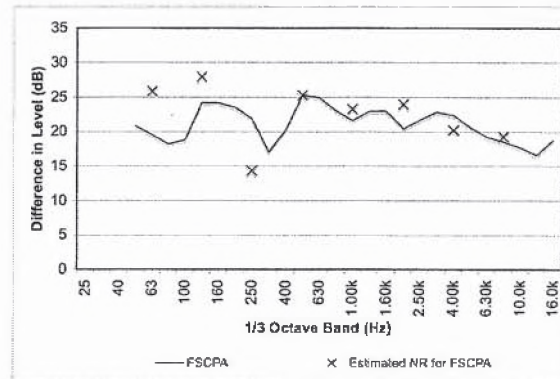


Figure 2. Calculated (X) and measured (-) Reverberant Field Noise Reduction at the Four Seasons Centre for the Performing Arts.

within the room are described mathematically as bounded (i.e. finite) planes. Thus, for a reflector, such as those making up the stage canopy at The Esplanade, the test of whether the sound goes past it or is reflected off it, is based on the intersection of a line and a plane. If the line intersects the plane within its defined boundaries the sound will reflect. If the line intersects outside the boundaries it will go past the reflector, in this case up into the acoustically absorbent flytower. The problem is that lines are infinitely thin. Acoustic waves, of course, are of finite dimension. Thus the computer model algorithm may be exaggerating the amount of sound that flows through the openings in the canopy. A comparison of the two prediction methods with the final full scale measured results is shown in Figure 3. The scale model predictions are surprisingly accurate.

The Esplanade opened in October 2005 and has quickly established a reputation as one of the best sounding rooms in Western Canada.

REFERENCES

1. American Society of Heating, Refrigerating and Air Conditioning Engineers (ASHRAE), Sound and Vibration Control, 2003 ASHRAE Handbook, pp. 47.1-47.5.
2. Grillon, V (1995) Auralisation dans les Maquettes: Traitement des Response Impulsionelles, Ph. D. Thesis, Univ. du Maine.
3. Polack, J.D., Marshall, A.H., Dodd, G. J. (1989) Digital Evaluation of the Acoustics of Small Models, J. Acoust. Soc. Am. Vol. 85, pp. 185-194
4. Summers, J.E., Torres, R.R., Shimizu, Y., Dalenbäck, B-I (2005) Adapting a randomized beam-axis-tracing algorithm to modelling of coupled rooms via late part ray tracing. J. Acoust. Soc. Am. Vol. 118, pp. 1491-1502.

ACKNOWLEDGEMENTS

I would like to thank Kiyoshi Kuroiwa for all his hard work on the scale and computer models. Our work on the Four Seasons Centre for the Performing Arts was in association with Sound Space Design. Bob Essert participated in the plenum measurements for that building and his sage advise on the topic is greatly appreciated.

COMPARISON OF SUBJECTIVE AND OBJECTIVE RATINGS OF INTELLIGIBILITY OF SPEECH RECORDINGS

Bradford N. Gover and John S. Bradley

Institute for Research in Construction, National Research Council, Ottawa, ON K1A 0R6, Canada
brad.gover@nrc-cnrc.gc.ca

1. INTRODUCTION

The intelligibility of speech recordings made in rooms and other spaces can be affected by a range of factors, including reverberation, noise, distance from talker to microphone, and properties of the microphone system itself. This paper presents some results regarding the evaluation of the intelligibility of speech recordings made under controlled conditions with a variety of microphone systems. Test speech sentences were recorded, and the intelligibility of those recordings was determined by a subjective listening test. Additionally, STIPA, a form of the Speech Transmission Index intended to predict intelligibility for electroacoustic systems [1] was determined for each recording condition.

2. METHOD

Recordings of test speech sentences [2] were made under controlled conditions in 4 test spaces having widely varying acoustical properties: see Table 1.

Test Space	Volume (m ³)	Noise (dBA)	RT (s)	Description
C	148	46.1	1.5	Reverb chamber with added absorption.
K	77	49.9	0.4	Domestic space.
R	892	67.3	–	Large, noisy.
T	–	63.8	0.05	Pickup truck.

Table 1: Descriptions of test spaces. The noise in each was generated via playback of recorded noise over loudspeakers.

In each space, a small loudspeaker played the test speech and the STIPA test stimulus at a fixed level, and recordings were made at 3 recording positions with each of 7 microphone systems, some in several different configurations. In all, 83 unique recordings were made, 44 of which were 2-channel. The 2-channel recordings were also analyzed as 1-channel, resulting in a grand total of 83 + 44 = 127 recordings. Each recording contained 5 unique test sentences, each of which was rated by 10 participants in a subjective intelligibility test. A total of 40 subjects participated, and the testing was approved by the NRC Research Ethics Board (O-REB Protocol 2006-47). One at a time, participants listened over headphones to the recorded sentences. After each, they repeated to the test operator the words they understood, as well as their judgments on a 7-

point scale of “How difficult did you find it to understand the speech?” (1=Extremely Difficult, 7=Not Difficult At All) and “How would you rate the quality of this speech recording?” (1=Low Quality, 7=High Quality). The fraction of words correctly identified was determined for each sentence, and for a particular recording, the average score was determined from 50 responses (10 subjects × 5 sentences).

3. RESULTS

The intelligibility results for recordings made with four of the microphone systems at one location within each test space are shown in Fig. 1. These devices all used omnidirectional microphones, and differed in terms of size, preamplification, and processing. The black bars indicate the average intelligibility score for the 1-channel recording made with device D_i , in configuration C_j , in position M_k , for the test space indicated (C, K, R, or T). The light grey bars are the scores for the 2-channel recording, where one existed. An asterisk at the left indicates that the difference between 1 and 2-channel scores was significant ($p < 0.05$).

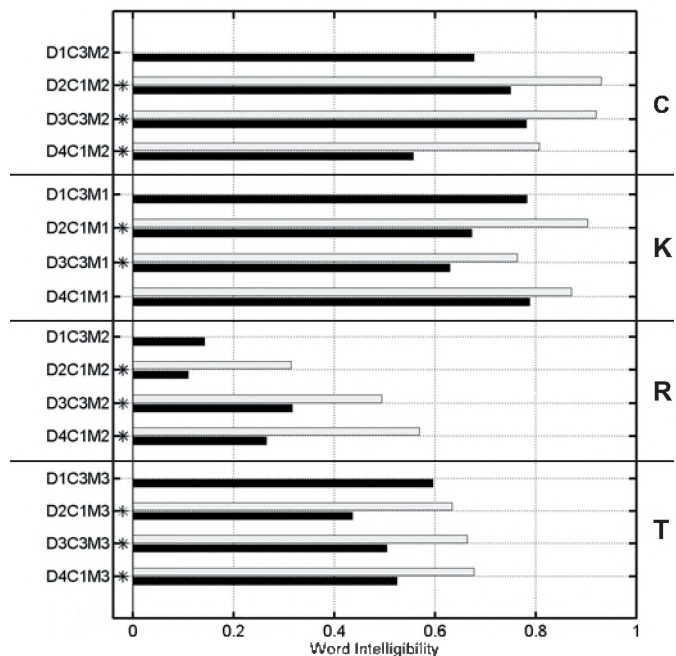


Figure 1: Selected word intelligibility scores: black bars for 1-channel, light grey bars for 2-channel. An asterisk at left implies a significant difference between the two ($p < 0.05$).

Within each test space, the variation in score indicates the variation with recording system at a fixed location: among 1-channel recordings, a substantial difference in intelligibility of almost 0.2 (20%) can result.

The scores for the 2-channel recordings were always higher than the corresponding 1-channel recordings. This is further demonstrated in Fig. 2, which plots the 2-channel score versus the 1-channel score for all 44 such recording conditions tested. The 2-channel intelligibility scores were on average 0.13 (13%) higher.

The judgments of difficulty and of quality are plotted versus intelligibility score in Fig. 3 for all 83 1-channel measurement cases. There is the expectation that as intelligibility increases; a sense of difficulty will decrease [3], and presumably, a sense of quality will increase. This is seen in the figure. Only for cases with intelligibility greater than about 0.8 (80%) were ratings greater than 4 (i.e., on the “Not Difficult”, “High Quality” side of “Neutral”).

Figure 4 shows the intelligibility scores plotted against STIPA for the 83 1-channel recordings. Overall, the correlation is not very high ($R^2=0.35$), but the breakdown by test space shows that it is lowest for test space R ($R^2=0.21$) and highest for test space K ($R^2=0.71$). The accuracy of STIPA as an objective predictor of speech intelligibility is not guaranteed. In some noise and reverberation conditions, it does not accurately predict intelligibility.

4. CONCLUSIONS

For a single recording location, the intelligibility of speech recordings varied by up to 0.2 (20% word score) depending on recording device type.

The intelligibility of 2-channel recordings was significantly higher than corresponding 1-channel recordings, by an average of 0.13 (13%).

Ratings of difficulty and quality improved (i.e., decreased, increased respectively) as intelligibility scores increased.

STIPA was not generally well correlated with subjective intelligibility, but for a subset of the data (from particular test spaces), the relationship is stronger.

REFERENCES

- [1] IEC 60268-16 “Objective rating of speech intelligibility by speech transmission index,” IEC Switzerland (2003).
- [2] “IEEE recommended practice for speech quality measurements,” IEEE Trans. Aud. Electroacoust., **17** (1969).
- [3] Kobayashi *et al.*, “Optimum speech level to minimize listening difficulty in public spaces,” J. Acoust. Soc. Am., **121** (2007).

ACKNOWLEDGEMENTS

Thanks to M. Stinson, G. Daigle, J. Quaroni, and R. Hartwig of NRC Institute for Microstructural Sciences for assistance and guidance in making the measurements.

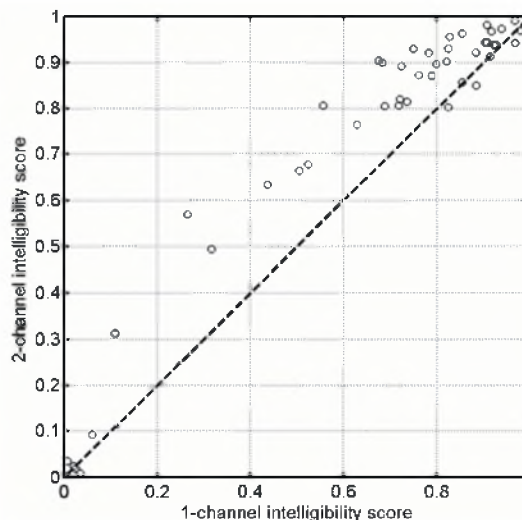


Fig 2: Intelligibility scores for 2-channel recordings versus corresponding 1-channel recordings for 44 cases. The dashed line indicates where the points would lie if equal.

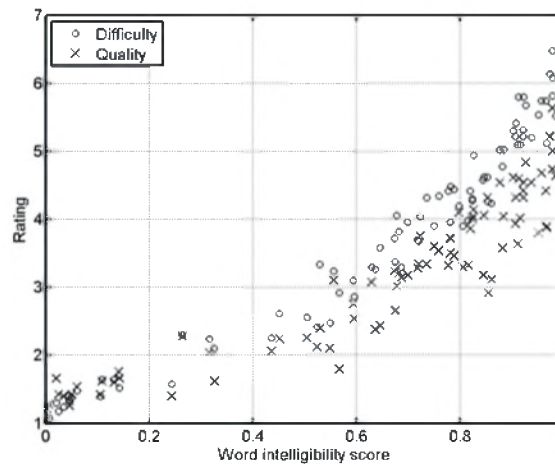


Fig 3: Ratings of Difficulty (1=Extremely Difficult, 7=Not Difficult At All) and Quality (1=Low Quality, 7=High Quality) versus intelligibility scores.

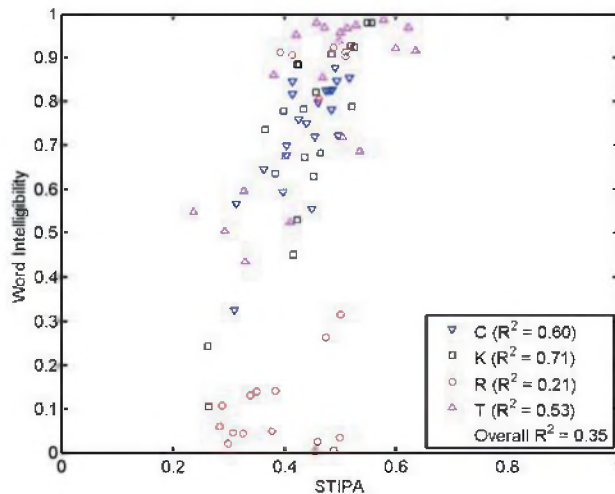


Fig 4: Intelligibility score versus STIPA for all 83 1-channel recordings, broken down by test space (C, K, R, and T).

EFFECTS OF STRUCTURAL FLANKING ON APPARENT STC OF STEEL STUD WALL

Clair W. Wakefield, and Andrew P. Williamson

Wakefield Acoustics Ltd., 301-2250 Oak Bay Avenue, Victoria, B.C., Canada, V8R 1G5 email: nonoise@shaw.ca

1. INTRODUCTION

As acoustical consultants in Victoria, with its booming condominium market, Wakefield Acoustics Ltd. is often asked to conduct field tests of the Sound Transmission Class (STC) of demising walls within both newly-constructed and converted condominium buildings. The issuance of an occupancy permit often depends on achieving STC 50. Such tests present many challenges including the presence of background noise, small room sizes - often preventing valid Transmission Loss (TL) measurements in the lower frequency bands and the difficulty, particularly when testing corridor walls, in finding a wall section not fatally compromised by sound leakage via the suite's entry door. This often results in a bathroom serving as the receiving space while the adjacent corridor serves as the source space. Considerable effort must be expended to control leakage using temporary barriers (gypsum board, batt insulation etc.) placed over doorways. In a recent such test in a new concrete building not only did airborne noise leakage need to be suppressed but it was later discovered that structure-borne flanking - primarily via junctions between the test wall (a bathroom wall containing the tub) and its adjoining side walls - significantly limited the wall's sound insulation performance.

This paper presents the results of the above-described field test and discusses the effects of flanking transmission on the test results.

2. TEST CONDITIONS AND METHOD

The demising wall which separated the bathroom and entry/kitchen area of the test suite (#206) from the corridor was constructed as follows:

- 2 layers 16 mm Type X gypsum board,
- 152 mm steel studs @ 400 mm o.c.,
- 152 mm fiberglass batt insulation,
- 16 mm Type X gypsum board,
- 6 mm cement board.

Figure 1 shows the layout of the test wall in relation to the corridor (source space), bathroom (receiving space) and the suite entry.

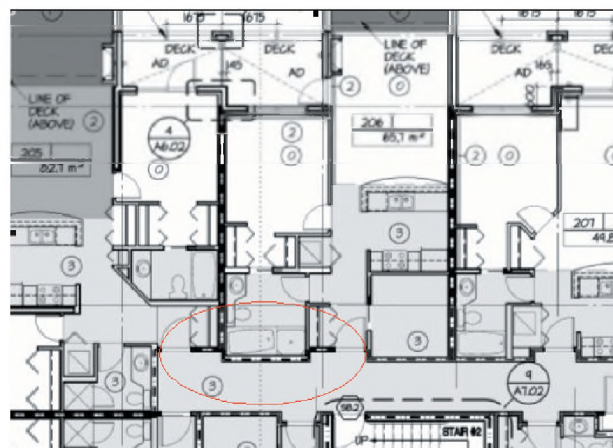


Figure 1; Layout of ASTC Test in Suite 206 showing Corridor Bathroom, Suite 206 Entry to right and Suite 205 Entry to Left.

To the extent possible given the small size of both the source (corridor) and receiving (bathroom) spaces, the Apparent STC test was carried out in accordance with ASTM E 336-05. A powerful loudspeaker fed with steady broad-band noise was placed in the corridor and average sound pressure levels were measured with a Larson-Davis Model LD2800 Real Time Analyzer at five locations on either side of the test wall using the swept microphone technique. The same system was used to measure the reverberation times in the receiving room.

After some experimentation, airborne sound leakage via the suite entry door was effectively eliminated by covering both the suite entry door and the door connecting the entry to the subject bathroom with layers fiberglass batt insulation and gypsum board. In addition, the perimeter of door between the entry and the bathroom was sealed with heavy tape. Fortunately, access to the bathroom for test purposes could be gained via a second door leading to the master bedroom.

3. RESULTS

3.1 Initial Test Results - Apparent STC 46

The initial test of the corridor wall yielded an Apparent STC (ASTC) of 46 (see Figure 2) whereas the 2006 BC Building Code (see Walls Number S9a and S9b rates this construction at STC 57 to 59. The mos

significant TL deficiencies were not in the lower 1/3-octave bands (125 to 250 Hz.) as is often the case, but rather between 1,250 and 3,150 Hz. These mid-to-high frequency TL deficiencies were not felt to be due to air-gap leakage since the TL performance recovered again in the 4,000 Hz. 1/3-octave band.

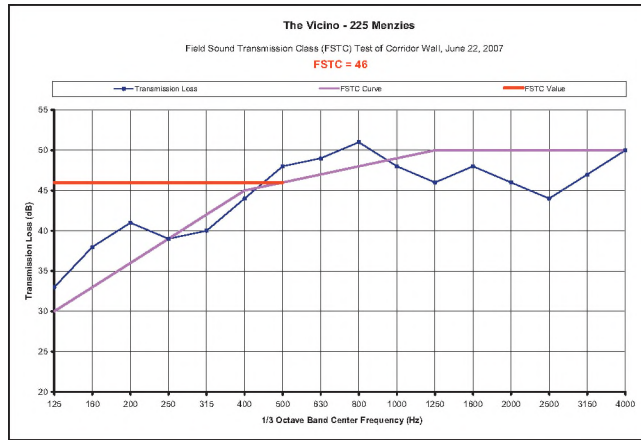


Figure 2; Results of Initial Apparent STC (ASTC) Test of Corridor Wall Showing Mid-High Frequency TL Deficiencies

Suspecting that construction flaws might be responsible for these TL deficiencies, a section of wall was opened up on the bathroom side to confirm the presence of cavity insulation and the absence of any structural bridging (by waste pipes etc.) across the cavity. No such construction flaws were discovered. This then left the possibility that structural flanking was the culprit, an opinion that was subsequently reinforced by a conversation with a specialist in this area – Dr. Trevor Nightingale of the NRC.

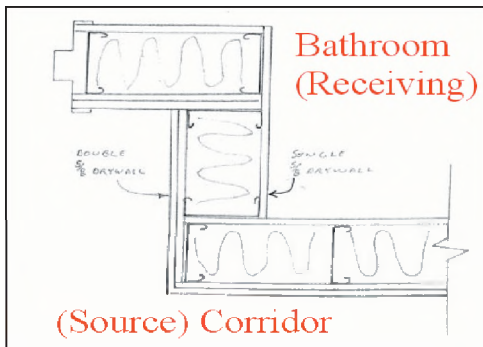


Figure 3; Detail of Junction between Corridor Test Wall and Side Wall showing Bridging of Wall Cavity by Gypsum Board.

As seen in Figure 3, the wall cavity is blocked off with one or two layers of gypsum board at each corner - apparently for flame spread prevention, but also likely for convenience during construction. Gypsum board then bridges the cavity at the corners and allows structure-borne sound to pass through it more efficiently than would be the case if the only connections were provided by lightweight steel studs.

3.2 Final Test Results - Apparent STC 50

Upon verification of the basic construction of the corridor wall, a second test was conducted to confirm the initial result. The section of wall board and cement board (about 1 m by 1m) removed for inspection purposes had been replaced but the small gaps around its perimeter had not been repaired (mudded) as the surface was to be tiled. Unexpectedly, this retest revealed TL improvements of 5 to 6 dB in the 1,000 to 4,000 Hz. range and an increase in ASTC from 46 to 50.

3.3 Near Field SPL Scans of Room Surfaces

At the time of the second test, a series of spatially averaged SPL measurements were made within about 50 mm the various bathroom wall surfaces to explore their relative significance to the overall sound radiation into the space. Figure 4 shows the various 1/3-octave band SPL spectra obtained. Note the consistency of the sound levels particularly at and above 1000 Hz., indicating that the level of induced vibration in the two side walls were not significantly different from those in the test wall.

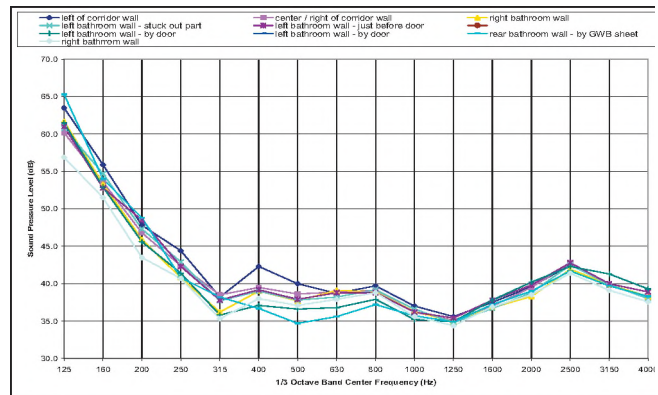


Figure 4; Results of Near-Field SPL Scans Over Wall Surfaces

4. DISCUSSION

These tests have shown that flanking transmission via sidewalls can result in differences between the ASTC's and lab-rated STC's of steel stud and gypsum board walls larger than indicated by the familiar 3 to 5 point "rule of thumb". Here flanking was aggravated by the small size of the test wall (i.e., relatively small ratio of area-to-perimeter) and also by the fact that portions of the side walls adjoining the corridor were exposed to the source sound field. These results also support the notion that the Building Code should be modified to better address structural flanking transmission in real buildings. Such revisions could presumably focus on specifying appropriate connectivity details rather than simply advising designers/builders to apply a safety margin of 5 STC points when selecting a wall since they won't be able to achieve lab results in the field.

MEASUREMENT OF THE PERFORMANCE OF SOUND LEVEL METERS USING IEC 61672-3:2006

Peter Hanes

Institute for National Measurement Standards, National Research Council Canada,
1200 Montreal Rd., Ottawa, Ontario, Canada, K1A 0R6 • peter.hanes@nrc-cnrc.gc.ca

1. INTRODUCTION

1.1 IEC 61672

IEC 61672-1:2002¹ provides specifications for sound level meters (SLMs) and was recommended for use in Canada by the Canadian Standards Association in CSA Z107.10² in 2006. IEC 61672-1:2002 generally specifies tighter tolerance limits than previous standards, and requires that measurement uncertainties are taken into account when testing conformance³.

IEC 61672-3:2006⁴ provides the first internationally agreed methods for measuring the performance of individual SLMs. Because of the limited extent of the measurements, even if the results of the measurements are successful, no general conclusion about the conformance of the SLM to the specifications of IEC 61672-1 can be made unless evidence of pattern approval of the model of SLM is publicly available. Pattern approval tests are specified in IEC 61672-2⁵ but are in practice only performed in countries where legal requirements exist for testing a model of SLM before it may be sold.

1.2 Measurements required by IEC 61672-3

A calibrated sound calibrator is applied in order to determine the overall sensitivity at a reference level (for example, 94 dB) at a single frequency (usually 1 kHz).

The indicated sound level with no input signal is noted; this corresponds to the level of self-generated noise in the SLM.

The difference in the response to a steady 1 kHz sinusoidal signal when switching between different time weightings and frequency weightings is measured.

One frequency weighting response relative to 1 kHz is determined using acoustical signals at 125 Hz and either 4 kHz or 8 kHz. This provides a simple test of the performance of the microphone.

Frequency weightings A, C and Z (if available) relative to 1 kHz are determined for the frequency range from 63 Hz to 8 kHz or 16 kHz (depending on performance class) by applying sinusoidal electrical signals and adjusting the

results for the acoustical influence of the microphone, case and any accessories.

The level of an applied 8 kHz sinusoidal signal is varied over the entire linear operating range. The differences between the indicated sound levels and the anticipated levels are determined. The level linearity errors caused by switching the SLM to other level ranges are also measured.

The response of the SLM to toneburst signals of durations as short as 0.25 ms is measured, and compared with the theoretical ideal response. Accurate toneburst response is crucial for measurement of sounds of short duration.

The indicated peak C sound level in response to single cycle and half cycle sinusoidal electrical signals is measured and compared with the theoretical ideal response.

For SLMs capable of displaying time-average sound level only, the levels of positive and negative half-cycle input signals that first give overload indications are compared. The SLM should respond equally to signals of positive and negative polarity. The indicator should latch on until reset.

2. APPLICATION TO OLDER INSTRUMENTS

While Part 3 of IEC 61672 was intended for use in testing sound level meters that are designed to meet the requirements of Part 1, the measurement methods are also useful for determining the performance of older SLMs. NRC-INMS does not perform conformance tests of acoustical instruments, but does provide a measurement service for its clients that closely follows the methods of Part 3.

Five SLMs that were manufactured prior to 2002 were measured using the methods of Part 3. Measurements of frequency weighting at some additional frequencies using acoustical and electrical input signals were also attempted, but the results are not considered here; measurements of frequency weighting A at the lowest frequencies are not always possible because of the limited extent of the linear operating range of the SLM.

All the instruments were well-maintained examples of relatively expensive instruments from well-known manufacturers. Instruction manuals were available; most contained adjustment data and typical microphone frequency responses. Some sensible selection of levels and settings at which the measurements were performed was required. Because the SLMs were designed to conform to the specifications of previous standards and because the individual examples are not necessarily representative of their models, the instruments are identified here only by their year of manufacture and claimed performance Type.

3. RESULTS

The majority of the SLMs performed adequately for the majority of the measurements. A summary of the results is shown in Table 1.

The results most often exceed the tolerance limits of IEC 61672 for the toneburst response measurements. The 1997 Type 2 SLM performed poorly in response to any toneburst of duration less than 200 ms. The response of the 1980 Type 1 SLM in response to a 200 ms toneburst when using the S time weighting was just outside the IEC 61672 tolerance limits, but the SLM performed adequately for shorter toneburst durations and when using the F time weighting. The 1977 Type 1 SLM performed poorly in three of the five toneburst response measurements.

The level linearity error of the 1980 Type 1 SLM exceeded the IEC 61672 tolerance limits only when attempting to indicate the reference SPL on its most-sensitive (lowest) level range. The same SLM gave a level difference in the overload indication test of about four times the tolerance limit of IEC 61672.

4. CONCLUSIONS

Existing sound level meters did not necessarily become obsolete on the publication of IEC 61672-1 in 2002. However, it is quite possible that models of SLMs that have not been successfully pattern evaluated according to IEC 61672-2 could perform poorly by current standards, especially in response to signals of short duration.

Measurement using the methods of IEC 61672-3 provides the best basis for determining confidence in the performance of an individual SLM. IEC 61672-3 should be recommended for use in Canada with appropriate guidance on its use with respect to older SLMs. Measurement standards in Canada should be updated where appropriate to require at least that the performance of an individual SLM has been measured according to the methods specified in IEC 61672-3.

REFERENCES

- ¹IEC 61672-1 Ed. 1, Electroacoustics – sound level meters – Part 1: Specifications (2002)
- ²CSA Z107.10-06 Guide for the use of acoustical Standards in Canada (2006)
- ³G. S. K. Wong, L. Wu, and P. Hanes, “The current status of international standards for sound level meters” *Canadian Acoustics*, 30(3), 110-111 (2002)
- ⁴IEC 61672-3 Ed. 1, Electroacoustics – sound level meters – Part 3: Periodic tests (2006)
- ⁵IEC 61672-2 Ed. 1, Electroacoustics – sound level meters – Part 2: Pattern evaluation tests (2003)

ACKNOWLEDGEMENTS

Lixue Wu and George Wong assisted in the development of the measurement procedure. The Acoustics and Signal Processing Group of the NRC Institute for Microstructural Science provided some of the SLMs.

Table 1. Summary of results. ✓ indicates that the results do not exceed the tolerance limits of IEC 61672; ✗ indicates that the results exceeds the tolerance limits of IEC 61672; ... indicates that the SLM does not provide this capability.

Sound level meter	1997 Type 2	1996 Type 1	1984 Type 1	1980 Type 1	1977 Type 1
Measurement					
Time & frequency weightings at 1 kHz	✓	✓	✓	✓	✓
Frequency weighting – acoustical input	✓	✓	✓	✓	✓
Frequency weighting – electrical input	✓	✓	✓	✓	✓
Level linearity – reference level range	✓	✓	✓	✓	✓
Level linearity – including range control	✓	✓	✓	✗	✓
Toneburst response	✗	✓	✓	✗	✗
Peak C sound level	...	✓	✓	✓	✓
Overload indication	...	✓	✓	✗	...

IMPROVED REPEATABILITY FOR CALIBRATION OF SHOCK ACCELEROMETERS

Lixue Wu

Institute for National Measurement Standards, National Research Council Canada
1200 Montreal Rd., Ottawa, Ontario, Canada K1A 0R6

1. INTRODUCTION

A previous study of the NRC system for calibration of shock accelerometers investigated the effect of mass loading on the system using a vibrometer [1]. At that time, the repeatability of the measurements was limited by the resolution of the instrumentation in use. Further investigation of the effect of mass loading effect will use improved instrumentation: a reference accelerometer replaces the vibrometer for sensing the shock pulse motion, and a high-speed and high-resolution (14-bit) A/D conversion card is used to record the waveforms of the outputs of the accelerometers. This paper describes the signal processing techniques that can then applied to the recorded waveforms to extract acceleration peak values.

2. CALIBRATION METHOD

An upward-moving pneumatically-operated projectile, as illustrated in Fig. 1, provides a simple means for the comparison shock calibration of accelerometers. A pressure release mechanism controls the moving speed of the projectile. The shock acceleration is created by the projectile impacting on an anvil that has pads attached to its bottom surface. A wide range of shock pulse amplitudes and durations can be generated by controlling the drive pressure and the mass of the target (anvil and accelerometers).

2.1 Mass loading

Mass loading affects the sensitivity of an accelerometer. In order to calibrate the accelerometer under test for a particular load, dummy masses (steel cylinders) can be mounted using studs between the accelerometer under test and the reference accelerometer (refer to Fig. 1). The mass loading effect can be corrected if mass loading correction curves are published by manufacturers [1]. These curves, however, may not be applicable to shock acceleration.

A torque wrench is used to secure the mass and accelerometers to the anvil with a specified torque (typically 2 N·m). In this arrangement the top accelerometer has no mass load and the bottom accelerometer is loaded by a mass that is the sum of the cylinder mass and the mass of the top accelerometer.

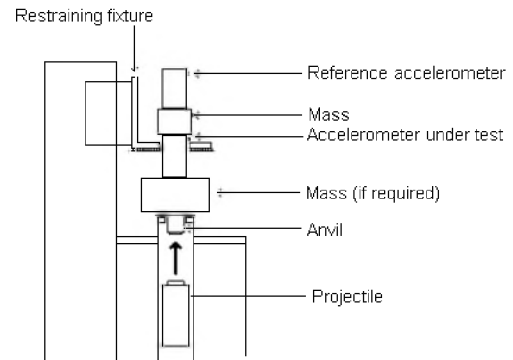


Fig. 1. Arrangement for shock accelerometer calibration.

2.2 Accelerometer sensitivity

Let $S_t(a, m)$ and $S_b(a, m)$ be the voltage sensitivities at shock amplitude a and mass load m for the top and bottom accelerometer including charge amplifiers, respectively. Let V_t and V_b be the peak voltage outputs of the charge amplifiers for the top and bottom accelerometers, respectively. Assume that $S_t(a_i, 0)$ is known. (The reference accelerometer is calibrated at discrete shock amplitudes with no mass load.) Since $V_t = a S_t(a, 0)$, one can control the drive pressure to the projectile to achieve $a_i = V_t / S_t(a_i, 0)$ within a predefined tolerance. Further assume that the assembly of the mass load and the accelerometers is rigid enough that relative motion between the top and bottom accelerometer is negligible. Thus, the output of the charge amplifier for the bottom accelerometer is given by $V_b = a_i S_b(a_i, m)$. That is,

$$S_b(a_i, m) = S_t(a_i, 0) V_b / V_t.$$

2.3 Instrumentation

The instrumentation used to measure the ratio of the peak voltage outputs is shown in Fig. 2. The trigger of the digitizer is set to upward slope and one half of the expected pulse amplitude. The trigger event position is set to 50% (designating 50% of the record length to be pre-trigger samples and 50% of the record length to be post-trigger samples). Using this setting, any DC bias of the output signal can be detected from the pre-trigger samples and then removed.

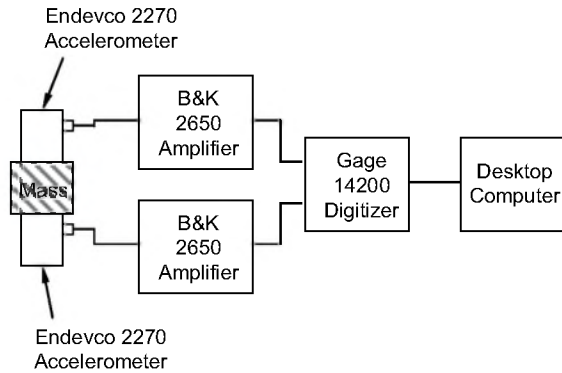


Fig. 2. Arrangement of instrumentation.

2.4 Measurement repeatability

The repeatability of the measurement of peak voltage ratio V_b/V_t is one of the major contributions to the measurement uncertainty of V_b/V_t . Therefore, signal processing methods for processing the recorded signals to improve three aspects of the voltage ratio measurement have been investigated.

DC bias

DC bias exists in recorded signals. With no motion (except environmental vibrations) on accelerometers, the outputs of the charge amplifiers were recorded by the digitizer and further studied for the time variance of the DC bias. It was found that DC bias remains almost constant over a period of equal to the length of the shock pulse (a few milliseconds). Thus, the DC bias estimated from the pre-trigger samples (corresponding to no accelerometer motion) can be used to correct for the DC bias in the post-trigger samples.

Waveform distortion

Damage to the pads which are attached to the bottom of the anvil causes distortion in the shock waveforms and therefore contributes to the poor repeatability of the voltage ratio measurements. The damage to the pads is not always visible. A likelihood test is therefore used to examine the similarity of two pulses recorded. One of the pulses is rescaled and time-shifted to compensate for the gain- and phase-differences between the two measuring channels. The minimum mean squared error between the two waveforms is then calculated for optimal scale factor and time shift. This minimum mean squared error is then compared to a preset limit to decide whether the recorded signals are acceptable.

Noise

Environmental noise (such as external vibration and the interference from power line or radio frequency sources) and inherent noise (such as Johnson and preamplifier noise) also contribute to the poor repeatability

of the voltage ratio measurements. Band pass filters can be used to remove noise to some extent. To further reduce the effect of noise, a polynomial function of variable order is applied to model the waveform around the peak of the pulse. The model parameters (polynomial coefficients) are found by minimising the mean squared error between the polynomial function and the recorded waveform. The peak value is then calculated using the polynomial function.

3. RESULTS

Shown in Fig. 3 are example plots of recorded waveforms and their polynomial model functions (in dark lines). The one having lower peak is the output from the reference accelerometer.

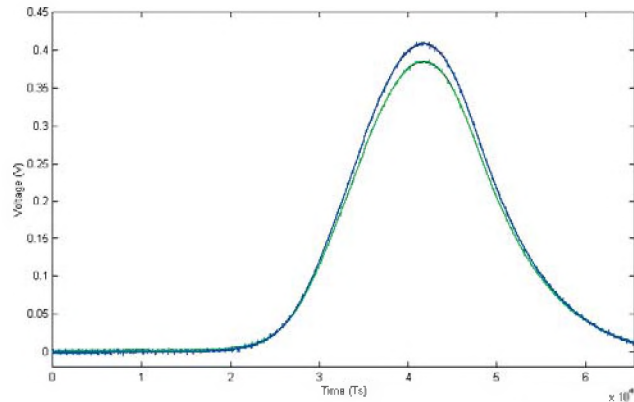


Fig. 3. Plots of recorded waveforms and their model functions, where T_s is the sampling interval and $T_s = 1/50 \mu s$.

The measurement data for ten voltage ratio measurements are listed in Table 1. The standard deviation of the measurements V_b/V_t is 0.016 % with shock amplitudes controlled within ± 0.75 % of a_t for a mass load of 40 g.

Table 1. Measurement data for mass load of 40 g

V_t	V_b	V_b/V_t	V_t	V_b	V_b/V_t
0.3839	0.4077	1.0620	0.3838	0.4077	1.0622
0.3836	0.4073	1.0618	0.3854	0.4093	1.0619
0.3829	0.4066	1.0619	0.3864	0.4104	1.0621
0.3877	0.4118	1.0622	0.3836	0.4074	1.0620
0.3857	0.4097	1.0623	0.3858	0.4096	1.0618

4. CONCLUSION

In the previous study of mass loading effect, the variance of the measured shock sensitivity was up to 1 %. Replacing the 8-bit A/D converter by the 14-bit digitizer and implementing the three signal processing methods reduces the variance of the measured shock sensitivity significantly.

REFERENCES

- [1] Wu, L., Wong, G.S.K., Hanes, P., Ohm, W.S. (2004). The effect of mass loading on the sensitivity of shock accelerometers. *Canadian Acoustics*, 32 (3), 96-97.
- [2] Sill, Robert D. Mass loading in back-to-back reference accelerometers. Technical Paper 310, Endevco Corporation.

A NEW METHOD OF ACOUSTICAL REMOTE EVALUATION OF DEFECTIVE STRUCTURES AND MATERIAL CHARACTERIZATION

Mfoumou, E.^{1,2}, Hedberg, C.¹, Kao-Walter, C.¹, and Narayanswamy, S.²

¹Dept. of Mech. Eng., Blekinge Institute of Technology, SE 371 79, Karlskrona, Sweden

² Dept. of Mech. & Ind. Eng., Concordia University, 1515 St. Catherine W., Montreal, Qc, H3G2W1 Canada

1. INTRODUCTION

This study aims at showing the feasibility of a remote monitoring of structures for a progressive damage assessment as well as material characterization using a simple and inexpensive experimental setup. The method is based on a remote acoustic excitation of transverse vibrations on a membrane using an ordinary broadband low frequency loudspeaker, and the measurement of the response using a Laser Doppler Vibrometer (LDV). Small rectangular strips of aluminium foil (6.35 μm thick), Low Density Polyethylene (LDPE 25μm thick), Paperboard (PPR 100 μm thick) or a combination of these materials were considered. The samples were tested using the implemented Low Frequency Vibration-Based Technique (LFVBT), showing that remote damage monitoring and material characterization are feasible with this method. Theoretical modeling is also developed to correlate the experimental results obtained. This yields a new method for Non Destructive Testing (NDT) of sheet-like materials.

2. METHOD

2.1 Governing equation and steady-state vibration

The theoretical analysis in this study uses the theory of vibrating membrane with account of intrinsic elasticity, governed by the equation [1]:

$$\frac{\partial^2 \xi}{\partial t^2} - c^2 \left(\frac{\partial^2 \xi}{\partial x^2} + \frac{\partial^2 \xi}{\partial y^2} \right) + d^2 \left(\frac{\partial^2}{\partial x^2} + \frac{\partial^2}{\partial y^2} \right) \xi = \frac{p(x, y, t)}{\rho h} \quad (1)$$

Here ξ - is the displacement normal to the plane (xy) coincident with the equilibrium position of membrane, c - is the velocity of propagation of bending waves at zero intrinsic elasticity defined below, p - is external pressure on the surface of the membrane, ρ , h - are density and thickness of the material, and:

$$c = \sqrt{T/(\rho h)}; \quad d^2 = \frac{Eh^2}{12\rho(1-\nu^2)} \quad (2)$$

Where E , T and ν are the elastic modulus, tensile force per unit length of the edge, and the poisson's ratio.

The frequency equation with fixed-fixed boundary conditions was derived [2] to obtain the vibration frequency of each bending mode as follows:

$$\omega_{mn} = c \sqrt{\left(\frac{\pi n}{a}\right)^2 + \left(\frac{\pi m}{b}\right)^2} \left\{ 1 + \frac{d^2}{2c^2} \left[\left(\frac{\pi n}{a}\right)^2 + \left(\frac{\pi m}{b}\right)^2 \right] \right\} \quad (3)$$

a , b are the dimensions of the membrane, m and n are the mode numbers.

2.2 Local density variation: addition of mass

Let the mass m' be attached to the sheet and assume its size to be small in comparison with the wavelength of bending wave.

This mass vibrates together with the membrane and yields the following equation of natural frequencies [3]:

$$\omega_{mn} = \Omega_{mn} \sqrt{\frac{1 + \frac{d^2}{c^4} \Omega_{mn}^2}{1 + 2\beta_0 \frac{m'}{M} \cos^2\left(\pi n \frac{x_0}{a}\right) \cdot \sin^2\left(\pi m \frac{y_0}{b}\right)}} \quad (4)$$

where $M = \rho hab$ - is the mass of the membrane, $\beta_0 = 1$, $\beta_q = 2$ ($q > 1$), and Ω_{mn} is the natural frequency of the unloaded membrane.

One can see that the local load shifts down the natural frequency. The shift is determined by the ratio of loading mass and the mass of membrane m'/M . This shift can be detected only if the special mode is excited which has the loop neighboring the point x_0 , y_0 of the location of the loading mass. Evidently, the weight placed in the node cannot shift the frequency of the corresponding mode.

2.3 Young's modulus from dynamic measurement

From equation (2) relating the velocity of bending wave and the tensile load T , one can easily derive the following:

$$c = \sqrt{T/(\rho h)} = \sqrt{E\varepsilon/\rho} \quad (5)$$

where ε is the longitudinal strain.

Inserting equation (5) into equation (3) with no account of intrinsic elasticity, and solving for normal modes along the length of the specimen yield [2]:

$$f_{0n}^2 = \frac{E \cdot n^2}{4 \cdot \rho \cdot b^2} \cdot \varepsilon \quad (6)$$

where f_{0n} is the resonance frequency of mode $0n$ in Hz. E , n and ρ being all constants for a given measurement, the square resonance frequency is linearly proportional to the strain. As a consequence, dynamic Young's modulus is extracted from the slope of the curve.

Equation (6) offers an idea of how one can estimate Young's modulus of a material from a dynamic measurement using as inputs the longitudinal strain and the measurement of the corresponding resonance frequency in flexural mode.

3. EXPERIMENT AND RESULTS

The function generator provides an input voltage (peak to peak) of a sine signal to the loudspeaker. The acoustic field excited by the loudspeaker vibrates the sample. Laser detection of the surface vibrational response of the sample is accomplished with the laser vibrometer. The vibrometer used in this study makes high-fidelity and absolute measurements of surface displacement over a bandwidth of DC to 50 kHz. The measured response is monitored by the oscilloscope; this allows the detection of the maximum surface displacement, corresponding to a normal mode, which is related to the mechanical properties of the material, or carries information on any structural change in the sample under investigation. The setup is shown in figure 1.

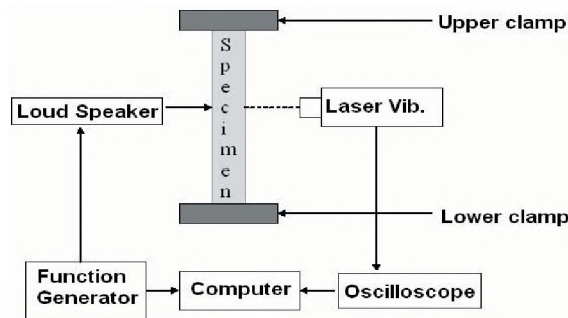


Figure 1: Experimental setup

Small strips are successively added in the middle of the sample and the fundamental frequency change is monitored. The result is shown in figure 2, together with a plot of equation (4), in terms of first mode relative frequency shift with respect to percentage of added mass. A good agreement is observed between experimental and analytical results.

For a varying strain (or extension) within elastic region of the material, equation (6) was plotted using experimental data for each sample. The slope of the line obtained, according to equation (6), allows the extraction of Young's modulus. The result is shown on figure 3 for paperboard, for different specimen lengths. Extended results for Al foil, LDPE, and laminates are published in [4].

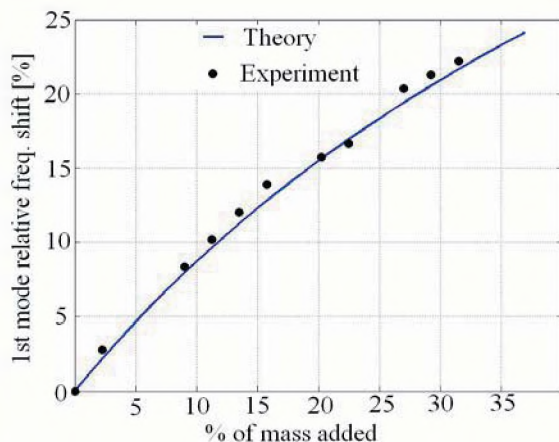


Figure 2: 1st mode relative frequency shift

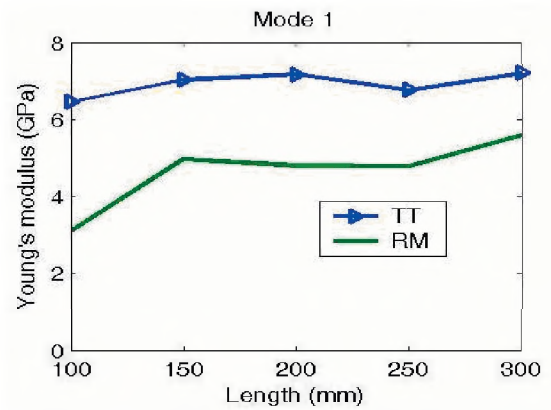


Figure 3: Young's modulus from static & dynamic tests. TT = tensile test, RM = resonance method.

4. CONCLUSION AND DISCUSSION

The theory developed above offers the ability to detect an inhomogeneity in form of added mass using a frequency shift measurement. In other words, we use *acoustic weighing* of the specimen. We have also demonstrated the feasibility of Low Frequency Vibration-Based Technique for dynamic characterization of sheet materials. As they are both frequency measurements, one can expect that the sensitivity of this technique will be acceptable for non-destructive testing of sheet materials.

The observation that changes in structural properties cause changes in vibration frequencies is the impetus for using modal methods for health monitoring and material characterization. However, the method presented in this paper is certainly liable to some improvements. Thus, the combination of constitutive models and optimization algorithms [5] in a future investigation may lead to improvement of the suitability of the presented method for nondestructive characterization of vibrating sheets.

REFERENCES

- [1]: Landau L. D., and Lifshitz E. M., (1979). *Theory of Elasticity*, 3rd edition, Pergamon.
- [2]: Mfoumou, E., Hedberg, C., and Kao-Walter, S., (2006). *Static Versus Low Frequency Dynamic Elastic Modulus Measurement of Thin Films*, Electronic Journal "Technical Acoustics", www.ejta.org, 2006:17.
- [3]: Mfoumou E.; Hedberg C.; Koa-Walter S.; (2007). *Vibration-Based Damage Detection and Evaluation of Sheet Material using a Remote Acoustic Excitation*, in print for journal publication, *Acoustical Physics*, #5 - 2007.
- [4]: Mfoumou E.; Koa-Walter S. and Hedberg C.; *Remote Acoustic Monitoring of Thin Laminates*, 4th International Conference on Condition Monitoring, Harrogate, UK, 2007. ISBN: 978-1-901892-22-2.
- [5]: Genovese K., Lamberti L., Pappalettere C.; (2005). *Mechanical Characterization of Hyperelastic Materials with Fringe Projection and Optimization Techniques*, *Optics and Lasers in Engineering* 44, 423-442.

FREQUENCY ANALYSIS OF THE ACOUSTIC PRESSURE OF NONLINEAR STANDING WAVES

Majid Nabvai, M.H. Kamran Siddiqui, and Javad Dargahi
 Department of Mechanical and Industrial Engineering, Concordia University
 1455 de Maisonneuve Blvd. West, Montreal, Quebec, Canada H3G 1M8

1. INTRODUCTION

Analytical, numerical and experimental analysis of linear and nonlinear standing acoustic waves in time and space domains have been extensively investigated in the recent years¹⁻³. When the amplitude of acoustic standing wave is infinitesimal, the acoustic wave can be described by linear laws. However, when the acoustic wave is driven into large amplitude oscillations, the equations of motion are nonlinear and the nonlinear effects could distort originally harmonic waves, shift the resonance frequency, and transform acoustic energy into higher harmonic components⁴. In this paper, we have examined the acoustic pressure inside a nonlinear standing wave resonator in the frequency domain, and the effect of nonlinearity on the frequency spectrum of the pressure signal through numerical and experimental investigations.

2. METHOD

The description of nonlinear acoustic waves in a viscous, heat-conducting fluid in 1-D is obtained using the following equation⁵,

$$\rho_0 u_{tt} = \gamma p_0 \frac{1}{(1 + u_x)^{\gamma+1}} u_{xx} + b u_{txx}, \quad (1)$$

$$b = \kappa \left(\frac{1}{c_V} - \frac{1}{c_P} \right) + \frac{4}{3} \mu + \mu_B$$

where u is the particle displacement, ρ_0 and p_0 are the static density and pressure, respectively, μ and μ_B are the shear and bulk viscosities, κ is the coefficient of thermal conduction and $\gamma = c_P/c_V$ is the ratio of specific heats at constant pressure and constant volume. This nonlinear differential equation is solved numerically using an effective finite difference method (FDM) without truncation. The following initial and boundary conditions are applicable,

$$\begin{aligned} u(0, t) &= u_0 \sin(\omega t) \quad , \quad u(L, t) = 0, \\ u(x, 0) &= 0 \quad , \quad u_t(x, 0) = 0. \end{aligned} \quad (2)$$

The acoustic pressure p' , can be evaluated from u using

$$p' = \frac{p_0}{(1+u_x)^\gamma} - p_0.$$

In the experimental part of this study, we have developed a setup to measure high-amplitude pressure inside the standing wave tube. The setup consists of a rigid-walled tube of adjustable length, a driving system to excite the standing wave inside the tube, and data acquisition system (see Fig. 1). The acoustic pressure is measured using a quarter-inch condenser microphone cartridge Model 377A10 PCB Piezotronics. The pressure signal from the microphone was acquired via a 16-channel data acquisition card (PCI-6036E, National Instruments) using the LabView data acquisition software. The measurements were made at five different locations along the channel center axis, at different excitation voltages. The numerical model requires maximum diaphragm displacement (u_0) for the boundary condition (see Eq. 2). A Bruel & Kjaer laser vibrometer is used to measure this parameter for different loudspeaker driver intensities.

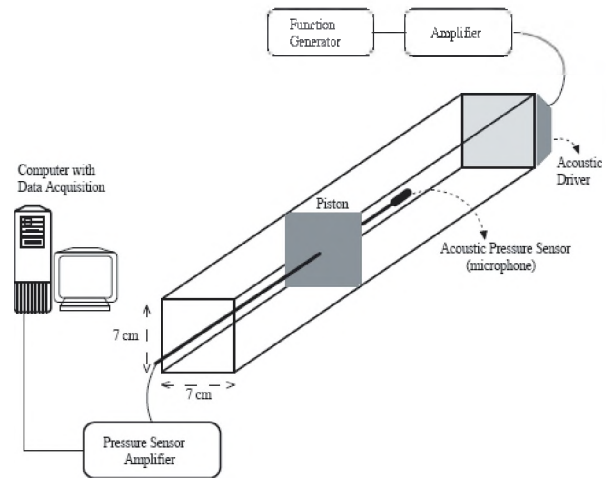


Figure 1: Schematic of the experimental setup and instrumentation.

3. NUMERICAL RESULTS

The frequency spectrum for the numerical and experimental pressure at different axial distances for $u_0=175 \mu\text{m}$ and resonance frequency of $f=1024 \text{ Hz}$ are shown in Fig. 2. It can be seen that there is a good agreement between the numerical and experimental data in frequency domain. The existence of the higher harmonics in the frequency spectrum

shows that in nonlinear acoustic resonators, acoustic energy is transformed into higher harmonic components. The plot shows that the fundamental mode is dominant at all spatial locations except at $x = 8.5$ cm, i.e. the middle of the channel (the location of the theoretical pressure node), where the second harmonic is dominant. The reason for this trend is that the pressure node is not fixed in time and space. That is, during a wave period, the pressure node oscillates about the theoretical pressure node. The frequency of oscillation is twice the resonance frequency. It is because of this oscillation the large amplitude second harmonic mode of pressure manifested at the location of theoretical pressure node in Fig. 2. The plot also shows that except at $x = 8.5$ cm, the magnitude of second harmonic from experimental results is higher than the numerical results. Vanhille and Campos-Pozuelo¹ studied the pressure amplitude at different harmonics at the center of the reflector. They also observed that the experimentally obtained pressure amplitude at second harmonic is overall higher than the numerical one. Using the verified model presented here, we can analyze the frequency spectrum of the pressure and particle velocity signals at different frequencies and excitation amplitudes from linear to finite-amplitude nonlinear cases.

REFERENCES

- [1] Vanhille C., Campos-Pozuelo C. (2005). Numerical and experimental analysis of strongly nonlinear standing acoustic waves in axisymmetric cavities. *Ultrasonics*, 43, 652-660.
- [2] Bednarik M., Cervenka M. (2006). Nonlinear standing wave in 2D acoustic resonators. *Ultrasonics*, 44, 773-776.
- [3] Nabavi M. Siddiqui K. Dargahi J. (2007). Numerical and experimental analysis of finite-amplitude nonlinear standing waves in time and space. *Int. Cong. on Ultrasonics (ICU 2007)*, Vienna, Austria.
- [4] Ilinskii Y.A., Lipkens B., Zabolotskaya E.A. (2001). Energy losses in an acoustical resonator. *J. Acoustical Society of America*, 109, 1859-1870.
- [5] Vanhille C., Campos-Pozuelo C. (2000). A High-order finite difference algorithm for the analysis of standing acoustic waves with finite but moderate amplitude. *J. Computational Physics*, 165, 334-353.

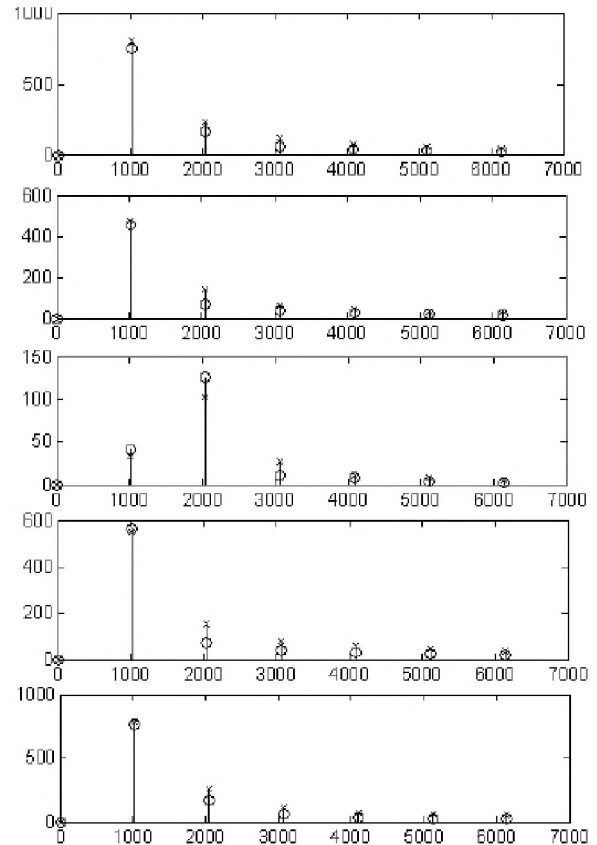


Figure 2: Frequency spectrum of the acoustic pressure for $u_0 = 175 \mu\text{m}$ at (a) $x = 17\text{cm}$, (b) $x = 13\text{ cm}$, (c) $x = 8.5\text{ cm}$, (d) $x = 5\text{ cm}$ and (e) $x = 1\text{ cm}$. \circ , numerical; \times , experimental. Vertical axis, pressure in Pa; Horizontal axis, frequency in Hz. x is measured from the driver end of the resonator.

RAY TRACE MODELING OF MULTIPATH IN ULTRASOUND POWER MEASUREMENT SYSTEM

Lixue Wu

Institute for National Measurement Standards, National Research Council Canada
1200 Montreal Rd., Ottawa, Ontario, Canada K1A 0R6

1. INTRODUCTION

The measurement of ultrasonic power in liquids (commonly water) is based on the measurement of the radiation force using a gravimetric balance. A schematic representation of the INMS ultrasound power measurement system is shown in Fig. 1. A conical target submerged in water is suspended using thin wires from a small hook at the bottom of an electronic balance. The transducer with its active surface submerged in water is positioned coaxially above the target. The radiation force generated by the transducer that impinges on the target is measured by the electronic balance [1].

Additional lateral absorbers that line the wall of the water tank reduce, but do not completely eliminate, reflections at the walls of the tank. In the above arrangement, there are two assumptions: 1) the ultrasonic beam is a plane wave; and 2) the target is large enough that the entire ultrasonic beam is intercepted. The acoustic power radiated from the transducer can be then related to the radiation force measured by the electronic balance [2].

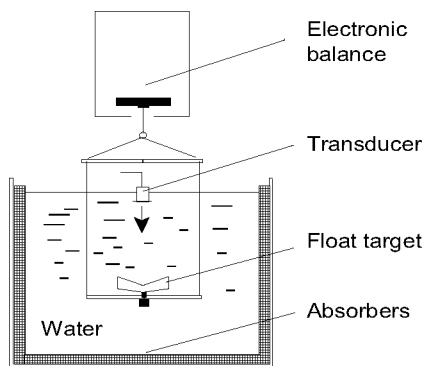


Fig. 1. Schematic diagram of the ultrasound power measurement system.

Multipath, the propagation phenomenon by which ultrasound waves reach the target by two or more paths, exists in such a system. The main causes of multipath are

reflections from the imperfect absorbers at the tank walls and from the water surface. In ultrasound power measurements, multipath can cause constructive and destructive interference and affect the quality of measurements. In this paper a ray tracing ultrasound model is described that calculates the ultrasound pressure at some point in a water tank remote from an ultrasound source. The method parallels the process of geometric optics and assumes constant ultrasound speed in water. The discussion of an experiment results shows the validation of the ray trace modeling method. An algorithm is also presented that finds the optimal measurement settings (water depth and target distance) for an existing ultrasound power measurement system to minimize the effect of multipath.

2. MULTIPATH MODELING

2.1 Assumptions

The temperature variations in water are less than $0.05\text{ }^{\circ}\text{C}$ under laboratory conditions. These variations result in sound speed variations less than 168 ppm. With such a small value one can assume constant sound speed in water. Thus, sound propagation takes place in straight line paths. The wavelength of the ultrasound radiation is much smaller than the target and absorbers so that no scattering occurs in water. With these assumptions, a ray trace model that parallels the process of geometric optics can be used to model the ultrasound propagation [3]. Shown in Fig. 2 is an illustration of the ray traces that occur for different water levels. Raising the water level can prevent the reflected sound wave from reaching the target.

2.2 Ultrasound source images

The formation of multiple images of an ultrasound source due to the reflecting surfaces can further simplify the calculation. The source images due to the reflecting target for two different transducer positions are illustrated in Fig. 3. Only half of the images are shown because of cylindrical symmetry of the measurement system. When the distance of the target from the transducer increases, the ultrasound beam begins to diverge as shown by the dashed lines in Fig. 3. Source images due to secondary reflections from the target are not considered because of the high absorption of the material from which the absorbers are made.

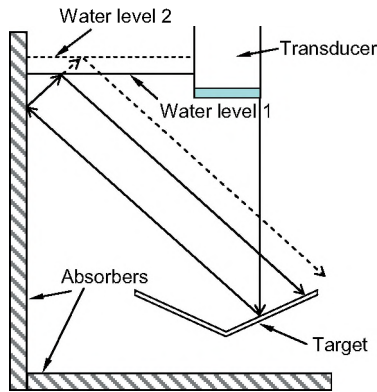


Fig. 2. An illustration of ray traces for different water levels.

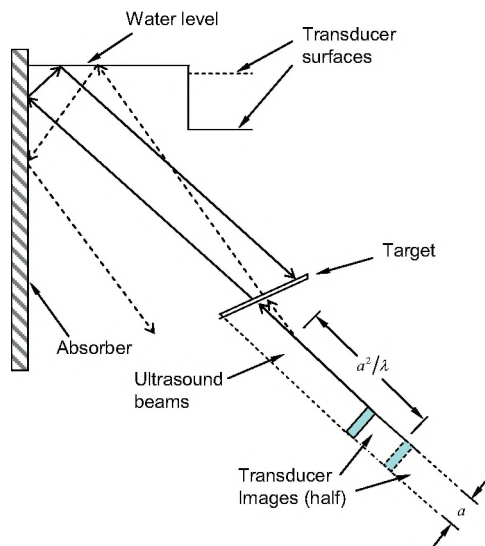


Fig. 3. An illustration of sound source images by the reflecting target for different transducer positions.

2.3 Ultrasound pressure calculation

The returning beam is always parallel to the incident beam as shown in Fig. 3 because of the geometry of reflection surfaces (the water level is perpendicular to absorber). Varying the water level and the transducer position may shift the returning beam apart from the incident beam, preventing it from reaching the target. When the returning beam does impinge on the target the ray trace model can calculate the ultrasound pressure of the returning reflections on the target. The most recent edition of international standard IEC 61161:2006-12 [2] requires that returning reflections do not contribute to more than 1 % of the overall measured power.

3. OPTIMIZATION ALGORITHM

An optimum water level and transducer position that minimize the effect of multipath on the measured ultrasound power can be found. An optimization algorithm has been developed based on the ray trace model. For a given water level and transducer position, the algorithm can calculate the additional radiation force due to the returning beam intercepted by the target. An exhaustive search of all possible water levels and transducer positions can find the optimal setting. The algorithm assumes a perfect disc transducer with uniform velocity movement over its surface. Water attenuation, reflection coefficients of the absorber, and transducer beam shape (depending on whether the target is within near zone or far zone) are incorporated into the algorithm.

4. VERIFICATION

An experiment was setup at 1 MHz for verifying: 1) transducer beam shape; 2) incident beam (reflections from the target) shape; 3) returning beam (reflections from absorber or water surface) shape and 4) ultrasound pressure of returning reflections at the target. A broadband needle hydrophone (Mediscan, No. 82), diameter = 1.25 mm, with a wide angular response was added to the existing ultrasound power measurement system. A tone-burst signal was fed to the transducer so that the direct waves and reflections can be distinguished by their different arrival times at the hydrophone. The hydrophone outputs were recorded by a digital oscilloscope for comparison with those calculated by the ray trace model.

5. DISCUSSION

The experimental data show that the measured beam shapes are within ± 5 mm of those calculated by the ray trace model. Considering the spatial resolution of the hydrophone and the accuracy of its positioning system (no 3D translation table), this is good agreement. The measured sound pressures of returning reflections at the target do not agree well with those calculated by the model. This is due to the constructive and destructive interference of the secondary reflection from the target. If the hydrophone is placed 2 cm above the target, the secondary reflection from the target can then be separated. In this case, the measured ultrasound pressures of returning reflections are within ± 14 % of those calculated by the model.

REFERENCES

- [1] Wong, G.S.K., Wu, L. (2002). High power ultrasound standard. *Journal of the Acoustical Society of America*, vol. 111 (4), 1791-1799.
- [2] International Electrotechnical Commission (2006). IEC 61161 Ed. 2.0 b:2006, Ultrasonics - Power measurement - Radiation force balances and performance requirements. International Electrotechnical Commission, Geneva.
- [3] Coates, R.F.W., (1990). *Underwater acoustic systems*. Macmillan, London.

MONTE CARLO SIMULATION FOR CALCULATION OF UNCERTAINTY IN RECIPROCITY CALIBRATION OF MICROPHONES

Peter Hanes

Institute for National Measurement Standards, National Research Council Canada,
1200 Montreal Rd., Ottawa, Ontario, Canada, K1A 0R6 • peter.hanes@nrc-cnrc.gc.ca

1. INTRODUCTION

1.1 Reciprocity technique

Reciprocity calibration of the sensitivity level of a Laboratory Standard microphone is the means by which national measurement institutes provide traceability to the SI for acoustical measurements. The pressure reciprocity technique¹ requires the measurement of the electrical transfer impedance of coupled pairs from a set of three microphones and the calculation of the acoustic transfer impedance of the microphone pairs. The acoustic transfer impedance depends on the dimensions of the microphones and coupler, the acoustical properties of the microphones, the properties of the air in the coupler and the prevailing environmental conditions. Even with the well-defined geometry of LS1P and LS2P (Laboratory Standard) microphones², the model used for the calculation of acoustic transfer impedance is complicated.

1.2 Determination of measurement uncertainty

Calculation of the measurement uncertainty by determination of sensitivity coefficients and standard uncertainties for each input quantity³ for the reciprocity technique is a time-consuming task. About 50 quantities that contribute to the uncertainty have been identified, many of which appear several times in the model. The sensitivity coefficients and standard uncertainties vary with frequency.

Monte Carlo simulation is a numerical technique that can be used to propagate the distributions of the input quantities using the calculation model in order to estimate the distribution of the outputs⁴. It can provide a standard uncertainty and a coverage interval for a desired level of confidence (typically 95 %) for the pressure sensitivity levels, without intermediate determination of sensitivity coefficients.

2. IMPLEMENTATION

Calculation software has been developed at NRC-INMS to compute the pressure sensitivity levels from the input data using the model of acoustic transfer impedance specified in IEC 61094-2:1992¹. Corrections for the effect of radial wave motion in a plane-wave coupler⁵ were also programmed. The software was validated by comparing its

output against that of commercially-available software⁶ and (at two frequencies only) a Microsoft Excel spreadsheet.

The NRC-INMS software was further developed to allow the calculation of the associated measurement uncertainty by Monte Carlo simulation.

The number of Monte Carlo trials to be performed in the simulation is determined by the requirements for the resolution of the uncertainties (here, two significant figures). In this exercise, standard uncertainties were determined from the results of 10^5 trials.

The effect on the pressure sensitivity level of the distributions of individual input quantities to the model can be found by fixing all other input quantities at their best estimates. The effects of all input quantities were estimated for both LS1P and LS2P microphones at selected frequencies.

3. RESULTS

Typical pressure sensitivity levels for one LS1P microphone from reciprocity measurements are shown in Fig. 1.

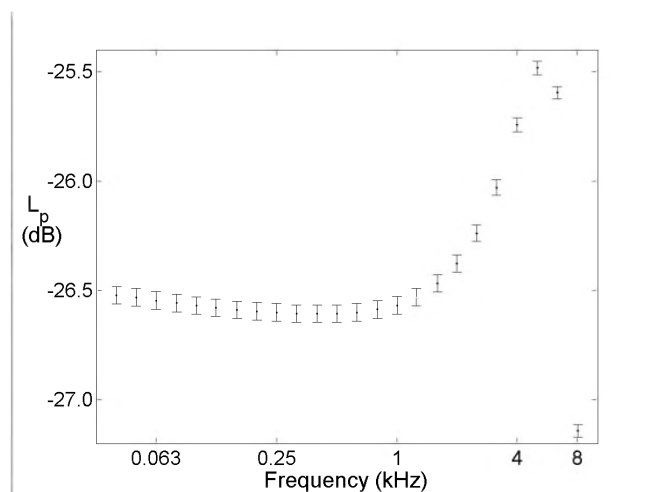


Fig. 1. Pressure sensitivity level of a typical LS1P microphone. Vertical bars indicate measurement uncertainty as the extent of the coverage interval for 95 % level of confidence.

A typical approximation to the probability density function for sensitivity level at one frequency is shown in Fig. 2.

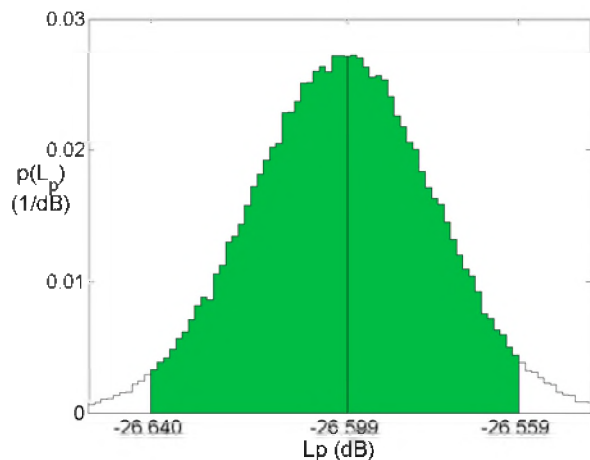


Fig. 2. Approximation to the probability distribution for the pressure sensitivity level of an LS1P microphone at 0.25 kHz, calculated by Monte Carlo simulation (10^5 events). The abscissa labels indicate the expected value and the extent of the coverage interval for 95 % level of confidence (shaded area).

The standard uncertainties were computed for frequencies at one-third-octave intervals from 40 Hz to 8 kHz (LS1P) or 20 kHz (LS2P); values for selected frequencies are listed in Table 1.

Table 1. Standard uncertainty in pressure sensitivity level computed by Monte Carlo simulation at selected frequencies for LS1P and LS2P microphones.

Frequency (kHz)	$u(L_p)$ (dB) for LS1P	$u(L_p)$ (dB) for LS2P
0.063	0.020	0.013
0.25	0.021	0.013
1	0.020	0.013
4	0.017	0.012
8	0.014	0.011
16	...	0.017
20	...	0.029

4. DISCUSSION

The standard uncertainties in Table 1 are in the expected ranges for the method and equipment used. The greatest contribution to the standard uncertainty at low frequencies is the uncertainty of the equivalent volume of the diaphragm when determining the acoustic impedance of the microphone. This contribution reduces as frequency increases. This pattern of frequency dependence confirms

the results of a previous uncertainty determination based on use of partial derivatives of the model⁷.

As the frequency approaches the resonance frequency of the diaphragm (about 8 kHz for LS1P or 23 kHz for LS2P) the greatest contributions arise from the unpredictability of radial wave motion and of viscous losses in the coupler.

Other significant uncertainty contributions are due to uncertainty in the sensitivity to static pressure of LS1P microphones, uncertainty in the reference value for speed of sound in dry air, and uncertainty in measurement of voltage ratio for electrical transfer impedance. The contributions from input quantities such as lengths and diameters of coupler and microphones are tightly controlled through precise dimensional measurements.

Evaluation of individual components enables future research and development work to focus on potential areas for improvement in uncertainty. Definition of the distributions of the input quantities and the implementation of the Monte Carlo simulation are subject to continuous improvement.

5. CONCLUSIONS

Probability distributions for pressure reciprocity levels of Laboratory Standard microphones can be determined using Monte Carlo simulation. The technique shows potential for use in determining measurement uncertainties for ‘primary’ acoustical standards.

REFERENCES

- ¹IEC 61094-2 Ed. 1, Electroacoustics – measurement microphones – Part 2: Primary method for pressure calibration of laboratory standard microphones by the reciprocity technique (1992)
- ²IEC 61094-1 Ed. 2, Electroacoustics – measurement microphones – Part 1: Specifications for laboratory standard microphones (2000)
- ³BIPM, IEC, IFCC, IUPAC, IUPAP and OIML, Guide to the expression of uncertainty in measurement (1995)
- ⁴BIPM JCGM, Evaluation of measurement data – Supplement 1 to the “Guide to the expression of uncertainty in measurement” – Propagation of distributions using a Monte Carlo method (Draft, September 2006)
- ⁵K. Rasmussen, “Radial wave-motion in cylindrical plane-wave couplers” *Acta Acustica*, **1**, 145-151 (1993)
- ⁶E. Sandermann Olsen & K. Rasmussen, “MP.EXE microphone pressure sensitivity calibration calculation program version 3.00” Technical University of Denmark, Department of Acoustical Technology, Internal report PL-14 (1999)
- ⁷P. Hanes, L. Wu, W-S. Ohm and G.S.K. Wong, “Calculation of uncertainty in calibration of microphones by the pressure reciprocity technique” *J. Acoust. Soc. Am.*, **113**, 2219 (2003)

ACKNOWLEDGEMENTS

Won-Suk Ohm programmed the first version of the code for the calculation of the radial wave motion correction.

A THEORETICAL STUDY ON USING PVDF IN THE ACOUSTIC MICROPUMP FOR BIOMEDICAL APPLICATIONS

Majid Nabvai, M.H. Kamran Siddiqui, and Javad Dargahi

Department of Mechanical and Industrial Engineering, Concordia University
1455 de Maisonneuve Blvd. West, Montreal, Quebec, Canada H3G 1M8

1. INTRODUCTION

In the recent years micropumps have been extensively developed to manipulate fluids in a small scale. With the increasing demand of the medical fields, micropumps have been applied to biomedical applications^{1,2}. Various micropumps with different actuation principles, such as piezoelectrics, shape memory alloys, electrostatics, thermal actuation and magnetics, have been investigated in the last decade³. For biomedical applications, micropumps are predestinated due to their small size, small power consumption, no moving parts, no frictional losses, no lubrication required, perfect isolation of the fluid from the outside environment, no chance of fluid contamination and consequently, better biocompatibility.

Acoustic standing wave micropump which achieves a pumping action using the properties of standing waves is a new type of micropump. A standing wave micropump consists of a chamber and an acoustic driver (see Fig. 1). The chamber has a fluid inlet and outlet through which the pumped fluid enters and exits. The excitation driver provides excitation energy to establish a standing wave in the chamber. The excitation source is matched with the pumped fluid and with the length of the excitation chamber so that a traveling wave generated by the excitation source is reflected upon itself within the chamber to create the standing wave. The frequency of oscillation of the excitation source and the length of the pump chamber are configured together so that this arrangement forms a resonant cavity where acoustic standing waves are established in the fluid. The length of the pump chamber should be equal to an integer times half the wavelength of the acoustic wave and the pump housing acts as a resonant cavity having a standing wave pattern set up inside. The standing wave results in one or more pressure nodes and pressure anti-nodes within the chamber. The number of nodes and anti-nodes depends upon the length of the chamber and the frequency of oscillation of the excitation source. Generally, the pressure at a pressure node is relatively constant at approximately the same level as the undisturbed pressure of the fluid while the pressure at a pressure anti-node fluctuates above and below the undisturbed pressure level. The inlet and outlet may be placed proximate to the pressure nodes and anti-nodes of the chamber, respectively. Due to significantly large pressure inside the cavity at the pressure

anti-node, the fluid is discharged through the outlet. As the fluid discharges, there is a reduction in the fluid mass inside the tube which will cause a reduction in the static pressure.

The pressure will now be lower than the pressure of the inlet fluid. As a result the fluid will be sucked into the tube. A check valve must be placed at the outlet to prevent the pumped fluid from re-entering the chamber during low pressure portions of the cycle at the pressure anti-node. However, a valveless version of this micropump is also capable of pumping fluid.

Among different actuation methods, PZT actuation is promising due to its simple structure, high output power density and high actuation strength. However, lack of biocompatibility is the main drawback of PZT for biomedical applications. Whereas PVDF (Polyvinylidene fluoride) is a medical grade material and compatible with the biofluids. The aim in this paper is to theoretically show that PVDF in bimorph configuration is an appropriate material as an actuator in the acoustic micropump.

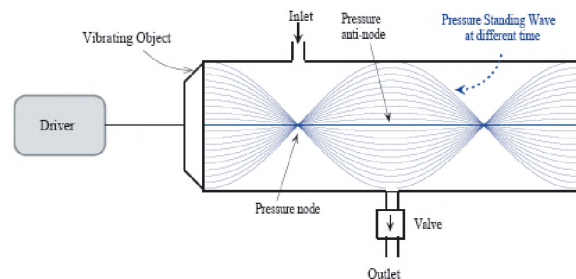


Figure 1: The schematic of the standing wave micropump.

2. BIMORPH PVDF ACTUATOR

The pumping action of the acoustic micropump is related to the maximum pressure fluctuation inside the pump chamber.

The larger pressure fluctuation, the higher flow rate of the micropump. To achieve higher pressure fluctuation we need larger value of maximum vibrational displacement (u_0). Typically the value of u_0 between 10 to 100 μm is required. In the following we have shown that this value of u_0 can be achieved using an appropriate configuration of PVDF film as an actuator.

The values of length change (δl) and width change (δt) of a PVDF film can be obtained using $\delta l = d_{31}lV/t$, $\delta t = d_{33}V$, where V is excitation voltage, l and t are length and thickness of the PVDF film, respectively, and d_{31} and d_{33} are piezoelectric strain coefficients for the drawn and thickness directions, respectively. Typical value for these parameters is about 2×10^{-11} m/V. The maximum thickness of commercially available PVDF films is limited to 110 μm . Obviously, even for large value of excitation voltage the change in thickness of a single layer of PVDF film is not sufficiently large to produce enough vibrational displacement to excite high-amplitude standing wave inside the micropump chamber. Therefore, a two-layer bimorph PVDF actuator is considered for actuation of the micropump, as shown in Fig. 2. The layer A and B are glued together using a low viscosity epoxy and a parallel electrical connection is made in order to form a bimorph actuator configuration to increase the vibrational displacement. In the bimorph configuration, an applied voltage causes one PVDF film to expand, whereas the other unit contracts causing the entire multi-layer PVDF film to deflect in one direction or the other. The bimorph configuration converts small length changes into sizable transverse deflection.

As a feasibility study, mathematical calculations of the maximum vibrational displacement have been performed with the bimorph PVDF actuator for $V=1000$ V, $l=2$ cm and $t=110$ μm . The resultant values of δl and δt are 3.64 and 0.02 μm , respectively. Referring to Fig. 3, in bimorph configuration the values of α , R and x can be calculated, $\alpha = \delta l/t = 0.033$ rad, $R = (l - \delta l)/\alpha = 604.89$ mm, $x = R \cos(\alpha/2) = 604.807$ mm. The maximum vibrational displacement of the bimorph PVDF actuator is obtained using $u_0 = R - x = 82.6$ μm . It is observed that sufficiently large vibrational displacement can be obtained using the bimorph PVDF configuration.

REFERENCES

- [1] Jang L., Kan W. (2007) Peristaltic piezoelectric micropump system for biomedical applications. *Biomedical Microdevices*, 9, 619-626.
- [2] Hsu Y., Lin S., Hou S. (2007) Development of peristaltic antithrombogenic micropumps for in vitro and ex vivo blood transportation tests. *Microsystem Technology*, 14, 31-41.
- [3] Zhang C., Xing D., Li Y. (2007) Micropumps, microvalves, and micromixers within PCR microfluidic chips: Advances and trends. *Biotechnology Advances*, 25, 483-514.

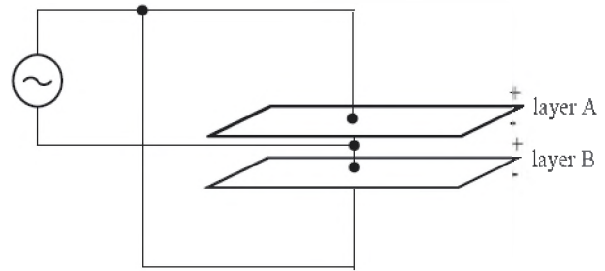


Figure 2: Configuration of a bimorph PVDF actuator.

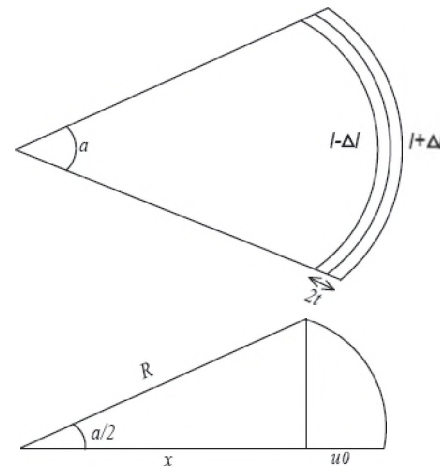


Figure 3: Deflection of the bimorph PVDF actuator in the thickness direction.

IMPEDANCE TUBE CHARACTERIZATION OF ELASTIC PROPERTIES OF EXPANDING FOAMS

Fabien CHEVILLOTTE et Raymond PANNETON

GAUS, Department of mechanical engineering, Université de Sherbrooke, Québec, Canada, J1K 2R1

Fabien.Chevillotte@USherbrooke.ca, Raymond.Panneton@USherbrooke.ca

1. INTRODUCTION

Many authors worked on the propagation of acoustical and elastic waves in elastic open-cell porous materials. The energy carried by the waves is dissipated through structural damping loss, viscous loss (due to relative motion between the two phases), and thermal loss [1]. In the case of elastic closed-cell foams, there is no relative motion between the fluid and the solid phases. Consequently, the only energy dissipation mechanisms are the structural damping and thermal losses [2]. From the Biot's theory [3], only the elastic compression and shear waves now propagate in the closed-cell foams. In this case, few specific models were proposed to study the acoustic dissipation within this type of foams. The most common way of modelling these foams is to use a solid model with equivalent elastic properties. Even if the core of these foams is made of closed cells (i.e., no propagation of acoustical waves in the core), their surface may show open cells and irregularities (e.g., exploded cells). In this case, the surface may be seen as a thin resistive layer showing some surface sound absorption.

To account for the surface sound absorption of closed-cell foams, a model was worked out by one of the authors [4]. In this work, it was shown that closed-cell foams show resonant sound absorption (i.e., sound absorption at elastic resonances) with residual surface absorption (apart from resonances). To model this type of acoustic behaviour, the closed-cell foams are modelled as a two-layer material: a resistive layer covering a core made of an equivalent solid with bulk elastic properties. The bulk elastic properties account for the structural damping and thermal losses. The resistive surface layer is characterized by its static airflow resistivity. While the resistivity can be easily identified, the key element in the proper use of this so-called "surface absorption solid model" is the fine characterization of the bulk elastic properties.

The main objective of this work is to develop a method, based on sound absorption measurements, for the characterization of the bulk elastic properties of closed-cell foams –more especially those from heat expanding foam process [4]. This paper is organized as follows. In section 2, the theory behind the method is first reminded for the sliding edge condition for which the bulk's modulus and damping loss factor can be deduced. These results were worked out in previous works [5]. Then, the method is extended to the bonded edge condition which additionally allows the identification of the Poisson's ratio. In section 3,

the method is experimentally tested for characterizing the bulk elastic properties of foam with the bonded edge condition. Then, sound absorption predictions using the identified bulk elastic properties are compared to impedance tube results. Finally, section 4 concludes this work.

2. THEORY

2.1 Sliding edge condition

The sliding edge condition is an ideal case for the characterization of the bulk elastic properties. The method was previously developed by considering this boundary condition [5]. Two main results are recalled in this section.

- a) The 1st natural frequency is linked to the bulk modulus by:

$$f_1 = \frac{\omega_1}{2\pi} = \frac{1}{4L} \sqrt{\frac{K_b}{\rho_1}} \quad (1)$$

- b) The sound absorption coefficient at the resonance is linked to the bulk damping loss factor. Assuming that the damping loss factor is low enough ($\eta < 1$), the surface impedance can be approximated by Eq.(2). The optimal and reduced damping loss factors are then introduced by Eqs.(3) and (4), and the absorption coefficient at the resonance is linked to the bulk damping loss factor by Eq. (5).

$$Z_s(\omega_1) \cong \frac{1}{2} \rho_1 \omega_1 L \eta \quad (2)$$

$$\eta_{op} = \frac{2Z_0}{\omega_1 \rho_1 L} \quad (3)$$

$$\eta_r = \frac{\eta}{\eta_{op}} \quad (4)$$

$$\alpha(\omega_1) = 1 - \left| \frac{\eta_r - 1}{\eta_r + 1} \right|^2 \quad (5)$$

2.2 Bonded edge condition

Considering a bonded edge condition and a hard backing, the first compression resonance depends on the

shape factor s and Poisson's ratio ν . This frequency is expressed in function of the first natural frequency of the sliding case:

$$f_1^b = c_b(\nu, s) \cdot f_1. \quad (6)$$

The factor c_b is called the bonded edge correction factor. This coefficient only depends on the shape factor and Poisson's ratio. When the Poisson's ratio is assumed to be known, the bulk modulus and Young's modulus can be deduced from the first natural frequency by using Eq. (6).

With this bonded edge condition, the sound absorption coefficient at the resonance still reaches a maximum for an optimal damping loss factor. The sound absorption coefficient can still be expressed by Eq. (5) but the optimal damping loss factor is no more defined by Eq. (3). This optimal factor is linked to that of the sliding case by:

$$\eta_{lop}^b = \frac{\pi \cdot s}{c_b} \cdot m(c_b) \cdot \eta_{op} + b(c_b). \quad (7)$$

Thus, knowing the shape factor and Poisson's ratio, the bonded correction factor can be calculated and the method can be extended to the bonded edge condition. The bulk modulus and Young's modulus are deduced from the first natural frequency and the bulk damping loss factor is deduced from the sound absorption coefficient at the resonance peak.

3. EXPERIMENTAL RESULTS

The method is now experimentally tested on a sample with a bonded edge condition. Three samples of a different length are required for computing the Poisson's ratio [6]. Here, each foam samples were carefully and directly heat expanded in a hollow cylinder having a 29-mm inner diameter.

The sound absorption coefficient is now computed with the equivalent solid model and compared to impedance tube measurements in Fig. 1. The correlation with measurements is good, especially at the resonance peak. The surface absorption model [4] is used in order to correct the underestimation of the predicted absorption. The residual variation between these latter predictions and measurements may be attributed to the fact that the real elastic parameters of the expanded foam are not necessarily constant with the frequency.

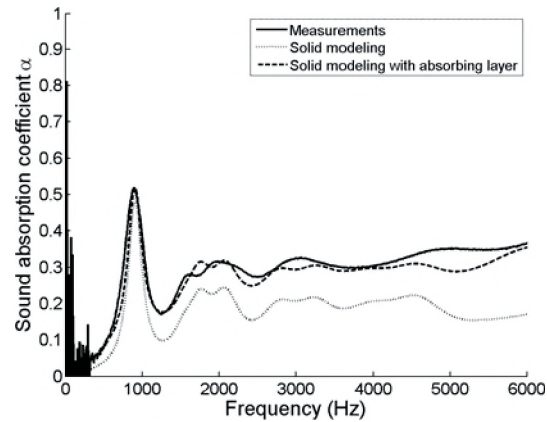


Figure 1: Normal sound absorption coefficient of the heat expanded foam.

4. CONCLUSION

In this work, a method was proposed to determine the bulk elastic properties of soft equivalent solids or closed-cell foams from simple impedance tube absorption tests. The method was tested experimentally with success in laboratory. It has revealed that the properties found with the proposed method can be used in the surface absorption solid model worked out in reference [4] to yield good correlations with measurements.

However, the accuracy of the method relies mostly on the proper control of the mounting conditions in the impedance tube. This is actually the most important limitation of the method, especially on small sample diameters for which the absorption measurement is very sensitive to boundary conditions. Further tests are required to validate the robustness of the proposed method.

REFERENCES

- Allard, J.F. (1993). Propagation of sound in porous media. Modeling sound absorbing materials (Elsevier applied science).
- Ingard, U. (1994). Notes on sound absorption technologies (Noise Control Fundation, NY).
- Biot, M. (1956). "The theory of propagation waves in a fluid-saturated porous solid. I. Low frequency range. II. Higher frequency range," J. Acoust. Soc. Am. 28, 168-191.
- Wojtowicki, J.-L., Panneton, R (2005). "Improving the efficiency of sealing parts for hollow body network," SAE Tech. Paper, Doc# 2005-01-2279.
- Chevillotte, F., Panneton, R., Wojtowicki, J.-L., Chaut, C. (2007). "Characterization of the bulk elastic properties of expanding foams from impedance tube absorption tests," SAE Tech. Paper, Doc# 2007-07-2191.
- Chevillotte, F., Panneton, R. (2007). "Elastic characterization of closed cell foams from impedance tube absorption tests," submitted to J. Acoust. Soc. Am. (05/2007).

ACKNOWLEDGEMENTS

This work was supported by Henkel technologies, NSERC Canada, FQRNT Quebec, and NCE Auto21.

EFFECT OF MEAN FLOW ON THE ACOUSTIC TRAPPED MODES OF A CAVITY-DUCT SYSTEM

K. Awny, and S. Ziada

Department of Mechanical Engineering, McMaster University,
Hamilton, Ontario, Canada

1. INTRODUCTION

Flow-induced acoustic resonance in cavities, which is known to occur in numerous engineering applications, can cause hazardous noise levels, and in some cases catastrophic failure due to acoustic fatigue of the cavity structure [1]. Having the cavity attached to a confined domain reduces the acoustic radiation, resulting in “trapped acoustic modes” which are highly susceptible to self-sustaining acoustic resonance, even at moderate subsonic Mach number flow. In such configuration, the interaction between the acoustic field and the flow vorticity is the main source of acoustic power production.

In many previous studies, the acoustic field used in estimating the acoustic power was calculated at zero flow velocity, which ignores the effect of the mean flow on the resonant acoustic field. In this paper, the effect of mean flow on the embedded trapped acoustic mode of a two-dimensional cavity mounted at the middle of a rectangular duct is investigated numerically as a step toward improving the prediction of acoustic power.

The cavity-duct geometry is shown schematically in Fig. 1. Both cavity length (l) and depth (d) are taken to be $1/6 H$, where H is the height of the duct. The duct length is slightly longer than 6 times the height to minimize the effect of the duct length and the ends boundary conditions on the shape of the acoustic mode. For all simulations, the direction of air flow is from the left to the right.

2. PROBLEM FORMULATION

2.1 Governing equations

The numerical method is based on solving the Acoustic Perturbation Equations (APE) developed by Ewert & Schroder [2]. The Acoustic Perturbation Equations account for the convection and refraction of the acoustic perturbation wave by the mean flow. However, it doesn't support the vorticity wave. This prevents the excitation of the hydrodynamic instability in the cavity free shear layer. As the coupling between the mean flow and the acoustic perturbation is outside the scope of this paper, aerodynamic sources are not considered in the solution. The APE system

for multidimensional domain without source terms can be written as follow:

$$\frac{\partial p'}{\partial t} + \bar{c}^2 \nabla \cdot \left(\bar{\rho} \mathbf{u}^a + \bar{\mathbf{u}} \frac{p'}{\bar{c}^2} \right) = 0 \quad (1)$$

$$\frac{\partial \mathbf{u}^a}{\partial t} + \nabla (\bar{\mathbf{u}} \cdot \mathbf{u}^a) + \nabla \left(\frac{p'}{\bar{\rho}} \right) = 0 \quad (2)$$

Where p' is the acoustic pressure perturbation, \mathbf{u}^a is the acoustic particle velocity vector, $\bar{\mathbf{u}}$ is the mean velocity, $\bar{\rho}$ is the mean density and \bar{c} is the mean acoustic speed, which is set to 340 m/s. The mean flow quantities used in the solution are calculated using the Reynolds Averaged Navier-Stokes equations Solver.

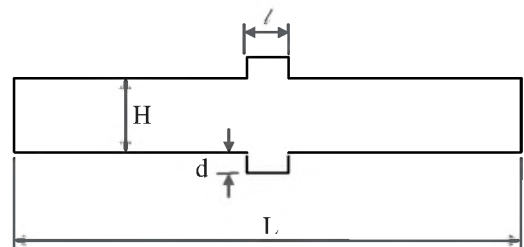


Fig. 1. Cavity-Duct Geometry

2.2 Numerical algorithm

To solve the 2-D governing equations, a CAA code is developed. The spatial derivatives are calculated using the optimized prefactored compact scheme [3]. The time derivatives are calculated using 5/6 stage low dissipation and dispersion Runge-Kutta scheme in the 2N-Storage form [4]. A 6th order filter is also applied at each stage of the Runge-Kutta scheme to eliminate spurious short-wavelength disturbances that the numerical grid can't resolve. Regarding the boundary conditions, at the walls, the normal velocity is set to zero. At the duct ends, the acoustic pressure is set to zero which simulates a complete reflection of the acoustic wave. This condition is chosen because the main duct is sufficiently long to consider the actual radiation of the trapped modes to be negligible.

3. RESULTS AND DISCUSSION

In this part, the first trapped mode in the transverse direction to the flow, which is equivalent to the empty duct first transverse mode, is studied. The resonance mode is simulated at zero flow and at Mach numbers of 0.1, 0.2 and 0.3 based on the average velocity at the inlet of the duct. For each case, the resonance frequency is determined from the domain response to a narrow band external perturbation. The external perturbation is introduced to the domain as a velocity fluctuation at the cavity top and bottom floors in the normal direction to the wall. The top and bottom floors oscillate out of phase to excite the first transverse mode. Figure 2 shows the change of the resonance frequency with the Mach number. The first transverse mode resonance frequency experiences consistent drop as the Mach number increases. The rate of frequency decrease appears to be proportional to the square of the Mach number. Similar behavior was observed during a current experimental study focusing on aerodynamic excitation of transverse acoustic modes of axi-symmetric cavity-duct system.

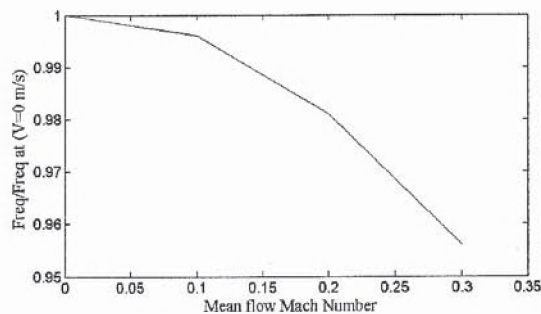


Fig. 2. Resonance frequency change with the Mach number

To obtain the mode shape, the domain is excited at the resonance frequency using sinusoidal normal velocity perturbation introduced also at the cavity floors. The amplitude of the acoustic pressure increases as the simulation progress in time. The simulation stops when the change in the pressure amplitude from one cycle to the next is less than 1%.

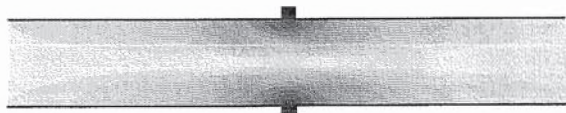


Fig. 3. Mode shape of the first transverse resonance

Figure 3 shows the first transverse mode shape at zero flow velocity in term of the contours of the acoustic pressure amplitude, as the darkness of the contours is an indication of the amplitude. As can be seen, the high pressure area is confined to the cavity. From analyzing the pressure amplitude values along the axial direction, it is observed that the pressure amplitude drops exponentially as we move

away from the cavity. This is in a full agreement with the theoretical trend of trapped wave pressure drop. For the other mean flow Mach numbers, the mode shape remains similar to the zero flow velocity case.

Although the mode shape doesn't change with the velocity, the instantaneous pressure oscillation changes as a longitudinal phase difference starts to appear and increases with the Mach number. Figure 4 shows the longitudinal phase of the pressure oscillation for different Mach numbers. The midpoint of the top cavity floor is considered the reference point in the phase calculation.

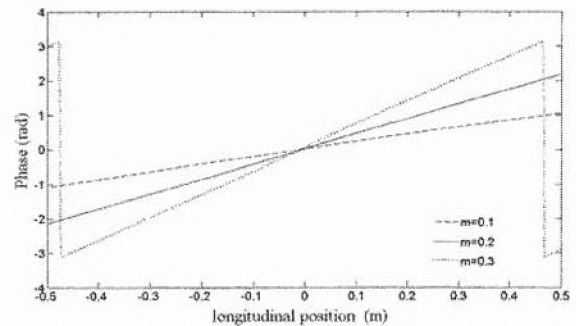


Fig. 4. Longitudinal phase change of acoustic pressure

4. CONCLUSION

This study shows that the developed CAA code is capable of simulating the convection and refraction effect of the mean flow on the acoustic resonance modes. The simulation results show that the acoustic resonance frequency decreases with the square of the mean flow Mach number. Also, it shows that the pressure mode shape doesn't change significantly in the range of the studied Mach number. However, due to the acoustic wave convection by the mean flow, a phase shift starts to develop in the streamwise distribution of acoustic pressure as the Mach number is increased.

5. REFERENCES

- [1] Rockwell, D.; "Oscillations of Impinging Shear Layers"; *AIAA J.*, 21(5):645-664, 1983.
- [2] Ewert, R., Schroder, W., "Acoustic perturbation equations based on flow decomposition via source filtering," *journal of computational physics*, 188: 365-398, 2003.
- [3] Ashcroft, G., Zhang, X., "Optimized prefactored compact schemes," *journal of computational physics*, 190: 459-477, 2003.
- [4] Stanescu, D., Habashi, W. G., "2N-Storage low dissipation and dispersion Runge-Kutta scheme for computational acoustics," *journal of computational physics*, 143: 674-681, 1998.

A NUMERICAL STUDY ON THE EFFECT OF VIBRATOR SHAPE ON THE DEVELOPMENT OF NONLINEAR STANDING WAVES IN A 2-D ACOUSTICAL RESONATOR

Majid Nabvai, M.H. Kamran Siddiqui, and Javad Dargahi

Department of Mechanical and Industrial Engineering, Concordia University
1455 de Maisonneuve Blvd. West, Montreal, Quebec, Canada H3G 1M8

The 2-D nonlinear standing wave equation can be written in the conservative form as,

1. INTRODUCTION

In the recent years linear and nonlinear standing acoustic waves in one-dimensional (1-D) and two-dimensional (2-D) resonators have been extensively investigated numerically, mathematically and experimentally.¹⁻³ To establish acoustic standing wave, we need a chamber and a vibrator. In all of the previous study, the vibrator of the acoustical resonator was assumed to be a constant shape vibrating piston. However, in the real applications different shape of the vibrator may be used to excite the resonator. In the present study the objective is to numerically analyze the effects of different shape of the vibrator on the pressure and velocity profile in 2-D nonlinear standing wave resonator.

2. METHOD

The wave equation for high-amplitude nonlinear acoustic waves in a thermo-viscous fluid is derived from the basic equations of fluid mechanics (continuity and Navier-Stokes equations) along with an appropriate state equation which can be written in 2-D as,

$$\frac{\partial \rho}{\partial t} + \frac{\partial(\rho u)}{\partial x} + \frac{\partial(\rho v)}{\partial y} = 0, \quad (1)$$

$$\rho \frac{Du}{Dt} + \frac{\partial p}{\partial x} = \frac{\partial \tau_{xx}}{\partial x} + \frac{\partial \tau_{yx}}{\partial y}, \quad (2)$$

$$\rho \frac{Dv}{Dt} + \frac{\partial p}{\partial y} = \frac{\partial \tau_{yy}}{\partial y} + \frac{\partial \tau_{xy}}{\partial x}, \quad (3)$$

$$p = c_0^2 \rho - \kappa \left(\frac{1}{c_v} - \frac{1}{c_p} \right) \left(\frac{\partial u}{\partial x} + \frac{\partial v}{\partial y} \right). \quad (4)$$

where, $\frac{D(\cdot)}{Dt} = \frac{\partial(\cdot)}{\partial t} + u \frac{\partial(\cdot)}{\partial x} + v \frac{\partial(\cdot)}{\partial y}$, and

$$\begin{aligned} \tau_{xx} &= \left(\frac{4}{3}\mu + \mu_B \right) \frac{\partial u}{\partial x} + \left(-\frac{2}{3}\mu + \mu_B \right) \frac{\partial v}{\partial y}, \\ \tau_{yy} &= \left(\frac{4}{3}\mu + \mu_B \right) \frac{\partial v}{\partial y} + \left(-\frac{2}{3}\mu + \mu_B \right) \frac{\partial u}{\partial x}, \\ \tau_{xy} &= \tau_{yx} = \mu \left(\frac{\partial u}{\partial y} + \frac{\partial v}{\partial x} \right). \end{aligned} \quad (5)$$

In the above equations u and v are the velocity components, ρ is density, p is pressure, c_0 is small-signal sound speed, μ and μ_B are the shear and bulk viscosities, κ is the coefficient of thermal conduction and $\gamma = c_p/c_v$ is the ratio of specific heats at constant pressure and constant volume.

$$U_t + AU_x + BU_y = CU_{xx} + DU_{yy} + EU_{xy}, \quad (6)$$

where,

$$U = \begin{bmatrix} \rho \\ u \\ v \end{bmatrix}, A = \begin{bmatrix} u & \rho & 0 \\ c_0^2 \rho^{\gamma-2} & u & 0 \\ 0 & 0 & u \end{bmatrix},$$

$$B = \begin{bmatrix} v & 0 & \rho \\ 0 & v & 0 \\ c_0^2 \rho^{\gamma-2} & 0 & v \end{bmatrix}, C = \begin{bmatrix} 0 & 0 & 0 \\ 0 & \nu b/\rho & 0 \\ 0 & 0 & \nu/\rho \end{bmatrix},$$

$$D = \begin{bmatrix} 0 & 0 & 0 \\ 0 & \nu \rho & 0 \\ 0 & 0 & \nu b/\rho \end{bmatrix}, E = \begin{bmatrix} 0 & 0 & 0 \\ 0 & 0 & \nu(b-1)/\rho \\ 0 & \nu(b-1)/\rho & 0 \end{bmatrix},$$

where ν is the kinematic viscosity and b indicates the total effect of viscosity and thermal conductivity of the fluid as well as the wall absorption, and can be obtained as, $b = 2c_0^3 a/\omega^2 \nu$, where, $\omega = 2\pi f$ and a is the total absorption coefficient which is the sum of thermoviscosity absorption coefficient and wall absorption coefficient.⁴ a is expressed as $a = a_{\nu} + a_{wall}$, where,

$$\alpha_{\nu} = \frac{\omega^2 \nu}{2c_0^3} \left(\frac{4}{3} + \frac{\mu_B}{\mu} + \frac{\gamma-1}{P_r} \right) \text{ and } \alpha_{wall} = \sqrt{\frac{\omega \nu}{8c_0^2}} \left(1 + \frac{\gamma-1}{\sqrt{P_r}} \right) \frac{\rho}{\lambda}$$

and $P_r = \mu c_p \kappa$ is the Prandtl number⁴.

Eq. 6 is an unsteady nonlinear equation and must be solved using an appropriate numerical scheme and initial and boundary conditions. Combination of a second-order finite difference scheme and a second-order Runge-Kutta time stepping scheme provides an accurate and fast-solver numerical model which can predict pressure, particle velocity and density along the highly nonlinear standing wave resonator filled with a thermoviscous fluid with no restriction on the nonlinearity level and the type of fluid. The fluid is assumed to be initially at rest and excited by the harmonic motion of a diaphragm at $x=0$ at the frequency f (see Fig. 1). Assuming L and H to be the length and width of the tube, respectively, the following initial and boundary conditions are applicable,

$$\begin{aligned} u(0, y, t) &= G(y, t), \quad u(L, y, t) = v(x, 0, t) = v(x, H, t) = 0, \\ u_y(x, 0, t) &= u_y(x, H, t) = v_x(0, y, t) = v_x(L, y, t) = 0, \\ \rho_x(0, y, t) &= \rho_x(L, y, t) = \rho_y(x, 0, t) = \rho_y(x, H, t) = 0, \\ u(x, y, 0) &= v(x, y, 0) = 0, \quad \rho(x, y, 0) = \rho_0. \end{aligned} \quad (7)$$

where $0 < x < L$, $0 < y < H$ and $G(y, t)$ represents shape and time-dependent excitation function of the diaphragm.

3. NUMERICAL RESULTS

To investigate the effects of the diaphragm shape on the pressure and velocity waveforms of an acoustic resonator, three different shapes are considered for the diaphragm which are, constant shape vibrating piston, circular shape and cosine shape, hereinafter referred to as cases A, B and C, respectively. These three shapes are illustrated in Fig. 1, where, u_0 is maximum velocity of the diaphragm. All simulations are conducted in air at 25°C with the following thermo-physical properties, $c_0 = 343.4$ m/s, $\rho_0 = 1.2$ kg/m³, $\nu = 1.84 \times 10^{-5}$ N.s/m², $\mu_B = 0.6 \times \mu$ and $\gamma = 1.401$. The frequency of the diaphragm is set equal to 1 kHz for all cases.

Fig. 2 depicts the variations of pressure and particle velocity over one standing wave period for u_0 equal to 0.1 and 10 m/s for cases A, B and C. At $u_0 = 0.1$ m/s, standing wave inside the resonator is linear, whereas, at $u_0 = 10$ m/s, the standing waves is nonlinear. As shown in Fig. 2, the shapes of the pressure and particle velocity are the same for the different shapes of the vibrator. However, the maximum amplitudes of pressure and velocity vary with the shape of vibrator. For the same maximum vibrational velocity of the diaphragm, the amplitudes of the pressure and velocity for constant shape vibrating piston are largest and for cosine shape are smallest.

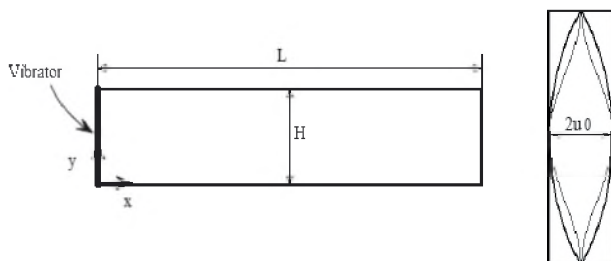


Figure 1: Schematic of the model.

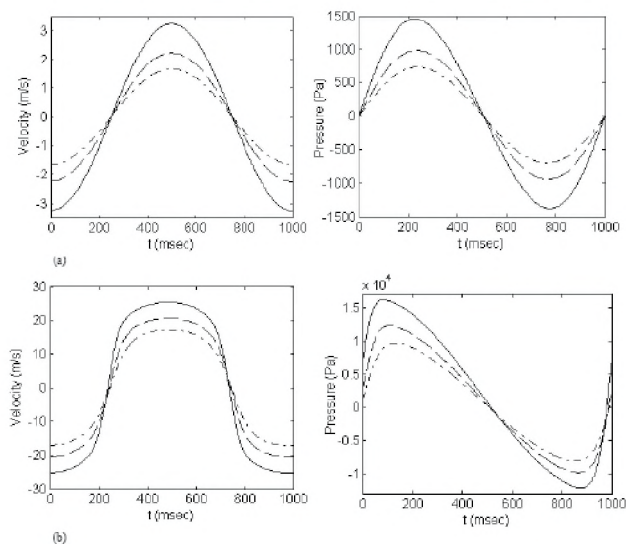


Figure 2: The variation of the pressure and particle velocity over one standing wave period for (a) $u_0 = 0.1$ and (b) 10 m/s. case A, solid line; case B, dash line; case C, dash-dot line.

REFERENCES

- [1] Vanhille C., Campos-Pozuelo C. (2004). Numerical simulation of two-dimensional nonlinear standing waves. *J. Acoustical Society of America*, 116, 194-200.
- [2] Bednarik M., Cervenka M. (2006). Nonlinear standing wave in 2D acoustic resonators. *Ultrasonics*, 44, 773-776.
- [3] Nabavi M., Siddiqui K., Dargahi J. (2007). Numerical and experimental analysis of finite-amplitude nonlinear standing waves in time and space. *Int. Cong. on Ultrasonics (ICU 2007)*, Vienna, Austria.
- [4] Blackstock D.T. (2000). *Fundamentals of physical acoustics*. Wiley-Interscience publication.

IN-PLANE FREE VIBRATION OF CIRCULAR DISKS USING CHARACTERISTIC ORTHOGONAL POLYNOMIALS IN RAYLEIGH-RITZ METHOD

Salem Bashmal¹, Rama Bhat, and Subash Rakheja

¹Dept. of Mechanical and Industrial Engineering, Concordia University, 1455 De Maisonneuve Blvd. W., Montreal, Quebec, Canada, H3G 1M8, s_bashm@encs.concordia.ca

1. INTRODUCTION

The out-of plane flexural vibrations of the circular disks has been analytically investigated under different boundary conditions using several approximate methods, see for example Rao (1999). In comparison, only a few studies have been carried out on the vibrations within the plane of the disk. However, in many engineering applications involving circular disks, such as railway wheels, grinding wheels, disk brakes etc, in-plane vibrations can play a prominent role causing disk noise and vibration.

Predictions of the in-plane natural frequencies have been treated in a few references. Holland (1966) used trigonometric and Bessel functions to study the free in-plane vibration of circular disks with free edges and presented frequency parameters for different values of Poisson's ratio. Ambati et al (1976) investigated the in-plane vibrations in annular disks with free boundaries. Recently, Farag and Pan (2003) analyzed the modal characteristics of in-plane vibrations of solid disk with clamped outer edge. These studies were carried out for a limited set of boundary conditions. Irie et al. (1984) examined the in-plane vibrations in circular and annular disks using transfer matrix formulation. Natural frequencies were obtained for several radius ratios of annular disks with combinations of free and clamped conditions at the inner and outer edges.

The main objective of the present paper is to provide the natural frequencies of circular disks subject to various combinations of boundary conditions, with relative ease and acceptable accuracy. Most of the studies concerning disk vibrations expressed the mode shapes as a series summation of Bessel functions in the radial direction. In the present analysis, boundary characteristic orthogonal polynomials, first introduced by Bhat (1985) are used as the admissible functions. These functions have some advantageous features such as relative ease of generation and integration, diagonal mass matrix and diagonally dominant stiffness matrix.

The approach presented in this paper is straightforward but more general than the approaches presented previously in the literature. Starting from the constitutive laws and stress-strain relations, the integral expressions for strain and kinetic energies of the disk are presented in polar coordinates. The Rayleigh-Ritz method is employed to solve for the eigenvalues. The radial and circumferential displacement components are expressed in terms of

trigonometric functions in the circumferential direction and boundary-characteristic orthogonal polynomials in the radial direction. The frequency parameters are presented for circular disks with different boundary conditions. The accuracy of the eigenvalues is ascertained through comparisons with the existing results from the literature.

2. THEORY

In this section, the in-plane characteristic of a non-rotating circular disk is investigated using the Rayleigh-Ritz method. The material of the disk is assumed to be isotropic with mass density ρ , Young's modulus E and Poisson ratio ν . Let the outer radius of the disk be R , the inner radius be R and the thickness of the disk be h . the radial and circumferential displacement components of a material point on the disk are denoted by u_r, u_θ , respectively.

The expressions for the maximum values of strain and kinetic energies of the disk in polar coordinates are expressed in terms of displacements as:

$$V = \frac{1}{2} \int_0^R \int_0^{2\pi} \frac{E}{1-\nu^2} \left\{ \left(\frac{\partial u_r}{\partial r} \right)^2 + 2\nu \left(\frac{u_r}{r} \frac{\partial u_r}{\partial r} + \frac{1}{r} \frac{\partial u_\theta}{\partial \theta} \frac{\partial u_r}{\partial r} \right) + \left(\frac{u_r}{r} \right)^2 + 2 \frac{u_r}{r^2} \frac{\partial u_\theta}{\partial \theta} + \frac{1}{r^2} \left(\frac{\partial u_\theta}{\partial \theta} \right)^2 + \frac{1}{2} (1-\nu) \left(\frac{1}{r} \frac{\partial u_r}{\partial \theta} + \frac{\partial u_\theta}{\partial r} - \frac{u_\theta}{r} \right)^2 \right\} r dr d\theta \quad (1)$$

$$T = \frac{1}{2} \int_0^R \int_0^{2\pi} (\dot{u}_r^2 + \dot{u}_\theta^2) \rho r dr d\theta \quad (2)$$

The free in-plane vibrational response is assumed to have a sinusoidal variation around the disk. Introducing the non-dimensional parameter $\xi = r/R$, the maximum displacements of the disk may be expressed in the form:

$$u_r(\xi, \theta, t) = \sum_n^{\infty} U_n(\xi) \cos(n\theta) e^{-j\omega t} \quad (3)$$

$$u_\theta(\xi, \theta, t) = \sum_n^{\infty} V_n(\xi) \sin(n\theta) e^{-j\omega t} \quad (4)$$

where n is the circumferential wave number. In this analysis, an orthogonally generated set, based on the work of Bhat (1985), are used to express the radial component of the displacements $U_{n,m} = \sum_m \bar{U}_{n,m} \phi_m(\xi)$ and $V_{n,m} = \sum_m \bar{V}_{n,m} \phi_m(\xi)$. The trial function is chosen to satisfy the boundary conditions at the inner and outer edges of the disk.

As an alternative approach, orthogonal polynomials generated for free conditions can be used as trial functions for the clamped case through the use of artificial springs. Disks are assumed to have elastically restrained boundaries, which require simply adding the energy stored in the springs to the strain energy expressions given in equation (1). The clamped boundary condition is achieved when the springs constants approach infinity. This approach is useful for systems composed of various types of components. For systems in which flexible joints exist between components, the artificial springs are assigned the actual values of stiffness for the joints.

The assumed solutions -equations (3) and (4)- are substituted into the energy equations (1) and (2). Both equations are integrated with respect to θ from $\theta=0$ to $\theta=2\pi$.

Minimizing the natural frequencies with respect to the arbitrary coefficients $\bar{U}_{p,q}$ and $\bar{V}_{p,q}$, results in the following

$$\left\{ \begin{matrix} [K] - \Omega^2 [M] \\ \bar{U}_{p,q} \\ \bar{V}_{p,q} \end{matrix} \right\} = \{0\} \quad (5)$$

where $\Omega^2 = \rho \omega^2 R^2 (1 - \nu^2) / E$

The solution of this eigenvalue problem yields the natural frequencies and mode shapes.

3. RESULTS

The energy expressions derived previously are used to obtain the modal characteristics of the disk. The results of the above computations are tabulated for several boundary conditions. The frequency parameters are compared with other results available in the literature to assess the accuracy of the present study. Table 1 presents the dimensionless frequencies for solid disk with free conditions while Table 2 gives the natural frequencies for clamped disks. The results

obtained by the present method are in full agreement with those of other studies, which indicates the accuracy of this method. The frequency parameters are the largest for the clamped-clamped disks, and become smaller in that order for the free-clamped disks, the clamped-free disks and free-free disks. With the increase of the radius ratio, the parameters monotonically increase except for the free-free disks.

Table 1. Frequency parameters for free conditions (numbers in brackets are from Holland (1966)).

(m,n)	1	2	3
1	(1.6176) 1.6175	(3.5291) 3.5289	(4.0474) 4.0472
2	(1.3877) 1.3928	(2.5112) 2.5146	(4.5208) 4.5561
3	(2.1304) 2.1303	(3.4517) 3.4515	(5.3492) 5.349

Table 2. Frequency parameters for clamped conditions using artificial springs (numbers in brackets are from Farag and Pan (2003)).

(m,n)	1	2	3
1	(1.9441) 1.9442	(3.1126) 3.1131	(4.9104) 4.9098
2	(3.0185) 3.0186	(4.0127) 4.0128	(5.7398) 5.7401
3	(3.9116) 3.9118	(4.9489) 4.9491	(6.5537) 6.5542

REFERENCES

- Rao, J. (1999). Dynamics of Plates, Narosa Publishing House.
- Holland, R. (1966). Numerical studies of elastic-disk contour modes lacking axial symmetry. Journal of Acoustical Society of America, vol 40, no 5, 1051-1057.
- Ambati, G. (1976). In-plane vibrations of annular rings. Journal of Sound and Vibrations, vol 47, no 3, 415-432.
- Farag, N., Pan, J. (2003). Modal characteristics of in-plane vibration of circular plates clamped at the outer edge. Journal of the Acoustical Society of America, vol 113, no 4, 1935-1946
- Irie, T., Yamada and Muramoto Y. (1984). Natural frequencies of in-plane vibration of annular plates" Journal of Sound and Vibrations, vol 97, no 1, 171-175.
- Bhat R. (1985). Natural frequencies of rectangular plates using characteristic orthogonal polynomials in Rayleigh-Ritz Method. Journal of Sound and Vibrations, vol 102, no 4, 493-499.

DESIGN OPTIMIZATION OF THE OF AN AUTOMOTIVE THERMOACOUSTIC AIR CONDITIONING SYSTEM

Hadi Babaei, Kamran Siddiqui

Dept. of Mechanical and Industrial Engineering, Concordia University, 1455 De Maisonneuve Blvd. W., Quebec, Canada, H3G 1M8 h_babaei@alcor.concordia.ca

1. INTRODUCTION

Concerns about global warming, pollution and the depletion of ozone layer due to CFC refrigerants have urged researchers to find alternatives to conventional engines and refrigerators. Some recent advancement in the field of thermoacoustics have revolutionized the way many conventional devices operate. Thermoacoustics deals with the conversion of heat into sound energy and vice versa. A heat-driven thermoacoustic refrigerator (HDTAR) can be considered as a new source of renewable energy with no moving part and no hazardous materials. A HDTAR is comprised of a thermoacoustic heat engine which converts heat into acoustic work and a thermoacoustic refrigerator which utilizes this acoustic work as an input to produce refrigeration. Thus, by applying this technology, any source of heat particularly the industrial waste heat could be utilized for cooling purposes. One of the potential applications of HDTAR is the automotive air conditioning system in which the engine waste heat could be used for air conditioning purposes. Zoontjens *et al.* [1] investigated the feasibility of using such devices as the air conditioning system of an automotive. They concluded that the thermoacoustic refrigeration is the most appealing of all the alternative refrigeration technologies considered in their studies. They used the computer program DeltaE [2] to design and propose a HDTAR for automotive air conditioning systems. In the present study, an alternative device is designed and optimized with higher overall efficiency of that of proposed by Zoontjens *et al* [1]. This device is also simulated by DeltaE to verify the results.

2. METHODOLOGY

A comprehensive algorithm has been developed by the authors (described elsewhere) to design and optimize heat-driven thermoacoustic refrigeration systems. This algorithm is applied to design and optimize a HDTAR capable of providing 30 w of cooling power at 2°C. The four heat exchangers of the device are optimized to improve the efficiency of the system and to make them practical [3]. Finally, the computer code DeltaE is used to simulate the device. The data obtained from DeltaE simulations are used for comparison with the design of Zoontjens *et al.* [1] and discussion.

3. RESULTS

Figure 1 shows the schematic of the designed and optimized HDTAR. Helium is considered as the working gas at the mean pressure of 700 kPa. The HDTAR has the total length of 1.25 m and the cross sectional area of 0.012m². A half wavelength standing acoustic wave with the resonance frequency of about 400 Hz is produced by the engine stack (the stack on the left side in Figure 1). The variation of the acoustic power along the axial coordinate of the resonator is shown in figure 2. The thermoacoustic engine can theoretically produce 25.3 W of acoustic power by utilizing 159 W of waste heat from the automobile engine. Although the temperatures of the waste heat in an automotive engine range from 200°C to 600°C [4], for the present case, the temperature of waste heat is considered to be 260°C. About 7.3 W of the produced acoustic power is consumed by the refrigerator stack (the stack on the right side in Figure 1) to provide the desired cooling power of 30 W at 2°C. Figure 2 also shows the dissipation of some acoustic power in the resonator.



Fig. 1. Schematic of the designed HDTAR. All dimensions are in millimeters.

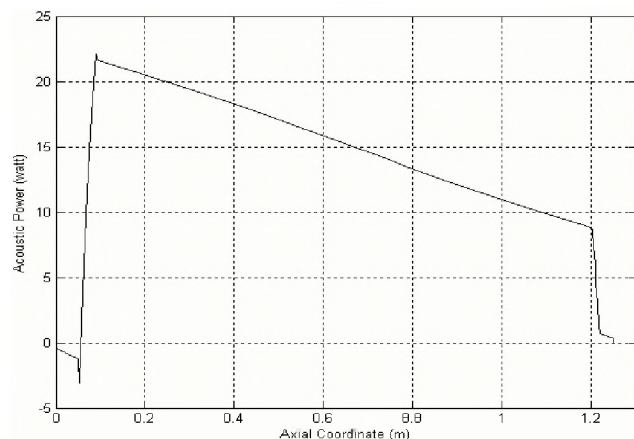


Fig. 2. Variation of acoustic power along the resonator

The device is designed to have the maximum pressure amplitude of 21 kPa. The drive ratio (DR) which is the ratio

of the pressure amplitude to mean pressure is about 3% which is within the linear range of the thermoacoustic theory. Thus, the available thermoacoustic model which has been developed by linearizing the governing equations [5, 6] can be used to predict the behavior of the given thermoacoustic device with reasonable accuracy.

Figure 3 shows the schematic of the apparatus proposed by Zoontjens *et al* [1]. The parameters of the two numerically designed apparatuses are compared in Table 1.

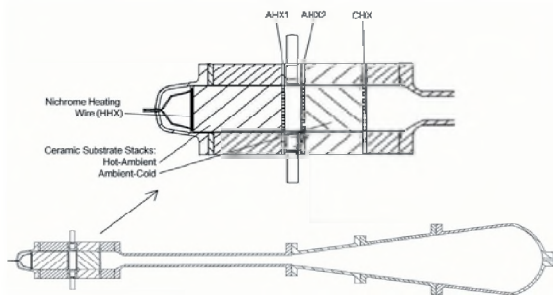


Fig. 3. Schematic of the apparatus proposed by Reference 1.

The results in Table 1 show that the device proposed in the present study is capable of providing the same cooling power (i.e. 30 W) as of that proposed by Zoontjens *et al* [1] with almost half of the heat input. Thus, the overall efficiency of the present design is 8.8% higher than that of Zoontjens *et al* [1]. The power density in a thermoacoustic device is proportional to DR^2 ; meanwhile, there is no theoretical model to predict the behavior and the performance of a thermoacoustic device in the nonlinear range ($DR > 0.03$). It could be concluded that the proposed design in this study is more reliable and predictable since the apparatus of Zoontjens *et al* [1] is designed using a linear model for $DR = 26.5\%$ that correspond to highly nonlinear regime.

4. CONCLUSION

A HDTAR is theoretically designed for automotive air conditioning application. The device receives 159 W of waste heat from the automotive engine and produces 30 W of cooling power. The overall efficiency of the designed device is 8.8% higher than the previously designed thermoacoustic device by Zoontjens *et al* [1] for automotive air conditioning. The results indicate that since HDTAR devices utilize the available waste heat from the automotive engine to cool down the automotive interior, even at relatively low efficiency these devices could still reduce the amount of fuel used in the conventional automotive air conditioning systems.

By designing a thermoacoustic system operating at higher hot heat exchanger temperatures, optimizing the shape of the resonator [7] and using working gases with lower Prandtl number [8], the theoretical efficiency of the

proposed system can improve to the higher values. With higher efficiencies, these devices have a very strong potential to replace the existing automotive air conditioning systems thus providing environmental as well as economical benefits to the society.

Apparatus Characteristics	Proposed in the present study	Proposed by Zoontjens <i>et al.</i>
Working gas	Helium	Helium
Mean pressure (kPa)	700	700
Drive ratio (%)	3	26.5
Frequency (Hz)	400	256
Cooling power (W)	30	30
Cooling temperature (°C)	2	2
Ambient heat exchangers temperature (°C)	27	27
Estimated required waste heat for engine (W)	159	300
Hot heat exchanger temperature (°C)	260	450
Overall efficiency (%)	18.8	10

Table 1. Comparison between two numerically designed devices.

REFERENCES

- Zoontjens, L., Howard, C., Zander, A. and Cazzolate, B (2005). Feasibility Study of an Automotive Thermoacoustic Refrigerator. Proceedings of *Acoustics*, Busselton, Australia, November 9-11.
- Ward, W.C. and Swift, G.W (1994). Design environment for low-amplitude thermoacoustic engine. *J. Acoustic Soc Am.* **95**, 3671-3674.
- Babaei, H., Siddiqui, K (2007). Design Optimization for (Parallel Plate) Heat Exchangers in thermoacoustic Devices. CAA Annual Conference, Montreal, Canada, October 9-12.
- Johnson, V.H., (2002). Heat generated cooling opportunities in vehicles. Society of automotive engineers, 1969-1974.
- Swift, G.W. (2002). Thermoacoustics: A unifying perspective for some engines and refrigerators. The Acoustical Society of America, Melville, NY.
- Swift, G.W. (1995). Thermoacoustic engines and refrigerators. *Physics Today* **48**, 22-28.
- Bao R., Chen G., Tang K., Jia, Z. and Cao, W. (2006). Influence of resonance tube geometry shape on performance of thermoacoustic engine. *Ultrasonics* **44**, 1519-1521.
- Belcher, J.R., Slaton, W.V., Raspet, R., Bass, H.E. and Lightfoot, J. (1999). Working gases in thermoacoustic engines. *J. Acoust. Soc Am.* **105**, 2677-2684.

RADIATION BY A SUBMERGED CYLINDRICAL SHELL IN RESPONSE TO AN EXTERNAL NON-STATIONARY ACOUSTIC PULSE

Serguei Iakovlev

Department of Engineering Mathematics and Internetworking, Dalhousie University, Halifax, Nova Scotia, Canada B3J 2X4
Serguei.Iakovlev@Dal.Ca

1. INTRODUCTION

Submerged circular cylindrical shells are very common in ocean engineering, and their analysis under various loading conditions has received a considerable attention over the past few decades. The present work concerns with the analysis of the acoustic field induced around such a shell when it is subjected to an external non-stationary acoustical pulse, or a very weak shock wave, and when no internal fluid is present. A detailed review of the relevant literature can be found in [1]. The problem is not new, and some of its aspects have been addressed as early as the 1950-1960s [2], with a number of studies concerned with more subtle fluid-structure interaction effects appearing in the last decade, e.g. [3]. It appears, however, that the fully evolved radiated field induced during the interaction has not been considered in enough detailed as of yet, which is the main goal of this presentation.

2. MATHEMATICAL APPROACH

The fluid is assumed to be irrotational, inviscid, and linearly compressible, and is therefore governed by the wave equation. The shell is assumed to be thin enough so that the linear theory of shells can be used, and, additionally, Love-Kirchhoff hypothesis is assumed to hold true as well; the respective shell equations can be found in [4]. The motion of the fluid is coupled to that of the shell through the dynamic boundary condition on the interface, and, additionally, we assume the zero conditions at the infinity, periodicity conditions with respect to the angular coordinate, and the zero initial conditions.

A mixed analytical-numerical solution has been developed, where the separation of variables was used in combination with the Laplace transform technique to obtain the diffraction and radiation pressure in modal form, and the finite differences were employed to obtain the harmonics of the shell surface displacements, with subsequent coupling of the two parts. The details can be found in [5]. The simulated images based on the solution developed were compared to the available experimental ones [3], and an excellent agreement was observed.

3. RESULTS AND CONCLUSIONS

A steel shell submerged into water was considered, and its thickness and radius were assumed to be 0.005 m

and 0.5 m, respectively. The interaction with a cylindrical incident wave [5] with the rate of exponential decay of 0.0001314 s, and the pressure in the front of 10 kPa, was analyzed. For the system's parameters considered, it takes about 0.714 ms for the incident wave to move over the shell.

The interaction has been simulated, and the images of the dynamic pressure pattern in the fluid have been generated. Figures 1 and 2 show the acoustic field during the early interaction, $t=0.286$ ms. Two images depicting different pressure ranges are shown – figure 1 captures the entire range of the pressure observed, while figure 2 shows a low-magnitude close-up to ensure that all pressure components are visible equally well.

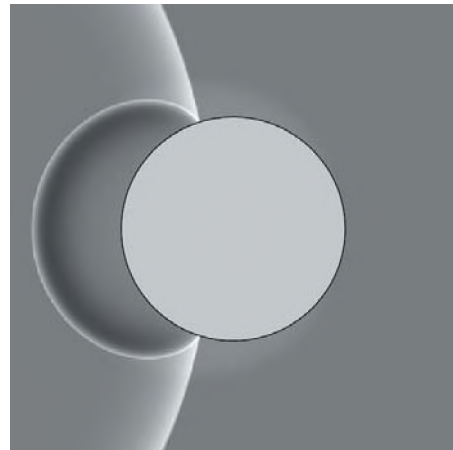


Figure 1. The acoustic field during the early interaction. The pressure of 10 kPa corresponds to the white half-tone, and -7.5 kPa to the black one.

One can see that two different components of the acoustic field can be clearly identified: the high-magnitude component corresponding to the incident and diffracted waves (we refer to it as the “scattered field”), and the low-magnitude component corresponding to the radiation of the elastic waves propagating in the shell into the fluid (we refer to it as the “shell-induced field”). We particularly emphasize that the former waves propagate with the velocity equal to the acoustic speed in the fluid, whereas the latter is a “head wave” which, due to the fact that the acoustic speed in the shell is much higher than that in the fluid, propagates far ahead of the incident front.

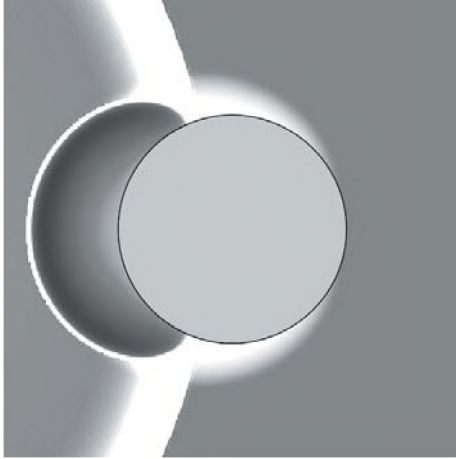


Figure 2. The low-magnitude close-up of the acoustic field during the early interaction. The pressure of 1 kPa and above corresponds to the white halftone, and -7.5 kPa to the black one.

The results observed are not new, and have been reported before, both experimentally and numerically, e.g. [3]. However, it appears that only the early interaction has been investigated in the work published (i.e., at the instants when the incident front has not yet moved into the shadow zone, and when the elastic waves have not completed their first full circumferential passage around the shell). Our objective is to look at the acoustic field during the late interaction, and to focus on the shell-induced field that results from the multiple passages of the elastic waves around the shell. We also note that in the experiments [3, figure 6], two different shell-induced waves were observed, S_o and A_o (symmetric and antisymmetric Lamb waves, respectively), whereas here we only observed one of them, S_o . This is due to the limitations of the shell model employed, but it does not appear to be a detrimental drawback of the study since the most rapidly propagating (and, therefore, most practically interesting) component, S_o , is captured really well.

Figure 3 shows the fully evolved shell-induced wave system during the late interaction, $t=1.61$ ms; the incident wave is not shown, only the location of its front. By the instant depicted, the incident wave moved over, and more than the diameter away from, the shell. There are five wavefronts propagating upstream and downstream visible in the snapshot, F1-F5. Each of these wavefronts corresponds to an individual passage of the elastic waves around the shell, and the highest pressure in the fronts corresponds to the superpositions of the elastic waves at the head ($\theta=0$) and tail ($\theta=\pi$) points of the shell. Thus, the images of the radiated field taken during the late interaction allow one to see the entire evolution of the dynamics of the process (as far as the radiation by the shell is concerned) in a single shot, which makes them a very useful analysis tool. We also note that due to the mentioned difference in the acoustic speeds, the

first radiated front propagates considerably ahead of the scattered one (in the present case, the time difference is about 0.39 ms). This feature becomes particularly important when the response time is critical – when there are other structures located upstream of the primary shock-responding one, detecting the shell-induced field prior to the arrival of the incident wave itself allows for some extra time to take the measures necessary.

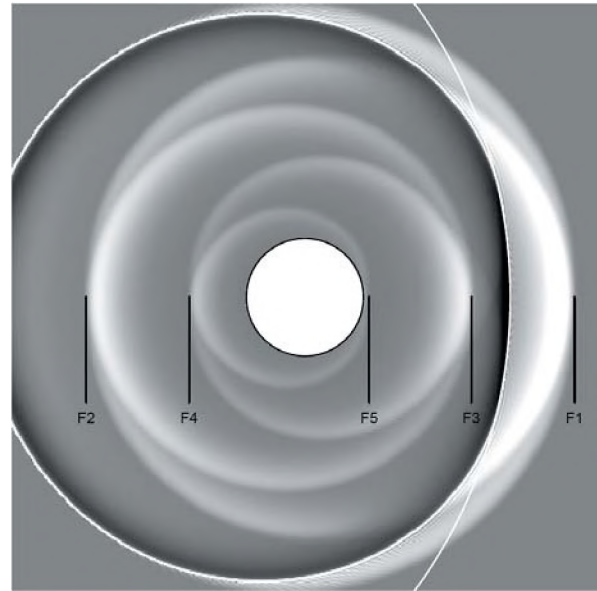


Figure 3. The fully-evolved radiated wave system, late interaction.

REFERENCES

1. Iakovlev, S. External shock loading on a submerged fluid-filled cylindrical shell, *Journal of Fluids and Structures* 22, 2006, 997-1028.
2. Geers, L. T. Excitation of an elastic cylindrical shell by a transient acoustic wave, *Journal of Applied Mechanics* 36, 1969, 459-469.
3. Ahyi, A. C., Pernod, P., Gatti, O., Latard, V., Merlen, A., and Uberall, H. Experimental demonstration of the pseudo-Rayleigh A_o wave, *Journal of the Acoustical Society of America* 104, 1998, 2727-2732.
4. Junger, M. C. and Feit, D. *Sound, structures, and their interaction*, 1972, MIT Press, Cambridge, USA.
5. Iakovlev, S. Interaction between a submerged evacuated cylindrical shell and a shock wave. Part I: Diffraction-radiation analysis, submitted to *Journal of Fluids and Structures*, 2007.

ACKNOWLEDGEMENTS

The author gratefully acknowledges the financial support of the Natural Sciences and Engineering Research Council (NSERC) of Canada, the Killam Trusts, and the Faculty of Engineering, Dalhousie University. The assistance of Ryan Barnes is gratefully acknowledged as well.

DESIGN OPTIMIZATION OF PARALLEL PLATE HEAT EXCHANGERS IN THERMOACOUSTIC DEVICES

Hadi Babaei, Kamran Siddiqui

Dept. of Mechanical and Industrial Engineering, Concordia University, 1455 De Maisonneuve Blvd. W., Quebec, Canada, H3G 1M8, h_babaei@alcor.concordia.ca

1. INTRODUCTION

Cooling by sound is a new environmentally friendly technology developed rapidly during the past three decades. The refrigeration system based on this technology is called thermoacoustic refrigeration. Due to inherent simplicity, reliability and no hazardous materials, thermoacoustic refrigeration systems have a strong potential to replace conventional refrigeration systems. However, at present, these devices have lower efficiency mainly attributed to the poor understanding of the fundamental processes and technical immaturity to design different components of these devices. Thus, significant efforts are needed to improve the fundamental understanding of the thermoacoustic process, and the role/impact of the main components of these devices on the overall performance. This will lead to the development of efficient devices that will benefit the society from environmental as well as economical perspectives.

One of the main components of a thermoacoustic device is the heat exchanger. Heat exchangers are used to exchange heat with the warm and cold environments external to the device. However, the impact of heat exchanger design on the thermoacoustic process and the overall performance of the device are not well understood. In the present study, parallel plate heat exchangers of a thermoacoustic refrigerator with an acoustic driver and a heat-driven thermoacoustic refrigerator are optimized theoretically by using the second law of thermodynamics and the computer code DeltaE which solves the one dimensional wave equation in a geometry defined by the user. DeltaE is a great tool to simulate and predict the behavior of thermoacoustic devices in the linear range of the acoustic wave [1]. The manufacturing issues are also considered for the optimized heat exchangers to facilitate easy fabrication and thus, practical usage.

2. METHODOLOGY

To have minimum working gas flow disturbance in the vicinity of stack edges and heat exchangers, some studies have recommended that the heat exchangers should have the same porosity as that of the stack [2]. However, to keep the same porosity as the stack, the plate spacing in parallel plate heat exchangers needs to be reduced which results in increasing the entropy generation due to viscous effects quadratically [3]. Thus, it could be inferred that

keeping the same porosity for the heat exchangers as that of the stack is not an optimized choice. A better design choice for parallel plate heat exchangers is investigated in the present study by applying the analysis developed by Ishikawa and Hobson [4] which is based on the second law of thermodynamics for the time-averaged entropy generation in parallel plate heat exchangers of thermoacoustic devices. The effects of plate thickness, spacing and the porosity of parallel plate heat exchangers on the performance of the two thermoacoustic devices are investigated using DeltaE. Swift [5] recommended that the optimum length of a heat exchanger is equal to the peak to peak gas displacement at the heat exchanger location. In this study, the length of the cold heat exchangers and the refrigerator ambient heat exchangers are assumed equal to the gas peak to peak displacement at the cold heat exchanger locations and the length of the hot heat exchanger and the engine ambient heat exchanger are assumed equal to the gas peak to peak displacement at the engine ambient heat exchanger location.

3. RESULTS

A thermoacoustic refrigerator is designed with the air as the working gas. The mean pressure is considered to be atmospheric with the resonance frequency of 140 Hz. The sketch of the designed device is shown in Figure 1. The overall length and cross sectional area of the device are 1.22 m and 0.0132 m^2 , respectively. This device could provide 3 watt of cooling power at 9°C .



Fig. 1. Sketch of the thermoacoustic refrigerator with air, all dimensions are in millimeters

In the first simulation by DeltaE, the blockage ratio of the heat exchangers is assumed equal to that of the stack (BR=0.8). Through the second law analysis and by assuming the plate thickness of the heat exchangers equal to their length (i.e. 3.6 mm), the porosity of the heat exchangers is optimized. The optimized blockage ratio for the cold heat exchanger and ambient heat exchanger are estimated 0.56 (plate spacing 4.6 mm) and 0.345 (plate

spacing 1.9 mm), respectively. The heat exchangers with modified blockage ratio are used to simulate the same apparatus by DeltaE. The results of the two simulations are summarized in table 1. The results show that with the optimized heat exchangers whose porosity is less than that of the stack, the overall performance of the thermoacoustic refrigerator is increased by 16%.

Cases	BR same as stack	BR optimized based on second law
Required acoustic power(w)	2.28	1.97
Dissipated acoustic power in the stack(w)	0.88	0.88
Dissipated acoustic power in the CHX(w)	0.17	0.01
Dissipated acoustic power in the AHX(w)	0.16	0.02
Ratio of the dissipated acoustic power in HXs to required acoustic power	14.4%	1.52%
Overall coefficient of performance	1.31	1.52

Table 1: simulation results for the thermoacoustic refrigerator

A heat driven thermoacoustic refrigerator is also designed with helium as the working gas at the mean pressure of 7 atm. The resonance frequency is 400 Hz. The sketch of the designed device is shown in Figure 2. The overall length and cross sectional area of the device are 1.25 m and 0.012 m², respectively. This device could provide 30 watt of cooling power at 2°C.



Fig. 2. Sketch of the heat driven thermoacoustic refrigerator with helium, all dimensions are in millimeters

The same procedure is used to optimize the heat exchangers of the second device. That is, the device is simulated first by assuming the blockage ratio of all heat exchangers to be the same as the stack i.e. 0.8. Then the blockage ratio of the heat exchangers is changed to optimize the design based on the second law analysis. The simulation results for both cases are presented in Table 2. Similar to the first refrigerator, the results show that for the heat-driven thermoacoustic refrigerator, with the optimized heat exchangers whose porosity is less than that of the stack, the overall performance of the thermoacoustic refrigerator is

increased by 35%. The modified blockage ratio of hot heat exchanger, engine ambient heat exchanger, cold heat exchanger and refrigerator ambient heat exchanger are 0.13, 0.19, 0.32 and 0.20, respectively.

Cases	BR same as stack	BR optimized based on second law
Required heat energy (w)	215	159
Produced acoustic power in engine stack (w)	35.1	25.2
Dissipated acoustic power in the CHX/Ref. AHX (w)	2.49/2.66	0.23/0.67
Dissipated acoustic power in the HHX/Eng. AHX(w)	5.15/3.28	1.82/0.57
Ratio of the dissipated acoustic power in HXs to produced acoustic power	38.7%	13%
Overall efficiency	14%	18.9%

Table 2: simulation results for the heat driven thermoacoustic refrigerator

4. DISCUSSION

The present study shows that parallel plate heat exchangers with the same porosity as that of the stack are not optimized due to higher acoustic power dissipation. Furthermore, they are not practical from manufacturing aspect. It is also been shown that the porosity of the optimized parallel plate heat exchangers is lower from that of the stack which also reduces the manufacturing challenges.

REFERENCES

1. Ward, W.C. and Swift, G.W (1994). Design environment for low-amplitude thermoacoustic engine. *J. Acoustic Soc Am.* **95**, 3671-3674.
2. Tijani, M.E.H., Zeegers, J.C.H. and De Waele, A.T.A.M (2002). Design of thermoacoustic refrigerators. *Cryogenics* **42**, 49-57.
3. Ishikawa, H., Mee, D.J. (2002). Numerical investigations of flow and energy fields near a thermoacoustic couple. *J. Acoust. Soc Am.* **111**, 831-839.
4. Ishikawa, H., and Hobson, P.A. (1996). Optimisation of heat exchanger design in a thermoacoustic engine using a second law analysis. *International Communications in Heat and Mass Transfer* **23**, 325-334.
5. Swift, G.W. (1988). Thermoacoustic engines. *J. Acoust. Soc Am.* **84**, 1145-1179.

EFFECT OF BOUNDARY CONDITIONS ON STRING INHARMONICITY

Chien-Yu Chen and Rama B. Bhat

Department of Mechanical and Industrial Engineering, Concordia University,
1455 de Maisonneuve Blvd. W., Montreal, Quebec, H3G 1M8, Canada

ABSTRACT

In studying the vibration of and sound from stringed musical instruments, the string is always considered to be completely fixed. However, this does not reflect the reality, especially for instruments such as guitar and violin where the player presses the strings with fingers. From the results obtained, it is clear that a partially fixed string will produce inharmonicity which will introduce some degree of beat phenomenon. This indicates an important aspect that has not been discussed extensively previously. In this paper, a simple mathematical model has been developed to represent a fixed-partially fixed string. The parameters that cause inharmonicity are discussed and the beat phenomenon between fundamental and inharmonic partials is studied.

1. INTRODUCTION

In classical analysis of string vibrations, the boundary condition has always been set as fixed. However, in many real cases, they are being attached in many ways, which do not always guarantee a completely fixed situation. In this study, the effect of partially fixed string is analyzed which leads to some degree of inharmonicity. This may explain the source of inharmonic partials in some stringed musical instruments such as guitar and violin where the strings are pressed with fingers while playing.

2. BASIC EQUATION

The string is modeled as fixed at one end and partially fixed at the other as shown in Figure 1. The spring stiffness (k) represents the partially fixed nature of the string. When k is infinite, it is equivalent to fixed-fixed string. The wave equation in the string is given by [1]:

$$T \frac{\partial^2 y}{\partial x^2} = \rho \frac{\partial^2 y}{\partial t^2} \quad (1)$$

where L is the string length, T is the tension applied, and ρ is the string mass per unit length.

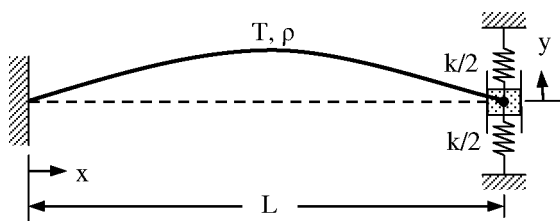


Fig. 1. The string model

The boundary conditions are [2]:

$$\text{At } x = 0 \quad y(0, t) = 0 \quad (2a)$$

$$\text{At } x = L \quad -ky(L, t) = T \sin \theta \approx T \frac{dy}{dx} \quad (2b)$$

Applying the boundary conditions to the wave equation, the frequency equation is obtained as:

$$\tan(\tau L) = -\frac{T\tau}{k} \quad (3)$$

where $\tau = \omega/c$ and $c = \sqrt{T/\rho}$ is the speed of wave traveling. The natural frequencies (ω_n) of the system obtained by solving Eq. (3) as shown in Figure 2, are:

$$\omega_n = c\tau_n \quad (4)$$

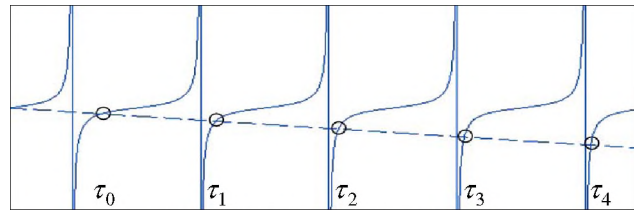


Fig. 2. Graphical solution of Eq. (3)

3. RESULTS

Solving Eq. (3) for various stiffness and string lengths with constant tension, the results are tabulated in

Table 1 where f_0 and f_i are the fundamental frequency and the partials, respectively.

Table 1. Inharmonicity with respect to stiffness (k) and string length (L) with constant tension (T)

Stiffness (k)	Ratio	String length (L)			
		0.25m	0.50m	1.00m	5.00m
5 N/m	f_2 / f_1	2.984	2.974	2.953	2.796
	f_3 / f_1	4.972	4.954	4.906	4.648
	f_4 / f_1	6.959	6.933	6.867	6.500
	f_5 / f_1	8.947	8.913	8.827	8.352
	f_6 / f_1	10.935	10.893	10.788	10.204
50 N/m	f_2 / f_1	2.877	2.778	2.609	2.158
	f_3 / f_1	4.776	4.597	4.289	3.408
	f_4 / f_1	6.680	6.423	5.976	4.697
	f_5 / f_1	8.585	8.253	7.673	6.000
	f_6 / f_1	10.493	10.082	9.371	7.303
500 N/m	f_2 / f_1	2.348	2.169	2.064	2.032
	f_3 / f_1	3.790	3.422	3.179	3.053
	f_4 / f_1	5.257	4.710	4.324	4.063
	f_5 / f_1	6.733	6.009	5.483	5.084
	f_6 / f_1	8.213	7.315	6.652	6.105
5000 N/m	f_2 / f_1	2.005	2.002	1.992	2.010
	f_3 / f_1	3.021	3.006	2.990	3.020
	f_4 / f_1	4.048	4.012	3.988	4.020
	f_5 / f_1	5.087	5.023	4.984	4.949
	f_6 / f_1	6.132	6.035	5.984	6.040
∞ N/m	f_2 / f_1	2.000	2.000	2.000	2.000
	f_3 / f_1	3.000	3.000	3.000	3.000
	f_4 / f_1	4.000	4.000	4.000	4.000
	f_5 / f_1	5.000	5.000	5.000	5.000
	f_6 / f_1	6.000	6.000	6.000	6.000

Tension applied (T) = 100 N

From Table 1, it clearly indicates that the inharmonicity is higher when string length (L) is shorter and stiffness (k) is lower. Also, at low stiffness, the partials are shown to be shifted from their respective harmonic positions to values that are close to odd multiples of the fundamental frequency.

4. DISCUSSION

In classical string vibration analyses, boundary conditions have always been set as fixed which may not correspond to the reality. In current study, the results indicate that the boundary condition has a very significant effect on the behavior of the string by introducing inharmonicity which in turn affects the sound produced. This study finds that the combination of short string with

low stiffness in partially fixed string will shift the partials away from their harmonic positions. In the ultimate inharmonic case, the partials are moved to frequencies that are close to odd multiples of the fundamental value.

5. REFERENCES

- [1] L. E. Kinsler, and A. R. Frey (2000). Fundamentals of acoustics. Fourth Edition, John Wiley & Sons, New York, NY
- [2] S. S. Rao (2004). Mechanical Vibrations. Fourth Edition, Prentice Hall, Upper Saddle River, NJ
- [3] H. Fletcher, E. D. Blackham, and R. Stratton (1962). Quality of Piano Tones. Journal of the Acoustical Society of America, 34(6) 749-761

A REVIEW OF NOISE IMPACTS FROM OFFSHORE OIL-GAS PRODUCTION ACTIVITIES ON THE MARINE BIOTA

Sharmin Sultana and Zhi Chen

Dept. of Building, Civil & Environmental Engineering, Concordia University, 1455 de Maisonneuve, Quebec, Canada, H3G1M8, zhichen@alcor.concordia.ca

1. INTRODUCTION

Marine noise originates from vessel traffic, oil-gas exploration activities, machinery and propeller noise, research activities, military sonar, and dredging [1]. Although noise pollution is not directly fatal, it adversely affects the regular and natural biota activities [2]. For example, the recent expansion of petroleum exploration in the coastal area poses a threat on the regional ecosystem.

In details, noise may come from three offshore oil-gas exploration and extraction activities: [i] exploration stage - mapping subsurface geology and resource reservoir using seismic operation with the release of compressed air from an array of airgun, drilling exploration and wells delineation for feasibility study; [ii] construction stage - preparing drilling pad, establishing drilling platform, drilling and completion of extraction wells, installing wellhead, other utility construction accessories; [iii] operation and maintenance [3].

It was discussed that noise from offshore drilling operation can hardly impact the marine lives compared to seismic noise [4]. Reported impacts from marine noise pollution can be summarized as: egg-larvae mortality, feeding and breeding problem, stress, damage of tissue and organs, masking, hearing loss, behavioral changes, communication problem, and the like [1,2,5]. The issue of marine noise impacts on biota is a relatively new research field which is in need of extensive efforts to quantify the impacts and support the related management.

2. A SURVEY AND DISCUSSION

In this section, previous studies on marine noise and its impacts related to offshore oil and gas activities are discussed with respect to monitoring and experimental investigations, modeling and risk assessment, and proposed mitigation measures.

2.1 The effects of noise on marine biota

Numerous observations have been reported on the effects of noise on marine biota. For example, the uses of sound by marine mammals are adapting to the ambient environment and navigation, communication and sensing, e.g. echolocation for tracking prey, mating and group interaction, vocalization and avoid predators [2,6]. Noise pollution affects marine mammals and fish to experience pathological effects, behavioral changes, and feeding-

mating-breeding-nursing disruptions [5]. Temporary and permanent hearing loss, damage of tissue, trauma, stress, and food chain disruptions are also other possible impacts due to noise pollution from anthropogenic activities such as oil-gas production operations [7]. High intensity sound from such activities causes masking problem which is quite serious as it conceals the communicative sounds as well as biologically important sounds [1].

2.2 Monitoring and experimental studies

Experimental studies were mainly conducted in biological lab together with field monitoring actions by governmental and industrial agencies. For example, an archival acoustic recording tag called DTAG had been developed to monitor and track the behavioral changes and responses of less visible deep diving marine mammals with built-in sensors in the Mediterranean Sea and the Gulf of Mexico [8]. Impacts of anthropogenic noise e.g. oil and gas drilling noise on nervous and immune systems of marine mammals, e.g. whale and dolphin, were tested by analyzing their blood samples before and after the exposure to seismic sound [9]. For high-level sound, norepinephrine, epinephrine, dopamine, γ -glutamyltransferase levels increased while alkaline phosphatase decreased in white whale body. For dolphin, aldosterone increased and monocytes decreased after exposure to impulse sound, for tonal sound, the neural-immune changes were minimal. Shallow water ambient noise experiments were conducted in Eastern Canadian waters to show their temporal and spatial variations due to whale song, wind, shipping and drilling activities in oil platform [10]. Long term monitoring is vital for critical and sensitive species in areas of concern such as restricted migratory routes, spawning area, feeding-breeding-nursing grounds, and resting places [11].

2.3 Modeling and risk assessment

The relevant modeling studies include sound propagation modeling, simulation of the perceived sound by marine animal and consequent impacts on biota. It was shown that seismic sound amplitude originating from the trial of exploring oil-gas reserves decreases logarithmically with water depth from the source; at the greater distances, the amplitude diminishes and frequency spectrum broadens; attenuation is also influenced by ocean depth and other physical characteristics e.g. temperature, salinity, density, bed roughness [12]. A mathematical model was developed to predict oil industry generated acoustic noise propagation

into the sea sensed by mammals [13]; acoustic parameters e.g. peak pressure, peak-to-peak pressure, root mean square pressure, and sound pressure spectral level were measured in this study.

A multidisciplinary study was undertaken by the US Navy to develop a software workbench by integrating expertise from acoustics, oceanographic modeling, marine mammal biology, oceanography, naval operations, and environmental compliance; it was intended for simulating animal movement, estimating received acoustic time series along animal's track, predicting hearing loss related temporary threshold shifts (TTS) [14]. To demonstrate the noise impacts from sonar, shipping, oil exploration and drilling activities on marine environment, a time series stimulator was implemented fully incorporating Doppler effects to predict actual time series of a moving mammal and its auditory changes at lower frequencies [15].

2.4. Mitigation efforts

Several mitigation measures have been proposed to ensure the balance between resource extractions and maintaining good environmental poise. It stated that: (i) if any sensitive and critical species are present within the operation area, industrial activities can be delayed until suitable conditions are achieved (ii) even in the desirable condition, operations can be started gradually for warning the species; and (iii) visual observations can be scheduled every after a certain period [5]. New technologies have been reported being used to ensure efficient resource extraction activities. For example, new acoustical transducer systems, digital communication with system-tuned code-decode algorithms, smaller and more sensitive seismic instruments could be used for environmentally friendly offshore oil and gas activities [6]. Other reported remedies are with case-by-case scenarios, which include controlling seismic operations, uniform application of regulatory procedures, establishing larger exclusion zone, imposing moratorium where necessary, discovering alternative energy sources [7].

2.5 Regulatory aspects

The survey in this study indicates that noises from anthropogenic activities including offshore oil-gas exploration operations have much potential to endanger the marine biota, which are usually regulated. For example, there are extensive regulatory frameworks in the North America related to anthropogenic noise impacts on marine mammals including Marine mammal Protection Act, 1972; Endangered Species Act, 1973; and National Environmental Policy Act, 1969 [16]. It is regulated on, for instance, [i] the harassment of special fishes are prohibited; [ii] conservation of plants and animals listed as endangered or threatened should be promoted; and [iii] the environmental review of project activities including seismic operations is required.

3. CONCLUSION AND FUTURE MANAGEMENT

A survey and discussion have been conducted in this paper to address possible impacts on the marine biota resulting from offshore industrial activities, mainly oil-gas

extraction activities. It indicates that effective management tools can greatly reduce the concerned problems. In response to the required future research needs, a technical framework is proposed based on a state-of-the-art review as given in Figure 1.

Technological innovations including new monitoring and warning systems, better transducer, more sensitive seismic device, tuned systems, and underwater telemetry can help in better maintaining the desired marine ecological conditions. While modeling the sound propagation, background sound sources are often neglected which could be incorporated to quantify the relevant risks and impacts. More case-by-case analysis with direct field investigations needs to be carried out with enough collected samples. The governmental agencies will continue to play an important role in the management action and decision-making with more scientific studies being promoted.

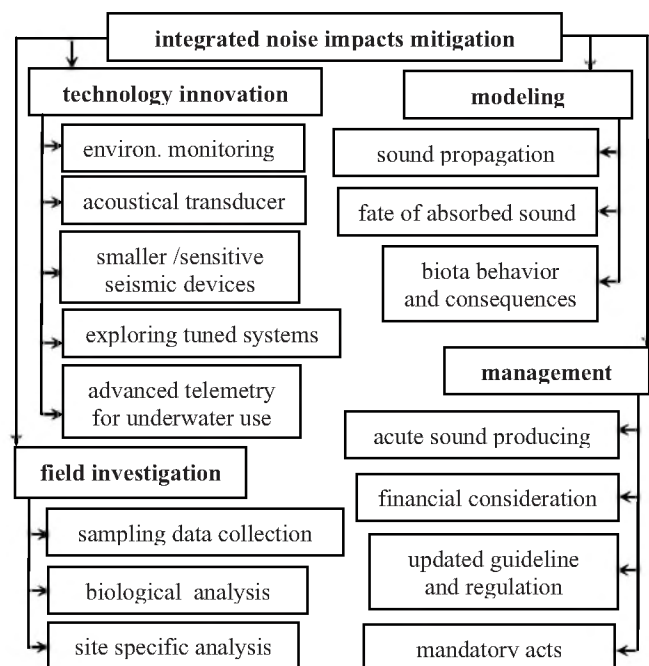


Fig. 1. A technical framework.

REFERENCES

1. Simmonds M., Dolman S., and Weilgart L. (2004). 'Oceans of noise'. WDCS Science Report.
2. Hildebrand J. (2004). 'Impacts of anthropogenic sound on Cetaceans'. IWC/SC/56/E13.
3. US Army Corps of Engineers (2005). 'Known and potential environmental effects of oil and gas drilling activity in the Great Lakes'. Chicago District.
4. Hurley G., and Ellis J. (2004). Environmental effects of exploratory drilling offshore Canada'. Prepared for The CEAA, RAC.
5. Farrell P. (2005). 'Trim 3D marine seismic survey environment plan'. The Woodside group of Companies, Australian Energy.
6. Stocker M. (2002). 'Fish, mollusks, and other sea animals, and the impact of anthropogenic noise in the marine acoustical environment'. Prepared for Earth Island Inst.
7. Cummings J., and Brandon N. (2004). 'Sonic impact: A precautionary assessment of noise pollution from ocean

- seismic surveys'. *Acous. Ecol. Inst.*, Greenpeace USA, June 2004.
8. Johnson M.P., and Tyack P.L. (2003). 'A digital acoustic recording tag for measuring the response of wild marine mammals to sound'. *IEEE J. of Oceanic Eng.*, 28(1), 3-12.
 9. Romano T.A., Keogh M.J., Kelly C., Feng P., Berk L., Schlundt C.E., Carder D.A., and Finneran J.J. (2004). 'Anthropogenic sound and marine mammal health: measures of the nervous and immune systems before and after intense sound exposure'. *Can. J. Fish. Aquat. Sci.* 61: 1124-1134.
 10. Hazen M.G., and Desharnais F. (1997). 'The eastern Canada shallow water ambient noise experiment'. *Oceans '97, MTS/EEE, Conf. Proc.*, v1, 471-476, Oct. 6-9, v1.
 11. Antarctic Treaty Consultative Meeting (2007). 'Taking action on marine noise in the Southern Ocean'. New Delhi.
 12. CEF Consultants Ltd. (2005). 'Strategic environmental assessment of Misaine Bank'. Prepared for CNOPB.
 13. Pedersen C.B., Hovem J.M., and Dong H. (2005). 'A model for predicting propagation of anthropogenic acoustic noise in the sea'. *Oceans - Europe 2005*, 293-298.
 14. Shyu H. J., and Hillson R. (2006). 'A software workbench for estimating the effects of cumulative sound exposure in marine mammals'. *IEEE J. of Oceanic Eng.*, 31(1), 8-21.
 15. Siderius M., and Porter M.B. (2006). 'Modeling techniques for marine-mammal risk assessment'. *IEEE J. of Oceanic Eng.*, 31(1), 49-60.
 16. Pierson M.O., Wagner J.P., Langford V., Birnie P., and Tasker M.L. (1998). 'Protection from, and mitigation of, the potential effects of seismic exploration on marine mammals'. *Proc. of the Seismic and Marine mammals Workshop, London, 23-25 June 1998*.

EDITORIAL BOARD / COMITÉ EDITORIAL

ARCHITECTURAL ACOUSTICS: ACOUSTIQUE ARCHITECTURALE:	Vacant		
ENGINEERING ACOUSTICS / NOISE CONTROL: GÉNIE ACOUSTIQUE / CONTROLE DU BRUIT:	Colin Novak	University of Windsor	(519) 253-3000
PHYSICAL ACOUSTICS / ULTRASOUND: ACOUSTIQUE PHYSIQUE / ULTRASONS:	Werner Richarz	Aercoustics	(416) 249-3361
MUSICAL ACOUSTICS / ELECTROACOUSTICS: ACOUSTIQUE MUSICALE / ELECTROACOUSTIQUE:	Annabel Cohen	University of P. E. I.	(902) 628-4331
PSYCHOLOGICAL ACOUSTICS: PSYCHO-ACOUSTIQUE:	Annabel Cohen	University of P. E. I.	(902) 628-4331
PHYSIOLOGICAL ACOUSTICS: PHYSIO-ACOUSTIQUE:	Robert Harrison	Hospital for Sick Children	(416) 813-6535
SHOCK / VIBRATION: CHOCS / VIBRATIONS:	Li Cheng	Université de Laval	(418) 656-7920
HEARING SCIENCES: AUDITION:	Kathy Pichora-Fuller	University of Toronto	(905) 828-3865
HEARING CONSERVATION: Préservation de L'Ouïe:	Alberto Behar	A. Behar Noise Control	(416) 265-1816
SPEECH SCIENCES: PAROLE:	Linda Polka	McGill University	(514) 398-4137
UNDERWATER ACOUSTICS: ACOUSTIQUE SOUS-MARINE:	Garry Heard	DRDC Atlantic	(902) 426-3100
SIGNAL PROCESSING / NUMERICAL METHODS: TRAITMENT DES SIGNAUX / METHODES NUMERIQUES:	David I. Havelock	N. R. C.	(613) 993-7661
CONSULTING: CONSULTATION:	Corjan Buma	ACI Acoustical Consultants Inc.	(780) 435-9172
ADVISOR: MEMBER CONSEILLER:	Sid-Ali Meslioui	Pratt & Whitney Canada	(450) 647-7339

831 sound level meter/real time analyzer

- Consulting engineers
- Environmental noise monitoring
- Highway & plant perimeter noise
- Aircraft noise
- General Surveys
- Community noise

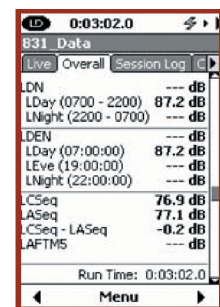
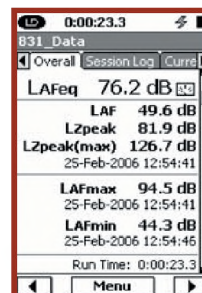
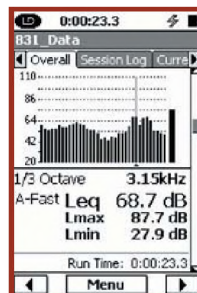
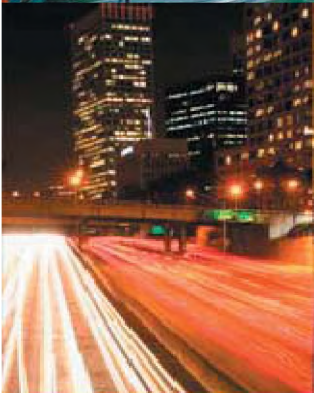
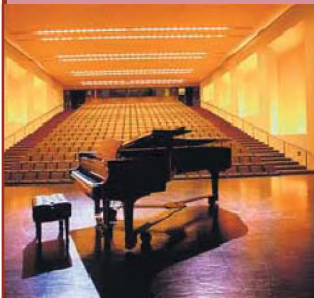
FEATURES

- Class 1/Type 1 sound level meter
- Small size with large display. Ergonomic
- User friendly operator interface
- 120MB standard memory expandable up to 2GB
- Single measurement range from 20 to 140 dB SPL
- Up to 16 hours of battery life
- Provided with utility software for instrument set-up and data download
- Field upgradeable
- AUX port for connection to USB mass storage & cellular modems



MEASUREMENT CAPABILITIES

- Real time 1/1 & 1/3 octave frequency analysis
- Simultaneous display of several noise measurements—ANY DATA (Leq, Lmax, Spectra, etc)
- Automatic logging of user selectable noise measurements (Leq, Lmax, Spectra, etc...)
- Exceedance logging with user selectable trigger levels
- Audio and voice recording with replay



BAYESIAN MATCHED-FIELD GEOACOUSTIC INVERSION

Stan E. Dosso

School of Earth and Ocean Sciences, University of Victoria, Victoria BC Canada V8W 3P6, sdosso@uvic.ca

1. INTRODUCTION

This paper describes a Bayesian approach to matched-field geoacoustic inversion, with emphasis on rigorous uncertainty estimation [1]–[3]. In a Bayesian formulation, the unknown geoacoustic model parameters are considered to be random variables constrained by the data and prior information, and the goal is to interpret the multi-dimensional posterior probability density (PPD). The approach is developed and illustrated for a shallow-water test site in the Mediterranean Sea.

2. THEORY

Let \mathbf{m} and \mathbf{d} represent the model and data vectors, respectively, with elements considered random variables that obey Bayes rule, which may be written

$$P(\mathbf{m} | \mathbf{d}) \propto L(\mathbf{m}, \mathbf{d})P(\mathbf{m}).$$

In the above equation, $P(\mathbf{m} | \mathbf{d})$ represents the PPD which quantifies the information content for the model parameters given both data information, represented by the likelihood function $L(\mathbf{m}, \mathbf{d})$, and prior information $P(\mathbf{m})$. The likelihood can typically be written $L(\mathbf{m}, \mathbf{d}) \propto \exp[-E(\mathbf{m}, \mathbf{d})]$, where E represents an appropriate data misfit function (considered later). The PPD can be written

$$P(\mathbf{m} | \mathbf{d}) = \frac{\exp[-\phi(\mathbf{m}, \mathbf{d})]}{\int \exp[-\phi(\mathbf{m}', \mathbf{d})] d\mathbf{m}'},$$

where the integration spans the parameter space and the generalized misfit, including data and prior, is given by

$$\phi(\mathbf{m}, \mathbf{d}) = E(\mathbf{m}, \mathbf{d}) - \ln P(\mathbf{m}).$$

The multi-dimensional PPD is typically characterized in terms of parameter estimates, uncertainties, and inter-relationships, as given by the maximum *a posteriori* (MAP) model, mean model, marginal probability distributions, and covariance/correlations defined

$$\hat{\mathbf{m}} = \text{Arg}_{\max} \{P(\mathbf{m} | \mathbf{d})\}$$

$$\bar{\mathbf{m}} = \int \mathbf{m} P(\mathbf{m} | \mathbf{d}) d\mathbf{m}$$

$$P(m_i | \mathbf{d}) = \int \delta(m_i - m'_i) P(\mathbf{m}' | \mathbf{d}) d\mathbf{m}'$$

$$C_{ij} = \int (m_i - \bar{m}_i)(m_j - \bar{m}_j) P(\mathbf{m} | \mathbf{d}) d\mathbf{m}.$$

For nonlinear problems, such as geoacoustic inversion, analytic solutions to the above optimization and integrations are not available, and numerical methods must be employed. Hybrid algorithms, such as adaptive simplex simulated annealing [1], which combine global and local methods, have proven effective for optimization. Integration can be carried out using Markov-chain Monte Carlo importance sampling methods, such as fast Gibbs sampling [2].

The data uncertainty distribution, which defines the likelihood function, must include both measurement errors (e.g., additive noise, instrument uncertainties) and theory errors (due to the simplified model parameterization and inexact theory). Since data uncertainties are generally not well known *a priori*, physically reasonable assumptions are required about the form of the distribution. In many practical cases, lack of specific knowledge of uncertainties suggests a simple distribution (e.g., Gaussian) be assumed with statistical quantities estimated from the data.

Let the complex acoustic pressure fields measured at an array of N sensors and F frequencies be given by $\mathbf{d} = \{\mathbf{d}_f, f=1, F\}$. Assuming the data errors are complex, circularly-symmetric, zero-mean Gaussian-distributed random variables which are uncorrelated from frequency to frequency but potentially correlated spatially with data covariance matrix \mathbf{C}_f at the f th frequency, the likelihood function is given by

$$L(\mathbf{m}, \mathbf{d}) \propto \prod_{f=1}^F \exp \left\{ [\mathbf{d} - A_f e^{i\theta_f} \mathbf{d}_f(\mathbf{m})]^T \mathbf{C}_f^{-1} [\mathbf{d} - A_f e^{i\theta_f} \mathbf{d}_f(\mathbf{m})] \right\}$$

where T indicates conjugate transpose, $\mathbf{d}_f(\mathbf{m})$ is the modeled acoustic pressure, and A_f and θ_f represent the unknown source spectrum. Maximizing the likelihood with respect to A_f and θ_f leads to

$$L(\mathbf{m}, \mathbf{d}) \propto \exp \left\{ -\sum_{f=1}^F \mathbf{d}_f^T \mathbf{C}_f^{-1} \mathbf{d}_f + \frac{|\mathbf{d}_f^T \mathbf{C}_f^{-1} \mathbf{d}_f(\mathbf{m})|^2}{|\mathbf{d}_f^T(\mathbf{m}) \mathbf{C}_f^{-1} \mathbf{d}_f(\mathbf{m})|} \right\}.$$

The data covariance matrices \mathbf{C}_f are generally not known *a priori*, but can be estimated from the autocovariance of the data residuals (difference between measured data and data computed for the MAP model estimate, applying maximum-likelihood source spectral estimates), under the assumption of ergodicity [3]. The validity of the covariance estimates and the assumption of Gaussian error processes can be examined by applying statistical tests to the data residuals,

standardized by the Cholesky decomposition (square root) of the inverse covariance matrix. For instance, the runs test can be applied to examine whether the estimated covariance matrices successfully decorrelates the residuals, and the Kolmogorov-Smirnov (KS) test can be applied to examine the Gaussianity of the residuals [3].

3. RESULTS

The geoacoustic experiment was carried out by the NATO Undersea Research Centre in the Mediterranean Sea off the west coast of Italy near Elba Island. The experiment consisted of recording acoustic signals from a transducer towed at approximately 12-m depth over a track with nearly range-independent bathymetry (water depth ~132 m). The source emitted a 0.5-s linear frequency-modulated signal over the band 300-800 Hz every 0.25 km. The signals were received at a bottom-moored vertical line array (VLA) of 48 hydrophones which spanned from 26-120-m depth with 2-m sensor spacing. The data set analyzed here consisted of 11 frequencies at 50-Hz intervals from 300-800 Hz recorded for a source-receiver range of approximately 3.85 km.

The experiment and the environmental and geometric parameters included in the model \mathbf{m} are illustrated in Figure 1. The acoustic source is at depth z and range r from the VLA in water of depth D . The geoacoustic parameters include the thickness h of an upper sediment layer with sound speed c_s , density ρ_s , and attenuation α_s , overlying a semi-infinite basement with sound speed c_b , density ρ_b and attenuation α_b . The SSP is represented by four unknown sound speeds c_1 - c_4 at depths of 0, 10, 50, and D m.

The Bayesian inversion applied bounded uniform prior distributions for all parameters. Wide bounds were applied for the geoacoustic parameters to limit the inversion to physically reasonable values but allow the acoustic data to determine the solution. For the SSP parameters, the bounds were ± 4 m/s about the measured sound speeds, representing calibration uncertainty and the effects of spatial and/or temporal variability. For the geometric parameters (D , r , z), the bounds represent small corrections due to imprecise knowledge of these experiment parameters.

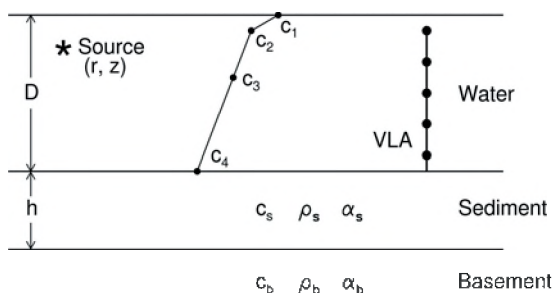


Fig. 1. Experiment geometry and model parameters.

Due to space limitations, inversion results are shown here only in terms of parameter marginal distributions (Figure 2). With the exception of the basement density, the geoacoustic

parameters are generally well determined, with the sediment thickness and basement sound speed particularly well resolved. The SSP parameters are less well determined, due to strong inter-parameter correlations (not shown). The geometric parameters are distributed near their nominal values. The KS test indicated no significant evidence against the assumption of Gaussian-distributed error processes, while the runs test suggested that the estimated data covariance matrices accounted for much, but not all, of the data error correlations.

REFERENCES

- [1] Dosso, S. E., M. J. Wilmut and A. L. Lapinski (2001). An adaptive hybrid algorithm for geoacoustic inversion. IEEE. J. Ocean. Eng., vol 26, 324-336.
- [2] Dosso, S. E. and P. L. Nielsen (2002). Quantifying uncertainty in geoacoustic inversion II: A fast Gibbs sampler approach. J. Acoust. Soc. Am., vol 111, 143-159.
- [3] Dosso, S. E., P. L. Nielsen and M. J. Wilmut (2006). Data error covariances in matched-field geoacoustic inversion. J. Acoust. Soc. Am., vol 119, 208-219.

ACKNOWLEDGEMENTS

The author thanks Peter Nielsen of the NATO Undersea Research Centre for providing the acoustic data and for helpful discussions.

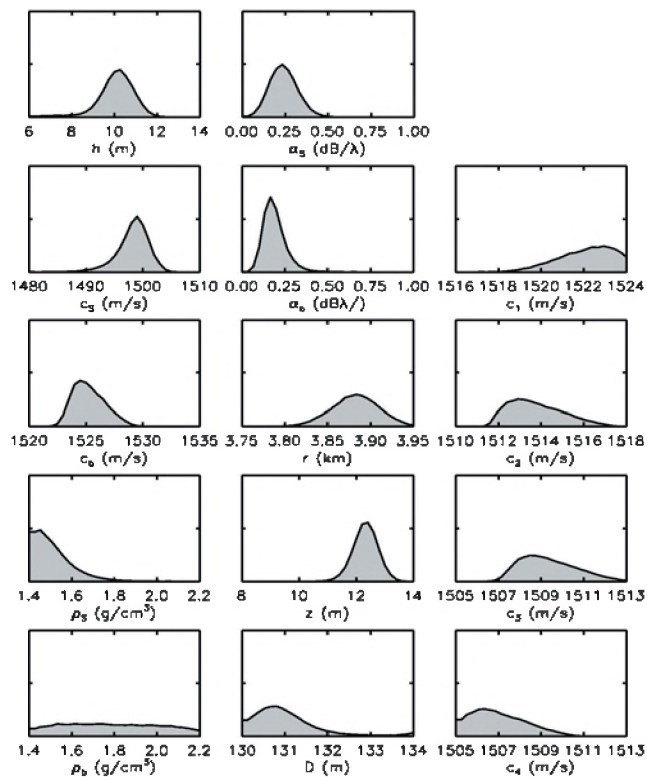


Fig. 2. Posterior Marginal probability distributions.

ASSESSMENT OF AIRCRAFT NOISE IMPACT ON RESIDENTIAL AREA

Z. Chen, W.B. Amer and J. Yuan

Dept. of Building, Civil & Environmental Engineering, Concordia University, 1455 de Maisonneuve West, Montreal, Quebec, Canada, H3G1M8, zhichen@bcee.concordia.ca

1. INTRODUCTION

With the flight frequencies increased recently, aircraft noise is associated with an increasing community concern. For example, Blackwell (2004) observed that noise pollution from aircrafts posed adverse impacts on workers in the airport and surrounding residents as well as their properties. The methods of assessing the noise impact in airport residential area have been proposed. For example, Janssens et al. (2006) proposed a model-based synthesis approach for vehicle and aircraft noise. Butikofer (2007) studied the concepts of aircraft noise calculations from the airport operation point of view. This paper includes a preliminary environmental assessment of the impacts (EIA) on the residential areas resulting from aircrafts activities in the Montreal international airport.

2. MATERIAL AND METHOD

2.1 Study area

The Dorval residential area, which is the closest to the Montreal Trudeau Airport, located approximately 19 kilometers from the downtown of Montreal is selected in this case study. There are numerous aircrafts of different Airlines companies, which serve at the airport, travel to various locations around the world. They are the most regular aircraft flying in and out of Montreal Trudeau Airport. Most of the flight traffics pass through the Dorval area as shown in Figure 1.

2.2 Method

According to Bram and Mills (2006), six steps are considered in an EIA regarding the aircraft noise. This study was conducted between February and May 2006. A portable Digital Sound Level Meter (Model TES-1351, GENEQ INC.) was used in this study for the field measurement. Field measurements and sociological surveys typically representing the residential areas focusing on 30 positions were undertaken to determine noise levels at different locations at the surrounding residential area of the airport. The distance from Airport to the selected sampling positions was ranging from 2 km to 11 km. The sampling and monitoring are carried out at representative locations during the morning, afternoon and evening in presence and absence of flights. The procedure was applied three times a day with 12 locations in the morning session, 9 in the afternoon, and 9 in the evening. In addition, the measurement for each

position was taken two times with and without the presence of flights.

Quality control of monitoring data is conducted according to the relevant procedures and guidelines. Levels of noise emissions and impact concerns were investigated following the aforementioned six steps. Local aircraft activities are assumed fixed-wing aircraft operations and ground operations used in this study (Goff and Novak 1977):

$$EN = d + (16.7) n \quad (1)$$

where, EN = effective number of operations; d = number of daytime operations (0700-2200); and n = number of nighttime operations (2200-0700).

With the collected measurement data, the equivalent sound level (L_{eq}), which is the measurement of sound energy over a period of time, is calculated (Canter 1996):

$$L_{eq} = 10 \times \log (10^{(L_{p1}/10)} \times t_1 + 10^{(L_{p2}/10)} \times t_2) \quad (2)$$

where, L_{p1} and L_{p2} are noise levels; and t_1 and t_2 are time fractions of measurement associated with L_{p1} and L_{p2} , respectively.

3. RESULTS AND DISCUSSION

3.1 Results

The noise levels recorded in the various locations in morning are shown in Table 1. In presence of a flight, the highest value was 86.4 dB (A) at Carson Avenue/ Elmridge Avenue while the lowest value was 54.4 dB (A) at Carson Avenue/ Boul Pine Beach. On the other hand, in absence of a flight the highest value was 68.9 dB (A) at Carson Avenue/ Elmridge Avenue and the lowest value was 52.1 dB (A) at Place Glenarry/ Boul Pine Beach. The highest L_{eq} was 82 dB (A) at Carson Avenue/ Elmridge Avenue, while the lowest was 53.3 dB (A) at Carson Avenue/ Boul Pine Beach.

The noise levels measured during the afternoon can be shown in a table similar to Table 1. In presence of a flight, the maximum value was 97.1 dB (A) at Clement Avenue/ Dawson Avenue, while the minimum value was 52.8 dB (A) at Boul Pine Beach/ Lakeshore drive. When there was no flight the highest value was 65 dB (A) at Dawson Avenue/ Allard Avenue, and the lowest value was 51.0 at Bord Du Luc. The highest L_{eq} was 84 dB (A) at Clement Avenue/ Dawson Avenue and the lowest L_{eq} was 52 dB (A) at Boul Pine Beach/ Lakeshore drive.

The noise levels observed during the evening can be shown in a table similar to Table 1. When there was a flight the maximum value was 91.5 dB (A) at Carson/ Allard Ave, while the lowest value was 66.1 dB (A). On the contrary, in absence of a flight, the highest value was 67.1 dB (A) at Carson/ Allard Ave, while the lowest value was 52.1 dB (A) at Lepage Ave/ 5th Avenue. The maximum value of Leq was 79 dB (A) at Carson/ Allard Avenue and the minimum value of Leq was 57 dB (A) at Lepage Ave/ 5th Avenue.

Table 1. Noise levels at morning at selected sample locations

#	Location	With Flight dB (A)	No flight dB (A)	L _{eq} dB-(A)
1	Dawson Ave / Fenelon	78.0	68.9	71
2	Dorval Sec. School	70.6	57.5	63
3	Kingsley / Elmridge	86.4	59.2	74
4	Carson Ave / Pine	54.4	53.2	53.3
5	Turcot Ave / Pine	75.2	59.3	64
6	Glenarry / Pine	81.4	52.1	68
7	Carson / Meredith Ave	76.1	63.0	66
8	St. Veronica's Church	75.7	69.3	70
9	Carson / Caledonia Ave	76.7	69.4	71
10	Place Hamilton/ Pine	62.5	55.0	57

3.2 Result analysis

Canadian standard for noise level in residential area is 45 - 55 dB (A)-Leq (Madhusoodanan Pillai 2000). Figures 1 and 2 give the visualized results for the study area for the conditions with and without flights over the sky, respectively. It clearly shows the effects from the aircrafts flying activities that additional 1 to 30 dB(A) were observed at locations in a range of less 1 to 8 km away from the airport. The annual number of taking off and landing flights at the airport is approximately 200,000 including domestic flights, cross border flights and international flights. Adverse effects on residential area fairly close to the airport can be observed when there are frequent flights taking off and landing.

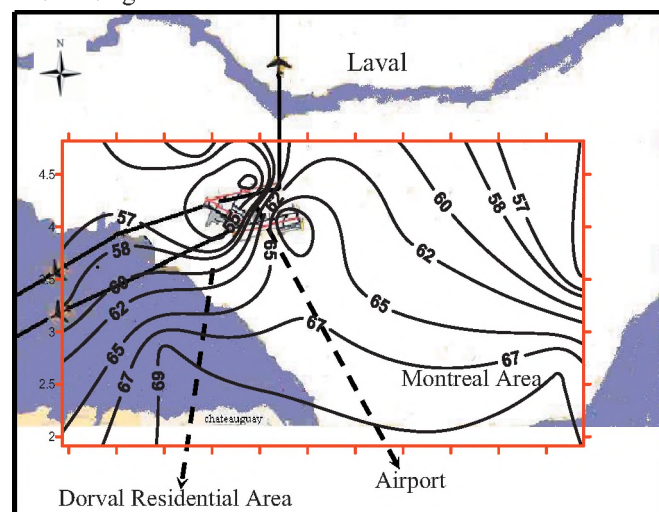


Fig. 1. Noise levels (dBA) in the morning with flights.

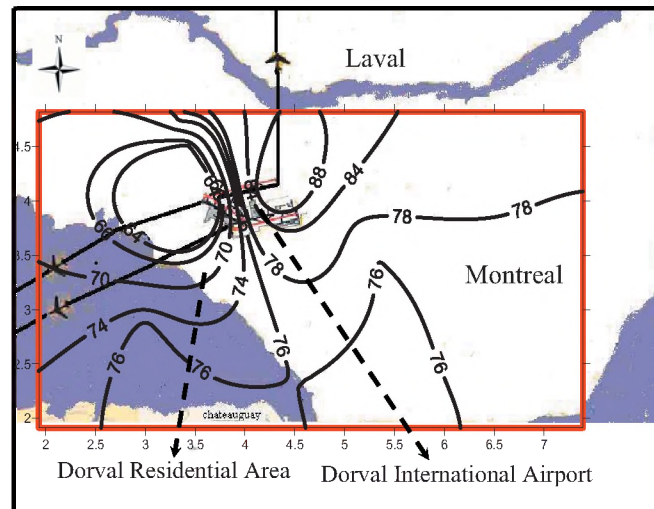


Fig. 2. Noise levels (dBA) in the morning without flights.

4. CONCLUDING REMARKS

The following conclusions are drawn from this study: (1) the background noise level in the Dorval area is relatively high compared to the national standard for residential area. With the recent expansion of Montreal airport, aircraft noise further worsens the condition; and (2) it indicates that there is marginal impact on the majority of the residential area away from the airport with the consideration of the background noise. However, the assessment shows that there are adverse effects on residential area fairly close to the airport when there are frequent flights taking off and landing.

REFERENCES

- Alexandre A., Wakstein C., Bugliarello G. and Barnes J. (1975). The Impact of Noise Pollution, Franklin, Philadelphia.
- Blackwell J. (2004). Noise Management and Protection of Hearing at Work, Work cover publications, New York.
- Bram F. and Mills D. (2006). Introduction to Environmental Impact Assessment: a guide to principles and practice: Oxford University Press, Oxford.
- Bram F. and Mills D. (2006). Introduction to Environmental Impact Assessment: a guide to principles and practice: Oxford University Press, Oxford.
- Butikofer, R. (2007) Concepts of aircraft noise calculations. Acta Acustica United With Acustica, 93, 253-262.
- Canter L.W. (1996). Environmental Impact Assessment, New York, McGraw-Hill.
- Garcia, A. (2001). Environmental Urban Noise, WIT press.
- Goff, R.J. and Novak, E.W. (1977). Environmental Noise Impact Analysis for Army Military Activities, User Manual. Construction Engineering Research Lab, Champaign Ill.
- Rubhera, R. (1997). Noise Pollution Associated with the Operation of the Dar es Salaam International Airport, Transportation Research Part D 4.
- Madhusoodanan Pillai, G. (2000). Standardizing noise. <http://www.kerala.gov.in/keralcaljan05/p17.pdf>

Note: The Second Author was a graduate student at Concordia.

SUIVI DU BRUIT AUDIBLE GÉNÉRÉ PAR UNE NOUVELLE LIGNE À HAUTE TENSION À 735 KV

Franck Duchassin¹, Claude Chamberland¹ et Blaise Gosselin²

¹Division Air et Acoustique, SNC-Lavalin Environnement inc., Québec, Canada, J4G 2R7

²Hydro-Québec TransÉnergie, Québec, Canada, H2L 4M8

Franck.Duchassin@snc-lavalin.com, Claude.Chamberland@snc-lavalin.ca, Gosselin.Blaise@hydro.qc.ca

1. INTRODUCTION

Dans le cadre du projet de construction de la ligne à 735 kV Saint-Césaire – Hertel, Hydro-Québec a mandaté SNC-Lavalin Environnement inc. pour réaliser un suivi de l'ambiance sonore engendré par la présence de la ligne. Ce suivi comprend des relevés du climat sonore effectués en 2001, avant la mise en service de la ligne puis en 2004, 2005 et 2006, années qui ont suivi la mise en service. Pour caractériser le bruit ambiant sous diverses conditions météorologiques, des relevés de bruit ont été effectués pour les conditions de temps sec, pendant et après une averse de pluie ainsi que pendant et après une averse de neige. Le présent article résume les principaux résultats mis en évidence dans le rapport d'étude de synthèse [1].

2. MÉTHODOLOGIE

Les relevés de bruit ont été effectués pendant les périodes calmes, de jour ou de nuit, en s'inspirant de la procédure corporative d'Hydro-Québec TET-ENV-P-CONT002 « *Mesure du bruit audible émis par les installations de TransÉnergie* ».

Pour chaque point et chaque condition météorologique, le bruit ambiant et les conditions météorologiques ont été retenus par intervalle de cinq minutes. Le niveau de pression acoustique continu équivalent (L_{Aeq}) et le niveau de dépassement de seuil de 95 pour cent (L_{A195}) ont été mesurés pour chaque bande de tiers d'octave de fréquence comprise entre 63 Hz et 12,5 kHz. Les conditions météorologiques mesurées sont la température moyenne, l'humidité relative moyenne, la direction du vent dominant, la vitesse moyenne du vent, la quantité totale de pluie et la pression barométrique instantanée. L'opérateur a consigné par écrit s'il y avait précipitation de pluie ou de neige, la couverture nuageuse, la condition du pavé (sec, mouillé ou enneigé), le nombre de véhicule circulant sur la route ainsi que tout autre événement sonore affectant le relevé.

2.1 Instruments

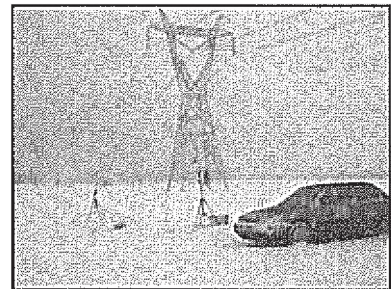
Les sonomètres utilisés sont conformes à la publication CEI 651, type 1 et ils ont été vérifiés une fois l'an afin d'assurer leur conformité aux normes. Lors des relevés pendant et après la pluie, un dessiccateur et un chapeau anti-pluie ont été ajoutés. Les conditions

météorologiques sur le site ont été obtenues avec une station météorologique portative calibrée sur une base annuelle.

2.2. Position des points de mesure

Quatre sites de mesure ont été retenus le long des tronçons Saint-Césaire – Hertel et des Cantons – Saint-Césaire de la nouvelle ligne Hertel – des Cantons pour réaliser le suivi du climat sonore.

Les relevés ont été effectués à 15 m et plus de la bordure de la route, à un point localisé à la limite de l'emprise de la ligne Hertel – des Cantons, soit à 40 m du centre de la ligne et à mi-portée entre deux pylônes.



Le microphone était à une hauteur de 1,5 m du sol et à plus de 3 m de toute surface réfléchissante (murs, obstacles et surface pavée). Les conditions météorologiques ont été mesurées à 2 m du sol.

2.3. Analyse

L'analyse des données avant et après la mise en service de la ligne a été faite selon les périodes de jour ou de nuit en fonction de chacune des conditions météorologiques suivantes : temps sec, pendant une averse de pluie, après une averse de pluie, pendant une averse de neige et après une averse de neige. Les périodes ayant un niveau de bruit L_{A195} et des conditions météorologiques stables ont été choisies. Pour chaque période choisie, les niveaux de bruit moyens et les conditions météorologiques moyennes ont été calculés.

Pour tous les sites de mesure et pour toutes les conditions météorologiques, l'analyse des relevés de bruit réalisés entre 2004 et 2006 concluait que l'indice L_{A195} est celui qui indique le mieux l'effet de la ligne 735 kV sur le bruit ambiant. Ainsi, la synthèse et les conclusions en découlant se basent principalement sur l'analyse de cet indice de bruit.

3. SYNTHÈSE DES RELEVÉS

Le bruit audible d'une ligne de transmission à haute tension apparaît normalement lors de précipitations. La présence d'eau autour ou sur les conducteurs provoque des décharges qui génèrent du bruit.

3.1. Niveau global du bruit ambiant

La figure 1 représente les moyennes des niveaux L_{AF95} (sites 1 à 4) en fonction des périodes de la journée, et ce, pour l'année 2001 (avant la mise en service de la ligne) et pour les années 2004 à 2006 (après la mise en service de la ligne).

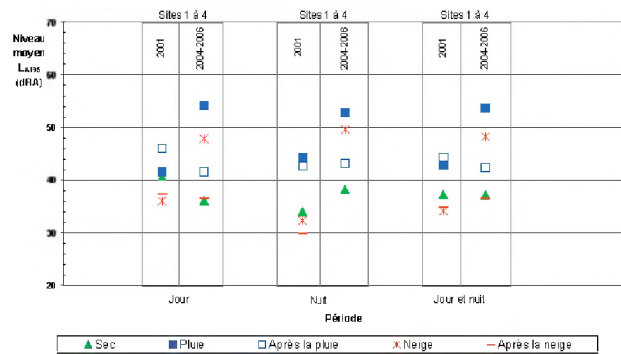


Fig. 1 : Niveaux moyens L_{AF95} mesurés aux sites 1 à 4 entre 2001 et 2006

Par temps sec, après une averse de pluie et après une averse de neige, les niveaux L_{AF95} moyens mesurés avant la mise en service de la ligne sont du même ordre de grandeur que ceux mesurés après la mise en service de la ligne. Lors de ces conditions météorologiques, le bruit généré par la ligne 735 kV n'a pas ou peu d'influence sur les niveaux de bruit ambiant mesurés. Par contre, pendant la pluie et pendant la neige, les niveaux L_{AF95} moyens mesurés après la mise en place de la ligne ont augmenté respectivement de 11 et 14 dBA. Le bruit généré par la ligne 735 kV a donc une influence significative sur les niveaux de bruit ambiant mesurés.

3.2. Spectre fréquentiel du bruit ambiant

Les spectres fréquentiels moyens des niveaux de bruit ambiant mesurés selon la condition météorologique, avant et après la mise en service de la ligne, ont été calculés. Lorsqu'il pleut ou neige, le crépitement, bruit à large bande de fréquence (800 Hz à 8 000 Hz) et le bourdonnement, bruit à caractère tonal à 120 Hz et 240 Hz, sont clairement audibles et identifiables sur les spectres fréquentiels moyens mesurés. Suite à la mise en service de la ligne 735 kV, les augmentations du niveau de bruit L_{AF95} entre 800 Hz à 8 000 Hz sont substantielles pendant la pluie et pendant la neige. Ces augmentations atteignent 20 dBA (pluie) et 30 dBA (neige) pour la bande de tiers d'octave de fréquence de 2 500 Hz.

Les figures 2 et 3 présentent respectivement les spectres fréquentiels moyens mesurés aux sites 1 à 4 pendant une averse de pluie et pendant une averse de neige.

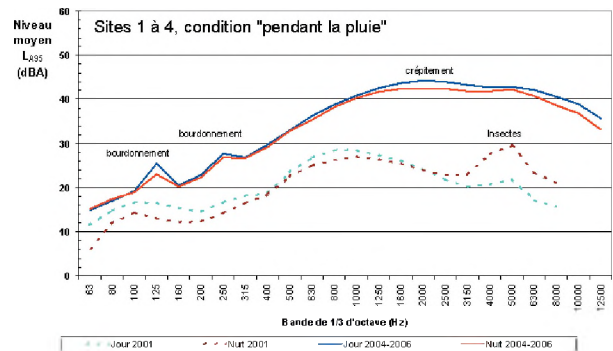


Fig. 2 : Spectres moyens L_{AF95} mesurés pendant la pluie

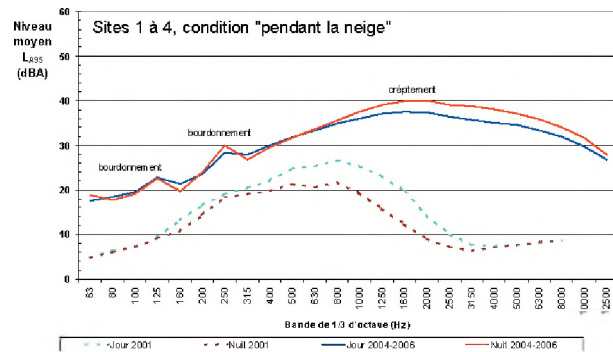


Fig. 3 : Spectres moyens L_{AF95} mesurés pendant la neige

Par temps sec, un léger crépitement de la ligne est perçu mais n'a pas ou peu eu d'influence sur les niveaux de bruit globaux moyens L_{AF95} . Après la pluie, le bourdonnement et le crépitement provenant de la ligne persiste mais à des niveaux suffisamment bas pour ne pas ou peu influencer les niveaux de bruit globaux moyens L_{AF95} . Enfin, après la neige, seul le crépitement provenant de la ligne persiste mais à des niveaux suffisamment bas pour ne pas ou peu influencer les niveaux de bruit globaux moyens L_{AF95} .

3.3 Transition avant et après des précipitations

La compilation des transitions entre deux conditions météorologiques montre que les écarts de niveaux de bruit mesurés varient de 6 à 16 dBA et que la durée de transition varie de 5 à 60 minutes. L'hypothèse retenue pour expliquer ces importantes variations est la variabilité des conditions météorologiques (quantité de précipitations, soudaineté du commencement ou de l'arrêt des précipitations, type de précipitations, humidité de l'air). Néanmoins, l'analyse de toutes les transitions observées entre deux conditions météorologiques nous permet de faire les constations suivantes : l'augmentation du niveau de bruit L_{AF95} lors du commencement d'une averse de pluie est, en général, plus rapide que la diminution du niveau de bruit L_{AF95} après la fin d'une averse; l'augmentation du niveau de bruit L_{AF95} lors du

commencement d'une averse de pluie dure en moyenne 15 minutes; la diminution du niveau de bruit L_{AF95} après la fin d'une averse de pluie ou de neige dure en moyenne 40 minutes.

3.4 Évolution du niveau de bruit ambiant dans le temps

Dans l'ouvrage « Transmission Line Reference Book » [3], il est mis en évidence que le bruit généré par les lignes à haute tension (345 kV et plus) diminue avec l'âge des conducteurs de la ligne. Les mesures réalisées entre 2004 et 2006 dans le cadre du suivi ne permettent pas de mettre en évidence un quelconque effet de l'âge des conducteurs sur le bruit généré par la ligne. Pour l'expliquer, les hypothèses suivantes sont avancées : les conditions météorologiques lors des mesures ne sont pas contrôlées et peuvent varier d'une année à l'autre (type et intensité des précipitations par exemple), la durée de la campagne de mesure (2004 à 2006) n'est peut-être pas suffisamment longue pour faire apparaître une tendance.

4. DISCUSSIONS ET CONCLUSIONS

Le bruit généré par la nouvelle ligne à haute tension à 735 kV Saint-Césaire – Hertel a une influence significative sur le bruit ambiant régnant à proximité de la ligne pendant les averses de pluie et de neige. Cette influence est peu significative par temps sec et avant et après les averses de pluie et de neige. Le bruit généré par la ligne est caractérisé par un crépitement et un bourdonnement. Suite au début des précipitations, le niveau de bruit augmente sur une durée moyenne de 15 minutes. Après l'arrêt des précipitations, le niveau de bruit diminue sur une durée moyenne de 40 minutes. Enfin, les résultats des mesures entre 2004 et 2006 ne permettent pas d'établir une tendance à la baisse ou à la hausse du bruit généré par la ligne en fonction de l'âge des conducteurs.

Le bruit généré par la ligne à haute tension à 735 kV a des caractéristiques particulières. L'influence du bruit généré par la ligne sur le bruit ambiant mesuré aux limites de l'emprise de la ligne s'avère significative uniquement lorsqu'il pleut ou lorsqu'il neige. L'exposition au bruit généré par la ligne est donc limitée en terme de durée.

Enfin, le critère de conception de la ligne Saint-Césaire – Hertel à 735 kV est de 55 dBA à la limite de son emprise lorsque les conducteurs sont mouillés mais qu'il n'y a aucune précipitation. Lorsque ces conditions ont pu être obtenues, pour tous les sites de mesure et pour toutes les périodes de la journée, les mesures du bruit ambiant montrent que le critère de conception est respecté.

RÉFÉRENCES

[1] SNC-Lavalin Environnement inc., *Boucle Montérégienne, ligne à 735 kV Saint-Césaire-Hertel, Climat sonore 2001 à 2006 avant et après la mise en service*, Juillet 2007

[2] Maruvada, P. Sarma, *Corona Performance of High-Voltage Transmission Lines*, Chapter 6 : Audible Noise, 164-175

[3] *Transmission Line Reference Book – 345 kV and above / Second Edition*, Electric Power Research Institute, Chapter 6 : Audible Noise, 267-318 (1982)

REMERCIEMENTS

Nous tenons à remercier Hydro-Québec TransÉnergie pour nous avoir permis de présenter les résultats de cette étude.

PYROK ACOUSTEMENT ACOUSTICAL PLASTERS CEILING AND WALL FINISHES

Designers and owners choose Pyrok Acoustement for their school and university projects because Pyrok provides:

- Decorative plaster finishes
- Superior sound absorbing performance
- Resistance to damage
- Low life cycle cost
- Non-combustible formulation



Perrot Memorial Library, Old Greenwich, CT



William Hart High School, Newhall, CA



High School for Physical City, New York, NY



Carmel Valley Recreation Center, San Diego, CA

CONTACT:

Howard Podolsky, Pyrok, Inc.

914-777-7070

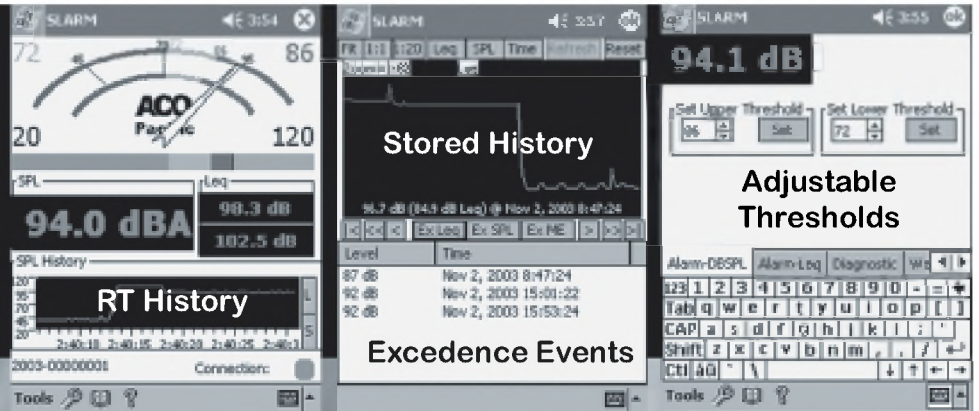
E-mail: info@pyrokin.com or

www.pyrokin.com

Noise Pollution

The SLARM™ Solution

PDA & Laptop
Displays
Wired
Wireless



The SLARM™ developed in response to increased emphasis on hearing conservation and comfort in the community and workplace incorporates ACOustAlert™ and ACOustAlarm™ technology. Making the SLARM™ a powerful and versatile sound monitoring/alarm system.

Typical Applications Include:

Community

- ◆ Amphitheaters
- ◆ Outdoor Events
- ◆ Nightclubs/Discos
- ◆ Churches
- ◆ Classrooms

Industrial

- ◆ Machine/Plant Noise
- ◆ Fault Detection
- ◆ Marshalling Yards
- ◆ Construction Sites
- ◆ Product Testing

FEATURES

- ✓ **Wired and Wireless (opt)**
- ✓ **USB, Serial, and LAN(opt) Connectivity**
- ✓ **Remote Display s and Programming**
- ✓ **SPL, Leq, Thresholds, Alert and Alarm Filters (A,C,Z), Thresholds, Calibration**
- ✓ **Multiple Profiles (opt)**
- ✓ **100 dB Display Range:**
- ✓ **20-120 dBSPL and 40-140 dBSPL**
- ✓ **Real-time Clock/Calendar**
- ✓ **Internal Storage: 10+days @1/sec**
- ✓ **Remote Storage of 1/8 second events**
- ✓ **7052S Type 1.5™ Titanium Measurement Mic**



2604 Read Ave., Belmont, CA 94002 Tel: 650-595-8588 FAX: 650-591-2891
www.acopacific.com acopac@acopacific.com

ACOustics Begins With ACO™

REDUCTION OF NOISE GENERATING FLOW FLUCTUATIONS IN HYDRAULIC SYSTEMS DRIVEN BY SWASH PLATE PUMPS THROUGH IMPROVED PORT PLATE DESIGN

M. Chikhalsouk and R.B. Bhat

Concordia University –Department of Mechanical and Industrial Engineering, Montreal, Quebec, H3G 1M8;

INTRODUCTION

Flow fluctuations in hydraulic systems driven by swash plate pumps generate noise. A swash plate pump contains a finite number of pistons arranged in a cylinder block. Motion of each piston is separated by a phase difference of $(2\pi/9)$ Rad. The total pump flow is the sum of individual cylinder flows. An improved port plate design is proposed and analyzed for the pump flow characteristics.

PUMP PERFORMANCE

The flow should rise gradually as the cylinder port and the port plate delivery slot overlap during the pump action, in order to avoid undesirable flow fluctuations [1]. Delivery stroke starts when the piston is at its top dead center and ends when it is at its bottom dead center. The second stroke of the cylinder cycle is the suction stroke at which the cylinder does not contribute in generating fluid flow. Bernoulli principle is used to characterize the mathematical relationship between the cylinder delivery pressure and the corresponding flow rate. By considering a stream line path, which starts when the stream leaves the cylinder delivery port and ends at the port plate delivery slot, the cylinder delivery pressure, its flow rate and the porting area are considered and studied. The cylinder pressure variation with time can be given as

$$p_k(\phi) = \frac{B}{V_{ck}(\phi)} Q_k(\phi) \quad (1)$$

where

$$Q_k(\phi) = \text{sign}(p_k - p_d) c_d A_d \sqrt{\frac{2}{\rho} |p_k - p_d|} \quad (2)$$

$$V_{ck}(\phi) = A_p (0.5I_c + c_t \cos(\phi)) \quad (3)$$

$$A_d = 2[\pi r_d^2 \theta_1 - (0.5h_1 b_1)] + \left[\frac{h_g b_g}{2}\right] \quad (4)$$

Eq. (1), (2), (3) and (4) represent the cylinder delivery pressure change rate, cylinder delivery flow rate, cylinder fluid volume and the groove delivery area in the overlapping zone, respectively. Proper port plate design can lead to the best pump performance with minimum flow fluctuations.

PORT PLATE

The pump has two kidney-shaped ports that control the fluid

traffic in/out the cylinder [2]. The current designs come with a shallow silencing groove or without groove. Fig. 1 shows the port plate general configuration. The delivery section was divided into 5 zones. The pump flow rate and porting area are simulated and presented in Fig. 2 and 3, the dashed line corresponding to the conventional design. From the result of simulation, the design experiences pressure overshooting twice in the delivery stroke, where the overshooting leads to maximum flow fluctuation, which is the source of high levels of noise.

NEW PORT PLATE

The need to reduce, or eliminate the overshooting can be achieved at the design level. The current designs experience an overshooting. The overshooting occurs at the beginning and end of the overlapping zones. The proposed design suggests utilizing a pair of deep silencing grooves in the beginning and end of the slot. These grooves help in achieving a gradual rise in the pressure, where the pressure increases as the cylinder leaves its T.D.C. This design can grant the pressure more time to rise gradually and to reach the value of load without any overshooting. Also, the triangular shape of the groove helps in achieving a smooth transitional pressure.

Fig. 1 illustrates the general configuration of the new design, the dashed line showing the proposed silencing grooves. The simulation results are presented in Figs. 2 and 3, with the solid line. From Fig. 3, it is seen that the pump flow fluctuation decreases remarkably. This reduction will be reflected on noise levels of the hydraulic system resulting in a quieter hydraulic system.

DISCUSSION

It is clear that the new design can eliminate the pressure overshooting and the flow rate fluctuations. Further work is needed to assess the extent of noise level reduction with the introduction of the proposed silencing grooves.

REFERENCES

1. Khalil M., Bhat R. (2003), "Performance Investigation of the Swash Plate Axial Piston Pumps with Conical Cylinder Blocks", PhD thesis, Concordia University, Montreal, Canada.
2. Manring D and Yihong Z. (2001), "The Improved Volumetric-Efficiency of and Axial-piston Pump Utilizing a Trapped-Volume Design", *Journal of Dynamic Systems, Measurement, and Control*, Vol.123, pp. 479-488.

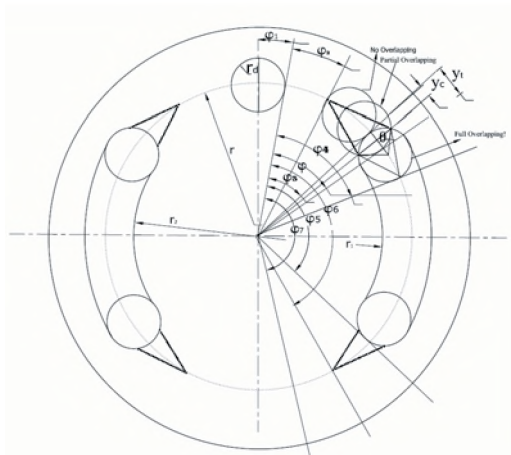


Fig. 1: General configuration for the port plate, (the dashed line for the groove, and the solid for the Non-groove plate)

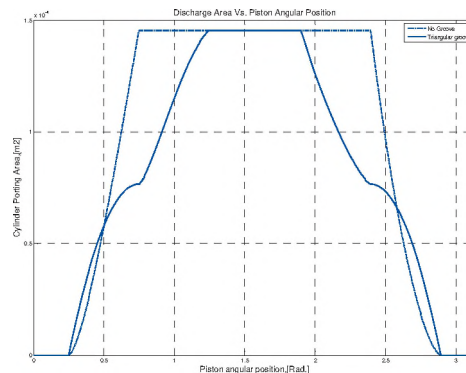


Fig. 2: Delivery area, dashed line for Non-groove and solid line for the new design

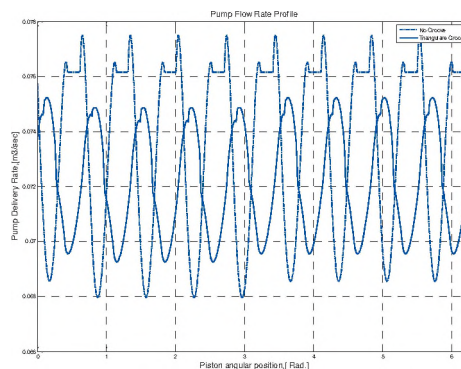
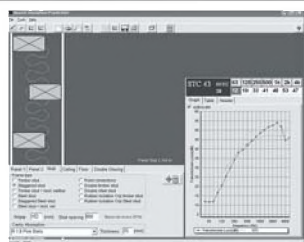


Fig. 3: Pump flow rate, dashed line for Non-groove and solid line for the new design



INSUL



INSUL is an easy to use software tool for predicting airborne sound insulation of simple or complex partitions consisting of various materials &

structural systems, floors and glazing and impact sound insulation of concrete floors. It can be used to quickly evaluate new materials and systems or to investigate the effects of changes to existing designs. (It models partitions using theoretical work of Sharp, Cremer and others.) Input is simple and intuitive with drop down menus and an on-screen picture of your construction.

Trial Version: www.navcon.com/insul.htm

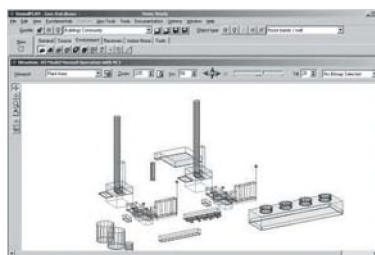
Navcon Engineering Network

Phone: 714-441-3488

Email: forschner@navcon.com



SoundPLAN



SoundPLAN is a graphics oriented noise prediction program used for noise planning, noise assessment & the development of noise mitigation measures. The database and management structure allows for a quick

& easy generation of variants for small & complex noise models (i.e., Road & Railroad Projects, Industrial Plants, Quarry & Mines Operation, Power Plants, Amusement Parks, Wind Farms, Manufacturing Buildings/Rooms & Enclosures).

SoundPLAN is based upon 30+ standards such as ISO 9613, Concawe, Nord2000, FHWA RD 77-108, TNM™2.5, FRA, VDI 3760. It generates traceable result tables and professional looking maps visualizing the input & output data. Noise Control & Optimization Tools include Noise Barrier Design and Industrial Noise Control Planning.

Please visit us www.navcon.com/soundplan.htm for more information. Occasional users please check out **SoundPLAN essential**.

Characterization of Sound Emitted by Wind Machines Used For Frost Control

Vince Gambino, B.A.Sc., P.Eng, Tony Gambino, Engineering Technician
Aercoustics Engineering Ltd., 50 Ronson Drive, Suite 165, Toronto, ON, Canada M9W 1B3

Hugh W. Fraser, M.Sc., P.Eng.
Ontario Ministry of Agriculture, Food & Rural Affairs, Box 8000, Vineland, ON L0R 2E0

Introduction

Wind machines are tall (~ 10m high), fixed-in-place, engine-driven fans that pull warm air down from high above ground during a strong thermal inversion¹, raising air temperatures around cold-sensitive crops such as grapes and tender fruits, thereby protecting crops from cold-injury. Fan diameters are typically about 5.4 m to 6.0 m and fan RPM ranges from 375 to 525. A single machine covers about 10 acres of crops as it rotates slowly over 360 degrees at a rate of about 4.5 to 6.5 minutes per revolution.



Figure 1: Typical wind machine in a vineyard

The number of wind machines has about double annually from a handful in the late 1990's to more than 425 in 2006². proliferation of wind machines has occurred mainly in Niagara-on-the-Lake's (NOTL) grape growing area has led to noise complaints: 'it sounds like a helicopter'; 'there's a droning-sound', 'it's a thumping-sound', 'my dishes are vibrating', and 'it is worse upstairs in the bedrooms'.

There are no environmental impact controls for wind machines in Ontario. Farmers are protected from nuisance complaints under Ontario's *Farming and Food Production Protection Act, 1998*, providing that the nuisance is created as a result of a normal farm practice. A 3-year applied research project commenced in November 2005 to establish best environmental management practices so the use of

wind machines would be limited to those times when absolutely needed to protect crops from damage. One part of this project entailed the characterization of the sound as discussed in this paper.

Noise Generation by Wind Machines

As the orientation of the fan changes, so does the sound pressure level at a fixed point in the far field. The expected pattern is illustrated in figure 2.

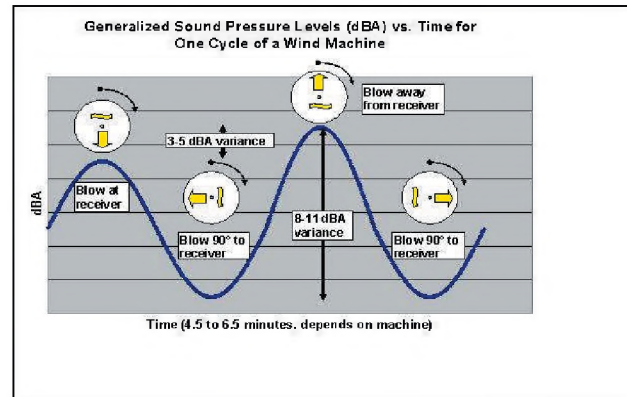


Figure 2: SPL vs. time over one rotation cycle

The sound levels vary in a sinusoidal fashion, the period being of the order of a few minutes; level changes of up to 11 dBA have been measured. The highest levels are observed when the machine blows away from the receiver. .

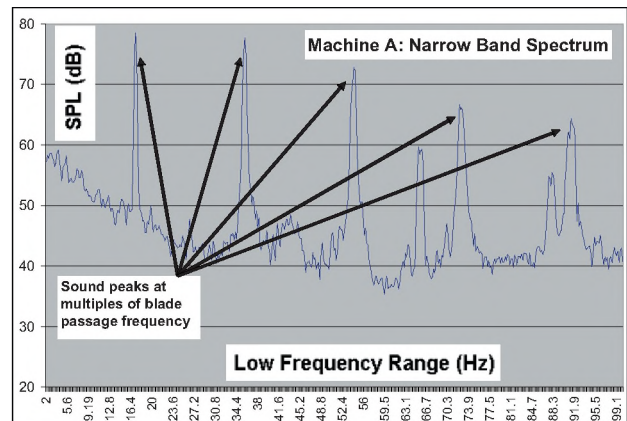


Figure 3: Narrow band spectrum of a wind machine.

The predominantly low frequency sounds can penetrate homes and excite a variety of acoustic-standing waves and structural-resonant modes within any given dwelling space. This may lead to annoyances that are at times perceived to be worse inside than outside^{3,4}.

Figure 4 shows the amplitude time history measured inside a dwelling⁵. The data is presented in with different weightings. A strong correlation is observed between the vibration velocity (as measured on an interior dwelling wall) and infrasound levels measured (dBG)⁶. In contrast, the dBA levels do not track the level changes with any degree of consistency.

Conclusions

A limited number of measurements have been conducted and it is clear that there is still much to be studied about the various operating scenarios under which this equipment is operated. However, the following conclusions can be drawn about wind machines.

- Noise from wind machines is due to both aerodynamic and mechanical effects, but aerodynamic sounds are deemed to be the most significant.
- There is evidence of low frequency blade slapping or impulsive sounds, during little to no winds (<5kph) and especially in the presence of mild to moderate ambient winds (5 to 10kph).
- The A-weighting descriptor has deficiencies in depicting noise from wind machines.

- Low frequency and infrasonic energy from wind machines is capable of exciting components such as floors, walls roofs and windows that comprise a building structure, thus causing increased annoyance potential.
- Perceptible infrasound is present at some receptors that are in proximity to wind machines.

References

1. Shaw, T. 2001. Final Report: Wind Machine Technology to Optimize Vineyard Conditions. Brock University, ON.
2. Fraser, H.W., K. Slingerland, H. Fisher, K. Ker, 2006. *Infosheet: Wind Machines for Protecting Grapes and Tender Fruit from Cold Injury*. Ontario Ministry of Agriculture, Food and Rural Affairs, 2006.
3. Shepherd, K.P. and H. Hubbard, 1990. *Physical Characteristics and Perception of Low Frequency Noise From Wind Turbines*. Noise Control Engineering Journal, Vol. 36, Number 1.
4. Hubbard, H. 1982. Noise Induced Vibration and Human Perception. Noise Control Engineering Journal.
5. Gambino, V., Gambino, T., Richarz W., Tremblay, D. Report, 2006: Preliminary Sound Level Measurements of Three Periodic Wind Machines. AERCOUSTICS Engineering Limited and Ontario Ministry of Agriculture, Food and Rural Affairs
6. ISO 7196: 1995. Acoustics-Frequency Weighting characteristics for infrasound measurements.

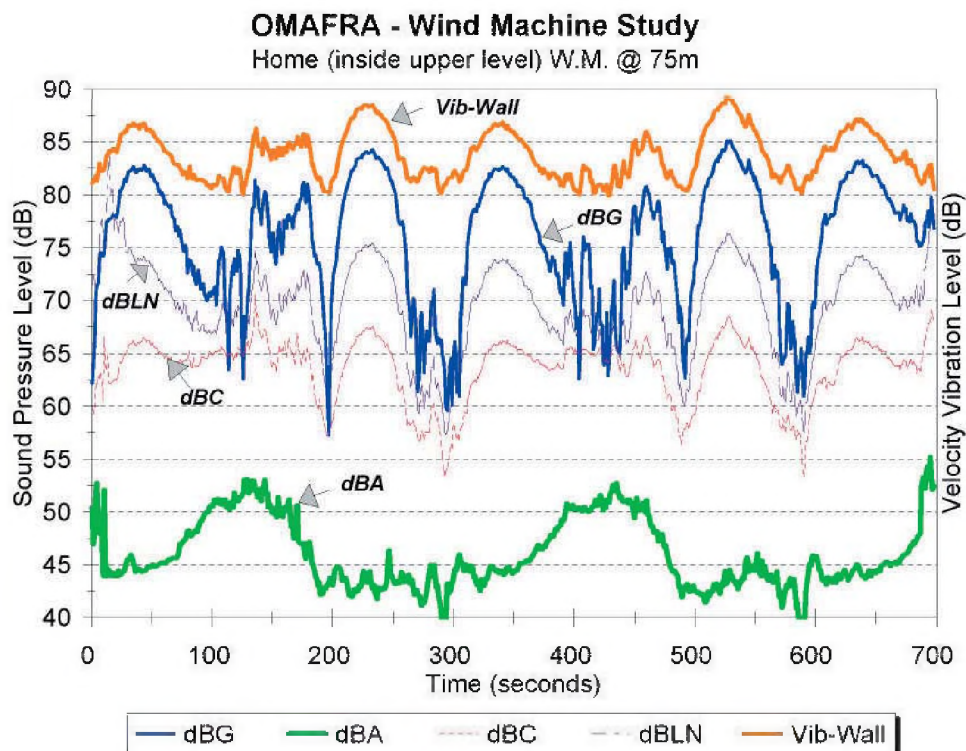


Figure 4: Weighted SPLs (A, C, G, Lin, & Vel.) vs. time over two cycles of a wind machine

WIND TURBINE NOISE AND METEOROLOGICAL INFLUENCES

Ramani Ramakrishnan¹ and Nicholas Sylvestre-Williams²

1. Ryerson University, Department of Architectural Science, 350 Victoria St.; Toronto, ON
2. Ryerson University, Department of Mechanical Engineering, 350 Victoria St.; Toronto, ON

INTRODUCTION

Wind turbines and wind farms produce power from the forces of wind. The prevailing wind, in addition, generates ambient sound levels that can mask the no-wind ambient sound levels. It has been argued that such masking may not be a real phenomenon and is influenced by meteorological wind classes. A simple analysis is presented based on a three-month wind conditions during the summer in a typical Ontario location.

NOISE IMPACT ASSESSMENT

The Ontario Ministry of the Environment (MOE) has implemented a very simple procedure to assess the noise impact of a wind farm, consisting of a group of wind turbines [1]. The process is: a) identify the locations of the wind turbines within the wind farm as well as all the sensitive receptors within an influence zone of 1 km; b) calculate the noise levels of the wind turbine from the posted sound power data of the turbine at each wind speed; c) the turbine sound power data is evaluated as per the IEC standard procedures and referenced to the 10 m high wind speed [2]; d) evaluate the noise levels at all identified receptor locations by using a standardized propagation model such as ISO-9613 Part II; e) establish the ambient sound levels at each 10 m high wind speed from the data provided in Reference 1; and f) establish the noise impact by comparing the sound levels established in Steps (d) and (e) above.

The procedure applied by MOE is simple in its intention and assumed neutral wind conditions. The procedures also allowed the potential masking effect of the prevailing wind noise. The above aspects provided an avenue for criticism based on the work of van Den Berg [3]. One of the main contentions of Reference 3 is that the IEC method of estimating power referenced to the 10 m high wind speed is flawed because the actual hub-high wind speed can be higher than predicted by the typical logarithmic wind profiles. The sound power levels of the turbines and thereby, the wind farm, can be higher than predicted during stable and very stable wind classes, a usual night time phenomenon. The wind speed measurements of Botha was conducted at four different sites and showed contradicting results of speeds with heights [4]. The wind speed variation with height is, therefore, strongly dependent on local terrain conditions. The assertive contention of van Den Berg was thus seen to be not valid for all locations even if the meteorology condition was in the very stable class. The field studies of Howe and McCabe showed large variations in receptor location noise levels [5].

The main conclusion evident from the results of the previous work is that the local conditions such as the terrain

variations, and wind directions have strong dominance on the resulting noise levels generated by wind farms. To investigate the influences of local conditions on the generated noises levels, a simple simulation study was conducted. The details of the model are described below.

MODELLING AND SIMULATION

A 10 km square area near Lake Huron was chosen for the simulation. The chosen location was within a km of an Environment Canada's weather station. Twenty-one wind turbines, capacity of 1.8 mW each, were spaced at 500 metres apart within the 10 sq.km wind farm. The noise levels at eight points of receptions from 500 m to 2 km distances from the wind farm boundary, four in the easterly direction and four in the northerly direction, were evaluated using the software, CADNA-A. A schematic detail of the wind farm with 21 turbines and 8 receptor locations is shown in Figure 1.

Meteorological data, wind speed and direction, were obtained as one-hour averages from the weather station, near the wind farm. The data is summarized in Figures 2 thru' 5. The wind rose data of Figure 2 shows that maximum speed levels were mostly from the lake (225°-NE; and 330° -SW) and the evening and night time average wind speeds are not substantially lower than the day-time wind speeds. The averaged wind speed for three summer months showed that local conditions in Ontario have preponderance of neutral classes compared to stable and very stable classes, disproving one of the main contentions of Reference 3.

The wind speed data for Ontario was adjusted using the results of Reference 4 for the flat terrain sites. The wind speed variation with heights for these two Australian sites didn't follow the IEC Standard's logarithmic wind profiles. The wind speeds at 10 m high were converted to a hub-height of 80 m (shown in Table 1A) and then reconverted back to the 10 m high wind speeds (Table 1B). The results show that at night time, it may be possible to have a higher than expected wind speeds at the hub, thereby generating more noise levels than expected.

Table 1. Wind Speed Data, m/sec. (References 2 and 4)

A) 80 m high wind speeds;

Wind Speed @ 10 m	4	8	12
Day	5.6	11.2	16.8
Night - IEC	5.6	11.2	16.8
Night - Botha	7.2	14.4	21.6

B) 10 m high wind speeds;

Wind Speed @ 80 m	7.2	14.4	21.6
Night - IEC	5.1	10.3	15.4
Night - Botha	4	8	12

The above wind speed changes indicate that for a typical 1.8 mW turbine the sound power levels can increase by .2 dBA at 4 m /sec, by 3 dBA at 8 m/sec and actually decreases at 12 m/sec speeds at 10 m height.

The noise level generated by the wind farm (21 turbines) at the eight locations were evaluated for four different wind conditions: A – all downwind propagation; B- wind is from the west; C – wind is from 225°; and D – wind is from 330°. The results are presented in Table 2 for one north and one east receptor respectively. The results show that noise level variations of ± 5 dBA can be expected depending on the local meteorological conditions.

Table 2. Noise Levels at Point of Reception, dBA

Condition and Wind Speed @ 10 m	4 m/sec	8 m/sec	12 m/sec
A - East – 500 m	40.8 dBA	46.7 dBA	47.6 dBA
A - North -500 m	40.0 dBA	45.9 dBA	46.8 dBA
B - East – 500 m	45.7 dBA	46.7 dBA	52.9 dBA
B - North -500 m	41.2 dBA	45.9 dBA	48.4 dBA
C - East – 500 m	44.8 dBA	51.2 dBA	52.0 dBA
C - North -500 m	44.8 dBA	50.7 dBA	51.5 dBA
D - East – 500 m	44.3 dBA	50.8 dBA	51.6 dBA
D - North -500 m	34.2 dBA	40.1 dBA	40.5 dBA

SUMMARY AND CONCLUSIONS

Simple simulation model applying local meteorological conditions to a typical wind farm was generated to evaluate point of reception noise levels. The results show that local conditions do not follow any set patterns and there can be substantial variations in evaluated noise levels.

REFERENCES

1. Ministry of the Environment, “Interpretation for Applying MOE NPC Technical Publications to Wind Turbine Generators.” PIBS 4709e, 6 July, 2004.
2. International Standard, IEC 61400-11. “Wind Turbine Generator Systems – Part 11: Acoustic Noise Measurement Techniques.” Edition 2.1, 2006-11.
3. G.P. van den Berg, “The Sounds of High Winds: the effect of atmospheric stability on wind turbine sound and microphone noise.” Doctoral dissertation, University of Goringern, Netherlands, May 2006.
4. P. Botha, “The Use of 10 m Wind Speed Measurements in the Assessment of Wind Farm Developments.” Proceedings of Wind Turbine Noise 2005, Berlin, October 2005.
5. B. Howe and N. McCabe, “Assessment of Noise and Infrasound at the Pubnico Point Wind-Energy Facility, Nova Scotia.” Proceedings of 2007 Spring Conference on Environmental and Occupational Noise, Banff, Alberta, May 2007.

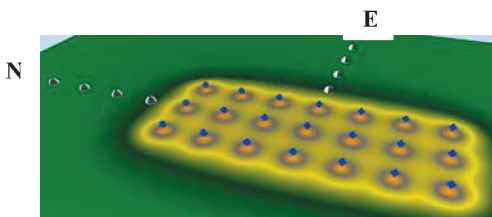


Figure 1. Wind Farm Model – Blue marks 1.8 mW turbine; Black arrow – receptor locations 500 m apart.

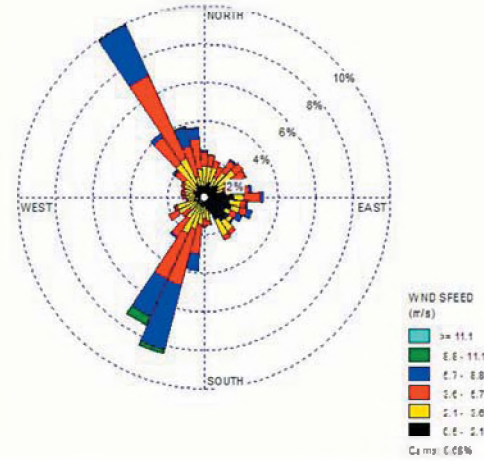


Figure 2. Wind Rose Data of the 10 m high wind speed over three months.

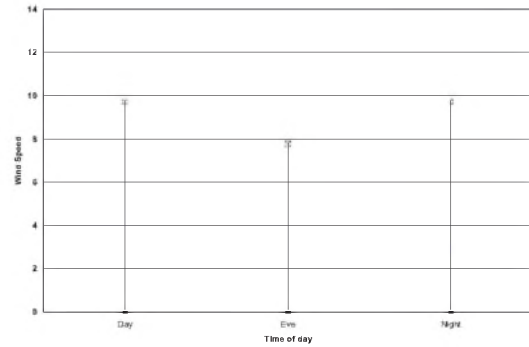


Figure 3. Wind Speed Data at 10 m high for June 2006.

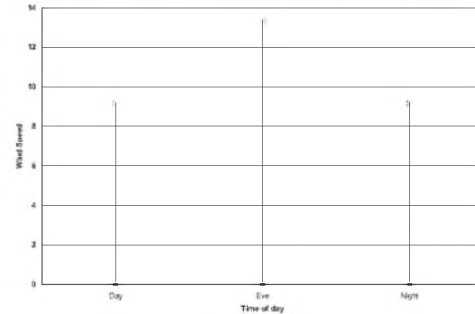


Figure 4. Wind Speed Data at 10 m high for July 2006.

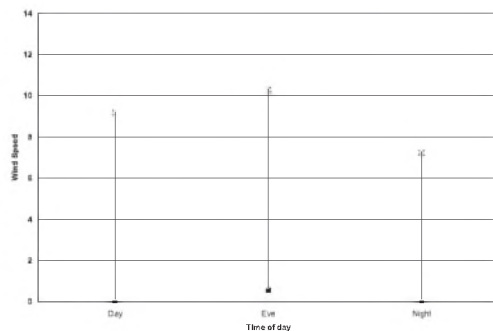


Figure 5. Wind Speed Data at 10 m high for August 2006.

IMPULSE NOISE EXPOSURE DURING PERSONAL WEAPONS TESTING ON AN OUTDOOR SHOOTING RANGE

Ann Nakashima and Yushi Hu

Defence Research and Development Canada – Toronto, 1133 Sheppard Ave West, Toronto, ON, M3M 3B9
ann.nakashima@drdc-rddc.gc.ca

1. INTRODUCTION

High-level impulse noise from firearms and blasts are a concern in military operations. Although the auditory hazard due to impulse noise exposure has been investigated extensively by many research groups, there are still differences between the criteria listed by different governing bodies. The Occupational Health and Safety Administration (OSHA) states that impulsive or impact noise exposure shall not exceed 140 dB peak sound pressure level. Other standards use the 8-hour integrated average of the A-weighted sound pressure level, Leq8, which is applied the same way for continuous and impulsive noise (e.g. ISO 1999). The Canada Labour Code limit for Leq8 is 87 dBA (MOL, 1991). There has been considerable research on temporary hearing threshold shift (TTS) immediately after exposure to a noise impulse or a series of impulses. Exposure limits based on the TTS have also been proposed (NATO, 2003). It is often not practical to take these measurements in practice, because it would require unoccluded exposures to high noise levels.

Canadian Forces (CF) army members, or any CF personnel who are being deployed overseas, are required to complete weapons qualifications, called Personal Weapons Tests (PWT). The noise exposure will be different for the shooters, the personnel in the butts (the shielded area from which the targets are raised and lowered), and the Range Safety Officer (RSO). It was of interest to measure the noise levels on the range at the firing line and in the butts to estimate the exposure levels for all range personnel.

2. METHOD

2.1 Description of the Personal Weapons Tests

Measurements were taken on two occasions over three days of personal weapons testing at Canadian Forces Base Borden (CFB Borden) in May 2007. The shooters performed PWT 1 and 2 using the C7 service rifle and 9 mm service pistol. PWT 1 for the rifle involves shooting at a target in the prone, kneeling, sitting and standing positions at a distance of 100m. In PWT 2, rapid and snap shooting (target exposure is time-limited) are tested at 200m. For the pistol, PWT 1 tests shooting from 15m in the standing position, and PWT 2 tests shooting from 15, 20 and 25m in the standing, kneeling and sitting positions. To pass the tests, shooters must achieve a minimum grouping on the target (pattern created by firing numerous bullets at the same point of aim on a target).

2.2 Measurement Procedure

Measurements were taken using a Larson Davis LxT sound level meter with a high pressure microphone at the firing line, and a Quest 1900 sound level meter in the butts. Digital recordings were also made with Sony PCM-M1 portable digital audio tape (DAT) recorders. Separate recordings were taken for each application of each test. The length of time required for each application was generally between 60 and 90 seconds for the rifle and between 30 and 60 seconds for the pistol. Between each application, there were less noisy periods while the butts personnel scored the groupings and the shooters received their instructions.

On the first day of testing, measurements were taken of one group of five shooters who performed PWT 1 and 2 for both the C7 rifle, and six shooters for the 9 mm pistol. The measurements were taken a few meters behind the shooters on the firing line (where the RSO stands), and in the butts. The tests took approximately 4.5 hours in total to complete. On the third day of testing, measurements were taken of one group of four and one group of five shooters who performed PWT 1 and 2 for the rifle only; this took approximately 3 hours. Measurements were taken approximately 30 cm from the ear of one of the shooters, and in the butts. Because the shooters wore the provided earplugs, it was not possible to take in-ear measurements.

3. RESULTS

Sample C7 rifle data for one of the PWT 1 applications are shown in Table 1 for the shooter, RSO, and butts. During this application, each of the five shooters fired five rounds in the standing position at a distance of 100m from the target. For the "Shooter" data, the microphone was held approximately 30 cm from the head of the shooter. The exposure time during this application was approximately one minute. In all cases, the peak levels exceeded the 140 dB OSHA limit for unprotected exposure to impulses. The time signal and 1/3 octave band spectrum for this application are shown in Figures 1 and 2, respectively.

Table 1. Sample data for the C7 rifle during a PWT 1 application (five rounds fired from 100 m)

	Leq (dBA)	Lpeak (dB SPL)
RSO	104.2	148.3
Shooter	112.9	154.7
Butts	90.2	140.8

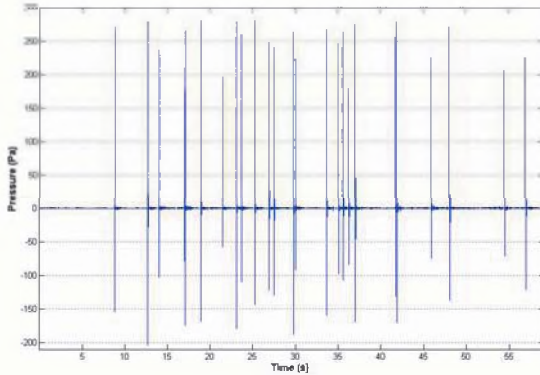


Figure 1. Time signal of a PWT 1 application using the C7 rifle.

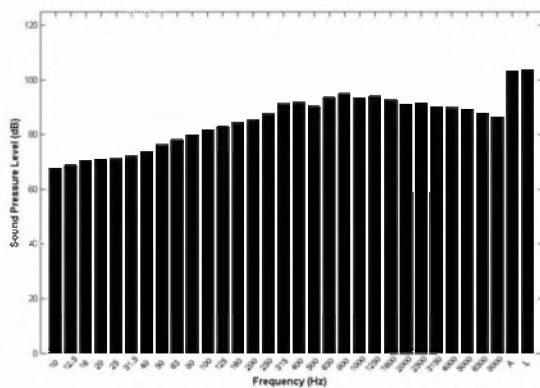


Figure 2. 1/3 octave band spectrum of a PWT 1 application using the C7 rifle.

Sample data for the 9 mm pistol during a PWT 1 application (six shooters), in which 10 rounds were fired from a distance of 15 m from the target, are shown in Table 2. The exposure time for this application was approximately 45 seconds. The peak levels for the RSO and shooter were similar to those of the rifle, and exceeded the 140 dB OSHA limit. The peak level in the butts was below the limit at 134.5 dB.

Table 2. Sample data for the 9 mm pistol during a PWT 1 application (10 rounds fired from 15 m)

	Leq (dBA)	Lpeak (dB SPL)
RSO	101.0	148.4
Shooter	111.5	155.6
Butts	96.1	134.5

Of the 4.5 hours of testing that were observed on the first day, there was approximately 37 min of shooting. The Leq for the RSO during that 37 min was 106 dBA, or approximately 97 dBA over 4.5 hours. For the shooters on the third day of testing, the Leq for the 26 min of shooting was 113 dBA, or 104 dBA over 3 hours. In the butts, the Leq for the shooting time was 94 dBA, or 85 dBA over 3

hours. The exposures for the RSO and the shooters were well above the Leq8 limit of 87 dBA using the 3 dB exchange rate.

4. DISCUSSION

It is difficult to assess the noise hazard on a live fire range without disturbing operations. In particular, it was not possible to take TTS measurements immediately after each application, nor was it possible to take in-ear noise measurements underneath the earplugs that were provided to the range personnel. Noise dosimeters do not have the capability to capture impulse noise, and thus will tend to underestimate the noise exposure. Since the RSO, shooters and butts personnel were all exposed to noise impulses in excess of 140 dB, hearing protection would have been required according to the OSHA standard. However, according to the Canada Labour Code limit of 87 dBA for Leq8, and using the 3 dB exchange rate, hearing protection would not have been required for the butts personnel.

It was observed that some of the range personnel inserted their earplugs improperly due to lack of training, or intentionally so that they can better hear the RSO. The reduced attenuation due to improper insertion may not be sufficient to reduce the noise exposure to safe levels (Abel et al, 1982). One possible solution is to use non-linear earplugs which allow natural listening for non-hazardous noises (i.e., speech), but provide attenuation for high-level impulses.

REFERENCES

- Abel, SM, Alberti, PW and Riko, K (1982). "User fitting of hearing protectors: Attenuation results," in Personal Hearing Protection in Industry, edited by PW Alberti (Raven, New York) pp. 315-322.
- ISO 1999 (1990). Acoustics – Determination of occupational noise exposure and estimation of noise-induced hearing impairment.
- MOL (1991). "Canada Labour Code, Part VII, Levels of sound." Canada Occupational and Safety Regulations, Ministry of Labour, Ottawa, ON.
- NATO (2003). Reconsideration of the effects of impulse noise. RTO Human Factors and Medicine Panel, Technical Report TR-017.

ACKNOWLEDGEMENTS

The authors wish to thank Capt Eric Drolet of the Canadian Forces Environmental Medical Establishment (CFEME) and the CFEME personnel who participated in the range exercises for their support and co-operation during the measurements.

THE SOUND THAT VORTICES WITHIN VORTICES MAKE

Georgios H. Vatistas

Dept. of Mechanical and Industrial Engineering, Concordia University, Montreal, Quebec, Canada, H3G 1M8

1. INTRODUCTION

Vortices being interwoven into the fabric of fluid mechanics appear in the majority of naturally occurring and industrial flows. In technology these are either produced deliberately to accomplish the task, improve the function of devices, or emerge as a parasitic bi-product of fluid motion. As they are transported by the main flow, they may deform, impinge on solid surfaces, or interact with other vortices producing sound. Because of this they are often called the voice of fluid motion. In the greater part of situations their presence in the flow produce vibrations and noise and the designer strives to suppress them.

Vortex-body interaction has been in the forefront of aeroacoustic research for many years. Most of the contributions consider vortices of the zero-circulation Taylor's type. Much less is however known about the noise generated by deforming intense vortices. Recently, several contributions¹⁻³ appeared in the technical literature with respect to the acoustics produced by non-zero circulation, intense, concentrated vortices (most of the vorticity resides within the core) like the $n = 2$ model⁴.

Another important vortex manifestation that appears to have been neglected in aeroacoustical research is noise produced by interacting satellite vortices that are known to spawn inside a parent vortex. The present paper focuses on this feature.

Humans have noticed since the ancient times that domesticated and wild animals change dramatically their behavior in front of an impending disaster, such as severe storms like hurricanes and tornadoes. Is subaudible sound the messenger of the imminent danger? In 1996, Bedard from NOAA Boulder Colorado, while assessing some sensitive microphones detected a low frequency sound emanating from an unknown source. With the aid of radar, he located the presence of some tornadoes in the area. Tracking them down he discovered that their location appeared to correspond to the site of the detected infrasound. In a relatively recent article⁵, Bedard has attributed the unusual acoustical manifestation to waves produced inside the vortex cores. In antithesis to the ~ 60 km range of a tornado-warning radar system, the detection limit via the new infrasound device could now exceed 100 km. Alike to the noise produced in vortex chambers the experiments performed in a laboratory simulated tornado revealed that the sounds produced were pretty irritating. Is this sound quality that makes the animals to be agitated and aware of the impending danger?

The aim of this paper is to brief the acoustical community about some new developments in vortex dynamics (particularly on satellite vortices/waves inside a parent vortex) that are relevant to the sound produced by intense concentrated eddies.

2. VORTICES/WAVES

2.1 The polygonal core shapes of whirlpools

Past experimental studies⁶ have shown that under prevailing conditions, waves on the free surface of a liquid vortex produced in the apparatus shown in Fig. 1, exhibit the fundamental characteristics of Kelvin's equilibrium patterns. The rotary motion imparted to the fluid by the disk, generates a centrifugal force field, which pushes the liquid towards the container's wall. The receding liquid exposes part of the surface of the disk to air whereby, the line of intersection between the surfaces of the solid disk, the liquid, and air outlines the core shape. In order to bring the patterns into relief, the liquid was colored with a blue water-soluble dye. For very low rotational disk speeds it is expected that the water vortex core remains circular expanding and contracting in time ($n = 0$, breathing mode). Increasing its rotation, the vortex transfers into another state characterized by a precessing circular core ($n = 1$). A further increase of disk speed (ω_d) yields progressively cores with elliptical ($n = 2$), triangular ($n = 3$), square ($n = 4$), pentagonal ($n = 5$), and hexagonal ($n = 6$) shapes, see Fig. 2. No heptagonal shape was formed. Since the interval of

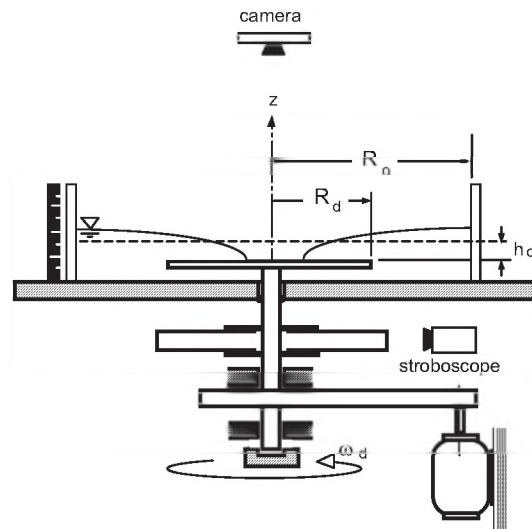


Figure 1. The experimental apparatus.

endurance of the stationary states decreases with n , if $n = 7$ exists in theory it must be critically stable. As the disk speed increases well beyond $n = 6$ amplification of dynamical noise will eventually wipe out the sharp spectral peaks.

The source of the waves appearing on the liquid interface has been now attributed to the presence of revolving satellite vortices, which give the event a dual wave/vortex nature.

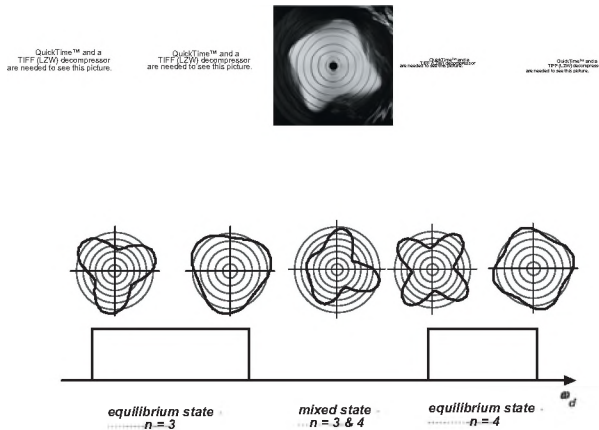


Figure 2. Spectrum of core patterns.

2.2 The solitron

The solitary wave in rotation (or solitron) experiments were conducted in a transparent cylindrical reservoir having a circular outlet, fixed on the bottom plate. The wave of Fig. 3 appeared as the liquid level dropped to a specific height. Among some other interesting things we now find that the evolution of the cylindrical soliton depends strongly on the original residual vorticity of the liquid inside the tank. Furthermore, the height of the single interfacial wave increases if a jolt is applied to the container along the lateral direction prior to the wave development.

QuickTime™ and a
TIFF (LZW) decompressor
are needed to see this picture.

Figure 3. The solitary wave.

2.2 The resonating vortex

Our tests have also revealed that in tall vortices and for certain disk speeds a spectacular episode appeared. Initially the core was relatively calm having the expected inverted bell-like shape and an almost circular interfacial surface in every elevation. Past this stage, the vortex started to form in time polygons of different shapes on the disk surface in an indiscernible manner but giving the impression that it was searching in vain to find a stationary state. Failing to do so, a good portion of the core transformed into an elliptical cross-sectional form, and the liquid surface began to undulate. The minor axis of the ellipse was then shortened and the major was elongated while the free-surface sloshing behavior intensified. Finally, the free liquid surface was pinched near the center of rotation forming two vortices. Subsequently, the eddy was destroyed and the liquid interface returned to its initial calm condition. This phenomenon was repeated without any external stimulus. These experiments reveal that the phenomenon is highly sensitive to spin history, see Fig. 4. Given the disk speed the

sloshing only happens within a specific interval of initial liquid heights.

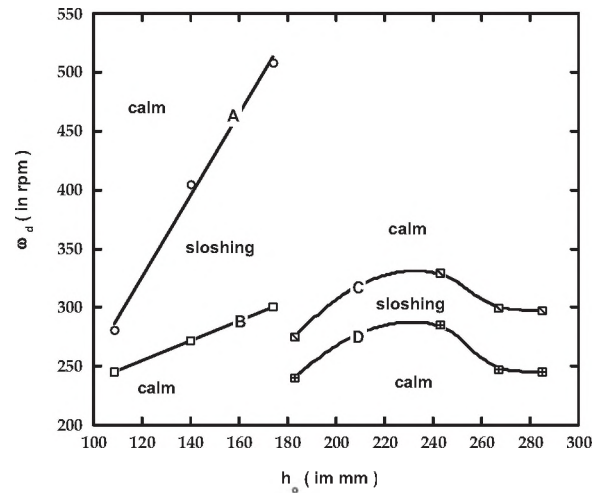


Figure 4. Spectrum of resonance.

3. CONCLUSIONS

Several vortex/wave phenomena, pertinent to the sound produced by intense, concentrated, vortices, were described. Hopefully, this presentation will capture the interest of the acoustical community so that by incorporating these effects into the current aeroacoustical simulations, it will yield an adequate insight into a phenomenon, which is of significance to science and technology.

REFERENCES

- Povitsky, A., Zheng, T.H., and Vatisias, G.H. "Effect of vortex profile on sound generation in a non-uniform flow", *Math. Comput. Simulat.*, **65** (4-5): 447-468 (2004).
- Casey L. Burley, et al. "Rotor wake vortex definition—evaluation of 3-C PIV results of the HART-II study", *Aeroacoustics*, **5** (1): 1-38 (2006).
- Zheng, T. H., Vatisias, G.H., and Povitsky, A. "Sound generation by a street of vortices in a nonuniform flow", *Phys. Fluids* **19**: 037103 (2007).
- Vatisias, G.H., Kozel, V. and Minh, W. "A Simpler model for concentrated vortices" *Exp. Fluids*, **11** (1): 73-76 (1991).
- Bedard Jr., A. J. "Low-Frequency Atmospheric Acoustic Energy Associated with Vortices Produced by Thunderstorms", *Month. Weather Rev.*, **133**: 241- 263 (2005).
- Vatisias, G.H. "A Note on Liquid Vortex Sloshing and Kelvin's Equilibria". *J. Fluid Mech.* **217**, 241-248 (1990).

AN INDEX OF HETEROGENEITY OF SOUND ABSORBING POROUS MATERIALS

Yacoubou SALISSOU and Raymond PANNETON

GAUS, Department of mechanical engineering, Université de Sherbrooke, Québec, Canada, J1K 2R1

Yacoubou.Salissou@USherbrooke.ca, Raymond.Panneton@USherbrooke.ca

1. INTRODUCTION

Important intrinsic properties of a sound absorbing porous material are its characteristic impedance, complex wave number, dynamic density, and dynamic bulk modulus. The latter two dynamic properties are of utmost importance when modeling a porous material as an equivalent fluid. Acoustical methods have been developed for measuring these dynamic properties. The traditional standing wave method¹ was the first proposed. Nowadays, the two-cavity method by Utsuno *et al.*², the three-microphone method by Iwase *et al.*³, and the transfer matrix method by Song and Bolton⁴ are commonly used. However, some issues remain unsolved. In fact, all the aforementioned methods assume through-thickness homogeneity (TTH or symmetry) of the porous medium. Unfortunately, there exists no mean of quantifying simply the TTH of porous material.

In this paper, an index of heterogeneity is worked out and discussed. The calculation of this TTH index only requires impedance tube measurements (ASTM E1050, ISO 10534) of the acoustical surface impedance on both faces of the tested material backed by the rigid termination of the tube. To verify the validity of this TTH index, a two-layer rigid frame porous system representing a single porous layer with a sudden change in its physical properties is studied. Following the two-cavity method, the sound absorption coefficient, complex wave number, and characteristic impedance of this equivalent single layer are computed in the normal and inverted positions (i.e., when both sides of the material are facing successively the incident wave).

2. WHY AN INDEX OF HETEROGENEITY?

We restrict our analysis to the potential impact of the TTH on the normal acoustical surface impedance. The analysis may easily be extended to other bulk properties. For the composite material shown in Fig. 1, let Z_{AB} be the normal acoustic surface impedance of the composite layer backed by a rigid wall with side A facing the incident sound wave, and Z_{BA} the normal acoustic surface impedance when side B is facing the incident sound wave. For a homogeneous medium, Z_{AB} is equal to Z_{BA} ; *a priori*, this is not the case for a heterogeneous medium. The question arising from this is, *where does homogeneity stop?*

Let us consider three motionless frame porous composite samples, each made up as shown in Fig. 1. The Johnson-Lafarge macroscopic parameters^{5,6} and the dimensions of

Table 1: Foam parameters used for the composite samples

Property (symbol)	Foam1	Foam2	Foam3	Foam4	Units
Porosity (Φ)	0.97	0.96	0.90	0.99	
Static airflow resistivity (σ)	87 000	86 900	15843	10 900	Ns/m ⁴
Tortuosity (α_∞)	2.52	2.32	1.32	1.02	
Viscous characteristic length (Λ)	37	29	83	100	μm
Thermal characteristic length (Λ')	119	112	132	130	μm
Static thermal permeability (k'_e)	0.004	0.003	0.002	0.002	mm ²
Thickness	25	15	10	50	mm

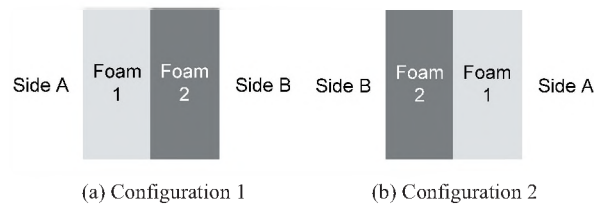


Figure 1: Composite porous sample made up from two porous layers. (a) Configuration 1 or “Normal configuration” when side A is facing the incident sound wave. (b) Configuration 2 or “inverted configuration” when side B is facing the incident sound wave

the foams used in the composites are given in Table 1. The three samples S1, S2 and S3 are respectively made from foam1/foam2, foam3/foam4, and foam1/foam4. The bulk dynamic properties of these samples have been simulated using the two-cavity method. Simulations were made for both normal and inverted configurations. From results shown in Figs. 2 and 3, it is obvious that sample 3 is heterogeneous, and sample 1 homogeneous (sample 1 is not shown since results for both configurations overlap). On the other hand, the answer is less obvious for sample 2. Indeed, comparing its absorption coefficients suggests assuming this material homogeneous. However, characteristic impedance curves seem to yield different conclusion, considering their deviations.

3. AN INDEX OF HETEROGENEITY

The heterogeneity of a material can be quantified by the average relative standard deviation (ARSD) of a bulk property measured respectively in both normal and inverted configurations. For a bulk property P , the ARSD writes,

Table 2: Bulk property ARSDs of the three composite samples

	Sample 1	Sample 2	Sample 3
ΔZ_s (%)	2.61	16.65	59.01
ΔZ_c (%)	2.60	15.63	58.89
Δk (%)	0.84	7.03	19.69
$\Delta \alpha$ (%)	1.02	2.15	19.72

Table 3: Range of foam parameters for the 50 composite samples

Property (symbol)	Range of values	Units
Porosity (Φ)	0.7-0.99	
Static airflow resistivity (σ)	1000-499000	Ns/m ⁴
Tortuosity (α_∞)	1.01-2.99	
Viscous characteristic length (Λ)	14-300	μm
Thermal characteristic length (Λ')	50-500	μm
Static thermal permeability (k'_o)	0.002-0.01	mm ²
Thickness	10-50	mm

$$\Delta P = \min \left[\frac{1}{n} \sum_{i=1}^n \left| \text{abs} \left(\frac{P_{\text{ref}}(\omega_i)}{P_{AB}(\omega_i)} \right) - 1 \right|; \frac{1}{n} \sum_{i=1}^n \left| \text{abs} \left(\frac{P_{BA}(\omega_i)}{P_{AB}(\omega_i)} \right) - 1 \right| \right]$$

P_{AB} and P_{BA} are the measured bulk property P when side A and B of the composite are facing the incident sound wave respectively, and ω_i is the i^{th} frequency. The ARSD values range between 0 (for ideal homogeneous material) and 1.

Table 2 gives the various bulk property ARSDs for the three composite samples (ΔZ_s for the surface impedance, $\Delta \alpha$ for the absorption coefficient, ΔZ_c for the characteristic impedance, and Δk for the complex wave number). From these results, it seems the ARSD is a good basis for a TTH index due to its sensitivity to heterogeneity.

In order to identify the most sensitive bulk property to TTH, we have computed the ARSD of the three latter bulk properties as a function of the one for the surface impedance for 50 different composites. The composites were made up from a combination of two foams having macroscopic parameters randomly selected in the ranges listed in Table 3. From Fig. 4, the ARSDs of the surface impedance and characteristic impedance seem to be equal. Moreover, these properties appear to be more sensitive to the heterogeneity of the material. Hence, the surface impedance ARSD is a good TTH index. As a criterion of heterogeneity, a TTH index of 5% is suggested as the threshold for heterogeneity.

ACKNOWLEDGEMENTS

N.S.E.R.C., REGAL, and ALCAN supported this work.

REFERENCES

¹ Scott, Proc. Phys. Soc. London, 58, 358-368 (1946)
² Utsumo *et al.*, J. Acoust. Soc. Am., 86, 637-643 (1989)
³ Iwase *et al.*, Intersound 98, New Zealand. (1998)
⁴ Song and Bolton, J. Acoust. Soc. Am., 107, 1131-1152 (2000)
⁵ Johnson *et al.*, J. Fluid. Mech., 176, 379-402 (1987)
⁶ Lafarge *et al.*, J. Acoust. Soc. Am., 102, 1995-2006 (1997)

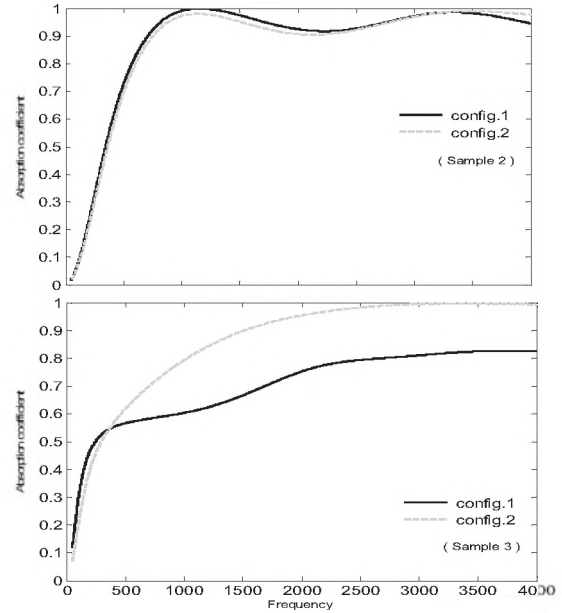


Fig. 2: Sound absorption coefficient of samples 2 and 3

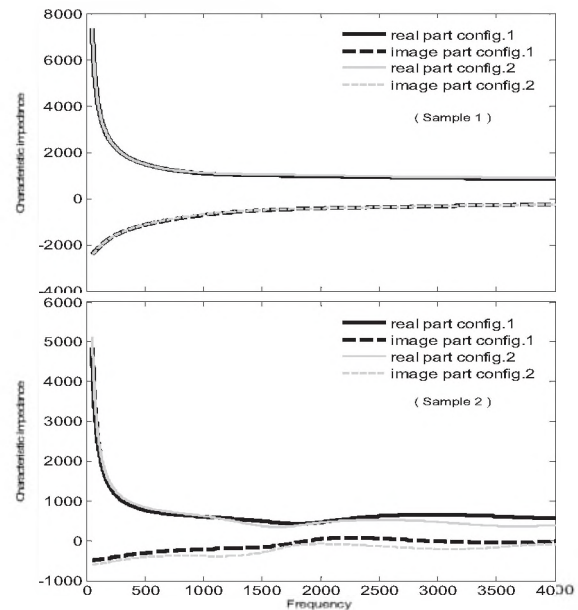


Fig. 3: Characteristic impedance of samples 1 and 2

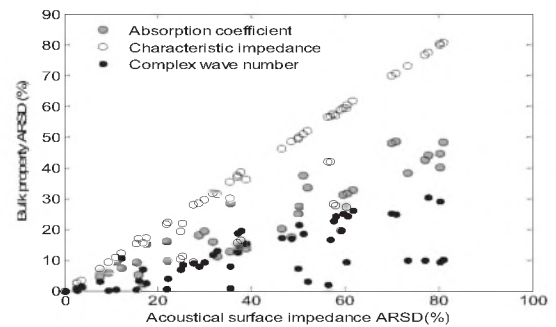


Fig. 4: Bulk property ARSD versus surface impedance ARSD

A NEW 3D FINITE ELEMENT FOR SANDWICH STRUCTURES WITH A VISCOELASTIC CORE

Kamel AMICHI and Noureddine ATALLA

¹Dept. of Mechanical Engineering, Université de Sherbrooke, 2500 Boulevard Université, Sherbrooke, Que., Canada J1K 2R1

1. INTRODUCTION

Nowadays, noise and vibrations control is a major concern in several industry fields such as aeronautics and automobile. The reduction of noise and vibrations is a major requirement for performance, sound quality and customer satisfaction. Passive damping technology using viscoelastic materials is classically used to control the vibration. The steel industry proposes damped sandwich panels with thin layer of viscoelastic core (Metal/Polymer/Metal). This type of structures has appeared recently as a viable alternative to classical add-on or spray-on treatments. It has been shown that this class of materials enables manufacturers to cut weight and cost while providing noise, vibration and harshness performance. This motivated the development of prediction methods for their vibration and acoustic indicators. Initially, analytical techniques were developed to predict the performance of damped sandwich panels with classical boundary conditions. The fundamental work in this field was pioneered by Ross, Kerwin and Ungar (RKU) [1] who used a three-layer model to predict damping in plates with constrained layer damping treatments. Kerwin [2] was the first to present a theoretical approach of damped thin structures with constrained viscoelastic layer. He presented the first analysis of the simply supported sandwich beam using a complex modulus to represent the viscoelastic core. Several authors (DiTaranto [3], Mead and Markus [4]) extended Kerwin's work using his same basic assumptions. Six-order equations of motion were developed in term of axial displacements by DiTaranto [3] for the unsymmetrical three-layer beam, and this was subsequently refined [4]. However, these analytical solutions are only appropriate for simple structures such as beams or plates with simple boundary conditions. In practice it is often necessary to design damped structures with complicated geometry, complex loadings and non-uniform features such as material discontinuities. Consequently, it is natural to consider the finite element method (FEM) to represent correctly the physics of such complicated problem. However existing finite elements methods necessitate the use of plate-solid-plate models which are computationally expensive.

In this paper a new sandwich finite element model has been developed. It allows for both symmetrical and unsymmetrical configurations. The rotational influence of the transversal shearing in the core on the skins behaviours, ensure a displacements consistency over the interfaces

between the viscoelastic core and the elastic skins; thus resulting in an accurate representations of the physics. Validation examples, consisting on sandwich structure with various geometrical and mechanical behaviours, have been conducted to demonstrate the validity and accuracy of the developed element to (i) estimate the modal resonances; (ii) the frequency response functions and (iii) the damping loss factors. Validations were performed versus both analytical and classical Finite elements models using MSC/Nastran® (Nastran).

2. FINITE ELEMENT FORMULATION

The displacement field of the skins is based on the Love-Kirchhoff's assumptions but is corrected to account for the rotational influence of the transversal shearing in the core. The Mindlin model is used to describe the displacement field of the core. The rotation effects of the transversal shearing in the core as well as the bending of the panel are described by the rotations γ_x and γ_y angles and the transversal displacement w .

The displacements fields of each of the three layers are written as follows:

$$\begin{cases} U_1 = U_{20} - z\theta_x + z_2\psi_x \\ V_1 = V_{20} - z\theta_y + z_2\psi_y \\ W_1 = W \end{cases} \begin{cases} U_2 = U_{20} - z\theta_x + z\psi_x \\ V_2 = V_{20} - z\theta_y + z\psi_y \\ W_2 = W \end{cases} \begin{cases} U_3 = U_{20} - z\theta_x + z_3\psi_x \\ V_3 = V_{20} - z\theta_y + z_3\psi_y \\ W_3 = W \end{cases}$$

Where the following notations are used:

$$\psi_x = \theta_x + \gamma_x \text{ and } \psi_y = \theta_y + \gamma_y$$

z_2 and z_3 are the distance between the reference axis and the lower and upper faces of the core, respectively..

The generalized displacements u is related to an elementary degrees of freedom vector q_e witch contain four degrees of freedom per node in the case of the beam and seven for the plate. In the latter case, these are the transverse displacement w , the two rotations of the face sheets θ_x and θ_y , the two rotations related to the transversal shearing in the core ψ_x and ψ_y and the in-plane displacements u_{20} and v_{20} of the middle planes of these face sheets. To account for the curvature, rotational degrees of freedom around the normal to the plan of the beam or plate are added. This result in nine degrees of freedom per node for both cases: u_{20} , v_{20} , w , θ_x , θ_y , θ_z , ψ_x , ψ_y , ψ_z .

3. RESULTS

3.1 Sandwich ring

A damped sandwich ring of axial length b and a single point load applied in the radial direction is investigated in this example. Figure 1 and table 1 gives the associated dimensions and material properties. In the following, indices 1 and 3 refer to the skins and 2 to the core.

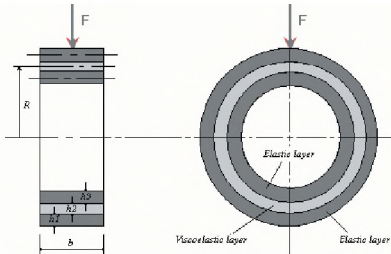


Fig. 1. Sandwich ring

Table 1. Ring's configurations and the material's properties used for the numerical validation

$R=0.1015835\text{m}$; $b=0.01\text{m}$; $h_1=h_3=1.52\text{mm}$; $h_2=0.127\text{mm}$			
$E_1 = E_3$ (Pa)	7.037×10^{10}	$E_2 = 7.037 \times 10^5$ (Pa)	
$\nu_1 = \nu_3$	0.3	ν_2	0.49
$\rho_1 = \rho_3$ (kg/m ³)	2770	ρ_2 (kg/m ³)	970
$\eta_1 = \eta_3$.0001	η_2	.3

Figure 2 resents the comparisons between the present finite element model and a classical finite elements model using Nastran. The Nastran model uses solid finite elements for the core and shell finite elements (with offset option) for the skins. Excellent agreement is observed. Both the resonance frequencies and the resonance amplitudes of the first six modes are accurately estimated.

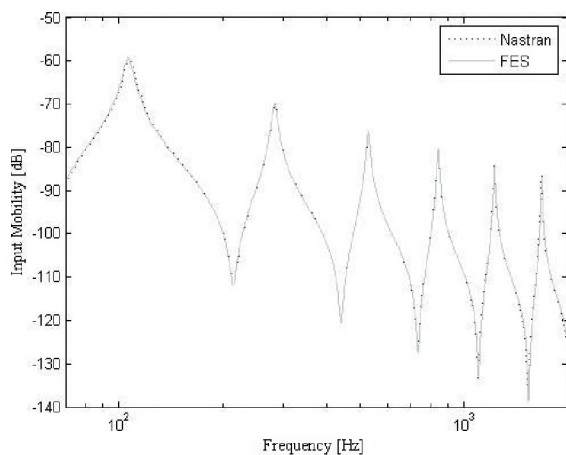


Fig. 2. Input mobility (dB) of a sandwich ring. Numerical validation: (—) finite element sandwich; (-----) Msc. Nastran

3.2 Simply supported sandwich plate

This section compares the modal frequencies of free vibration predicted by an existing analytical solution [5] and finite element method (Nastran) [6], to those predicted by the developed element for a simply supported sandwich plate with symmetric isotropic aluminium skins and a viscoelastic core. The complex shear modulus of the core is

assumed constant over the frequency range. The geometrical and physical parameters of the plate are presented in Table2

Table 2. Plate's configurations and the material's properties used for the numerical validation.

$L_x=304.8\text{mm}$; $L_y=348\text{mm}$; $h_1=h_3=0.762\text{mm}$; $h_2=0.254\text{mm}$			
$E_1 = E_3$ (Pa)	6.89×10^{10}	$E_2 = 2.67008 \times 10^6$ (Pa)	
$\nu_1 = \nu_3$	0.3	ν_2	0.49
$\rho_1 = \rho_3$ (kg/m ³)	2737	ρ_2 (kg/m ³)	999
$\eta_1 = \eta_3$.0	η_2	.5

Table 3. Comparison of natural frequencies and loss factors of a symmetric sandwich with isotropic face-plates.

	Analytical		Nastran (10x12 elements)		FES (10x12 elements)	
	f (Hz)	Eta	f (Hz)	Eta	f (Hz)	Eta
1	60.3	0.190	57.4	0.176	58.24	0.171
2	115.4	0.203	113.2	0.188	114.44	0.191
3	130.6	0.199	129.3	0.188	130.44	0.189
4	178.6	0.181	179.3	0.153	176.96	0.168
5	195.7	0.174	196.0	0.153	196.59	0.165

Compared to the analytical results, it is observed that the present finite element (FES) is more accurate than NASTRAN for the same number of elements. This is corroborated by other tests. Moreover, a substantial savings in computation time is achieved. However, current challenges, fir using the new element to model real life applications, concerns in its interface with classical plate and solid elements.

4. CONCLUSION

A new sandwich finite element for laminated steels has been introduced. It allows for both symmetrical and unsymmetrical configurations. Validation comparisons of the presented approach versus analytical and numerical methods were presented. These studies show that the proposed element sandwich is accurate for the modeling of the studied laminated steels.

REFERENCES

- [1] Ross D, Ungar EE, Kerwin EM. Damping of flexural vibrations by means of viscoelastic laminate. In: Structural Damping. New York: ASME, 1959.
- [2] Kerwin EM. Damping of flexural waves by a constrained viscoelastic layer. Journal of the Acoustic Society of America 1959; 31(7):952-62.
- [3] DiTaranto R. A. Theory of vibratory bending for elastic and viscoelastic layered finite length beams. Journal of Applied Mechanics 1965; 87: 881-886.
- [4] Mead D. J. and Markus S. The forced vibration of a three-layer, damped sandwich beam with arbitrary boundary conditions. Journal of Vibration and Acoustics 1969; 10(2):163-175.
- [5] Abdulhadi F. 'Transverse Vibrations of Laminated Plates With Viscoelastic Layer Damping'. Rochester, MN: IBM System Development Division, 1971.
- [6] Johnson CD, Kienholz DA. 'Finite element prediction of damping in structures with constrained viscoelastic layers'. AIAA Journal 1981; 20(9):1284-90.

INVERSE ACOUSTICAL CHARACTERIZATION OF POROUS MEDIA

Ali Hamoudi and Raymond Panneton

GAUS, Department of mechanical engineering, Université de Sherbrooke (Qc), Canada, J1K 2R1

1. INTRODUCTION

Porous materials constitute a practical solution for noise abatement in many mechanical engineering applications. For this reason, several models were developed to study their acoustic behavior. These models are based on the use of viscous and thermal macroscopic parameters linked to the morphology of the material.

In this research work, the six-parameter model by Johnson-Lafarge is used to describe the viscous and thermal dissipations of acoustic waves in the porous material. The model is especially well suited to study these dissipations in the high frequency range. The six macroscopic parameters of the model are: the open porosity (ϕ), the static airflow resistivity (σ), the tortuosity (α_∞), the viscous characteristic dimension (Λ), the thermal characteristic dimension (Λ'), and the static thermal permeability (k'_0). From this choice, the technological problem one is facing is how to measure these parameters.

Several methods have been developed in the past. One can refer to references 1 and 2 for a review. The main objective of this paper is to focus on the use of the acoustical inversion technique as introduced by one of the authors [2]. This technique is only based on measurements performed in an impedance tube following standard ASTM E1050. Compared to the previous study, this inversion is not limited to only three parameters. This time, we attempt to characterize the whole set of parameters of the model. Also, the sensitivity of the method to random noise during measurements is addressed with a view to determine a confidence level.

2. METHOD

2.1 Johnson-Lafarge equivalent fluid model

Under acoustical excitations, if the frame of the porous material is assumed motionless, then the material can be modeled as an equivalent fluid. Under harmonic excitations, the Helmholtz equation governs the propagation of the compression waves in this equivalent fluid. This equivalent fluid is described by its dynamic density and dynamic bulk modulus. Both dynamic properties are related to the macroscopic parameters of the material, and depend on the frequency of excitation. In the Johnson-Lafarge model [3,4], these dynamic properties write

$$\tilde{\rho} = \rho_0 \alpha_\infty \left(1 - j \frac{\sigma \phi}{\omega \rho_0 \alpha_\infty} \sqrt{1 + j \frac{4 \alpha_\infty^2 \eta \rho_0}{\sigma^2 \phi^2 \Lambda^2} \omega} \right)$$

and

$$\tilde{K} = \frac{\gamma P_0}{\gamma - (\gamma - 1) \left(1 - j \frac{8 \eta}{\omega \text{Pr} \Lambda'^2 \rho_0} \sqrt{1 + j \frac{\omega \text{Pr} \Lambda'^2 \rho_0}{16 \eta}} \right)^{-1}}$$

where ρ_0 , η , and γ are the density, viscosity, and specific heat ratio of the saturating air, Pr is the Prandtl number, and P_0 is the static pressure.

From these two dynamic properties, one can deduce the normal incidence acoustic surface impedance of a porous sample of thickness d by

$$Z_{sn}^{\text{model}} = -j \cdot \frac{\sqrt{\tilde{\rho} \tilde{K}}}{\phi} \cdot \cot \left(\omega \sqrt{\frac{\tilde{\rho}}{\tilde{K}}} d \right).$$

2.2 Inverse technique of characterization

The characterization following the proposed inverse technique consists in computing the difference (or residual) between the experimental data and the data predicted by the model. Then, the unknown macroscopic parameters are adjusted so that the residual is minimized.

Consequently, the difficulty of the problem is to correctly minimize the following residual function by using an algorithm of descent:

$$R(\mathbf{X}) = Z_{sn}^{\text{model}}(\mathbf{X}) - Z_{sn}$$

with

$$\mathbf{X} = \{ \phi, \sigma, \alpha_\infty, \Lambda, \Lambda', k'_0 \}$$

In a first time, R is linearized around an initial point \mathbf{X}_0 thanks to the first order Taylor formula. Defining the jacobian matrix of R by H , this yields:

$$R(\mathbf{X}) = R(\mathbf{X}_0) + \mathbf{H} \times d\mathbf{X}$$

By solving this equation, $d\mathbf{X}$ is found, and a new point is deduced. The operation is repeated until $d\mathbf{X}$ tends to zero - this corresponds to a minimum of R , and to the corresponding set of parameters.

3. RESULTS

Initially, the strategy to test the inverse method was not considering noise in the measurement of Z_{sn} . In this noiseless case, the results were very conclusive for a broad range of materials. The range of the material properties are given in Table 1.

When random noise is considered in Z_{sn} , the conclusion is different for some materials. The most important impact of noise on the inversely found parameters occurs for the thermal characteristic length. This parameter was found to be very sensitive to noise, more especially when its true value is large. This is shown in Figure 1, where the error on the found Λ' is plotted in function of the error on Z_{sn} for different values of Λ' . One can note the inversion procedure yields a larger error (always underestimate) on Λ' as the error on Z_{sn} increases. This error increases much more rapidly than the error on Z_{sn} and as Λ' is larger.

4. DISCUSSION

From Figure 1, one can conclude that it may be difficult to obtain a good estimate of the thermal characteristic length with an acoustical inverse method if noise is not sufficiently controlled. To obtain a higher degree of accuracy on Λ' using the inverse approach, it is necessary to base the inversion procedure on an acoustical measurement that is more sensitive to the thermal characteristic length. More indications will be given at the conference.

REFERENCES

1. J.F. Allard (1993). *Propagation of sound in porous media. Modelling sound absorbing materials* (Elsevier applied sciences).
2. Y. Atalla and R. Panneton, "Inverse acoustical characterization of open-cell porous media using impedance tube measurements," *Canadian Acoustics* 33 (1), 11-24 (2005).
3. D. L. Johnson, J. Koplik, and R. Dashen, "Theory of dynamic permeability and tortuosity in fluid-saturated porous media," *J. Fluid Mechanics* 176, 379-402 (1987).
4. D. Lafarge, Sound propagation in porous materials having a rigid frame saturated by gas, (in French). Ph.D. Dissertation, Université du Maine, 1993.

Table 1 : Range of parameters

Parameter	Lower bound	Upper bound
ϕ	0.6	1
σ	3000 Ns/m ⁴	100000 Ns/m ⁴
α	1	7
Λ	15 μm	500 μm
Λ'	15 μm	500 μm

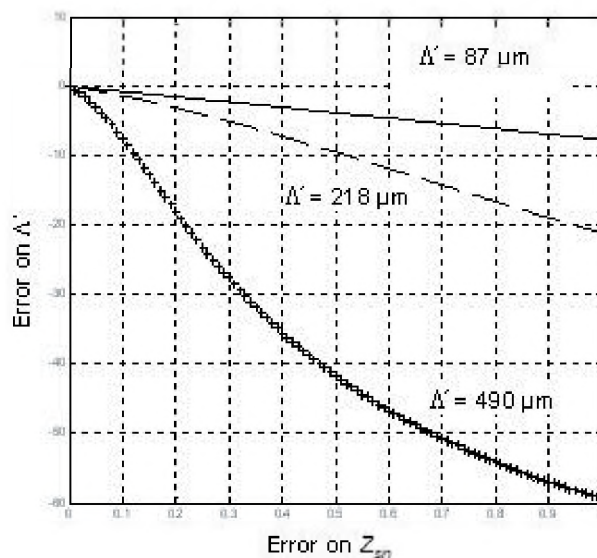


Figure 1 : Error on inversely found Λ' in function of the error on Z_{sn}

Modeling of general laminate composite structures with viscoelastic layer

Sebastian Ghinet and Nouredine Atalla

Universite de Sherbrooke, Departement of Mechanical Engineering
2500 Boulevard Universite, Sherbrooke, QC, J1K 2R1, Canada

1. INTRODUCTION

Damped multilayer structures such as flat panels are largely used in automotive and aerospace constructions. Most papers in the field treat isotropic structures¹ with damped layers or patches in symmetrical or asymmetrical sandwich configurations. The increasing requirements of accuracy have encouraged important improvements¹⁻³ in the modeling approaches. The industry development of new multilayer damped configurations (not necessarily of a symmetric sandwich nature) favors the use of general laminate models². Moreover, the new iterative identification algorithms, used for the characterization of the viscoelastic materials' dynamic properties, require a tremendous amount of computational effort³. These methods³ update successively the complex eigenvalues and eigenvectors until required accuracy is achieved. It is worth pointing out that accurate and fast numerical solutions are imperatives for such applications.

This paper describes the modeling of reasonably thick general composite laminate plates and beams with linear viscoelastic damping. The principal aim is the fast and accurate modeling of such structures for low to high frequencies. The problem is solved by discrete laminate method in a wave approach context. The discrete laminate approach assumes each layer described by a Reissner-Mindlin displacement field which leads to equilibrium relations accounting for membrane, transverse shearing, bending and full inertial terms. Each layer accounts for orthotropic plies orientations. The discrete description of each layer allows for accurate handling of thin/thick laminates and sandwich panels over the audible frequency range. In particular, at high frequencies the combination of (i) propagating wavelength characteristics (short wavelengths) and (ii) the layout's physical properties (certain layers are much stiffer than adjoining ones) may result in decoupled out-of-phase movement of stiff layers. Such phenomena are correctly captured by the discrete laminate approach.

2. THEORY

This study deals with layouts of an unlimited number of composite and viscoelastic layers. Figure 1 represents the global geometrical configuration of a composite panel (Figure 1.a) and a composite beam (Figure 1.b) with side dimensions L_x and L_y and total thickness h . The layered construction is considered, in general, asymmetrical. The

origin of the coordinates system is defined on a reference surface passing through the middle thickness as represented in Figure 1.

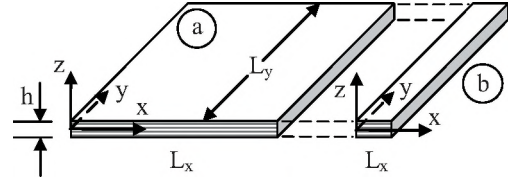


Figure 1. Global geometrical configuration. Flat laminated composite panel (a), and laminated composite beam (b) of L_x and L_y side dimensions and h total thickness.

Membrane and bending displacements as well as shearing rotation are generally expected to act in each layer; the displacement field of any i^{th} discrete layer of the panel is of Mindlin's type.

The resultant stress forces and moments of any layer are defined in Ref. [5]. There are three interlayer forces along x , y , and z directions between any two layers. Consequently, the total number of interlayer forces is $3(N-1)$ where N is the number of layers.

For any i^{th} layer there are five equilibrium equations:

$$\begin{aligned} N_{x,z}^i + N_{xy,y}^i + F_x^i - F_x^{i-1} &= m_y^i u_{,tt}^i + I_{z2}^i \varphi_{x,tt}^i \\ N_{zy,z}^i + N_{y,y}^i + F_y^i - F_y^{i-1} &= m_x^i v_{,tt}^i + I_{z2}^i \varphi_{y,tt}^i \\ Q_{x,x}^i + Q_{y,y}^i + F_z^i - F_z^{i-1} &= m_z^i w_{,tt}^i \\ M_{x,x}^i + M_{xy,y}^i - Q_x^i + z^i F_x^i - z^{i-1} F_x^{i-1} &= I_2^i \varphi_{x,tt}^i + I_{z2}^i u_{,tt}^i \\ M_{zy,z}^i + M_{y,y}^i - Q_y^i + z^i F_y^i - z^{i-1} F_y^{i-1} &= I_2^i \varphi_{y,tt}^i + I_{z2}^i v_{,tt}^i \end{aligned} \quad (1)$$

Rotational inertia, in-plane, bending as well as transverse shearing effects are accounted for in each layer. Also, orthotropic ply's directions are used for any lamina composing a layer. The expressions of the transverse shear stress forces Q_i , the in-plane stress forces N_i , the inertial terms I_i , and the stress moments M_{ij} of each layer are defined in Ref. [5].

2.1. Dispersion relation

For any layer, the dynamic equilibrium equations are rewritten using equations (1) with appropriate algebraic manipulations and has $5N+3(N-1)$ variables regrouped in a hybrid displacement-force vector $\langle e \rangle$. Next, the system is expressed in the form of a generalized polynomial complex eigenvalue problem:

$$k_c^2 [A_2] \{e\} - jk_c [A_1] \{e\} - [A_0] \{e\} = 0; \quad (2)$$

where, $k_c = \sqrt{k_x^2 + k_y^2}$, $j = \sqrt{-1}$ and $[A_0]$, $[A_1]$, $[A_2]$ are real square matrices (in the absence of damping) of dimension $5N+3(N-1)$ defined in Ref [5].

Relation (2) has $2(5N+3(N-1))$ complex conjugate eigenvalues and represents the dispersion relations of the laminated composite structure. The matrices in relation (2) become complex when viscoelastic layers compose the layout.

The pure arithmetically real solution with the highest amplitude corresponds, in the case of thin isotropic structures, to the bending wavenumber. This solution has three asymptotical behaviors for sandwich configurations: pure bending at low frequencies, core's transversal shearing at mid-frequencies and pure bending of skins at high frequencies.

In the following, the first propagative solution (of highest amplitude) is retained and used to illustrate applications of the proposed model. This propagative solution corresponds to transversal displacements motion (bending for the thin structures' case) accompanied by in-plane and transversal shearing internal deformations.

2.2. Equivalent loss factor

The propagating solutions and the associated eigenvectors of the relation (2) are used to express the strain energy U_n of the hybrid problem. Next, the equivalent loss factor of a panel or beam with N layers, associated to the n^{th} propagating wave is expressed as:

$$\eta_n = \frac{2}{\pi} \int_0^{\pi/2} \frac{\sum_{k=1}^{N_{lay}} \eta_k U_n^k}{U_n} d\varphi = \frac{2}{\pi} \int_0^{\pi/2} \frac{\sum_{k=1}^{N_{lay}} \eta_k v_n^T Re[\lambda_n A - B] v_n}{v_n^T Re[\lambda_n A - B] v_n} d\varphi \quad (3)$$

where, the matrices A and B are given in Ref. [5].

Relation (3) compute the total damping loss factor of a composite laminate as the average of the angular distributions of the damping loss factor over a quart of the wavenumber space with respect to the heading directions.

2.3. Numerical results and validation

Examples of comparisons to experimental and spectral finite elements results are presented and discussed in this section. Figure 2 presents the comparisons between experimental results⁶ and the present discrete laminate approach. Excellent agreement is observed. The resonance frequencies and the resonance amplitudes of the first four modes are accurately estimated.

The next configuration concerns very thin laminated steel beam with a constrained viscoelastic layer, representative of laminated steel used in automobiles. Damping loss factor is computed using the present approach and spectral finite element model presented in Ref. [2], and the results are plotted in Figures 3. Excellent agreement is observed in Figure 3 between the analytical discrete laminate and spectral finite elements approaches.

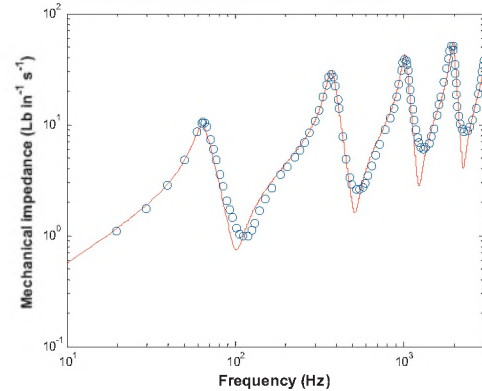


Figure 2. Driving point mechanical impedance of a sandwich beam (Sun and Lu⁶, Fig. 4.3, Pag.173). Experimental validation: (—) Discrete laminate; (o) Experimental.

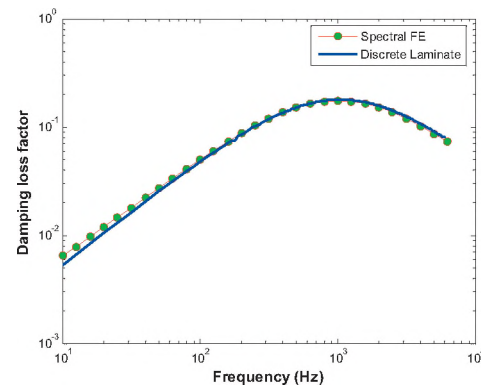


Figure 3. Damping loss factor of a cantilever sandwich beam.

3. CONCLUSIONS

The modeling of thick composite laminated plates and beams with linear viscoelastic damping layers was described. A theoretical approach has been developed so as to fulfill a present need for fast and accurate numerical models generally dedicated to optimization and inverse characterization applications. The problem was solved by analytical discrete laminate method in a wave approach context. The model has been successfully validated with experimental and numerical results. Moreover, the model was applied to the calculation of the structural loss factor associated to the bending wave-type.

References:

1. Mead D.J. "A comparison of some equations for the flexural vibration of damped sandwich beams", *J. Sound Vib.*, 83(3), 363-377, (1982).
2. Shorter P.J. "Wave propagation and damping in linear viscoelastic laminates", *J. Acoust. Soc. Am.*, 115(5), 1917-1925, (2004).
3. Miles R. N. and Reinhall P. G. "An analytical model for the vibration of laminated beams including the effects of both shear and thickness deformation in the adhesive layer". *J. of Vib. and Acoustics*, 108 (1986), 56-64.
4. Mead D. J. "The measurement of the loss factors of beams and plates with constrained and unconstrained damping layers: A critical assessment", *J. Sound Vib.*, Vol 300, Issues 3-5, 6 March 2007, Pages 744-762.
5. Ghinet S. PhD Thesis, Université de Sherbrooke, "Statistical energy analysis of the transmission loss of sandwich and laminate composite structures", June, 2005.
6. Sun C. T. and Lu Y. P. "Vibration damping of structural elements", Prentice Hall PTR, 1995.

SYMMETRY OF VISCOUS PERMEABILITY TENSOR IN POROUS MEDIA

C. Perrot, F. Chevillotte, and R. Panneton

GAUS, Department of Mechanical Engineering, Université de Sherbrooke, Canada, (Qc) J1K 2R1

1. INTRODUCTION

This paper reports parts of recent simulation results [1] carried out in order to illustrate a rather theoretical and somewhat non intuitive property of the viscous permeability tensor in porous media: considering periodic porous structures in the long wavelength limit, even if the structure is anisotropic, its acoustical properties will remain isotropic, i.e. : the velocity fields are qualitatively different in principal directions of a porous structure showing different local arrangements to an incident acoustic wave; however, they remain identical on average. The practical importance of this property is that it can be used to assess the validity and accuracy of numerical simulations in the emerging field of bottom-up approaches for microstructure optimization of sound absorbing materials. This paper is organized as follows. In Sec. 2 the basic equations used to describe the physical properties of a porous material are presented at the macroscale of day-to-day engineering applications. In Sec. 3 a short description of the permeability tensor symmetry property is given from the standpoint of the equations governing the physics at the pore scale, i.e. microscale. In Sec. 4, numerical results in porous structures with hexagonal symmetry are presented to illustrate the previous property. Good agreement between theory and numerical experiment is found.

2. MACROSCOPIC DESCRIPTION

This Sec. deals with the classical description of the flow of a viscothermal fluid in a motionless homogeneous porous structure. The statistical properties of the porous frame can be defined in homogenization volumes with dimensions much smaller than the wavelength of the acoustic waves that propagate in the saturating fluid. The microscopic quantities that describe the flow (pressure p , velocity \mathbf{v}) present variations at the microscopic scale in the homogenization volume. To smooth out these variations and leave only the macroscopic variations, fluid-phase average is introduced ($\langle \cdot \rangle$). At a given frequency, a fundamental relation called the generalized Darcy law in memory of its pioneering work [2] and defined as $\Phi \langle \mathbf{v}_i(\omega) \rangle = - [k_{ij}(\omega)/\eta] \mathbf{grad}_j \langle p \rangle$, is linking the gradient of the macroscopic pressure to the macroscopic velocity. Here, Φ is the open porosity, η is the viscosity of the fluid, and $k_{ij}(\omega)$, previously defined and studied by Johnson et al. [3], is the second order dynamic viscous permeability tensor only depending on frequency and on the geometry of the porous structure.

3. PERMEABILITY TENSOR SYMMETRY

As discussed in Ref. [4], describing the periodic oscillating flow created in a porous medium by an external unit harmonic pressure gradient, one has to solve in the fluid volume Ω_f the following set of scaled equations (unsteady Stokes problem):

$$\frac{-i\omega}{\nu} \mathbf{w} = -\nabla \pi + \Delta \mathbf{w} + \mathbf{e} \quad \text{in } \Omega_f, \quad (1)$$

$$\nabla \cdot \mathbf{w} = 0 \quad \text{in } \Omega_f, \quad (2)$$

$$\mathbf{w} = 0 \quad \text{in } \partial\Omega, \quad (3)$$

where \mathbf{e} is a unit vector, $\nu = \eta/\rho_0$, ρ_0 is the air density at rest, and $\mathbf{w} = \mathbf{v} / |\mathbf{grad} \langle p \rangle| \eta$ is the scaled velocity field (in m^2). The solution to the problem (1)-(3) is fixed by adding the condition that π is a spatially stationary or periodic field. This problem is relevant to sound propagation as long as the wavelength is large enough for the saturating fluid to behave as an incompressible fluid in volumes of the order of the homogenization volume (a period in the case of periodic structure).

The demonstration proposed in Ref. [1] states that, by using three individual solicitation vectors \mathbf{e}^i in three perpendicular directions, with components $\mathbf{e}_{ij} = \delta_{ij}$, $k_{ij}(\omega)$ can be written in a symmetrical form in i and j :

$$k_{ij}(\omega) = -\frac{i\omega\phi}{\nu} \langle \mathbf{w}^j \cdot \mathbf{w}^i \rangle + \phi \left\langle \left(\frac{\partial}{\partial x_m} \mathbf{w}^j \right) \cdot \frac{\partial}{\partial x_m} \mathbf{w}^i \right\rangle. \quad (4)$$

This shows that the viscous permeability tensor is symmetric, $k_{ji} = k_{ij}$. As a consequence, there exists a system of orthogonal axes, the principal axes, where the tensor has only diagonal elements different from zero. If the medium presents the trigonal, the tetragonal, and the hexagonal symmetry, the axis of symmetry Z must coincide with one of the principal axes and the invariance of the system through some discrete rotations along this axis necessarily means that the two transverse eigenvalues of the tensor are the same (transverse isotropy). In particular, the static permeability k_{0ij} has value k_{0z} along axis Z , and unique values k_{0p} for all directions orthogonal to Z .

$$\begin{bmatrix} k_{011} & k_{012} \\ k_{021} & k_{022} \end{bmatrix} = \phi \begin{bmatrix} \langle \mathbf{w}_{01}^1 \rangle & \langle \mathbf{w}_{01}^2 \rangle \\ \langle \mathbf{w}_{02}^1 \rangle & \langle \mathbf{w}_{02}^2 \rangle \end{bmatrix} = \begin{bmatrix} 4.9420 & 0 \\ 0 & 4.9353 \end{bmatrix} \times 10^{-8} \text{ m}^2 \quad (5)$$

4. NUMERICAL SIMULATIONS

Parameters k_0 is important for the prediction of the acoustic properties of porous media. The constraint which exists when the structure has the uniaxial symmetry can provide a test for the precision of the simulations. An example is given in that Sec. where the static permeability k_{0P} is evaluated in a hexagonal porous structure. As an illustration, we show in Fig. 1 the two components of the static scaled patterns obtained for excitation along the two principal directions in the plane perpendicular to the axis of symmetry of the periodic geometry. This yields the tensor written in Eq. (5). The relative differences found for the horizontal and vertical directions are less than 0.13 %. Also, the non-diagonal terms are numerically equal to zero. These results are consistent with the theory presented in Section 3, and, as a consequence, prove the validity of our numerical implementation. Finally, these results provide, in the limit of the precision of the finite element method, a numerical illustration of the symmetry property of the viscous permeability tensor reported in Section 3. In a plane perpendicular to the axis of a porous material with hexagonal symmetry, viscous permeability tensor is reduced to a constant diagonal element.

5. CONCLUSION

In conclusion, a simple proof has been proposed of a somewhat non-intuitive property of the dynamic viscous permeability tensor. As long as the wave length is much larger than the pore sizes, for periodic porous structures with hexagonal symmetry presenting different local configurations to a wave propagating in different directions in the plane perpendicular to the axis of symmetry, the permeability tensor is diagonal and constant in the different directions. This property can notably be used for error estimation of numerical computation.

REFERENCES

[1] Perrot C., Chevillotte F., Panneton R., Allard J. F. and Lafarge D. (2007). Symmetry of viscous permeability tensor in porous media. Submitted to Wave Motion.
 [2] Darcy H. (1856). Les Fontaines Publiques de la Ville de Dijon, Victor Dalmont, Paris.
 [3] Johnson D. L., Koplik J., and Dashen R. (1987). Theory of dynamic permeability and tortuosity in fluid-saturated porous media. J. Fluid Mech. 176, 379-402.
 [4] Lafarge D. (2006). Milieux poreux et poreux stratifiés. Modèles linéaires de propagation, in Matériaux et acoustique 1, M. Bruneau and C. Potel eds., Lavoisier, Paris.

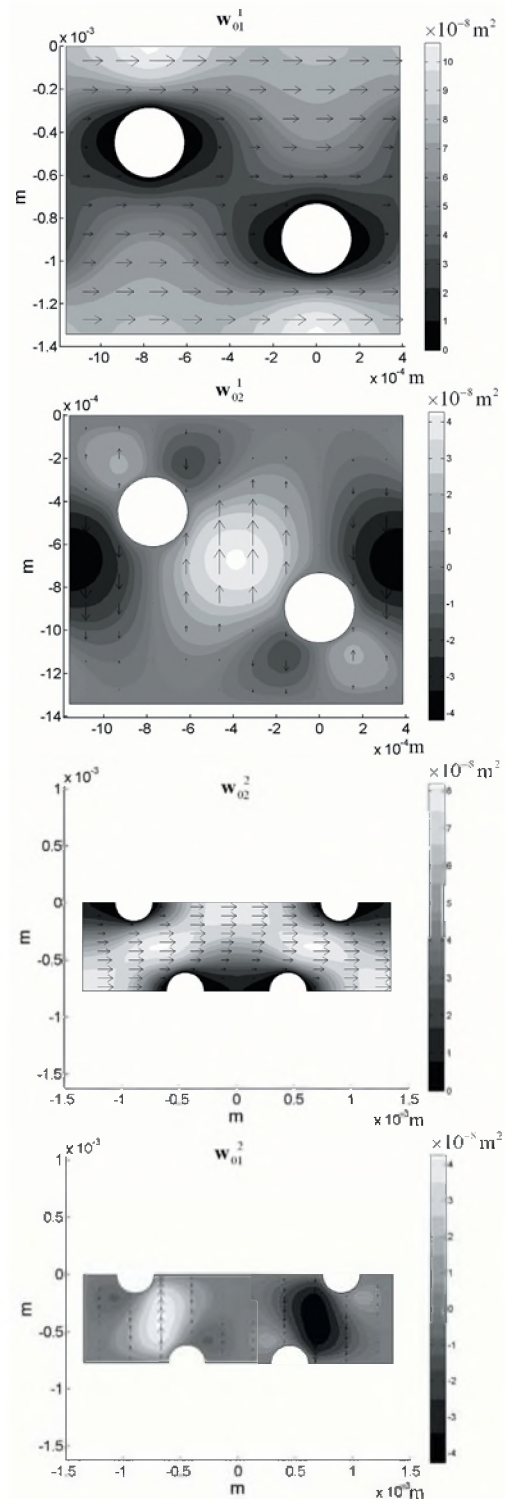


Fig. 1. Static scaled velocity fields obtained by solving the steady-Stokes problem in principal directions of an hexagonal periodic porous structure.

DAMPING AND QUALITY FACTOR OPTIMIZATION IN MEMS MICRORESONATORS

Gino Rinaldi, Muthukumaran Packirisamy, Ion Stiharu
Optical Microsystems Laboratory, CONCAVE Research Centre
Concordia University, Montreal, CANADA H3G 1M8

1. INTRODUCTION

Micro-Electro-Mechanical-Systems (MEMS) resonators are used in many applications ranging from bio-medical to space exploration [1-3]. In this regard, boundary conditioning is a way of modeling the integrated characteristics of material, geometry, boundary support, and operating conditions on the elastic property of suspended microstructures [4, 5]. For microresonators, the effects of damping will affect the dynamic response of suspended microcantilever type devices, where damping in general may be due to structural and or squeeze film effects. An important issue involved in these developments is to characterize the interaction of the resonating structure with the thin gas layer between the structure and its supporting substrate [6].

The performance of many MEMS devices can be improved by tuning the quality factor (Q) of the dynamic system [7]. A high Q can increase the scanning angle of a micromachined optical scanner and the sensitivity of a micromachined microphone [8]. On the other hand, damping can be used to reduce the oscillation of an accelerometer at resonance, and to reduce the settling time of various types of sensors and actuators [9]. In this work, a method using cutouts [10, 11] to tune the dynamic response of the microcantilever and improve the Q of the resonating microdevice is presented.

2. MODEL

The dynamic characteristics of micromachined structures, such as resonant frequency and damping coefficient are usually influenced by air. This squeezed-film effect will introduce an equivalent lumped variable damper and spring model as shown in Figure 1, where the equation of motion for the vibrating structure is given by

$$M\ddot{x} + C\dot{x} + Kx = 0 \quad (1)$$

where M is the mass, C the damping coefficient and K the stiffness of the system.

The variable nature of the stiffness and damping in this model, as shown in Figure 1, is directly related to the geometry of the cutout. In this regard, the cutout will affect both the stiffness and the damping of the microsystem, and the Q is directly proportional to the reduction in the damping of the microsystem.

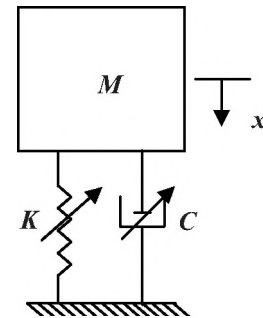


Fig. 1. Lumped mass model of a variable spring-damper resonating microstructure.

Two damped microcantilever models are investigated experimentally in this work. In this first model as shown in Figure 2, the microcantilever cutouts are of equal size for three different microcantilever lengths, while in the second model as shown in Figure 3, the microcantilever length is constant and the slot length is varied. A microscope image of these two cutout models applied to atomic force microscope (AFM) microcantilevers is shown in Figure 4.

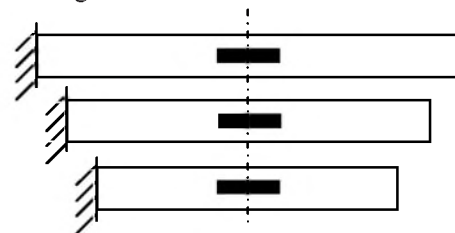


Fig. 2. Top view of three microcantilevers of various lengths with equal cutouts.

The experimental results were obtained by using a non-contact optical test method in which the natural frequencies of the resonating microcantilevers were obtained [12]. A piezo-stack was used for the base excitation in which a swept sinusoidal frequency approach was used. The experimental resonance responses obtained are presented in Figure 5.

3. DISCUSSION

The resonance responses obtained show that the damping can be reduced significantly by the inclusion of a cutout in the microcantilever. The sharpness of the

resonance may also be affected by the geometry of the cutout. In this regard, cutouts may be used to tune the frequency response of a given microcantilever, and also to reduce the squeeze film damping in the microsystem.

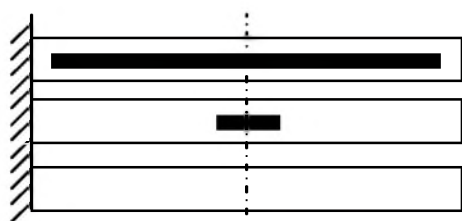


Fig. 3. Top view of three microcantilevers of the same lengths with various cutouts.

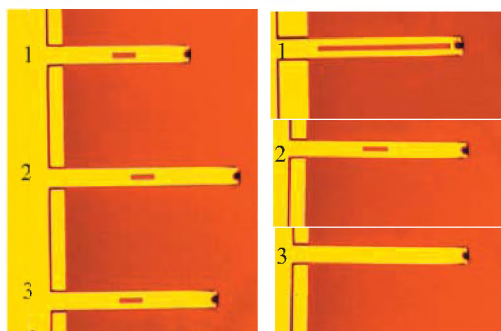


Fig. 4. Left: Microscope image of top view of three AFM microcantilevers of various lengths with equal cutouts. Right: Top view of three AFM microcantilevers of the same lengths with various cutouts.

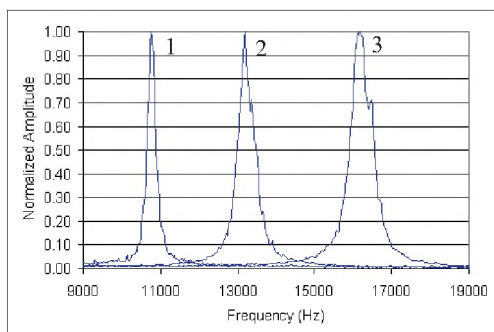
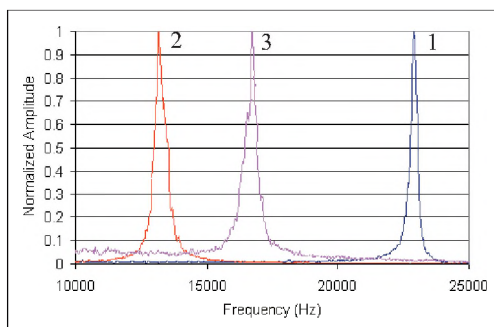


Fig. 5 Top: Frequency responses of three AFM microcantilevers as shown in Fig. 4 (left). Bottom: Frequency responses of three AFM microcantilevers as shown in Fig. 4 (right).

4. CONCLUSION

An experimental investigation into the damping and Q, of resonating AFM microcantilevers has been presented. It was shown that the resonance response and Q can be favourably tuned with the choice of appropriate cutout geometry, where the increase in Q is directly related to the reduction in damping of the microsystem.

REFERENCES

1. Raiteri, R., Grattarola, M., Butt, H.J., Skladal, P. (2001) "Micromechanical cantilever-based biosensors", *Sensors and Actuators: B*, 79, 115-126
2. Riesenber, R., Nitzsche, G., Wuttig, A., Harnisch, B. (2001) "Micro spectrometer and MEMS for space", 6th ISU Annual International Symposium, Smaller Satellites: Bigger Business, Strasbourg, France, May 21-23
3. Su, M., Li, S., Dravid, V.P. (2003) "Microcantilever resonance-based DNA detection with nanoparticle probes", *Biochemical and Biophysical Research Communications*, 304, 98-100
4. Rinaldi, G., Packirisamy, M., Stiharu, I. (2005) "Multiparameter synthesis of microsystems", Proceedings of SPIE, International Conference on Photonic Devices, Toronto, Ontario, Canada September 12-14
5. Packirisamy, M., Bhat, R.B., Stiharu, I. (1999) "Boundary conditioning technique for structural tuning", *Journal of Sound and Vibration*, 220, 847-859
6. Zhang, C., Xu, G., Jiang, Q. (2004), "Characterization of the squeeze film damping effect on the quality factor of a microbeam resonator", *Journal of Micromechanics and Microengineering*, 14, 1302-1306
7. Cheng, C.-C., Fang, W. (2005) "Tuning the quality factor of bulk micromachined structures using squeezed-film damping", *Microsystem Technologies*, 11, 104-110
8. Lin, H.-Y., Fang, W. (2000) "Torsional mirror with an electrostatically driven lever-mechanism" the IEEE Optical MEMS 2000, Kauai, Hawaii, August, 113-114
9. Greywall, D.S., Busch, P.A., Walker, J.A. (1999) "Phenomenological model for gas-damping of micro mechanical structures", *Sensors and Actuators: A*, 72, 49-70
10. Rinaldi, G., Packirisamy, M. and Stiharu, I. (2007) "Dynamic analysis of slotted MEMS cantilevers", *International Journal of COMADEM*, 10, 13-19
11. Rinaldi, G., Packirisamy, M. and Stiharu, I. (2006) "Tuning the dynamic behaviour of cantilever MEMS based sensors and actuators", *Sensor Review*, 27, 142-150
12. Rinaldi, G., Packirisamy, M. and Stiharu, I. (2006) "Dynamic testing of micromechanical structures under thermo-electro-mechanical influences", *Measurement*, 40, 563-574

MEMS BASED ACOUSTIC PRESSURE MEASUREMENTS

Gino Rinaldi, Muthukumaran Packirisamy, and Ion Stiharu

Optical Microsystems Laboratory, CONCAVE Research Center
Department of Mechanical & Industrial Engineering
CONCORDIA UNIVERSITY, Montreal, CANADA H3G 1M8

1. INTRODUCTION

Dynamic pressure measurements are a promising new approach to obtain diagnostic characteristics where pressure variations may be used to extract hardware performances. In this regard, pressure sensor designers agree that in-situ measurements would enable performance extractions currently unavailable with conventional pressure sensors. This paper proposes using Micro-Electro-Mechanical-Systems (MEMS) microphones as pressure sensors for monitoring dynamic pressure variations. Shown in Figure 1 is a cross-section of a Knowles acoustics SiSonic microphone [1]. It is a free-floating design with 36 support posts and one physical connection to the diaphragm. Shown in Figure 2 is an image of the SiSonic microphone diaphragm, support posts and connections.

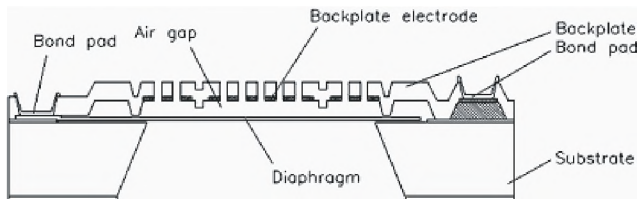


Fig. 1. Cross-section of SiSonic MEMS microphone [1].

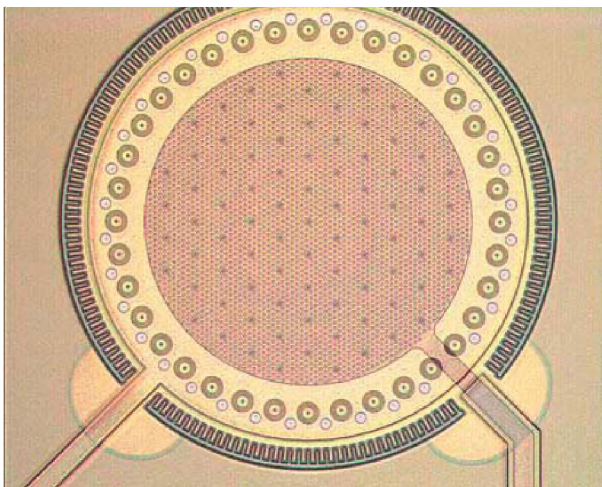


Fig. 2. SiSonic MEMS microphone diaphragm [1].

MEMS pressure sensors combine high sensitivity with small size/weight packaging that would enable in situ monitoring of pressure flows. Current pressure sensor technology for engine applications, for example, makes use of magnetic captors or torque sensors. While the sensitivity and selectivity of these types of sensors is satisfactory, problems are encountered with their reliability and the drift from the calibrated point. Packaging is to some extent heavy in part due to the sensor qualification requirements. In this capacity, MEMS pressure sensors satisfy several important criteria, namely, small size/weight, robustness, easily integrated with electronics, low power consumption and low cost. In this paper MEMS microphones are used to monitor the pressure variations of rotating axial fans.

2. EXPERIMENT

Described in this section is the experimental setup and equipment used for the MEMS based pressure sensor. The experiments consisted of measuring the pressure variation of several DC fans [2, 3] having maximum rotational frequencies $\sim 4000\text{Hz}$. Shown in Figure 3 is a 5 bladed DC axial fan used in the experiments. The white lines seen on the fan blades were used for stroboscopic measurements of the fan speed.

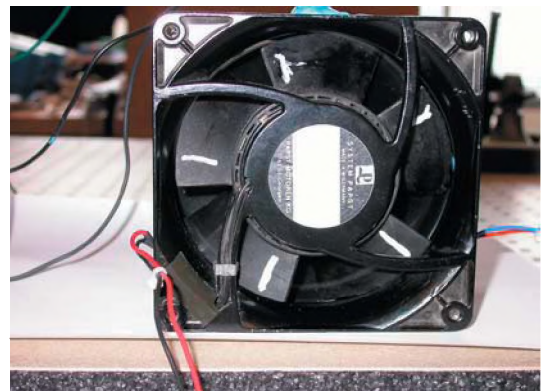


Fig. 3. Fan with 5 blades.

The pressure variations were measured using both an ultra-miniature electret microphone [3] and MEMS microphone

[1] for comparison. In the course of the experiments no differences were seen between these two technologies. In all of the experiments, pressure measurements were taken directly over the fan blades through a hole in the axial fan casing. Shown in Figure 4 is a Papst [2] technology fan with an electret [4] microphone mounted over the fan blades. A double fan configuration is also analyzed as shown in Figure 6 with a MEMS acoustic sensor mounted in between the two fans.

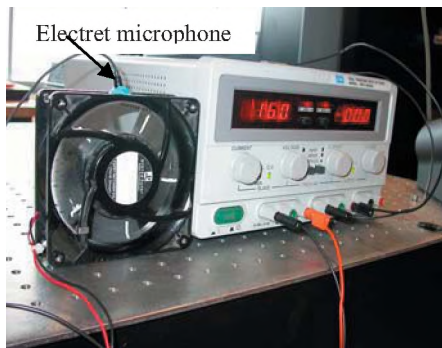


Fig. 4. Fan and power supply. White lines on the fan blades were used for stroboscopic measurement of the fan speed.

3. RESULTS

Shown in Figure 5 is an FFT [5] carpet plot of the fan speed and frequency (fundamental and harmonics). The frequency is a function of the blade passage across the plane of the sensor. These results were repeated for higher rotational velocities and frequencies (~4000Hz) with excellent signal-to-noise ratios obtained with the sensor.

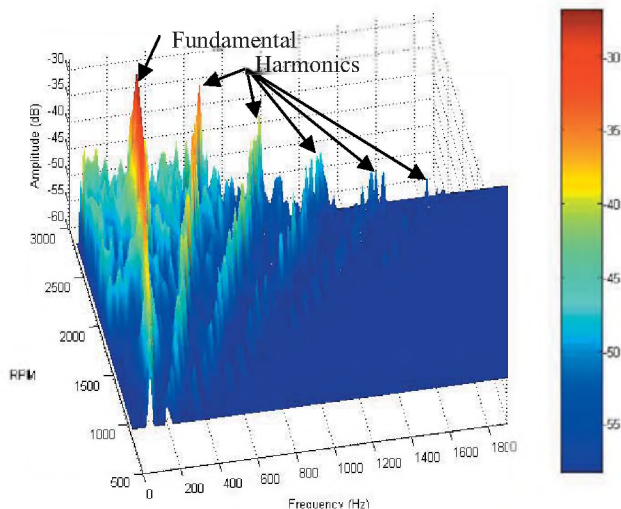


Fig. 5. FFT carpet plot of the fan rotation as a function of the pressure variation created by the fan blade passage. The fundamental mode and harmonics are visible.

The results obtained for the double fan scheme are given in Figure 7.

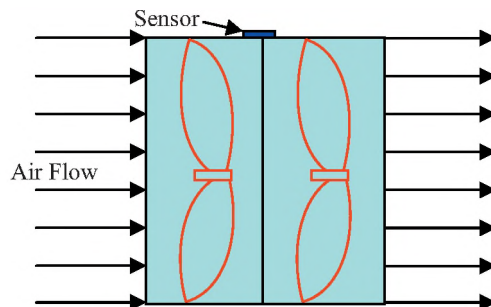


Fig. 6. Double fan configuration with an acoustic pressure sensor placed at the mid point of the two fans.

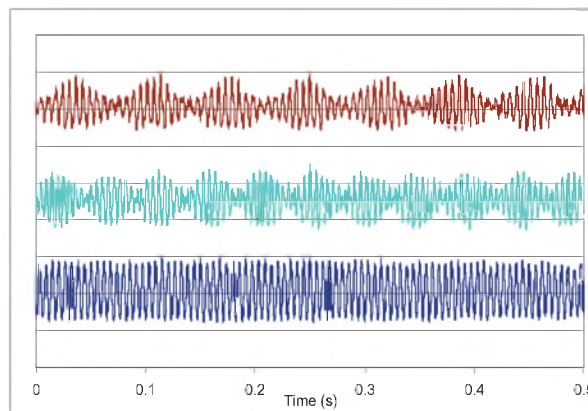


Fig. 7. Pressure plots for a two fan configuration taken at the midpoint of the two fans. Top: F1 speed > F2 Middle: F2 speed > F1. Bottom: F1 speed = F2.

5. CONCLUSION

The possibility of integrating MEMS based acoustic pressure sensors in rotating machinery such as fans has been presented. MEMS offer small size with great sensitivity and reliability at a reduced cost. In this regard, their suitability for in-situ measurements of active flow systems such as generated by rotating fans makes them an excellent diagnostic tool by virtue of the information extracted from the pressure signal obtained.

REFERENCES

1. Knowles Acoustics, Technical Data Sheets, SiSonic Microphones SPM0102ND3, SPM0103ND3, www.knowlesacoustics.com
2. EBM-Papst, Technical Data Sheet, 4100N Series Tubeaxial Fan, www.ebmpapst.us
3. Delta Electronics, Technical Data Sheet, PFB Series DC Brushless Fan, www.delta.com.tw
4. NexxTech, Technical Data Sheet, 3303013 Ultra-Miniature Microphone, www.nexxtech.com
5. Bruel Kjaer Sound & Vibration, Technical Data Sheet, Signal Analyzer Unit 2035, www.bksv.com

ABSTRACTS FOR PRESENTATIONS WITHOUT SUMMARY PAPERS

AEROACOUSTICS

H.S. Ribner and Aero Acoustics at UTIAS (Invited Talk)
Werner Richarz, Aeroacoustics, Toronto.

Herbert S. Ribner came to the University of Toronto Institute for Aerophysics in 1956. Here he established one of the centers of excellence in aerodynamically generated noise. The first research efforts were directed at boundary layer noise. Subsequently, he turned his attention to jet noise. His insight into the physics of unsteady flows and mathematical ability led to what appear to be simple models and theories that describe all the observed features of (sub-sonic) jet noise within the framework of Lighthill's acoustic analogy. The paper is a perspective of the many contributions to aero-acoustics made at the University of Toronto Institute for Aerospace Studies.

Valve Noise Control
Sid-Ali Meslioui, Pratt & Whitney, Longueuil, Quebec

In gas turbine engines such as turbofans, turboshafts and turboprops, a significant amount of compressed air is dumped out the engine at off design conditions to ensure a continuous safe operation. The design of the bleed flow discharge system varies from one engine to another, but it essentially uses a controlled valve for flow regulation. The discharged bleed air is at high velocity and high pressure, creating a loud noise at low power conditions, undesirable for noise certification and cabin comfort. The noise control engineering of such a problem usually consists of designing an acoustic muffler device, even though its acoustic and mechanical performance may deteriorate with time making the muffler life, weight and cost a frequent issue. Alternatively, the valve noise can be reduced by introducing devices to gradually relieve the high pressure across the valve, and / or minimize the intensity of the turbulence produced. This can be achieved by using a perforate screen or unconventional valve design. This paper presents design and test results of a few noise devices successfully used to reduce valve noise.

MUSIC COGNITION AND MUSICAL ACOUSTICS

Emotion recognition and Autistic Spectrum Disorders (ASD):
Can music help?

E. Quintin, A. Bhatara, C. Frombonne, H. Poissant and Daniel Levitin, University of Montreal

Individuals with autistic spectrum disorders (ASD) exhibit a heightened interest in music and above average auditory processing abilities (Heaton, 2005). Baron-Cohen et al. (2000) believe that hypo-functioning of the amygdala may explain the social and emotional deficits in ASD such as a diminished sensitivity to fear. Happy and sad music can be identified as

such by individuals with ASD (Heaton et al., 1999) but their recognition of scary and peaceful music should be impaired, as observed in patients with damage to the amygdala (Gosselin et al., 2005). Thus, we asked teenagers with ASD (N=15) and typically developing (TD) teenagers (N=15) with comparable musical knowledge and ability to describe musical excerpts using one of the 4 following emotions: happy, sad, scared or peaceful. A diagnosis group effect was observed ($p < .001$), the ASD group being less accurate than the TD group, but no interaction effect between diagnosis group and intended emotion was found. A significant interaction effect between diagnosis group and VIQ was identified ($p < .05$). Post-hoc analyses failed to find a diagnosis group differences when the four emotions were considered separately (all $p > .05$). Thus, our results replicate Heaton and colleagues' (1999) observations that individuals with ASD can identify happy and sad music. However, our results fail to support Baron-Cohen and colleagues' (2000) amygdala theory of autism, which states that individuals with ASD exhibit impaired fear recognition. It is possible that music represents a specific domain where the amygdala theory of autism does not hold.

Vikrutha Panchama Scales in Carnatic Music Containing both Fourth and Diminished Fifth
Rama Bhat, Concordia University, Montreal

The Carnatic classical music system which is prevalent in South India uses 12 semitones within an octave, as in Western classical music. There are seven syllables in the solfa system named S, R, G, M, P, D, and N (pronounced Sa, Ri, Ga, Ma, Pa, Da, and Ni, respectively). The first note S, and the perfect fifth P, are fixed in frequency in a melody scale according to convention. In any fundamental melody scale (parent raga), either the perfect fourth M1 or the augmented fourth M2 will be present exclusively. The second, third, sixth and the seventh notes can have three variations, some of which overlap as follows: R1 (minor second), R2 = G2 (major second), R3 = G2 (minor third), G3 (major third), D1 (minor sixth), D2 = N1 (major sixth), D3 = N2 (minor seventh), N3 (major seventh). With the above notation and using each solfa symbol S, R, G, M, P, D, N only once in the ascending order, traditionally 72 fundamental melody scales have been formed. Each one of them can have many derived scales excluding some notes, or using the notes in a convoluted fashion.

This paper presents 36 new fundamental melody scales for the first time, by using both perfect fourth (M1) and the augmented fourth (M2) in the same fundamental melody scale. Since the augmented fourth (M2) is also the diminished fifth, the perfect fifth is discarded and the unused solfa syllable P is attached to the diminished fifth. By varying the solfa syllables R, G, D, N as before will give 36 new fundamental melody scales. This will bring the total fundamental melody scales to 108.

Subharmonic Effects in Some Musical Instruments

Alfred Hanssen, Øistein Hanssen and Mari Kimura, Heidi Hindberg and Yngve Birkelund
University of Tromsø, Technical Dept., Norway

For some musical instruments, it is possible to excite oscillations that are not part of the normal group of harmonically related partials. In this presentation, we will show results on so-called subharmonic generation in some non-standard transversal flute instruments, and in bowed instruments. These subharmonic components may fall below the normal fundamental (hence their name), and there may be generated spectral components between the ordinary partials. We provide high-quality measurements and state-of-the-art spectral analysis of data from two different types of transversal flutes. These are the Korean membrane flute called a Taegum, and a Norwegian flute made of a vascular plant related to Hogweed. In both cases, we show that material properties are responsible for the subharmonic components. We also present recent violin data which has a rich subharmonic structure. The explanation lies probably within an excitation of torsional wave modes on the violin string. Finally, we attempt to connect the analysis of these instruments to Helmholtz' notion of roughness and inharmonicity of sound.

HEARING SCIENCES

Is it the Pits? Noise Exposure of Opera Musicians

Ewen Macdonald Alberto Behar and Willy Wong
IBBME, University of Toronto

A previous noise exposure survey involving the Canadian Opera Company followed several musicians over the course of rehearsals, dress rehearsals, and performances of two operas (Lee, Behar, Wong, and Kunov, 2005). The results showed that, by itself, the musicians' activity associated with the opera posed no hazard to their hearing. Since then, the Canadian Opera Company has moved to a new venue. Thus, a new study was conducted to examine whether the new venue would have an effect on noise exposure. Measurements were taken during three performances of five different operas using five dosimeters attached to music stands in the orchestra pit. Details of the measurements and results will be presented along with interpretation regarding the effects of venue, opera, and location in the orchestra on noise exposure of musicians.

Validation of an NVH Simulator Compared to Traditional Laboratory Experiment

Colin Novak and Helen Ule
University of Windsor, Windsor, Ontario

Recently, sophisticated NVH simulators have been developed to provide an alternative approach to conventional listening tests done in a laboratory. For automotive applications, this approach often includes visual inputs via a video screen, audio inputs through headphones, and user interaction with audio and visual scenes through a steering wheel and a throt-

tle. These methods of product evaluation provide significant benefits to the vehicle NVH process by allowing listeners to experience free-driving conditions in a virtual environment. On the other hand, these methods have not been verified in terms of psychoacoustic attributes particularly in comparison to conventional jury testing techniques. The goal of the study was to perform a series of listening experiments in a listening room with and without the NVH simulator. Subsequently it was found that the auditory attributes derived from the two listening conditions were very different suggesting that the NVH simulator provided better estimates of attribute scales compared to the traditional evaluation methods without the use of a simulator.

Development of Temporary Threshold Shift (TTS) Detector for use in iPods and other Portable Audio Devices

Chantal Laroche, Christian Giguère, Les Blomberg, Joëlle Séguin and Valérie Lizée, University of Ottawa, Ottawa

Portable audio devices have raised concerns regarding the consequences of exposure to high levels of amplified music on hearing health. Following an exposure to loud sounds, it is common to experience tinnitus and temporary threshold shifts (TTS). The objective of this long term study is to develop a user-administered measure of TTS to be included in portable audio devices in order to increase user awareness of the hazardous effects of loud music on hearing and to help foster safer listening practices. By comparing the number of tones (varying in sound pressure level by a given step size) heard prior to and following the listening session, users could determine if TTS has occurred, and if so, the magnitude of this threshold shift. Through a series of 5 steps (1: Effect of battery life on sound levels emitted from portable audio devices; 2: Attenuation and maximum output provided by various types of earphones; 3: Linearity of audio portable devices; 4: Repeatability of earphone placement in human subjects; 5: Validation of the approach in noisy backgrounds), this study will seek to determine the optimal parameters to be used (frequency of test signal, step size, threshold measurement approach), as well as the feasibility and repeatability of the approach. Results from steps 1 to 4 will be presented.

Blink Reflex and Auditory-Speech Perception in Prelingually Cochlear Implanted Children

Hessameddin Shafaghat, Lida Shafaghat, Parvaneh Abbassalipour, Saeed Hassanzadeh and Ahmad Daneshi
Iran

This study is intended to demonstrate that Blink Reflex or Auropalpebral Reflex evaluation can be used as a prognostic factor for the assessment of auditory and speech perception levels in prelingually cochlear implanted children. In an observational, analytic, prospective study conducted at a single cochlear implant rehabilitation center on 85 prelingually cochlear implanted children, the presence or absence of the Blink reflex (BR) was evaluated and the results of auditory and speech perception tests were compared in the two

groups. To obtain the BR, 4 electrodes were applied in both the Nucleus & the MED-EL systems and then stimulated by the current levels higher than the previously detected Most comfortable level of the patient until the reflex appeared. Auditory and Speech perception levels were measured using the Vowels - confusion test and the Categorization of Auditory perception Scale. The Mean results of auditory and speech perception tests were significantly higher in reflex "positive (R+) compared with reflex-negative (R-) patients. This study shows that (R-) prelingually cochlear implanted children are not optimally suitable candidates for cochlear implantation. However if this group are implanted, other rehabilitation methods should be incorporated into their rehabilitation program to achieve better results and maximize the efficacy of their prothesis.

NOISE

Modeling Aircraft Cabin Noise with Statistical Energy Analysis (SEA)

Andrew Wareing, Bombardier Aerospace, Toronto

Designing aircraft for lower passenger cabin noise and reduced weight is a considerable challenge that requires sophisticated prediction capabilities. A methodology of predicting aircraft cabin noise using Statistical Energy Analysis (SEA) is presented. Confidence in the method has been developed from simple transmission loss models of fuselage sections, to full aircraft cabin models in flight (cruise) conditions. Model validation is shown for transmission loss tests, ground tests on full aircraft, and noise surveys performed in flight at cruise conditions. Future work will focus on increasing model fidelity, the improved characterization of the turbulent boundary-layer noise source, and validating the prediction of noise transmission paths.

Acoustic Echo Cancellation and Noise Removal in the Automobile

Phil Hetherington, QNX Software Systems

Despite hundreds of technical advances in AEC and NR, deploying such algorithms into the automobile remains challenging and the space continues to offer ground fertile for innovation. Our group has been involved in the research, development, and integration of novel handsfree algorithms for the automobile for 7 years. Over 15 car manufacturers, 60+ vehicle platforms, and 70+ patents later we are quite confident that there is quite a lot of fertile ground remaining! Why is there still room for improvement? First, the combination of far-field speech in very dynamic and extreme noise will easily push past the upper limit of advanced NR techniques. Second, the wide variation in coupling between a microphone and powerful automotive speakers, combined with the variability in high noise and dynamics of room response will often violate the assumptions made by most AEC algorithms.

Third, downstream processing on GSM and CDMA phones and networks often poses as our devil in the details. Fourth, the expectations of high voice quality while perfectly understandable and desirable are often impractically and unattainably high. Fifth, the optimum conditions for good quality are rarely if ever afforded as aesthetics, cost, and other considerations often take precedence. Finally, even in the most expensive cars, there are significant constraints on processor usage due to cost, power (heat), and size requirements, and more importantly the need to run multiple applications in the vehicle, including simultaneous navigation and route calculation, speech recognition, and rear seat entertainment systems.

SEA based model for the prediction of the acoustic performance of machine enclosures

H. Neliise, F. Sgard and N. Atalla

IRSST, Montreal, Quebec

The use of enclosures to control the noise radiated by machines is a popular solution. By selecting carefully the various materials and dimensions for the enclosures up front during the design stage, it is usually possible to come up with an efficient solution at minimal cost. To achieve this objective, predictive models can be of great help. This paper presents the development of a simple tool for the prediction of the acoustic performance of enclosures. The tool is based on the statistical energy analysis (SEA) for the prediction of the acoustic field inside the aperture and the acoustic transmission across the various elements of the enclosure. The SEA technique can be improved by other methods (finite-element, method of images, ray-tracing, etc.) in order to better simulate the non-diffuse nature of the field inside the enclosure. Some of these approaches are investigated. The calculation results are compared to experimental results carried out in a semi-anechoic room on rectangular and L-shape enclosures. The comparisons between the models and the experimental results show good correlations for most of the tested configurations. The effect of openings, acoustic absorbing treatments and location of the source are investigated both experimentally and theoretically and discussed.

Integration of Turbulent Boundary Layer (TBL) by using Plate-Backed Cavity to Study the Various TBL Models

Emmanuel Levitte and Nouredine Atalla

University of Sherbrooke, Sherbrooke, Quebec

For many years, reducing cabin noise has been a major concern for aircraft manufacturers. Low noise levels in cars and planes have become important sale arguments since they have a major impact on passengers comfort. The broader scope of the presented work is geared at better predicting cabin noise during cruising flight which is mainly due to Turbulent Boundary Layer (TBL) excitation. In this paper, a plate-backed cavity is used to study the problem. A modal based approach is used to calculate the input power from the TBL to the plate and

the vibration and cavity responses. The model is validated by comparison with (i) SEA (Statistical Energy Analysis) in the case of the Cockburn and Roberston TBL model and (ii) experimental data found in the literature will be also presented. Finally, a comparison between several TBL models (Chase, Corcos, Efimtsov, Smol'yakov and Trachenko) is presented together with an assessment of the contributions of resonant and non-resonant different transmission paths for the TBL excitation.

BUILDING ACOUSTICS

Noise Control Provisions in Canada's Building Codes

T. Nightingale and D. Quirt

National Research Council of Canada, Ottawa

In 2005, NRC published the new "objective-based" version of the National Building Code of Canada. Provincial and territorial codes based on this model have already come into use in many provinces, and most others will follow over the next year. This talk will explain how the Codes have changed in the context of noise control in multi-dwelling buildings, and outline further changes that are being considered for the next cycle of revisions (which is already underway). These proposed changes have implications for both the research and standards development community, and for design professionals including acoustical consultants. This session will continue a dialogue to support progress on improved noise control regulations for buildings.

Using Annoyance and Loudness Ratings of Transmitted Speech and Music to Evaluate Measures of Sound Insulation

Hyeon Ku Park, John Bradley and Brad Gover

National Research Council, Montreal Rd. Ottawa Canada,

Measures of airborne sound insulation were evaluated in terms of their correlations with subjective ratings of the acceptability of transmitted sounds. Listeners heard speech and music sounds played through 20 different simulated walls and in the presence of a constant 35 dBA ambient noise. In different experiments, they rated how disturbing the sounds were in terms of either annoyance or loudness. The results for music and speech sounds are compared and the new subjective ratings of the annoyance and loudness of speech sounds are compared to previous tests in terms of the intelligibility of speech sounds transmitted through simulated walls. The results show that the ISO Weighted Sound Reduction Index (Rw) and ASTM Sound Transmission Class (STC) ratings were more successful in these tests than in a previous test using speech intelligibility scores and that they predict annoyance to speech sounds better than annoyance to music sounds. While mid-frequency sounds were most important for predicting responses to speech sounds, the low and high-frequency extremes were most important for music type sounds. In general sound insulation rating measures that are more successful for speech

sounds are different from those that are more successful for music sounds.

Acoustics, Noise & Vibration Issues for Technology Research & Manufacturing

Todd Busch, B. C.

Technologically advanced buildings contain research instrumentation and/or processes that are sensitive to vibration and noise. Vibration amplitudes that are imperceptible to people can completely compromise the research and manufacturing activities within a facility. Noise levels for current generation research instrumentation often need to be on the order of those found in low-noise recording studios that are borderline perceptible to people. Internal spaces within technologically advanced buildings that need to be evaluated to attain the necessary acoustical performance also include offices, classrooms, auditoria, and seminar rooms. Environmental noise adversely affects surrounding communities with potential annoyance and complaints to the owners, occupants, and government agencies. Environmental noise problems should be remedied, even when applicable noise ordinance standards are not exceeded. To avoid inadequate performance, costly liability claims, and potential abandonment of deficient buildings, thorough attention to the location of a building relative to external sources must be considered, along with internal layout, structural design, and building systems.

INSTRUMENTATION, SIGNAL PROCESSING AND TECHNIQUES

Optical Audio Reconstruction for Stereo Phonograph Records using White Light Interferometry

Beinan Li, Simon de Leon, and Ichiro Fujinaga

McGill University

This paper presents the first Optical Audio Reconstruction (OAR) approach for restoring the acoustic signals of stereo phonograph records. OAR uses precision metrology and digital image processing to obtain and convert groove contour data into digital audio for access and preservation. This contactless and imaging-based approach has considerable advantages over the traditional mechanical methods, such as the capability to extract audio from broken records. Past efforts on monophonic phonograph records have been successful. However, no attempts on 33rpm long-playing stereo records (LPs) have been reported yet. By using a white light interferometry optical profiler, we are able to extract stereo audio information encoded in the 3D profile of the phonograph record grooves. First the desired disc area was scanned by our profiler and the 3D images of the disc surface are obtained. The disc grooves containing audio information are then unwrapped and their horizontal and vertical undulations are converted into audio signals. The result of extracting a short musical excerpt from a 33rpm LP record is presented.

Effect of Demographics on Subjective Jury Testing of an Automotive Application

Helen Ule and Colin Novak

University of Windsor, Windsor, Ontario

Subjective jury testing has become an integral part of product development for the automotive industry. The process of jury testing facilitates the use of human subjects to perform listening tests in order to evaluate the quality and character of product sound. The information derived from such tests is particularly important for manufacturers of big ticket items, such as the competitive pickup truck market, as the perceived quality of the sound produced by these vehicles is of great importance and can dictate what attracts or detracts a potential customer. The jury testing methods explored in this study used the Paired Comparison and Semantic Differential approaches to evaluate major competitor's pickup truck products. The goal of the study was to compare the results of the subjective tests to the results obtained by different demographic groups. It was determined that with demographic information provided by the subjects, the results amongst the different groups do not necessarily coincide with society's perception as a whole.

COMPUTATIONAL ACOUSTICS

Modeling transient wave propagation with retarded boundary potentials and waveguide meshes

Simon de Leon and Gary Scavone, McGill University

A numerical method based on the retarded potential technique for the solution of the Kirchhoff equation in arbitrary volumes is presented. These volumes are bounded by unstructured triangular meshes generated by the GPL toolbox Distmesh. Transient motion across the mesh surface is governed by digital waveguide junctions adapted for an unstructured topology and coupled with the boundary values of the pressure field. In doing so, we are able to achieve fully coupled simulations of transient, linear acoustic systems. The use of this method to extract time domain response characteristics of acoustic spaces and struck musical instruments is illustrated, along with an outline of possible future work and applications.

Sound Propagation in Nonstationary, Inhomogeneous and Dispersive Media

Alfred Hanssen, University of Tromsø, Norway

A number of simplifying assumptions are conventionally employed when modeling propagation of sound fields. Among the standard assumptions are that the medium is limited to be statistically stationary, homogeneous and dispersionless. In this presentation, we will show that if we assume that the sound field belongs to the harmonizable class of random fields, then it is possible to relax these limiting assumptions. In particular, we will show that a very elegant generalization of resonance theory appears. The generalization leads to sev-

eral second order moment functions, or spectral correlation functions, that can be used to describe the sound field in various combinations of space, time, wavenumber and frequency coordinates. Finally, we will explain how microphone array measurements can be employed to derive high-quality estimates of all second order moment functions involved. Applications are abundant in all branches of acoustics, and especially those circumstances where the sound propagation channel is far from ideal would benefit from the formulation described in this presentation. Useful geometrical interpretations of the theory will be offered to ease the understanding.

ENVIRONMENTAL ACOUSTICS

Performance Parameters for Selecting Equipment to Characterize Sound and Weather Conditions in Remote Natural Environments

Todd Busch, B. C.

Attempts to quantify the characteristics of the natural world and the potentially intrusive effects of people have been made using concurrent measurement of sound and weather conditions in remote natural environments. Discussed here are the experiences of the author in terms of what is absolutely necessary in order to deliver quality data to the organizations that fund these efforts. For sound level meters the crucial issues include dynamic range, internal electronic noise floor performance, memory capacity for a given configuration, and the need to correlate variations of sound at different frequencies with natural and human activity. One complicating issue in low-noise environments is differentiating between sound measurement data that can be attributed to wind at a microphone diaphragm that varies in conjunction with sound that can be attributed to wind-induced motion of surrounding trees and foliage. Another is the need to associate logarithmic sound level data with linear weather data such as wind speed and direction.

MICRO AND NANO ACOUSTICS

Static Modeling of multiple-electrostatically deformable microbridges

Y. Li, M. Packirisamy, Rama Bhat, Concordia University

An analytical approach to predict the static behavior of double clamped and microfabricated microbridges subjected to electrostatic fields of multiple electrostatic actuators is presented in this paper. The boundary support conditions of the micro-machined structures are modeled with artificial rotational springs. The static behavior of the microbridge is modeled with energy based approach using boundary characteristic orthogonal polynomials. The deflection of the microbridge are also presented and compared with the experimental results. The proposed method is simple and can be easily extended to complicated configurations which are suitable for adaptive optics applications.

Hearing: Anatomy, Physiology, and Disorders of the Auditory System, By A. R. Møller Elsevier, 2006, List price: \$\$\$ USD (hardcover), ?? pp., ISBN: ??

Hearing: Anatomy, Physiology, and Disorders of the Auditory System offers a broad introduction to the field. It includes sections on the ear (divided into 4 chapters), central auditory system (4 chapters), and hearing disorders (3 chapters). Chapters feature an abstract, an introduction, a hierarchy of sub-headings, and a multitude of drawings, figures and boxed topics, all contributing to the quintessential course textbook feel.


The author intended his book for “otologists, audiologists, neurologists and researchers in the field of hearing” (Preface). That would be accurate, if the important qualifier “novice” had been prepended. Hearing will be useful chiefly for students new to the field. The level of presentation, repetitive style, and combination of very broad scope with relatively brief length (300 pages, but with more figures than text) simply do not produce enough depth of coverage to make the book worthwhile for the more seasoned members of the auditory community.

Take Chapter 3, “Physiology of the Cochlea”, as an example. Otoacoustic emissions receive barely 2 pages of treatment. The central problem with OHC somatic motility-based theories of cochlear mechanics, namely that amplification of basilar membrane vibrations increases with sound frequency, despite the concomitant increase in viscous damping, and decrease in the driving AC receptor potentials (due to the low-pass RC filtering of the cell membrane), is not brought up. Neither is the more recent but well-established finding that hair cell stereocilia bundles also function as active force generators. Such omissions will not necessarily concern the beginning reader, of course. Still, the level of presentation is such that no hearing researcher, at least, is likely to find much interesting material anywhere in the book.


How then would the student, or the instructor of an introductory course, rate *Hearing*? The guess is, only average. The greatest strength of the book is undoubtedly its breadth. Nearly every topic likely to be of future interest is at least mentioned (the notable exception being psychoacoustics, which receives almost no coverage). The accuracy of the content and the clarity of the presentation are good enough, but not great. The biggest problem for this reviewer, and potentially for the student, is that the book does not do enough “teaching” from first principles. It does a fair job of describing facts but not of explaining them. For comparison, *An Introduction to the Physiology of Hearing* by J.O. Pickles (Academic Press, 1988) and *An Introduction to the Psychology of Hearing* by B.C.J. Moore (Elsevier, 2003) are almost as broad in scope, but offer much deeper insight into the auditory system for

students and more seasoned researchers alike. The somewhat broader range of topics in the new text from Møller is not enough to recommend it over the above-mentioned classics.

Dr. Martin Pienkowski
University of Western Ontario




**WESTERN
ELECTRO-ACOUSTIC
LABORATORY**

A division of Veneklasen Associates, Inc. 

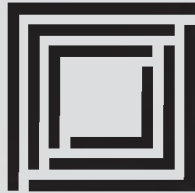
ACOUSTICAL TESTING & MEASUREMENTS

Laboratory Testing	
Sound Transmission Loss, STC	ASTM E-90* (ISO 140*)
Sound Absorption, NRC	ASTM C-423* (ISO 354*)
Calibration of Microphones	ANSI SI-10*
Acoustic Power	ANSI S12-32
<i>Full Anechoic Chamber Measurements also available</i>	
Field Testing	
Noise Reduction, NIC, FSTC	ASTM E-336*
Impact Sound Transmission, FIIC	ASTM E-1007*
Building Facades	ASTM E-996*

*NVLAP Accredited



TEL: 661.775.3741 FAX: 661.775.3742
25132 Rye Canyon Loop Santa Clarita, CA 91355
www.weal.com



E.I. Williams STEEL DIVISION BUILDING SOUND SOLUTIONS

Designers & Manufacturers of Noise Enclosures and Industrial Silencers

We specialize in custom-built silencers and noise enclosures for your specific dimensional and operational requirements.

- ◆ Rotary Positive Blower Intake & Discharge Silencers
- ◆ Pod Silencers for Rotary Positive Blowers
- ◆ Combination Silencers for Rotary Positive Blowers
- ◆ Fan Silencers
- ◆ Centrifugal Compressor Silencers
- ◆ Vent Silencers
- ◆ Engine Silencers
- ◆ Noise Enclosures...

Tel: (905) 428-0950 Toll Free: 1-877-840-3347 Fax: (905) 428-8343 Email: info@silencer.biz

**E.I. Williams Industries - 264 Fairall Street, Ajax, Ontario, Canada L1S 1R6
VISIT OUR WEB SITE AT: WWW.SILENCER.BIZ**

West Caldwell Calibration Laboratories, Inc.
uncompromised calibration
Web site: www.wccl.com E-mail: info@wccl.com

Head Office: 1575 State Route 96, Victor, NY 14564
Phone: 585-586-3900 Fax: 585-586-4327
Branch Office: 220 Rutherford Rd. S. Suite 210, Brampton, ON L6W 3J6
Phone: 905-595-1107 Fax: 905-595-1108

A SINGLE SOURCE LABORATORY

for Calibration and Repair of Sound, Vibration, and Electronic Test Instrumentation

SPECIALIZING IN:

- Accelerometers
- Microphones
- Sound Level Meters
- Field Calibrators
- Audiometric Equipment
- Vibration Meters
- Frequency Analyzers
- Vibration Test Equipment

OUR AUTOMATED FACILITY ASSURES YOU OF:

- Calibrations Traceable to N.I.S.T.
- Certification: ISO 9001:2000
- Accreditation: ISO/IEC 17025:2005
- Compliance: ISO 10012-1, MIL-STD-45662A, ANSI/NCSL 2540-1-1994
- Superior Workmanship
- Complete Test Documentation
- Quick Turnaround time:
 - 48 Hour Calibration Service Available for an Additional Fee
 - 5-10 Days Standard Turnaround



Authorized Calibration and Repair Center for

- Rion • Ono-Sokki • Scantek Inc.

We service equipment manufactured by:

- ACO Pacific*
- Brüel & Kjær*
- CEL*
- Dytran*
- Endevco*
- Fluke
- G.R.A.S.*
- Hewlett-Packard
- Larson Davis*
- Metrosonics*
- Norsonic*
- Norwegian Electric*
- PCB*
- Rion*
- Simpson
- Syminex*
- Quest
- and others

FREE INITIAL OR NEXT CALIBRATIONS COMPLIMENTS FROM WCCL

Your cost of the instrument will be manufacturers list price.

* We will be pleased to order any instrument for you from the manufacturers marked with an **

OTHER SERVICES INCLUDE:
• Custom System Integration

Just Showing Off

Type 2250

You've heard about it from colleagues, or glanced at it in an advertisement. The look is perfect Brüel & Kjær - *simply unmistakable*.

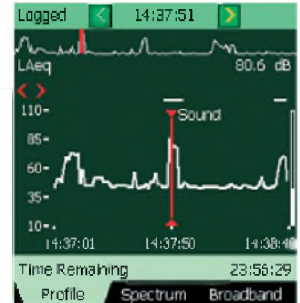
Unparalleled performance and more integrated applications. This powerful tool was built just for you to help do your work better and faster!

Like the great green sound level meters of the past, Type 2250 has become an industry standard, setting sales records worldwide.

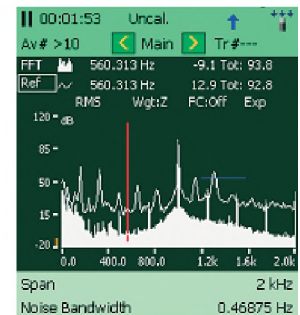
Don't take our word for it, just listen to what our customers have to say.

- "...after spending a few days with my new 2250 all I can say is "wow." This is a product done right. Not only is it extremely easy to use (and has a great long-lasting battery) the documentation and software is excellent. The 2250 represents Brüel & Kjær at its best."

For more details please contact your local sales representative or go to bksv.com



Noise Profiles



6400 Line FFT



Reverberation Time

HEADQUARTERS: DK-2850 Nærum · Denmark · Telephone: +4545800500
Fax: +4545801405 · www.bksv.com · info@bksv.com

USA: 2815 Colonnades Court · Norcross, GA 30071
Toll free (800) 332-2040 · www.BKhome.com · bkinfo@bksv.com

Type 2250: *Easy, Safe, Clever!*

Brüel & Kjær 

NEWS / INFORMATIONS

CONFERENCES

If you have any news to share with us, send them by mail or fax to the News Editor (see address on the inside cover), or via electronic mail to stevenb@aciacooustical.com

2007

2-7 September 19th International Congress on Acoustics (ICA2007), Madrid Spain. (SEA, Serrano 144, 28006 Madrid, Spain; Web: www.ica2007madrid.org)

9-12 September: ICA2007 Satellite Symposium on Musical Acoustics (ISMA2007). Barcelona, Spain. Web: www.isma2007.org

9-12 September: ICA2007 Satellite Symposium on Room Acoustics (ISMA2007). Sevilla, Spain. Web: www.isra2007.org

17-19 September. 3rd International Symposium on Fan Noise. Lyon, France. Web: www.fannoise2007.org

19-21 September. Autumn Meeting of the Acoustical Society of Japan. Kofu, Japan. Web: www.asj.gr.jp/index-en.html

20-22 September: Wind Turbine Noise 2007, Lyon, France. Web: www.windturbinenoise2007.org

24-28 September. XIX Session of the Russian Acoustical Society. Nizhny Novgorod, Russia. Web: www.akin.ru

3-5 October. Pacific Rim Underwater Acoustics Conference, Vancouver, Canada. Web: <http://pruac.apl.washington.edu/>

9-12 October. Canadian Acoustical Association Annual Conference. Montreal, Canada. Web: <http://www.caa-aca.ca>

17-18 October. Institute of Acoustics Autumn Conference, Oxford, UK. Web: <http://www.ioa.org.uk/viewupcoming.asp>

22-24 October. Noise-Con 2007. Reno, Nevada, USA. Web: www.inceusa.org/nc07/index.asp

28-31 October. IEEE International Ultrasonics Symposium, New York, NY, USA. Web: http://ewh.ieee.org/conf.ius_2007

14-16 November. 14th Mexican International Congress on Acoustics. Leon, Guanajuato, Mexico. Email: sberista@hotmail.com

November 27 - December 02: 154th Meeting of the Acoustical Society of America. New Orleans, LA, USA. Web: www.asa.aip.org

09-13 December. IEEE Automatic Speech Recognition and Understanding Workshop. Kyoto, Japan. Web: www.asru2007.org

2008

March 31 - April 04. International Conference on Acoustics, Speech, and Signal Processing (IEEE ICASSP 2008). Las Vegas, Nevada, USA. Web: www.icassp2008.org

17-18 April. Swiss Acoustical Society Spring Meeting. Bellinzona (Tessin), Switzerland. Web: www.sga-ssa.ch

CONFÉRENCES

Si vous avez des nouvelles à nous communiquer, envoyez-les par courrier ou fax (coordonnées incluses à l'envers de la page couverture), ou par courriel à stevenb@aciacooustical.com

2007

2-7 septembre 19e Congrès international sur l'acoustique (ICA2007), Madrid Spain. (SEA, Serrano 144, 28006 Madrid, Spain; Web: www.ica2007madrid.org)

9-12 septembre: ICA2007 Satellite Symposium sur Musical Acoustics (ISMA2007). Barcelona, Spain. Web: www.isma2007.org

9-12 septembre: ICA2007 Satellite Symposium sur Room Acoustics (ISMA2007). Sevilla, Spain. Web: www.isra2007.org

17-19 septembre. 3rd International Symposium on Fan Noise. Lyon, France. Web: www.fannoise2007.org

19-21 septembre. Autumn Meeting of the Acoustical Society of Japan. Kofu, Japan. Web: www.asj.gr.jp/index-en.html

20-22 Septembre: Wind Turbine Noise 2007, Lyon, France. Web: www.windturbinenoise2007.org

24-28 septembre. XIX Session of the Russian Acoustical Society. Nizhny Novgorod, Russia. Web: www.akin.ru

3-5 octobre. Pacific Rim Underwater Acoustics Conference, Vancouver, Canada. Web: <http://pruac.apl.washington.edu/>

9-12 octobre. Canadian Acoustical Association Annual Conference. Montreal, Canada. Web: <http://www.caa-aca.ca>

17-18 octobre. Institute of Acoustics Autumn Conference, Oxford, UK. Web: <http://www.ioa.org.uk/viewupcoming.asp>

22-24 octobre. Noise-Con 2007. Reno, Nevada, USA. Web: www.inceusa.org/nc07/index.asp

28-31 octobre. IEEE International Ultrasonics Symposium, New York, NY, USA. Web: http://ewh.ieee.org/conf.ius_2007

14-16 Novembre. 14th Mexican International Congress on Acoustics. Leon, Guanajuato, Mexico. Email: sberista@hotmail.com

novembre 27 - décembre 02: 154th Meeting de l'Acoustical Society d'America. New Orleans, LA, USA. Web: www.asa.aip.org

09-13 décembre. IEEE Automatic Speech Recognition and Understanding Workshop. Kyoto, Japan. Web: www.asru2007.org

2008

mars 31 - avril 04. International Conference on Acoustics, Speech, and Signal Processing (IEEE ICASSP 2008). Las Vegas, Nevada, USA. Web: www.icassp2008.org

17-18 avril. Swiss Acoustical Society Spring Meeting. Bellinzona (Tessin), Switzerland. Web: www.sga-ssa.ch

29 June - 04 July: Joint Meeting of European Acoustical Association, Acoustical Society of America, and Acoustical Society of France. Paris, France. Web: www.sfa.asso.fr/en/index.htm

7-10 July: 18th International Symposium on Nonlinear Acoustics (ISNA18). Stockholm, Sweden. E-mail: benflo@mech.kth.se

27-30 July. Noise-Con 2008. Dearborn, MI, USA.

27-31 July. 10th Mechanics of Hearing Workshop. Keele University, UK. Web: www.mechanicsofhearing.com

28 July - 1 August: 9th International Congress on Noise as a Public Health Problem. Mashantucket, Pequot Tribal Nation, (CT, USA). Web: www.icben.org

25-29 August. 10th International Conference on Music Perception and Cognition. Sapporo, Japan. Web: <http://icmpc10.typepad.jp>

08-12 September: International Symposium on Underwater Reverberation and Clutter. Lerici, Italy. Web: <http://isurc2008.org>

15-17 September: International Conference on Noise and Vibration Engineering (ISMA2008). Leuven, Belgium. Web: www.isma-isaac.be

16-18 September: Underwater Noise Measurement. Southampton, UK. Web: www.ioa.org.uk/viewupcoming.asp

22-26 September: Interspeech 2008 - 10th ICSLP, Brisbane, Australia. Web: www.interspeech2008.org

26-29 October: Interspeech 2008, Shanghai, China. Web: www.interspeech2008.org

01-05 November. IEEE International Ultrasonic Symposium. Beijing, China. Web: www.ieee-uffa.org/ulmain.asp?page=symposia

2009

23-26 August: Interspeech 2009, Ottawa, Canada.

23-27 August: International Congress on Acoustics 2010. Sydney, Australia. Web: www.acoustics.asn.au

06-10 September: Interspeech 2009. Brighton, UK. Web: www.interspeech2009.org

2010

23-27 August: International Congress on Acoustics 2010. Sydney, Australia. Web: www.acoustics.asn.au

26-30 September: Interspeech 2010. Makuhari, Japan. Web: www.interspeech2010.org

29 juin - 04 juillet: Joint Meeting d'European Acoustical Association, Acoustical Society d'America, et Acoustical Society du France. Paris, France. Web: www.sfa.asso.fr/en/index.htm

7-10 juillet: 18th International Symposium sur Nonlinear Acoustics (ISNA18). Stockholm, Sweden. E-mail: benflo@mech.kth.se

27-30 juin. Noise-Con 2008. Dearborn, MI, USA.

27-31 juillet. 10th Mechanics of Hearing Workshop. Keele University, UK. Web: www.mechanicsofhearing.com

28 juillet - 1 août: 9th International Congress sur Noise as a Public Health Problem. Mashantucket, Pequot Tribal Nation, (CT, USA). Web: www.icben.org

25-29 août: 10th International Conference on Music Perception and Cognition. Sapporo, Japan. Web: <http://icmpc10.typepad.jp>

08-12 septembre: International Symposium on Underwater Reverberation and Clutter. Lerici, Italy. Web: <http://isurc2008.org>

15-17 septembre: International Conference on Noise and Vibration Engineering (ISMA2008). Leuven, Belgium. Web: www.isma-isaac.be

16-18 septembre: Underwater Noise Measurement. Southampton, UK. Web: www.ioa.org.uk/viewupcoming.asp

22-26 septembre: Interspeech 2008 - 10th ICSLP, Brisbane, Australia. Web: www.interspeech2008.org

26-29 Octobre: Interspeech 2008, Shanghai, China. Web: www.interspeech2008.org

01-05 novembre. IEEE International Ultrasonic Symposium. Beijing, China. Web: www.ieee-uffa.org/ulmain.asp?page=symposia

2009

23-26 août: Interspeech 2009, Ottawa, Canada.

23-27 août: International Congress sur Acoustics 2010. Sydney, Australia. Web: www.acoustics.asn.au

06-10 septembre: Interspeech 2009. Brighton, UK. Web: www.interspeech2009.org

2010

23-27 août: International Congress sur Acoustics 2010. Sydney, Australia. Web: www.acoustics.asn.au

26-30 septembre: Interspeech 2010. Makuhari, Japan. Web: www.interspeech2010.org

NEWS

We want to hear from you! If you have any news items related to the Canadian Acoustical Association, please send them. Job promotions, recognition of service, interesting projects, recent research, etc. are what make this section interesting.

OTTAWA NOISE SPECIALIST JOINS BOARD OF THE ACOUSTICAL SOCIETY OF AMERICA

Melville, NY, July 15, 2007 — Michael R. Stinson, group leader for the Acoustics & Signal Processing Group in the Institute for Microstructural Sciences at the National Research Council of Canada, has been elected a Member of the Executive Council of the Acoustical Society of America (ASA), headquartered in Melville, NY. He took office on 6 June 2007. "I was pleased and honored to have been elected to the ASA Executive Council," Stinson said. "I look forward with some excitement to serving the Society in this new capacity."

Dr. Stinson has been active in the ASA for many years. He was elected a Fellow of the Society in 1990 and has served as Associate Editor of the *Journal of the Acoustical Society of America* (JASA), as Chair of the Technical Committee on Noise, and as Technical Program Chair for the ASA's 1993 meeting held in Ottawa. He is currently an Associate Editor for *JASA Express Letters*.

Dr. Stinson's research activities have spanned a broad range of technical activities. He has studied the acoustics of the human ear canal in support of hearing aid design and has investigated the properties of materials used to control noise. Dr. Stinson has studied the physical mechanisms that affect how sound propagates through the atmosphere. He has also studied the use of arrays of microphones, for videoconferencing and surveillance.

Stinson received B.Sc. and M.Sc. degrees in physics from Simon Fraser University, and a Ph.D. in physics from Queens's University, Kingston, Ontario. He has been an adjunct professor at University of Waterloo since 1997 and was a visiting associate research scientist in Otolaryngology at Columbia University, New York, from 1986 to 1994. He is a Distinguished Corresponding Member of the Institute of Noise Control Engineering.

The Acoustical Society of America is the premier international scientific society in acoustics devoted to the science and technology of sound. Its 7000 members worldwide represent a broad spectrum of the study of acoustics. ASA publications include the *Journal of the Acoustical Society of America*—the world's leading journal on acoustics, *Acoustics Today* magazine, books, and standards on acoustics. The Society also holds two major scientific meetings per year. For more information about the Society visit our website, <http://asa.aip.org>

EXCERPTS FROM "WE HEAR THAT...", IN ECHOS, ASA

James West received the 2006 National Medal of Technology at the White House on July 27. Jim, who is a professor at Johns Hopkins University and a former president of ASA, was recognized "for co-inventing the electret microphone while working with Gerhard Sessler at Bell Labs in 1962. Ninety percent of the two billion microphones produced annually and used in everyday items such as telephones, hearing aids, camcorders, and multimedia computers employ electret technology."

Jan Achenbach received the National Medal of Science at the White House on July 27. Jan, who is a professor at Northwestern University and an ASA Fellow, was recognized for "seminal contributions to engineering research and education in the area of wave propagation in solids and for pioneering the field of quantitative non-destructive evaluation."

Patricia Kuhl, Professor of Speech and Co-Director of the University of Washington Institute for Learning and Brain Sciences, received an Outstanding Alumni Achievement award from the University of Minnesota.

EXCERPTS FROM "SCANNING THE JOURNALS", IN ECHOS, ASA

An invited review of **Lord Rayleigh's contributions to acoustics** by D. Murray Campbell appears in the July issue of *Acoustical Science and Technology*. The paper begins with a brief biography, followed by discussions of some of Rayleigh's more important Acoustics papers, including his first on the theory of resonances, the Rayleigh disc, his energy-based approach to the study of vibrating systems (widely known as Rayleigh's principle), and Rayleigh waves that propagate on the surfaces of elastic solids (and now form the basis of surface acoustic wave (SAW) devices).

Clownfish are prolific singers that produce a wide variety of sounds, and their **sound producing mechanism** is the subject of a paper in the 18 May issue of *Science*. An unusual sonic ligament, responsible for a rapid lower jaw elevation, is the key. The ligament, acting as a cord, forces the mandible to turn around, which forces the mouth to close. Sound results from the collisions of the jaw teeth, transferring energy to the jaws that radiate the sound. Clownfish produce a wide variety of sounds, described as "chirps" and "pops" with energy between 450 and 800 Hz.

According to an article entitled "How the **brain can hear shapes**" in the 26 May issue of *New Scientist*, seeing may depend less on our eyes than we thought. When you identify an object's shape, a particular part of your brain called the lateral-occipital tactile-visual area (LOtv) "lights up." At first this area was thought to be purely visual, but several years ago it was shown that touch can also activate it. Now it has been discovered that "hearing" a shape can also activate it (see following article in *Nature Neuroscience*). Researchers taught seven sighted volunteers to use a device called "The voice," which converts visual details into sound, using pitch to represent up and down, and volume to reflect brightness. They then performed MRI scans of the volunteers' brains, plus those of two expert blind users of the device,

The lateral-occipital tactile-visual area (LOtv) is activated when objects are recognized by vision or touch. A paper in *Nature Neuroscience*, the LOtv is also activated in sighted and blind humans who recognize objects by extracting shape information from **visual-to-auditory sensor** substitution soundscapes (see previous article in *New Scientist*). Recognizing objects by their typical sounds or learning to associate specific soundscapes with specific objects do not activate this region.

Various aspects of the **quartz tuning fork** are discussed in a paper in the May issue of *American Journal of Physics*. Its original purpose was a high quality factor resonator for use as a stable frequency reference, but it has also seen more exotic applications in

sensing and scanning probe microscopy. The paper discusses how to tune the quality factor by injecting energy in phase with the current at resonance (quality factor increase) or out of phase (quality factor decrease). The principle of shear force scanning probe microscopy is demonstrated on a simple profiler. The interaction between the tuning fork and the surface under investigation influences the current through the tuning fork by perturbing the resonance frequency of the prong in contact with the sample.

Waves generated deep inside the Sun and other stars help astronomers see the hidden core where energy-producing fusion reactions occur, according to an article in the 15 June issue of *Science*. These waves, similar in some ways to seismic waves on Earth, come in two main types: gravity waves or "g modes" that are driven by buoyancy, and pressure waves or "p modes," which are **sound waves**. It is possible to understand what is happening inside the Sun by observing the oscillations produced on the solar surface by these modes. P modes are trapped in the Sun's outer layers and only a few penetrate below a fractional radius of 0.2 into the core of the Sun. G modes, on the other hand, are trapped in the core as well as in the radiative zone.

The "**effective mass of an oscillating spring**" is the subject of a paper in the February issue of *The Physics Teacher*. Measured values for the mass presented in the paper are in good agreement with those calculated using a simple model. The calculation and experimental observations are made with varying number of coils oscillating. The oscillation period is proportional to the number of active coils.

Some of the ways in which weather in one part of the world affects others is explained by a model based on planetary waves, according to note in the 3 June issue of *Nature Physics*. The interacting **planetary waves**, in particular the interaction of four resonant clusters, each composed of three modes, explains why intraseasonal oscillations affect both the Northern and Southern hemispheres and why these oscillations are more observable in winter.

Shake a can of mixed nuts and the "**Brazil nut effect**" often brings the largest nuts to the top, an article in the July issue of *Physics World* reminds us. However the "reverse Brazil-nut effect" (see Winter 2005 issue of *ECHOES*) often occurs in containers with particles of different sizes and densities when the larger particles are heavy enough to push the smaller particles out from beneath them or when the shaking is violent enough that gaps between smaller particles become large enough for the large particles to fall through. Now researchers have observed an abrupt transition between the two effects. A glass tube with a mixture of glass spheres 1.4 mm in diameter and brass spheres 2.4 mm in diameter was shaken at 20 Hz. At the end of one hour, a reverse-Brazil nut state was observed, with nearly all the large spheres sinking to the bottom of the tube, but after about 25 hours of shaking, the larger brass spheres suddenly started drifting upwards and within an hour were all at the top of the tube where they remained for the next 180 hours. It is believed that the change was caused by increased friction between the spheres which became scratched and scuffed after hours of vibration. They repolished the scuffed spheres in an ultrasonic cleaner, and again the brass spheres started off at the bottom of the tube for 25 hours before rising again to the top.

Accuracy & Low Cost— Scantek Delivers Sound & Vibration Instruments

Scantek offers two integrating sound level meters and real-time octave-band analyzers from CESVA that make measurements quickly and conveniently. The easy to use SC-30 and SC-160 offer a single dynamic range of 100dB, eliminating any need for range adjustments. They simultaneously measure all the functions with frequency weightings A, C and Z. Other features include a large back-lit screen for graphical and numerical representation and a large internal memory.

The SC-30 is a Type 1 precision analyzer while the SC-160 Type 2 analyzer offers the added advantages of lower cost and NC analysis for real-time measurement of equipment and room noise. Prices starting under \$2,000, including software.

Scantek delivers more than just equipment. We provide solutions to today's complex noise and vibration problems with unlimited technical support by acoustical engineers that understand the complex measurement industry.

Scantek

Sound and Vibration
Instrumentation & Engineering

7060 Oakland Mills Road • Suite L
Columbia, MD 21046
800•224•3813
www.scantekinc.com
info@scantekinc.com

SC-30 / SC-160 Applications

- Machinery Noise
- Community Noise
- HVAC Acoustics
- Room Acoustics & Reverb Time
- Noise Criteria (NC) (SC-160)

CESVA

We sell, rent, service, and calibrate sound and vibration instruments.



INSTRUCTIONS TO AUTHORS FOR THE PREPARATION OF MANUSCRIPTS

Submissions: The original manuscript and two copies should be sent to the Editor-in-Chief.

General Presentation: Papers should be submitted in camera-ready format. Paper size 8.5" x 11". If you have access to a word processor, copy as closely as possible the format of the articles in *Canadian Acoustics* 18(4) 1990. All text in Times-Roman 10 pt font, with single (12 pt) spacing. Main body of text in two columns separated by 0.25". One line space between paragraphs.

Margins: Top - title page: 1.25"; other pages, 0.75"; bottom, 1" minimum; sides, 0.75".

Title: Bold, 14 pt with 14 pt spacing, upper case, centered.

Authors/addresses: Names and full mailing addresses, 10 pt with single (12 pt) spacing, upper and lower case, centered. Names in bold text.

Abstracts: English and French versions. Headings, 12 pt bold, upper case, centered. Indent text 0.5" on both sides.

Headings: Headings to be in 12 pt bold, Times-Roman font. Number at the left margin and indent text 0.5". Main headings, numbered as 1, 2, 3, ... to be in upper case. Sub-headings numbered as 1.1, 1.2, 1.3, ... in upper and lower case. Sub-sub-headings not numbered, in upper and lower case, underlined.

Equations: Minimize. Place in text if short. Numbered.

Figures/Tables: Keep small. Insert in text at top or bottom of page. Name as "Figure 1, 2, ..." Caption in 9 pt with single (12 pt) spacing. Leave 0.5" between text.

Line Widths: Line widths in technical drawings, figures and tables should be a minimum of 0.5 pt.

Photographs: Submit original glossy, black and white photograph.

Scans: Should be between 225 dpi and 300 dpi. Scan: Line art as bitmap tiffs; Black and white as grayscale tiffs and colour as CMYK tiffs;

References: Cite in text and list at end in any consistent format, 9 pt with single (12 pt) spacing.

Page numbers: In light pencil at the bottom of each page. Reprints: Can be ordered at time of acceptance of paper.

DIRECTIVES A L'INTENTION DES AUTEURS PREPARATION DES MANUSCRITS

Soumissions: Le manuscrit original ainsi que deux copies doivent être soumis au rédacteur-en-chef.

Présentation générale: Le manuscrit doit comprendre le collage. Dimensions des pages, 8.5" x 11". Si vous avez accès à un système de traitement de texte, dans la mesure du possible, suivre le format des articles dans *l'Acoustique Canadienne* 18(4) 1990. Tout le texte doit être en caractères Times-Roman, 10 pt et à simple (12 pt) interligne. Le texte principal doit être en deux colonnes séparées d'un espace de 0.25". Les paragraphes sont séparés d'un espace d'une ligne.

Marges: Dans le haut - page titre, 1.25"; autres pages, 0.75"; dans le bas, 1" minimum; latérales, 0.75".

Titre du manuscrit: 14 pt à 14 pt interligne, lettres majuscules, caractères gras. Centré.

Auteurs/adresses: Noms et adresses postales. Lettres majuscules et minuscules, 10 pt à simple (12 pt) interligne. Centré. Les noms doivent être en caractères gras.

Sommaire: En versions anglaise et française. Titre en 12 pt, lettres majuscules, caractères gras, centré. Paragraphe 0.5" en alinéa de la marge, des 2 cotés.

Titres des sections: Tous en caractères gras, 12 pt, Times-Roman. Premiers titres: numéroter 1, 2, 3, ..., en lettres majuscules; sous-titres: numéroter 1.1, 1.2, 1.3, ..., en lettres majuscules et minuscules; sous-sous-titres: ne pas numéroter, en lettres majuscules et minuscules et soulignés.

Equations: Les minimiser. Les insérer dans le texte si elles sont courtes. Les numéroter.

Figures/Tableaux: De petites tailles. Les insérer dans le texte dans le haut ou dans le bas de la page. Les nommer "Figure 1, 2, 3,..." Légende en 9 pt à simple (12 pt) interligne. Laisser un espace de 0.5" entre le texte.

Largeur Des Traits: La largeur des traits sur les schémas technique doivent être au minimum de 0.5 pt pour permettre une bonne reproduction.

Photographies: Soumettre la photographie originale sur papier glacé, noir et blanc.

Figures Scanées: Doivent être au minimum de 225 dpi et au maximum de 300 dpi. Les schémas doivent être scannés en bitmaps tif format. Les photos noir et blanc doivent être scannées en échelle de gris tifs et toutes les photos couleurs doivent être scannées en CMYK tifs.

Références: Les citer dans le texte et en faire la liste à la fin du document, en format uniforme, 9 pt à simple (12 pt) interligne.

Pagination: Au crayon pâle, au bas de chaque page. Tirés-à-part: Ils peuvent être commandés au moment de l'acceptation du manuscrit.

The Canadian Acoustical Association l'Association Canadienne d'Acoustique



Application for Membership

CAA membership is open to all individuals who have an interest in acoustics. Annual dues total \$60.00 for individual members and \$20.00 for Student members. This includes a subscription to *Canadian Acoustics*, the Association's journal, which is published 4 times/year. New membership applications received before August 31 will be applied to the current year and include that year's back issues of *Canadian Acoustics*, if available. New membership applications received after August 31 will be applied to the next year.

Subscriptions to *Canadian Acoustics* or Sustaining Subscriptions

Subscriptions to *Canadian Acoustics* are available to companies and institutions at the institutional subscription price of \$60.00. Many companies and institutions prefer to be a Sustaining Subscriber, paying \$300.00 per year, in order to assist CAA financially. A list of Sustaining Subscribers is published in each issue of *Canadian Acoustics*. Subscriptions for the current calendar year are due by January 31. New subscriptions received before August 31 will be applied to the current year and include that year's back issues of *Canadian Acoustics*, if available.

Please note that electronic forms can be downloaded from the CAA Website at caa-aca.ca

Address for subscription / membership correspondence:

Name / Organization _____
 Address _____
 City/Province _____ Postal Code _____ Country _____
 Phone _____ Fax _____ E-mail _____

Address for mailing *Canadian Acoustics*, if different from above:

Name / Organization _____
 Address _____
 City/Province _____ Postal Code _____ Country _____

Areas of Interest: (Please mark 3 maximum)

- | | | |
|--|---|---|
| 1. Architectural Acoustics | 5. Psychological / Physiological Acoustic | 9. Underwater Acoustics |
| 2. Engineering Acoustics / Noise Control | 6. Shock and Vibration | 10. Signal Processing / Numerical Methods |
| 3. Physical Acoustics / Ultrasound | 7. Hearing Sciences | 11. Other |
| 4. Musical Acoustics / Electro-acoustics | 8. Speech Sciences | |

For student membership, please also provide:

 (University) (Faculty Member) (Signature of Faculty Member) (Date)

I have enclosed the indicated payment for:

- CAA Membership \$ 60.00
 CAA Student Membership \$ 20.00
 Institutional Subscription \$ 60.00
 Sustaining Subscriber \$ 300.00
 includes subscription (4 issues /year)
 to *Canadian Acoustics*.

Payment by: Cheque
 Money Order
 VISA credit card (Only VISA accepted)

For payment by VISA credit card:

Card number _____
 Name of cardholder _____
 Expiry date _____

Mail application and attached payment to:

 (Signature) (Date)

D. Quirt, Secretary, Canadian Acoustical Association, PO Box 74068, Ottawa, Ontario, K1M 2H9, Canada



Formulaire d'adhésion

L'adhésion à l'ACA est ouverte à tous ceux qui s'intéressent à l'acoustique. La cotisation annuelle est de 60.00\$ pour les membres individuels, et de 20.00\$ pour les étudiants. Tous les membres reçoivent *L'Acoustique Canadienne*, la revue de l'association. Les nouveaux abonnements reçus avant le 31 août s'appliquent à l'année courante et incluent les anciens numéros (non-épuisés) de *L'Acoustique Canadienne* de cette année. Les nouveaux abonnements reçus après le 31 août s'appliquent à l'année suivante.

Abonnement pour la revue *Acoustique Canadienne* et abonnement de soutien

Les abonnements pour la revue *Acoustique Canadienne* sont disponibles pour les compagnies et autres établissements au coût annuel de 60.00\$. Des compagnies et établissements préfèrent souvent la cotisation de membre bienfaiteur, de 300.00\$ par année, pour assister financièrement l'ACA. La liste des membres bienfaiteurs est publiée dans chaque issue de la revue *Acoustique Canadienne*. Les nouveaux abonnements reçus avant le 31 août s'appliquent à l'année courante et incluent les anciens numéros (non-épuisés) de *L'Acoustique Canadienne* de cette année. Les nouveaux abonnements reçus après le 31 août s'appliquent à l'année suivante.

Pour obtenir des formulaires électroniques, visitez le site Web: caa-aca.ca

Pour correspondance administrative et financière:

Nom / Organisation _____

Adresse _____

Ville/Province _____ Code postal _____ Pays _____

Téléphone _____ Téléc. _____ Courriel _____

Adresse postale pour la revue *Acoustique Canadienne*

Nom / Organisation _____

Adresse _____

Ville/Province _____ Code postal _____ Pays _____

Cocher vos champs d'intérêt: (maximum 3)

- | | | |
|---|-------------------------------|--|
| 1. Acoustique architecturale | 5. Physio / Psycho-acoustique | 9. Acoustique sous-marine |
| 2. Génie acoustique / Contrôle du bruit | 6. Chocs et vibrations | 10. Traitement des signaux / Méthodes numériques |
| 3. Acoustique physique / Ultrasons | 7. Audition | 11. Autre |
| 4. Acoustique musicale / Electro-acoustique | 8. Parole | |

Prière de remplir pour les étudiants et étudiantes:

(Université) (Nom d'un membre du corps professoral) (Signature du membre du corps professoral) (Date)

Cocher la case appropriée:

- Membre individuel \$ 60.00
 Membre étudiant(e) \$ 20.00
 Abonnement institutionnel \$ 60.00
 Abonnement de soutien \$ 300.00
(comprend l'abonnement à
L'acoustique Canadienne)

Méthode de paiement:

- Chèque au nom de l'Association Canadienne d'Acoustique
 Mandat postal
 VISA (*Seulement VISA*)

Pour carte VISA: Carte n° _____

Nom _____

Date d'expiration _____

Prière d'attacher votre paiement au formulaire d'adhésion. Envoyer à :

(Signature)

(Date)

Secrétaire exécutif, Association Canadienne d'Acoustique, Casier Postal 74068, Ottawa, K1M 2H9, Canada

The Canadian Acoustical Association l'Association Canadienne d'Acoustique



PRESIDENT PRÉSIDENT

Stan Dosso
University of Victoria
Victoria, British Columbia
V8W 3P6
(250) 472-4341
sdosso@uvic.ca

PAST PRESIDENT PRÉSIDENT SORTANT

John Bradley
IRC, NRCC
Ottawa, Ontario
K1A 0R6
(613) 993-9747
john.bradley@nrc-cnrc.gc.ca

SECRETARY SECRÉTAIRE

David Quirt
P. O. Box 74068
Ottawa, Ontario
K1M 2H9
(613) 993-9746
dave.quirt@nrc-cnrc.gc.ca

TREASURER TRÉSORIER

Dalila Giusti
Jade Acoustics
545 North Rivermede Road, Suite 203
Concord, Ontario
L4K 4H1
(905) 660-2444
dalila@jadeacoustics.com

EDITOR-IN-CHIEF RÉDACTEUR EN CHEF

Ramani Ramakrishnan
Dept. of Architectural Science
Ryerson University
350 Victoria Street
Toronto, Ontario
M5B 2K3
(416) 979-5000 #6508
rramakri@ryerson.ca
ramani@aiolos.com

WORLD WIDE WEB HOME PAGE: <http://www.caa-aca.ca>

Dave Stredulinsky
(902) 426-3100

ASSISTANT EDITOR RÉDACTEUR ADJOINT

Ralph Baddour
Department of Medical Biophysics
University of Toronto
rbaddour@uhnres.utoronto.ca

DIRECTORS DIRECTEURS

Alberto Behar
(416) 265-1816
behar@sympatico.ca

Tim Kelsall
(905) 403-3932
tkelsall@hatch.ca

Richard Peppin
(410) 290-7726
peppinr@scantekinc.com

Nicole Collison
(902) 426-3100, Ext. 94
nicole.collison@drdc-rddc-gc.ca

Anita Lewis
(403) 297-3793
anita.lewis@gov.ab.ca

Clair Wakefield
(250) 370-9302
nonoise@shaw.ca

Christian Giguère
613-562-5800 Ext. 3071
cgigure@UOTTAWA.CA

Vijay Parsa
(519) 661-2111 Ex. 88947
parsa@nca.uwo.ca

SUSTAINING SUBSCRIBERS / ABONNES DE SOUTIEN

The Canadian Acoustical Association gratefully acknowledges the financial assistance of the Sustaining Subscribers listed below. Their annual donations (of \$300.00 or more) enable the journal to be distributed to all at a reasonable cost.

L'Association Canadienne d'Acoustique tient à témoigner sa reconnaissance à l'égard de ses Abonnés de Soutien en publiant ci-dessous leur nom et leur adresse. En amortissant les coûts de publication et de distribution, les dons annuels (de \$300.00 et plus) rendent le journal accessible à tous nos membres.

ACI Acoustical Consultants Inc.

Mr. Steven Bilawchuk - (780) 414-6373
stevenb@aciacoustical.com - Edmonton, AB

Aercoustics Engineering Ltd

Mr. John O'Keefe - (416) 249-3361
aercoustics@aercoustics.com - Rexdale, ON

Dalimar Instruments Inc.

Mr. Daniel Larose - (514) 424-0033
daniel@dalimar.ca - Vaudreuil-Dorion, QC

Eckel Industries of Canada Ltd.

Mr. Bruce Allan - (613) 543-2967
eckel@eckel.ca - Morrisburg, ON

Hatch Associates Ltd.

Mr. Tim Kelsall - (905) 403-3932
tkelsall@hatch.ca - Mississauga, ON

Integral DX Engineering Ltd.

Mr. Greg Clunis - (613) 761-1565
greg@integraldxengineering.ca - Ottawa, ON

Jade Acoustics Inc.

Ms. Dalila Giusti - (905) 660-2444
dalila@jadeacoustics.com - Concord, ON

MJM Conseillers en Acoustique Inc.

MJM Acoustical Consultants Inc.
M. Michel Morin - (514) 737-9811
mmorin@mjm.qc.ca - Montréal, QC

OZA Inspections Ltd.

Mr. David Williams - (800) 664-8263x25
oza@ozagroup.com - Grimsby, ON

Pinchin Environmental Ltd.

(905) 363-0678; FAX: (905) 363-0681
info@pinchin.com - Mississauga, ON

Scantek Inc.

Mr. Richard J. Peppin, (410)-290-7726
peppinr@scantekinc.com - Columbia, MD

Soft dB Inc.

M. André L'Espérance - (418) 686-0993
contact@softdb.com - Sillery, QC

State of the Art Acoustik Inc.

Dr. C. Fortier - (613) 745-2003,
sota@sota.ca - Ottawa, ON

Valcoustics Canada Ltd.

Dr. Al Lightstone - (905) 764-5223
solutions@valcoustics.com
Richmond Hill, ON

Water & Earth Science Associates (WESA)

Dejan Zivkovic, M.Sc. - (905) 639-5789 x151
dzivkovic@wesa.ca - Burlington, ON

ACO Pacific Inc.

Mr. Noland Lewis - (650) 595-8588
acopac@acopacific.com - Belmont, CA

Bruel & Kjaer North America Inc.

Mr. Andrew Khoury - (514) 695-8225
andrew.khoury@bksv.com - Pointe-Claire, QC

Dodge-Regupol

Mr. Paul Downey - (416) 440-1094
pcd@regupol.com - Toronto, ON

Enviro Noise Control Corp.

Alex V. Tardecilla - (403) 279-2764
alex@enctech.net - Calgary, AB

HGC Engineering Ltd.

Mr. Bill Gastmeier - (905) 826-4044
info@hgcengineering.com - Mississauga, ON

J.E. Coulter Associates Ltd.

Mr. John Coulter - (416) 502-8598
jcoulter@on.aibn.com - Toronto, ON

JASCO Research Ltd.

Mr. Scott Carr - (902) 405-3336
scott@jasco.com - Halifax, NS

Novel Dynamics Test Inc.

Mr. Andy Metelka - (519) 853-4495
metelka@aztec-net.com - Acton, ON

Peutz & Associés

M. Marc Asselineau +33 1 45230500
marc.asselineau@club-internet.fr
Paris, FRANCE

Pyrok Inc.

(914) 777-7770; FAX: (914) 777-7103
info@pyrokinc.com - Mamaroneck, NY

SILEX Innovations Inc.

Mr. Mehmood Ahmed - (905) 612-4000
mehmooda@silex.com, Mississauga, ON

SounDivide Inc.

C.W. Ray Bakker - (877) 816-5435
ray.bakker@SounDivide.com - Calgary, AB

Swallow Acoustic Consultants Ltd.

Mr. John Swallow - (905) 271-7888
jswallow@jsal.ca - Mississauga, ON

Vibro-Acoustics

Mr. Tim Charlton - (800) 565-8401
tcharlton@vibro-acoustics.com
Scarborough, ON

West Caldwell Calibration Labs

Mr. Stanley Christopher - (905) 595-1107
info@wccal.com - Brampton

Acoustec Inc.

Dr. J.G. Migneron - (418) 834-1414
courrier@acoustec.qc.ca - St-Nicolas, QC

CDMca Ltd.

Jonas Sackanskis - (905) 265-7401
- Woodbridge, ON

Earth Tech Canada Inc.

Miroslav Ubovic - (905) 886-7022-x2215
noisevibration@earthtech.ca - Markham, ON

H.L. Blachford Ltd.

Mr. Dalton Prince - (905) 823-3200
amsales@blachford.ca - Mississauga, ON

Hydro-Quebec

M. Blaise Gosselin - (514) 840-3000x5134
gosselin.blaise@hydro.qc.ca - Montréal, QC

J.L.Richards & Assoc. Ltd.

Mr. Terry Vivyurka, P.Eng. - (613) 728-3571
mail@jlrichards.ca - Ottawa, ON

Mc SQUARED System Design Group

Mr. Wade McGregor - (604) 986-8181
info@mcsquared.com - North Vancouver, BC

Owens-Corning Canada Inc.

Mr. Salvatore Ciarlo - (800) 988-5269
salvatore.ciarlo@owenscorning.com -
St.Leonard, QC

Michel Picard

(514) 343-7617; FAX: (514) 343-2115
michel.picard@umontreal.ca - Brossard, QC

RWDI AIR Inc.

Peter VanDelden - (519) 823-1311
peter.vandelden@rwdi.com - Guelph, ON

SNC/Lavalin Environment Inc.

M. Jean-Luc Allard - (514) 651-6710
jeanluc.allard@snclavalin.com - Longueuil, QC

Spaarg Engineering Ltd.

Dr. Robert Gaspar - (519) 972-0677
gasparr@kelcom.igs.net - Windsor, ON

Tacet Engineering Ltd.

Dr. M.P. Sacks - (416) 782-0298
mal.sacks@tacet.ca - Toronto, ON

Wakefield Acoustics Ltd.

Mr. Clair Wakefield - (250) 370-9302
nonoise@shaw.ca - Victoria, BC

Wilrep Ltd.

Mr. Don Wilkinson - (905) 625-8944
info@wilrep.com - Mississauga, ON